COMISSÃO NACIONAL DE ENERGIA NUCLEAR-CNEN
CENTRO DE DESENVOLVIMENTO DA TECNOLOGIA NUCLEAR - CDTN Programa de Pós-Graduação em Ciência e Tecnologia das Radiações, Minerais e Materiais

UNIVERSIDAD DE SALAMANCA – USAL ESCUELA DE DOCTORADO "STUDII SALAMANTINI" Programa de Doctorado en Geología

TESE DE DOUTORADO

Origem e evolução dos depósitos de urânio na região noroeste da Província Uranífera de Lagoa Real, Bahia, Brasil

Camila Marques dos Santos

Orientadores/ Diretores:
Francisco Javier Rios (CDTN-BR)
Alexandre Raphael Cabral (UFMG-BR)
Clemente Recio (USAL-ES)

Dezembro 2020

COMISSÃO NACIONAL DE ENERGIA NUCLEAR - CNEN
CENTRO DE DESENVOLVIMENTO DA TECNOLOGIA NUCLEAR - CDTN
Programa de Pós-Graduação em Ciência e Tecnologia das Radiações, Minerais e Materiais

UNIVERSIDAD DE SALAMANCA – USAL ESCUELA DE DOCTORADO
"STUDII SALAMANTINI" Programa de Doctorado en Geología

Origem e evolução dos depósitos de urânio na região noroeste da Província Uranífera de Lagoa Real, Bahia, Brasil

Camila Marques dos Santos

Tese apresentada ao Curso de Pós-Graduação em Ciência e Tecnologia das Radiações, Minerais e Materiais (CDTN-Brasil), como requisito parcial à obtenção do título de Doutor em Ciência e Tecnologia dos Minerais e Meio Ambiente, e à *Escuela de doctorado* da *Universidad de Salamanca* (USAL-Espanha) como requisito parcial à obtenção do título de *Doctor en Geología*.

Área de concentração – CDTN: Ciência e Tecnologia dos Minerais e Meio Ambiente.

Línea de investigación – USAL: Caracterización geoquímica e isotópica de rocas, minerales, y de productos de consumo humano para establecer procedencia y justificar denominaciones de origen.

Belo Horizonte, Dezembro de 2020

Agradecimentos

Ao CDTN por prover a estrutura física para o desenvolvimento desta tese, aos pesquisadores e funcionários do CDTN e PGCDTN.

A Coordenação de Aperfeiçoamento de Pessoal de Nível Superior - Brasil (CAPES) pelo apoio financeiro provendo a bolsa de doutorado, em especial pela bolsa do Programa de Doutorado Sanduíche no Exterior (Pr. n° 88882.442551/2019-01).

Às Industrias Nucleares do Brasil na pessoa do geólogo Evando Carele e do técnico Ailton, Coordenador de Geologia e Supervisor de Lavra, respectivamente, que sempre nos acompanham nas etapas de campo e prontamente nos atendem quando necessário.

Ao time de orientadores Dr. Francisco Javier, Dr. Alexandre Cabral e Dr. Clemente Recio. Ao Dr. Francisco Javier que me acompanhou durante toda a pós-graduação. Obrigada pela paciência, compreensão e incentivo durante estes anos. Ao Dr. Alexandre Cabral por ter aceitado encarar esse trabalho, por ter engrandecido essa tese com discussões, apoio e abrindo portas. Ao Dr. Clemente Recio por ter me recebido muito bem em Salamanca e pela disposição em ajudar. O convívio diário com todos vocês certamente foi um aprendizado à parte.

Aos Drs. Michael Wiedenbeck e Alexander Rocholl por terem me recebido no GFZ-Potsdam, pela atenção e discussões durante e após as análises de SIMS. Ao Dr. Adrian Boyce pelo auxilio durante as analises de isótopos estáveis na SUERC em Glasgow. Aos técnicos dos laboratórios de preparação de amostras da UERJ (LGPA) e UFOP pelo grande auxílio.

À Dr. Kathryn Cutts pelas incansáveis correções e discussões nos manuscritos e por me auxiliar a lidar com o submundo das revistas científicas.

Aos colegas do Laboratório de Caracterização Mineralógica e Metalogênese (LCMM) – Lucilia, Mônica, Lucas, Tiago, Nilo, Anna Luíza e Jefferson – por compartilhar discussões, idéias, fofocas, piadas e cafeína durante todos esses anos.

À minha família que mesmo distante, e não fazendo muita idéia do que tudo isso se trata, sempre me apoiou.

Aos amigos de sempre e aos novos que compartilharam momentos comigo e ajudaram direta ou indiretamente com o desenvolvimento desse trabalho.

RESUMO

A Província Uranífera de Lagoa Real (PULR) está localizada a norte do Orógeno Araçuaí na porção invertida do Aulacógeno do Paramirim. A PULR é representada principalmente pelas rochas de 1,75 Ga da Suíte Intrusiva Lagoa Real (SILR), comumente denominadas de Granito São Timóteo, que são intercaladas com lentes métricas de albitito. Os albititos são os principais portadores da mineralização de urânio e podem ou não estar mineralizados. Este estudo aborda os principais aspectos das rochas dos depósitos Gameleira I (AN 35), Barreiro (AN 31) e Barrinha (AN 34) localizados na região noroeste da PULR, assim como apresenta novos dados petrográficos, geoquímicos e isotópicos. A SILR é geoquímicamente caracterizada pelo seu caráter metaluminoso, alcalino, reduzido, ferroan e nos diagramas de discriminação geotectônica mostra características de granitos do tipo-A, intraplaca e A2. Nos depósitos estudados a SILR é representada pela facies hipersolvus álcali-feldspato granito, em que predomina ortoclásio pertítico, hedembergita, hastingsita, biotita e titanita. Os parâmetros de cristalização calculados indicam temperatura do *líquidus* mínima de 900 ºC e tardi-magmática entre 660-690 ºC. As rochas da SILR são convertidas em albititos através de dois principais processos que se desenvolveram sob regime predominantemente dúctil. O primeiro ocorreu antes da Orogenia Brasiliana e corresponde às alterações sódico-cálcica e ferro-cálcico-magnesiana que permitiram a cristalização de albita, clinopiroxênio de composição variada (hedembergita–augita–diopsídio–aegirina-augita), titanita, andradita e magnetita a partir da assembleia magmática do Granito São Timóteo. Estas alterações também são acompanhadas por dessilicificação. Este primeiro estágio desenvolveu-se sob variáveis condições de fugacidade de oxigênio e em alta temperatura (680–400 ºC), provavelmente durante o estágio tardi-magmático da SILR. O segundo estágio de alteração abrange os estágios sin a pós colisionais relacionados à Orogênese Brasiliana. Neste estágio ocorreram as alterações potássica retrógrada e cálcica tardia sob condições de facies anfibolito a xisto-verde. A alteração potássica é representada pela precipitação de uma assembleia retrógrada, principalmente anfibólio e biotita, cuja composição é comandada pelo clinopiroxênio precursor. Os geotermômetros baseados na composição do anfibólio indicam temperatura entre 650 e 400 ºC e pressão entre 3 e 0.9 kbar. A alteração cálcica tardia, por sua vez, foi responsável pela precipitação de epidoto, allanita e calcita e desenvolveu-se sob regime dúctil-ruptil com máxima temperatura de 300 ºC. A uraninita é intercrescida com titanita e zircão sob a forma de *veinlets* concordantes à foliação e está

hospedada principalmente nos albititos com diopsídio. Esta uraninita tem idade em torno de 580 Ma, coincidente ao estágio sin-colisional. A química da uraninita (baixa razão U/Th e alto conteúdo de Y) atesta temperatura de cristalização maior que 450 ºC. Durante o estágio tardi a pós-colisional da orogenia Brasiliana (530–450 Ma) a mineralização foi redistribuída como disseminações, associadas principalmente à assembleia retrógrada, e alterada para as espécies de U^{+6}, como a uranofana. Os dados obtidos neste trabalho aliados à literatura mostram que as idades da titanita e do zircão da assembleia de minério são mais antigas e mais variadas que as idade da uraninita. Esta variabilidade não representa um artefato, pois resultam coincidentes aos múltiplos eventos de rifteamento ocorridos no Aulacógeno do Paramirim entre ~1750 e 580 Ma. Este fato mostra o caráter multi-estágio da mineralização de U, que ocorreria em diversos momentos e motivado por múltiplos eventos geotectônicos, tendo seu fim no Ediacarano durante a orogenia Brasiliana. A assinatura geoquímica do minério é marcada por alto conteúdo de U, V, Nb, Ta, Zr/Hf, Mg e Na. O Granito São Timóteo pode ter sido fonte de U, mas a influencia de rochas vulcânicas também deve ser considerada. Os dados de isótopos de oxigênio e de hidrogênio mostram que os fluidos são empobrecidos em $\delta^{18}O_{smow}$, o que denota a influencia de água meteórica nos estágios finais de alteração.

Palavras-chave: depósitos de urânio, albititos, química mineral, geocronologia, Província Uranífera de Lagoa Real

ABSTRACT

The Lagoa Real uranium province (LRUP) is localized at the northern portion of Araçuaí orogen in the inverted portion of Paramirim aulacogen. The LRUP is represented by the rocks of ca. 1.75 Ga of Lagoa Real intrusive suite (LRIS), also known as São Timóteo Granite, which are interlayered with metric pods and lenses of albitite. The albitite rocks are the main ore host may be mineralized or barren. This study covers the main geological aspects of the northwestern portion of LRUP represented by Gameleira I (AN 35), Barreiro (AN 31) and Barrinha (AN 34) deposits, presenting new petrographical, mineral chemistry, geochronological and whole-rock geochemical data. The LRSI is characterized as metaluminous, alkaline, reduced and ferroan. In the diagrams of geotectonic discrimination LRSI is A-type, intraplate and A2. In the studied deposits, LRSI is represented by the facies hypersolvus alkali-feldspar granite, which predominates perthitic orthoclase, hedenbergite, hastingsite, biotite and titanite. The calculated crystallization parameters indicate minimum liquidus temperature of 900 ºC and late-magmatic temperature between 660-690 ºC. The LRIS rocks are converted into albitite through two main stages of alteration, which developed under predominantly ductil regime. The first occurred before the Brasiliano orogeny and corresponds to the sodic-calcic and iron-calcic-magnesian alterations, which resulted in the crystallization of albite, clinopyroxene of variable composition (hedenbergite–augite–aegirine-augite), titanite, andradite and magnetite over the magmatic assemblage of São Timóteo Granite. These alterations are also acompanied by desilicification. The first stage developed under variable oxygen fugacity conditions and high temperature (680–400 ºC), probably during the late-magmátic stage of LRSI. The second alteration stage covers the syn-to-pos collisional phase related to Brasiliano orogeny and resulted in the potassic and late calcic alterations. The potassic alteration is represented by the crystallization of a retrograde assemblage, mainly amphibole and biotite, which composition have been controlled by the clinopyroxene precursor. The geothermometers indicate temperature between 650 and 400 ºC, and pressure between 3 and 0.9 kbar. The late calcic alteration, in turn, was responsible by the epidote, allanite and calcite precipitation and developed under ductil-to-brittle regime and maximum temperature of 300 ºC. Uraninite is intergrown with titanite and zircon veinlets concordantly to foliation. This assemblage is associated with diopside-bearing albitite. Uraninite give precise age of 580 Ma, coincident with Brasiliano sin collisional stage. Uraninite chemistry (low U/Th ratio and high Y contents)

attests for high temperature of crystallization (> 450 ºC). During the Brasiliano tardi-to-post collisional stages (530–450 Ma), mineralization was redistributed as disseminations, associated mainly to retrograde assemblage, and altered to U^{+6} species, i.e. uranophane. Geochronological data obtained in this work and from literature shows that titanite and zircon ages are older and variable than those from uraninite. This variability is not an artefact, as the ages are coincident with the multiple rift events occurred in the Paramirim aulacogen between ~1750 and 580 Ma. The results, therefore, show the multistage character of uranium mineralization, which had the onset during multiple geodynamic events, but ended in the Ediacaran during the Brasiliano orogeny. The ore geochemical fingerprint is characterized by high U, V, Nb, Ta, Zr/Hf, Mg and Na contents. The São Timóteo Granite is a presumable U source, but volcanic rocks associated to the rifting events should also be considered. Oxygen and hydrogen isotope data show that fluids were impoverished in $\delta^{18}O_{smow}$, which shows the influence of meteoric water during the final stages of alteration.

Keywords: uranium deposits, albitites, mineral chemistry, geochronology, Lagoa Real uranium province.

SUMÁRIO

CAPÍTULO 1 – INTRODUÇÃO

1.1 APRESENTAÇÃO

A Província Uranífera de Lagoa Real (PULR), alvo da presente pesquisa, está situada no centro-sul do estado da Bahia, nas proximidades dos municípios de Caetité e Lagoa Real. Geologicamente está inserida na porção intracontinental do orógeno Araçuaí-Oeste Congo (Fig. 1). É a 6º maior reserva de urânio do mundo e a única a ser explorada no Brasil e na América do Sul.

A história de prospecção de U em Lagoa Real data da década de 70 e desde então vários trabalhos acadêmicos e relatórios internos vêm sendo elaborados com o objetivo de elucidar as questões que envolvem a formação dos depósitos e a caracterização das rochas, mas após anos de estudos diversas questões permanecem não respondidas. Desta forma, a presente tese foi elaborada com o objetivo de caracterizar geologicamente a porção noroeste da PULR a partir do estudo de três depósitos: Barreiro (Anomalia 31), Gameleira I (Anomalia 35) e Barrinha (Anomalia 34). Para isto este projeto foi elaborado em cotutela com a *Universidad de Salamanca* e desenvolvido entre fevereiro de 2016 e novembro de 2020. Durante este período foram desenvolvidos estudos de petrografia, geoquímica de minerais e rocha total, além de estudos isotópicos. Esta pesquisa envolveu também uma etapa de oito meses de estágio *sandwich* na *Universidad de Salamanca*, além de visitas a centros de pesquisa para obtenção de dados, a dizer: *German Reserch Centre for Geoscience*s (GFZ) em Potsdam – Alemanha e *Scottish Universities Environmental Research Centre* (SUERC) em Glasgow.

Esta tese foi elaborada seguindo o modelo de tese integrada a partir de artigos científicos, cujo corpo central é baseado em quatro artigos científicos apresentados na forma de capítulos. Os capítulos principais da tese são precedidos por dois capítulos introdutórios que apresentam e discutem as motivações da pesquisa. O capítulo final sumariza as conclusões alcançadas na tese como um todo.

Os artigos apresentados são os seguintes:

Capítulo 3: WHOLE-ROCK CHEMISTRY OF THE GAMELEIRA I URANIUM DEPOSIT, LAGOA REAL, BRAZIL. Artigo publicado no periódico CHEMIE DER ERDE. Este artigo apresenta dados inéditos de petrografia e geoquímica do furo 10 do depósito Gameleira I. O trabalho tem o objetivo principal de descrever petrograficamente os principais tipos de albititos, mineralizados e estéreis, e suas rochas encaixantes, além de

caracterizar o comportamento geoquímico destas rochas em profundidade utilizando o Furo 10 como estudo de caso. Referido no texto como Marques et al., 2020a

Capítulo 4: LAGOA REAL URANIUM PROVINCE: A CASE OF "*ÉTAGEMENT TEMPOREL*". Artigo submetido ao periódico ECONOMIC GEOLOGY e encontra-se em fase de revisão. Este trabalho apresenta dados petrográficos e geocronológicos inéditos U-Pb (SIMS e LA-ICP-MS) em titanita e zircão e idade química da uraninita, com o objetivo de determinar os eventos de formação dos depósitos e especular sobre sua história evolutiva. Este trabalho foi fundamental para definir o caráter multi-estágio dos depósitos. Referido no texto como Marques et al., 2020b

Capítulo 5: MAJOR- AND TRACE-ELEMENT CONTENTS OF TITANITE FROM MAGMATIC TO URANIUM ORE ASSEMBLAGES, LAGOA REAL URANIUM PROVINCE, BAHIA STATE, BRAZIL: KEY DIAGNOSTIC GEOCHEMICAL FEATURES. A titanita é uma importante fase mineral na PULR, pois é comum em todas as rochas e também está associada à assembleia de minério. Este artigo apresenta uma caracterização química a partir de análises de elementos maiores e traço neste mineral com o objetivo de traçar as características químicas desta importante fase mineral. Este artigo encontra-se em fase de revisão pelos autores e é referido no texto como Marques et al., 2020c

Capítulo 6: EVOLUTION OF THE NORTHWEST LAGOA REAL URANIUM DEPOSITS, BRAZIL: CONSTRAINTS FROM MAGMATIC TO HYDROTHERMAL ASSEMBLAGE. Este artigo traz um estudo de química mineral das principais fases minerais que ocorrem tanto nas rochas magmáticas quanto nos seus produtos de alteração, e na assembleia de minério, com o objetivo de traçar os principais *trends* químicos e especular as condições termodinâmicas que influenciaram na formação desses minerais e que podem ter influencia na formação do minério. Este trabalho ainda traz novos dados de isótopos estáveis e outros dados de geocronologia da uraninita. Referido no texto como Marques et al., 2020d

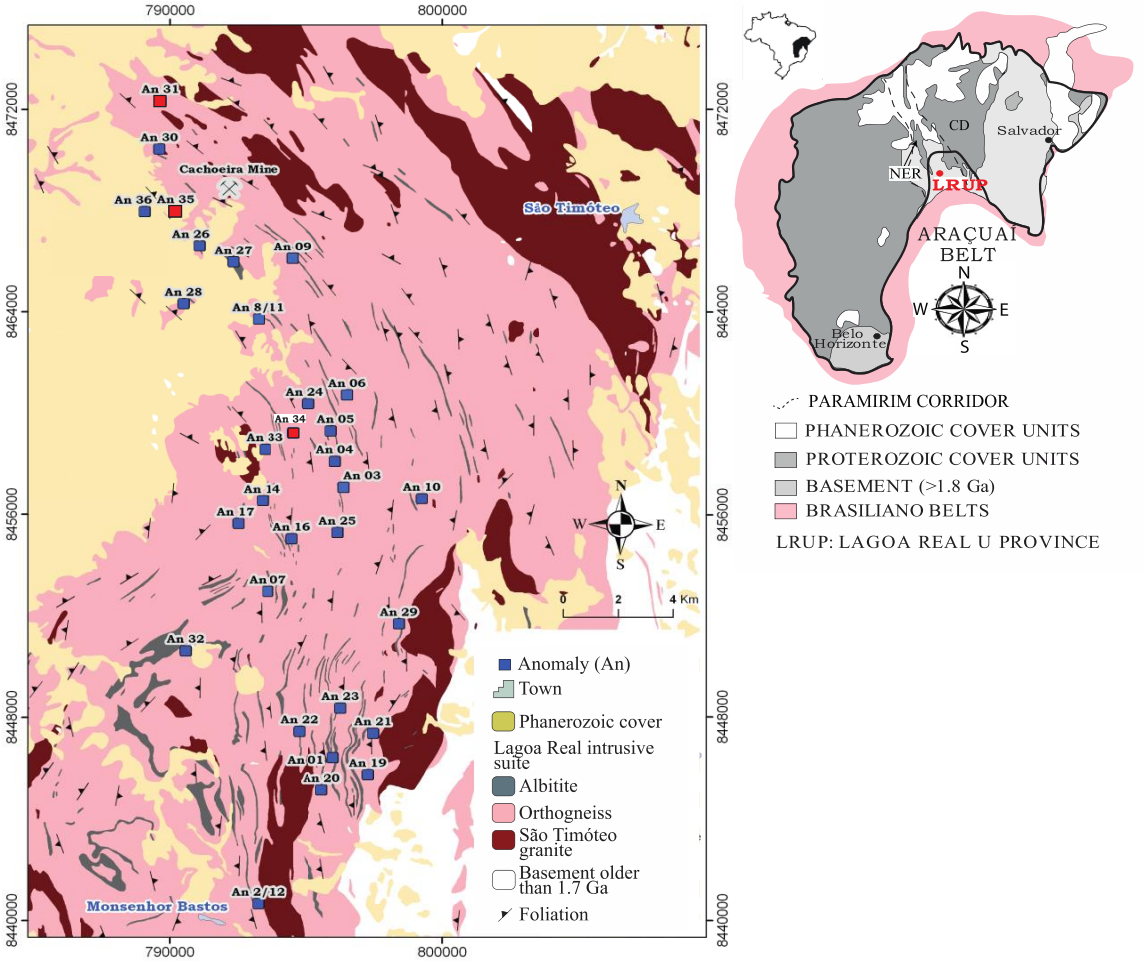

Fig. 1: Mapa geológico da Província Uranífera de Lagoa Real elaborado por Costa et al. (1985) mostrando a distribuição das principais anomalias uraníferas e evidenciando as anomalias estudadas (cor vermelha).

1.2 NATUREZA DO PROBLEMA E JUSTIFICATIVA

A PULR constitui uma das mais importantes províncias uraníferas da classe metassomática associada a albititos e vem sendo palco de pesquisas desde a década de 80. Porém com o declínio da prospecção do U no Brasil, a discussão em torno da metalogênese de depósitos de U tem sido arrefecida. Apesar de ser uma província com considerável número de estudos acadêmicos, ainda permanecem algumas incertezas acerca do seu modelo metalogenético. As principais incertezas são a respeito da relação entre metamorfismo, metassomatismo e mineralização, e quanto à idade da mineralização. Esta última de fundamental importância para a discussão do modelo do depósito. A diversificada ocorrência de tipos de albititos, as texturas e a paragênese de minério também são pouco registrados na literarura. Além disso, a grande extensão da PULR e diversidade de rochas metassomáticas mostram a necessidade de estudos setorizados. Trabalhos anteriores mostraram peculiaridades em diferentes setores

como, por exemplo: diferentes características de fluidos entre a região norte e sul da província (Oliveira et al, 2012), mineralização associada à rochas de composição máfica e na presença de quartzo, bem diferente do comum (Prates et al., 2011), ocorrência de metassomatitos variados (oligoclasitos, epidositos e anfibolitos; Chaves, 2013; Cruz et al., 2007; Souza, 2009), regiões com conteúdos anômalos de Th (AN32) (INB).

A área escolhida para este projeto localiza-se na região NW da PULR que vem sendo palco de estudos pelo LIFM-CDTN, pois contêm importantes anomalias de U, principalmente o depósito Gameleira I, que deve se tornar mina nos próximos anos. Ademais, a região apresenta áreas prospectáveis, uma vez que se acham parcialmente recobertas por sedimentos tércio-quaternários que constituem dificuldades aos levantamentos aerogamaespectrométricos e que podem mascarar a presença de urânio ou mesmo camuflar as denominadas "jazidas cegas", como é o caso do próprio depósito Gameleira I. Este estudo pode então ajudar a entender o comportamento do urânio naquela região.

Desta forma o considerável avanço das técnicas analíticas desde o primeiro *boom* da pesquisa do U, pretende-se obter novas informações acerca da assembléia de ganga e de minério, das condições termodinâmicas de alteração e mineralização, bem como novos resultados geocronológicos. Estes dados permitirão um avanço na compreensão dos processos de formação e evolução dos depósitos de urânio na região NW da PULR, e dos depósitos de U associados à albititos de maneira geral.

1.3 LOCALIZAÇÃO E ACESSO DA PROVÍNCIA URANÍFERA DE LAGOA REAL (PULR)

A PULR está localizada na porção centro-sul do estado da Bahia, entre os distritos de Lagoa Real e Caetité a 246 km de Vitória da Conquista e 647 km de Salvador. Partindo de Salvador, o acesso dá-se pela BR-346 até a cidade de Feira de Santana, em seguida pelas BR-116, até Vitória da Conquista e BR-030, até Caetité. A partir de Caetité, são necessários 28 km seguindo pela BR-122 até Maniaçu e 12 km por uma estrada não pavimentada, mas de boa qualidade até a Unidade de Concentração de Urânio (URA) (Fig. 2).

Está inserida na Folha Caetité (SD-23-Z-B-III), ocupando uma área de 1200 km^2, delimitada pelas coordenadas 42º07'30'' – 42º22'30'' W e 13º45'00'' - 14º07'30'' S.

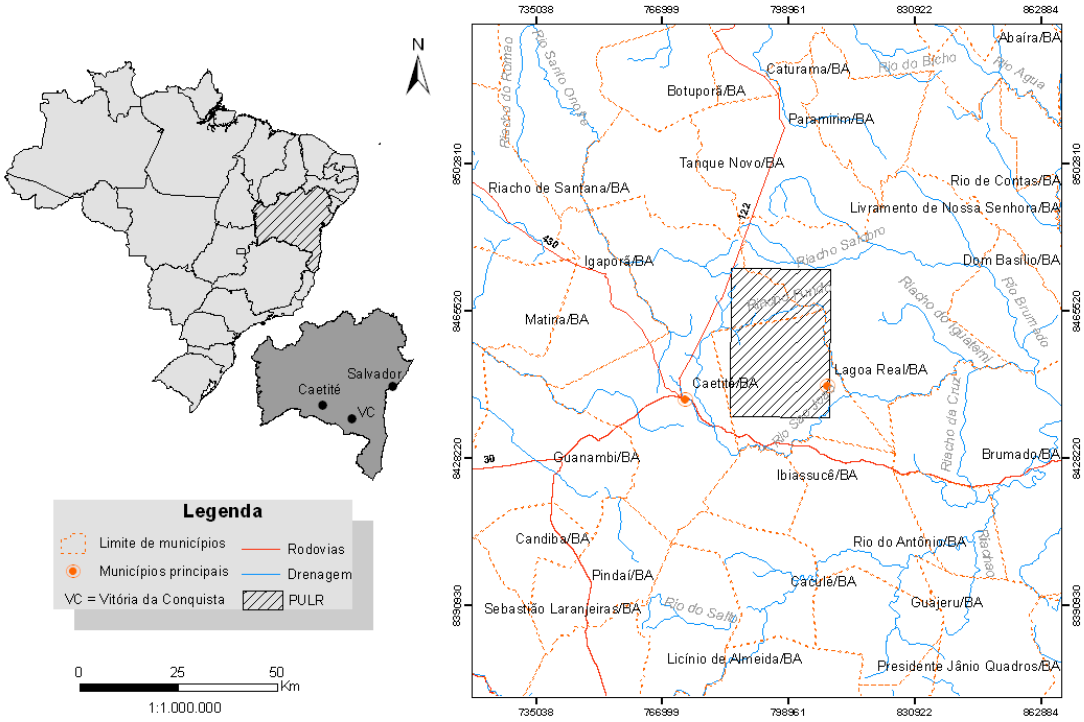

Fig. 2: Mapa de localização da Província Uranífera de Lagoa Real (PULR).

1.4 OBJETIVOS DO ESTUDO

O principal objetivo é esclarecer o processo de formação dos albititos e a gênese da mineralização de urânio na porção noroeste da PULR no intuito de definir a cronologia e condições termodinâmicas dos processos. contribuir para o conhecimento da metalogênese da PULR e de depósitos de U hospedados em albitito.

Para atingir os objetivos gerais foram estabelecidos os seguintes objetivos específicos:

- Caracterização petrográfica da assembleia magmática e hidrotermal através de estudos de 7 furos de sondagem das anomalias 31, 34 e 35;
- Caracterização química de elementos maiores por microssonda eletrônica na assembléia mineral metamórfica/metassomática e nos minerais de urânio;
- Caracterização química de elementos traço em titanita;
- Determinação da idade dos albititos e da mineralização utilizando dados geocronológicos U-Pb (SIMS e LA-ICP-MS) em zircão e em titanita, e idade química por microssonda eletrônica da uraninita;

- Determinação isotópica dos fluidos e condições físico-químicas sob as quais a mineralização e a alteração ocorreram, através de isótopos estáveis em minerais selecionados.

CAPÍTULO 2 – REVISÃO BIBLIOGRÁFICA

2.1 CONTEXTO GEOLÓGICO REGIONAL DA PROVINCIA URANÍFERA DE LAGOA REAL – AULACÓGENO DO PARAMIRIM

O Aulacógeno do Paramirim (AP) ocupa a porção leste do Cráton do São Francisco, a sua porção sul está parcialmente inserida no Orógeno Araçuaí (Fig. 1) nas regiões do vale do Paramirim, do Rio São Francisco e da Chapada Diamantina. Originalmente chamado de Aulacógeno do Espinhaço (Costa & Inda 1982), o Aulacogeno do Paramirim (after Pedrosa-Soares et al. 2001) foi nucleado por volta de 1,78 Ga e corresponde a uma bacia do tipo rift-sag invertida, com idade de inversão Ediacarana. Suas unidades de preenchimento registram desde a formação da bacia até sua modificação, inversão e eventos climáticos que ocorreram entre o Estateriano e o Ediacarano (˜1778 e 480 Ma) (Alkmim & Martins-Neto 2012; Pedrosa-Soares & Alkmim 2011; Guimarães et al. 2012; Guadagnin & Chemale Jr. 2015).

As regiões do Espinhaço Setentrional, a oeste, e da Chapada Diamantina, a leste são separadas pelo vale do Paramirim que expõe o embasamento do bloco Paramirim (Fig. 3). Este embasamento deve agido como um *horst* durante a evolução do aulacógeno implicando na formação de duas sub-bacias quase independentes que foram individualizadas no fim do Paleoproterozoico e permaneceram desta maneira até o fim do Neoproterozoico (Jardim de Sá, 1981; Costa & Inda, 1982; Dominguez, 1993; Danderfer Filho & Dardenne, 2002; Schobbenhaus, 1996; Cruz & Alkmim, 2006; Alkmim & Martins-Neto, 2012). As unidades litoestratigráficas de ambas sub-bacias serão resumidamente discutidas a seguir e a coluna estratigráfica mostrada na Fig. 4 seguindo a classificação estratigráfica designada por Guimarães et al., (2012) com atualizações descritas em Cruz & Alkmim, (2017).

O embasamento do AP compreende: i) Granitoides de idade Paleo-, Meso-, Neoarqueanas com enclaves granuliticos anfibolíticos parcialmente migmatizados e gnaissificados, ii) greenstone belts arqueanos (Cunha et al., 2012; Cruz et al., 2014, 2017), iii) sequencias metavulcanosedimentares e granitoides Siderianos-Orosirianos (Cruz et al., 2017).

2.1.1 Supergrupo Espinhaço e rochas plutônicas associadas

- *Sub-bacia Espinhaço Setentrional*

O preenchimento da bacia inicia-se com a deposição das rochas siliciclásticas e metavulcânicas dacíticas a riolíticas do Supergrupo Espinhaço que extende-se entre 1, 77 e

0,9 Ga (Schobbenhaus and Kaul, 1971, Guimarães et al., 2008, Loureiro et al., 2009, Guimarães et al., 2012, Danderfer-Filho et al., 2015, Guadagnin et al., 2015) e é subdividido na Formação Algodão e nos grupos Oliveira dos Brejinho e São Marcos que ocorrem ao longo do flanco leste na parte nordeste do Espinhaço Setentrional.

O Grupo Oliveira dos Brejinhos é subdividido nas formações São Simão, Pajeú e Sapiranga (Guimarães et al. 2012). A formação São Simão é composta por riolitos, riodacitos e rochas piroclásticas datadas de 1731 ±5 e 1740 ±10 Ma (Danderfer Filho et al. 2009, 2015). A Formação Pajeú é separada desta por uma superfície erosional e consiste em conglomerados lacustrinos, arcósios e pelitos, sobreposta por arenitos eólicos, lacustrinos e aluviais e pelitos da Formação Sapiranga (Guimarães et al., 2008). Guadagnin & Chemale Jr. (2015) obtiveram dois grupos de idades de proveniência para as rochas deste grupo: uma entre 2,17 e 2,07 Ga e outra entre 1,81 e 1,73 Ga.

O Grupo São Marcos é formado em sua unidade inferior pela Formação Bomba, composta por lavas riolíticas e traquíticas de afinidade alcalina ferroana de idade entre 1,58 e 1,56 Ma (Danderfer Filho et al. 2009, dos Santos et al., 2020), seguida das Formações Bom retiro e Riacho do Bento que consistem em arenitos eólicos que gradam para arenitos marinhos e pelitos. A unidade superior deste grupo é formada pela Formação Mosquito que compreende pelitos e arenitos deltaicos (Danderfer Filho 2000; Loureiro et al. 2009; Danderfer Filho et al. 2009).

- *Sub-bacia Chapada Diamantina*

Este sub-domínio é formado predominantemente pelo Supergrupo Espinhaço, representados pela Formação Serra da Gameleira e pelos grupos Rio dos Remédios, Paraguaçu e Chapada Diamantina, além das rochas plutônicas intrusivas da Suíte Intrusiva Lagoa Real (SILR) e albititos uraníferos associados, alvos deste trabalho.

Na Formação Serra da Gameleira predominam arenitos eólicos que gradam lateralmente para conglomerados aluvais, arenitos lacustrinos e pelitos de idade mínima de 1,75 Ga dada pela idade das rochas vulcânicas sobrepostas do Grupo Rio dos Remédios - (Danderfer Filho et al. 2009; Schobbenhaus et al. 1994; Babinski et al. 1994) e idade máxima de 2040 Ma dada pela idade metamórfica mais jovem documentada nas rochas do embasamento.

A sucessão de lavas ácidas e sedimentos lacustrinos e aluviais do Grupo Rio dos Remédios é subdividido nas Formações Novo Horizonte na base, Lagoa de Dentro e Ouricuri do Ouro no topo. A Formação Novo Horizonte é formada por tufos, lavas e rochas epiclásticas de composição dacítica, riolítica e andesítica (McReathet al. 1981; Guimarães

et al. 2008) da idade 1752 ± 4 a 1748 ± 4 Ma (Schobbenhaus et al., 1994 & Babinski et al., 1994). A Formação Lagoa de Dentro é formada por arenitos interacamadados e pelitos contendo lentes de conglomerados que gradam para arenitos e conglomerados arcosianos da Formação Ouricuri do Ouro (Guimarães et al., 2012).

A cristalização da Suíte Intrusiva Lagoa Real (after Arcanjo et al., 2005), comumente conhecida como Granito São Timóteo, ocorreu por volta de 1, 75 Ga (Turpin et al., 1988; Cordani et al., 1992). Esta é a principal litologia na área da PULR que extende-se por cerca de 200 km e é constituída por rochas de textura porfirítica e/ou granulação grossa, dispostos principalmente nas facies álcali-feldspato granito, e hastingsita sienito/sienogranito. Estão associados a charnoquitos, anfibolitos e corpos pegmatíticos.

De acordo com Machado (2008), Amorim (2012) e Marques et al., (2020a), geoquímicamente estas rochas possuem características de granitos tipo-A ferroanos, reduzidos, metaluminosos de alto-K da série cálcico alcalina a álcali-cálcica. São geralmente enriquecidos em SiO_2 e K_2O, elementos incompatíveis, ETRL e empobrecidos em ETRP com alta razão FeOt/(FeOt + MgO). Possuem alto conteúdo de Nb, Zr, ETR, U, Th e razão Th/U maior que a taxa crustal (Maruejol et al., 1989; Marques et al., 2020a). Estas rochas geralmente estão metamorfizadas e convertidas em augen gnaisses, protomilonitos e ultramilonitos com pouca ou nenhuma modificação química em relação ao protólito.

Maruejol (1989) distinguiu duas principais facies para o Granito São Timóteo na área da PULR: i) um grupo de baixa sílica, menos fracionado e *subsolvus*, e ii) um grupo de alta sílica, mais fracionado e *hipersolvus*. A facies *hipersolvus* estaria espacialmente concentrada na porção oeste e em pequenas regiões no sul da PULR, enquanto a *subsolvus* ocupa a região mais leste. Geoquimicamente há um enriquecimento em Si, K, U Th, ETR, Rb, Nb e Y e empobrecimento em Ca, Mg, Ba, Sr, V dos granitos *subsolvus* para os *hipersolvus*.

O Grupo Paraguaçu é dividido nas Formações Mangabeira e Açuruá. A Formação Mangabeira é composta por pelitos e arenitos marinhos que gradam para eólicos e fluviais. A idade mínima de deposição é definida pelas idades de cristalização de diques máficos que cortam esta unidade datados de 1514 ± 22 e 1501 ± 9 Ma (Babinski et al. 1999; Silveira et al. 2013). Estes diques máficos correspondem a diques e *sills* gabroicos, de característica continental intraplaca e afinidade toleítica e ocorrem na Chapada Diamantina.

O Grupo Chapada Diamantina é formado por três formações e ocupa uma grande parte do aulacógeno. A porção inferior é dada pelos arenitos e conglomerados diamantíferos da Formação Tombador (Magalhães et al. 2014, 2016) que gradam para pelitos marinhos e lentes de carbonato da Formação Caboclo. Separado das unidades inferiores por uma

inconformidade regional ocorrem conglomerados diamantíferos e arenitos, pelitos com intercalações de depósitos eólicos da Formação Morro do Chapéu (Dominguez, 1993; Loureiro et al. 2009), porém a classificação estratigráfica desta formação é controversa (Schobbenhaus, 1996 e Guimarães et al. 2008).

2.1.2 Grupo São Onofre, Supergrupo São Francisco e magmatismo associado

Ocorre no Espinhaço Setentrional e na Chapada Diamantina e, juntamente com o Grupo Macaúbas (Pedrosa-Soares *et al.*, 2011a) representa o sistema de bacias precursoras do Orógeno Araçuaí depositados entre 850 e 675 Ma (Bitencourt et al., 2019 e Santana, 2016, respectivamente).

O rifteamento toniano é marcado pela colocação de diques e sills de composição gabroica e afinidade toleítica colocado entre 934 ± 4 Ma e 854 ± 23 (Loureiro et al., 2009, Danderfer Filho et al., 2009).

O Grupo Santo Onofre com idade máxima de 875 Ma é subdividido nas Formações Serra da Garapa e Boqueirão (after Bitencourt et al., 2019). A Formação Serra da Garapa consiste em arcósios marinhos, quartzo arenitos, arenitos ferruginosos e conglomerados que gradam para pelitos hematíticos, carbonáceos e manganesíferos com lentes de dolarenitos estromatolíticos (Guimarães et al. 2012). Por fim, na Formação Boqueirão predominam pelitos hematíticos e grafíticos com arenitos, conglomerados e brechas subordinados (Danderfer Filho 2000; Guimarães et al. 2012) interpretados como leques aluviais em transição a uma plataforma marinha rasa.

O Supergrupo São Francisco é formado pelo Grupo Una, que por sua vez engloba as formações Salitre e Bebedouro. Na Formação Bebedouro foram descritas por Guimarães (1996) uma série de litofácies com diamictitos diversos, pelitos, arenitos e uma camada de calcarenitos e dolarenitos representando a capa carbonática dolomítica. Esta associação foi interpretada por aquele autor como depositados em ambiente subaquático com fluxo de lama, correntes de turbidez e vento em ambiente gracial marinho depositados entre 1000 e 900 Ma (Brito-Neves et al. 1980; Macedo & Bonhome 1981, 1984). A Formação Salitre, por sua vez, é formada por uma sequencia de rochas pelíticas a carbonáticas interpretadas como uma sequencia de raseamento ascendente em rampa carbonática influenciada por onda e maré (Leão & Dominguez 1992; Leão et al. 1992). Macedo & Bonhome (1984); Toulkeridis et al. (1999) definiram que a idade de deposição ocorreu entre 750 e 850 Ma.

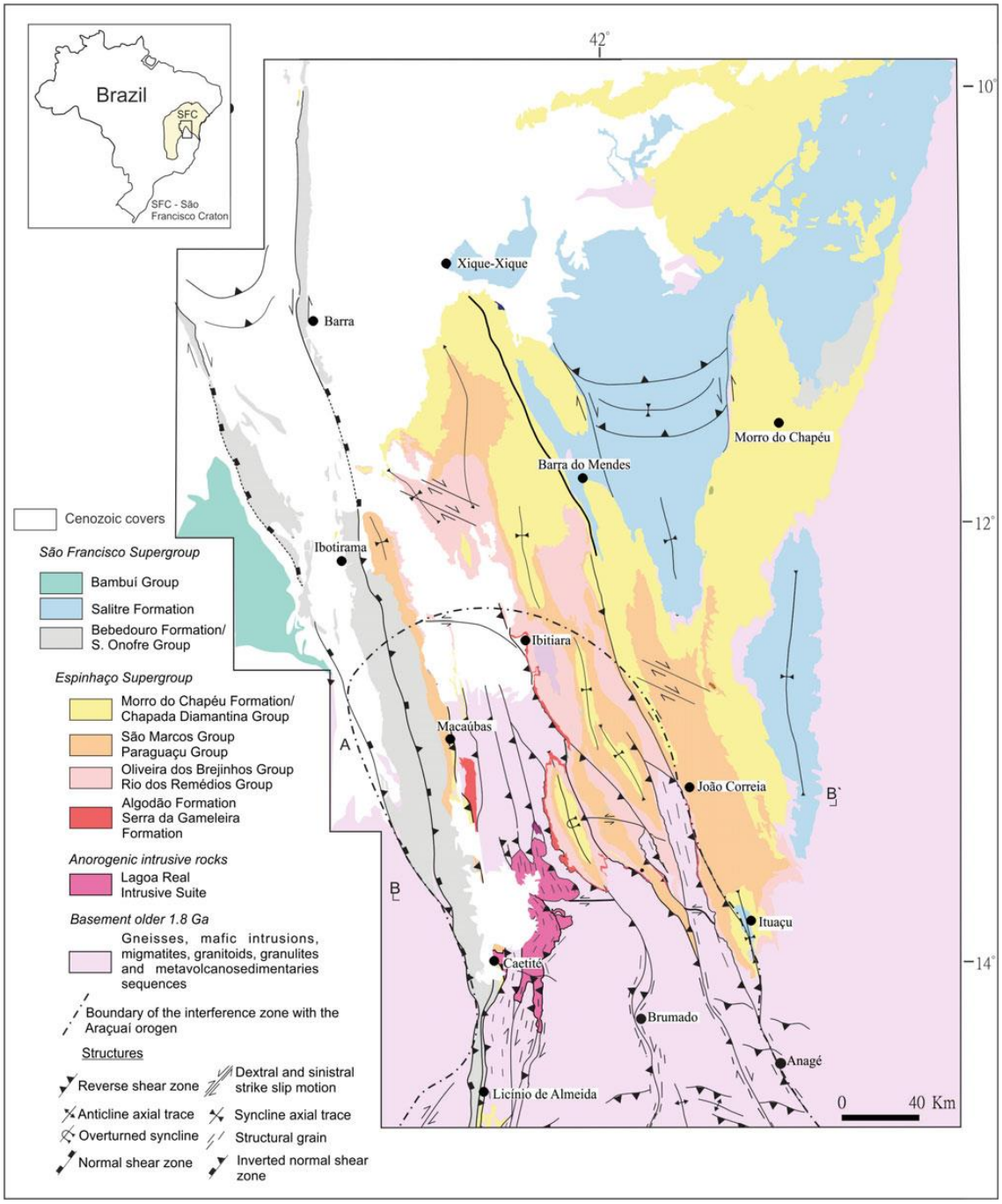

Fig. 3: Mapa geológico do Aulacógeno do Paramirim *in* Cruz & Alkmin, 2017.

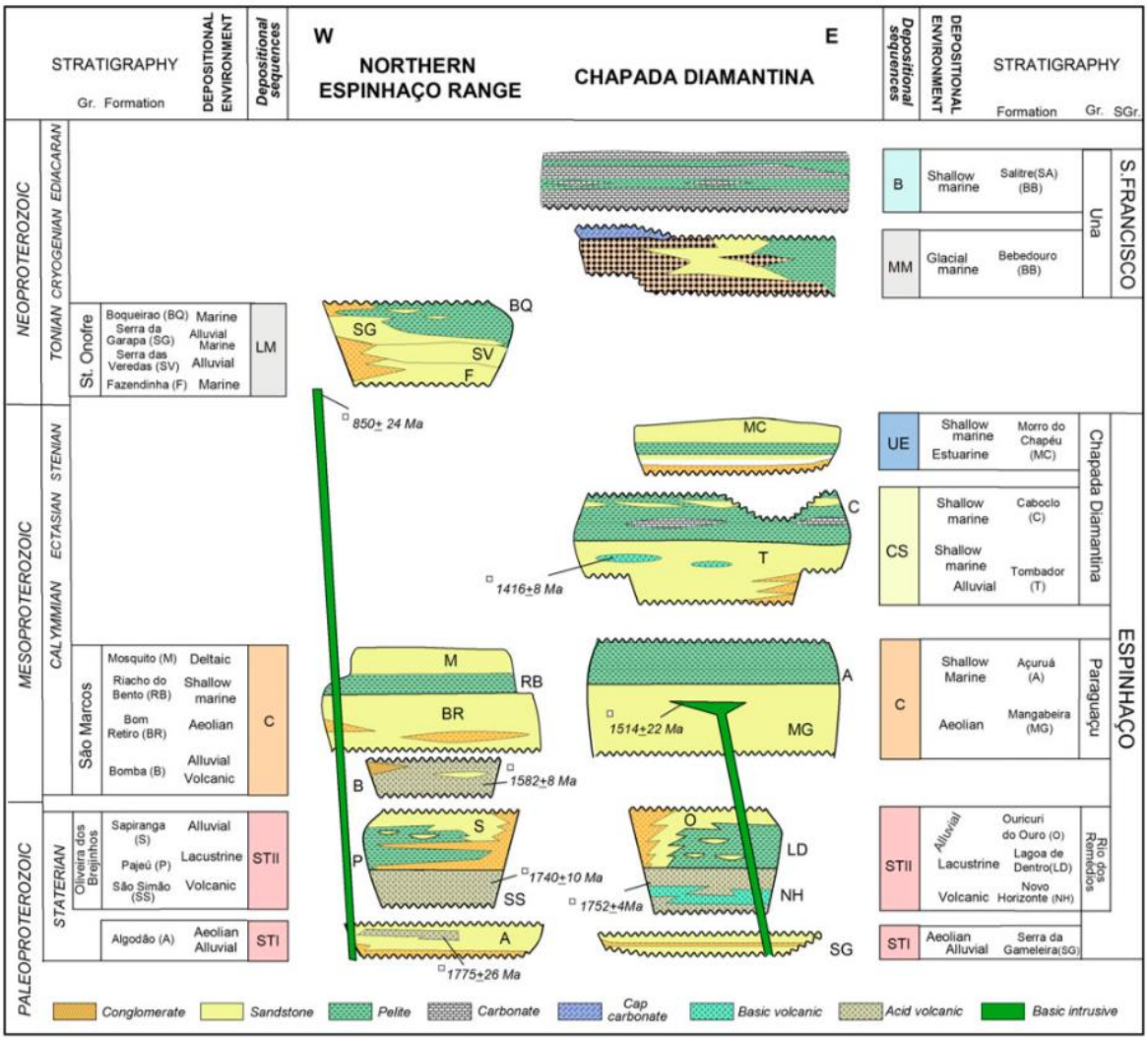

Fig. 4: Carta estratigráfica das sub-bacias Espinhaço Setentrional e Chapada Diamantina do Aulacógeno do Paramirim. Sequencias deposicionais: STI – Estateriano I; STII – Estateriano II; C – Calimiano; CE – Calimiano- Esteniano; UE – Espinhaço Superior; LM – Santo Onofre; MM – Bebedouro; B – Salitre. Os números indicam idade de cristalização ou as idades detríticas mais jovens em zircão. (*in* Cruz & Alkmin, 2017).

2.1.3 Evolução Tectônica do Aulacógeno do Paramirim

Apesar de amplamente estudado, vários autores divergem quanto à evolução tectônica do Aulacógeno do Paramirim, principalmente quanto à natureza, idade e significado tectônico das suas unidades de preenchimento. Apesar disto, de acordo com os dados geocronológicos disponíveis na literatura e compilados em Cruz & Alkmin, (2017), o AP possui pelo menos oito sequencias limitadas por inconformidades, que significam distintos pulsos de subsidência ao longo da sua evolução entre 1,7 Ga e por volta de 0,49 Ga, no período

Ediacarano. Cruz & Alkmin (2017), sintetizaram estas seis sequencias da seguinte maneira (ver Fig. 5):

I. Estateriano I: compreende as Formações Algodão e Gameleira e marcam o início da sedimentação do Espinhaço em 1775 Ma .
II. Estateriano II: após o primeiro pulso de subsidência da fase anterior houve renovação do tectonismo extensional por volta de 1740 Ma dando início a esta nova fase. Nesta, ocorreu a deposição dos Grupos Oliveira dos Brejinhos e Rio dos Remédios, bem como novo plutonismo da Suíte Lagoa Real.
III. Calimiano: deposição dos grupos São Marcos e Paraguaçu entre 1575 e 1420 Ma e intrusão de diques e sills máficos na região da Chapada Diamantina.
IV. Calimiano-Esteniano: deposição do Grupo Chapada Diamantina iniciada por volta de 1420 Ma

A partir do Calimiano a bacia Espinhaço experienciou ampla expansão desde a formação do Grupo Paraguaçu até a deposição da Formação Tombador por volta de 1420 Ma. Loureiro et al. (2009) e Guimarães et al. (2012) argumentam que esta acumulação representa eventos maiores de *sagging*. Entretanto, a ocorrência de magmatismo ácido marcados através da presença de basaltos riolíticos e intrusões máficas por volta de 1,5 Ga associadas àquelas sequencias, indicam que houve um evento de rifteamento que antecedeu o evento Calimiano. A ausência de dados geocronológicos dificulta correlacionar a Formação Morro do Chapéu e o Supergrupo São Francisco nos eventos descritos, porém, por não conter afinidades litológicas com as unidades subjacentes, a Formação Morro do Chapéu é enquadrada como uma sequencia superior do Supergrupo Espinhaço.

V. Toniano: Os grupos Santo Onofre, Bebedouro e Salitre representam três sequencias do Supergrupo São Francisco limitadas por inconformidades. Segundo Danderfer Filho (2000), o Grupo Santo Onofre representa um novo evento de rifteamento ocorrido no período Toniano, coevo à abertura da bacia Macaúbas no Orógeno Araçuaí.

As idades das formações Bebedouro e Salitre ainda são alvo de debate, porém Pedrosa-Soares et al. (2011) e Kuchenbecker et al. (2015) associam os depósitos glaciogênicos da Formação Bebedouro ao Criogeniano com idade mínima de 740 ± 40 Ma (Babinski et al. 2007), idade da capa carbonática na Bacia do São Francisco, por outro lado Caxito et al. (2012) defende idade de 630 Ma para estes depósitos. A Formação Salitre é aparentemente associada a eventos de transgressão marinha correlata ao Grupo Bambuí, na bacia do São

Francisco, porém a idade deste grupo é alvo de incertezas. Fosséis descritos por Warren et al. (2014) indicam idade de deposição por volta de 550 Ma.

VI. Inversão do Aulacógeno do Paramirim: a idade de inversão do aulacógeno é produto de extenso debate. Enquanto Jardim de Sá (1978, 1981), Costa & Inda (1982) e Cordani et al. (1992) defendem que a inversão ocorreu durante o Mesoproterozóico, Danderfer Filho (1990, 2000), Danderfer Filho et al. (1993), Cruz & Alkmim (2006), Guimarães et al. (2008) e Loureiro et al. (2009) postulam uma idade Ediacarana-Cambriana, baseados nos dados estruturais que indicam que a deformação compressional, resultado da inversão, afetou os Supergrupos Espinhaço e São Francisco.

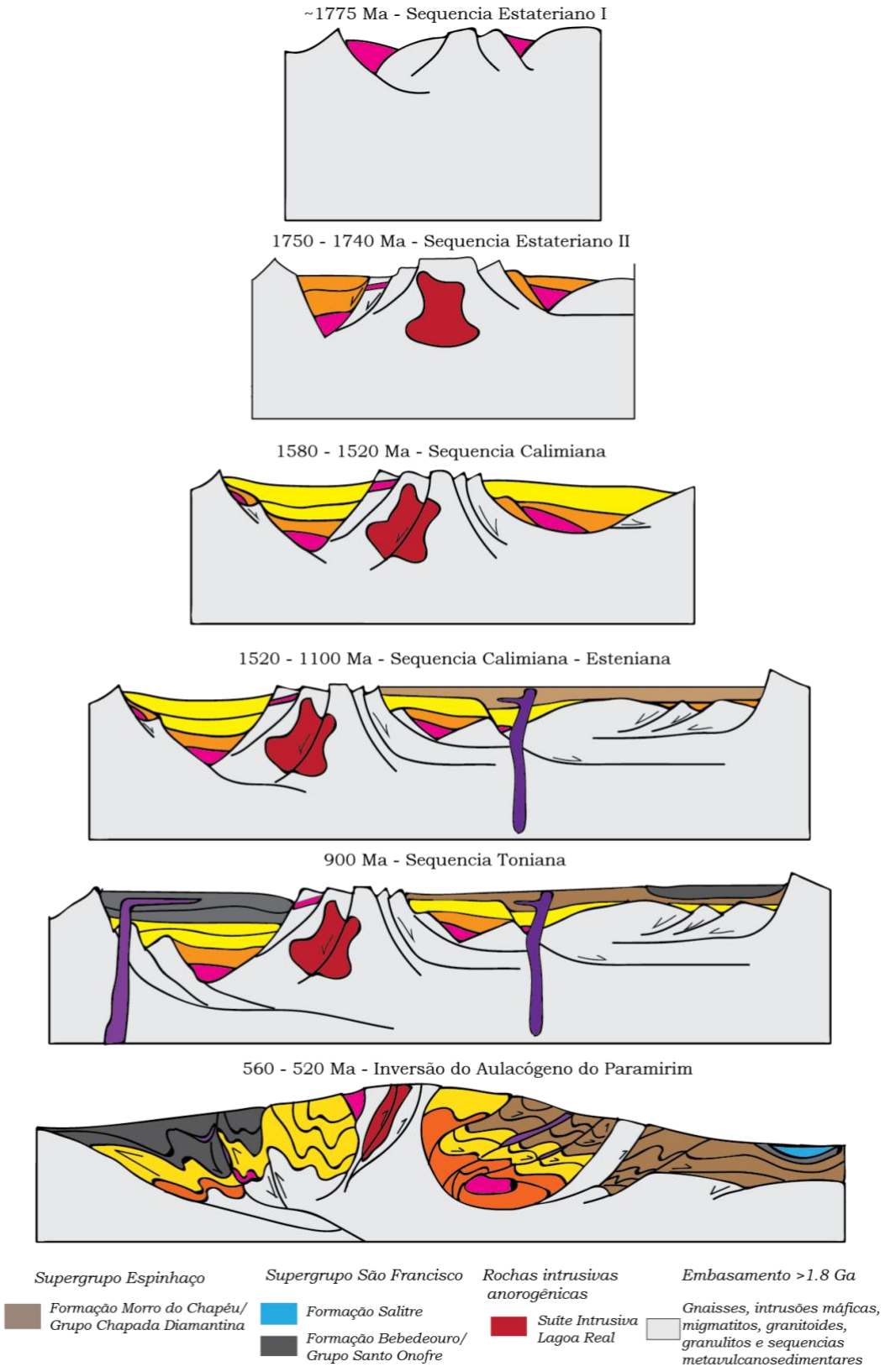

Fig. 5: Desenho esquemático da evolução do Aulacógeno do Paramirim. Modifcado de Cruz & Alkmin (2017).

2.2 PROVÍNCIA URANÍFERA DE LAGOA REAL: ATUAL ESTADO DO CONHECIMENTO

A descoberta de urânio em Caetité e adjacências ocorreu a partir de levantamento aerogeofísico realizado pela CGA (Centro de Geofísica Aplicada) para o DNPM, estes dados foram repassados à CNEN, que posteriormente comunicou à Nuclebrás (Cruz et al., 2008). A Nuclebrás então estabeleceu um programa de pesquisa e prospecção que resultou na confirmação das anomalias de urânio, além disso, outras anomalias foram constatadas por Geisel et al. (1978) através de levantamento autoportado. Em seguida, uma série de projetos de mapeamento ocorreram entre os anos de 1975 e 1985: Bahia (Pedreira et al., 1975), Projeto Letos (Costa *et al*., 1976); projetos Brumado-Caetité (Moraes *et al*., 1980) e Projeto Lagoa Real (Costa *et al*., 1985). A partir destes diversos trabalhos de levantamento geológico, além de sondagem, cubagem, avaliação de recursos, a Nuclebrás estabeleceu áreas de interesse. Hoje, a PULR é explorada e explotada pelas INB – Indústrias Nucleares do Brasil, antiga Nuclebrás, e no ano de 2000, Lagoa Real passou a produzir concentrado de urânio. O período de cava a céu aberto foi estimado em 12 anos, após este período a lavra deveria ocorrer de forma subterrânea (Cruz et al., 2008), porém esta ultima etapa ainda não ocorreu e a exploração passou a ocorrer a partir da Mina Engenho (Anomalia 09) em 2019.

A PULR encontra-se na porção sul e invertida do Aulacógeno do Paramirim (Fig. 1) afetada pela deformação *far-field* do orógeno Araçuaí. Ocupa uma área de 35 km de extensão e 5 km de largura, contendo 38 anomalias uraníferas que encontram-se em diferentes níveis de detalhamento, das quais oito (8) são atualmente consideradas depósitos economicamente viáveis e somente duas tornaram-se minas. A PULR contém 94.000 toneladas de minério de U_3O_8 com teor médio de 2700 ppm. Até hoje, foram retiradas 5.000 toneladas minério, a partir de sete corpos de minério da mina Cachoeira (Anomalia 13), que esteve em operação à céu aberto até 2014. Em dezembro de 2020 a mina Engenho (Anomalia 09) está prevista para entrar em operação.

A área da PULR concentra principalmente as rochas da SILR e diversas rochas metassomáticas representadas principalmente pelos albititos, mas também por oligoclasitos, microclinitos e epidositos, e conjuntamente também são denominados Complexo Lagoa Real. Todas estas rochas podem estar cortadas discordante ou concordantemente por corpos de diabásio e anfibolitos. Os corpos de albitito são lenticulares, descontínuos, maciços ou gnaissificados e estão preservados como *pods* em meio às rochas granito-gnáissicas da SILR com contatos transicionais ou abruptos. Os corpos de albititos possuem dimensões variadas,

entre metros a centenas de metros (<480 m, Ribeiro et al., 1984), e em conjunto delineiam uma estrutura regional helicoidal (Fig. 6), denominada Arco de Lagoa Grande (Stein et al. 1980, Sobrinho et al. 1980, Ribeiro et al. 1984, Costa et al. 1985).

Os corpos de albititos são os principais portadores da mineralização, e estão variavelmente mineralizados. De acordo com Lobato & Fyfe (1990) e Maruejol (1989) a mineralização tem preferencia por albititos sem quartzo, contendo principalmente hedenbergita + granada. Lobato & Fyfe (1990) ainda descrevem a forte associação espacial entre uraninita e magnetita martitizada. Lobato (1985), Maruejol (1989), Cruz (2004), Chaves (2013) descrevem ocorrência de uraninita associada a albita, piroxênio, biotita, titanita e magnetita martitizada. Lobato (1985) registrou também epidositos portadores da mineralização.

Os primeiros dados geocronológicos obtidos nas rochas de Lagoa Real foram gerados por Turpin et al., (1988) e Cordani et al., (1992) cujos resultados serviram de base para formular as primeiras hipóteses. Estes dados isotópicos são discutidos em detalhe no Capítulo 4.

Neste sentido, Fyfe (1979, apud Brito *et al.* 1984), Stein *et al.* (1980), Sobrinho *et al.* (1980), Lobato (1985), Maruèjol (1989), Cruz (2004) e Chaves (2013) formularam algumas hipóteses a partir das suas investigações.

Fyfe (1979, apud Brito *et al.* 1984) propôs que o metassomatismo e a deformação foram processos concomitantes e que o cavalgamento das rochas do Supergrupo Espinhaço pelo embasamento teria gerado um gradiente de temperatura que mobilizaria fluidos contidos nos poros dos metassedimentos. Como consequência deste aumento de temperatura, fluidos contidos nos poros dos metassedimentos passariam para o estágio supercrítico, permitindo o alçamento do bloco do embasamento e facilitando o desenvolvimento de falhas de empurrão e de fraturas hidráulicas. Os fluidos seriam, desta forma, injetados nas zonas e fraturas do embasamento, provocando o metassomatismo sódico e a formação dos corpos de albititos mineralizados em urânio.

Stein *et al.* (1980) propuseram que o metassomatismo que originou os albititos precedeu a principal fase de deformação registrada nessas rochas. Dados geocronológicos obtidos em uraninita resultaram em idades de 820 Ma e 540 Ma. Entretanto, baseados nos depósitos de U da Ucrânia estes autores interpretaram que a formação dos albititos e da mineralização de urânio teria se dado entre 1,80 e 1,5 Ga e as idades de 820 Ma e 540 Ma, seriam resultados de processos de remobilização. O metassomatismo seria então relacionado à formação de bacias sedimentares, acompanhada de extenso vulcanismo e os fluidos alcalinos

provenientes de granitos tardios ao Evento Transamazônico teriam sido responsáveis pelo metassomatismo. A fonte do urânio seriam as rochas clásticas dos depósitos vulcanossedimentares de idade arqueana distribuídos no embasamento da região ou a partir de rochas magmáticas colocadas durante o Paleoproterozóico. Por fim, durante o Brasiliano o urânio teria sido reconcentrado ao longo de falhas reativadas.

Para Brito et al., (1984), Raposo & Matos., (1982) e Maruèjol (1989) o processo de formação dos albititos deve ter se dado a partir de duas principais fases metassomáticas, que seriam metassomatismo sódico seguido de metassomatismo cálcico.

Segundo Maruèjol (1989) o granito São Timóteo teria passado por uma alteração tardi-magmática que resultaria em aumento nos conteúdos de ETR, Y, Nb, e F. O metassomatismo sódico-cálcico teria ocorrido em seguida, porém somente 300 Ma após a colocação do granito, em 1,4 Ga, provavelmente motivado pelo vulcanismo ácido representado pelos corpos de anfibolito que possuem ampla ocorrência na área. Os fluidos seriam aquosos, oxidantes e de alta temperatura (400–500 ºC), que lixiviariam urânio dos minerais acessórios dos granitos. O metamorfismo Brasiliano conduziria a recristalização da assembleia mineral e reequilibraria as inclusões fluidas

Lobato (1985) e Lobato & Fyfe (1990) definiram apenas um metassomatismo sódico, que teria se desenvolvido concomitantemente à mineralização e deformação brasiliana. O metassomatismo teria ocorrido preferencialmente ao longo de zonas de cisalhamento e as transformações texturais estariam associadas a reações metamórficas de oxidação e desidratação. Estas reações seriam acompanhadas por uma fase fluida oxidante, rica em sódio e urânio. A precipitação da uraninita teria sido controlada pela redução do fluido via oxidação dos minerais máficos e as transformações metassomáticas teriam ocorrido principalmente por: 1) recristalização da assembléia mineral juntamente com desidratação e oxidação da hastingsita para produzir hedembergita e granada com consumo de SiO_2. Restrita formação de albita e remoção de quartzo. Alta fugacidade de oxigênio controlada pelo FMQ *buffer*; 2) intensa albitização dos feldspatos. Formação de aegirina-augita e completa desilicificação. Limitada formação de uraninita inclusa em albita e piroxênio; 3) oxidação da aegirina-augita e da magnetita dando origem a andradita e hematita, respectivamente. Ampla precipitação de uraninita como inclusões em andradita e óxidos. Fugacidade do oxigênio controlada pelo HM *buffer*; 4) incipiente a moderada alteração do piroxênio para anfibólio. Estabilidade do quartzo é restabelecida. Diminuição de temperatura e alterações tardias com calcita, biotita, e prehnita, wollastonita e vesuvianita.

As reações progressivas teriam se processado na fácies epidoto-anfibolito, com temperatura entre 500 e 600 ºC e pressão inferior a 4 kbar. A mineralização de urânio teria se desenvolvido por fluidos quentes (~500 – 550 ºC) e oxidantes, além disso, as rochas mineralizadas e não mineralizadas teriam similares valores de isótopos de oxigênio, -3,7 – +2,6‰ e -0,8 – +7,3‰, respectivamente. Baseados na razão isotópica $^{87}Sr/^{86}Sr$ os autores sugeriram que os fluidos são derivados das rochas do Supergrupo Espinhaço, adjacentes às rochas do complexo granítico-gnáissico Lagoa Real. Estes fluidos teriam sido expelidos durante evento metamórfico, e devem ter sido responsáveis pela mineralização de urânio. Recentemente Lobato et al., (2015) obteve idade de 960 Ma (U-Pb; La-ICP-MS em titanita) e concluiu que os processos de metassomatismo e mineralização teriam ocorrido nessa idade.

Cruz (2004) também atribui a formação dos albititos como sendo resultado da deformação das rochas granitoides, porém constatou a partir de estudos microestruturais que há um evento metassomático sódico precoce à deformação e que se ocorreu via desenvolvimento de pertitas metassomáticas. Este evento seria responsável pela albitização, porém a individualização dos corpos de albititos, teria ocorrido via recristalização sintectônica durante o Brasiliano. O metamorfismo Brasiliano seria responsável também concentração de urânio nas zonas de cisalhamento. Estes autores identificaram na área da PULR três eventos de metassomatismo (Ms_1, Ms_2 e Ms_3) e um de metamorfismo, que se subdivide em prógrado e retrógrado, associados a três fases deformacionais distintas (D_a, D_p e D_e). Estes eventos teriam se processado da seguinte maneira:

1) Metassomatismo *Ms_1* que é de natureza predominantemente sódica e subordinadamente cálcica. Ocorreu anteriormente às fases de deformação e provocou a albitização dos granitóides São Timóteo (*sensu latu*). Esta fase teria sido impulsionada pela presença de intrusões graníticas anorogênicas, como o granito de Potiraguá (Silva *et al.* 2002), associadas à fase de abertura do rifte Macaúbas, por volta de 1 e 0,8 Ga. Estes granitos teriam sido a fonte de fluidos ricos em sódio e em elementos menores, assim como por captar o urânio das rochas encaixantes, como anteriormente proposto por Maruèjol (1989).

2) Metassomatismo *Ms_2* / Metamorfismo progressivo *$M1_p$* / *Sin-Dp_1*: nesta fase predomina a assembléia constituída por quartzo, albita, microclina, oligoclásio, andradita–grossularita, almandina, hastingsita, hedembergita, aegirina-augita, titanita, uraninita, magnetita e hematita. Este evento estaria associado com a inversão do Aulacógeno do Paramirim e promoveu a gnaissificação do Granito São Timóteo e a individualização dos corpos de albititos, microclinitos e oligoclasitos A geração da trama foi acompanhada por

reações de oxidação. Esta fase teria ocorrido em condições de facies anfibolito entre 600 e 650 ºC.

3) Metassomatismo *MS_3* / Metamorfismo regressivo *M_1r_1 /Sin-Dp_2*: Possui associação mineralógica constituída por actinolita/tremolita, mica branca, quartzo e clorita. Esse evento marca a nucleação das grandes zonas de cisalhamento rúptil-dúcteis durante a fase de deformação Dp_2. Esta fase se desenvolveu em condições de facies xisto-verde entre 300 e 550 ºC.

4) Metamorfismo regressivo *M_1r_2/ Sin-De*: Está associado com a nucleação de zonas de cisalhamento normais e levou a formação de uma associação metamórfica regressiva tardia, sin- M_1r_2, constituída por epidoto, calcita e quartzo. Esta fase teria ocorrido em condições de facies epidoto-anfibolito entre 500 e 550º.

Chaves (2013) classifica os albititos como sienitos sódicos metamorfizados, a partir de suas observações petrográficas e estudos litogeoquímicos, que mostraram haver nestas rochas textura magmática preservada caracterizada principalmente pela ocorrência de anti-pertita. Foram observadas ainda, albita e augita rica em possíveis *melt inclusions* nas porções com textura magmática preservada. Para este autor, a ausência de quartzo nos sienitos uraníferos e de texturas que caracterizem dissolução de quartzo, confrontam a presença de metassomatismo sódico nestas rochas. Ao lado disso, os *trends* diferentemente lineares quanto ao conteúdo de álcalis para os albititos e gnaisses *vs* anfibolitos, confrontariam a idéia de mobilização destes elementos durante o metamorfismo, contradizendo a hipótese de formação dos "albititos" a partir do metassomatismo sódico do Granito São Timóteo. Desta forma, os *trends* geoquímicos e a clara associação entre albititos e anfibolitos sugerem ao invés de metassomatismo, uma origem comum a estas rochas. A evolução destas rochas se daria através de cristalização fracionada por diferenciação magmática a partir de um magma básico álcali-diorítico para um magma sienítico intermediário. Os anfibolitos corresponderiam então a dioritos metamorfizados e são considerados representantes da fase menos evoluída, e os representantes finais dessa diferenciação seriam dados pelo quartzo sienitos. Estes sienitos, então, teriam sido submetidos a um metamorfismo de alto grau na fácies anfibolito revelado pela associação oligoclásio + andradita. O epidoto e a biotita surgiriam de um novo estágio metamórfico menos intenso que outrora substituindo os minerais pré-existentes.

Datações químicas e isotópicas foram apresentadas em Chaves et al., (2008; 2009) em minerais variados como titanita, zircão, uraninita, epidoto e allanita. A titanita contendo altos conteúdos de U hospedadas nos albititos mostrou idades variando entre 2,0 Ga e 0,5 Ga.

Os dados geocronológicos (U/Pb; LA-ICP-MS - zircão) obtidos por este autor nos microclina gnaisses mostraram intercepto superior de 2,0 Ga ± 78 Ga que foi interpretado como sendo idade de cristalização do protólito destas rochas. Já os sienitos metamorfizados mostraram intercepto superior que resulta em idade de 1,9 Ga, interpretados como a idade de cristalização e/ou influência do metamorfismo Orosiriano, e um intercepto inferior de 483 Ma, que marcaria o metamorfismo Brasiliano. Os dados obtidos para a uraninita (datação quimica) associadas à andradita e epidoto indicariam que a primeira população teria idade de 1,8 Ma, o que representaria o pico do metamorfismo que se deu, então no Paleoproterozóico, enquanto a segunda população resultou em idade de 605 Ma e representaria uma cristalização durante o evento metamórfico Brasiliano, concordante com a idade encontrada para o sienito uranífero, já mencionada anteriormente. A partir de observações petrográficas e dados de química mineral este autor concluiu que a titanita magmática seria o principal mineral portador de urânio. Este mineral seria a principal fonte de deste elemento, que deve ter sido liberado durante os eventos metamórficos, seja por processos de controle redox ou não.

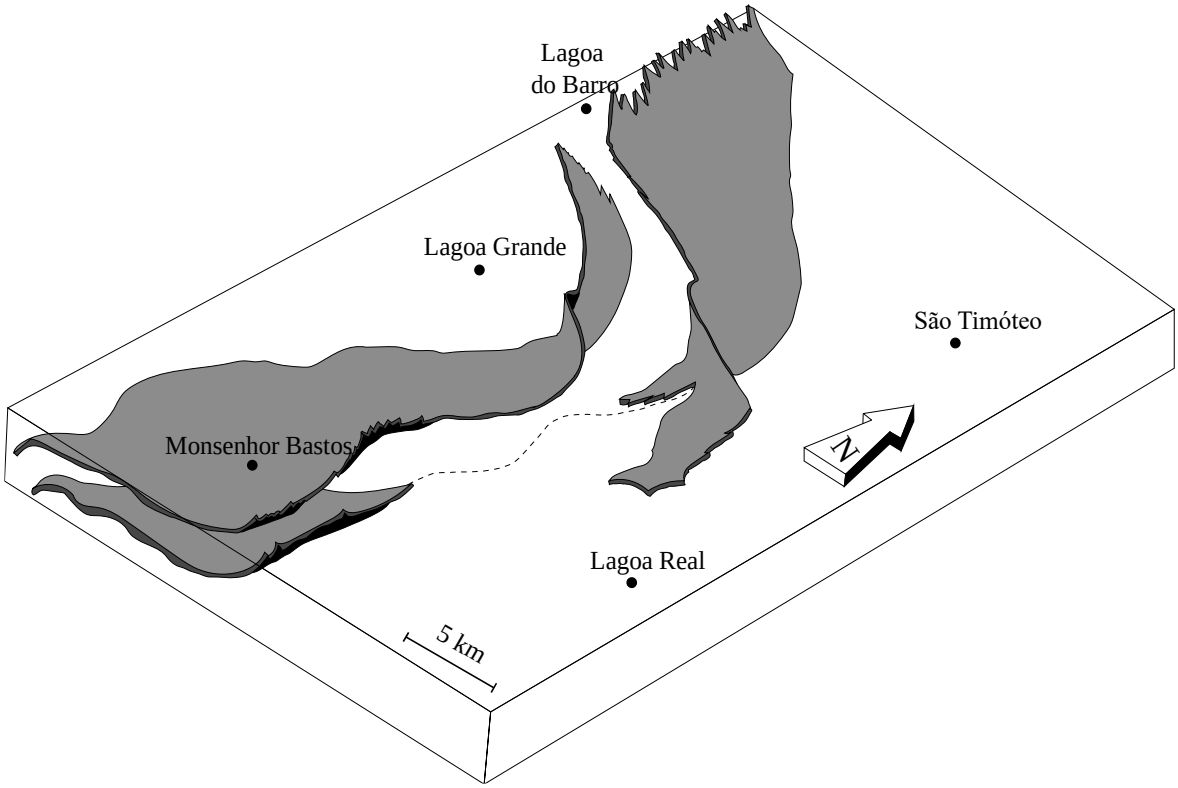

Fig. 6: Bloco diagrama mostrando a disposição dos corpos de albitito na área da PULR (Costa et al., 1985)

2.3 REFERÊNCIAS

Arcanjo, J.B., Marques-Martins, A.A., Loureiro, H.S.C., Varela, P.H.L. 2005. Projeto Vale do Paramirim, Bahia: geologia e recursos minerais. Salvador, Companhia Baiana de Pesquisa Mineral-CBPM. Série Arquivos Abertos, 22, 82p.

Alkmim FF, Martins-Neto, M. (2012). Proterozoic first-order sedimentary sequences of the São Francisco craton, eastern Brazil. Marine and Petroleum Geology 33(1): 127–139.

Amorim, L.E.D. O Granito São Timóteo No Perfil Monsenhor Bastos, Província Uranífera De Lagoa Real. 146p. Dissertação (Mestrado em Ciência e Tecnologia das Radiações, Minerais e Materiais) – Centro Desenvolvimento da Tecnologia Nuclear, Belo Horizonte, 2012.

Babinski, M., Brito-Neves, B.B., Machado, N., Noce, C.M., Ulhein, A., Van Schumus, W.R. 1994. Problemas na metodologia U/Pb em zircões de vulcânicas continentais: o caso do Grupo Rio dos Remédios, Supergrupo Espinhaço, no estado da Bahia. XXXVIII Congresso Brasileiro de Geologia, Boletim de Resumos Expandi- dos, v.2, p. 409–410.

BABINSKI, M., PEDREIRA, A., BRITO-NEVES, B.B., VAN-SCHMUS, W.R. 1999. Contribuição à geocronologia da Chapada Diamantina. 7o Simpósio Nacional de Estudos Tectônicos, Anais, p. 118–121.

Babinski, M., Vieira, L.C., Trindade, R.I.F. 2007. Direct dating of the Sete Lagoas cap carbonate (Bambuí Group, Brazil) and implications for the Neoproterozoic glacial events. Terra Nova, 19, 401–406.

Bitencourt, C.N., Cruz, S.C.P., dos Anjos Cruz, V., Pedrosa-Soares, A.C., Paquette, J.L., Alkmim, A.R., Barbosa, J.S.F., 2019. Rifting events in the southern sector of the Paramirim Aulacogen, NE Brazil: New geochronological data and correlations for the São Francisco–Congo paleocontinent. Precambrian Res. 326, 417–446. https://doi.org/10.1016/j.precamres.2018.12.005

BRITO W., RAPOSO C. & MATOS E.C. 1984. Os albititos uraníferos de Lagoa Real. In: SBG, Cong. Bras.Geol., 33, Anais, p. 1475-1488

Brito-Neves, B.B., Cordani, U.G., Torquato, J.R. 1980. Evolução geocronológica do Precambriano no estado da Bahia. In: Inda, H.A. D. and Duarte, F.B. (eds.) Geologia e Recursos Minerais do Estado da Bahia, 3, SME-COM, p. 1–101.

Caxito, F.A., Halverson, G.P., Uhlein, A., Stevensson, R., Dias, T.G., Uhlein, G.J. 2012. Marinoan glaciation in eastern Central Brazil. Precambrian Research, 203, 38–58.

CHAVES, A.O. (2013). New geological model of the Lagoa Real uraniferous albitites from Bahia (Brazil). *Central European Journal of Geosciences*, *5*(3), 354-373.

CORDANI, U.G., IYER, S.S., TAYLOR, P.N., KAWASHITA, K., SATO, K., MCREATH, I. 1992. Pb-Pb, Rb-Sr, and K-Ar sistematic of the Lagoa Real uranium province (south-central Bahia, Brazil) and the Espinhaço Cycle (ca. 1.5–1.0 Ga). Journal of South American Earth Sciences, 1, 33-46

CRUZ SCP, ALKMIM FF (2006) The tectonic interaction between the Paramirim Aulacogen and the Araçuaí belt, São Francisco craton region, Eastern Brazil. Anais da Academia Brasileira de Ciências 78 (1): 151–173.

CRUZ, S. C. P., ALKMIM, F. F., LEITE, C. M. M., EVANGELISTA, H. J. CUNHA, J. C., MATOS, E. C., NOCE, C. M., MARINHO, M. M., 2007c. Geologia e arcabouço estrutural do Complexo Lagoa Real, Vale do Paramirim, Centro-Oeste da Bahia. Revista Brasileira de Geociên- cias, 37(4, suplemento), 28–146.

Cruz, S.C.P., Miranda, L.L.F., Veiga, P.M. O., 2008. Província Uranífera de Lagoa Real, Bahia. Companhia Baiana de Pesquisa Mineral-CBPM/Companhia de Pesquisa, 60p.

Cruz, S.C.P., Barbosa, J.S.F., Barbosa, A.C., Jesus, S.S.G.P., Medeiros, E.L.M., Figueiredo, B.S., Menezes-Leal, A.B., Lopes, P., Souza, J.S., 2014. Mapeamento Geológico e Levantamentos de Recursos Minerais das Folhas Espinosa e Guanambi (Escala 1:100.000). Programa de Levantamentos Geológicos Básicos, Convênio CPRM-UFBA-FAPEX, Salvador, BA, 253p.

Cruz, S.C.P., Alkmim, F.F., 2017. The Paramirim Aulacogen. In: Heilbron, M., Cordani, U.G., Alkmim, F.F. (Orgs.). Regional Geology Reviews. Springer International Publishing, 97–11

Cruz, S.C.P., Barbosa, J.S.F., Marinho, M.M., Peucat, J.J., Paquette, J.L., 2017. Quantas sequências metavulcanossedimentares pré-estaterianas existem a oeste do lineamento Contendas Mirante – Jacobina? Novos dados e correlações regionais. In: SBG, XVI Simpósio Nacional de Estudos Tectônicos e X International Symposium on Tectonics, Salvador, Boletim de Resumos Extendidos, Salvador, Anais, 120-123.

COSTA L.A.M. & INDA H.A.V. 1982. O Aulacógeno do Espinhaço. Ciências da Terra 2, 13–18.

COSTA, P. H. de O.; ANDRADE, A. R. F. de; LOPES, G. A.; SOUZA, S. L. de. Projeto Lagoa Real: mapeamento geológico, 1:25000, texto e mapas. Companhia Baiana de Pesquisa Mineral, Salvador, v. 1, 1985

COSTA, Luiz Alfredo Moutinho da et al. Projeto LETOS (Leste do Tocantins / Oeste do São Francisco): Relatório Final. DNPM: Rio de Janeiro, v.1A, 1976.

Cunha, J.C., Barbosa, J.S.F., Mascarenhas, J.F., 2012. Greenstone Belts e Sequências Similares. In: Geologia da Bahia: Pesquisa e Atualização. Coordenação Geral: Johildo Barbosa, cap IV, p. 203–326.

DANDERFER FILHO, A. AND DARDENNE, M.A. 2002. Tectonoestratigrafia da Bacia Espinhaço na porção centro-norte do Cráton do São Francisco: registro de uma evolução poliistórica descontínua. Revista Brasileira de Geociências, 4, 449–460.

Danderfer Filho, A., DeWaele, B., Pedreira, A., Nalini, H.A. 2009. New geochronological constraints on the geological evolution of Espinhaço basin within the São Francisco Craton-Brazil. Precam- brian Research, 170, 116–128.

Danderfer Filho, A., Lana, C., Nalini-Júnior, H.A., Costa, A.F.O. 2015. Constraints on the Statherian evolution of the intraplate rifting in a Paleo-Mesoproterozoic paleocontinent: New stratigraphic and geochronology record from the eastern São Francisco craton. Gondwana Research, 28, 668–688.

Danderfer Filho, A. 2000. Geologia sedimentar e evolução tectônica do Espinhaço Setentrional, estado da Bahia. Unpl. PhD Thesis, Universidade Federal de Brasília, Brasilia, 220p.

DOMINGUEZ, J.M.L. (1993). As coberturas do Cráton do São Francisco: Uma abordagem do ponto de vista da análise de bacias. In: Dominguez, J.M.L. and Barbosa, J.S.F. (eds) O Cráton do São Francisco, SGM, pp. 137–155.

dos Santos, C., Danderfer Filho, A., Queiroga, G. N., Zincone, S. A., De Castro, M. P., & Lana, C. C. (2020). Ferroan alkalic volcanism associated with Calymmian rifting in the Paramirim aulacogen, São Francisco craton, Brazil: New insights from lithofacies analysis and evidence of mantle-derived alkaline H2O-rich metasomatic fluids affecting ancient crustal materials. *Precambrian Research*, *340*, 105632.

Fyfe, W. S., 1979, The geochemical cycle of uranium: Royal Soc. Aqueous [London] Philos. Trans., v. 291A, p. 432-452.

Guadagnin F., Chemale Jr. F., Magalhães A.J., Santana A., Dussin I., Takehara, L. 2015 Age constraints on crystal-tuff from the Espinhaço Supergoup – Insight into the

Paleoproterozoic to Mesoproterzoic intracratonic basin cycles of the São Francisco craton. Gondwana Research, 27, 363–376.

GUADAGNIN, F. AND CHEMALE JR. F. 2015. Detrital zircon record of the Paleoproterozoic to Mesoproterozoic cratonic basins in the São Francisco Craton. Journal of South American Earth Sciences, 60, 104–116.

Guimarães J.T.; Santos R.A.S.; Melo R.C. (Orgs.). 2008. Geologia da Chapada Diamantina Ocidental. In: Guimarães J.T., Santos R.A., Melo R.C. Projeto Ibitiara – Rio de Contas. Companhia Baiana de Pesquisa Mineral-CBPM, Salvador, Arquivos Abertos 31, 64 p.

Guimarães, J.T. 1996. A Formação Bebedouro no Estado da Bahia: Faciologia, Estratigrafia e Ambiente de Sedimentação. Unpl. Master Thesis, Instituto de Geociências, Universidade Federal da Bahia, Salvador, 155p.

GUIMARÃES, J.T., ALKMIM, F.F., CRUZ, S.C.P. 2012. Supergrupos Espinhaço e São Francisco. In: Barbosa, J.S.F., Mascarenhas, J.F. M., Corrêa-Gomes, L.C., Domingues, J.M.L. (eds.). Geologia da Bahia. Pesquisa e Atualização de Dados. Salvador, Companhia Baiana de Pesquisa Mineral-CBPM, v. 2, p. 33–86.

JARDIM DE SÁ, E.F. 1981. A Chapada Diamantina e a faixa Santo Onofre: Um exemplo de tectônica intraplaca no Proterozóico Médio do Cráton São Francisco. In: Inda, H.A.A.V., Marinho, M.M., Duarte, F.B. (eds) Geologia e Recursos Minerais do Estado da Bahia, Textos Básicos, 4, SME/COM, pp. 111–120.

Kuchenbecker, M., Pedrosa-Soares, A.C., Babinski, M., Fanning, M. 2015. Detrital zircon age patterns and provenance assessment for pre-glacial to post-glacial successions of the Neoproterozoic Macaúbas Group, Araçuaí orogen, Brazil. Precambrian Research 266, 12–26.

Leão, Z.M.A.N., Dominguez, J.M.L., 1992. Plataformas carbonáticas precambrianas: o exemplo da Formação Salitre, Proterozóico Superior, Estado da Bahia, 37th Congresso Brasileiro de Geologia, Anais, p. 45–452.

Leão, Z.M.A.N., Dominguez, J.M.L., Camargo, S.L. 1992. Sedi- mentação carbonática marinha rasa no Pré-Cambriano: sobre a validade de aplicação de modelos de fácies desenvolvidos para o Fanerozóico. Simpósio de Geologia de Minas Gerais, 4, Anais, p. 103–104.

LOBATO, LM. Metamorphism, metassomatism and mineralization at Lagoa Real, Bahia, Brazil. PhD dissertation, University of Western Ontario, 1985

LOBATO, L., & FYFE, W. (1990). Metamorphism and mineralization at Lagoa Real, Bahia, Brasil. *Econ. Geol*, *5*, 968-989.

LOBATO, L.M., PIMENTEL, M.M., CRUZ, S.C.P., MACHADO, N., NOCE, C.M., ALKMIM, F.F. 2015. Geochronology of the Lagoa Real uranium district, Brazil: Implications for the age of the uranium mineraliza- tion. Journal South American Earth Sciences, 58, 129–140.

Loureiro H.S.C., Bahiense I.C., Neves J.P., Guimarães J.T., Teixeira L. R., Santos R.A., Melo R.C. (Org.). 2009. Geologia e recursos minerais da parte norte do corredor de deformação do Paramirim: (Projeto Barra – Oliveira dos Brejinhos). Companhia Baiana de Pesquisa Mineral-CBPM, Salvador, Série Arquivos Abertos 33, 113 p.

Macedo, M.H., Bonhome, M.G. 1984. Contribuição a cronoestratigrafia das Formações Caboclo, Bebedouro e Salitre na Chapada Dia- mantina (BA) pelos métodos RB-Sr e K-Ar. Revista Brasileira de Geociências, 3, 153–163.

Macedo, M.H.F., Bonhome, M.G. 1981. Datação Rb-Sr e K-Ar das formações Bebedouro e Caboclo na Chapada Diamantina. 1o Simpósio sobre o Cráton do São Francisco, Anais, p. 98–99.

Machado, G. S. (2008). Geologia da porção sul do complexo Lagoa Real, Caetité, Bahia. *Trabalho final de Graduação, Instituto de Geociências, Universidade Federal da Bahia, Salvador*.

MAGALHÃES, A.J.C., SCHERER, C.M.S., RAJA GABAGLIA, G.P., BÁLLICO, M. B., CATUNEANU, O. 2014. Unincised fluvial and tide-dominated estuarine systems from the Meso-proterozoic Lower Tombador Formation, Chapada Diamantina basin, Brazil. Journal South American Earth Science, 56, 68–90.

MAGALHÃES, A.J.C., RAJA GABAGLIA, G.P., SCHERER, C.M.S., BÁLLICO, M. B., GUADAGNIN, F., BENTO FREIRE, E., SILVA BORN, L.R., CATUNEANU, O. 2016. Sequence hierarchy ina Mesoproterozoic interior sag basin: from basin fill to reservoir scale, the Tombador Formation, Chapada Diamantina Basin, Brazil. Basin Research, 26, 393–432

Marques, C., Cabral, A. R., Rios, F., 2020a. Whole-rock chemistry of the Gameleira I uranium deposit, Lagoa Real, Brazil. Chemie der Erde. In press.

MARUÉJOL, P. Métasomatose alcaline et minéralisation uranifères: les albitites du gisement de Lagoa Real (Bahia, Brésil) et exemples complémentaires de Xihuashan (SE Chine), Zheltorechensk (Ukraine) e Chuling Khola (Népal central). 1989. 428p. Tese (Doutorado) - Centre du Recherche sur la Geologie de l'uranium, Nancy, 1989

McReath, I., Jardim de Sá, E.F., Fryer, B.J. 1981. As vulcânicas ácidas da região da Bacia do rio Paramirim-Bahia. In: Inda, H.A.V. Marinho, M.M., Duarte, F.P. (eds) Geologia e Recursos Minerais do Estado da Bahia, Textos Básicos, 4, SME/COM, pp. 120–130.

MORAES, et al. Projeto Brumado Caetite: Relatório Final da 1ªFase. Salvador: CPRM, 1980 9 v.

OLIVEIRA, L. A. R., DE SOUZA, A. D. S., RIOS, F. J., DE OLIVEIRA CHAVES, A., AMORIM, L. E. D., YARDLEY, B., ... & PRATES, S. P. (2012). Estudo de inclusões fluidas em minerais associados à mineralização uranífera de três jazidas da província uranífera de lagoa real, bahia–brasil. Revista geonomos, 2(20).

PEDREIRA, A.J.; ARCANJO, J.B.; PEDROSA, C.J.; OLIVEIRA, J.E.; SILVA, B.C.E. 1975. Projeto Bahia - Relatório Final - Geologia da Chapada Diamantina. Salvador, DNPM/CPRM, 2 volumes, (inédito)

PEDROSA-SOARES, A. C., NOCE, C. M., WIEDEMANN, C. M., & PINTO, C. P. (2001). The Araçuaı-West-Congo Orogen in Brazil: an overview of a confined orogen formed during Gondwanaland assembly. *Precambrian research,110* (1), 307-323.

PEDROSA-SOARES, A. C. AND ALKMIM, F. F. 2011. How many rifting events preceded the development of the Araçuaí-West Congo orogen? Geonomos, 12, 244–251.

Prates, S.C, Freitas, M. E., Matos, E. C, Alves, J. V., Garcia, L. R. A. 2011 A GARNET AND URANINITE RICH ROCK FOUND IN THE LAGOA REAL URANIUM PROVINCE PRELIMINARY STUDIES. International Nuclear Atlantic Conference. INAC. Belo Horizonte.

Raposo, C. e de Matos, E.C. (1982). Distrito uranifero de Laqoa Real - "A historia de um examplo". Soe. Bras. Geol., Anais 32° Conqr. Bras. Geol. 5_, 2035-2047.

Santana, A.V., 2016. Análise estratigráfica em alta resolução em rampa carbonática dominada por microbiolitos, Formação Salitre, Bacia de Irecê, Bahia. Ph.D. Thesis. Universidade Federal de Brasília, Brasília.

Silva, L. C., Armstrong, R., Noce, C. M., Carneiro, M. A., Pimentel, M., Pedrosa-Soares, A.C., Leite, C. A., Vieira, V. S., Silva, M. A., Paes, V. J. C., Cardoso Filho, J.M. 2002. Reavaliação da evolução geológica em terrenos pré-cambrianos brasileiros com base em novos dados U-Pb SHRIMP, Parte II: Orógeno Araçuaí, Cinturão Mineiro e Cráton do São Francisco Meridional. *Rev. Bras. Geoc.,* 32: 513-528.

SILVEIRA, E.M., SÖDERLUND, U., OLIVEIRA, E.P., ERNST, R.E., MENEZES LEAL, A.B. 2013. First precise U-Pb baddeleyite ages of 1500 Ma mafic dykes from the São Francisco Craton, Brazil, and tectonic implications. Lithos 174: 144 –156.

SOUZA, A. S. (2009). Inclusões Fluidas nos Minerais Associados à Mineralização Uranífera da Jazida do Engenho (Anomalia 09), Província Uranífera de Lagoa Real-Bahia. Dissertação de Mestrado em Ciência e Tecnologia das Radiações, Minerais e Materiais. Centro de Desenvolvimento da Tecnologia Nuclear, Belo Horizonte.

SCHOBBENHAUS, C. 1996. As tafrogêneses superpostas Espinhaço e Santo Onofre, estado da Bahia: Revisão e novas propostas. Revista Brasileira de Geociências, 4: 265–276.

Schobbenhaus C., Kaul, P.T. 1971. Contribuição à Estratigrafia da Chapada Diamantina Bahia-Central. Mineração e Metalurgia, 53 (315): 116–120.

STEIN, J. H., NETO, A. M., DRUMOND, A., & ANGEIRAS, A. G. (1980). Nota preliminar sobre os processos de albitização uranífera de Lagoa Real (Bahia) e sua comparação com os da URSS e Suecia. In *Congresso Brasileiro de Geologia* (Vol. 31, pp. 1758-1775).

TURPIN, L., MARUEJOL, P., & CUNEY, M. (1988). U-Pb, Rb-Sr and Sm-Nd chronology of granitic basement, hydrothermal albitites and uranium mineralization (Lagoa Real, South-Bahia, Brazil). *Contributions to Mineralogy and Petrology*, *98*(2), 139-147.

Toulkeridis T., Babinski M., Buchwaldt R., Brito Neves B.B., Todt W., Santos R. 1999. Are varangian or sturtian the glacial deposits on the São Francisco cráton? Evidence from determination of sedimentary rocks and minerals of the Neoproterozoic Una Group. In: South American Symposium on Isotope Geology, 2, Cordoba, Anais, p. 453–456.

Warren LV, Quaglio F, Riccomini C, Simões MG, Poiré DG, Strikis NM, Aneli LE, Strikis, P.C. 2014. The puzzle assembled: Ediacaran guide fossil Cloudina reveals an old proto-Gondwana seaway. Geology, 5, 391–394.

CAPÍTULO 3 – WHOLE-ROCK CHEMISTRY OF THE GAMELEIRA I URANIUM DEPOSIT, LAGOA REAL, BRAZIL

Camila Marques*[a,b], Alexandre Raphael Cabral[c,d], Francisco Javier Rios[d]

[a] Programa de Pós-Graduação em Ciência e Tecnologia das Radiações, Minerais e Materiais. Centro de Desenvolvimento da Tecnologia Nuclear (CDTN),

[b] Programa de Doctorado em Geología. Departamento de Geología, Facultad de Ciencias, Universidad de Salamanca

[c] Centro de Pesquisas Professor Manoel Teixeira da Costa (CPMTC), Instituto de Geociências, Universidade Federal de Minas Gerais (UFMG)

[d] Centro de Desenvolvimento da Tecnologia Nuclear (CDTN/CNEN-MG)

*corresponding author

Artigo publicado no *Geochemistry*

Disponível online no link https://doi.org/10.1016/j.chemer.2020.125677

Abstract

The Lagoa Real uranium (U) province, referred to as Lagoa Real, is located in Bahia state, northeastern Brazil. Lagoa Real has ~112,000 metric tonnes of U_3O_8 and an average grade of 2700 ppm, being one of the largest U deposits in the world and the largest in Brazil. Despite its economic and strategic importance, there are gaps in the geological knowledge of the Lagoa Real U deposits. One of them is the lack of extensive whole-rock chemical data sets. Here, we present whole-rock chemical analyses for major and trace elements, including the rare-earth elements (REE), from barren country rocks to uraniferous ore shoot, systematically sampled from an exploratory drill hole in the Lagoa Real uranium province, Brazil. The chemical data indicate that albitite rocks, with and without uraniferous mineralisation, cannot result from sodic syenitic magmatism, as proposed by recent studies, but from sodic metasomatism of a granitic protolith, as previously suggested. Petrographical and geochemical evidence supports the idea that the Lagoa Real albitite rocks are the metasomatic product of the granitic country rock, known as the São Timóteo granite. Their ore-mineral assemblages and geochemical characteristics share similarities with albitite-hosted U deposits worldwide.
Keywords: whole-rock chemistry; Lagoa Real uranium province; chemical profile; albitite; sodic metasomatism

3.1 INTRODUCTION

The Lagoa Real (U) province represents the world's sixth largest U reserve, being the most important in Brazil. Located in southern Bahia, in the northern part of the Araçuaí orogen, the province is approximately 35 km long and has 38 uraniferous anomalies along three semi-arched lineaments (Fig. 7). The province contains a total reserve of ~112,000 metric tons and average grade of 2700 ppm of U_3O_8 (Brito et al., 1984; Matos et al., 2003; Matos and Villegas, 2010). Its uraniferous mineralisation is spatially associated with lens-shaped albite-rich rocks, known as albitite. They are enclosed in the granite–gneiss rocks of the Lagoa Real intrusive suite, known as São Timóteo granite. Albitite rocks have abundant plagioclase, albite ± oligoclase, and a variety of subordinate minerals, such as garnet, clinopyroxene and amphibole, making up different calcic–sodic mineral assemblages.

Albitite-hosted U deposits, also referred to as Na-metasomatite and albitite-type deposits by Bruneton and Cuney (2016) and Wilde (2013), respectively, are characterised by discontinuous U-rich occurrences over several tens of kilometres hosted in extensive deformation corridors (Cuney, 2009), hosted by granitoids or metavolcanic strongly albitised rocks. Albitisation is generally early in relation to ore deposition and the main uranium ore are fine-grained uraninite and brannerite, which are associated to hydrothermal zircon and Ti-rich mineral (Polito, 2009; Alexandre, 2010; Cuney 2012; Wilde, 2013). This class of U deposit collectively holds as much U as the better-known unconformity-type deposits – i.e., over 1 million tonnes of U_3O_8 (Wilde, 2013), yet studies on albitite-type U deposits are comparatively sparse and, consequently, their genetic model is uncertain. Lagoa Real and Kirovograd–Krivoi Rog district, Ukraine, have traditionally been considered the most representative cases of the albitite type. More research is thus required to better understand their genesis and to develop exploration strategies.

In Lagoa Real, albitite rocks have generally been regarded as the result of metasomatic overprint on granitic–gneissic rocks of the São Timóteo granite. The metasomatic overprint mainly led to Na enrichment and silica depletion (Lobato and Fyfe, 1990; Maruejol, 1988). However, there has been a recent attempt to explain their genesis through a magmatic model in which albitite rocks would be derived from sodic syenitic magmatism (Chaves, 2013). Such contrasting views exemplify the lack of consensus regarding the origin of the Lagoa Real albitite rocks, notwithstanding numerous studies (Geisel Sobrinho et al., 1980; Lobato, 1985; Fuzikawa et al., 1988; Maruejol, 1988; Lobato and Fyfe, 1990; Cruz, 2004; Chaves, 2013; Lobato et al., 2015).

Similarly to the other albitite-hosted U systems, Lagoa Real occurs in a high-grade metamorphic terrane. Its poor exposition has contributed to unsolved questions, mainly about the processes leading to albitite genesis and U mineralization. The lack of consensus also comes from the paucity of published whole-rock chemical data for trace elements, particularly the rare-earth elements (REE) and the high-field-strength elements, from albitite rocks. One of the Lagoa Real uraniferous anomalies, Gameleira I, is poorly exposed. Recent exploration for uraniferous mineralisation at Gameleira I has made available fresh rocks from diamond drill holes. One of the exploratory drill holes, DDH-10, was sampled for whole-rock chemistry of albitite rocks, the results of which are presented and discussed in order to better constrain the albitite genesis, and to provide geochemical characteristics of altered rocks and ore shoots in the context of albitite-related U deposits.

3.2 GEOLOGICAL SETTING

Lagoa Real is situated in northern part of the Ediacaran–Cambrian Araçuaí orogen (Fig. 32; Almeida, 1977), in the Paramirim aulacogen (Alkmim et al., 2006; Pedrosa-Soares et al., 2001, 2007, 2008; Pedrosa-Soares and Wiedemann-Leonardos, 2000). Meso- to Neoarchaean tonalite–trondjemite–granodiorite (TTG) terrane, K-rich granitic rocks and greenstone belts comprise the basement within and around the Paramirim aulacogen (Barbosa et al., 2013; Leal et al., 1996; Martin et al., 1997; Nutman and Cordani, 1993; Peucat et al., 2002; Santos-Pinto et al., 2012). The aulacogen represents a partially inverted rift-sag basin, the metasedimentary cover of which accumulated at ca. 1.78 Ga (Cruz and Alkmim, 2007; Schobbenhaus, 2017). The metasedimentary cover forms two morphotectonic domains, the Serra do Espinhaço and the Chapada Diamantina, which evolved as two almost independent sub-basins by the end of the Neoproterozoic (Cruz and Alkmim, 2017). Two lithostratigraphic sequences have been individualised in the metasedimentary cover: the Espinhaço Supergroup (ca. 1.77 Ga to ca.1.14 Ga; Danderfer Filho et al., 2015 and Babinski et al., 1993, respectively) and the Neoproterozoic São Francisco Supergroup (ca. 850 Ma to 675 Ma; Bitencourt et al., 2019 and Santana, 2016, respectively).

An igneous suite of porphyritic and coarse-grained hastingsite-bearing syenite, syenogranite and alkali granite intruded the Paramirim basement. This suite of Statherian plutonic rocks is commonly known as the São Timóteo granite, but also as the Lagoa Real intrusive suite (Arcanjo et al., 2005), and it is part of a large silicic igneous province that erupted from ca.1.79 to 1.70 Ga in the São Francisco–Congo palaeocontinental block (Magalhães et al.,

2018; and references therein). The São Timóteo granite is characterised as metaluminous, high-K and Fe-rich calc-alkaline series of anorogenic origin (Teixeira, 2000; Machado, 2008; Amorim, 2012), the crystallisation of which took place between 1.77 and 1.74 Ga (Turpin et al., 1988; Cordani et al., 1992; Lobato et al., 2015).

Two geochronological groups of gabbro, diabase and diorite, of tholeiitic composition and continental intraplate affinity, intruded the Espinhaço Supergroup as sills and dykes (Arcanjo et al., 2005; Menezes et al., 2012). The oldest group, located in the eastern part of the Serra do Espinhaço, has ages of 1579 ± 15 Ma (Santos et al., 2020), 1514 ± 22 Ma (Babinski et al., 1999), 1507 ± 7 Ma (Silveira et al., 2013), 1496 ± 3.2 Ma and 1492 ± 16 Ma (Guimarães et al., 2008; Loureiro et al., 2009). The youngest group, situated in the eastern and western parts of the Serra do Espinhaço, comprises ages of 934 ± 14 Ma (Loureiro et al., 2009) and 854 ± 23 Ma (Danderfer et al., 2009).

Tectonic overprint on the São Timóteo granite is expressed as Ediacaran shear zones (Alkmim et al., 2006; Cruz and Alkmim, 2006), which consist mainly of gneisses derived from Lagoa Real suite intrusive rocks and albitite rocks, but also of epidosites, oligoclasites, microclinites, amphibolites, and diabases bodies of uncertain origin, which, excepting diabase, lie concordantly with regional rocks (Costa, 1985; Cruz et al 2007). Albitites host most of the uraniferous mineralisation of Lagoa Real, but ore shoots also occur in epidosite and oligoclasite (Cruz, 2004; Maruejol, 1988). Albitite bodies are discontinuous, massive or gneissified, fusiform and variable in length, ranging from metric to hundred of metres (<480 m; Ribeiro et al., 1984). Ore shoots have disseminated uraninite crystals, 5–25 μm across, commonly found in spatial association with andradite and hedenbergite, specifically at the margins of aegirine, albite, hastingsite, biotite, calcite and hematite (Lobato and Fyfe, 1990). Different ages have been proposed for the uraniferous mineralisation – e.g., ca. 1.4 Ga (Turpin et al., 1988); ca. 0.95 Ga (Lobato et al., 2015).

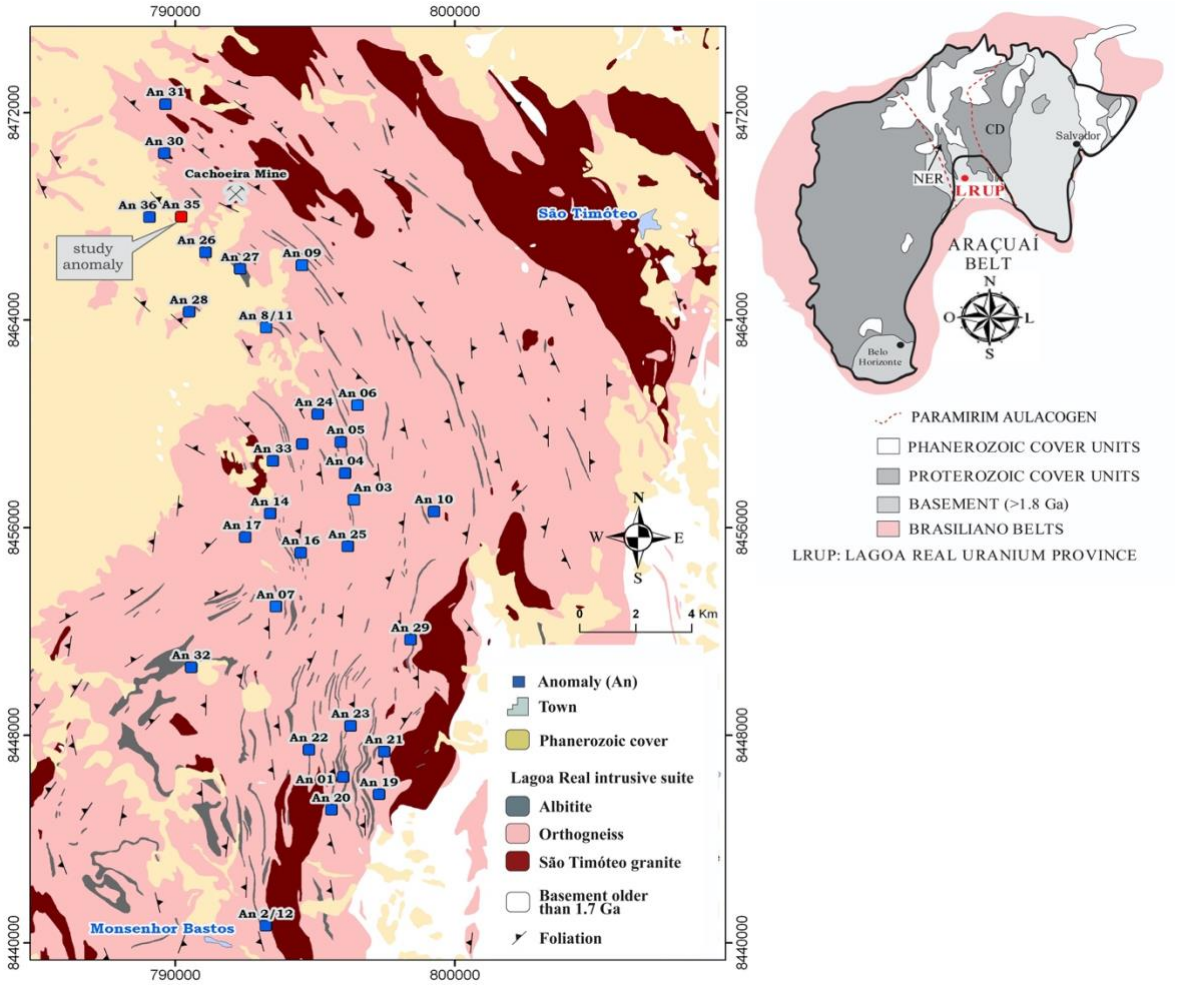

Fig. 7: Geological map of the Lagoa Real uranium province, abbreviated as LRUP in the inset (right), showing the distribution of U anomalies and the location of the Cachoeira U deposit. The map is adapted from Costa et al. (1985). Abbreviations: NER, Northern Espinhaço Range; CD, Chapada Diamantina.

3.3 METHODS

Fifteen samples from diamond drill hole (DDH) F10 were collected for whole-rock chemical analyses, which were performed at Bureau Veritas, Vancouver, Canada. Drill-core samples were crushed and then pulverised using a tungsten-carbide mill. Major elements were determined from a 0.2-g pulp sample split, fused at 1,000 °C with $LiBO_2$ flux. The molten bead was digested in 5% HNO_3, the solution of which was analysed by inductively coupled plasma–optical emission spectrometry (ICP–OES). Most of trace elements and all the REE were measured by inductively coupled plasma–mass spectrometry (ICP–MS), using reference materials STD-SO-18 and STD-SO-19. Loss-on-ignition was determined on sample splits of 1 g, ignited at 1,000 °C. Measurements for Ag, As, Bi, Cd, Cu, Mo, Ni, Pb,

Sb, Tl and Zn were from samples splits of 0.25 g, digested in a $HF–H_2O–HClO_4–HNO_3$ solution at fuming temperature and taken to dryness. Their residues were then solubilised in 50% HCl and analysed by ICP–MS.

3.4 RESULTS

3.4.1 Petrography

Fig. 8 schematically illustrates granitic rocks and albitite rocks that were intercepted by DDH F10. The granitic rocks are divided into two major types: (i) hypersolvus alkali-feldspar granite (HAFG); (ii) augen gneiss, which corresponds to deformed HAFG (HAFG-gneiss). Macroscopically, the HAFG has a coarse-grained hypidiomorphic fabric, >5 mm across and grey in colour. This fabric appears deformed and coloured to reddish shades in the HAFG-gneiss. The HAFG rocks are composed of K-feldspar (~60 vol.%), quartz (~30 vol.%), clinopyroxene, amphibole, biotite, titanite, ilmenite, zircon and apatite. The latter are individually variable in abundance, amounting to ~10% of modal volume. Phenocrystals of K-feldspar are the main mineral phase characterising a hypersolvus facies of granite (Fig. 9A). Amphibole is bluish green and forms interstitial aggregates in spatial association with Fe–Ti oxides, apatite, zircon and biotite. Amphibole envelops clinopyroxene and is replaced by biotite (Fig. 9B). The Fe–Ti oxides are titanite and ilmenite that form corona-like aggregates.

Gneissic rocks are porphyroclastic. Their main porphyroclast is K-feldspar, which is embedded in a recrystallised matrix of fine-grained feldspar and quartz. Accounting for up to ~40% of modal volume, K-feldspar contains plagioclase patches that grade to subgrains (Fig. 9C). In some reddened portions of the HAFG-gneiss, plagioclase is widespread and reaches ~20% of modal volume, acquiring a cloudy appearance due to alteration to sericite, fluorite and carbonate (Fig. 9D). Together, the porphyroclasts and recrystallised matrix form core-and-mantle domains that define the augen fabric of the HAFG-gneiss (Fig. 9E). Quartz is abundant, >30% vol.%, and occurs as ribbons. Amphibole and biotite are foliation-forming minerals. The former has inclusions of titanite and ilmenite with corona microfabric. Santos (2016) observed that feldspar in the HAFG-gneiss tends to become more sodic in composition with increasing strain.

Albitite rocks are divided into three major types on the basis of subordinate minerals, which have gradational contacts in DDH F10: (i) garnet-bearing albitite (GRAAB), composed of albite, garnet, clinopyroxene, calcite and titanite; (ii) magnetite-bearing albitite

(MAAB), made up of albite, magnetite, clinopyroxene, amphibole, biotite and titanite; (iii) and biotite-bearing albitite (BIAB), which has biotite, albite, zircon and titanite. Uraniferous mineralisation in DDH-F10 is hosted within pervasively foliated magnetite-bearing albitite, where uraninite is included in titanite and also has a close spatial association with zircon.

Albitite rocks display polygonal granoblastic and porphyroclastic fabrics (Fig. 10A), isotropic or foliated. Albite accounts for 60–80 vol.% of these rocks. All albitite varieties have common features regarding albite occurrence. The mineral occurs as: i) medium- to coarse-grained porphyroclasts with polysynthetic twinning, or chessboard twinning; ii) fine-grained granoblastic crystals of polygonal shapes, mostly without twinning.

Garnet-bearing albitite has light-green clinopyroxene, light-pink garnet and albite as the main mineral constituents. In the most foliated portions, clinopyroxene is well developed and accounts for ~15 vol.% of the rock; in less deformed portions, reliquial bluish-green amphibole is replaced by clinopyroxene. Carbonate coexists with garnet and clinopyroxene. Alkali-feldspar and quartz are either absent or in trace amounts. Magnetite, if any, is a trace mineral. Titanite forms aggregates of subhedral to euhedral crystals that are spatially associated with clinopyroxene and garnet.

Magnetite-bearing albitite consists of bluish-green amphibole, light-green clinopyroxene, magnetite partially oxidised to hematite ("martite"), light-green or brown biotite and albite. This variety of albite has spatial association with ore shoot in DDH F10. Clinopyroxene and green biotite are concentrated in bands with magnetite and titanite (Fig. 10B). Rarely observed, amphibole is replaced by clinopyroxene. Alkali feldspar and quartz are either in trace amounts or absent. Both minerals are found where planar anisotropy is well developed as gneissic foliation, along which quartz is ribboned. Titanite forms corona-like aggregates with ilmenite. Aggregates of allanite and magnetite occur near U-mineralised intervals. Green biotite and carbonate fill veinlets that cross-cut the rock matrix.

Biotite-bearing albitite has abundant biotite, ~20 vol.%, as a foliation-forming mineral (Fig. 10C). Two types of biotite have been identified: brown biotite and green biotite. The brown variety is found as medium-grained replacements of ferromagnesian minerals. The green variety occurs as fine-grained lamellae in albite. Minerals such as pyroxene, amphibole, titanite and magnetite are either rarely observed or absent. Zircon crystals are included in brown biotite.

Uranium ore is hosted in magnetite-bearing albitite as lenticular, weakly foliated domains that are spatially associated with diopside and actinolite concentrations (mineral composition according to Santos, 2016). Diopside occurs as relicts within actinolite, which

in turn overprinted by albite (Fig. 10D). The rock has fine-grained crystals of uraninite, ~5 μm across, invisible to the naked eye. The mineral is altered to uranophane and a U–Ca–Ti–Si-bearing mineral. Uraninite grains occur within titanite and in its immediate vicinity (Fig. 10E, F), as well as close to martitised magnetite and zircon. It is remarkable that fine-grained crystals of zircon are concentrated along albite and titanite grains (Fig. 4G). Uranophane is included in titanite (Fig. 10F). Zircon is generally fractured and porous, partially overgrown by zircon.

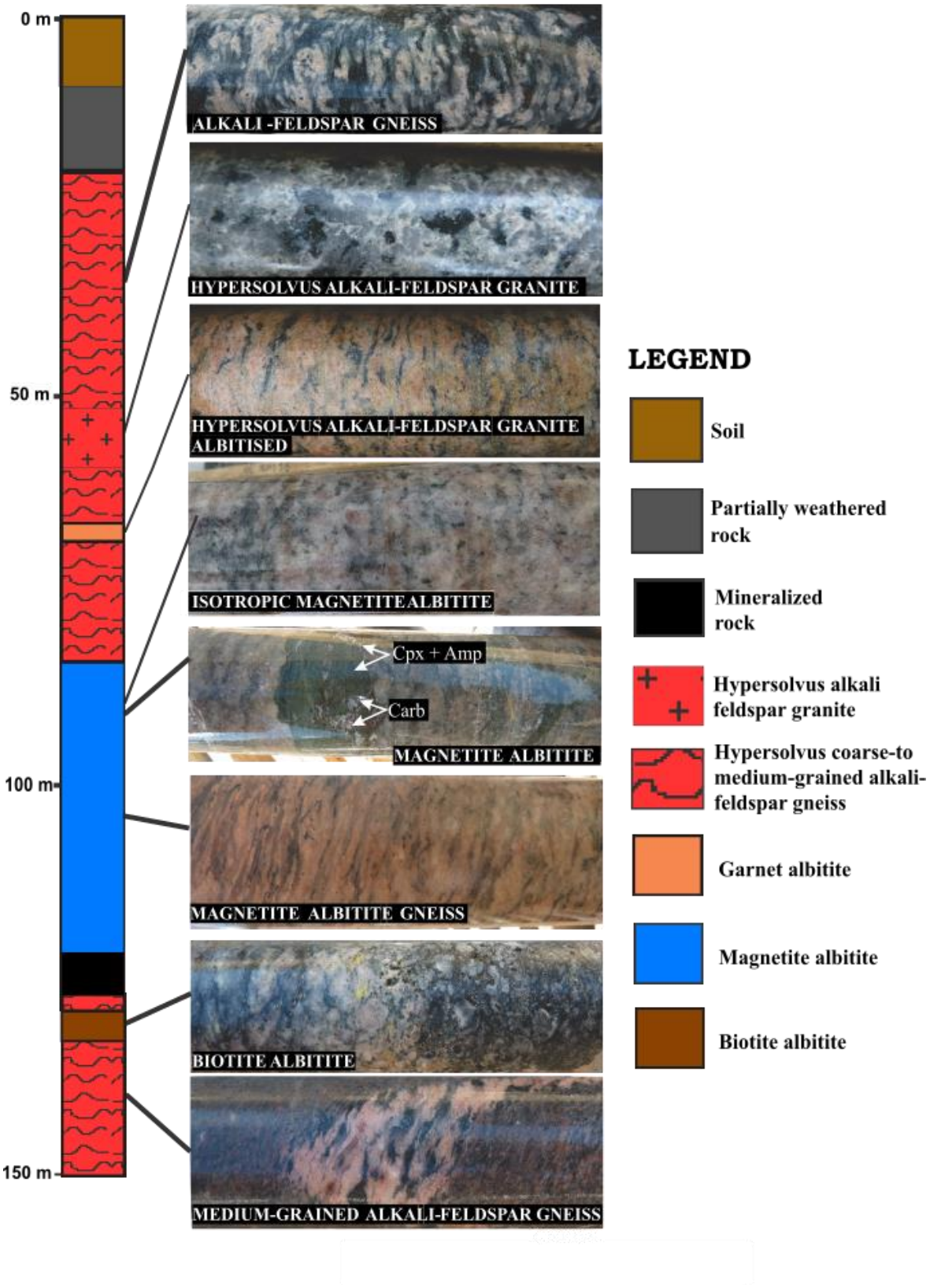

Fig. 8. Simplified drill-core log of DDH-F10 and photographs of main rock types. Drill-core diameter is NQ – i.e., diameter of ~4.8 cm – in all photographs.

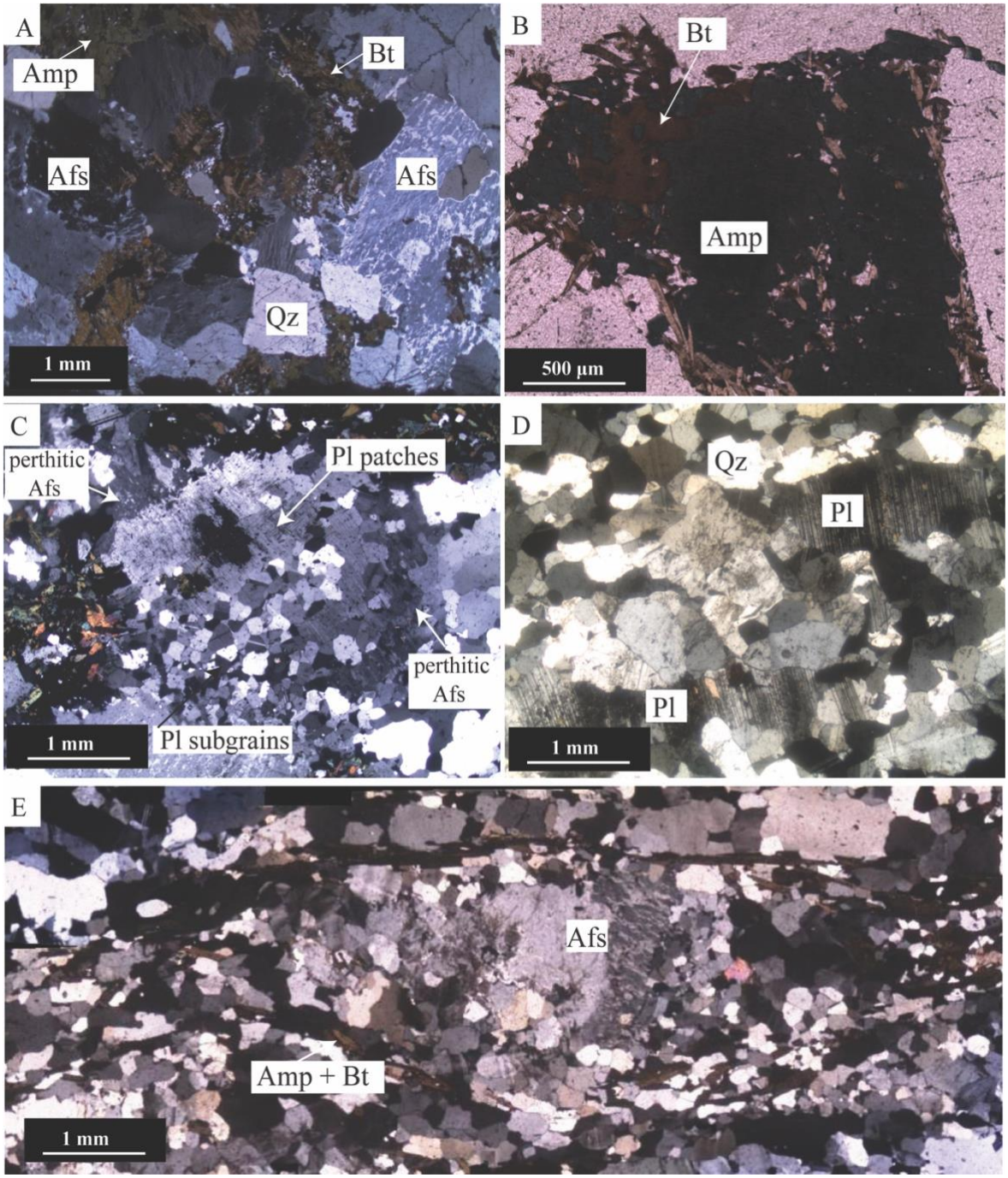

Fig. 9**.** Transmitted-light photomicrographs of granitic-gneissic rocks of the São Timóteo granite, either in plane-polarised light (PPL), or cross-polarised light (CPL). Mineral abbreviations are according to Whitney and Evans (2010). A) General fabric of hypersolvus alkali-feldspar granite showing coarse-grained crystals of perthitic K-feldspar and interstitial quartz, spatially associated with amphibole and biotite; CPL. B) Relicts of green amphibole, replaced by biotite in hypersolvus alkali-feldspar granite; PPL. C) Typical fabric of K-feldspar replacement by plagioclase in granitic-gneissic rocks. Note a rim of perthitic K-feldspar (Afs) with a core of altered plagioclase (Pl patches), which is converted into plagioclase subgrains; CPL D) Albitised granite with medium-grained sericitised

plagioclase, recognised by its dirty appearance; CPL. E) Augen microstructure of perthitic K-feldspar porphyroclast (Afs), in gneissic rock of the São Timóteo granite; CPL.

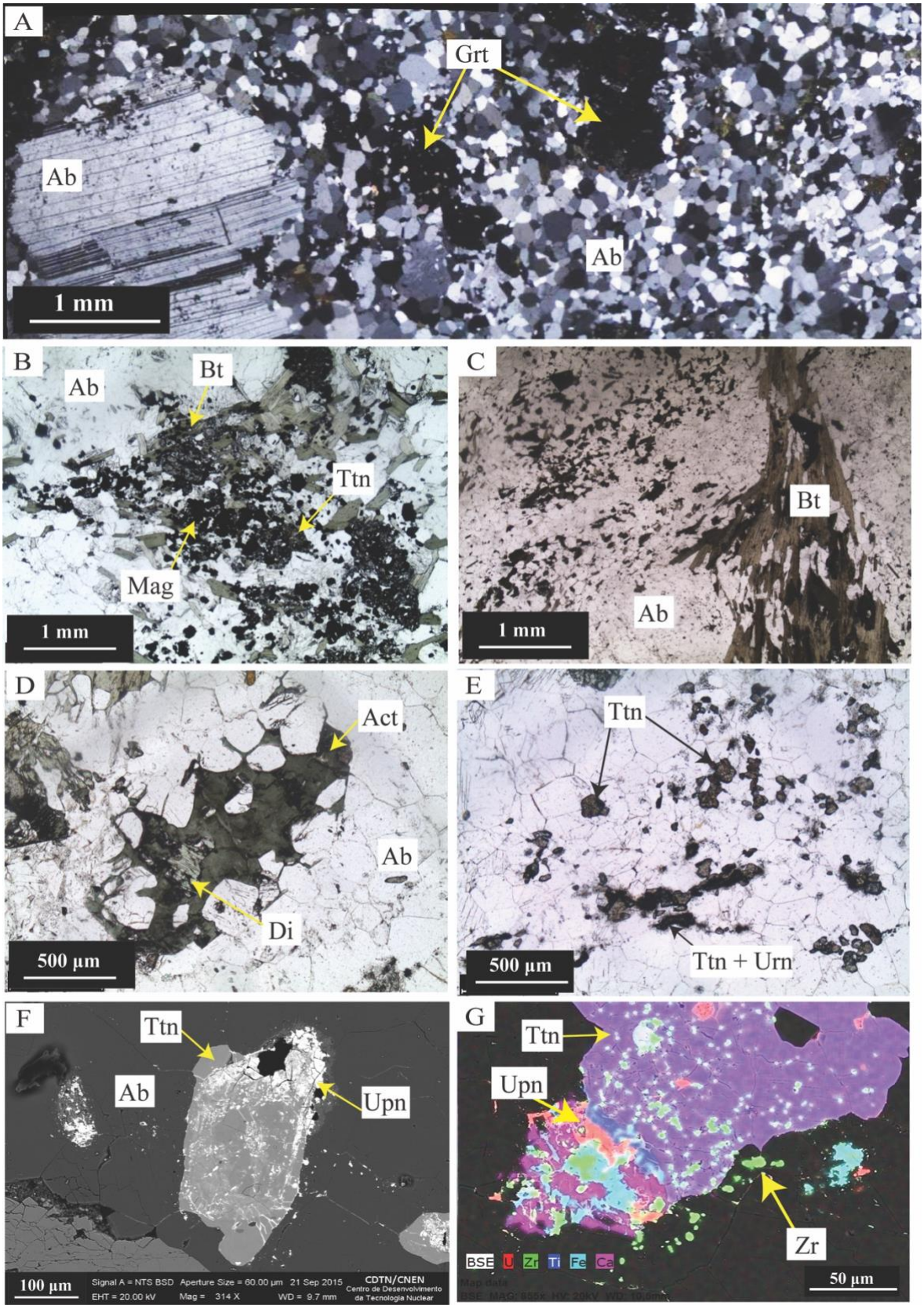

Fig. 10. Transmitted-light photomicrographs and backscattered-electron (BSE) images. Mineral abbreviations are according to Whitney and Evans (2010); for abbreviations PPL and CPL, see caption of Figure 3. A) General fabric of albitite, showing a porphyroclast of twinned (Ab) in a matrix of untwined, granoblastic albite; CPL. B) Magnetite-bearing albitite, in which magnetite occurs in the vicinity of green biotite and titanite; PPL. C) Biotite-bearing albitite, in which biotite is the main foliation-forming mineral; PPL. D) Relict of diopside within actinolite in ore-shoot albitite; PPL. Note that actinolite partially surrounds albite grains. E) Titanite and uraninite are typical minerals of ore-shoot albitite; PPL. F) BSE image of uranophane-hosting titanite from ore-shoot albitite. Note that uranophane fills microfractures in titanite and also along grain boundaries in the albitite matrix. G) X-ray maps for U, Zr, Ti, Fe and Ca. Zirconium concentrations indicate zircon crystals included in, and in the vicinity of, titanite and uranophane. Ca-rich domains represent titanite and Fe-rich domains are hematite.

3.4.2 Geochemistry

Concentrations of major and trace elements in DDH F10 are reported in Table 1, while Fig. 11 shows the main vertical geochemical variations. The São Timóteo granite, HAFG, and its gneissic varieties, HAFG-gneiss, have high K_2O contents, about 5 wt%, and SiO_2 contents between about 71 and 75 wt%, while other major elements are relatively low – i.e., TiO_2 (0.26–0.53 wt%), MgO (0.06–0.10 wt%), CaO (0.76–1.72 wt%), Na_2O (2.4–3.3 wt%) and P_2O_5 (0.03–0.07 wt%). Albitite rocks have at least 7 wt% Na_2O, whereas CaO contents are variable, between 0.8 and 4.4 wt%, depending on the amount of amphibole, pyroxene and/or garnet. The U-mineralised interval of DDH F10 and its immediately adjacent albitite rocks have the highest contents of MgO and Al_2O_3, between ~1.5 and 1.8 wt%, and between ~17 and 18 wt%, respectively, but SiO_2 contents as low as 62 wt%. In general, all samples show a positive correlation between Al_2O_3 and Ga, where the highest contents of Ga are in the ore shoot and samples adjacent to it (Fig. 12).

Granitic rocks and gneissic varieties are plotted in the discriminating diagrams Fig. 13. They plot in the granite field in the multicationic diagram of De La Roche et al. (1980), excepting one sample of partially albitised rock that plots in the syenite field (Fig. 13A). The rocks are metaluminous (Fig. 13B), according to Shand's index (Shand, 1950), alkaline (Fig. 13C; Sylvester, 1989), reduced (Fig. 13D; Dall'Agnol and Oliveira, 2007), as well as ferroan (Fig. 13E; Frost et al., 2001). They can further be classified as A-type (Fig. 13F; Whalen et al., 1987), with within-plate signature (Fig. 13G; Pearce et al., 1984). The classification of

Eby (1992) also indicates strong crustal contamination for the São Timóteo rocks (Fig. 13H; A2 field). The results are similar to those obtained by Teixeira (2000), Machado (2008) and Amorim (2012) for Lagoa Real suite intrusive rocks.

In DDH F10, albite-bearing varieties of HAFG and HAFG-gneiss are marked by a pinkish overprint due to fine-grained hematite. The latter is spatially associated with plagioclase replacement with fine-grained muscovite – i.e., sericite. Increasing contents of albite and/or oligoclase imprint a whitish appearance to the rock; the higher the Na_2O content (~5–7 wt%), the smaller the K_2O content (from 2.5 wt% down to 0.80 w%).

In addition to U in the ore shoot, Zr is considerably enriched, the highest content of which is found in the biotite albitite immediately underneath the ore shoot (1364 ppm Zr). This enrichment in Zr is decoupled from Hf, as expressed by a Zr/Hf ratio of 64 (Table 1). Vanadium contents increase from below the detection limit of <8 ppm at 94 m to 117 ppm at 124.5 m, where the uraniferous ore shoot is, and then reach the highest content, 634 ppm V, in the biotite albitite underlying the ore shoot.

Chondrite-normalised REE patterns exhibit moderately inclined slopes (Fig. 14), decreasing from La to Sm, with negative anomalies of Eu* (Eu* = 0.4 – 0.7 for granitic-gneissic rocks and Eu* = 0.4 – 0.5 for albitite rocks; see Table 1). Gently descending segments from Gd to Dy are followed by essentially flat segments from Ho to Lu. Albitite and granitic-gneissic rocks show similar light REE contents – i.e., ΣLREE = 315 – 556 ppm for the former, ΣLREE = 221 – 479 ppm for the latter. Ore-shoot sample ALB04 shows the highest LREE contents. The degree of fractionation of a REE pattern can be expressed by the concentration of a LREE against that of a heavy REE, normalised to their chondrite values (Rollinson, 1978). Applying the ratio La/Yb_N, it results that both groups have a similar degree of fractionation. Granitic-gneissic samples have La/Yb_N ratios between ~9 and 13, and albitite rocks are between ~6 and 14. The REE patterns of albitite rocks are indistinguishable from those of the HAFG and HAFG-gneiss, independently of U mineralisation.

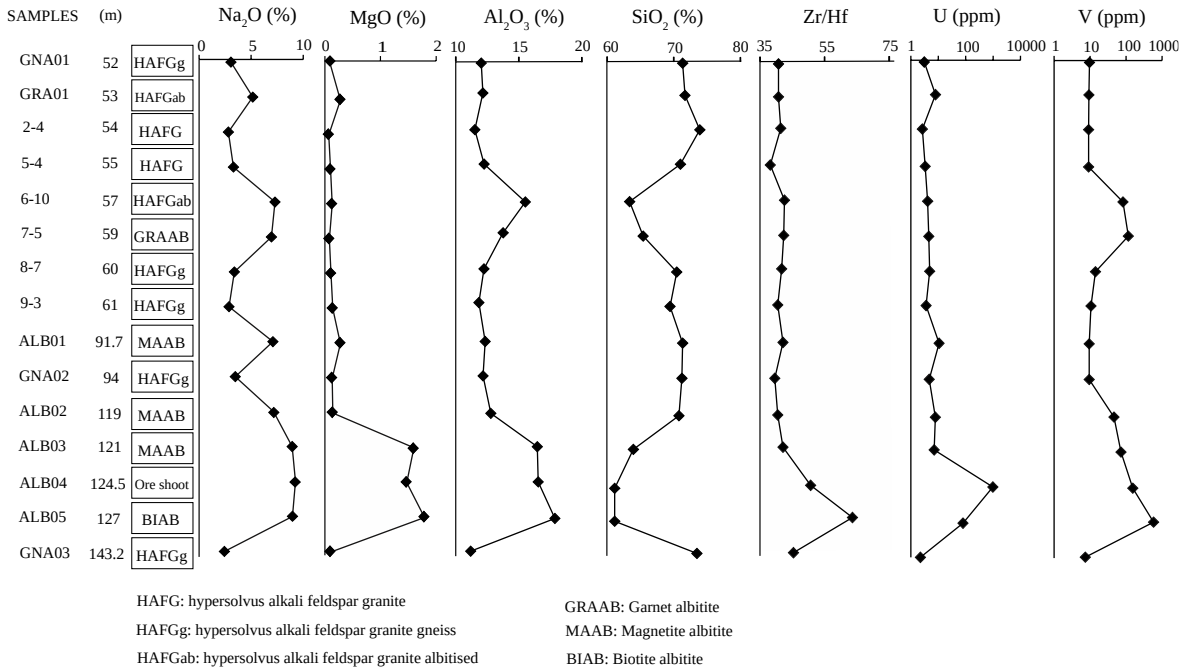

Fig. 11**.** Elemental contents vs. depth for a variety of rock types in DDH F10 (Fig. 2, Table 1).

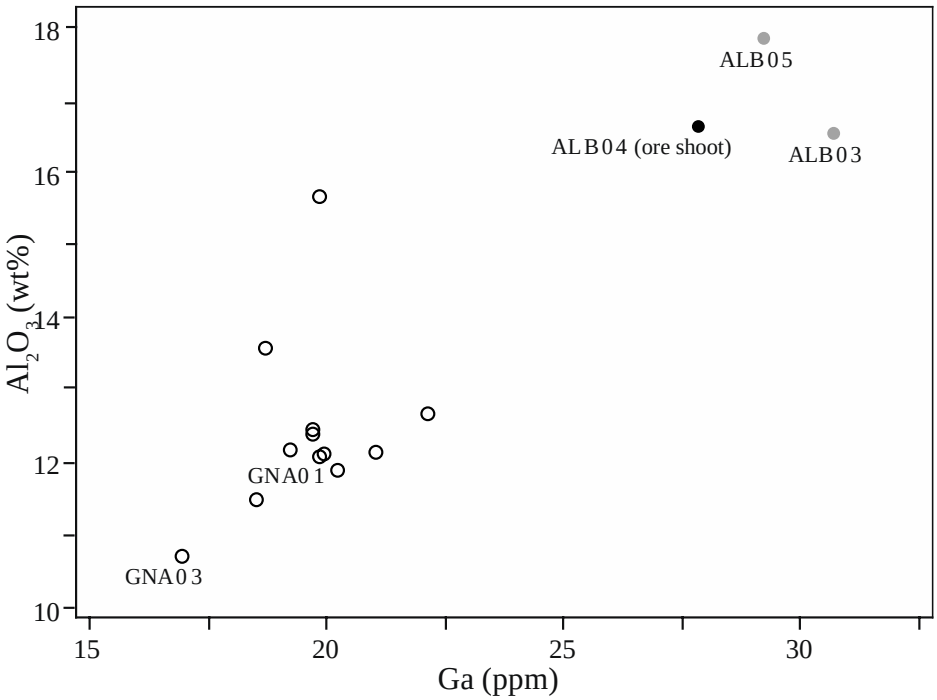

Fig. 12. Diagram of Al_2O_3 (wt%) vs. Ga (ppm) for rocks shown in Figure 2. Samples from the ore shoot and its immediately adjacent wall rock are indicated in black and grey, respectively, and labelled. White circles represent barren rock samples; the upper- and lowermost samples of the drill-core interval shown in Figure 5, respectively GNA01 and GNA03, are also labelled.

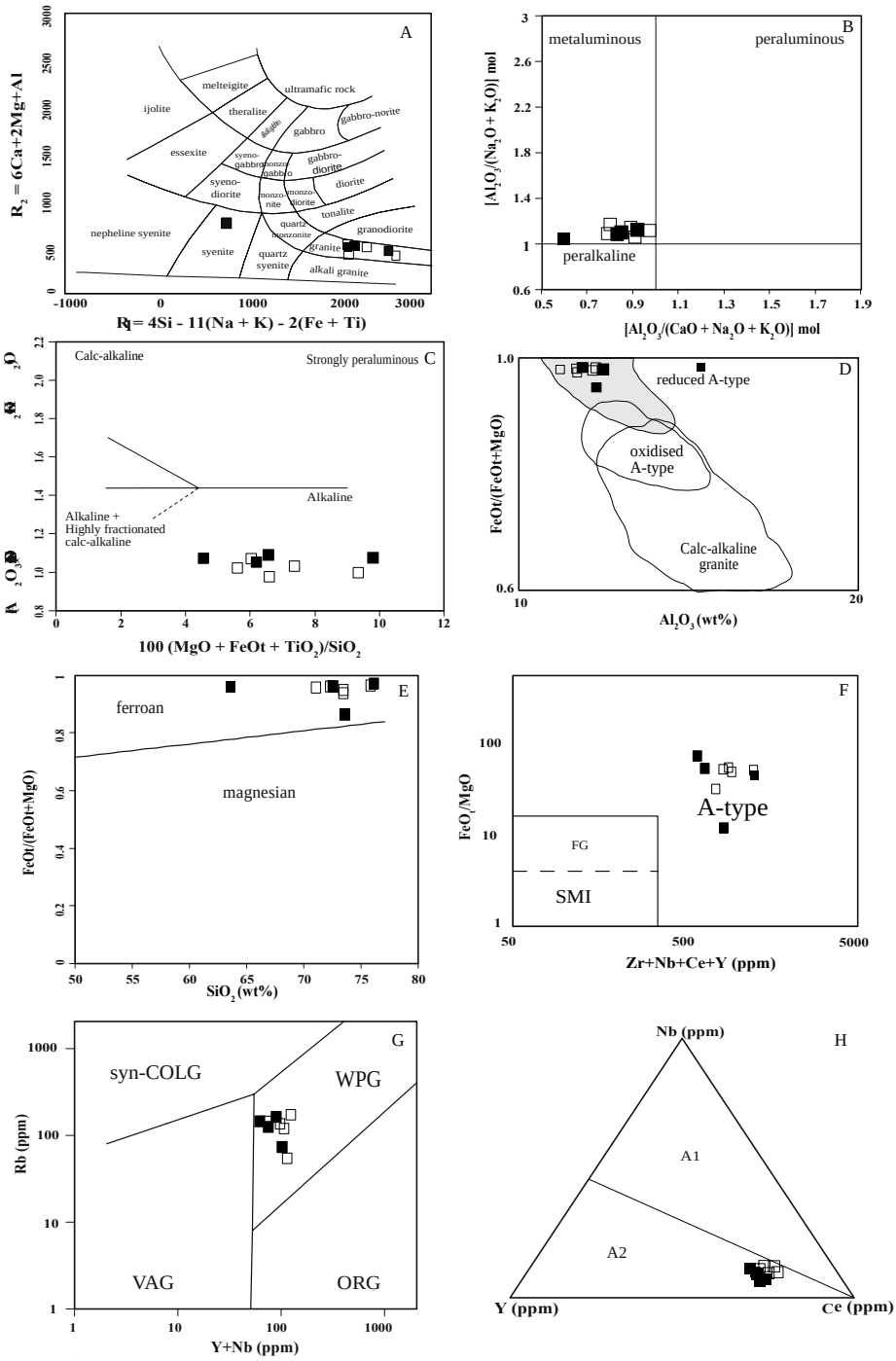

Fig. 13**.** Discriminating geochemical and geotectonic diagrams for granitic-gneissic rocks of the São Timóteo granite. A) Multicationic diagram from De La Roche et al. (1980). B) Shand's index (Shand, 1950). C) Diagram of 100∗(MgO + FeOt + TiO_2)/SiO_2 vs. (Al_2O_3 + CaO)/ (FeOt + Na_2O + K_2O) for granitic rocks (Sylvester, 1989). D) Distinction between oxidised and reduced granitic rocks (Dall'Agnol and Oliveira, 2007). E) Diagram of SiO_2 vs. total FeO/ (total FeO + MgO) from Frost et al. (2001). F) Diagram for discrimination of A-type granite (Whalen et al., 1987); FG = fractionated granite (S, I); SMI = not-fractionated granite (S, M and I). G) Diagram of Y + Nb vs. Rb (Pearce et al., 1984). H) Ternary diagram

of Y vs. Nb vs. Ce (Eby, 1992); A1 = represents mantle source granite and A2 = represents crustal or mantle-derived granite with crustal contamination. Black squares represent undeformed hypersolvus alkali-feldspar granite (HAFG) samples and empty black square are HAFG gneiss.

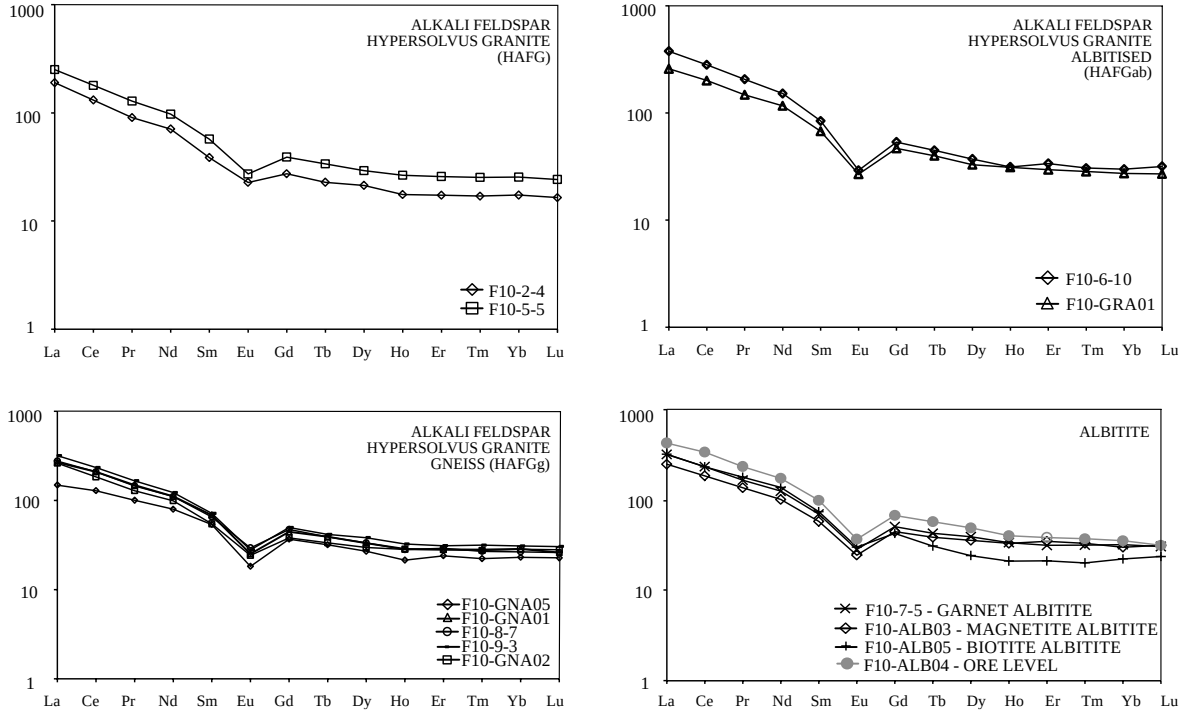

Fig. 14. Chondrite-normalised REE patterns for rocks sampled from DDH F10 (Fig. 2). Chondrite values used for normalisation are from Boyton (1984).

3.5 DISCUSSION

Despite uncertainties regarding the origin of albitite rocks in Lagoa Real, most of the data published so far give support to the idea that they are the metasomatic product of the country rock – i.e., the São Timóteo granite. Lines of evidence for the metasomatic origin include the concordant and gradational contacts of albitite bodies, as well as oligoclasite and microclinite, with the regional foliation of the country rock (Brito et al., 1984; Raposo et al., 1984; Cruz, 2004), and the occurrence of transitional rocks with less albite (<60 vol.%) and more quartz (>5 vol.%) than the albitite *strictu sensu* (Lobato et al., 1983; Lobato and Fyfe, 1990). Cruz (2004), based on microstructural criteria, argues that albitisation started prior to tectonic overprint, whereas isolated bodies of albitite formed during the Neoproterozoic Brasiliano orogeny through syntectonic recrystallisation of partially albitised K-feldspar to albite. Geochemical mass balance carried out by Lobato and Fyfe (1990) shows albitite rocks

as originated from the depletion of SiO_2, K_2O, Rb and Ba, with estimated volume loss of ~10%, and enrichment in Na_2O, Fe_2O_3, Sr, Pb, V and U in relation to granitic-gneissic rocks. Geochronological data for albitite zircon points to crystallisation age of ~1.7 Ga (Turpin, 1988; Cordani et al., 1992; Lobato et al., 2015), which cannot be distinguished from that of the São Timóteo granite, indicating it could be the protholith of albitite rocks.

On the other hand, Chaves (2013) presents petrographical arguments in favour of a magmatic origin for the albitite rocks: antiperthite in albitite rocks, quartz absence in U-bearing albitite and lack of quartz-dissolution features. Chaves (2013) also describes Na-rich melt inclusions in albitite and reports ages for albitite-hosted zircon of ~1.8 Ga, arguing that the albitite genesis is unrelated to the São Timóteo granite, but linked to an Orosirian sodic magmatism.

Discussion about geochronological data is beyond the scope of this paper. However, some of our observations are similar to those described by Lobato and Fyfe (1990) and Cruz (2004). Contacts between granitic-gneissic rocks and albitite are gradational, and plagioclase contents are relatively high in some granitic-gneissic rocks (albitised gneiss, Fig. 9D), where K-feldspar exhibits microfabrics of albite replacement (Fig. 9C).

Geochemical modelling by Chaves (2013), involving the São Timóteo granite and albitite rocks, considers Zr as immobile to build Pearce diagrams, which show two distinct linear trends: one is albitite vs. amphibolite, the other is albitite vs. the granitic-gneissic rocks of São Timóteo. The latter is taken by Chaves (2013) as evidence against alkali-metal mobilisation, while the former is considered to depict albitite and amphibolite as comagmatic in origin.

Zirconium should remain tightly coupled to Hf in geological processes, a *CHarge-and-RAdius-Controlled* (CHARAC) geochemical behaviour, which is characterised by Zr/Hf values between 26 and 46 (Bau, 1996). Non-CHARAC behaviour is typically found in aqueous solutions (Bau, 1996), where Zr and Hf decouple from each other. The ore-shoot sample, F10-ALB04, has 0.13 wt% U and its Zr/Hf ratio is 49, and sample F10-ALB05 has 85 ppm U and its Zr/Hf ratio is 64. Both samples show non-CHARAC behaviour (Fig. 15), suggesting fractionation of Zr from Hf due to hydrothermal fluid overprint. All other samples have essentially constant Zr/Hf ratios (Fig. 11), within the CHARAC range (Fig. 15). The lack of Hf data in previous works hinders further application of Zr/Hf ratios to Lagoa Real. As for quartz dissolution, it would have led to a relative increase in Al_2O_3, and relative decrease in SiO_2, contents in the uraniferous ore shoot and its vicinities, where the highest Ga contents are found (Fig. 12). Gallium correlations with increasing Al_2O_3 contents point

to residual concentrations due to silica leaching (Hieronymus et al., 2001). Therefore, Al and Ga remained immobile during the evolution of Lagoa Real rocks. Applying the same Pearce diagrams used by Chaves (2013), but replacing Zr by Al and Ga (Fig. 16), two distributions become apparent: (i) SiO_2 and K_2O contents decrease, but Na_2O contents increase, in granitic-gneissic rocks; (ii) albitite rocks show roughly constant Na_2O/Al_2O_3 and Na_2O/Ga ratios, in a plateu-like fashion (Fig. 16), due to SiO_2 leaching from, and relative Al_2O_3 and SiO_2 enrichment, in granitic-gneissic rocks. Moreover, note that two samples which correspond to albitised granite have intermediary behaviour in diagrams and rocks do not show distinct trends as reported by Chaves (2013).

Silica depletion is also indicated in the geochemical profile, along which SiO_2 contents abruptly decrease in the wall-rock albitite, immediately adjacent to the ore shoot (Fig. 11). The absence of petrographical evidence of quartz dissolution in albitite rocks can be attributed to quartz dissolution with concomitant albite precipitation.

Another problem with the Pearce-diagram approach carried out by Chaves (2013) is the interpretation of amphibolite as a mafic rock that is genetically associated with albitite rocks, without any petrographical and geochemical arguments. Even if assuming it as correct, there are at least four possibilities to consider in respect of the geological evolution of the Paramirim aulacogen, which experienced multiple intracratonic rift cycles (Cruz and Alckmin, 2017; and references therein), recorded as mafic magmatism at ca. 1.5 Ga, ca. 1.4 Ga, ca. 1.3 Ga and between 930 and 850 Ma (Babinski et al., 1999; Guimarães et al., 2008; Loureiro et al., 2009; Danderfer et al., 2009; Silveira et al., 2013; dos Santos et al., 2020). Without age constraints and geochemical data, the amphibolite in question could be related to any of those aforementioned ages.

Taking both hypotheses into consideration, metasomatic vs. magmatic, the similarity of REE patterns for the granitic rocks and those for the albitite rocks can be interpreted in two scenarios. Scenario 1 presupposes that the albitite rocks originated from the São Timóteo granite by sodic metasomatism (Lobato and Fyfe, 1990; Maruejol, 1988). In this scenario, the similarity of REE patterns indicates that the sodic metasomatism and later alterations did not significantly mobilise the REE, or that the REE were inherited from the São Timóteo granite. Scenario 2 requires a magmatic origin for the albitite rocks – i.e., Na-rich syenitic magmatism (Chaves, 2013). The magmatic scenario implies that both granitic and Na-rich syenitic magmas have equivalent REE patterns. If realistic, the alkaline character of Na-rich syenitic magmatism should be reflected in Nb/Y ratios above unity (Winchester and Floyd, 1977). The Nb/Y ratio, an indicator of alkalinity, is nearly constant, between 0.5 and 0.7, in

all samples analysed (Table 1). Therefore, scenario 2 is deemed unlikely, while scenario 1 is favoured. The albitite rocks have chondrite-normalised REE patterns that are similar to their protolith, the São Timóteo granite.

Our data, therefore, support the concept that the albitite rocks are the product of hydrothermal alteration of the granitic country rocks, known as the Lagoa Real intrusive suite or the São Timóteo granite, as previously proposed (e.g., Maruejol., 1988, Lobato and Fyfe, 1990; Cruz, 2004).

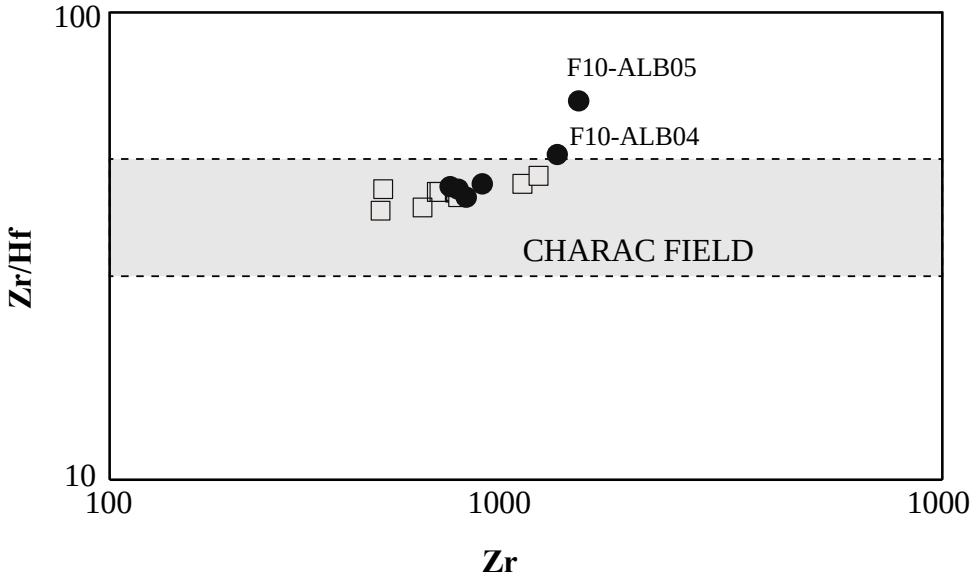

Fig. 15**.** Diagram of Zr/Hf vs. Hf. showing the CHARAC field (Bau, 1996). Squares are granitic-gneissic samples and black circles are albitite rocks. Fractionation of Zr from Hf is noticeable in the ore-shoot sample (F10-ALB04), but it is strongest in the immediately adjacent wall rock (F10-ALB05). Squares are granitic-gneissic samples and black circles are albitite rocks.

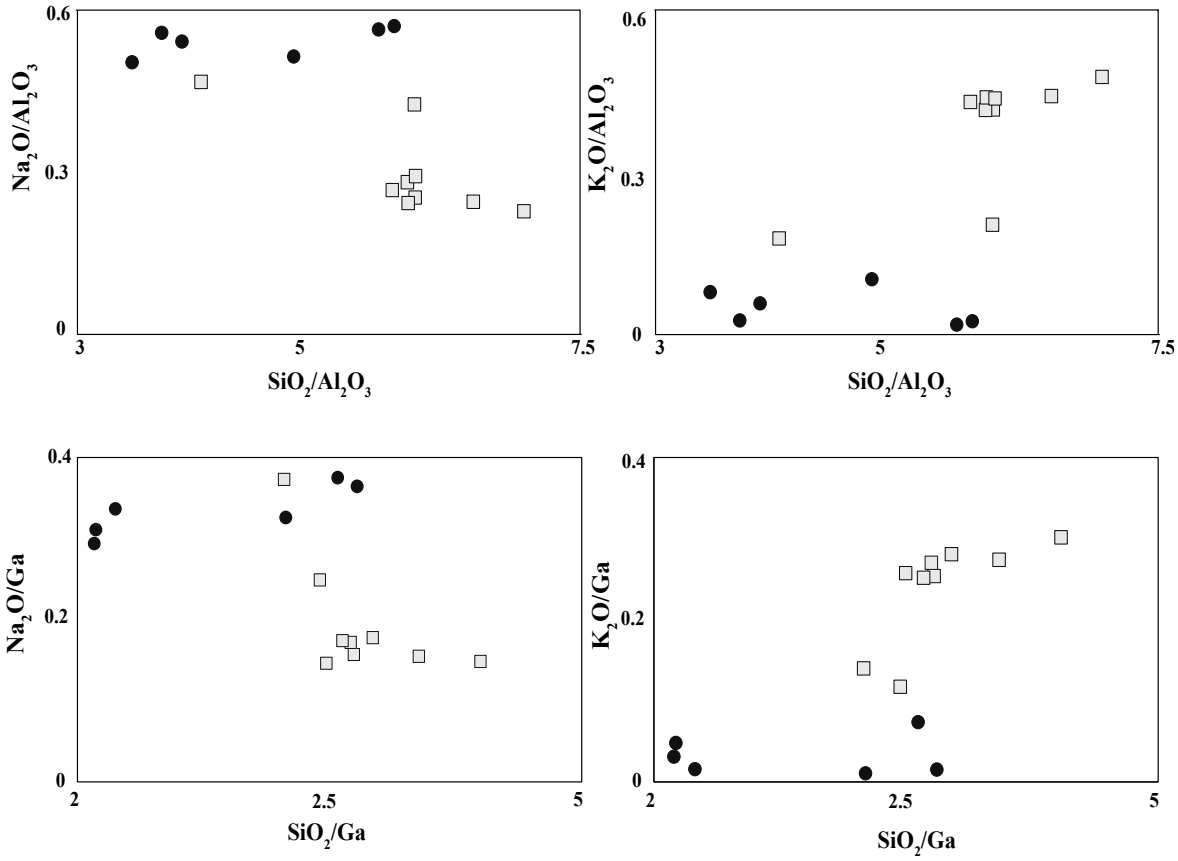

Fig. 16**.** Pearce diagrams of SiO_2, Na_2O and K_2O, against Al_2O_3 and Ga, which are typically immobile. Squares are granitic-gneissic samples and black circles are albitite rocks. The diagrams show trends of Na_2O enrichment and SiO_2 and K_2O loss from granitic-gneissic rocks of the São Timóteo to albitite rocks. Squares are granitic-gneissic samples and black circles are albitite rocks.

3.5.1 Mass balance

In order to check relative losses and gains in altered rocks, histograms were drawn for different rock types, normalised to the least altered granite sample, F10-5-5 (Fig. 17). For this discussion, only differences above 50% are considered and the minerals cited below refer to those also identified by Lobato and Fyfe (1990), Maruejol (1988) and Cruz (2004).

All samples gained Na and lost K in almost the same proportions, which is likely related to the replacement of K-feldspar (Fig. 9C) and biotite by albite. There is also a general loss of Ba and Rb, possibly following K, given that these elements have similar ionic radius. Calcium is remarkably enriched in garnet-bearing albitite, being attributed to calcic garnet and clinopyroxene – i.e., andradite and hedenbergite, respectively. Calcium loss in biotite-bearing albitite is related to the replacement of calcic minerals by biotite. Silica loss is widespread, but minor (~10%; ~0.9 in Fig. 17).

Biotite-bearing albitite should depict a prominent K gain, represented by the replacement of pre-existing amphibole and clinopyroxene by biotite (Fig. 10C). In the histogram of Figure 11, however, the expected enrichment is not observed because of normalisation against granite, a K-rich rock. Excepting F10-7-5 sample which has high K_2O (1.3%) by its high K-feldspar contents, other types of albitite contain ~0.5 wt% K_2O, whereas the biotite-albitite sample has 1.4 wt% K_2O (Table 1). Other elements follow the relative K gain, such as U, Pb, V and Zr gain. High Zr contents find their mineralogical expression as zircon inclusions in biotite.

Magnesium gain is conspicuous in magnetite-bearing albitite, as anticipated by the presence of magnesian silicates – i.e., edenite, Mg-hedenbergite and Mg-biotite. In particular, the U-ore shoot has diopside and actinolite. Vanadium, U, Zr, Hf, Nb and Ta are enriched in almost all samples, but they are striking in the U-ore shoot and its spatially associated biotite-bearing albitite.

In general, our study has similarities with the work published by Lobato and Fyfe (1990), who show that albitite rocks are poor in SiO_2, K_2O, Rb and Ba, but rich in Na_2O, Fe_2O_3, Sr, Pb, V and U in relation to granitic-gneissic rocks. Those authors also indicate that U has positive correlation with V.

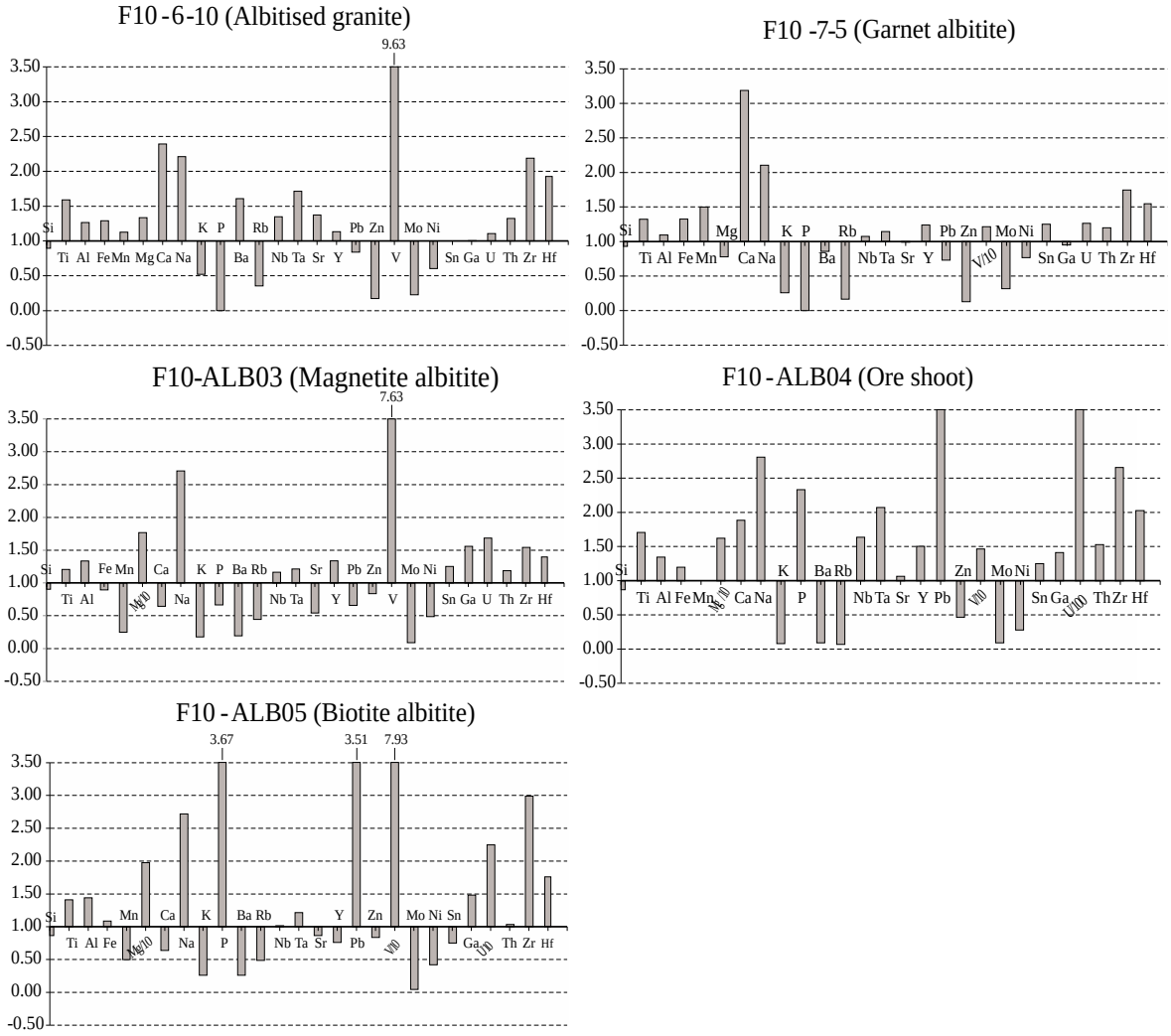

Fig. 17**.** Depletion and enrichment factors for rock types of the Gameleira I deposit. Ratio 1:1 is indicated in bold.

3.5.2 Ore geochemical fingerprint

Fig. 18A shows that albitite rocks, mainly the U-ore shoot and its neighbour sample (ALB05), are enriched in V. The V enrichment seems to be commom in U deposits. Vanadium is present in only small amounts in felsic rocks (~20 ppm), but in larger amounts in mafic igneous rocks (~250 ppm). Like U, V is a redox-sensitive element, occurring in nature in three oxidation states, +3, +4 and +5 (e.g., Taylor and Van Staden, 1994). This explains the usual correlation between U and V in U deposits, especially in the sandstone-hosted class, in which case the V enrichment is generally attributed to the dissolution of Fe–Ti oxides, such as ilmenite and magnetite, from which V is released and transported by brines. During its long history of 1.3 Ga, the Paramirim aulacogen had periods of sedimentary deposition and intrusion of mafic sills and dykes in response to rifting events.

The higher Nb (48 ppm) and Ta (2.9) contents of the ore shoot, also points out to the influence of a mafic source. Therefore, vanadium could have been sourced from those mafic intrusions, but a precise connection cannot currently be indicated.

In addition to V, our study also shows that U is coupled with Zr fractionation from Hf in aqueous fluids (Fig. 15), as indicated by the presence of fine-grained hydrothermal zircon in the vicinity of U minerals (Fig. 10G). On the other hand, the REE pattern for the U-ore shoot suggests that these elements were not fractionated during hydrothermal alteration (Fig. 8).

Vanadium enrichment and Zr mobility are a common geochemical characteristic of all documented albitite-hosted U deposits worldwide – e.g., Valhalla, Australia (Polito, 2009); Skal deposit, Mount Isa region, Australia (Wilde et al., 2013); Aricheng South occurrence, Guyana (Alexandre, 2010); Kirovograd and Novoukrainka deposits, central Ukraine (Cuney et al., 2012). Albitite-hosted U deposits show also depletions in Si, K, Ba and Rb relative to the host rocks, and enrichments in Na, Ca, U, Zr, P, V, Y and Sr. Interestingly, REE immobility during hydrothermal processes has been reported for Ukrainian U deposits (Cuney, 2012). The Gameleira I deposit has ore-mineral assemblages that are analogous to those described from other albitite-hosted U deposits (Wilde, 2013): fine-grained uraninite (<50 μm), presence of hydrothermal zircon and a Ti-rich mineral, which is titanite at Gameleira I. It is important to note that Lobato and Fyfe (1990) showed that uranium mineralization is mostly associated to andradite and hedenbertite paragenesis in Lagoa Real, however it is not the case in Gameleira I deposit. Aforementioned characteristics show that Gameleira I deposit is similar to albitite-hosted U deposits worldwide.

3.5.3 Presumable U source and deposition mechanism

In Lagoa Real, granitic-gneissic rocks have U contents, between 2.3 and 8.5 ppm, that are marginally higher than the crustal average (2.7 ppm; Cuney, 2014), as already noted by Lobato and Fyfe (1990). Their Th/U ratios vary from 1.9 to 6.1, beyond the crustal average of 3.9 (Cuney, 2014; Fig 12B). As pointed out by Cuney (2014), metaluminous high-K granitic rocks can be an effective U source if U is hosted in uraninite, or if the main U-bearing silicate mineral became metamict after hydrothermal fluid overprint. As uraninite has not been described in the São Timóteo granite, the latter hypothesis is further considered. In brief, there is evidence for increasing U loss from titanite from the country rock to albitised rocks (Santos, 2018). Uranium could, at least partially, have been sourced from

accessory minerals, i.e. zircon, in the São Timóteo granite. However, as well as for V, a mafic source should not be discarded.

Mechanisms of U deposition were evaluated by Lobato and Fyfe (1990), who proposed U precipitation in response to fluid reduction by magnetite oxidation. We have observed a spatial association between uraninite and martitic hematite at the DDH-F10 drill hole. Such an association makes their precipitation mechanism aplicable to our case. Albitisation, quartz dissolution and Zr transport suggest alkaline fluid conditions (Aja et al., 1995; Pouchon et al., 2001), which favour U solubility as hydroxyl complexes (Romberger, 1984). Oxygen-isotope results in silicatic assemblage from São Timóteo gneisses and albitite rocks suggest a trend towards lighter isotopic values, which are compatible with meteoric or basinal fluids that reached ~500 ºC (Lobato and Fyfe, 1990).

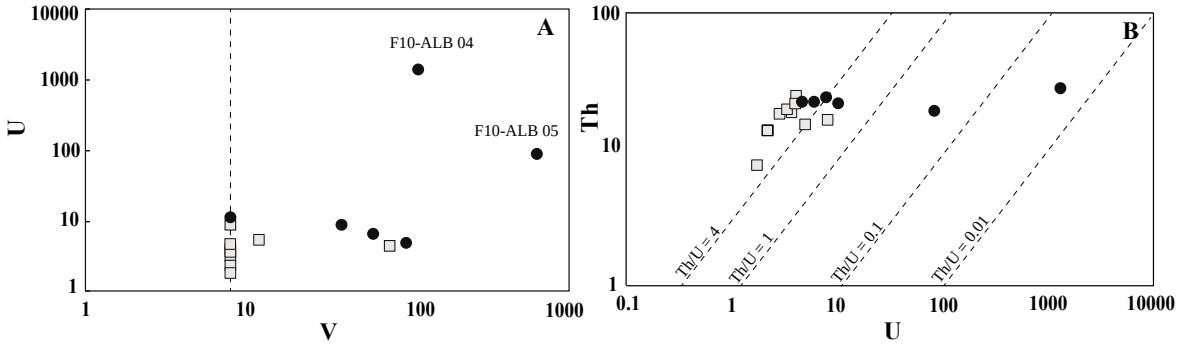

Fig. 18**.** A) Diagram of U vs. V; dashed line corresponds to the minimum detection limit of V (8 ppm). B) Diagram of Th vs. U. Thorium is not correlated with U enrichment. Granitic-gneissic rocks of the São Timóteo granite have Th/U ratios mostly above the crustal average (Th/U = 4). Squares are granitic-gneissic samples and black circles are albitite rocks.

3.6 CONCLUSIONS

This work is the first to present a whole-rock chemical profile of an exploratory drill hole in the Lagoa Real U province of Brazil. Samples were systematically collected from the granitic country rock to the uraniferous ore shoot. Concentrations of major and trace elements, including the REE, were determined. The data indicate that albitite rocks, one type of which, the magnetite-bearing albitite, typically hosts the uraniferous mineralisation of Lagoa Real. Geochemical and petrographical data show that albitite rocks cannot be explained by Na-rich syenitic magmatism. The albitite rocks have chondrite-normalised patterns and Nb/Y ratios that point to derivation from the granitic country rock by sodic metasomatism, in agreement with earlier works. Geochemical gains and losses, as well as ore-mineral assemblages, are similar to albitite-hosted U deposits worldwide.

Table 1: Whole-rock geochemical analyses of samples from diamond-drill-hole (DDH) F10, Gameleira I uranium deposit

SAMPLE	ROCK	SiO2 (%)	TiO2	Al2O3	Fe2O3	Mn	MgO	CaO	Na2O	K2O	P2O5	LOI	U (ppm)	Th	Th/U	Pb	Zr	Hf	Zr/Hf
HAFGg	F10-GNA01	72.63	0.36	12.07	4.20	0.11	0.09	1.39	3.05	5.01	0.03	0.60	3.0	18.3	6.1	17.2	618.6	15.0	41.2
HAFGab	F10-GRA01	72.82	0.39	12.12	4.32	0.08	0.27	1.35	5.15	2.45	0.04	0.60	8.5	16.3	1.9	7.4	631.2	15.4	41.0
HAFG	F10-2-4	75.01	0.26	11.48	3.57	0.08	0.06	1.11	2.81	5.05	0.03	0.30	2.3	13.9	6.0	14.5	459.8	11.0	41.8
HAFG	F10-5-4	71.94	0.34	12.38	4.27	0.08	0.09	1.38	3.30	5.31	0.03	0.60	3.8	18.6	4.9	15.5	456.1	12.1	37.7
HAFGab	F10-6-10	64.31	0.54	15.66	5.51	0.09	0.12	3.30	7.30	2.76	0.00	0.00	4.2	24.6	5.9	13.0	998.2	23.3	42.8
GRAAB	F10-7-5	66.82	0.45	13.55	5.66	0.12	0.07	4.40	6.95	1.37	0.00	0.30	4.8	22.3	4.6	11.3	795.7	18.7	42.6
HAFGg	F10-8-7	71.73	0.46	12.06	4.82	0.09	0.10	1.61	3.39	5.00	0.05	0.40	5.2	15.4	3.0	14.4	690.9	16.7	41.4
HAFGg	F10-9-3	70.68	0.53	11.87	5.79	0.10	0.13	1.72	2.88	5.19	0.07	0.70	3.5	19.7	5.6	8.6	696.5	17.3	40.3
MAAB	F10-ALB01	72.59	0.41	12.45	5.14	0.04	0.27	0.80	7.09	0.29	0.04	0.60	10.6	21.6	2.0	3.0	669.9	15.9	42.1
HAFGg	F10-GNA02	72.73	0.36	12.16	3.92	0.07	0.12	0.79	3.48	5.30	0.04	0.60	4.2	21.0	5.0	18.0	564.3	14.5	38.9
MAAB	F10-ALB02	72.07	0.43	12.67	5.27	0.05	0.13	0.79	7.14	0.22	0.04	0.90	8.3	23.8	2.9	3.1	732.2	18.2	40.2
MAAB	F10-ALB03	65.06	0.41	16.53	3.82	0.02	1.59	0.89	8.94	0.94	0.02	1.50	6.4	22.1	3.5	10.2	702.5	16.9	41.6
Ore shoot	F10-ALB04	62.42	0.58	16.63	5.11	0.08	1.46	2.60	9.26	0.42	0.07	0.90	1341.3	28.4	0.0	134.5	1211.5	24.5	49.4
BIAB	F10-ALB05	62.25	0.48	17.84	4.63	0.04	1.78	0.88	8.97	1.38	0.11	1.10	85.4	19.2	0.2	54.4	1364.2	21.3	64.0
HAFGg	F10-GNA03	74.76	0.43	10.70	4.61	0.10	0.09	0.76	2.43	5.08	0.03	0.60	1.8	7.6	4.2	6.6	1084.4	24.3	44.6

SAMPLE	ROCK	La	Ce	Pr	Nd	Sm	Eu	Gd	Tb	Dy	Ho	Er	Tm	Yb	Lu	Eu/Eu*	LREE	HREE	La/Yb	Ba	Rb
HAFGg	F10-GNA01	82.9	170.0	18.15	66.8	13.39	1.85	11.52	1.86	10.68	2.05	5.93	0.91	5.99	0.84	0.46	353.1	39.78	9.33	812	150.1
HAFGab	F10-GRA01	80.1	162.1	18.02	69.8	13.16	1.97	12.09	1.89	10.60	2.23	6.20	0.92	5.69	0.87	0.48	345.2	40.49	9.49	412	76.9
HAFG	F10-2-4	59	106.2	11.03	42.5	7.53	1.67	7.08	1.08	6.87	1.26	3.64	0.55	3.63	0.53	0.70	227.9	24.64	10.96	798	146.6
HAFG	F10-5-4	77.9	145.1	15.70	58.4	11.16	2.00	10.11	1.60	9.40	1.90	5.42	0.82	5.32	0.78	0.58	310.3	35.35	9.87	840	163.1
HAFGab	F10-6-10	117.0	227.4	25.15	91.0	16.41	2.14	13.84	2.12	11.97	2.25	7.09	0.99	6.24	1.02	0.43	479.1	45.52	12.64	1350	57.8
GRAAB	F10-7-5	98.2	187.7	20.11	74.7	13.55	2.08	13.05	2.02	12.58	2.41	6.58	1.02	6.68	0.98	0.48	396.3	45.32	9.91	719	27.0
HAFGg	F10-8-7	85.9	169.3	17.78	66.4	12.72	2.16	12.26	1.85	10.77	2.02	6.10	0.87	5.55	0.84	0.53	354.3	40.26	10.43	934	122.0
HAFGg	F10-9-3	98.6	189.1	20.24	73.6	13.97	2.05	12.86	1.97	12.30	2.33	6.51	1.02	6.44	0.98	0.47	397.6	44.41	10.32	895	172.7
MAAB	F10-ALB01	106.4	216.9	23.73	88.3	16.04	2.23	13.73	2.12	11.85	2.27	6.44	0.88	5.84	0.87	0.46	453.6	44.00	12.28	49	12.5
MAAB	F10-GNA02	81.3	148.7	15.70	59.6	10.64	1.78	9.85	1.59	9.54	2.03	5.88	0.89	5.92	0.90	0.53	317.7	36.60	9.26	1119	137.1
MAAB	F10-ALB02	99.2	193.3	21.41	79.8	15.57	1.98	13.71	2.22	12.55	2.52	7.48	1.07	6.97	1.07	0.41	411.3	47.59	9.60	42	3.9
MAAB	F10-ALB03	76.6	148.5	16.56	60.5	11.25	1.80	11.50	1.83	11.48	2.37	7.30	1.07	6.24	1.01	0.48	315.2	42.80	8.28	164	72.6
Ore shoot	F10-ALB04	131.6	271.4	28.41	103.6	19.23	2.70	17.39	2.71	15.76	2.88	8.04	1.20	7.36	1.01	0.45	556.9	56.35	12.05	76	11.2
BIAB	F10-ALB05	98.8	186.8	21.65	82.1	14.40	2.20	11.01	1.46	7.78	1.51	4.44	0.65	4.64	0.76	0.53	406.0	32.25	14.36	219	79.6
HAFGg	F10-GNA03	46.2	103.9	12.24	47.8	10.49	1.34	9.55	1.51	8.66	1.54	5.02	0.72	4.81	0.73	0.41	222.0	32.54	6.48	443	118.3

SAMPLE	ROCK	Zn	Nb	Ta	Sr	Y	Zn	V	Mo	Ni	Sn	Ga	Cs	As	Au	Bi	Cd	Cu	Se	Tl	Nb/Y
HAFGg	F10-GNA01	89	34.3	1.4	115.5	54.0	89	<8	3.4	6.4	3	19.8	1.9	1.2	8.9	<0.1	<0.1	13.1	0.7	0.5	0.64
HAFGab	F10-GRA01	46	34.1	1.6	77.4	57.5	46	<8	1.7	5.0	4	21.0	0.8	0.7	20.0	<0.1	<0.1	6.7	<0.5	0.2	0.59
HAFG	F10-2-4	71	23.0	1.2	102.4	34.4	71	<8	2.2	4.3	2	18.5	1.7	<0.5	8.1	<0.1	<0.1	11.5	<0.5	0.3	0.67
HAFG	F10-5-4	86	29.6	1.4	112.8	52.9	86	<8	2.2	4.3	4	19.7	2.1	<0.5	4.4	<0.1	0.1	18.8	<0.5	0.4	0.56
HAFGab	F10-6-10	15	39.9	2.4	154.7	59.9	15	77	0.5	2.6	4	19.8	0.1	<0.5	2.8	<0.1	<0.1	8.2	<0.5	<0.1	0.67
GRAAB	F10-7-5	11	31.8	1.6	111.7	65.5	11	97	0.7	3.3	5	18.7	<0.1	<0.5	13.6	<0.1	0.3	23.3	1.1	<0.1	0.49
HAFGg	F10-8-7	56	39.2	1.9	120.1	55.3	56	12	4.1	3.8	4	19.9	0.6	<0.5	3.6	<0.1	<0.1	22.7	<0.5	0.1	0.71
HAFGg	F10-9-3	106	40.2	2.0	120.1	65.9	106	<8	3.7	3.9	4	20.2	2.7	<0.5	7.8	<0.1	<0.1	23.8	<0.5	0.6	0.61
MAAB	F10-ALB01	19	33.3	1.8	39.8	59.8	19	<8	0.6	3.1	4	19.7	<0.1	<0.5	16.0	<0.1	<0.1	3.9	<0.5	<0.1	0.56
MAAB	F10-GNA02	22	34.7	1.8	132.4	53.8	22	<8	5.4	4.5	4	19.2	0.4	1.7	8.1	0.3	<0.1	23.1	0.7	0.2	0.64
MAAB	F10-ALB02	30	39.3	2.3	81.5	64.2	30	39	0.8	4.1	5	22.1	<0.1	0.5	5.4	<0.1	<0.1	4.4	<0.5	<0.1	0.61
MAAB	F10-ALB03	72	34.4	1.7	61.3	70.7	72	61	0.2	2.1	5	30.7	1.4	<0.5	9.4	<0.1	<0.1	3.7	<0.5	0.4	0.49
Ore shoot	F10-ALB04	40	48.4	2.9	120.0	79.5	40	117	0.2	1.2	5	27.8	<0.1	<0.5	4.2	<0.1	<0.1	3.1	1.0	<0.1	0.61
BIAB	F10-ALB05	72	30.1	1.7	97.5	40.2	72	634	0.1	1.8	3	29.2	1.6	0.9	7.6	<0.1	0.1	6.0	<0.5	0.3	0.75
HAFGg	F10-GNA03	76	29.9	1.2	62.7	43.7	76	<8	2.6	6.3	1	16.9	0.6	0.6	19.2	<0.1	<0.1	8.9	<0.5	0.2	0.68

HAFG: hypersolvus alkali feldspar granite; HAFG: hypersolvus alkali feldspar granite gneissified; HAFGab: hypersolvus alkali feldspar granite albitised: GRAAB: garnet albitite; MAAB: magnetite albitite; BIAB: biotite albitite

3.7 REFERENCES

Almeida, F.F.M., 1977. O Cráton do São Francisco. Revista Brasileira de Geociências 7, 349–364.

Aja, S.U., Wood, S.A., Williams-Jones, A.E., 1995. The aqueous geochemistry of Zr and the solubility of some Zr-bearing minerals. Applied Geochemistry 10, 603–620.

Alexandre, P. 2010. Mineralogy and geochemistry of the sodium metasomatism-related uranium occurrence of Aricheng South, Guyana. *Mineralium Deposita*, *45*(4), 351-367.

Alkmim, F.F., Marshak, S., Pedrosa-Soares, A.C., Peres, G.G., Cruz, S.C.P., Whittington, A., Carlos Pedrosa-Soares, A., Gravina Peres, G., Cruz, S.C.P., Whittington, A., 2006. Kinematic evolution of the Araçuaí–West Congo orogen in Brazil and Africa: Nutcracker tectonics during the Neoproterozoic assembly of Gondwana. Precambrian Research 149, 43–64. https://doi.org/10.1016/j.precamres.2006.06.007

Amorim, L.E.D. O Granito São Timóteo No Perfil Monsenhor Bastos, Província Uranífera De Lagoa Real. 146p. Dissertação (Mestrado em Ciência e Tecnologia das Radiações, Minerais e Materiais) – Centro Desenvolvimento da Tecnologia Nuclear, Belo Horizonte, 2012.

Arcanjo, J., Marques-Martins, A., Loureiro, H.S., Varela, P.H., 2005. Projeto Vale do Paramirim, Bahia: geologia e recursos minerais. Companhia Baiana de Pesquisa Mineral-CBPM, Salvador.

Babinski, M., Van Schmus, W.R., Chemale Jr., F., Brito Neves, B.B., Rocha, A.J.D. 1993. Idade isocrônica Pb/Pb em rochas carbonáticas da Formação Caboclo em Morro do Chapéu. In: Pedreira, A.J., Misi, A., Dominguez, J.M.L. (eds.), II Simpósio sobreo Craton do São Francisco. Brazilian Geological Society, Salvador, p. 160–16

Barbosa, N.D.S., Teixeira, W., Leal, L.R.B., Leal, A.B. de M., 2013. Evolução crustal do setor ocidental do Bloco Arqueano Gavião, Cráton do São Francisco, com base em evidências U–Pb, Sm–Nd e Rb–Sr. Geologia USP,.Série Científica 13, 63–88. https://doi.org/10.5327/Z1519-874X201300040004

Bau, M., 1996. Controls on the fractionation of isovalent trace elements in magmatic and aqueous systems: evidence from Y/Ho, Zr/Hf, and lanthanide tetrad effect.

Contributions to Mineralogy and Petrology 123, 323–333. https://doi.org/10.1007/s004100050159

Bitencourt, C.N., Cruz, S.C.P., dos Anjos Cruz, V., Pedrosa-Soares, A.C., Paquette, J.L., Alkmim, A.R., Barbosa, J.S.F., 2019. Rifting events in the southern sector of the Paramirim Aulacogen, NE Brazil: New geochronological data and correlations for the São Francisco – Congo paleocontinent. Precambrian Res. 326, 417–446. https://doi.org/10.1016/j.precamres.2018.12.005

Brito, W., Raposo, C., Matos, E.C. De, 1984. Os albititos uraníferos de Lagoa Real, in: Anais Do XXXIII Congresso Brasileiro de Geologia, Rio de Janeiro, 1984.

Bruneton, P., Cuney, M. Geology of uranium deposits. In: Uranium for Nuclear Power. Woodhead Publishing, 2016. p. 11-52.

Boyton W.V., 1984. Geochemistry of the rare earth elements: meteorite studies, in: Rare Earth Element Geochemistry. Elsevier, pp. 63–114.

Chaves, A. de O., 2013. New geological model of the Lagoa Real uraniferous albitites from Bahia (Brazil). Central European Journal of Geosciences 5, 354–373. https://doi.org/10.2478/s13533-012-0134-7

Cordani, U.G., Iyer, S.S., Taylor, P.N., Kawashita, K., Sato, K., McReath, I., 1992. Pb–Pb, Rb–Sr, and K–Ar systematics of the Lagoa real uranium province (south-central Bahia, Brazil) and the Espinhaço Cycle (ca. 1.5–1.0 Ga). Journal of South American Earth Sciences 5, 33–36.

Costa, P.H.O., Andrade, A.R.F., Lopes, G.A., Souza, S.L., 1985. Projeto Lagoa Real: mapeamento geológico 1:25000, textos e mapas. Companhia Baiana de Pesquisa Mineral-CBPM/ Empresas Nucleares Brasileiras (NUCLEBRAS), Salvador.

Cruz, S.C.P., 2004. A interação tectônica entre o Aulacógeno do Paramirim e o Orógeno Araçuaí-Oeste Congo. Tese de Doutorado, Departamento de Geologia, Universidade Federal de Ouro Preto, Ouro Preto. https://doi.org/85-230-0108-6

Cruz, S.C.P., Alkmim, F.F., 2006. The tectonic interaction between the Paramirim aulacogen and the Araçuaí belt, São Francisco craton region, Eastern Brazil. Anais da Academia Brasileira de Ciências 78, 151–173. https://doi.org//S0001-37652006000100014

Cruz, S.C.P., Alkmim, F.F., 2007. A história de inversão do aulacógeno do Paramirim contada pela sinclinal de Ituaçu, extremo sul da Chapada Diamantina (BA). Revista Brasileira de Geociências 37, 92–110.

Cruz, S. C. P., Alkmim, F. F. D., Leite, C. M. M., Evangelista, H. J., Cunha, J. C., Matos, E. C., Noce, C. M., Marinho, M. M. (2007). Geologia e arcabouço estrutural do Complexo Lagoa Real, Vale do Paramirim, Centro-Oeste da Bahia. Revista Brasileira de geociências 37 (4, suplemento), 28–146.

Cruz, S.C.P., Alkmim, F.F., 2017. The Paramirim Aulacogen, in: Heilbron, M., Cordani, U.G., Alkmim, Fernando F. (Eds.), São Francisco Craton, Eastern Brazil: Tectonic Genealogy of a Miniature Continent, Regional Geology Reviews. Springer International Publishing, Cham, p. 326. https://doi.org/10.1007/978-3-319-01715-0

Cuney, M., 2009. The extreme diversity of uranium deposits. Mineralium Deposita, 44(1), 3.

Cuney, M., Emetz, A., Mercadier, J., Mykchaylov, V., Shunko, V., Yuslenko, A., 2012. Uranium deposits associated with Na-metasomatism from central Ukraine: A review of some of the major deposits and genetic constraints. Ore Geology Reviews 44, 82–106. https://doi.org/10.1016/j.oregeorev.2011.09.007

Cuney, M. 2014. Felsic magmatism and uranium deposits. Bulletin de la Société Géologique de France, 185(2), 75-92

Dall'Agnol, R., Oliveira, D.C., 2007. Oxidized, magnetite-series, rapakivi-type granites of Carajás, Brazil: implications for classification and petrogenesis of A-type granites. Lithos 93, 215–233.

Danderfer, A., de Waele, B., Pedreira, A.J., Nalini, H.A., 2009. New geochronological constraints on the geological evolution of Espinhaço basin within the São Francisco Craton-Brazil. Precambr. Res. 170, 116–128.

Danderfer Filho, A., Lana, C.C., Nalini Júnior, H.A., Costa, A.F.O., 2015. Constraints on the Statherian evolution of the intraplate rifting in a Paleo-Mesoproterozoic paleocontinent: New stratigraphic and geochronology record from the eastern São Francisco craton. Gondwana Res. 28, 668–688. https://doi.org/10.1016/j.gr.2014.06.012

De La Roche, H., Leterrier, J. T., Grandclaude, P., & Marchal, M. 1980. A classification of volcanic and plutonic rocks using R1-R2-diagram and major-element analyses—its relationships with current nomenclature. Chemical Geology, 29(1), 183-210.

Eby, G. N. 1992. Chemical subdivision of the A-type granitoids: petrogenetic and tectonic implications. Geology, 20(7), 641-644.

Frost, B.R., Barnes, C.G., Collins, W.J., Arculus, R.J., Ellis, D.J., Frost, C.D., 2001. An geochemical classification for granitic rocks. Journal of Petrology 42, 2033–2048.

Fuzikawa, K., Alves, J., Maruejol, P., Cuney, M., Kostonlayl, C., Poty, B., 1988. The Lagoa Real Uranium Province, Bahia state, Brazil: some petrographic aspects and fluid inclusion studies. Geochimica Brasiliensis 2, 109–118.

Geisel Sobrinho, E., Raposo, C., Alves, J. V, Brito, W.D., Vasconcelos, T.G., 1980. O distrito uranífero de Lagoa Real, Bahia, in: Congresso Brasileiro de Geologia, 31, Camboriú, Anais, pp. 1499–1512.

Guimarães, J.T., Santos, R.A., Melo, R.C., 2008. Geologia da Chapada Diamantina (Projeto Ibitiara-Rio de Contas). CBPM, Série Arqu. ed. Salvador, BA.

Hieronymus, B., Kotschoubey, B., Boulègue, J., 2001. Gallium behaviour in some contrasting lateritic profiles from Cameroon and Brazil. Journal of Geochemical Exploration 72, 147–163. https://doi.org/10.1016/S0375-6742(01)00160-1

Leal, L.R.B., Teixeira, W., Macambira, M.J.B., Cordani, U.G., Cunha, J.C., 1996. Evolução crustal dos terrenos TTGs Arqueanos do Bloco do Gavião, Cráton do São Francisco: geocronologia U–Pb (Shrimp) e Pb–Pb em zircões, in: Congresso Brasileiro de Geologia, 39, Salvador, Anais, pp. 539–541.

Lobato, L.M., 1985. Metamorphism, metasomatism and mineralization at Lagoa Real, Bahia, Brazil. Unpublished doctoral thesis, University of Western Ontario.

Lobato, L. M., Forman, J. M., Fuzikawa, K., Fyfe, W. S., & Kerrich, R. (1983). Uranium in overthrust Archean basement, Bahia, Brazil. The Canadian Mineralogist, *21*(4), 647-654.

Lobato, L.M., Fyfe, W.S., 1990. Metamorphism, metasomatism, and mineralization at Lagoa Real, Bahia, Brazil. Economic Geology 85, 968–989. https://doi.org/10.2113/gsecongeo.85.5.968

Lobato, L.M., Pimentel, M.M., Cruz, S.C.P., Machado, N., Noce, C.M., Alkmim, F.F., 2015. U–Pb geochronology of the Lagoa Real uranium district, Brazil: Implications for the age of the uranium mineralization. Journal of South American Earth Sciences 58, 129–140. https://doi.org/10.1016/j.jsames.2014.12.005

Loureiro, H.S.C., Bahiense, I.C., Neves, J.P., Guimarães, J.T., Teixeira, L.R., Santos, R.A., Melo, R.C., 2009. Geologia e recursos minerais da parte norte do corredor de deformação do Paramirim (Projeto Barra – Oliveira dos Brejinhos)., Série Arqu. ed. Salvador, BA.

Machado, G. S. 2008. Geologia da porção sul do complexo Lagoa Real, Caetité, Bahia. Trabalho final de Graduação, Instituto de Geociências, Universidade Federal da Bahia, Salvador.

Magalhães, J.R., Pedrosa-Soares, A., Dussin, I., Müntener, O., Pinheiro, M.A.P., Silva, L.C. da, Knauer, L.G., Bouvier, A.-S., Baumgartner, L., 2018. First Lu–Hf, $\delta^{18}O$ and trace elements in zircon signatures from the Statherian Espinhaço anorogenic province (Eastern Brazil): geotectonic implications of a silicic large igneous province. Brazilian Journal of Geology 48, 735–759. https://doi.org/10.1590/2317-4889201820180046

Martin, H., Peucat, J.J., Sabaté, P., Cunha, J.C., 1997. Crustal evolution in the Early Archaean of South America: example of the Sete Voltas massif, Bahia state, Brazil. Precambrian Research 82, 35–62.

Maruejol, P., 1988. Métasomatose alcaline et minéralisations uranifères : les albitites du gisement de Lagoa Real (Bahia, Brésil) et exemples complémentaires de Xihuashan (SE Chine), Zheltorechensk (Ukraine) et Chhuling Khola (Népal central). Ph.D. thesis, Centre de Recherches sur la Geologie de l'Uranium, Nancy, France.

Maruejol, P., Cuney, M., Fuzikawa, K., Netto, A.M., Poty, B., 1987. The Lagoa Real subalkaline granitic complex (South Bahia, Brazil): A source for uranium mineralizations associated with Na–Ca metasomatism. Revista Brasileira de Geociências 17, 578–594.

Matos, E.C., Silva, J.R.A., Rubini, L.A., 2003. Aprovíncia uranífera de Lagoa Real - garantia de fornecimento de concentrado de urânio (DUA) para as necessidades brasileiras. Rev. Geol. 16, 111–120.

Matos, E.C., Villegas, R.A.S., 2010. Exploration and mining activities in the uranium province of Lagoa Real, in: Uranium 2010: The Future Is U Proceedings Volume 1 and 2. The Canadian Inst of Mining, Metallurgy and Petroleum, Canada, p. 2v.

Menezes, R.C.L., Conceição, H., Rosa, M.D.L.D.S., Macambira, M.J.B., Galarza, M.A., Rios, D.C., 2012. Geoquímica e geocronologia de granitos anorogênicos Tonianos (ca. 914–899 Ma) da Faixa Araçuaí no sul do Estado da Bahia. Geonomos 20, 1–13.

Nutman, A.P., Cordani, U.G., 1993. SHRIMP U-Pb zircon geochronology of Archaean granitoids from the Contendas-Mirante area of the São Francisco Craton, Bahia, Brazil. Precambrian Research 63, 179–188.

Pearce, J. A.; Harris, N. B. W.; Tindle, A.C. Trace element discrimination diagrams for the tectonic interpretation of granitic rock. Journal of Petrology. 1984. 25, 956-983.

Pedrosa-Soares, A.C., Wiedemann-Leonardos, C.M., 2000. Evolution of the Araçuaí belt and its connection to the Ribeira belt, eastern Brazil, in: Tectonic evolution of South America, Rio de Janeiro. 31st International Geological Congress, pp. 265–285.

Pedrosa-Soares, A.C., Noce, C.M., Wiedemann, C.M., Pinto, C.P., 2001. The Araçuaı-West-Congo Orogen in Brazil: an overview of a confined orogen formed during Gondwanaland assembly. Precambrian Research 110, 307–323.

Pedrosa-Soares, A.C., Noce, C.M., Alkmim, F.F., Silva, L.C., Babinski, M., Cordani, U., Castañeda, C., 2007. Orógeno Araçuaí: síntese do conhecimento 30 anos após Almeida 1977. Geonomos 15, 1–16.

Pedrosa-Soares, A.C., Alkmim, F.F., Tack, L., Noce, C.M., Babinski, M., Silva, L.C. da, Martins-Neto, M.A., 2008. Similarities and differences between the Brazilian and African counterparts of the Neoproterozoic Araçuaí-West Congo Orogen. Geological Society (London), Special Publication 294, 153–172.

Peucat, J.-J., Mascarenhas, J. de F., Barbosa, J.S.F., de Souza, S.L., Marinho, M.M., Fanning, C.M., Leite, C.M.M., 2002. 3.3 Ga SHRIMP U–Pb zircon age of a felsic metavolcanic rock from the Mundo Novo greenstone belt in the São Francisco craton, Bahia (NE Brazil). Journal of South American Earth Sciences 15, 363–373.

Polito, P.A., Kyser, T.K., Stanley, C., 2009. The Proterozoic, albitite- hosted, Valhalla uranium deposit, Queensland, Australia: a description of the alteration assemblage associated with uranium mineralization in diamond drill hole V39. Miner Deposita 44:11– 40. doi:10.1007/s00126-007-0162-2

Pouchon, M.A., Curti, E., Degueldre, C., Tobler, L., 2001. The influence of carbonate complexes on the solubility of zirconia: new experimental data. Progress in Nuclear Energy 38, 443–446.

Raposo, C., Matos, E.C. de, Brito, W., 1984. Zoneamento cálcico-sódico nas rochas da Província Uranífera de Lagoa Real, in: Anais Do XXXIII Congresso Brasileiro de Geologia, Rio de Janeiro, 1984

Ribeiro, C. I., Carvalho Filho, C. D., & Hashizume, S. 1984. As jazidas de urânio de Lagoa Real. In Congresso Brasileiro de Geologia (Vol. 33, pp. 1463-1474).

Rollinson, H. R. 1978. Using geochemical data: evaluation, presentation, interpretation. Routledge.

Romberger, S.B., 1984. Transport and deposition of uranium in hydrothermal systems at temperatures up to 300 °C: geological implications. In: DeVivo, B., Ippolito, F., Capaldi, G., Simpson, P.R. (Eds.), Uranium Geochemistry, Mineralogy, Geology, Ex- ploration and Resources. Institution of Mining and Metallurgy, London, pp. 12–17

Santana, A.V., 2016. Análise estratigráfica em alta resolução em rampa carbonática dominada por microbiolitos, Formação Salitre, Bacia de Irecê, Bahia. Ph.D. Thesis. Universidade Federal de Brasília, Brasília.

Santos, C.M., 2016. Petrografia, química mineral e litoquímica do albitito e das rochas granito-gnáissicas da anomalia 35, Província uranífera de Lagoa Real. Centro de Desenvolvimento da Tecnologia Nuclear.

Santos, C. M., Amorim, L. E D. A., Rios, F.J., Palmieri, H. L., Matos, E. C. 2018. Titanite as an important petrologic indicator from Gameleira I U-Deposit (Anomaly 35) Lagoa Real Uranium Province (LRUP), Bahia, Brazil. In: 15th Quadrennial International Association on the Genesis of Ore Deposits Symposium, Salta. 15th Quadrennial International Association on the Genesis of Ore Deposits Symposium.

dos Santos, C., Danderfer Filho, A., Queiroga, G. N., Zincone, S. A., De Castro, M. P., & Lana, C. C. (2020). Ferroan alkalic volcanism associated with Calymmian rifting in the Paramirim aulacogen, São Francisco craton, Brazil: New insights from lithofacies analysis and evidence of mantle-derived alkaline H2O-rich metasomatic fluids affecting ancient crustal materials. *Precambrian Research*, *340*, 105632.

Santos-Pinto, M., Peucat, J.-J., Martin, H., Barbosa, J.S.F., Fanning, C.M., Cocherie, A., Paquette, J.-L., 2012. Crustal evolution between 2.0 and 3.5 Ga in the southern Gavião block (Umburanas–Brumado–Aracatu region), São Francisco Craton, Brazil: a 3.5–3.8 Ga proto-crust in the Gavião block? Journal of South American Earth Sciences 40, 129–142.

Schobbenhaus, C., 2017. As tafrogêneses superpostas Espinhaço e Santo Onofre, estado da Bahia: Revisão e novas propostas. Revista Brasileira de Geociências 26, 265–276.

Shand S.J. 1950. Eruptive rocks their genesis, composition, classification and their relation to ore deposit. 4. ed., London, Thomas Murbyand, 488 p.

Silveira, E.M., Söderlund, U., Oliveira, E.P., Ernst, R.E., Leal Menezes, A.B., 2013. First precise U–Pb baddeleyite ages of 1500Ma mafic dykes from the São Francisco Craton, Brazil, and tectonic implications. Lithos 174, 144–156. https://doi.org/10.1016/j.lithos.2012.06.004

Sylvester, P.J., 1989. Post-collisional alkaline granites. Journal of Geology 97, 261–280.

Taylor, M., Van Staden, J., 1994. Spectrophotometric determination of vanadium(IV) and vanadium(V) in each other's presence. Rev. Anal. 119 (6), 1263–1276.

Teixeira, L.R., 2000. Relatório temático de litogeoquímica. Projeto Vale do Paramirim. Companhia Baiana de Pesquisa Mineral – CBPM/Companhia de Pesquisa de Recursos Minerais – CPRM, Salvador, Bahia, Brazil.

Turpin, L., Maruejol, P., Cuney, M., 1988. U-Pb, Rb-Sr and Sm-Nd chronology of granitic basement, hydrothermal albitites and uranium mineralization (Lagoa Real, South-Bahia, Brazil). Contributions to Mineralogy and Petrology 98, 139–147. https://doi.org/10.1007/BF00402107

Whalen, J. B., Currie, K. L., & Chappell, B. W, 1987. A-type granites: geochemical characteristics, discrimination and petrogenesis. Contributions to Mineralogy and Petrology, 95(4), 407–419.

Whitney, D. L., & Evans, B. W. (2010). Abbreviations for names of rock-forming minerals. American Mineralogist 95, 185–187.

Wilde, A., 2013. Towards a model for albitite-type uranium. Minerals 3, 36–48. https://doi.org/10.3390/min3010036

Winchester, J.A., Floyd, P.A., 1977. Geochemical discrimination of different magma series and their differentiation products using immobile elements. Chemical Geology 20, 325–343. https://doi.org/10.1016/0009-2541(77)90057-2

CAPÍTULO 4 – THE LAGOA REAL URANIUM PROVINCE, BRAZIL: A CASE OF "*ÉTAGEMENT TEMPOREL*"

Camila Marques[a,b*], Kathryn A. Cutts[c,d], Alexander Rocholl[e], Michael Wiedenbeck[f], Alexandre Raphael Cabral[g,h], Francisco Javier Rios[h]

[a]Programa de Pós-Graduação em Ciência e Tecnologia das Radiações, Minerais e Materiais. Centro de Desenvolvimento da Tecnologia Nuclear (CDTN/CNEN-MG). Av. Antonio Carlos 6627 – Universidade Federal de Minas Gerais – Campus Pampulha, 30270-901, Belo Horizonte, Minas Gerais, Brazil – camisgeo@gmail.com

[b]Programa de Doctorado em Geología. Departamento de Geología, Facultad de Ciencias, Universidad de Salamanca, Plaza de los Caídos, s/n, 37008, Salamanca, España

[c]Departamento de Geologia, Escola de Minas, Universidade Federal de Ouro Preto, Morro do Cruzeiro, 35400-000 Ouro Preto, MG, Brazil. Faculdade de Geologia, [d]Universidade do Estado do Rio de Janeiro, Rua São Francisco Xavier 524, Maracanã, Rio de Janeiro, 20550-900, Brazil – kathryn.cutts@gmail.com

[e]GFZ German Research Centre for Geosciences, Helmholtz Centre Potsdam, 14473 Potsdam, Germany – rocholl@gfz-potsdam.de

[f]GFZ German Research Centre for Geosciences, Helmholtz Centre Potsdam, 14473 Potsdam, Germany - michael.wiedenbeck@gfz-potsdam.de

[g]Centro de Pesquisas Professor Manoel Teixeira da Costa (CPMTC), Instituto de Geociências. Universidade Federal de Minas Gerais (UFMG), Av. Antonio Carlos 6627, 30270-901, Belo Horizonte, Minas Gerais, Brazil – arcabral@geol.igc.ufmg.br

[h]Centro de Desenvolvimento da Tecnologia Nuclear (CDTN/CNEN-MG). Av. Antonio Carlos 6627 – Universidade Federal de Minas Gerais – Campus Pampulha, 30270-901, Belo Horizonte, Minas Gerais, Brazil – javier@cdtn.br

[*]corresponding author

Artigo submetido ao periódico *Economic Geology*

Abstract

The Lagoa Real uranium province, referred to as Lagoa Real, is located in Bahia state, northeastern Brazil. Lagoa Real has around 112,000 metric tons of U_3O_8 and an average grade of 2700 ppm, being one of the largest U deposits in the world and the largest in Brazil. Despite a long history of research, the timing and generation of the deposits is uncertain. Uranium ore is hosted mainly by Na-rich gneissic rocks, known as albitite. Albitite occurs as pods within granite–gneiss rocks of the Lagoa Real intrusive suite that are distributed along NNW–SSE-striking shear zones. Here, we report new petrographical data and analytical work to determine the age of U mineralization and to elucidate the nature of the albitite protholith, using LA–ICP–MS for U–Pb dating of zircon and titanite, SIMS for U–Pb dating of zircon, and chemical dating of uraninite by EPMA. Zircon grains from albitite rocks yielded ages of ca. 1.74 Ga (LA–ICP–MS and SIMS data), which are identical to the age of emplacement of the host rock – i.e., the São Timóteo granite of the Lagoa Real intrusive suite. Detailed drill core descriptions and petrographical studies reveal a history of metasomatic alteration of the São Timóteo granite progressively through sodic, calcic-ferric, potassic-magnesian and finally calcic processes, which evolved mostly under a ductile regime. Uranium ore (uraninite + titanite ± zircon) precipitation is associated with the calcic-ferric and potassic-magnesian stages. Our results indicated a series of intermediate ages, between 1.7 Ga and 0.49 Ga, for ore-related titanite and zircon in agreement with previously reported ages. Ages obtained from uraninite indicate U precipitation likely occurred between 580 and 520 Ma, synchronous with the Brasiliano–Pan-African orogeny. To reconcile the obtained data, we propose that the intermediate ages represent fluid-flow episodes with concomitant U mineralization, which find geological expression as five discrete phases of tectonic extension that ended with the Brasiliano–Pan-African orogeny. The multi-stage character of U mineralization in Lagoa Real reflects "étagement temporel" (temporal superposition). Given U mobility and its endowment as "étagement temporel", it is not possible to determine when the main U-mineralizing stage took place, only that the U endownment continued until the Brasiliano–Pan-African orogeny. In contrast to preceding models, our results imply that the Lagoa Real U mineralization was a long-lived, multi-stage process spanning more than one billion years.

Keywords: Lagoa Real uranium province, U–Pb geochronology, uraninite chemical dating, multi-stage ore deposits

4.1 INTRODUCTION

The Lagoa Real uranium province (LRUP), hereinafter Lagoa Real, is located in southern Bahia state, in the eastern part of the São Francisco craton. The province is the sixth largest uranium (U) resource in the world, and the most important in Brazil. It is approximately 35 km long and contains 38 uraniferous anomalies along three semi-arched lineaments (Fig. 19). The Lagoa Real orebodies contain a total reserve of ~112,000 metric tons of U_3O_8 and an average grade of 2700 ppm (Brito et al., 1984; Matos et al., 2003; Matos and Villegas, 2010). Lagoa Real has been explored and mined by Indústrias Nucleares do Brasil (INB) since 1999. Annual production of about 300 tons of U concentrate was produced from seven orebodies in the Cachoeira mine. A new open-pit mine, the Engenho mine, will start operation in the next few years.

In Lagoa Real, U mineralization is spatially associated with albitite, a variety of Na-rich rock with abundant plagioclase (albite ± oligoclase) and variable proportions of iron–calcic–sodic mineral assemblages. Albitite hosts the main U mineralization, which is represented by fine-grained uraninite crystals included in garnet, pyroxene and titanite, or occurring at the grain boundaries of minerals, i.e. magnetite. Most genetic models propose that albitite is the product of metasomatic alteration of the São Timóteo granite, by sodium enrichment and silica depletion (Maruejol, 1988; Lobato and Fyfe, 1990). Alternatively, Chaves (2013) proposed that albitite rocks were emplaced during the Orosirian, at ca. 1.8 Ga, as Na-rich, quartz-free syenitic rocks as a result of the collision between the São Francisco and Congo landmasses. Despite a number of studies on the Lagoa Real U deposits (Geisel Sobrinho et al., 1980; Lobato, 1985; Fuzikawa et al., 1988; Maruejol, 1988; Lobato and Fyfe, 1990; Cruz et al, 2007; Chaves et al., 2007; Chaves et al., 2009; Oliveira, et al 2012; Lobato et al., 2015), there is no consensus regarding their genesis. Great uncertainties exist concerning the timing of the albitite-forming metasomatism and its U mineralization.

Geochronological studies in Lagoa Real have been conducted since the 1980s by means of different methods (Turpin et al., 1988; Cordani et al., 1992; Pimentel et al, 1994; Chaves et al., 2007; Chaves et al., 2009; Lobato et al., 2015), which are summarized in Appendix 1 - Table 1. Uranium mineralization and metasomatism were attributed to events at ca. 1.4 Ga by Turpin et al. (1988), based on U–Pb analyses of HNO_3-soluble fractions from heavy-liquid concentrates of minerals from U ores (magnetite, zircon and uraninite) and handpicked uraninite concentrates. Cordani et al. (1992), on the basis of

Rb–Sr whole-rock analyses, concluded that U was deposited between 1.5–1.2 Ga. Chaves (2007) published zircon U–Pb (LA–ICP–MS) analyses of three zircon grains that produced an upper intercept of ca. 1.8 Ga, which was interpreted as the crystallization age of a sodic syenite. More recently, Lobato et al. (2015) published a review of the TIMS-based geochronological work of Pimentel (1994), arguing that U-ore formation and hydrothermal alteration occurred at around 960 Ma. These different ages have resulted in contrasting models for the genesis of the Lagoa Real U mineralization, reflecting the difficulty in obtaining geologically significant data.

The relationship between U mineralization and geodynamic events, in terms of timing and tectonic setting bears important information for understanding not only the geological history of Lagoa Real, but also global events and periods of U concentration. The present work aims to elucidate the timing and setting of U mineralization based on U–Pb zircon dating by in-situ SIMS, and LA–ICP–MS methods, combined with chemical EPMA age dating of uraninite in albitite samples from two deposits in the northwest region of Lagoa Real. The results provide new insights on the temporal evolution of this economically important Brazilian U province, allowing comparison with other U deposits in the context of Western Gondwana.

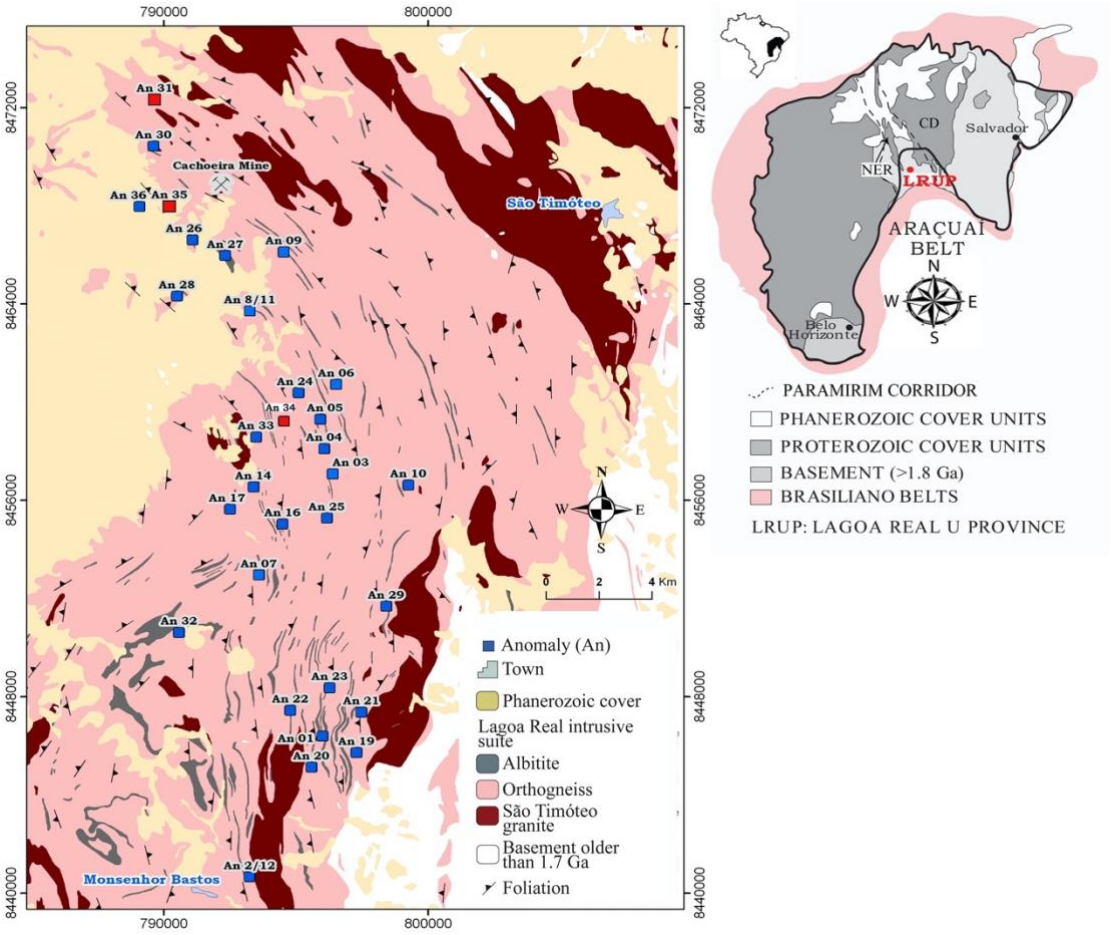

Fig. 19**.** Geological map of the Lagoa Real uranium province showing the distribution of uranium anomalies and the location of the Cachoeira mine (adapted from Costa et al., 1985). NER: Northern Espinhaço Range, CD: Chapada Diamantina

4.2 GEOLOGICAL SETTING

Lagoa Real is located in the northern part of the Neoproterozoic Araçuaí–West Congo orogenic system (AWCO), in a structure called the Paramirim Aulacogen (after Pedrosa-Soares et al., 2011) in the western sector of the São Francisco–Congo paleocontinent (Fig. 19; Alkmim et al., 2006; Pedrosa-Soares et al., 2008, 2007; Pedrosa-Soares and Wiedemann-Leonardos, 2000). The Paramirim Aulacogen is located in the northern sector of the AWCO and corresponds to a partially inverted rift-sag basin, filled with sediments that accumulated on the cratonic terrane from the Statherian (1775 ± 7 Ma; Danderfer Filho et al., 2015) through to the Cryogenian (675 Ma; Santana, 2016). Partial basin inversion occurred during the amalgamation of Gondwana in the Ediacaran–Cambrian Araçuaí orogen (Cruz and Alkmim, 2017).

The basement of the Paramirim Aulacogen, the Gavião block, is composed of: metagranitoids; orthogneiss rocks, often with Archean mafic and ultramafic migmatitic enclaves; greenstone belts; Paleoarchean, Neoarchean and Siderian–Rhyacian metavolcano-sedimentary sequences; and acidic, intrusive plutonic rocks of Siderian, Rhyacian and Orosirian ages (Bastos-Leal et al., 1998, 2000; Cordani et al., 1985, 1992; Cruz et al., 2012; Cruz et al., 2016; Cunha et al., 2012; Medeiros et al., 2017; Nutman and Cordani, 1993; Rosa et al., 2000; Santos-Pinto et al., 1998, 2012).

Anorogenic alkaline granitic rocks in Lagoa Real, defined as the Lagoa Real intrusive suite (Arcanjo et al., 2005) and commonly known as the São Timóteo granite, crystallized at ca. 1750 Ma based on U–Pb dating of zircon (Turpin et al., 1988; Cordani et al., 1992; Pimentel et al., 1994; Lobato et al., 2015; Amorim et al., 2020 - submitted). The São Timóteo granite consists of bodies of porphyritic and coarse-grained hastingsite-bearing syenite, syenogranite, and alkali granite. These are geochemically characterized as a reduced, ferroan A-type, A2 series, metaluminous, high-K and Fe-rich calc-alkaline series (Teixeira, 2000; Machado, 2008; Amorim et al., 2020; Marques et al., 2020a). These were deformed into protomylonites, mylonites and ultramylonites defined regionally as Cercado, Lagoa Grande and Caetité gneisses, respectively by Cruz et al (2007). The Lagoa Real intrusive suite, together with the Borrachudos and Catolé suites, and widespread meta-rhyolite and metamafic rocks in the Espinhaço domain, make up a silicic large igneous province (SLIP), which erupted on the São Francisco paleocontinent from ca. 1.79 Ga to 1.70 Ga (Magalhães et al., 2018, and references therein).

The metasedimentary cover units, the (Paleo- to Mesoproterozoic) Espinhaço Supergroup and the Neoproterozoic São Francisco Supergroup crop out in the northern Espinhaço and Chapada Diamantina regions, which are also called the western and eastern basins, respectively (Guimarães et al., 2012). They are separated by the Paramirim High (Cruz et al., 2012).

The Espinhaço Supergroup comprises a succession of metamorphosed siliciclastic rocks (i.e., metasandstones, metapelites and metaconglomerates) and subordinate metavolcanic rocks. The Supergroup has distinct facies in its northern and Chapada Diamantina sectors, and numerous studies have produced a multitude of different names and stratigraphic correlations (see Cruz and Alkmim, 2017, for a synopsis). Deposition of the Espinhaço Supergroup occurred from 1775 ± 26 Ma (U–Pb zircon age by LA–ICP–MS from felsic volcanic rocks; Danderfer Filho et al., 2015) to around 1140 Ma (carbonate, whole-rock Pb–Pb age; Babinski et al., 1993).

The São Francisco Supergroup comprises siliciclastic rocks of marine to alluvial origin, in addition to diamictite and carbonate that represent the Neoproterozoic Sturtian glacial event (ca. 715–650 Ma; Rooney et al., 2017). The São Francisco Supergroup was deposited between ca. 850 Ma (U–Pb age of detrital zircon; Bitencourt et al., 2019) to 675 Ma (U–Pb zircon age by ion microprobe, zircon; Santana, 2016).

Two groups of mafic sills and dikes intrude the Espinhaço Supergoup (Arcanjo et al., 2005; Menezes et al., 2012). These intrusions have tholeiitic composition and continental intraplate affinity. The oldest group is located in the Chapada Diamantina basin and has ages of 1514 ± 22 Ma (Babinski et al., 1999), 1501 ± 9 Ma (Silveira et al., 2013), 1492 ± 16 Ma and 1496 ± 3.2 Ma (Guimarães et al., 2008; Loureiro et al., 2009). The youngest group has ages of 934 ± 14 Ma and 854 ± 23 Ma (respectively, Loureiro et al., 2009, and Danderfer et al., 2009), and occurs in both the northern Espinhaço and Chapada Diamantina sectors. The latter are related to the Early Tonian rifting event that resulted in the formation of a large Neoproterozoic intracratonic basin, and deposition of the Macaúbas Group (Babinski et al., 2012; Moreira et al., 2020; Pedrosa-Soares et al., 2011a). This was the precursor basin of the Araçuaí orogen (Ediacaran to Cambrian). The Paramirim Aulacogen was partially inverted during the Ediacaran–Cambrian Araçuaí orogen (Cruz and Alkmim, 2006; Danderfer Filho, 2000, 1990; Danderfer Filho et al., 1993; Guimarães et al., 2008; Loureiro et al., 2009), when the São Francisco and Congo cratons collided. The zone that concentrates the majority of deformational structures is defined as the Paramirim corridor (Alkmim et al., 1993), which trends NNW. Its tectonic framework comprises contractional and extensional families of structures related to rift nucleation, reactivation and inversion of the aulacogen (Cruz et al., 2015).

4.3 THE URANIUM PROVINCE OF LAGOA REAL

Lagoa Real is located in the southern sector of the Paramirim corridor, where the Lagoa Real intrusive suite (LRIS) is exposed. The LRIS consists of A-type granitoids that enclose lens-shaped albite-rich rocks, henceforth referred to as albitite, the host rock of U deposits in Lagoa Real. Other metasomatic bodies also occur associated with the LRIS. These include epidosites, oligoclasites and microclinites, and are found interlayered with amphibolite and diabase bodies (Costa, 1985; Cruz et al, 2007). Albitite bodies are discontinuous, massive or gneissified, fusiform, and variable in length, ranging from metric to hundreds of metres (<480 m; Ribeiro et al., 1984). Albitite is a sodium-enriched rock dominated by plagioclase (albite ± oligoclase), and a variety of iron-calcic-silicate

mineral assemblages that include garnet, clinopyroxene, amphibole, epidote and titanite. Albitite pods have gradational or abrupt contacts with the LRIS granitoid rocks and, in general, are interpreted as the product of metasomatic alteration of the granite–gneiss country rock by sodium enrichment and silica depletion (Maruejol, 1988; Lobato and Fyfe, 1990). However, Chaves (2013) favored a magmatic origin for the albitites, as intrusive Na-rich, quartz-free syenitic rocks. Such contrasting views exemplify the lack of consensus regarding the origin of the Lagoa Real albitites, despite numerous studies (Geisel Sobrinho et al., 1980; Lobato, 1985; Fuzikawa et al., 1988; Maruejol, 1988; Lobato and Fyfe, 1990; Chaves, 2013)**.** Uranium mineralization is made up mainly of disseminated crystals of fine-grained uraninite (<5 m), which is highly concentrated in the most mylonitized zones, but uranophane and pitchblende have also been described as uranium ore. Lobato and Fyfe (1990) and Maruejol (1988) reported the preferential occurrence of uranium minerals in Fe^{3+}-rich garnet–hedenbergite-bearing albitites.

The regional, concordant intercalation of LRIS rocks with the metasomatic bodies of albitite, microclinites and oligoclasites, as well as the features of albitization in LRIS rocks, are the primary observations suggesting a common origin for these rocks (Cruz et al., 2007). However, the metamorphic overprint that resulted from the inversion of the aulacogen makes drawing of paragenetic sequence challenging.

The replacement of magmatic K-feldspar through development of metasomatic perthites was first described by Cruz et al. (2007). The albitization was interpreted as pre-metamorphic by these authors, as deformed rocks have no preferential orientation of perthites, in addition, new grains of albite cut the metasomatic perthites. The presence of recrystallized unaltered microcline near to altered feldspars is also an argument in favor of pre-kinematic character.

4.4 METHODS

4.4.1 Field work, petrography and SEM

Seven drill holes (DDH35-F10, DDH35-F16, DDH35-F12, DDH35-F33, DDH31-F11, DDH31-F04 and DDH34-F09) from the Gameleira I (AN35), Barrinha (AN34) and Barreiro (AN31) deposits were examined to determine the nature of the deposit host rocks, distribution and types of hydrothermal alteration, and mode of occurrence of the uranium ore. Petrographic investigations were conducted through the study of around 100 polished thin sections. These investigations were complemented by scanning electron

microscope (SEM) with coupled energy-dispersive X-ray spectrometer (EDS) analyses performed at the Centro de Desenvolvimento da Tecnologia Nuclear (CDTN), Brazil.

4.4.2 Geochronology

Zircon grains from the barren albitite (samples 3409 and 3510) that corresponds to calcic-ferric stage, and titanite grains from ore-bearing veinlets (sample TAR2) were extracted, mounted in resin and polished for U–Pb dating by means of laser ablation–inductively coupled plasma–mass spectrometry (LA–ICP–MS). Another sample (sample MAAB03) with ore-bearing veinlets had its fine-grained zircon dated in situ using a secondary-ion mass spectrometer (SIMS). In addition, chemical age dating by electron probe micro analysis (EPMA) of uraninite was conducted on samples MAAB03 and BCAB. Detailed information about geochronological analytical procedures are given in the Appendix 1.

4.5 RESULTS

4.5.1 Geology of Gameleira I (AN 35), Barrinha (AN 34) and Barreiro (AN 31) deposits.

Selected drill holes intercepted LRIS granitoids, albitite, and rarely amphibolite rocks (Fig. 20). The three studied deposits have similar rocks and mineralization style, because of this they are described together, and any differences between them are highlighted. Cross-sections of the studied drill-holes are presented in Fig. 21.

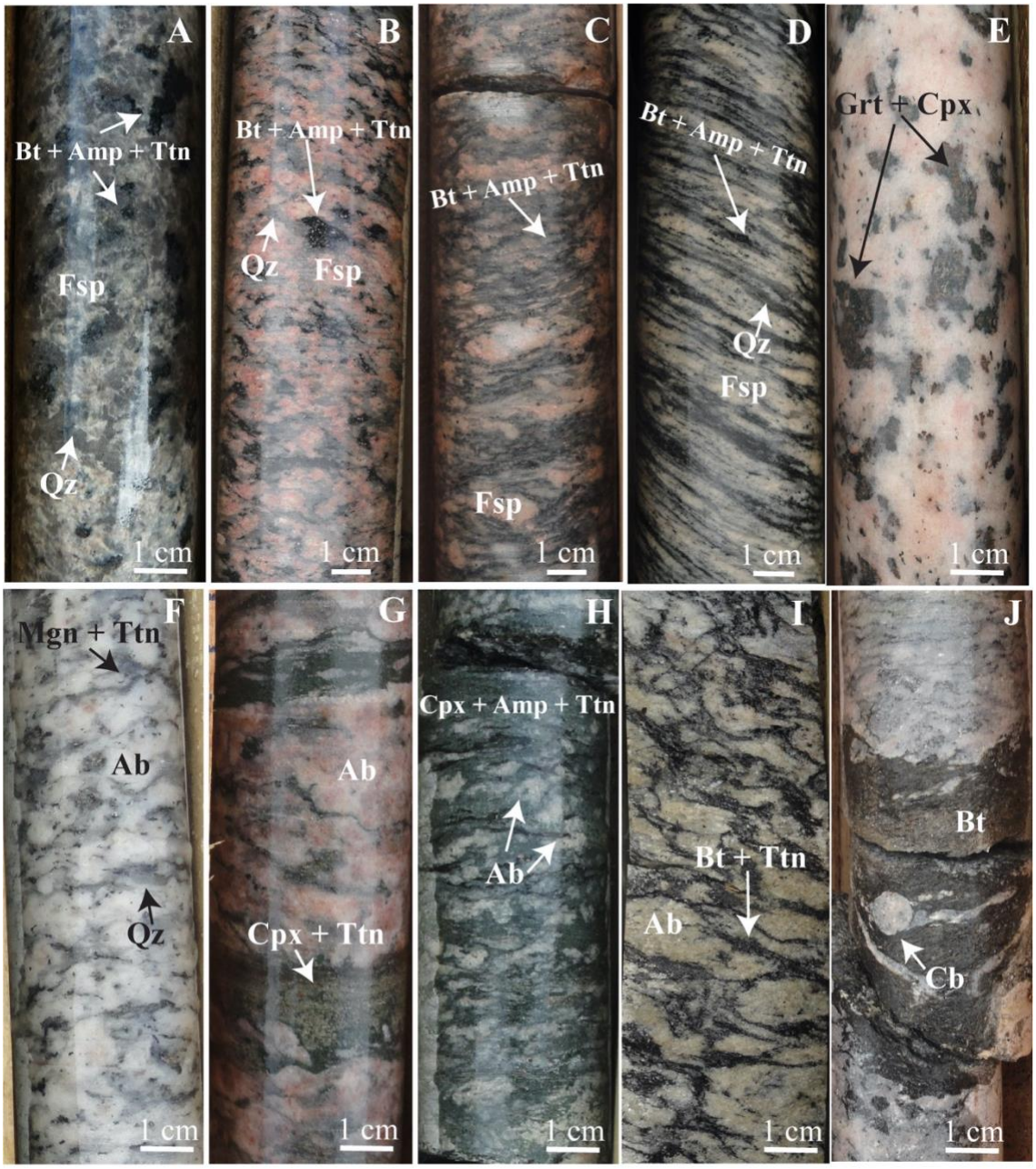

Fig. 20. Drill-core photographs of hydrothermally unaltered to altered rocks at Gameleira I, Barrinha and Barreiro deposits. A. Preserved unaltered and undeformed São Timóteo granite typically coarse-grained and grey in color. B. Weakly deformed São Timóteo granite with a discontinuous foliation showing signs of albitization represented by the pinkish color. C. São Timóteo gneiss showing augen-fabric and a pinkish color as a result of albitization. D. Striped São Timóteo gneiss with stretched crystals of feldspar and quartz. E. Massive garnet-rich albitite with andradite surrounded by Cpx II. F. Magnetite-rich albitite with low mafic contents. Magnetite and titanite are displaced mostly along the foliation. G. Cpx III and titanite concentrated in albitite portions. H. Cpx III ± amphibole II well developed in an augen-like albitite. I. Biotite-rich augen albitite

showing porphyroblasts of albite. J. Biotite-rich portions with deformed crystals of carbonate. *Bt* Biotite, *Amp* amphibole, *Ttn* titanite, *Fsp* Feldspar, *Qz* quartz, *Grt* garnet, *Cb* carbonate, *Ab* albite.

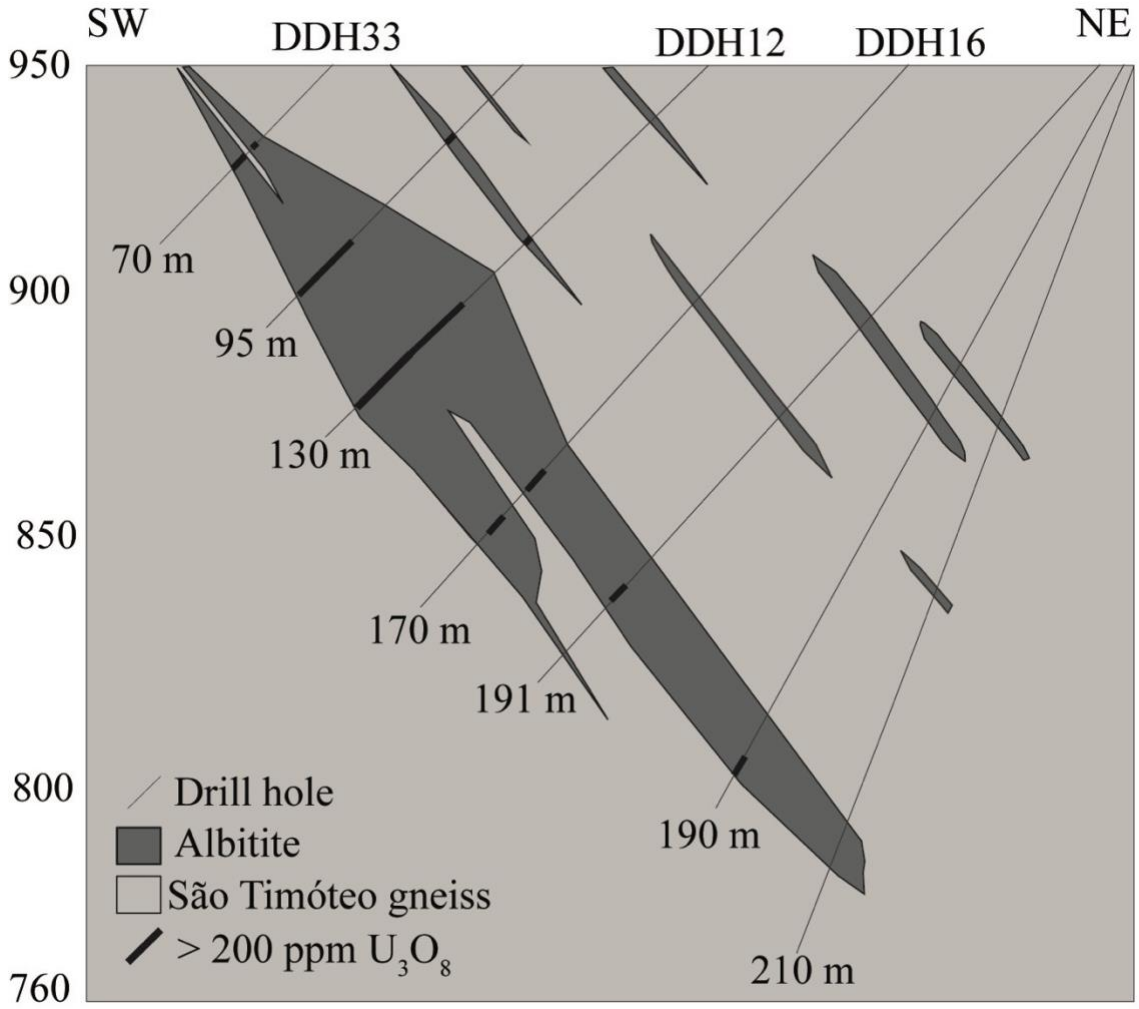

Fig. 21. Cross-section of the unexposed Gameleira I deposit.

Lagoa Real intrusive suite: the LRIS rocks are represented mainly by gneissic rocks, and rarely by the undeformed São Timóteo granite. The São Timóteo granite is typically isotropic, coarse grained and grey in color. It has a porphyritic texture with alkali feldspar phenocrystals of up to 2 cm (Fig. 20A). It grades into intervals of medium-grained protomylonitic gneisses with a discontinuous foliation (Fig. 20B), through to augen gneisses with a continuous foliation (Fig. 20C). In the Barrinha deposit the striped gneiss predominates with well-developed compositional layering between the quartz-feldspathic and mafic assemblages (Fig. 20D). The granitic-gneiss intervals have reddened portions, which sometimes occur close to the contact with the albitite rocks (Fig. 20B and C).

Petrographically, unaltered-to-altered rocks are divided into underformed São Timóteo granite, varieties of São Timóteo gneiss, and albitized gneiss.

São Timóteo granite: the São Timóteo granite is a coarse-grained rock, with grains attaining more than 5 mm across, in an inequigranular hypidiomorphic fabric. It is composed of K-feldspar (~60 vol.%), quartz (~30 vol.%), clinopyroxene, amphibole, biotite, titanite, ilmenite, zircon and apatite. The latter are individually variable in abundance, amounting to ~10% of the modal volume. Phenocrysts of K-feldspar are the main mineral phase in the absence of magmatic plagioclase, characterising it as a hypersolvus facies. Phenocrysts are medium to coarse in grain size, varying from 2 to 8 mm across and have patches of plagioclase connected with micro- to mesoperthites (Fig. 22A). Plagioclase patches are irregular in size and shape and may be twinned. Swapped albite rims or aggregates of intergranular albite occur at the contact between alkali-feldspar grains (Fig. 22B), mainly in undeformed, less altered granites. Quartz is either interstitial or included in alkali-feldspar crystals. Interstitial quartz is irregular and does not reach 1 mm across.

Amphibole is dark green (Amp I) and forms interstitial aggregates of either symplectic microstructure or tabular habit. The mineral envelops clinopyroxene (Cpx I) (Fig. 22C) and is replaced by biotite. The tabular amphibole is rich in fine-grained ilmenite inclusions along cleavage planes. Biotite and amphibole make up mafic patches, which may also comprise titanite, ilmenite, zircon, apatite and rarely observed allanite. Titanite manifests itself as aggregates surrounding ilmenite, composing a corona-like microstructure, which is interstitial or associated with amphibole.

São Timóteo gneiss: the magmatic hypidiomorphic fabric of the São Timóteo granite appears deformed in the gneissic rocks and results in a porphyroclastic texture. K-feldspar and plagioclase occur as porphyroclasts, which are embedded in a recrystallised matrix of medium-grained feldspar and quartz. The coupled development of plagioclase patches and mesoperthites resulted in partial to complete replacement of K-feldspar, forming porphyroclasts of plagioclase. The progressive recrystallization of porphyroclasts of plagioclase forms isolated grains with variable size. Together, porphyroclasts and recrystallized matrix form core-and-mantle domains that define the augen fabric (Fig. 22D). Subgrains and new grains of plagioclase are located along perthitic lamellae in K-feldspar or around plagioclase prophyroclasts and are variably sericitized (Fig. 22E and F). New grains of K-feldspar have tartan twinning. Aggregates of new grains and subgrains of quartz may preserve the outline of magmatic crystals of quartz or occur as

ribbons. Titanite forms on the rims of ilmenite with a corona-like texture. Amphibole, biotite and titanite-ilmenite are foliation forming minerals (Fig. 22D). The amphibole is intergrown with fine-grained titanite.

Albitized São Timóteo gneiss: in hand specimen, the albitized gneiss has pinkish to reddish tints (Fig. 22B and C). Mineralogically, it is similar to the São Timóteo granite and gneiss samples. The rock is characterized by the widespread occurrence of plagioclase (20% of modal volume) and strong decalcification of feldspar, observed through its replacement by calcite (Fig. 22G), epidote and minor fluorite (Fig. 22H). Sericite and hematite also overprint feldspar giving a cloudy apparence to the crystals. Albite crystals, fine to medium in grain size (<2 mm), display albite twinning and grain boundaries that are either rectilinear or lobate. Pyrite occurs, with magnetite inclusions and some chalcopyrite, in the interstices of amphibole crystals. Acessory allanite surrounds titanite, making up corona-like microstructures, which are spatially associated with thorite, pyrite and fluorcarbonate. Quartz occurs as aggregates of new grains or as ribbons, similar to the other non-albitized gneisses.

Metasomatic rocks: albitite rocks are further distinguished based on subordinate minerals: (i) garnet albitite; (ii) magnetite albitite; (iii) pyroxene-to-amphibole albitite, (iv) and biotite albitite, but mixed components are also observed. Albitite represents medium-to coarse grained, albite-rich rocks, which are massive, foliated or brecciated showing pinkish to whitish color. Garnet-bearing albitite is rare in the Gameleira I deposit, but occurs frequently in Barrinha, where it is represented by coarse-grained, massive (Fig. 20F) to foliated rocks (Fig. 20G), with transitional contacts in relation to São Timóteo gneisses. Magnetite albitite and pyroxene albitite are the most widespread albitite types and occur mainly in the Gameleira I deposit. Magnetite albitite is a foliated rock, preserved as lenses in unaltered LRIS gneisses or intercalated with pyroxene-bearing albitites, composed mainly of magnetite, titanite, and albite, with low modal contents of mafic minerals resulting in a predominantly white color (Fig. 20H). Pyroxene albitite is generally foliated. It grades from portions where pyroxene, amphibole and titanite define the foliation and are concentrated as centimetric levels (Fig. 20I), to augen gneisses with high modal volumes of green minerals (amphibole and pyroxene) plus titanite along the mylonitic foliation (Fig. 20J). Similarly to the pyroxene albitite, the biotite albitite has an augen fabric, with a mylonitic foliation defined by biotite, with albite preserved as porphyroclasts in augen form (Fig. 20K). Carbonate and chlorite veins are sparse. Monomineralic veins of biotites, or biotite plus carbonate were also observed (Fig. 20L).

Uranium mineralization is hosted within pervasively foliated albitite rocks as millimetric veinlets. These are mostly invisible to the naked eye and are concentrated in pyroxene- and biotite albitite types.

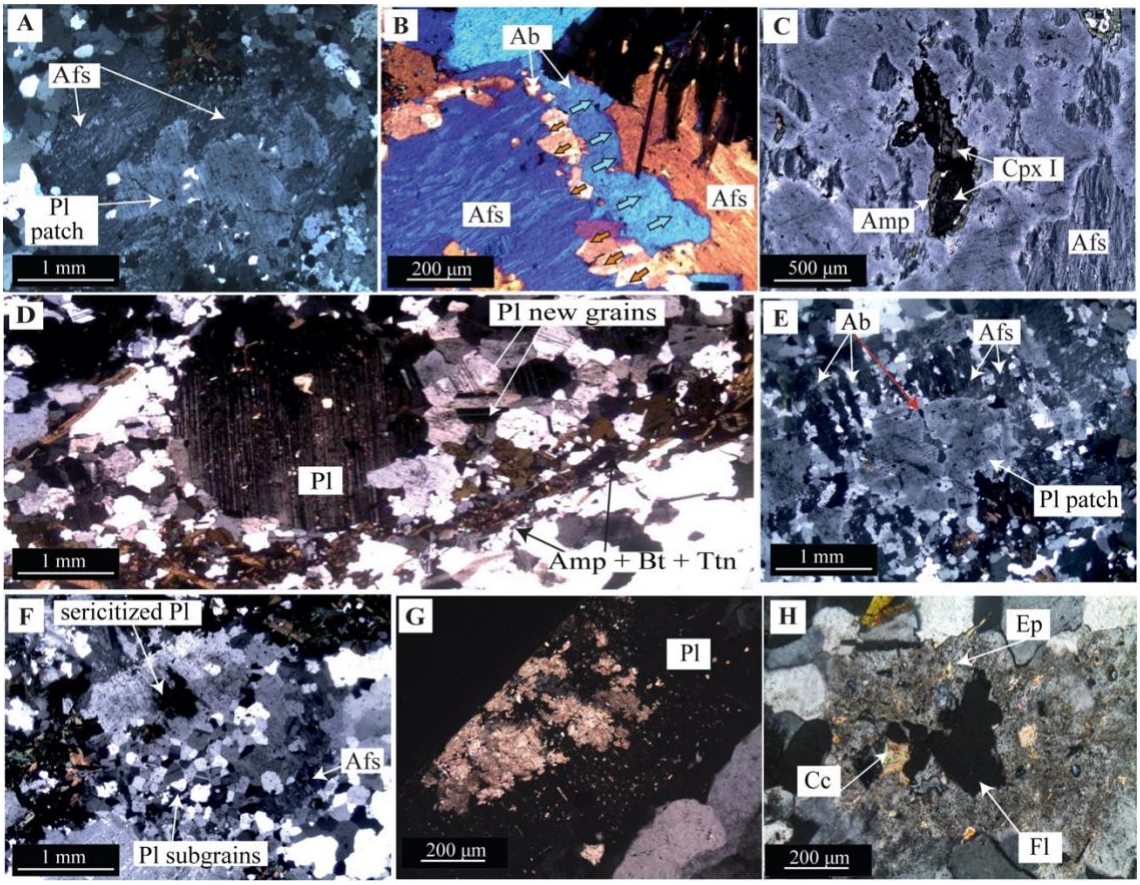

Fig. 22**.** Transmitted-light photomicrographs of altered to albitized granite-gneiss rocks of the São Timóteo granite in cross-polarized light (CPL). Mineral abreviations are according to Whitney and Evans (2010). A. Mesoperthitic K-feldspar with plagioclase patches in the core of the crystal. This texture represents one of the first stages of albitization in the São Timóteo rocks. B. Swapped albite rims along K-feldpar boundaries – CPL with quartz plate. C. Aggregate of Cpx I and Amp I, as core and rim, respectively, included in alkali feldspar. D. Plagioclase porphyroclast forming augen domain in the São Timóteo gneiss. The porphyroclast has tails of plagioclase subgrains. The augen domain is delineated by amphibole, biotite and titanite. E. Subgrains of plagioclase as an overprint on perthitic lamellae coupled with a plagioclase patch in the alkali-feldspar core. F. Sericitized plagioclase partially surrounded and cut by subgrains and new grains of albite. G. Carbonate overprint on plagioclase, which appears in black (at extinction). H. Plagioclase alterated to fluorite, carbonate and epidote.

4.5.2 Metasomatic temporal evolution of the albitite rocks

Shearing affected early to late parageneses and due to extensive recrystallization, accurate reconstruction of the early history of metasomatic alteration is challenging. However, petrographic observations in this work coupled with geochemical trends described by Santos et al., (2020) show that rocks can be related to four stages of metasomatic activity, which are summarized in Fig. 23. These include phases of sodic, calcic-ferric, potassic-magnesian and late calcic alteration, in addition to an infill stage recorded by calcite and sulphide precipitation as veinlets.

Sodic alteration: this stage is represented by the widespread presence of albite. All albitite varieties have features in common which together form polygonal granoblastic to porphyroclastic fabrics. Albite accounts for 60–80 vol.% of these rocks. The mineral occurs as: i) medium- to coarse-grained porphyroclasts with polysynthetic twinning, or chessboard twinning (Fig. 24A), which are variably kinked or present growth twinning; and, ii) fine-to medium-grained (200–250 μm) mostly untwinned, granoblastic crystals of polygonal shapes, which surround plagioclase porphyroclasts forming core-and-mantle textures. This albitization leaves residual grains of recrystallized primary K-feldspar associated with altered plagioclase (to carbonate, sericite, epidote), suggesting that this process was accompanied by intense plagioclase decalcification. During this stage, Cpx II precipitated (Fig. 24B) and probably quartz was partially dissolved, although dissolution textures are not strongly evident.

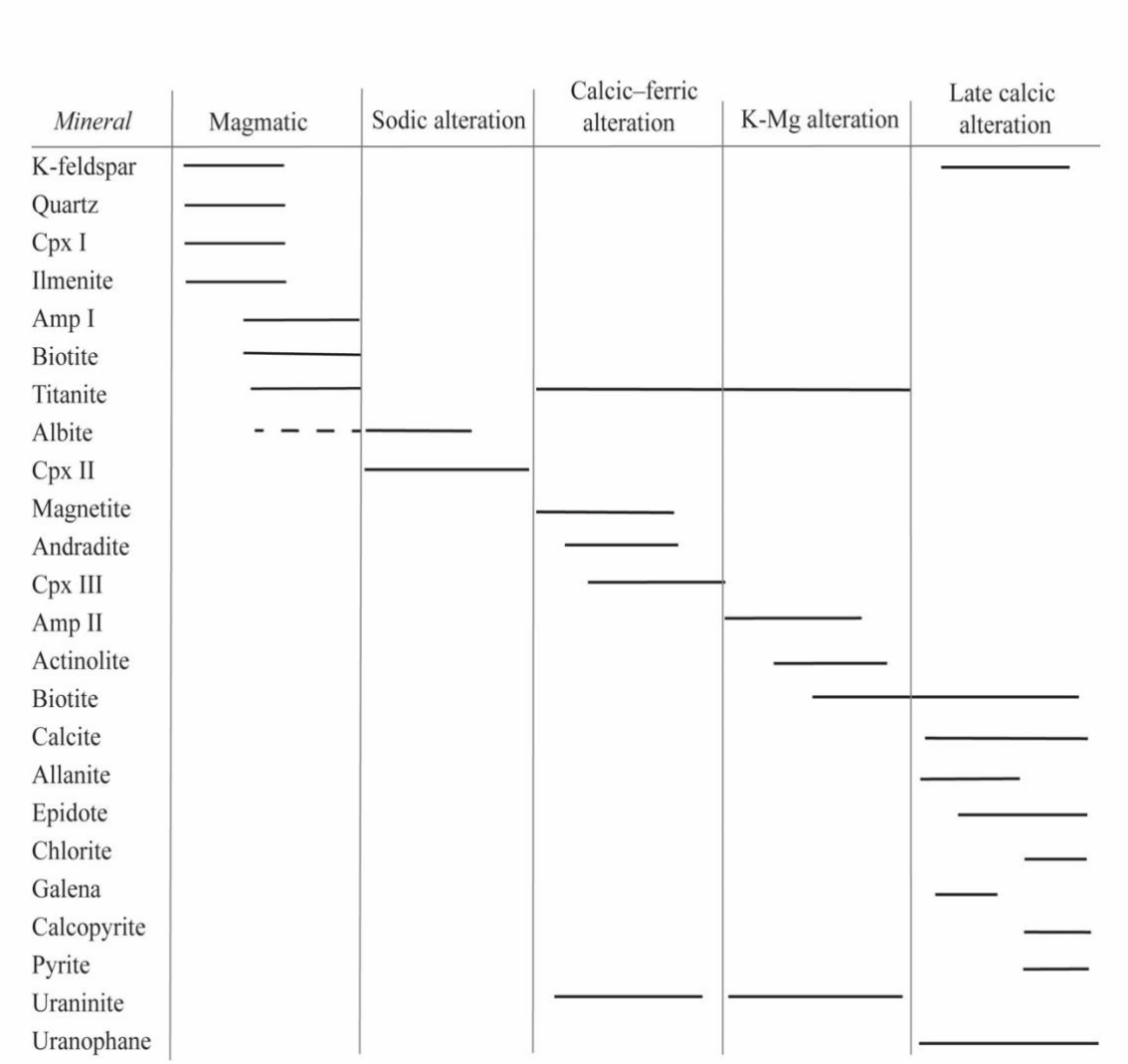

Fig. 23. Mineral parageneses in the host Lagoa Real suite intrusive rocks and albitites.

Calcic-ferric alteration: this alteration stage consists of the development of Cpx III, andradite, prismatic titanite and magnetite. Quartz and K-feldspar are trace or absent. Initially, andradite and magnetite replaced Amp I, Cpx II, albite and the corona-texture titanite, resulting in garnet- and magnetite-albitites. Later, Cpx III and prismatic titanite overprint the magnetite + andradite assemblage and this corresponds to portions where pyroxene-to-amphibole albitite are well developed, reaching 70% of the modal volume of the rock. Andradite is coarse-grained and is intergrown with fine-grained, prismatic titanite (Fig. 24C). Magnetite is fine-to-coarse grained, pervasively replaces the early assemblage, and is rimmed by titanite (Fig. 24D). Magnetite is strongly converted into hematite, however the timing of martitization is not clear. Uranium precipitation is related to this stage, which is shown by the presence of uraninite intergrown with the prismatic titanite associated with Cpx III as veinlets (Fig. 25).

Potassic-magnesian alteration: this stage is represented by the growth of amphibole II, actinolite (Amp III) and biotite. Amp II is largely produced by clinopyroxene (Cpx II and III) hydration, but also replaces albite. Amp II, in turn, is converted into actinolite (Fig. 24B), reaching the actinolite albitite composition (Fig. 24E). Biotite grains are brown or green in color and define a mylonitic foliation. Biotitization occurs after actinolite, and the biotite development overprints all amphiboles and clinopyroxenes from the early stages, forming biotite albitite. Biotite occurs associated with red-to-brown titanite and zircon (Fig. 24F).

Late calcic alteration: this final stage is represented by calcite, epidote, allanite, monazite, K-feldspar, chlorite and apatite precipitation. K-feldspar, apatite and chlorite occurrence are uncommon. K-feldspar replaces albite in association with epidote and galena. Epidotization coupled with allanite precipitation is the main remarkable feature of this stage (Fig. 24G). Fine-grained allanite develops in biotite clots with typical pleochroic halos or replaces titanite. Epidote grows after allanite, titanite, actinolite and biotite, forming halos around ore-bearing veinlets (Fig. 24G and H). This stage ended with calcite precipitation as this mineral is the most abundant veinlet fill. Carbonate replacement is either pervasive, substituting the matrix assemblage and well developed in K-Mg rich zones, or vein related where it is associated with the growth of pyrite and chalcopyrite denoting a ruptil character at the final stage (Fig. 24I).

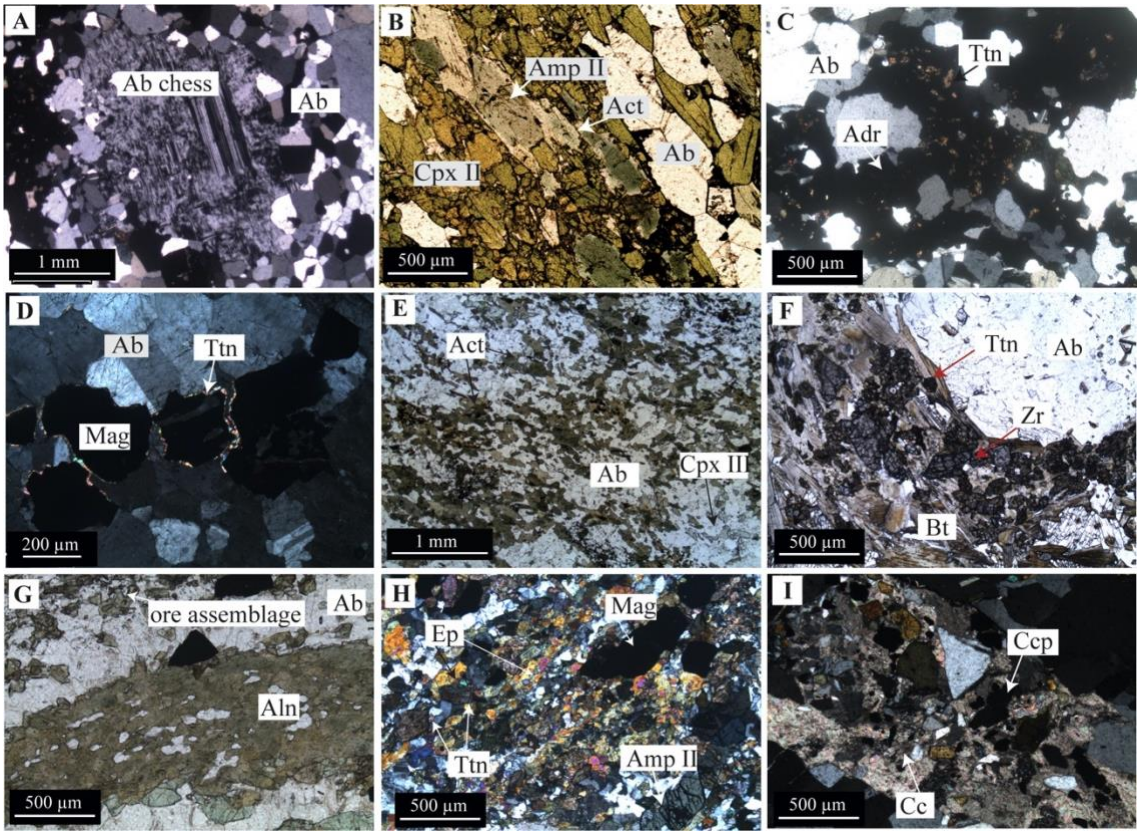

Fig. 24**.** Transmitted-light photomicrographs either in plane polarized light (PPL), or cross-polarised light (CPL) of albitite rocks. A. Porphyroclast of chessboard albite showing core-to-mantle texture with recrystallized untwinned albite grains. B. Cpx II recrystallized crystals converted into Amp II, which in turn is converted into actinolite at grain boundaries in the sodic assemblage. C. Andradite intergrown with titanite producing Ca-Fe alteration. D. Magnetite rimmed by a new titanite phase in Ca-Fe-rich zones. E. widespread actinolite formation producing actinolite albitite related to K-Mg alteration. Actnolite replaces Cpx III. F. Abundant biotite precipitated during K-Mg alteration. Biotite is associated with titanite and zircon. G. Widespread allanite and H. epidote (after allanite) replacement at the vicinities of ore-bearing veinlets forming halos of late calcic alteration. I. The infill stage is represented by carbonate and calcopirite.

Uranium mineralization style and ore assemblage: the uranium mineralization at the Gameleira I, Barreiro and Barrinha deposits is dominantly hosted by pyroxene- and actinolite-to biotite albitite bodies, which correspond to the Ca-Fe and K-Mg stages, respectively.

The ore assemblage associated with the Ca-Fe stage occurs as millimetric veinlets concordant with the foliation (Fig. 25A), in which very fine grained (< 5 µm) uraninite + zircon is intergrown with titanite (Fig. 25B). The evolution of ore paragenesis is better

constrained in lower strain regions, where uraninite occurs as rounded, unoriented crystals distributed homogeneously within titanite crystals (Fig. 25C and D). This indicates that uraninite is not an inclusion, but probably was exsolved from the titanite.

The presence of hydrothermal zircon inside veinlets is a remarkable feature of the ore assemblage. The zircon crystals are spatially associated with uraninite, also occurring as intergrowths with titanite (Fig. 25B and D). In general, fine-grained zircon (< 10 μm) occurs as rounded crystals, but zircon also occurs along albite grain boundaries as "gel-like" zircon (Fig. 25E) with uranophane inclusions. In the ore-bearing veinlets, magmatic zircon shows dissolution-reprecipitation textures represented by intense fracturing and microporosity in the core of crystals and overgrowth on the rims. Uranophane or uraninite fill some of these zircon fractures.

In the K-Mg zones, uraninite crystals are coarser (>10 μm) than those filling the veinlets. Uraninite is included in biotite, actinolite, titanite, and carbonate as rounded crystals with pleochroic halos (Fig. 25F). Despite occurring as disseminated crystals throughout the mineral assemblage, the greatest proportion of uraninite is found within titanite crystals.

Uranophane is observed as radial-fibrous crystals with anomalous interference colours, filling the interstitial spaces between actinolite, and along the cleavage planes of biotite and carbonate (Fig. 25G). Uranophane also mimetizes uraninite as rounded, fine-grained crystals included in titanite, zircon, and albite. Rarely, a U-Ti-Ca silicate occurs as inclusions in titanite or filling allanite fractures.

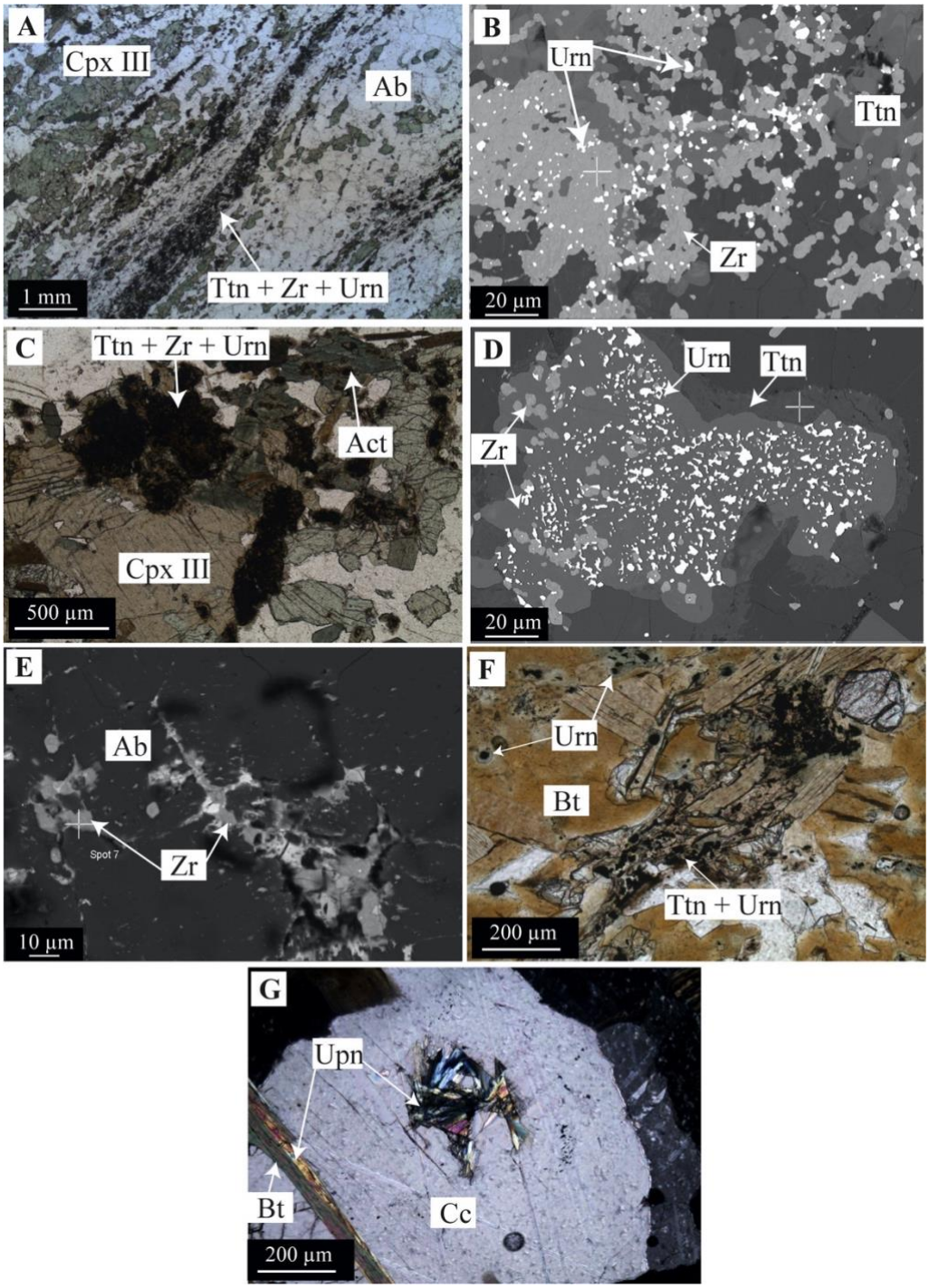

Fig. 25. Transmitted-light photomicrographs, either in plane polarized light (PPL) or cross-polarised light (CPL) and backscattered-eletron image (BSE) of the ore assemblage. A. Typical occurrence of the ore assemblage as veinlets of uraninite, titanite and zircon concordant with the foliation and spatially associated with Cpx III. B. BSE image of the ore assemblage present in the veinlets reveals the strong association of fine-grained uraninite and hydrothermal zircon. C. Outside the veinlets in less foliated portions of the rock, titanite rich in rounded uraninite crystals occurs. Note the strong preference of uraninite by titanite crystals (black spotted regions). D. BSE image of C, which shows

uraninite occurring as inclusions in titanite without orientation suggestive of exsolution. This process is accompanied by hydrothermal zircon precipitation. E. BSE image of the "gel-like" zircon filling grain boundaries of albite. F. Uraninite crystals included in biotite with pleochroic halos, and titanite related to K-Mg zones. Note that uraninite is coarser-grained here than in the veinlets, and despite widespread occurrence, uraninite concentrates preferentially in titanite. G. Uranophane filling biotite and carbonate cleavages.

4.6 GEOCHRONOLOGICAL RESULTS

In order to determine the origin of the albitite rocks and the timing of mineralization we investigated zircon grains of representative barren albitites (samples 3409 and 3510) and zircon, titanite and uraninite grains of mineralized albitites (sample MAAB03, TAR2 and BCAB). The data are listed in Appendix 1 – 1A to 1D.

4.6.1 Zircon U–Pb dating by LA–ICP–MS (barren, garnet albitites)

The barren samples 3409 and 3510, from the Barrinha and Gameleira I deposits respectively, are classified as garnet albitite and were chosen due to their transitional character with respect to the LRIS. This was based on the presence of relict magmatic Amp I and variable amounts of K-feldspar and quartz.

In sample 3409, zircon grains are generally prismatic and elongate (100 – 200 μm in length). CL images reveal homogeneous domains throughout the grains (Fig. 26, analysis SMPAB017), although some grains show dark cores, surrounded by light rims (Fig. 26, analysis SMPABC013). All data are given in Appendix 1A. Twenty-eight analyses were obtained from individual crystals and twenty of them are concordant (99 – 100%). The most concordant analyses yield a concordia age of 1736 ± 4 Ma (MSWD of concordance and equivalence: 0.56, n = 20; Fig. 27A). Six other analyses are discordant (95 – 98%), and two are reversely discordant (102 – 109%). Discordant analyses were mainly obtained from grain rims. Using the free regression function of Isoplot, twenty-six analyses define a discordia line with a calculated upper intercept of 1734 ± 8 Ma and lower intercept age of 914 ± 66 Ma (MSWD of 0.71; Fig. 27A).

Zircon grains in sample 3510 are mostly prismatic and elongate (100 – 200 μm in length). CL images reveal homogeneous domains throughout the grains (Fig. 26, analyses SMPAB048 and SMPAB079). Twenty-seven analyses were obtained from individual crystals, fourteen are concordant (~100%) and thirteen are discordant (94 – 102%).

Discordant points were generally obtained from grain rims. The concordant zircon analyses yield a concordia age of 1729 ± 6 Ma (MSWD of 2.7, *n* = 24; Fig. 27B), and the twenty-three analyses define a discordia line with a calculated upper intercept of 1722 ± 13 Ma and lower intercept age of 826 ± 55 Ma (MSWD of 3.6, *n* = 23; Fig. 27B).

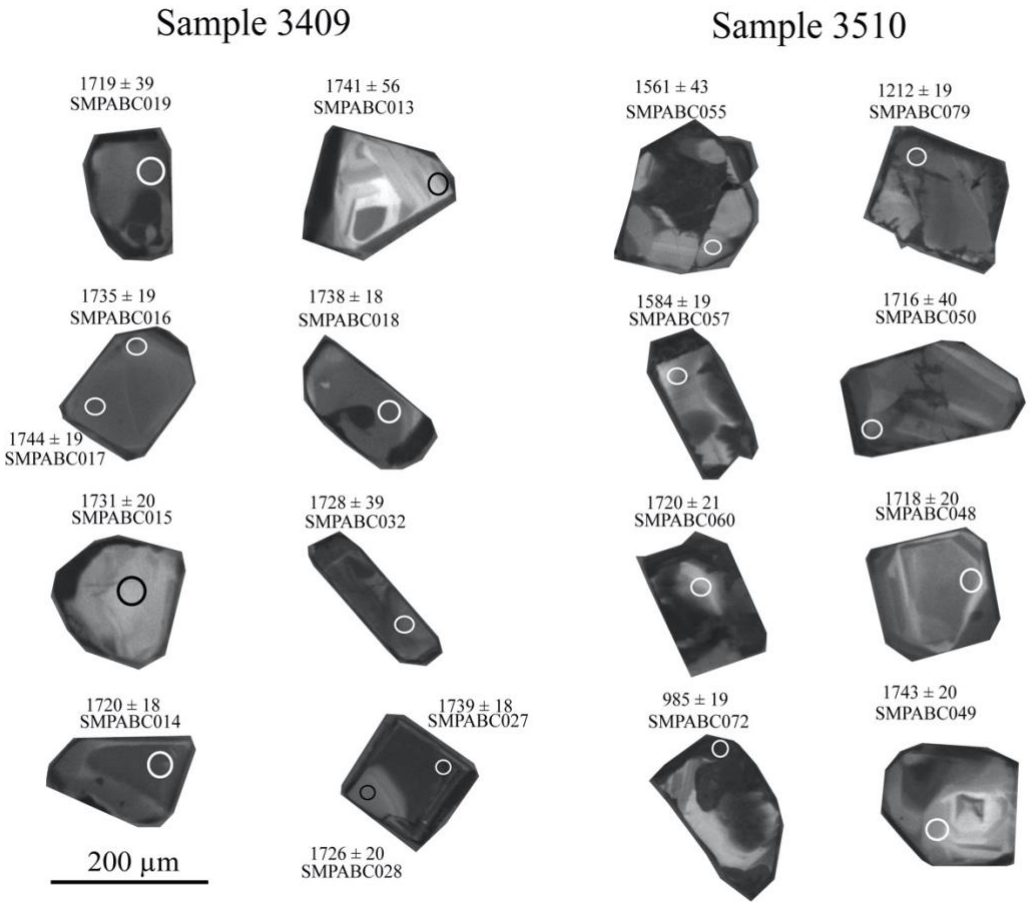

Fig. 26**.** Zircon cathodoluminescence images from samples 3510 and 3409. Analysis numbers and concordia ages age given for each spot in all samples

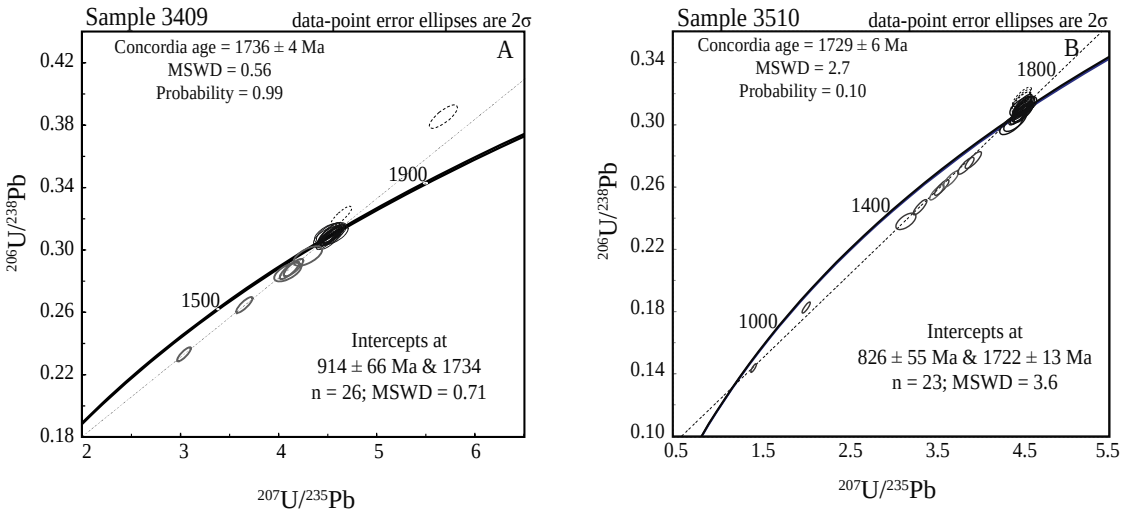

Fig. 27**.** A. Concordia plot for sample 3409 and 3510. Analyses given in black are ~100% concordant and used to produce the concordia age for this sample. Analyses in grey are 98–95% concordant and used along with the black analyses, to calculate the intercept age. The two dashed analyses are reversely discordant and not used in age calculations. B. Concordia plot for sample 3510. Black analyses are again the most concordant and used to calculate the concordia age, grey analyses are less concordant and used to calculate intercept ages and dashed analyses are reversely discordant and not used for age calculations

4.6.2 Zircon U–Pb dating of mineralized albitite by SIMS

Sample MAAB 03 was collected from drill hole F16 at 130 m depth in the Gameleira I deposit and corresponds to a mineralized pyroxene albitite from the Ca-Fe stage. This sample represents one of the typical styles of mineralization in Lagoa Real in which uraninite is concentrated in veinlets that are a few 100-µm wide, in close association with hydrothermal zircon. Uraninite from this sample was also analysed by electron microprobe analysis.

In order to target the age of U mineralization, SIMS analyses of zircon were conducted in situ, on a polished thin section in order to target grains inside the microshear zones (Fig. 25A), and results can be seen in Appendix 1 – 1B. However, the intense fracturing, small size and close association with fine-grained uraninite posed a challenge in carrying out zircon dating. In addition, the presence of fractures and uraninite inclusions were not easy to detect during the selection of spot areas. Fig. 28 shows the nineteen zircon grains analyzed, twelve analyses were made in prismatic grains, six in agglomerated crystals and one in a uraninite grain (Fig. 28G and H). Most of the data are discordant (85 – 118%),

with three analyses being reversely discordant. The primary reasons for discordance are the presence of fractures (i.e. Fig. 28N), or occasional mixed analysis of zircon and uraninite (Fig. 28C, analysis number 3 on Appendix 1 – 1B). The occurrence of mixed analyses is confirmed by the high U contents (11254 – 29911 ppm). In general, U contents are higher than those of zircon from the barren samples described above (3409 and 3510 samples; U = 46 – 642 ppm), but there is no clear relationship between U content and concordance. If the obviously mixed analyses are disregarded, U contents vary between 401 and 6486 ppm.

Three analyses are 100% concordant and have calculated $^{207}Pb/^{206}Pb$ ages of 1680 ± 13, 1264 ± 41 and 1179 ± 27 Ma. The location of these spots in the grains indicates that the ages of 1680 Ma (Fig. 28L) and 1264 Ma (Fig. 280G, H) may correspond to mixed analyses as they appear to be close to cracks, and only the 1179 ± 27 Ma age may be geologically significant.

The oldest obtained ages are indicated by analyses 5-5@3 and 5-20@1 with $^{207}Pb/^{206}Pb$ ages of 1707 ± 16 and 1742 ± 15, respectively. An age of ~1720 Ma is also observed as the upper intercept of the concordia plots (Fig. 29A and B).

The youngest obtained age is that which sampled uraninite. The U–Pb calibration based on RM zircon 91500 does not apply to uraninite. Therefore, both its U–Pb ages and U concentrations cannot be taken at face value, for example, the unrealistically high U concentration of 1153715 ppm = 115 %. However, there is a Zr signal in the analytical data of Area5-13-U@1, indicating that some zircon was co-analyzed with the uraninite. Two cases are possible: (i) The concurrently analyzed zircon stems from the rim. In this case, the 582 Ma $^{207}Pb/^{206}Pb$ age of the uraninite was not affected and, thus, represents a best-age estimate; (ii) The co-analyzed zircon stems from the old, central part with an age of at least 1264 Ma. In this case the $^{207}Pb/^{206}Pb$ age of the uraninite may theoretically be too old and would have to be corrected for the zircon contribution. Because of the drastic differences in U content between uraninite and zircon, less than 0.1 per mil of the radiogenic Pb is contributed by the zircon, meaning that the $^{207}Pb/^{206}Pb$ age of 582 ± 5 Ma is a good approximation of the age of uraninite crystallization. A young age of around 580 Ma is also supported by the lower discordia intercepts at 524, 560 and 615 Ma, respectively, in the zircon concordia plots (Fig. 29A, B, C). Note that the position of the discordia strongly depends on the data points included and that the intercepts have large errors of nearly 40%. The presented concordia plots include only the discordant data.

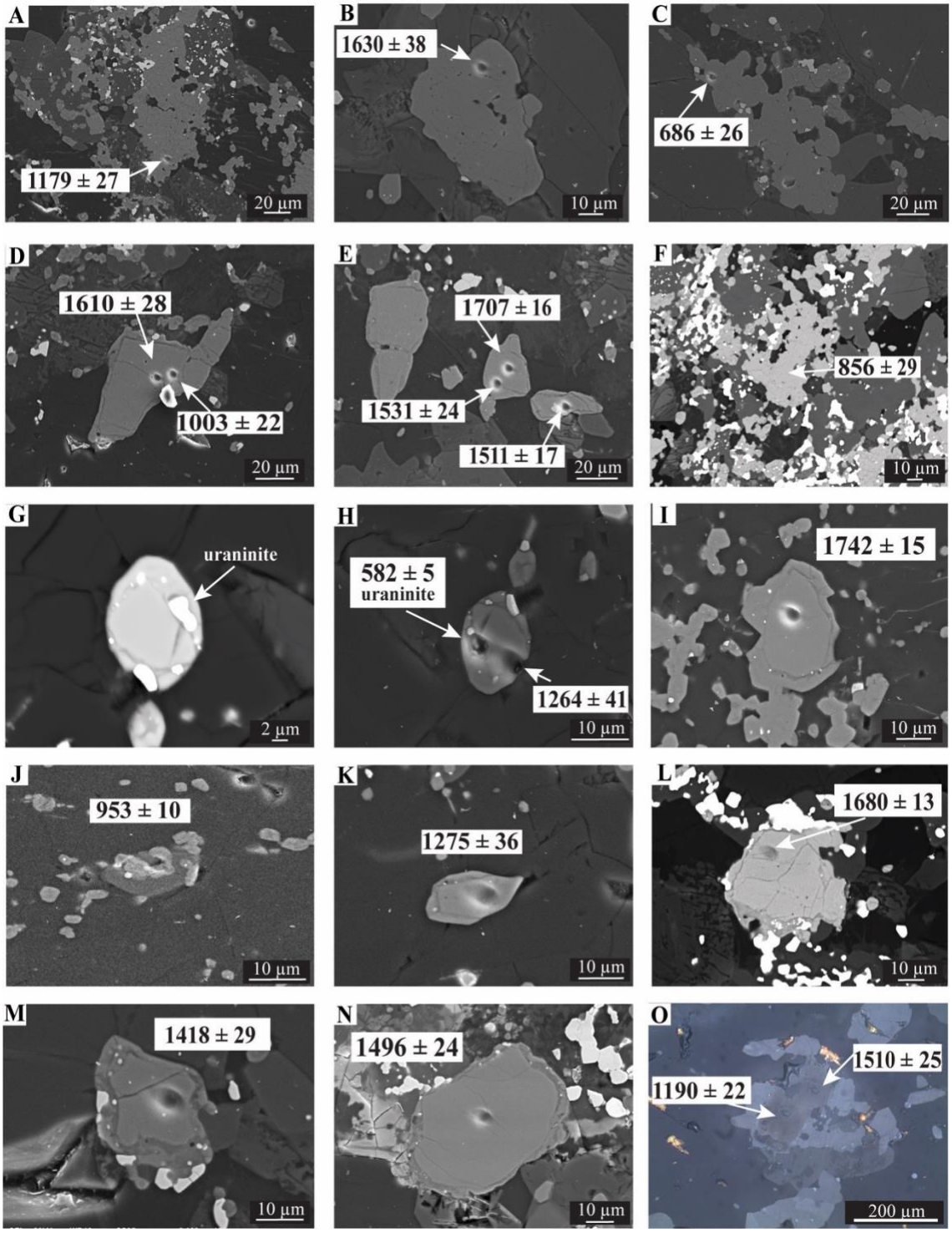

Fig. 28. Photomicrography, Secondary-electron image (SE) and backscattered-eletron image (BSE) of zircon crystals analysed by SIMS (sample MAAB03). The ages given are $^{207}Pb/^{206}Pb$ ages. A, B, C, D, E, I, J, K, M, N) SE image; F, G, H, L) BSE image and O) reflected-light photomicrograph in plane polarized light (PPL)

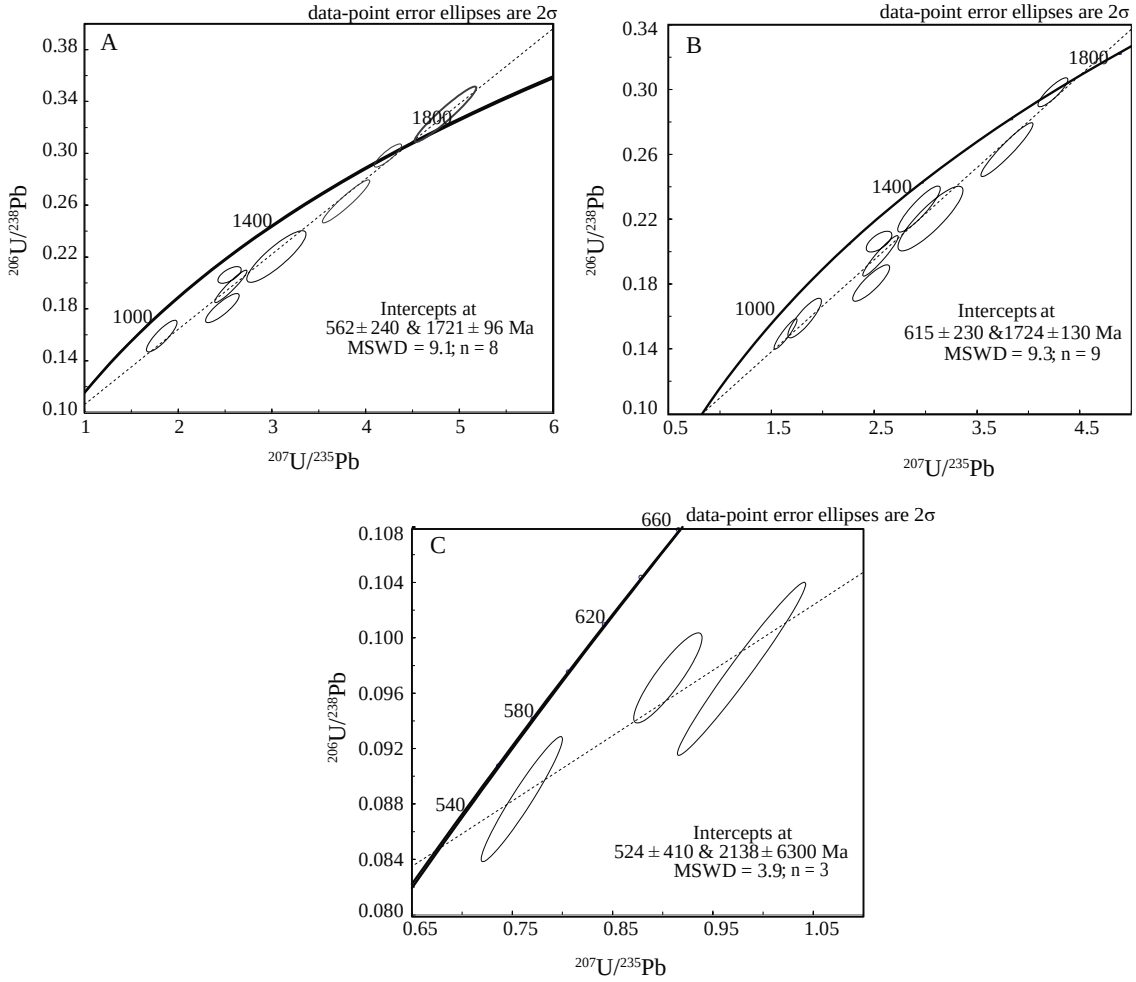

Fig. 29. Concordia plots of U–Pb data in sample MAAB03. A, B and C shows different concordia plots with lower intercept around 500 and 600 Ma depending on which data are plotted

4.6.3 Titanite dating by LA–ICP–MS – mineralized albitite

Sample TAR2, taken from the distal drill hole (F10) of the Gameleira I deposit, is a pyroxene albitite from the Ca-Fe stage. Similarly to sample MAAB03, this sample was selected because it represents the main style of mineralization, with uraninite occurring as veinlets. In this sample, titanite has inclusions of, and is intergrown with, uraninite and uranophane, and was investigated by LA-ICP-MS.

Titanite crystals are anhedral, intensely fractured and corroded, and up to 200 µm in size. BSE images reveal mostly homogeneous domains throughout the grains and the ubiquitous presence of uraninite inclusions.

Results are shown in Appendix 1 – 1C. Eighteen crystals were analyzed in sample TAR2. Eleven analyses are strongly discordant (58 – 516%) and eight analyses have concordance between 95 – 104%. Uranium and Pb contents are highly variable (U = 7 –

296 ppm; Pb = 7 – 189 ppm), and this variability is not related with discordance, but with age. Three concordant analyses (97 – 100%) have ages of 1461 ± 13, 2069 ± 23 and 2244 ± 14 Ma and five spot analyses (91 – 104% of concordance) give a weighted $^{207}Pb/^{206}Pb$ mean age of 1165 ± 21 Ma (MSWD of 1.6; Fig. 30).

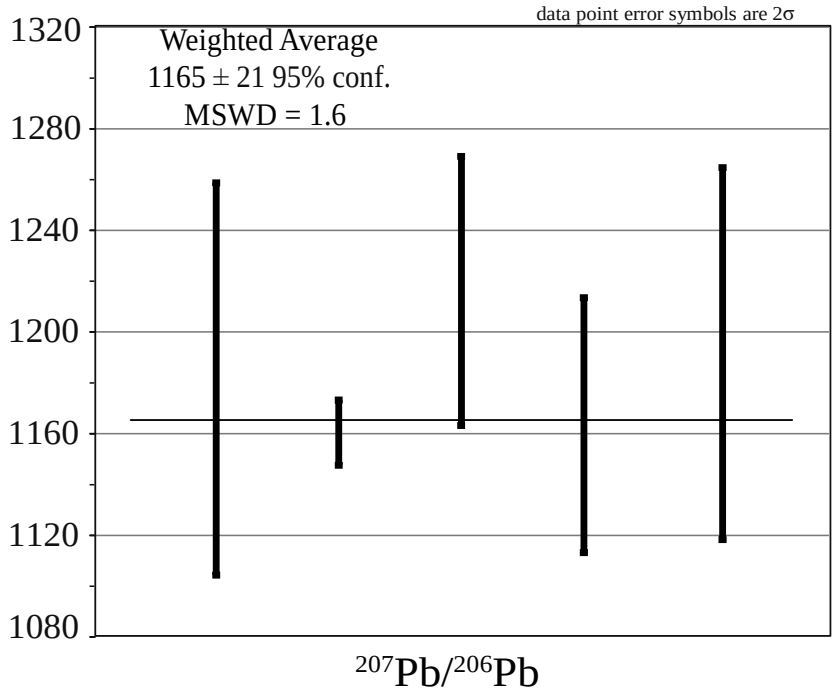

Fig. 30**.** Weighted average results for five concordant analyses of titanite (sample TAR2)

4.6.4 Uraninite chemical dating

Sample BCAB, collected from drill hole F16 at 145 m depth, of the Gameleira I deposit, is a biotite albitite. This rock contains biotite, albite, titanite and calcite, and represents the other mineralization style in which uraninite is associated with the K-Mg stage, and included in biotite, titanite and calcite. Uraninite in this sample, and sample MAAB03, were analyzed for major elements in order to obtain chemical ages. Electron-microprobe analyses are reported in Appendix 1 – 1D. The most remarkable chemical difference between the two occurrences of uraninite is related to the Y_2O_3 contents. Sample MAAB03 has between 1.62 to 3% of Y_2O_3, while in sample BCAB the values are between 0.4 and 0.8%. Despite variable contents of minor elements such as CaO and Y_2O_3, there is no discernible correlation between $\Sigma CaO + FeO + Al_2O_3 + SiO_2 + Y_2O_3$ and PbO or UO_2 (Fig. 31), indicating that these minor elements are most likely primary and do not affect the calculation of chemical ages. Chemical ages are similar for both samples and

are between 0.56 Ga and 0.48 Ga (average: 0.52 Ga; *n* = 7) for sample MAAB03, and between 0.55 Ga and 0.49 Ga (0.53 Ga on average *n* = 21) for sample BCAB.

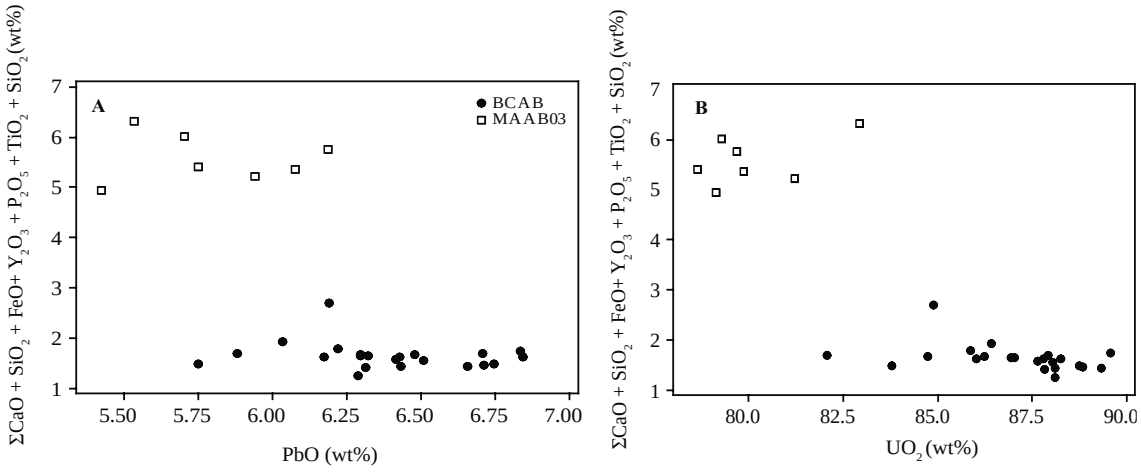

Fig. 31**.** Biplot of main chemical trends in uraninite. A. Sum of concentrations of variable elements in uraninite plotted *versus* PbO concentrations B. Sum of concentrations of variable elements in uraninite plotted *versus* PbO UO_2 concentrations. Note that there is any correlation between PbO, UO_2 and the other elements showing that uraninite was not submitted to U or Pb loss. The two different groups are differentiated by Y_2O_3. See text for more information.

4.7 DISCUSSION

4.7.7 Origin of albitite and age of mineralization

The history of geochronological studies in Lagoa Real is summarized in **Table 2**, with the investigations of Turpin et al. (1988) and Cordani et al. (1992) being first to attempt to constrain the age of granite emplacement, U deposition and metamorphism.

Table 2: Published geochronological data for the Lagoa Real Province. 1: Turpin et al. (1988); 2: Cordani et al. (1992), 3: Chaves et al. (2007) 4: Chaves. (2009) 5: Lobato et al. (2015); 6: Amorim et al. (2020).

Rock unit	Material	Method	Age	Reference
Basement				
Basement gneiss and migmatite	whole rock	Rb–Sr	2650 ± 100 (i. r. ¼ 0.712)	2
Basement gneiss and migmatite	biotite	K–Ar	538	2
Migmatite	amphibole	K–Ar	491	2
Charnockite	zircon	U–Pb	2047 ± 5	4
Lagoa Real suite intrusive				
Granitic rocks				
São Timóteo granite	zircon	U–Pb	1724 ± 5	1
São Timóteo granite	whole rock	Pb–Pb	1706 ± 107	2
São Timóteo granite	whole rock	Rb–Sr	1710 ± 45 (i. r. ¼ 0.7135)	2
São Timóteo granite	biotite	K–Ar	573	2
Lineated granite	whole rock	Rb–Sr	1280 ± 20 (i. r. ¼ 0.775)	2
Gneiss	whole rock	Rb–Sr	1629 ± 30 (i. r. ¼ 0.7104)	1
Orthogneiss	whole rock	Rb–Sr	1000 ± 60 (i. r. ¼ 0.722)	2
Orthogneiss	whole rock	Rb–Sr	1220 ± 130 (i. r. ¼ 0.723)	2
Gneiss	amphibole	K–Ar	503	2
São Timóteo granite	zircon	U–Pb	1746 ± 5	5
Albitized orthogneiss	whole rock	Rb–Sr	1520 ± 20 (i. r. ¼ 0.7221)	2
São Timóteo granite	zircon	U–Pb	1741 ± 4	6
Charnockite	zircon	U–Pb	1746 ± 5	6
Juazeirinho granite	zircon	U–Pb	1755 ± 5	6
Lagoa do Barro granite	zircon	U–Pb	1762 ± 9	6
Albitized gneiss	zircon	U–Pb	1740 ± 6 and 1742 ± 4	6
Albitite				
Albitite	Acid-soluble fractions of whole-rock, heavy mineral, and uraninite concentrate	U–Pb	1397 ± 9	1
Mineralized albitite	zircon	U–Pb	1744 ± 4	5
Mineralized albitite	titanite	U–Pb	956 ± 9	5
Mineralized albitite	titanite	U–Pb	384 ± 100	5
Metamorphosed syenite*	uraninite	U–Pb	605 ± 70	3
Metamorphosed syenite*	titanite	EMPA	2052 ± 80; 1701 ± 57;1488 ± 64; 1298 ± 69; 1108 ± 78; 978 ± 50	4
Metamorphosed syenite*	uraninite	EMPA	489 ± 7	4

* here refered as albitite

The LRIS, commonly referred to as the São Timóteo granite, are the most well understood rocks regarding their ages in Lagoa Real (Turpin et al., 1988; Cordani et al., 1992; Lobato et al., 2015; Amorim et al., 2020). According to these authors, the São Timóteo granite was emplaced at ca. 1.74 Ga, as a result of a rifting event, which produced acid-to-mafic magmatism in the southern, central and northern Espinhaço rift system. This event resulted in the deposition of the Espinhaço Supergroup as well. On the other hand, the age of U deposition and hydrothermal alteration are still controversial, ranging between roughly 1.9 and 0.5 Ga (Turpin et al., 1988, Cordani et al., 1992; Lobato et al., 2015; Chaves et al., 2007, 2009). This huge age range is mainly due to two factors: (i) the previously obtained data utilized unsuitable methods for such complex rocks, i.e. U–Pb in acid-soluble fractions derived from heavy-mineral concentrates, which produces mixed ages; ii) and the significant degree of U and Pb disturbance in both, zircon and titanite analyses (Lobato et al., 2015; present work), due to metasomatism and metamorphism. The consequence of these factors is a plethora of different genetic models for Lagoa Real with variable timing for ore deposition ranging from the Mesoproterozoic to the Ediacaran (**Table 2**, and references therein).

Initially, the albitites that host the Lagoa Real U deposits were considered to have formed as a result of metasomatic transformation of a magmatic rock. This suggestion was based mainly on field observations and genetic models of Ukrainian deposits, since no geochronological data were obtained (Brito et al., 1984; Raposo et al., 1984). This relationship was further developed following the work of Turpin et al. (1988) and Cordani et al. (1992), which were based on whole-rock Rb–Sr data and U–Pb analyses of acid-soluble fractions that produced intermediary ages, between 1.7 Ga and 570 Ma, for the albitites (**Table 2**). Lobato et al. (2015) reinvigorated the discussion by publishing U–Pb ages obtained by ID-TIMS from zircon in albitite that produced an upper intercept age of 1744 ± 4 Ma.

In our study, the two barren albitite samples 3409 and 3510 produced comparable concordia ages of 1736 ± 4 Ma and 1729 ± 6 Ma, respectively. In contrast, the zircon from the mineralized sample displays a wide range of apparent U–Pb ages. The oldest age obtained (with the smallest error) was also ca. 1740 Ma (Fig. 28I, analysis area5-20@1), with the SIMS analysis targeting the core of a ~40 µm zircon grain, yielding a $^{207}Pb/^{206}Pb$ age of 1742 ± 6 Ma, in good agreement with the São Timóteo emplacement ages published by Turpin et al. (1988; 1724 ± 5, U–Pb zircon), Cordani et al. (1992; 1710 ± 45, Rb–Sr whole rock), more recently by Lobato et al. (2015; 1746 ± 5, U–Pb zircon)

and Amorim et al. (2020; 1741 ± 4, U–Pb zircon). Therefore, the age of ca. 1.74 Ga obtained here from both the barren and mineralized albitite rocks indicates that the São Timóteo granite is the protolith of the albitite. This is strongly supported by the field relationships described in Cruz et al. (2007), showing that the metasomatic bodies are interlayered with the granite-gneiss rocks of Lagoa Real. The presence of transitional rocks with intermediate composition between granite-gneiss and albitite are also observed by this work and previously by Maruejol (1988) and Lobato and Fyfe (1990). The paragenetic sequence presented in Figure 5, and the geochemical trends (Lobato and Fyfe., 1990; Santos et al., 2020) also show that the metasomatism was accompanied mainly by SiO_2 and K_2O loss and Na enrichment, which is further support for the São Timóteo granite as the protolith of the albitite. Stein et al. (1980) determined the U–Pb age of uraninite grains extracted from ore samples at ca. 820 Ma, which they assigned to a stage of metasomatism and U remobilization. More recently, Lobato et al. (2015) obtained an upper intercept age of 956 ± 59 Ma based on TIMS U–Pb analyses of dissolved U-enriched titanite fractions from one sample of mineralized garnet-bearing albitite, and interpreted this as the age of hydrothermal alteration and U deposition. Lobato et al. (2015) argued that the high U contents of the titanite would indicate the age of U mineralization.

The present work shows lower intercept ages of 914 ± 66 Ma and 826 ± 55 Ma in the barren albitite from two different anomalies (samples 3409 and 3510; Fig. 27). These ages are within error similar to those reported by Lobato et al. (2015). However, in our study they are observed in the barren rocks. The occurrence of these similar ages in both mineralized and barren samples likely represents partial re-homogenization by the Brasiliano tectonothermal event (580 – 490 Ma). Similarly, the age of 1179 ± 27 Ma obtained by SIMS in zircon and the 1165 ± 21 Ma age obtained from titanite in sample TAR2 may be the result of U and Pb remobilization/enrichment.

Intermediate ages, between 1.74 Ga and the 0.58–0.49 Ga Araçuaí orogeny, are frequently observed in the metasomatized rocks of Lagoa Real. Cordani et al. (1992) reported several whole-rock Rb–Sr isochrons displaying ages of ca. 1520 Ma, 1280 Ma, 1220 Ma and 1000 Ma from albitized gneiss and albitite. Chaves et al. (2009) also reported five groups of chemical ages obtained in ore-related titanite (see **Table 2**). However, all these intermediate ages obtained before (Cordani et al., 1992; Chaves et al., 2009; Lobato et al., 2015) and the 1179 ± 27 Ma age obtained in this work are not random. They are synchronous with tectonic events that took place in the Paramirim Aulacogen,

which records several extensional events during its 1.1 Ga existence (see Cruz and Alkmim, 2017). The age of 1520 Ma (Cordani et al., 1992), for example, is coeval with 1.5 Ga acid magmatism that intruded the Espinhaço Supergroup (Babinski et al., 1999; Silveira et al., 2013). The 1179 Ma age is chronocorrelated with the 1140 ± 140 Pb-Pb carbonate ages of the Caboclo Formation (Babinski et al., 1993), which is interpreteted to be the age of reactivation and expansion of the Chapada Diamantina basin represented by deposition of the uppermost Espinhaço Supergroup (Chapada Diamantina group) rift-sag sequence (Pedrosa Soares et al., 2001; Chemale-Júnior et al., 2010; 2011). Ages between ca. 957 Ma and 850 Ma (ca. 960 Ma; Lobato et al., 2015; this work) record the initiation of the Santo Onofre–Macaúbas rift system, which is the precursor to the Araçuaí–West-Congo orogen, and the related mafic to felsic magmatism recorded in several regions of the São Francisco craton and Araçuaí–West-Congo orogen (Machado et al., 1989; Silva et al., 2008; Kuchenbecker et al., 2015; Alkmim et al., 2006, 2017; Menezes et al., 2012 ; Bitencourt et al., 2019).

This spread in geochronological data, suggests that movement of fluids in Lagoa Real is potentially related to multiple tectonic events that occurred in the Paramirim Aulacogen.

The SIMS analysis of uraninite obtained in this study produced an age of 582 ± 5 Ma and chemical EPMA dating of uraninite from two mineralized samples gave slightly younger average ages of 530 to 520 Ma (Appendix 1 – 1D). Overall, these results suggest that a U concentration event occurred in Lagoa Real at ca. 580–520 Ma, during the Brasilian-Pan African orogeny. This is also supported by the lower intercept ages from hydrothermal zircon in the mineralized sample, which are in the range of 615 – 524 Ma (Fig. 29). In addition, the high Y contents in uraninite are a typical characteristic of high-temperature (> 350 ºC, i.e. syn-metamorphic) uraninite (Mercadier et al., 2011; Eglinger et al., 2013, Frimmel et al., 2014). The Y contents indicate the presence of two uraninite groups in Lagoa Real: i) sample MAAB03 corresponds to veinlet-related uraninite (Fig. 25A), which has up to 1.6 wt% of Y_2O_3; and ii) sample BCAB where uraninite has Y_2O_3 < 0.8 wt%, is widespread and included in the late-stage assemblage (Fig. 25F). Despite both having high Y contents, similar to uraninite precipitated at elevated temperatures, the different Y contents may show that the early-stage, higher-Y uraninite was precipitated at higher temperatures than the later, low-Y uraninite, which potentially corresponds to lower T precipitation or redistribution during a late-stage process.

The intermediate ages (1740–490 Ma) consistently observed in the albitite rocks, especially those observed in titanite-related uraninite (this work; Chaves et al., 2007; 2009; Lobato et al., 2015), coupled with the uraninite data show that the Lagoa Real uranium mineralization is a product of successive episodes of crustal fluids induced metasomatism, influenced by rift events that took place in the Paramirim Aulacogen.

This is in agreement with the metallogenetic concept of "étagement temporel" (temporal superposition) proposed by Routhier (1967). In this concept, specific metals are repeatedly concentrated in the same area by different geological processes and at different times. However, in Lagoa Real it is not clear if most of the ore formed during one or more of the earlier events and experienced remobilization during subsequent hydrothermal events concluding with the Brasiliano-Pan African orogeny, or whether the ore formed through progressive episodic upgrading over 1.1 billion years reaching its maximum during the Brasiliano-Pan African event.

Therefore, our data support the idea that albitite corresponds to metasomatically altered São Timóteo granite, part of the Lagoa Real intrusive suite that was emplaced at ca. 1.74 Ga. Ore genesis probably is the consequence of cryptic and multiple episodes of uranium mineralization and remobilization related to tectonic events that occurred in the Paramirim Aulacogen, which ended between 580 to 520 Ma, synchronous with the Brasiliano-Pan African orogeny.

4.7.2 Uranium-mineralization episode and related geodynamic events in the Araçuaí orogen

In the Araçuaí orogen, the time interval of 580 to 520 Ma is marginally coincident with the 630–580-Ma Rio Doce magmatic arc, as documented by Lima et al. (2002) and Tedeschi et al. (2016). This corresponds to calcic-alkaline plutons with a pre-collisional volcanic arc signature. This range is also coincident with the lower interval of the 575–565 Ma event that represents the time of the largest production of syn-collisional crustal melts in the Araçuaí orogeny – i.e., leucogranites of the G2 granite supersuite (Gradim et al., 2014; Melo et al., 2017; Pedrosa-Soares et al., 2011a, 2011b; Peixoto et al., 2015; Richter et al., 2016). The age of 575 Ma likely records the climax of the syn-kinematic metamorphic event (Alkmim et al., 2017).

The Brazilian portion of the Araçuaí-West Congo Orogen records a massive circulation of magmatic/hydrothermal fluids related to its extensional collapse phase. This process was responsible for important ore deposits such as the giant Eastern

Brazilian Pegmatite Province (Pedrosa-Soares et al., 2011b), Au mineralization in the Southern Espinhaço Range and in the Quadrilátero Ferrífero (Cabral et al., 2013; Cabral and Zeh, 2015), and several meter to kilometer-scale quartz veins (Scholz et al., 2012, Gonçalves et al. 2019). Recently, Gonçalves et al. (2019) targeted hydrothermal minerals from quartz veins crosscutting rocks of the southern Serra do Espinhaço and the Araçuaí belt (south of the region investigated here), in order to determine the time interval of this widespread post-orogenic hydrothermal mineralization. The results of U–Pb dating of monazite, rutile and xenotime produce ages in the range of 515 to 495 Ma, which is in agreement with the ages of the main ore deposits in the AWCO and Southern Espinhaço (Pedrosa-Soares et al., 2011b; Scholz et al., 2012, Cabral et al., 2013; and Cabral and Zeh., 2015). This time interval is related to the extensional collapse of the Araçuai orogeny and multi-sourced fluid production from deep to shallow crustal levels that resulted in significant mineralization and affected an area of more than 400,000 km^2 along the eastern border of the São Francisco craton.

The interval between 580–495 Ma corresponds to a period of intense regional magmatic and metamorphic activity during the AWCO, the final stages of which resulted in widespread mineralization along the eastern border of the São Francisco craton and probably influenced the creation of Lagoa Real as an economic deposit either as the source of fluids, or of heat.

4.7.3 Uranium deposits related to the Brasiliano–Pan-African event

The class of U deposits known as the albitite-type (Wilde, 2013), or Na-metasomatism deposits (Cuney & Kyser, 2008), which include Kirovograd (Ukraine), Michelin (Canada), and Valhalla (Australia), along with the Lagoa Real deposits, have been linked to a global 1.8–1.5 Ga orogenic event by Wilde (2013) and Cuney (2010). These authors included the Lagoa Real province in this global context based on the data presented by Cordani et al., (1992) and Turpin et al., (1988).

In the context of Western Gondwana, Cuney (2010) also pointed out U deposits associated with the timing of the Brasiliano–Pan African orogeny that had resulted from the amalgamation of Gondwana. Examples of these include the São José de Espinharas and Itataia deposits, both in Brazil, in the Borborema Province (north of the study area), in addition to the Kitongo deposit, in the Central African fold belt. These deposits are associated with syn-orogenic magmatism between 0.59 to 0.47 Ga (Barbosa, 2012; Kouske et al., 2012; Veríssimo et al., 2016; Olivier et al., 2020). Eglinger et al. (2016)

correlated dozens of U occurrences in the Lufilian orogenic belt, Zambia, with the Brasiliano event. These are associated with periods of syn-orogenic burial to syn-orogenic exhumation at 0.54 to 0.53 Ga. Our data suggest that Lagoa Real should be included in this scenario, together with the aforementioned U deposits. This also highlights the importance of the Brasiliano event for the genesis of U deposits during the amalgamation of Gondwana.

4.8 CONCLUSIONS

The results of this study show that albitites, which host the U ore in Lagoa Real, are metasomatically altered granitic rocks that crystallized at ca. 1.74 Ga. This transformation was developed through sodic, calcic-ferric, potassic-magnesian and late calcic metasomatism, which resulted in uraninite precipitation associated with titanite and zircon. Ore genesis is the result of a 1.1 Ga long-lived process that involved multi-stage episodes of uranium mineralization and remobilization that ended between 580 to 520 Ma during the Brasiliano orogeny. This finding contrasts with previous studies, which suggested the U deposition event occurred as the result of a single event at 1.4 Ga (Turpin et al., 1988), between 1.5 Ga to 1.2 Ga (Cordani et al., 1992), at 1.8 Ga (Chaves, 2013) or at 960 Ma (Lobato et al., 2015). The construction of Lagoa Real as an economic uranium deposit is probably linked to the widespread multi-sourced fluid-flow event produced during the extensional collapse of the Araçuaí orogeny.

Similar to Lagoa Real, other uranium deposits occur in Western Gondwana linked to the Brasiliano–Pan-African orogeny. Taken together, these deposits highlight the importance of the Brasiliano–Pan-African event in the context of uranium deposits worldwide.

4.9 REFERENCES

Alkmim, F.F., Marshak, S., Pedrosa-Soares, A.C., Peres, G.G., Cruz, S.C.P., Whittington, A., Carlos Pedrosa-Soares, A., Gravina Peres, G., Cruz, S.C.P., Whittington, A., 2006. Kinematic evolution of the Araçuaí-West Congo orogen in Brazil and Africa: Nutcracker tectonics during the Neoproterozoic assembly of Gondwana. Precambrian Research 149, 43–64. https://doi.org/10.1016/j.precamres.2006.06.007

Alkmim, F.F., Brito Neves, B.B. de, Alves, J.A.C., 1993. Arcabouço tectônico do Cráton do São Francisco: uma revisão, in: Dominguez, J.M., Misi, A. (Eds.), O Cráton Do São Francisco. Sociedade Brasileira de Geologia, Salvador, pp. 45–62.

Alkmim, F.F., Pedrosa-Soares, A.C., Noce, C.M., Cruz, S.C.P., 2006. Sobre a Evolução Tectônica do Orógeno Araçuaí-Congo Ocidental. Geonomos 15, 25–43.

Alkmim, F.F., Kuchenbecker, M., Reis, H.L.S., Pedrosa-Soares, A.C., 2017. The Araçuaí Belt, in: São Francisco Craton, Eastern Brazil. Springer, pp. 255–276.

Amorim, L.E.D., Rios, F. J., Freitas, M. E., Cutts, K., Geraldes, M. C., Diniz, A. C. D., Matos, E. C. 2020. Zircon U-Pb geochronology of Paleoproterozoic Statherian intraplate A-Type magmatic associations of the Lagoa Real Uranium Province, São Francisco Craton (Bahia, Brazil). Journal of South American Earth Sciences. submitted.

Arcanjo, J.B.A., Martins, A.M., Loureiro, H.C., Delgado, I.M., Souza, J.D., Neves, J.P., Oliveira, J.E., Teixeira, L.R., Varela, P.H., Gomes, R.D., 2005. Vale do Paramirim, Bahia: Geologia e recursos minerais. Série Arq. Abertos 22.

Babinski, M., Pedrosa-Soares, A.C., Trindade, R.I.F., Martins, M., Noce, C.M., Liu, D., 2012. Neoproterozoic glacial deposits from the Araçuaí orogen, Brazil: Age, provenance and correlations with the São Francisco craton and West Congo belt. Gondwana Res. 21, 451–465. https://doi.org/10.1016/j.gr.2011.04.008

Babinski, M., Van Schmus, W.R., Chemale Jr, F., 1999. Pb–Pb dating and Pb isotope geochemistry of Neoproterozoic carbonate rocks from the São Francisco basin, Brazil: implications for the mobility of Pb isotopes during tectonism and metamorphism. Chem. Geol. 160, 175–199.

Babinski, M., Van Schmus, W.R., Chemale Jr., F., Brito Neves, B.B., Rocha, A.J.D. 1993. Idade isocrônica Pb/Pb em rochas carbonáticas da Formação Caboclo em Morro do Chapéu. In: Pedreira, A.J., Misi, A., Dominguez, J.M.L. (eds.), II Simpósio sobre o Craton do São Francisco. Brazilian Geological Society, Salvador, p. 160–16

Barbosa, B.M. de A., 2012. Estudo do potencial mineral para U-ETR com base na geoquímica e química mineral do Depósito Uranífero de São José de Espinharas (PB). Dissertação de Mestrado. Universidade Federal de Pernambuco.

Bastos-Leal, L.R., Teixeira, W., Cunha, J.C., Leal, A.B.M., Macambira, M.J.B., Rosa, M.L.S., 2000. Isotopic signatures of paleoproterozoica granitoids of the Gavião

block and implications for the evolution of the São Francisco craton, Bahia, Brazil. Rev. Bras. Geociências 30, 66–69.

Bastos-Leal, L.R., Teixeira, W., Cunha, J.C., Macambira, M.J.B., 1998. Archean tonalitic-trondhjemitic and granitic plutonism in the Gavião block, São Francisco Craton, Bahia, Brazil: Geochemical and geochronology characteristics. Rev. Bras. Geociências 2, 209–220.

Bitencourt, C.N., Cruz, S.C.P., dos Anjos Cruz, V., Pedrosa-Soares, A.C., Paquette, J.L., Alkmim, A.R., Barbosa, J.S.F., 2019. Rifting events in the southern sector of the Paramirim Aulacogen, NE Brazil: New geochronological data and correlations for the São Francisco–Congo paleocontinent. Precambrian Res. 326, 417–446. https://doi.org/10.1016/j.precamres.2018.12.005

Brito, W., Raposo, C., Matos, E.C. De, 1984. Os albititos uraníferos de Lagoa Real, in: Anais do XXXIII Congresso Brasileiro de Geologia, Rio de Janeiro, 1984.

Cabral, A.R., Zeh, A., 2015. Detrital zircon without detritus: a result of 496-Ma-old fluid–rock interaction during the gold-lode formation of Passagem, Minas Gerais, Brazil. Lithos 212–215, 415–427. https://doi.org/10.1016/j.lithos.2014.10.011.

Cabral, A.R., Eugster, O., Brauns, M., Lehmann, B., Rosel, D., Zack, T., de Abreu, F.R., Pernicka, E., Barth, M., 2013. Direct dating of gold by radiogenic helium: Testing the method on gold from Diamantina, Minas Gerais, Brazil. Geology 163–166

Chaves, A. O., Tubrett, M., Rios, F. J., Oliveira, L. A., Alves, J. V., Fuzikawa, K., Neves, J. M., Matos, E. C., Chaves, A. M. D. V., Prates, S. P., 2007. U-Pb ages related to uranium mineralization of Lagoa Real, Bahia-Brazil: tectonic implications. Revista de Geologia, 20(2), 141-156.

Chaves, A. O., Tubrett, M., Avelar, S. C., Rios, F. J., Sgarbi, G. N., Neves, J. M., Alves, J. V., Fuzikawa, K., Matos, E. C., Prates, S. P., 2009. Electron microprobe chemical U-Th-Pb and La-ICP-MS U-Pb dating of multiple hydrothermal and metamorphic events recorded in minerals of the Lagoa Real uraniferous albitites (Brazil). Pesquisas em Geociências, 36(2), 181-201.

Chaves, A. de O., 2013. New geological model of the Lagoa Real uraniferous albitites from Bahia (Brazil). Cent. Eur. J. Geosci. 5, 354–373. https://doi.org/10.2478/s13533-012-0134-7

Chemale-Júnior. F., Dussin I.A., Martins M.S., Alkmim F.F., Queiroga G., 2010. The Espinhaço Supergroup in Minas Gerais: A Stenian Basin? In: 7th South American Symposium on Isotope Geology, Brasília, p. 552-555.

Chemale-Júnior F., Dussin I., Alkmim F., Martins M.S., Queiroga G., Armstrong R., Santos M. 2011. Unravelling a Proterozoic basin history through detrital zircon geochronology: The case of the Espinhaço Supergroup, Minas Gerais, Brazil, Gondwana Research, doi: 10.1016/j.gr.2011.08.016.

Cordani, U.G., Iyer, S.S., Taylor, P.N., Kawashita, K., Sato, K., McReath, I., 1992. Pb-Pb, Rb-Sr, and K-Ar systematics of the Lagoa real uranium province (south-central Bahia, Brazil) and the Espinhaço Cycle (ca. 1.5-1.0 Ga). J. South Am. Earth Sci. 5, 33–36.

Cordani, U.G., Sato, K., Marinho, M.M., 1985. The geologic evolution of the ancient granite-greenstone terrane of central-southern Bahia, Brazil. Precambrian Res. 27, 187–213.

Costa, P.H.O., Andrade, A.R.F., Lopes, G.A., Souza, S.L., 1985. Projeto Lagoa Real: mapeamento geológico 1:25000, textos e mapas. Companhia Baiana de Pesquisa Mineral-CBPM/ Empresas Nucleares Brasileiras (NUCLEBRAS), Salvador.

Cruz, S.C.P., Alkmim, F.F., 2017. The Paramirim Aulacogen, in: Heilbron, M., Cordani, U.G., Alkmim, Fernando F. (Eds.), São Francisco Craton, Eastern Brazil: Tectonic Genealogy of a Miniature Continent, Regional Geology Reviews. Springer International Publishing, Cham, p. 326. https://doi.org/10.1007/978-3-319-01715-0

Cruz, S.C.P., Alkmim, F.F., 2007. A história de inversão do aulacógeno do Paramirim contada pela sinclinal de Ituaçu, extremo sul da Chapada Diamantina (BA). Revista Brasileira de Geociências. 37, 92–110.

Cruz, S. C. P., Alkmim, F. F. D., Leite, C. M. M., Evangelista, H. J., Cunha, J. C., Matos, E. C., Noce, C. M., Marinho, M. M., 2007. Geologia e arcabouço estrutural do Complexo Lagoa Real, Vale do Paramirim, Centro-Oeste da Bahia. Revista Brasileira de Geociências. 37, 128–146.

Cruz, S.C.P., Alkmim, F.F., 2006. The tectonic interaction between the Paramirim aulacogen and the Araçuaí belt, São Francisco craton region, Eastern Brazil. An. Acad. Bras. Cienc. 78, 151–173. https://doi.org//S0001-37652006000100014

Cruz, S. C. P, Alkmim, F.F., Pedreira, A., Teixeira, L., Pedrosa-Soares, A.C., Gomes, L.C.C., Souza, J.S., Leal, A.B.M., 2012. O Orógeno Araçuaí, in: Geologia Da Bahia. Pesquisa e Atualização de Dados. CBPM Salvador, pp. 131–178.

Cruz, S. C P, Peucat, J.J., Teixeira, L., Carneiro, M.A., Marques Martins, A.A., Santana, J. dos S., De Souza, J.S., Barbosa, J.S.F., Leal, Â.B.M., Dantas, E., Pimentel, M.,

2012. The Caraguataí syenitic suite, a ca. 2.7-Ga-old alkaline magmatism (petrology, geochemistry and U-Pb zircon ages). Southern Gavião block (São Francisco Craton), Brazil. J. South Am. Earth Sci. 37, 95–112. https://doi.org/10.1016/j.jsames.2011.11.006

Cruz, S. C. P., Alkmim, F. F., Barbosa, J. S. F., Dussin, I., Gomes, L. C. C., 2015. Tectonic inversion of compressional structures in the Southern portion of the Paramirim Corridor, Bahia, Brazil. Brazilian Journal of Geology, 45(4), 541-567

Cruz, S.C.P., Barbosa, J.S.F., Santos Pinto, M., Peucat, J.J., Paquette, J.L., Souza, J.S., Martins, V.S., Chemale Júnior, F., Carneiro, M.A., 2016. The Siderian-Orosirian magmatism in the Gavião Paleoplate, Brazil: U-Pb geochronology, geochemistry and tectonic implications. J. S. Am. Earth Sci. 69, 43–79.

Cuney, M., Kyser, K., 2008. Recent and not-so-recent developments in uranium deposits and implications for exploration. Mineral. Assoc. Can. Short Course Ser. 39, 97–116.

Cuney, M., 2010. Evolution of uranium fractionation processes through time: driving the secular variation of uranium deposit types. Econ. Geol. 105, 553–569.

Cunha, J.C., Barbosa, J.S.F., Mascarenhas, J.F., 2012. Greenstones Belts e Sequências Similares, in: Geologia da Bahia. Pesquisa e Atualização, CBPM Série Publicações Especiais. Salvador, pp. 203–325.

Danderfer, A., de Waele, B., Pedreira, A.J., Nalini, H.A., 2009. New geochronological constraints on the geological evolution of Espinhaço basin within the São Francisco Craton-Brazil. Precambr. Res. 170, 116–128.

Danderfer Filho, A., 2000. Geologia sedimentar e evolução tectônica do Espinhaço Setentrional, estado da Bahia. Unpubl. Ph.D. Thesis. Univ. Fed. de Brasília, UnB.

Danderfer Filho, A., 1990. Análise descritiva e cinemática do Supergrupo Espinhaço na região da Chapada Diamantina, BA. Unpubl. MsC Thesis, Univ. Fed. Ouro Preto, UFOP.

Danderfer Filho, A., Lagoeiro, L.E., Alkmim, F.F., 1993. O Sistema de dobramentos e empurrões da Chapada Diamantina (BA): Registro da inversão do Aulacógeno do Espinhaço no decorrer do Evento Brasiliano. SBG, II Simpósio sobre o Crát. São Fr. Tectônica e Met. An. 197–199.

Danderfer Filho, A., Lana, C.C., Nalini Júnior, H.A., Costa, A.F.O., 2015. Constraints on the Statherian evolution of the intraplate rifting in a Paleo-Mesoproterozoic paleocontinent: New stratigraphic and geochronology record from the eastern São

Francisco craton. Gondwana Res. 28, 668–688. https://doi.org/10.1016/j.gr.2014.06.012

Eglinger, A., André-Mayer, A. S., Vanderhaeghe, O., Mercadier, J., Cuney, M., Decrée, S., Feybesse, J., Milesi, J. P., 2013. Geochemical signatures of uranium oxides in the Lufilian belt: From unconformity-related to syn-metamorphic uranium deposits during the Pan-African orogenic cycle. Ore Geology Reviews, 54, 197-213.

Eglinger, A., Vanderhaeghe, O., André-Mayer, A. S., Goncalves, P., Zeh, A., Durand, C., & Deloule, E., 2016. Tectono-metamorphic evolution of the internal zone of the Pan-African Lufilian orogenic belt (Zambia): Implications for crustal reworking and syn-orogenic uranium mineralizations. Lithos, 240, 167-188.

Frimmel, H. E., Schedel, S., & Brätz, H., 2014. Uraninite chemistry as forensic tool for provenance analysis. Applied Geochemistry, 48, 104-121.

Fuzikawa, K., Alves, J., Maruejol, P., Cuney, M., Kostonlayl, C., Poty, B., 1988. The Lagoa Real Uranium Province, Bahia state, Brazil: some petrographic aspects and fluid inclusion studies. Geochim. Bras. 2, 109–118.

Geisel Sobrinho, E., Raposo, C., Alves, J. V, Brito, W.D., Vasconcelos, T.G., 1980. O distrito uranífero de Lagoa Real, Bahia. Congr. Bras. Geol. 31, 1499–1512.

Gonçalves, G. O., Lana, C., Buick, I. S., Alkmim, F. F., Scholz, R., & Queiroga, G., 2019. Twenty million years of post-orogenic fluid production and hydrothermal mineralization across the external Araçuaí orogen and adjacent São Francisco craton, SE Brazil. Lithos, *342*, 557-572

Gradim, C., Roncato, J., Pedrosa-Soares, A.C., Cordani, U., Dussin, I., Alkmim, F.F., Queiroga, G., Jacobsohn, T., Silva, L.C. da, Babinski, M., 2014. The hot back-arc zone of the Araçuaí orogen, Eastern Brazil: from sedimentation to granite generation. Brazilian J. Geol. 44, 155–180. https://doi.org/10.5327/Z2317-4889201400010012

Guimarães, J.T., Alkmim, F.F., Cruz, S.C.P., 2012. Supergrupos Espinhaço e São Francisco. Geol. da Bahia. Pesqui. e atualização dados 2, 33–86.

Guimarães, J.T., Santos, R.A., Melo, R.C., 2008. Geologia da Chapada Diamantina (Projeto Ibitiara-Rio de Contas). CBPM, Série Arqu. ed. Salvador, BA.

Kouske, A.P., Suh, C.E., Ghogomu, R.T., Ngako, V., 2012. Na-Metasomatism and Uranium Mineralization during a Two-Stage Albitization at Kitongo, Northern

Cameroon: Structural and Geochemical Evidence. Int. J. Geosci. 03, 258–279. https://doi.org/10.4236/ijg.2012.31028

Kuchenbecker, M., Pedrosa-Soares, A.C., Babinski, M., Fanning, M., 2015. Detrital zircon age patterns and provenance assessment for pre-glacial to post-glacial successions of the Neoproterozoic Macaúbas Group, Araçuaí orogen, Brazil. Precambr. Res. 266, 12–26.

Lima, S.A., Martins-Neto, M.A., Pedrosa-Soares, A.C., Cordani, U.G., Nutman, A., 2002. A Formação Salinas na área-tipo, NE de Minas Gerais: Uma proposta de revisão da estratigrafia da Faixa Araçuaí com base em evidências sedimentares, metamórficas e idades U-Pb SHRIMP. Rev. Bras. Geociências 32, 491–500.

Lobato, L.M., 1985. Metamorphism, metasomatism and mineralization at Lagoa Real, Bahia, Brazil. The University of Western Ontario.

Lobato, L.M., Fyfe, W.S., 1990. Metamorphism, metasomatism, and mineralization at Lagoa Real, Bahia, Brazil. Econ. Geol. 85, 968–989. https://doi.org/10.2113/gsecongeo.85.5.968

Lobato, L.M., Pimentel, M.M., Cruz, S.C.P., Machado, N., Noce, C.M., Alkmim, F.F., 2015. U-Pb geochronology of the Lagoa Real uranium district, Brazil: Implications for the age of the uranium mineralization. J. South Am. Earth Sci. 58, 129–140. https://doi.org/10.1016/j.jsames.2014.12.005

Loureiro, H.S.C., Bahiense, I.C., Neves, J.P., Guimarães, J.T., Teixeira, L.R., Santos, R.A., Melo, R.C., 2009. Geologia e recursos minerais da parte norte do corredor de deformação do Paramirim (Projeto Barra – Oliveira dos Brejinhos)., Série Arqu. ed. Salvador, BA.

Machado, N., Schrank, A., Abreu, F.R., Knauer, L.G., Almeida-Abreu, P.A., 1989. Resultados preliminares da geocronologia U-Pb na Serra do Espinhaço Meridional. Boletim Núcleo Minas Gerais-Sociedade Brasileira de Geologia 10, 171–174.

Machado, G. S. 2008. Geologia da porção sul do complexo Lagoa Real, Caetité, Bahia. Trabalho final de Graduação, Instituto de Geociências, Universidade Federal da Bahia, Salvador.

Magalhães, J.R., Pedrosa-Soares, A., Dussin, I., Müntener, O., Pinheiro, M.A.P., Silva, L.C. da, Knauer, L.G., Bouvier, A.-S., Baumgartner, L., 2018. First Lu-Hf, δ18O and trace elements in zircon signatures from the Statherian Espinhaço anorogenic province (Eastern Brazil): geotectonic implications of a silicic large igneous

province. Brazilian J. Geol. 48, 735–759. https://doi.org/10.1590/2317-4889201820180046

Maruejol, P., 1988. Métasomatose alcaline et minéralisations uranifères: les albitites du gisement de Lagoa Real (Bahia, Brésil) et exemples complémentaires de Xihuashan (SE Chine), Zheltorechensk (Ukraine) et Chhuling Khola (Népal central). Unp. Ph.D. thesis.

Matos, E.C., Silva, J.R.A., Rubini, L.A., 2003. A província uranífera de Lagoa Real - garantia de fornecimento de concentrado de urânio (DUA) para as necessidades brasileiras. Rev. Geol. 16, 111–120.

Matos, E.C., Villegas, R.A.S., 2010. Exploration and mining activities in the uranium province of Lagoa Real, in: Uranium 2010: The Future is U Proceedings Volume 1 and 2. The Canadian Inst of Mining, Metallurgy and Petroleum, Canada, p. 2v.

Medeiros, E.L.M., Cruz, S.C.P., Barbosa, J.S.F., Paquette, J.L., Peucat, J., Jesus, S.S.G.P., Barbosa, R.G., Brito, R.S., Carneiro, M.A., 2017. The Santa Izabel complex, Gavião Block, Brazil: components, geocronology, regional correlations and tectonic implications. J. South Am. Earth Sci. 80, 66–94.

Melo, M.G. de, Stevens, G., Lana, C., Pedrosa-Soares, A.C., Frei, D., Alkmim, F.F. de, Alkmin, L.A., 2017. Two cryptic anatectic events within a syn-collisional granitoid from the Araçuaí orogen (southeastern Brazil): Evidence from the polymetamorphic Carlos Chagas batholith. Lithos 277, 51–71.

Menezes, R.C.L., Conceição, H., Rosa, M.D.L.D.S., Macambira, M.J.B., Galarza, M.A., Rios, D.C., 2012. Geoquímica e geocronologia de granitos anorogênicos Tonianos (ca. 914–899 Ma) da Faixa Araçuaí no sul do Estado da Bahia. Geonomos 20, 1–13.

Mercadier, J., Cuney, M., Lach, P., Boiron, M. C., Bonhoure, J., Richard, A., Leisen, M., Kister, P., 2011. Origin of uranium deposits revealed by their rare earth element signature. Terra Nova, 23(4), 264-269.

Moreira, H.F., Danderfer, A., Costa, A.F.O., Bersan, S.M., Lana, C.C., Queiroga, G.N., 2020. Record of Early Tonian mafic magmatism in the central Espinhaço (Brazil): New insights for break-up of the Neoproterozoic landmass ancestor of São Francisco-Congo paleocontinent. Geosci. Front. https://doi.org/10.1016/j.gsf.2020.02.007

Nutman, A.P., Cordani, U.G., 1993. SHRIMP U-Pb zircon geochronology of Archaean granitoids from the Contendas-Mirante area of the São Francisco Craton, Bahia, Brazil. Precambrian Res. 63, 179–188.

Oliveira, L.A.R., Souza, A.S., Rios, F.J., Chaves, A.O., Lucas, E.D.A., Yardley, B., Banks, D., Matos, E.C., Freitas, M.E., Prates, S.P., 2012. Estudo de inclusões fluidas em minerais associados à mineralização uranífera de três jazidas da província uranífera de Lagoa Real, Bahia e Brasil. Geonomos 20 (2), 68–78.

Olivier, V., André-Mayer, A. S., Diondoh, M., Aurélien, E., Maryse, O., Moussa, I., & Marc, P., 2020. Uranium mineralization associated with late magmatic ductile to brittle deformation and Na–Ca metasomatism of the Pan-African A-type Zabili syntectonic pluton (Mayo-Kebbi massif, SW Chad). Mineralium Deposita, 1-23

Pedrosa-Soares, A.C., Alkmim, F.F., Tack, L., Noce, C.M., Babinski, M., Silva, L.C. da, Martins-Neto, M.A., 2008. Similarities and differences between the Brazilian and African counterparts of the Neoproterozoic Araçuaí-West Congo Orogen. Geol. Soc. London, Spec. Publ. 294, 153–172.

Pedrosa-Soares, A.C., Babinski, M., Noce, C., Martins, M., Queiroga, G., Vilela, F., 2011a. The Neoproterozoic Macaúbas Group, Araçuaí orogen, SE Brazil. Geol. Soc. London, Mem. 36, 523–534.

Pedrosa-Soares, A.C., de Campos, C.M.P., Noce, C.M., Silva, L.C. da, Novo, T.A., Roncato Júnior, J.G., Medeiros, S.R. de, Castañeda, C., Queiroga, G.N., Dantas, E., 2011b. Late Neoproterozoic–Cambrian granitic magmatism in the Araçuaí orogen (Brazil), the eastern brazilian pegmatite province and related mineral resources.

Pedrosa-Soares, A.C., Noce, C.M., Alkmim, F.F. De, Carlos, L., Babinski, M., Cordani, U., Castañeda, C., 2007. Orógeno Araçuaí: síntese do conhecimento 30 anos após Almeida 1977 15, 1–16.

Pedrosa-Soares, A.C., Wiedemann-Leonardos, C.M., 2000. Evolution of the Araçuaí belt and its connection to the Ribeira Belt, Eastern Brazil, in: Tectonic Evolution of South America. Sociedade Brasileira de Geologia São Paulo, pp. 265–310.

Peixoto, E., Pedrosa-Soares, A.C., Alkmim, F.F. de Dussin, I.A., 2015. A suture–related accretionary wedge formed in the Neoproterozoic Araçuaí orogen (SE Brazil) during Western Gondwanaland assembly. Gondwana Res. 27, 878–896.

Pimentel, M. M., Machado, N., & Lobato, L. M., 1994. Geocronologia U/Pb de rochas graníticas e gnáissicas da região de Lagoa Real, Bahia, e implicações para a idade

da mineralização de urânio. In SBG, Congresso Brasileiro de Geologia (Vol. 38, pp. 389-390)

Raposo, C., Matos, E.C. de, Brito, W., 1984. Zoneamento cálcico-sódico nas rochas da Província Uranífera de Lagoa Real, in: Anais do XXXIII Congresso Brasileiro de Geologia, Rio de Janeiro, 1984

Ribeiro, C. I., Carvalho Filho, C. D., & Hashizume, S., 1984. As jazidas de urânio de Lagoa Real. In: Anais do XXXIII Congresso Brasileiro de Geologia, Rio de Janeiro, vol. 3, pp. 1463–1474.

Richter, F., Lana, C., Stevens, G., Buick, I., Pedrosa-Soares, A.C., Alkmim, F.F., Cutts, K., 2016. Sedimentation, metamorphism and granite generation in a back-arc region: Records from the Ediacaran Nova Venécia Complex (Araçuaí Orogen, Southeastern Brazil). Precambrian Res. 272, 78–100.

Rooney, A. D.; Strauss, *J. V.; Brandon, A. D.; Macdonald, F. A., 2015. A Cryogenian chronology: Two long-lasting synchronous Neoproterozoic glaciations. Geology.* ***43*** *(5): 459–462.* doi*:*10.1130/G36511.1

Rosa, A.M.L.S., Conceição, H., Oberli, F., Meier, M., Martin, H., Macambira, M.B., Santos, E.B., Paim, M.M., Leahy, G.A.S., Bastos Leal, L.R., 2000. Geochronology (U-Pb/Pb-Pb) and isotopic signature (Rb-Sr/Sm-Nd) of the paleoproterozoic Guanambi Batholith, southwestern Bahia State (NE Brazil). Rev. Bras. Geociência 30, 062–06.

Routhier, P., 1967 Eassai critique sur les méthodes de la géologie. De I'objet & à la genése. Masson, Paris, 204 pp

Santana, A.V., 2016. Análise estratigráfica em alta resolução em rampa carbonática dominada por microbiolitos, Formação Salitre, Bacia de Irecê, Bahia. Unp. Ph.D. Thesis. Universidade Federal de Brasília, Brasília.

Santos, C. M., Cabral, A. R., Rios, F., 2020. Whole-rock chemistry of the Gameleira I uranium deposit, Lagoa Real, Brazil. Chemie der Erde. In press.

Santos-Pinto, M.., Peucat, J.J., Martin, H., Sabaté, P., 1998. Recycling of the Archaean continental crust: the case study of the Gavião Block, Bahia, Brazil. J. South Am. Earth Sci. Am. Earth Sci. 11, 487–498.

Santos-Pinto, M., Peucat, J.-J., Martin, H., Barbosa, J.S.F., Fanning, C.M., Cocherie, A., Paquette, J.-L., 2012. Crustal evolution between 2.0 and 3.5 Ga in the southern Gavião block (Umburanas-Brumado-Aracatu region), São Francisco Craton,

Brazil: a 3.5–3.8 Ga proto-crust in the Gavião block? J. South Am. Earth Sci. 40, 129–142.

Silva, L.C., Pedrosa-Soares, A.C., Teixeira, L.R., 2008. Tonian rift-related, A-type continental plutonism in the Araçuaí Orogen, eastern Brazil: New evidence for the breakup stage of the São Francisco–Congo Paleocontinent. Gondwana Research, 13,527–53

Scholz, R., Chaves, M.L.S.C., Krambrock, K., Pinheiro, M.V.B., Barreto, S.B., Menezes, M.G., 2012. Brazilian quartz deposits with special emphasis on gemstone quartz and its color treatment. In: Götze, Jens; Möckel, Robert. (Org.) (Ed.), Quartz, Deposits, Mineralogy and Analytics, 1st ed. Springer-Verlag, Heidelberg, pp. 139–156.

Silveira, E.M., Söderlund, U., Oliveira, E.P., Ernst, R.E., Leal Menezes, A.B., 2013. First precise U–Pb baddeleyite ages of 1500Ma mafic dykes from the São Francisco Craton, Brazil, and tectonic implications. Lithos 174, 144–156. https://doi.org/10.1016/j.lithos.2012.06.004

Stein, J.H., Netto, A.M., Drummond, D., Angeiras, A.G., 1980. Nota preliminar sobre os processos de albitização uranífera de Lagoa Real (Bahia) e sua comparação com os da URSS e Suécia, in: Congresso Brasileiro de Geologia. pp. 1758–1775.

Tedeschi, M., Novo, T., Pedrosa-Soares, A., Dussin, I., Tassinari, C., Silva, L.C., Gonçalves, L., Alkmim, F., Lana, C., Figueiredo, C., Dantas, E., Medeiros, S., De Campos, C., Corrales, F., Heilbron, M., 2016. The Ediacaran Rio Doce magmatic arc revisited (Araçuaí-Ribeira orogenic system, SE Brazil). J. South Am. Earth Sci. 68, 167–186. https://doi.org/10.1016/j.jsames.2015.11.011

Teixeira, L.R., 2000. Relatório temático de litogeoquímica. Projeto Vale do Paramirim. Companhia Baiana de Pesquisa Mineral–CBPM/Companhia de Pesquisa de Recursos Minerais – CPRM. Salvador, Bahia, Brasil.

Turpin, L., Maruejol, P., Cuney, M., 1988. U-Pb, Rb-Sr and Sm-Nd chronology of granitic basement, hydrothermal albitites and uranium mineralization (Lagoa Real, South-Bahia, Brazil). Contrib. To Mineral. Petrol. 98, 139–147. https://doi.org/10.1007/BF00402107

Veríssimo, C.U.V., Santos, R.V., Parente, C.V., De Oliveira, C.G., Cavalcanti, J.A.D., Nogueira Neto, J. de A., 2016. The Itataia phosphate-uranium deposit (Ceará, Brazil) new petrographic, geochemistry and isotope studies. J. South Am. Earth Sci. 70, 115–144. https://doi.org/10.1016/j.jsames.2016.05.002

Wilde, A. (2013). Towards a model for albitite-type uranium. Minerals, *3*(1), 36-48.

CAPITULO 5 – MAJOR- AND TRACE-ELEMENT CONTENTS OF TITANITE FROM MAGMATIC TO URANIUM ORE ASSEMBLAGES, LAGOA REAL URANIUM PROVINCE, BAHIA STATE, BRAZIL: KEY DIAGNOSTIC GEOCHEMICAL FEATURES.

Camila Marques dos Santos[a,b*]

[a]Programa de Pós-Graduação em Ciência e Tecnologia das Radiações, Minerais e Materiais. Centro de Desenvolvimento da Tecnologia Nuclear (CDTN/CNEN-MG). Av. Antonio Carlos 6627 – Universidade Federal de Minas Gerais – Campus Pampulha, 30270-901, Belo Horizonte, Minas Gerais, Brazil – camisgeo@gmail.com

[b]Programa de Doctorado em Geología. Departamento de Geología, Facultad de Ciencias, Universidad de Salamanca, Plaza de los Caídos, s/n, 37008, Salamanca, España

[*]corresponding author

Kathryn A. Cutts[c,d]

[c]Departamento de Geologia, Escola de Minas, Universidade Federal de Ouro Preto, Morro do Cruzeiro, 35400-000 Ouro Preto, MG, Brazil

Now at: [d]Universidade do Estado do Rio de Janeiro, Rua São Francisco Xavier 524, Maracanã Rio de Janeiro, 20550-900, Brazil – kathryn.cutts@gmail.com

Lucas Eustáquio Dias Amorim[e]

[e]Centro de Desenvolvimento da Tecnologia Nuclear (CDTN/CNEN-MG). Av. Antonio Carlos 6627 – Universidade Federal de Minas Gerais – Campus Pampulha, 30270-901, Belo Horizonte, Minas Gerais, Brazil – luckamorim@gmail.com

Alexandre Raphael Cabral[f]

[f]Instituto de Geociências. Universidade Federal de Minas Gerais. Av. Antonio Carlos 6627 – Universidade Federal de Minas Gerais – Campus Pampulha, 30270-901, Belo Horizonte, Minas Gerais, Brazil - arcabral@geol.igc.ufmg.br

Francisco Javier Rios[g]

[g]Centro de Desenvolvimento da Tecnologia Nuclear (CDTN/CNEN-MG). Av. Antonio Carlos 6627 – Universidade Federal de Minas Gerais – Campus Pampulha, 30270-901, Belo Horizonte, Minas Gerais, Brazil – javier@cdtn.br

Clemente Recio[h]

[h]Departamento de Geología, Facultad de Ciencias, Universidad de Salamanca, Plaza Caídos, s/n, 37008, España – crecio@usal.es

Keywords: Lagoa Real uranium province, titanite, trace elements, Zr-in-titanite geothermometry

Abstract

The Lagoa Real uranium province in Bahia, northeastern Brazil, is the leading uranium district for exploration in South America. It has 38 uraniferous anomalies that are hosted in lens-shaped albite-rich rocks, known as albitite, enclosed in the granite–gneiss rocks of the Lagoa Real suite intrusive. Titanite is a common mineral phase in both magmatic and hydrothermal rocks. Titanite microtextures and chemical compositions have been investigated from magmatic, barren and mineralized albitite rocks in order to constrain the magmatic and hydrothermal history in Lagoa Real and provide a better understanding of its geochemical characteristics. Three subtypes of titanite are documented based on microtexture and chemical composition: (i) primary magmatic; (ii) partially altered; and (iii) hydrothermal. Magmatic titanite is equilibrated with the magmatic assemblage and exhibits a corona-texture, surrounding ilmenite grains. It is defined by high Al, Zr/Hf, Th/U, HREE–Y contents, and low Fe, Ti and V concentrations. They additionally have low LREE/HREE fractionation ($[La/Yb]_N$= 0.05, average) and positive Eu anomalies indicating reducing conditions during magmatic crystallization. Partially altered titanite maintains the magmatic, chondrite-normalized REE pattern, but shows higher LREE/HREE fractionation ($[La/Yb]_N$ = 5.84, average) and Zr/Hf, V, in addition to lower HREE–Y contents, and variable Fe, Al and Th/U ratio (between 10 and 0). Hydrothermal titanite has a completely different chondrite-normalized REE pattern and higher contents of Fe, Ti and V, and lower concentrations of Al, Zr/Hf, Th/U and HREE–Y, in relation to magmatic titanite. In addition, it shows Th/U ratios <1, a common feature of hydrothermal titanite described in the literature. Based on Zr-in-titanite thermometry, formation temperatures for magmatic and partially altered titanite are estimated to be 670-690 ºC and 620-680 ºC respectively. Zirconium mobility during uranium precipitation makes the geothermometer unreliable in the mineralized samples. Although hydrothermal titanite is related to uraninite, it does not always show uranium enrichment. The progressive U loss in titanite highlights this mineral as a probable U source. Variations between positive and negative europium anomaly may indicate fluctuating oxygen fugacity during uranium precipitation event. This variation may also be related to the superposition of hydrothermal processes.

5.1 INTRODUCTION

Titanite ($CaTiSiO_5$) is one of the most common U–Th–bearing accessory minerals in magmatic and metamorphic rocks. It occurs in igneous rocks with high Ca/Al ratios, metamorphic rocks of mafic and calc-silicate compositions and may also be present as a detrital component in sedimentary rocks (e.g., Deer et al., 1982; Frost et al., 2001). The common occurrence of titanite, coupled with its high closure temperature (around 700 ºC; Frost et al., 2001) and low diffusion rate make it an important tool in the study of petrogenetic processes and geochronology (Della Ventura et al., 1999; Piccoli et al., 2000; Tiepolo et al., 2002; Prowatke and Klemme, 2005; Cherniak, 2006; Hayden et al., 2008; McLeod et al., 2010; Kohn, 2018).

Titanite is a repository of incompatible elements, including the rare-earth elements (REE) and the high field strength elements (HFSE). Additionally, titanite of different origins exhibits distinct trace element geochemistry serving a key role in understanding igneous, metamorphic and ore-forming processes (Storey et al., 2006; Horie et al., 2008; Smith et al., 2009; Li et al., 2010; Xie et al., 2010; Gao et al., 2012; Che et al., 2013; X. Deng et al., 2015; Xu et al., 2015; Guo et al., 2014; Fu et al., 2016; Liu et al., 2018; Olierook et al., 2019). Discriminating the different origins of titanite is thus particularly important for its use as a geochemical tracer and for interpreting its U–Pb age.

The Lagoa Real uranium province (LRUP), located in the south of Bahia state, Brazil, is the sixth largest uranium (U) resource in the world, and the most important in Brazil. It is approximately 35 km long and contains 38 uraniferous anomalies along three semi-arched lineaments (Fig. 1). The Lagoa Real orebodies contain a total reserve of ~112,000 metric tons of U_3O_8 and have an average grade of 2700 ppm (Brito et al., 1984; Matos et al., 2003; Matos and Villegas, 2010). The main lithology hosting this deposit is the Lagoa Real intrusive suite, which consists of granite-gneiss rocks that enclose pods of albite-rich rocks (hereafter referred to as albitite) in NW-SE shear-zones. Albitite is the main uranium host and is composed of a ferric-sodic-calcic assemblage made mainly by garnet, amphibole and clinopyroxene. Titanite is the most common Ti-bearing accessory mineral, and its occurrence is ubiquitous in all lithologies, occurring in magmatic rocks, and also in the hydrothermal products as part of the barren rocks or associated with ore assemblages. Chaves (2013) described the occurrence of a high-uranium titanite at the Cachoeira mine, and suggested its importance as a uranium source mineral. The uranium content in titanite was also used as an argument by Lobato et al. (2015) to debate the

uranium mineralization age based on titanite U–Pb geochronological data. However, no geochemical characterization of titanite in the host-granitoids, barren and ore-bearing rocks of the LRUP has been done until now. Geochemical information on titanite will enable its use as a geochemical tracer of alteration and ore-forming processes.

In this study, in-situ geochemical analyses were conducted to characterize titanite types and to elucidate their genesis. The main objective is to determine key diagnostic geochemical features of titanite that are related to alteration and uranium mineralization. Results from this study indicate the presence of three distinct types of titanite, and highlight the utilization of trace-element compositions in discriminating titanite of magmatic and hydrothermal origins, facilitating a more reasonable interpretation of the titanite U–Pb ages in future work.

5.2 GEOLOGICAL SETTING

Lagoa Real is located in the northern sector of the Neoproterozoic Araçuaí–West Congo orogenic system (AWCO), in a structure called the Paramirim Aulacogen (Fig. 32; Pedrosa-Soares and Wiedemann-Leonardos, 2000; Pedrosa-Soares et al., 2001, 2007, 2008; Alkmim et al., 2006). The Paramirim Aulacogen represents a rift, which formed in the Statherian (1775 ± 7 Ma; Danderfer Filho et al., 2015). Sediment deposition in this basin occurred from its formation in the Statherian through to the Cryogenian (675 Ma; Santana, 2016). The rift basin was partially inverted during the AWCO with the amalgamation of Gondwana. In the center of the Paramirim Aulacogen extensional structures are preserved, but both the northern and southern sections of the Aulacogen are affected by inversion (Cruz and Alkmim, 2017). The LRUP occurs within the southern inversion domain, which experienced thick-skinned deformation during the AWCO.

The basement of the Paramirim Aulacogen is composed of: Archean metagranitoid and orthogneiss rocks belonging to the Gaviao Block, often with mafic and ultramafic migmatitic enclaves; greenstone belts, consisting of Paleoarchean, Neoarchean and Siderian–Rhyacian metavolcano-sedimentary sequences; and finally acidic, intrusive plutonic rocks of Siderian, Rhyacian and Orosirian ages (Cordani et al., 1985, 1992; Marinho, 1991; Martin et al., 1991; Nutman and Cordani, 1993; Rosa et al., 2000; Peucat et al., 2002; Bastos-Leal et al., 1998, 2000; Cruz et al., 2012, 2016; Cunha et al., 2012; Santos-Pinto et al., 1998, 2012; Medeiros et al., 2017).

The Lagoa Real intrusive suite rocks (after Arcanjo, 2005) are known as the São Timóteo granite, and crystallized at ca. 1750 Ma (Turpin et al., 1988; Cordani et al., 1992;

Lobato et al., 2015). The São Timóteo granite consists of bodies of porphyritic and coarse-grained hastingsite-bearing syenite, syenogranite, and alkali granite crystallized in the hypersolvus and subsolvus conditions (Maruejol, 1989). These are geochemically characterized by authors (Maruéjol et al., 1987; Teixeira, 2000, Machado, 2008; Amorim, et al., 2020; Santos et al., 2020) as a metaluminous, ferroan, high-K and Fe-rich calc-alkaline series, reduced. They have also anorogenic, A2 and within-plate affinity.

Metasedimentary cover consists of the Paleo- to Mesoproterozoic Espinhaço Supergroup and Neoproterozoic São Francisco Supergoup (Danderfer and Dardenne, 2002; Misi and Veizer, 1996; Santana, 2016; Schobbenhaus, 2017; Bittencourt et al, 2019), which occur within two sub-basins, the western Espinhaço and the eastern Chapada Diamantina. The evolution of these rocks comprises five basin-forming, unconformity bounded events related to the evolution of the Paramirim Aulacogen, between the Statherian and the Cryogenian (Cruz and Alkmim, 2017; and references therein).

Two geochronological groups of gabbro/diabase and diorites, of tholeiitic composition and continental intraplate affinity, intruded the Espinhaço Supergoup as sills and dikes (Arcanjo et al., 2005; Menezes et al., 2012). The oldest group has ages of 1514 ± 22 Ma (Babinski et al., 1999), 1507 ± 7 Ma (Silveira et al., 2013), 1496 ± 3.2 Ma and 1492 ± 16 Ma (Guimarães et al., 2008; Loureiro et al., 2009), and is located in the eastern part of the Espinhaço range. The youngest group has ages of 934 ± 14 Ma and 854 ± 23 Ma (respectively, Loureiro et al., 2009 and Danderfer et al., 2009), and occurs in both eastern and western parts of the metasedimentary cover.

The Paramirim Aulacogen was inverted during the Ediacaran–Cambrian (Danderfer Filho 1990, 2000; Danderfer Filho et al. 1993; Cruz and Alkmim, 2007; Guimarães et al., 2008; Loureiro et al., 2009). The zone that concentrates most of these deformational structures is defined as the Paramirim corridor (Alkmim et al. 1993) and comprises an NNW-trending zone. Its tectonic framework comprises contractional and extensional families of structures related to aulacogen nucleation, reactivation and inversion (Cruz et al., 2015).

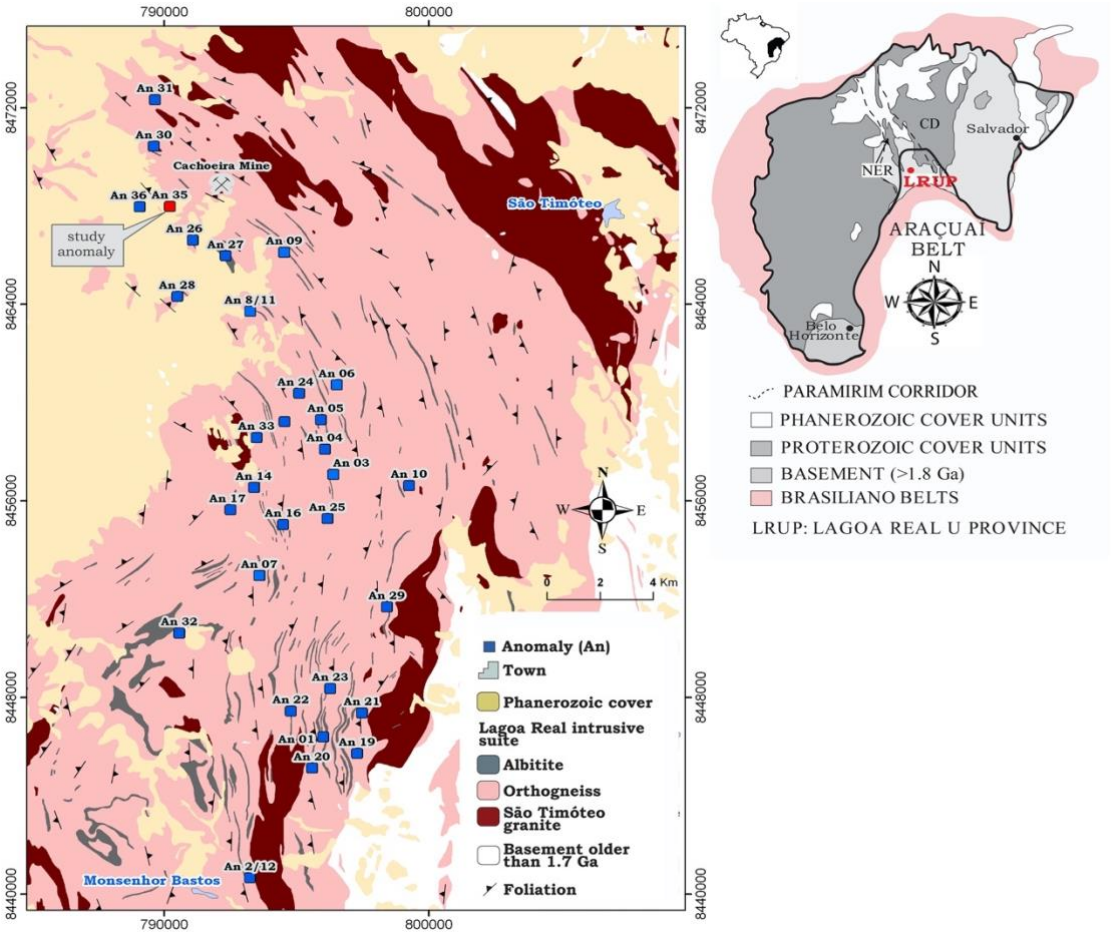

Fig. 32: Geological map of Lagoa Real uranium province showing distribution of uranium anomalies and the location of the Cachoeira mine (adapted from Costa, 1985). NER: Northern Espinhaço Range, CD: Chapada Diamantina

5.3 THE LAGOA REAL URANIUM PROVINCE

The Lagoa Real uranium deposits are spatially associated with albitites, which are sodium-enriched rocks dominated by plagioclase (albite ± oligoclase). The albitites are lens-shaped bodies hosted within the ca. 1.7 Ga A-type Sao Timoteo granitoids. Albitites have a variety of mineral assemblages that reflect different chemical compositions, in which sodium, calcium, iron and magnesium are dominant (Geisel Sobrinho et al., 1980; Raposo and Matos, 1984; Maruejol, 1989; Lobato and Fyfe, 1990; Chaves, 2013, Marques et al, 2020). In general, the albitites are thought to be the product of metasomatic alteration of the host Sao Timoteo granite-gneiss through sodium enrichment and silica depletion (Maruejol, 1989; Lobato and Fyfe, 1990, Marques et al, 2020). Maruejol (1989) and Lobato and Fyfe (1990) also observed that uranium mineralization is highly concentrated in the most mylonitized and oxidized zones, in association with the Fe^{3+}-rich garnet–hedenbergite albitite. Marques et al. (2020a) described three metasomatic

rocks in the DDH-F10 drill hole in the Gameleira I deposit, which encounters garnet-, magnetite- and biotite albitite. According Marques et al. (2020b), these rocks together with the pyroxene-to-amphibole albitites reflects a sequence of sodic-calcic, ferric-calcic-magnesian, potassic-magnesian and late calcic alteration stages. Having evolved under ductile regime. Later, infill stage occurred but this is rare. The ore is concentrated is associated with Ca-Fe-Mg and K-Mg stages as veinlets or disseminated ore. Uraninite is mostly hosted in titanite. Uranium correlates positively with V, Zr/Hf and Nb/Ta ratio (Marques et al. 2020a).

5.4 ANALYTICAL METHODS

Samples were collected from the Gameleira I deposit (Anomaly-35), a uranium prospect in the northwest part of Lagoa Real (Fig. 1). Samples GRA-01, 9-4, 7-1B, GNA 02 and ALB 05 were collected from the DDH-F10 in the distal zone of anomaly-35 in order to track chemical variations from non-altered into metasomatized rocks. They correspond to i) magmatic non-metasomatized rocks: hypersolvus alkali-feldspar granite (GRA-01) and its gneissified counterpart (9-4), ii) metasomatized rocks: garnet-bearing albitite (7-1B), magnetite-bearing albitite (GNA 02), and iii) ore shoot (mineralized sample): pyroxene-magnetite-bearing albitite (ALB 05). The complete description of the F-10 drillhole can be seen in Marques et al. (2020). Other mineralized samples were collected from the DDH-F11 and DDH-F12 drill hole. They correspond to biotite-bearing albitite (BIAB 129) and pyroxene-bearing albitite (POAB 05), respectively.

Electron microanalyses were then performed on polished thin sections at the Centro de Microscopia, Universidade Federal de Minas Gerais (UFMG), Brazil, using a JEOL JXA-8900RL. Analyses were collected using an accelerating voltage of 15 kV and a beam current of 20 nA, corresponding to a spot size of 5 μm. Elements and reference materials were (in parentheses) as follows: Na (jadeite), K (microcline), Mn (rhodonite), Mg (MgO), Ca (andradite), Fe (magnetite), Al (Al_2O_3), Si (quartz), F (fluorite), Cl (Cl-apatite). The *K*α X-ray lines of all elements were measured.

Spot analyses were carried out on feldspar, amphibole, pyroxene, biotite and titanite. Amphibole, pyroxene and biotite were classified according to the nomenclature of Leake et al., (2004), Morimoto, (1998) and Tischendorf et al., (1997) respectively. Amphibole analyses were recalculated using the Probe-Amph spreadsheet (Tindle and Webb, 1994). All data is included in Appendix 2.

Microanalyses using LA-ICP-MS (laser-ablation inductively-coupled plasma mass spectrometry) were performed in the Laboratory of Mass Spectrometry at the Centro de Desenvolvimento da Tecnologia Nuclear (CDTN – Minas Gerais, Brazil) and in the Chemistry and ICP Laboratory of the University of São Paulo (USP). Both laboratories use an ELAN 6100DRC, Perkin Elmer/ SciexTM quadrupole ICP-MS spectrometer, and a New Wave laser ablation system, model UP-213 A/F with a super cell. Titanite was sampled using a 40 µm laser spot with a hole depth of 30-60 µm. Measurements were carried out for the following elements: ^{27}Al, ^{44}Ca, ^{45}Sc, ^{51}V, ^{52}Cr, ^{63}Cu, ^{66}Zn, ^{69}Ga, ^{72}Ge, ^{85}Rb, ^{88}Sr, ^{89}Y, ^{90}Zr, ^{93}Nb, ^{135}Ba, ^{139}La, ^{140}Ce, ^{141}Pr, ^{146}Nd, ^{152}Sm, ^{151}Eu, ^{155}Gd, ^{159}Tb, ^{163}Dy, ^{165}Ho, ^{167}Er, ^{169}Tm, ^{172}Yb, ^{175}Lu, ^{178}Hf, ^{181}Ta, ^{208}Pb, ^{232}Th and ^{238}U. The reference materials NIST-610, NIST-612 and BHVO-2G (a USGS natural basaltic glass) were used as external calibration standards in both laboratories. Calcium (Ca) measured by EPMA was applied as an internal calibration standard, to correct drift and fractionation. Data acquisition, drift corrections and final data reduction were done using the SILLs software (Guillong et al., 2008). Results are included in Appendix 2 – 2A. Statistical calculations for detection limits of trace elements during analyses are shown in Appendix 2 – 2B.

5.5 SAMPLE MATERIAL

5.5.1 Hypersolvus alkali-feldspar granite (HAFG; sample GRA01) and related gneiss (HAFG gneiss; sample 9-4).

The GRA01 sample is a coarse-grained rock, grey to white in color (Fig. 33A). Petrographically, grains are more than 5 mm across and the rock has an inequigranular hypidiomorphic fabric. The rock contains perthitic K-feldspar, quartz, hastingsite, hedenbergite, biotite, titanite, ilmenite and zircon. Phenocrysts of perthitic K-feldspar (Or (=K/(K+Ca+Na)) = 91–98; see Supplementary Table 1 for the mineral chemical data) with lamellae or patches of albitic plagioclase (X_{Ab} (=Na/(Na+Ca+K)) = 0.76-93) are the main mineral phase (~50%). They are coarse-grained (from 2 to 8 mm). Quartz (~30%) is interstitial in alkali-feldspar crystals. Interstitial quartz is irregular and less than 1 mm across. Hedenbergite (X_{Mg} (=Mg/(Mg+Fe^{2+})) = 0.16–0.19) occurs rarely, surrounded by amphibole that forms corona-like textures. Hastingsite (X_{Mg} = 0.04) occurs with biotite (combined they make up ~20 % of the rock) forming interstitial aggregates, which also comprise titanite, ilmenite, zircon and apatite (Fig. 33B). Hastingsite can be symplectic

or tabular, both types are rimmed by radial biotite. Tabular shape hastingsite is integrown with fine-grained ilmenite. Biotite is Fe-rich with an X_{Mg} of 0.05–0.06.

Titanite is light brown in color and develops on the rims of fine-grained ilmenite forming a corona-like microstructure (Fig. 33C). Coronas of titanite on ilmenite are generally included in or in contact with amphibole (Fig. 33D). Ilmenite is volumetrically the most important component of such corona-like microstructures in the undeformed granite. Zircon may occur in contact with titanite–ilmenite coronas.

The mineralogy and modal proportions of sample 9-4 are almost identical to sample GRA01 except that clinopyroxene is absent and there are minor differences in texture. Sample 9-4 is a foliated medium-grained rock (<500 μm) with discontinuous gneissic banding (Fig. 33E). Hastingsite (X_{Mg} = 0.03–0.07) and biotite (X_{Mg} = 0.07–0.05) are foliation-forming minerals (Fig. 33E). K-feldspar (Or = 0.90–0.95, with one analysis of 0.69) occurs as porphyroclasts, which are surrounded by a matrix of recrystallized, fine-grained feldspar with tartan twinning. Plagioclase is albitic (X_{Ab}= 0.89–0.92) and occurs as fine-grained (<250 μm) polygonal shape crystals. Quartz occurs as ribbons in the felsic bands together with orthoclase. The occurrence of titanite in this sample is similar to that in sample GRA01. Titanite is light brown in color and occurs as a corona on ilmenite, but in this sample, titanite is associated with the mafic bands of the gneissic matrix (Fig. 33E) and the titanite coronas on ilmenite form elongated aggregates in which titanite is volumetrically dominant over ilmenite (Fig. 33F).

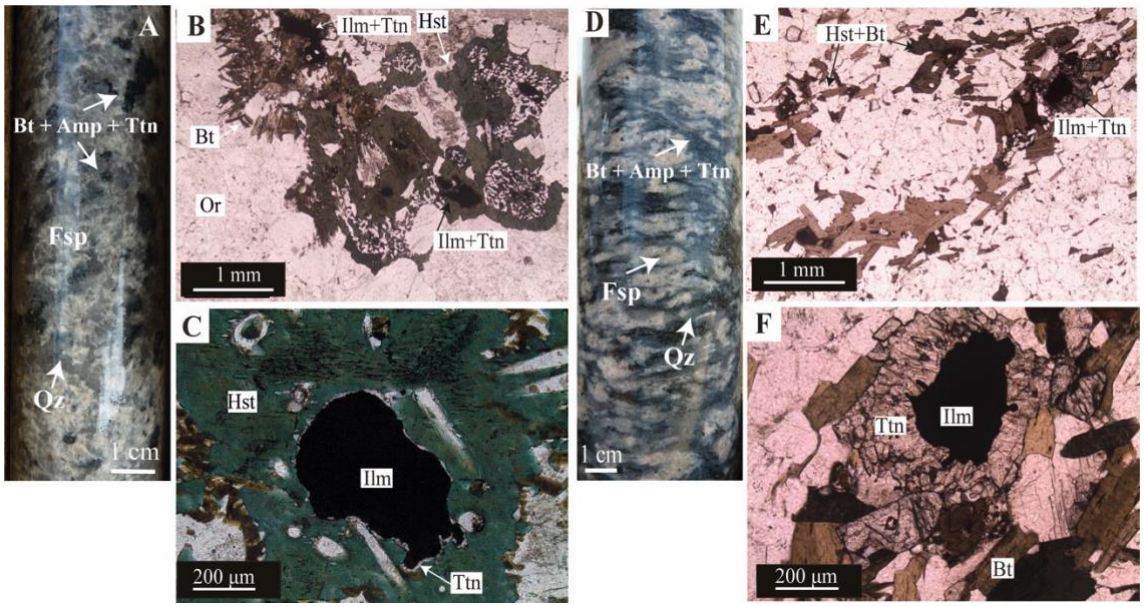

Fig. 33: Photomicrographs in plane-polarized transmitted light (PPL) and photographs of sample GRA01 (a – c) and 9-4 (d – f). a) Photograph of undeformed São Timóteo granite (sample GRA 01). b) Ilmenite–titanite corona-like microstructure in which ilmenite

predominates. c) Main occurrence of titanite in sample São Timóteo granite, it is mainly enclosed in hastingsite or surrounded by biotite. d) Photograph of sample 9-4 showing gneissic foliation. e) Titanite-ilmenite corona texture enclosed along foliation with biotite and hastingsite. f) Ilmenite–titanite corona-like microstructure in which titanite and ilmenite are in the same proportion. Hst: hastingsite, Ilm: ilmenite, Ttn: titanite, Bt: biotite, Ab: albite.

5.5.2 Barren albitite (sample 7-1B and GNA 02).

Both barren albitite samples are medium-grained and have a granoblastic polygonal texture. They consist of albitic plagioclase (70–90% modal, X_{Ab} =0.99-0.97) with ferric-calcic-magnesian assemblage constituted by amphibole, garnet and clinopyroxene (20–30%). Quartz, alkali-feldspar and magnetite are absent or minor.

Sample GNA 02 is isotropic, white in color in hand specimen (Fig. 34A). It is composed of albite, microcline (Or = 95–98), titanite, ilmenite, biotite, Mg-hedenbergite and Fe-edenite. Fe-edenite (X_{Mg} = 0.45–0.54) is replaced by Mg-hedenbergite (X_{Mg} = 0.43–0.71) and magnetite. Light-green biotite (X_{Mg} = 0.40–0.47) also occurs associated with titanite and magnetite as agglomerates (Fig. 34B). Titanite is light brown in color and occurs as a corona microstructure on ilmenite (Fig. 34C), similar to what is observed in the São Timóteo granite and gneiss samples. In sample GNA 02 titanite is volumetrically dominant over ilmenite. Both minerals occur associated with Fe-edenite, Mg-hedenbergite or biotite. This sample is considered to be a magnetite-bearing albitite. Sample 7-1B is weakly foliated and has a reddish color in hand specimen (Fig. 34D). This sample contains the minerals albite, K-feldspar, andradite, Fe-hedenbergite, hastingsite and carbonate. Hastingsite (X_{Mg} = 0.01–0.04), occurs rarely and is extensively replaced by Fe-hedenbergite (X_{Mg}= 0.12-0.03). The latter is associated with andradite (X_{And}(=Fe^{3+}/2) = 0.71-0.88) and titanite. Titanite is prismatic, light brown and without pleochroism (Fig. 34E). Titanite crystals are between 10 to 100 µm in length. Crystal outlines are euhedral, rhomboidal to elongate, and rounded. Titanite is commonly enclosed in andradite and hedenbergite with no clear genetic relationship with these minerals (Fig. 34F). This sample is classified as a garnet-bearing albitite.

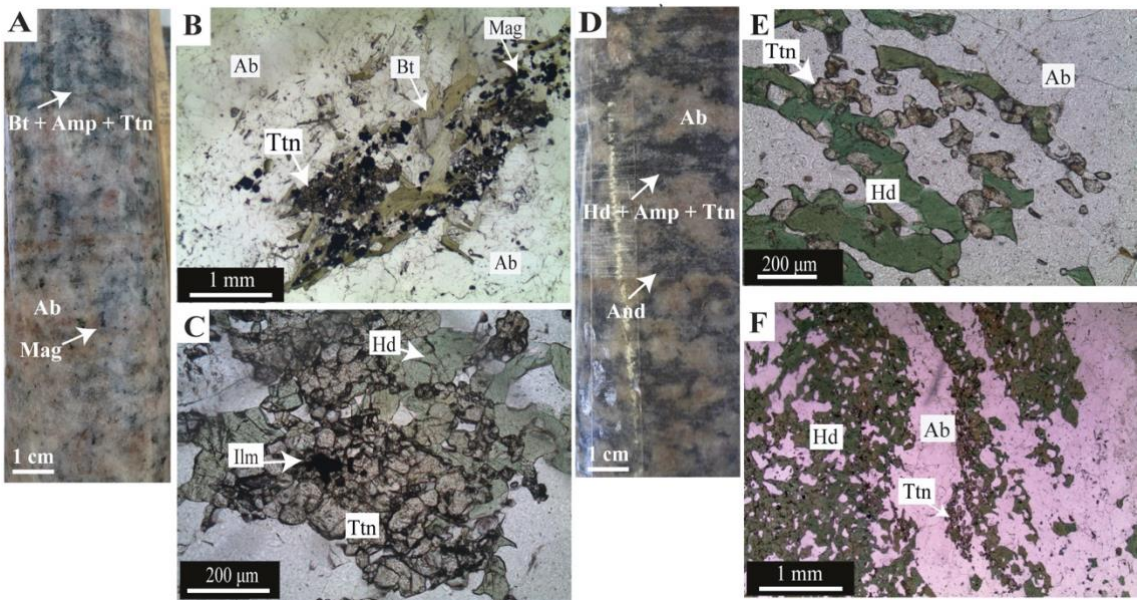

Fig. 34: Photomicrographs in plane-polarized transmitted light (PPL) and photographs of GNA 02 (a – d) and 7-1B (e – f) samples. a) Sample GNA 02 showing isotropic texture and red-to-white colour; b) Agglomerates of biotite, magnetite and titanite in magnetite-bearing albitite. c) Ilmenite–titanite corona-like microstructure in which titanite predominates in contact with hedenbergite. e) Foliated texture of sample 7-1B in which titanite forms brownish shoals of well-formed linked crystals associated with hedenbergite. f) Detailed view of the titanite texture which occurs as fine subhedral grains. Ttn: titanite, Ab: albite, Hd: hedenbergite; Ilm: ilmenite, Bt: biotite, Mag: magnetite.

5.5.3 Ore shoots (samples ALB 05, POAB 05 and BIAB 129).

Samples related to uranium ore shoots vary in microstructure and mineral assemblage. These constitute the ferric-calcic-magnesian and K-Mg stages. In these rocks, albite constitutes 70% to 80% of the modal volume, quartz and alkali-feldspar are absent or rare, clinopyroxene is present either as diopside or augite compositions. Actinolite, biotite and epidote, substitutes for clinopyroxene and albite, and the ore assemblage is located as veinlets or disseminated in rock.

Sample ALB 05 is a mineralized albitite (albite has $X_{Ab} = 0.99–0.97$) that is composed of diopside (7% modal, $X_{Mg} = 0.60–0.67$), actinolite (3% modal, $X_{Mg} = 0.58–0.77$), hematite (after magnetite), titanite, allanite, uraninite and uranophane. These minerals form an ore shoot within a magnetite-bearing albitite (GNA 02 sample). Hematite and allanite occur rarely. Actinolite replaces diopside (Fig. 35A). Titanite grains are

interstitial, between 50 and 300 µm in length and occur along albite grain boundaries (Fig. 35B); their color and microstructure are similar to those in the garnet-bearing albitite (sample 7-1B). However, the titanite occurring in the ore-shoot is intensely fractured, replaced by allanite and has inclusions <5 µm across, of zircon and uraninite, which is extensively altered to uranophane (Fig. 35C).

Sample POAB 05 is a pyroxene-bearing albitite mainly composed of diopside (20% modal, X_{Mg} = 0.68–0.73), actinolite (5% modal, X_{Mg} = 0.48–0.50), titanite, and biotite (3% modal, X_{Mg} = 0.68–0.69). Biotite and actinolite are replacive minerals and substitute mainly for diopside. Titanite is dark-reddish-to-brown, with weak pleochroism, and varies in diameter from 100 to 600 µm. Uranium mineralization is represented by uraninite, which occurs exclusively as inclusions in titanite (Fig. 35D). The uraninite has no distinct orientation, occurring as rounded crystals that are distributed homogeneously within all titanite crystals, this indicates that uraninite is not an inclusion, and may have been exsolved from titanite (Fig. 35E). In intensely deformed domains, titanite is associated with diopside, allanite, epidote and zircon, where its modal proportion is strongly increased (Fig. 35F).

Sample BIAB 129 is a biotite-bearing albitite. This sample has abundant biotite (20% modal, X_{Mg} = 0.76–0.77) and augite (5% modal, X_{Mg} = 0.84–0.86) as foliation-forming minerals, which surround albite porphyroclasts (X_{Ab} = 0.99–0.98). Carbonate fills fractures and interstitial spaces between the albite crystals. Biotite substitutes for augite. Titanite is prismatic, brownish to red in color, with strong pleochroism and occurs as single crystals or aggregates associated with biotite and zircon (Fig. 35G). It commonly contains ilmenite, uranophane and uraninite inclusions (Fig. 35H). Uranium ore consists of uraninite, coffinite and uranophane. Uraninite occurs chiefly as rounded crystals, which are included in titanite or are enclosed on contacts between titanite grains (Fig. 35H and I). These uraninite grains are surrounded by alteration halos composed by Si, Pb and Ti, which also fills the boundaries between titanite grains (Fig. 35I). Uranophane also occurs as rounded inclusions as a replacive mineral of uraninite in titanite or filling cleavages of carbonate and biotite. Coffinite fills cleavages in biotite.

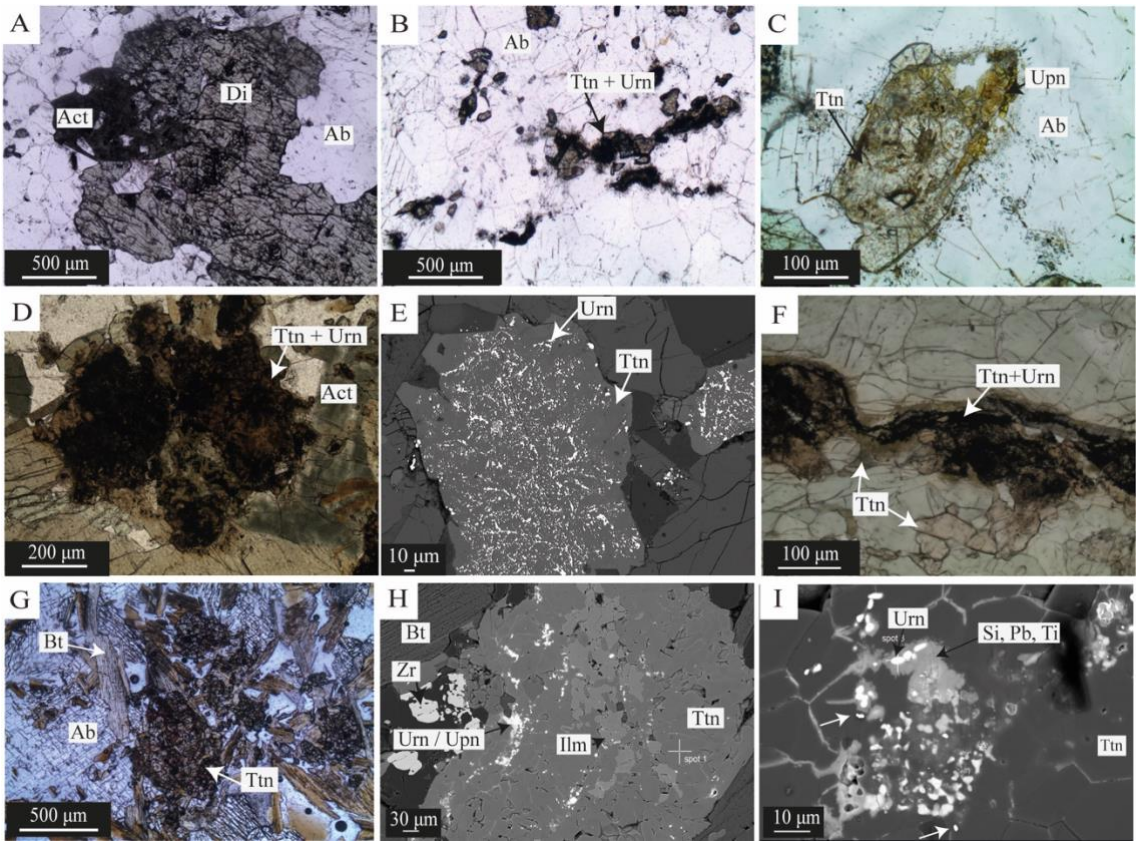

Fig. 35: Photomicrographs and backscattered images (BSE) of ore-related titanite textures (ALB 05, POAB 05 and BIAB 129 samples. a), b) and c) sample ALB 05, d), e) and f) sample POAB 05, and g), h) and i) sample BIAB 129. a), b), f) and g) are photomicrographs in plane-polarized transmitted light (PPL) and c), d), e), h) and i) are BSE images. Ab: albite, Ttn: titanite: Urn: uraninite, Upn: uranophane, Bt: biotite. a) Actinolite replacing diopside. Note that actinolite substitutes albite along grain boundaries. b) General aspect of ore assemblage in ALB 05 sample composed by sparse titanite in albite matrix. The black spots are composed by fine-grained uraninite or uranophane. c) Titanite crystal fractured and altered by uranophane. d) General aspect of the ore assemblage in sample POAB 05. Note that almost every uraninite crystal (white spots) is associated with titanite. e) Detailed image of titanite and uraninite. Note that uraninite is included in titanite as misoriented fine-crystals which suggests that uraninite exsolved from titanite. f) Extremely sheared portion in sample POAB 05, in which uraninite and titanite remain associated and enclosed along a micro shear zone. g) Titanite brownish in colour associated with biotite and zircon in sample BIAB 129. h) BSE image showing relationship between uraninite and titanite, in which uraninite is apparently included in titanite fractures or cleavages. i) Detailed image from h). Uraninite shows ambiguous relationships with titanite as it is enclosed in titanite cleavages and also as inclusions (red arrows) in titanite. Uraninite alteration can be seen by halos with a Si-Pb-

Ti composition that fill fractures and cleavages and which surrounds uraninite. Ttn: titanite, Ab: albite, Hd: hedenbergite; Di: diopside, Bt: biotite, Upn: uranophane, Act: actinolite, Zr: zircon, Ilm: ilmenite.

5.6 RESULTS

5.6.1 Compositional variability of major and trace elements in titanite

The major element results are given in Appendix 2 – 2C and trace element analyses results are given in the Appendix 2 – 2A.

Major elements. Calcium and Si contents of titanite are nearly constant in all rocks, ranging from 0.94 to 1.07 and 0.94 to 1.05 apfu, respectively. Titanite from the HAFG and HAFG gneiss (samples GRA-01 and 9-4 respectively) have the highest Al contents (0.17 to 0.24), but the lowest Ti contents (0.71 to 0.80) compared to the barren albitite rocks, which have scattered behavior in relation to these elements. On the other hand, titanite grains related to the uranium mineralization (i.e., samples ALB05, BIAB129 and POAB05) have the highest Ti contents (0.90 to 0.99), but the lowest Al contents (0.01 to 0.04).

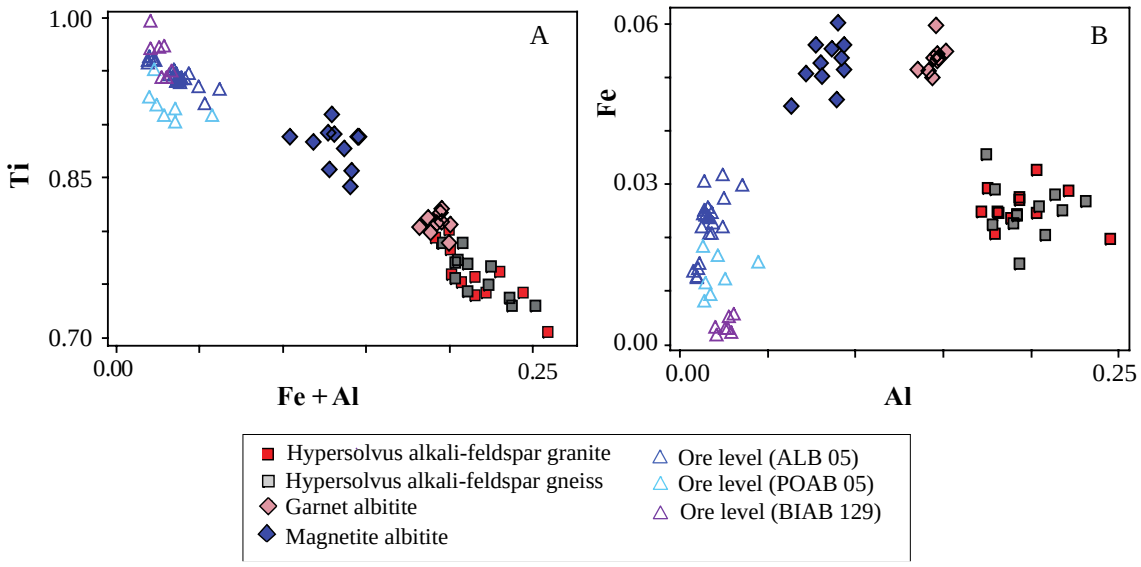

Fig. 36: Compositional variations of selected major elements in titanite in atoms per formula unit (apfu). a) Al + Fe vs. Ti. b) Al vs. Fe.

Rare earth elements and yttrium. The titanite from barren albitite sample GNA-02 and those spatially related to uranium mineralization – i.e., samples ALB05, BIAB129 and POAB05, have higher total REE contents (∑REE; GNA-02 = 4973 – 13178 ppm, average 10398 ppm; ALB05 = 1065 –22858 ppm, average 6638 ppm; POAB05 = 80 – 11561

ppm, average 3047 ppm; BIAB129 = 7096 - 19736 ppm, average 11066 ppm). The granite (HAFG) and related gneiss (HAFG gneiss, samples GRA-01 and 9-4), the barren albitite rocks (7-1B and GNA-02) and sample ALB 05 of the uranium-mineralized albitite have strong positive Eu anomalies ($Eu/Eu^*=Eu^*=Eu_N/\sqrt{(Sm_N*Gd_N)}$), for which average values are 1.65, 1.08, 1.28, 1.52 and 3.16, respectively. Cerium anomalies ($Ce/Ce^*=Ce^*=Ce_N/(0.5(La_N+Pr_N))$ are prominently negative for the aforementioned rocks (give values?). Ore shoot sample POAB 05 has a negative Eu anomaly (Eu* average = 0.4) and Ce* = 1.03, whereas the other ore shoot sample, BIAB 129 has both a positive Eu anomaly (1.12) and Ce* = 1.14.

The chondrite normalized REE pattern shows three main signatures for titanite: a) barren rocks (HAFG, HAFG gneiss, 7-1B and GNA-02) and one mineralized albitite (sample ALB 05) present a sub-horizontal profile, with a positive Eu anomaly, and negative Ce and Gd anomalies. Despite the similar REE patterns, this group shows different REE fractionation. The HAFG and HAFG gneiss have LREE/HREE between 0.23 and 0.38 and $(La/Yb)_N$ ratios of 0.05, indicating significantly low LREE/HREE fractionation. The barren albitite samples (7-1B and GNA-02) have slightly higher values (LREE/HREE = 0.47-0.51 and $(La/Yb)_N$ = 0.05 – 0.24), followed by the mineralized sample ALB05 (LREE/HREE = 2.9 and $(La/Yb)_N$ = 5.84). b) Titanite from the mineralized pyroxene-bearing albitite sample, POAB 05, is characterized by a wing-shaped pattern with a distinct negative Eu anomaly, lower LREE/HREE fractionation (0.54) and $(La/Yb)_N$ = 1.18. c) The mineralized biotite-bearing albitite sample, BIAB 129, does not have any distinctive anomaly; its ratios for LREE/HREE and $(La/Yb)_N$ are 2.39 and 3.47, respectively.

Titanite from the HAFG, HAFG gneiss and GNA-02 have the highest yttrium contents (Y = 3737 – 4936 ppm, average 4301 ppm; 1094 – 6182 ppm, average 4999 ppm; 3496 – 10223 ppm, average 6307 ppm, respectively). Sample POAB 05 also has high Y values and the values have a wide range (Y = 130 – 10944 ppm, average 4991 ppm). Sample 7-1B and some mineralized samples (ALB05 and BIAB129), have the lowest Y contents (7-1B = 1486 – 6615 ppm, average 2758 ppm; ALB05 = 331 – 4983 ppm, average 1346 ppm; BIAB129 = 1727 – 3627 ppm, average 2670 ppm). Variations of Y and ∑REE concentrations are to some extent consistent with each other.

Zirconium, hafnium and vanadium. The zirconium content is quite regular for all titanite grains. However, the amount of dispersion of values is variable and this can increase the average values. Titanite from the HAFG and HAFG gneiss have similar Zr

contents (average = 115 and 64 ppm, respectively), followed by 7-1B and GNA-02 (average = 154 and 98 ppm, respectively) whereas the mineralized samples have the highest values (average = 175, 267 and 401 ppm for samples ALB05, BIAB129 and POAB05, respectively).

On the other hand, the Hf content in titanite is different between samples. With the exception of sample 7-1B, the barren samples have the highest Hf contents (HAFG = 677 – 849 ppm, average 741 ppm; HAFG gneiss = 102 – 811 ppm, average 736 ppm; GNA-02 = 312 – 849 ppm, average 600 ppm). The garnet-bearing albitite (7-1B) has Hf amounts of 85 – 508 ppm (average 173 ppm). The mineralized samples have the lowest Hf contents (ALB05: 34 – 464 ppm, average 112 ppm; BIAB129: 3 – 11 ppm, average 9 ppm; POAB05: 1 – 26 ppm, average 3 ppm).

The barren samples, with the exception of the garnet-bearing albitite (7-1B), have the lowest V contents (HAFG = 9 – 22 ppm, average 13 ppm; HAFG gneiss = 4 – 31 ppm, average 16 ppm; GNA-02 = 18 – 55 ppm, average 31 ppm). Sample 7-1B has an intermediate range 474 – 2280 ppm of vanadium (average 867 ppm) and the mineralized samples have the highest V contents (ALB05: 1209 – 7677 ppm, average 3310; BIAB129: 4531 – 11195 ppm, average 6799; POAB05: 875 – 4359 ppm, average 2399 ppm).

Uranium, thorium and lead. The granite and gneiss (HAFG and HAFG gneiss, samples GRA-01 and 9-4 respectively) have similar ranges of U contents (HAFG: 20 – 43 ppm, average 27 ppm; HAFG gneiss: 11 – 29, average 22 ppm). Titanite from 7-1B, GNA-02 and the mineralized sample ALB05 have U contents below the detection limit and the other mineralized samples, BIAB129 and POAB05, have the highest values (2341 – 165525 ppm, average 27481 ppm; 10 – 1694 ppm, average 457 ppm, respectively).

Thorium and Pb behave similarly to each other. In general, the barren albitite samples have the highest concentrations of both elements. The HAFG (GRA-01) and HAFG gneiss (9-4) have equivalent ranges (HAFG = 297 – 508 ppm Th, average 383 ppm; 319 – 545 ppm Pb, average 411 ppm; HAFG gneiss = 2 – 491 ppm Th, average 251 ppm; 2.28 – 458 ppm Pb, average 234 ppm). Similarly, samples 7-1B and GNA-02 and the mineralized sample ALB 05 have comparable ranges (7-1B = 33 - 187 ppm Pb; average 187 ppm; 36 – 201 ppm Th, average 125 ppm; GNA-02 = 50 – 280 ppm Pb, average 124 ppm; 54 – 300 ppm Th; average 133 ppm; ALB05 = 46 – 328 ppm Pb, average 148 ppm; 50 – 323 ppm Th, average 158 ppm). In contrast, the other mineralized samples, BIAB129 has 313 – 7375 ppm Pb (average 982 ppm) and 20 – 882 ppm Th (average 201 ppm), and

POAB05 shows ranges between, 0 – 20 ppm Pb (average 9 ppm) and 0 – 39 ppm Th (average 0 ppm) for the same elements.

5.7 DISCUSSION

5.7.1 Titanite types: chemical and petrographical characteristics

Titanite is present in all of the rocks of Lagoa Real. The mineral occurs as part of the magmatic mineral assemblage of the São Timóteo granite, and the hydrothermal assemblage in the albitites, with different microstructures and mineral associations. However, the relationship of titanite regarding the magmatic, hydrothermal and uranium mineralization event(s) is ambiguous. Understanding the origin of titanite can thus provide important information for interpreting not only the nature of the uranium mineralization, but also geochronological data.

In our sample material, we observed three types of titanite in terms of petrographical texture: a) incolor aggregates, with corona-like microstructure on ilmenite (Fig. 33C), this type coexists mainly with hastingsite and biotite in granite sample (GRA-01); in mafic clots along the gneissic foliation in the gneissic sample (Fig. 33F; sample 9-4); and in the metamorphic/hydrothermal assemblage with Mg-hedenbergite, biotite and magnetite in albitite sample GNA02 (Fig. 34C); b) light-brownish prismatic aggregates in the garnet-bearing albitite (sample 7-1B), spatially associated with andradite, hedenbergite, calcite and magnetite (Fig. 34F); and c) red to brown crystals with strong pleochroism, with or without ilmenite inclusions, but hosting uraninite inclusions (sample ALB 05, POAB 05 and BIAB 129; Fig. 34B, 34E and 34H).

Sample GRA-01 shows weak hydrothermal alteration represented mainly by the replacement of K-feldspar as perthites and patches of albite. However, titanite in this sample is mostly in contact with hastingsite (Fig. 33D), which is part of magmatic assemblage. Titanite stability in granitic rocks is a function of oxygen fugacity, H_2O activity and temperature (Kohn, 2018). The low X_{Mg} (<0.2) in amphibole and biotite (indicating a high availability of Fe^{2+}, see Supplementary Table 1) attests to low oxygen fugacity conditions during São Timóteo crystallization according to classification of Anderson and Smith (1995). Amorim (2012) estimated temperature of crystallization of São Timóteo granite of around 900 ºC based on zircon saturation. High temperature and low oxygen fugacity conditions may have stabilized ilmenite rather than titanite in the hypersolvus facies of the São Timóteo granite. An increase of oxygen and water fugacity

during cooling can explain formation of titanite after ilmenite as a late-magmatic stage mineral in granite following the reaction (8) proposed by Frost et al., (2000):

7 $CaFeSi_2O_6$ (clinopyroxene) + 3 $FeTiO_3$ (ilmenite) + 5 SiO_2 (quartz) + 2 H_2O → 2 $Ca_2Fe_5Si_8O_{22}(OH)_2$ (Ca-amphibole) + 3 $CaTiSiO_5$ (titanite)

Previous studies have attempted to classify titanite according to major elements. Kowallis et al. (1997) proposed that the Fe/Al molar ratio could be used to distinguish titanite from different sources. Hydrothermal titanite and metamorphic titanite tend to have low Fe/Al ratios (0.1 – 0.5), whereas magmatic titanite is characterized by higher values (0.5 – >2.0). Che et al. (2013) suggested that magmatic titanite is depleted in Al and F, and enriched in Ti. A similar trend had already been observed by Broska et al. (2007), Morad et al. (2009) and Xie et al. (2010). Our data however shows that the late-magmatic titanite has high Al and F concentrations, and low Fe and Ti contents (Figure 5). In addition, the altered titanite follows a trend towards Al and F loss, but a Ti gain. Therefore, in our case, the major-element contents in isolation are not a good classification parameter. The high-Al contents in our titanite are likely related to the absence of Ca-rich plagioclase, which has a remarkable spatial association with high-Al titanite (X_{Al}>0.25; Oberti et al., 1991). Therefore, it is plausible that the low Fe/Al ratio of the titanite in the granite sample GRA-01 reflects excess Al in the hypersolvus facies of the Sao Timoteo granite.

The arguments listed above can explain formation of corona-like titanite in granitic-gneissic rocks, but the occurrence of titanite and ilmenite coronas in magnetite-bearing rock is not clear by petrographic observation itself, as titanite does not show clear relationship with the other minerals in these rocks. In addition, the magnetite albitite has a similar assemblage to the garnet-bearing albitite, composed mainly of hedenbergite + hastingsite + biotite, although titanite in the garnet albitite is prismatic and euhedral.
However, considering the rare-earth elements (REE) behavior and some selected traces, we can see some similarities and differences. In order to compare the titanite in the albitite samples (barren and mineralized) with the titanite from the granitic-gneiss samples (GRA 01, 9-4) we will call the latter **type-I** titanite.

The chondrite-normalized plots show two main patterns (Fig. 37). The first pattern consists of the hypersolvus alkali-feldspar granite (sample GRA-01; Fig. 33C), which is reproduced in titanite from the gneissic sample (sample 9-4; Fig. 33G), the magnetite-bearing albitite (sample GNA-02), the garnet-bearing albitite (7-1B) and one sample of the mineralized albitite (ALB05). Considering titanite type-I as a late-magmatic mineral,

this pattern can be interpreted as magmatic in origin what indicates that these samples have a common REE source. In addition to petrographical texture (Fig. 33C, Fig. 33F and Fig. 34B) and REE-chondrite-normalized pattern, sample GNA-02 shares similar values of Zr/Hf ratio, V, HREE and Y contents (Fig. 38A, B, C) with type-I titanite, so it should be included with this group. The garnet-bearing albitite (7-1B sample) and the mineralized sample ALB05 have higher Zr/Hf ratios and V contents, and lower HREE and Y contents than type-I titanite. Based on that, we interpret these to have **type-II** group titanite, corresponding to the titanite from samples 7-1B and ALB05. Type-II group titanite share similar REE-chondrite normalized patterns, but different contents of Zr/Hf ratios, V, HREE and Y in relation to type-I titanite. Here, it is possible to derive two implications from the preservation of the REE-chondrite normalized pattern in type-II titanite: the hydrothermal fluid did not erase the original magmatic signature of the titanite as the São Timóteo granite is the protolith of the albitite rocks and type-II titanite corresponds to partially altered type-I titanite as some aspects of their chemistry have been changed but the magmatic REE patterns are preserved; or the albitite-forming fluid was derived from a common magmatic source– i.e., hydrothermal fluids are late-magmatic. In addition, the hydrothermal process was able to progressively, from barren to mineralized albitite, adds V and leach Hf, HREE and Y in titanite, which will be further discussed in the following.

The titanite from the other uranium-mineralized albitite rocks (i.e., pyroxene- and biotite-bearing albitite of POAB 05 and BIAB 129, respectively, in which titanite hosts uraninite grains) show a second type of titanite REE pattern. These have completely different REE patterns compared to type-I and type-II titanite (Fig. 37), but are comparable to type-II titanite, mainly sample ALB 05, with respect to V, Zr/Hf, HREE, Y, Ti and Al concentrations (Fig. 36 and Fig. 38A, B, C). According to these different characteristics, this titanite is interpreted as **type-III**. Two interpretations are possible for type-III titanite: one is that it represents type-I titanite that was comprehensively altered – i.e., the magmatic REE signature of the pre-existing magmatic titanite was obliterated by that of the hydrothermal overprint. The other interpretation is that the type-III titanite is a hydrothermal precipitate, representing new titanite growth.

Titanite Th/U ratios may also be a good genetic indicator. In general, hydrothermal titanite contains lower Th/U (mostly < 1), whereas magmatic titanite is higher (Th/U > 1) (Aleinikoff et al., 2002; Che et al., 2013; Deng et al., 2015; Gao et al., 2012). The distribution of Th/U ratio in the studied titanite generations is shown in Fig. 39. Type-I

titanite has mostly Th/U ratio > 1 (average = 15, 10 and 0, for GRA-01, 9-4 and GNA 02 samples, respectively), however sample GNA 02 has Th/U < 1 (average = 0). Type-II titanite grains have a wide range of Th/U ratios (0 to 26), but the ore-related sample (ALB05) mostly has Th/U <<1, mainly due to U loss. The type-III titanite (from sample BIAB 129 and POAB05) has Th/U < 1 (average << 1) due to their high U contents. Therefore, despite the different REE-patterns between types II and III, most studied titanite from the albitite samples have Th/U ratios similar to the hydrothermal titanite.

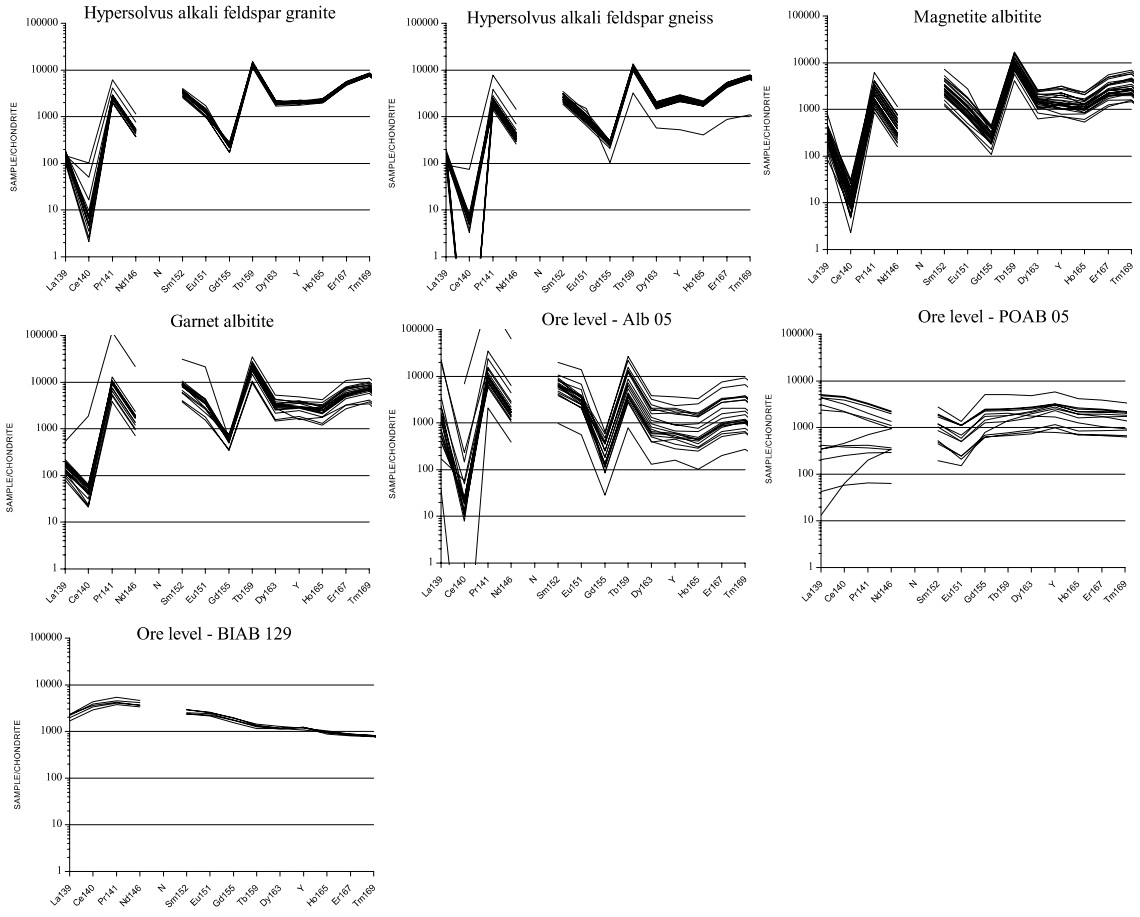

Fig. 37: Rare earth element chondrite normalized patterns in studied samples. Normalized to Boynton (1984).

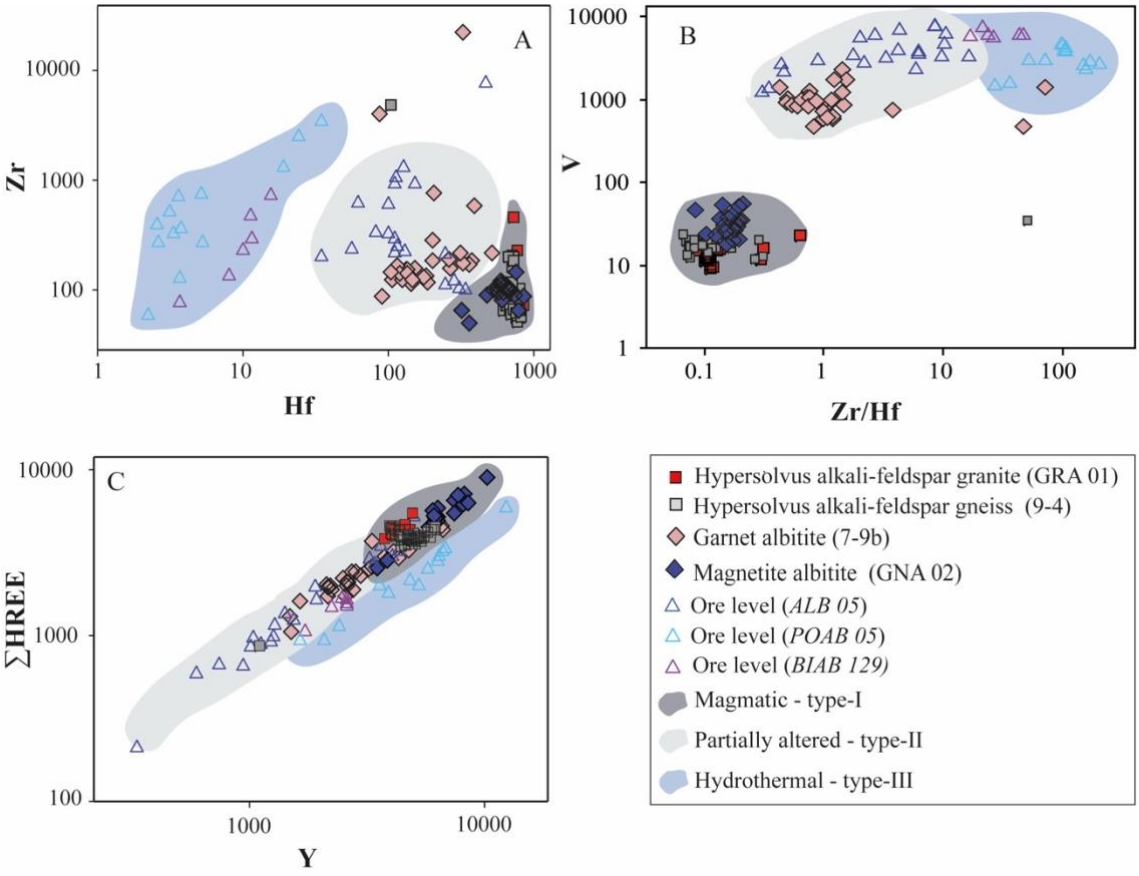

Fig. 38: Bivariate diagrams for selected trace elements. a) Zr vs. Hf b) V vs. Zr/Hf ratio. and c) ΣHREE vs. Y.

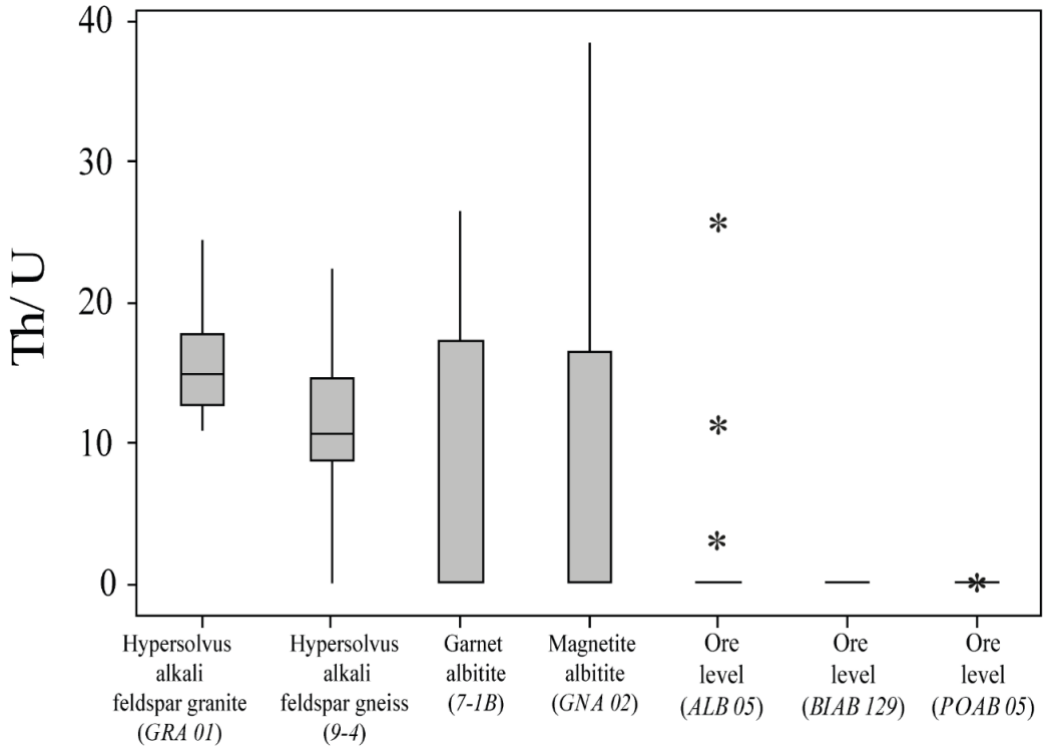

Fig. 39: Boxplot with Th/U ratio variation in studied samples.

5.7.2 Conditions of alteration and uranium precipitation

According to Franz and Spear (1985), the most common replacement that occurs in natural titanite is the coupled substitution: (Al, Fe^{3+}) + (F, $OH)^-$ ↔ Ti^{4+} + O^{2-} and this trend is observed in many other studies (see the summary in Cempírek et al., 2008). A strong negative correlation between Ti and Al + Fe^{3+} shown in Figure 4 indicates that the coupled substitution is the dominant mechanism on the Ti site. Figure 4 also illustrates that the trend describes the substitution from wall to mineralized rocks.

Kowallis et al. (1997) argued that Al and Fe^{3+} substitutions in titanite are regulated by factors such as variations in oxygen fugacity, pressure, and silica activity. The Fe-*vs*-Al diagram (Fig. 36A) describes a trend from granitic rocks having the highest Al and moderate Fe, moving to the barren albitite samples with moderate Al and the highest Fe values, through to the mineralized albitite samples which have the lowest Al and Fe contents. The lowest Fe^{3+} contents of uranium-related titanite against high Fe^{3+} contents of barren albitite may reflect fluctuating oxygen-fugacity conditions during the hydrothermal processes.

Oxygen fugacity exerts an influence on trace elements with different valences such as Ce and Eu (King et al., 2013). In the case of titanite, oxidation of Eu^{2+} into Eu^{3+} would inhibit its replacement for Ca^{2+} in the crystal lattice, creating distinct negative Eu anomalies (Horie et al., 2008). Another plausible explanation for negative Eu anomalies would be the preferential Eu incorporation into plagioclase, which results in a deficiency of Eu in the remaining magmas or fluids and, consequently, negative Eu anomalies in titanite crystallized from such magmas or fluids. Under oxidizing conditions, some Ce should exist as Ce^{4+}, and Ce would thus fractionate into titanite to a lesser extent than La^{3+}, Ce^{3+} and Pr^{3+} (e.g., Carlier and Lorand, 2008; Giannetti and Luhr, 1983; Henderson, 1980), making Ce anomalies in titanite another potential monitor of oxygen fugacity. Therefore, high fO_2 would make it difficult to incorporate Ce^{4+} into titanite, readily leading to negative Ce anomalies on the chondrite-normalized plots. Calculated Eu* and Ce* anomalies for studied samples are shown in Fig. 40.

Type-I titanite has a strong positive Eu anomaly indicating reducing conditions during the final stages of crystallization of the hypersolvus rocks from the Lagoa Real intrusive suite, but an increase in Eu as a result of the absence of plagioclase in the hypersolvus facies of the São Timóteo granite cannot be discounted. Harlov et al. (2006) suggested that the absence of magnetite during the replacement of titanite on ilmenite implied an

oxygen fugacity below the QFM buffer but above the iron-wüstite buffer. The same authors indicated that hydration reactions requiring high fH_2O were required to explain titanite reaction rims on ilmenite. Thus, the type-I titanite was likely generated under high fH_2O and low fO_2, below the QFM buffer. Titanite chemistry corroborate the reduced character of São Timóteo granite (ST), which is also shown in this work by the high Fe/(Fe+Mg) of amphibole and biotite (0.9 for both), and the high total rock analyses ((Fe/(Fe+Mg) = 0.8) according Marques et al. (2020a).

The type-II and GNA 02 sample titanite also have positive europium anomalies similar to the magmatic titanite. However, this titanite is Fe^{3+}-rich and occurs associated with hastingsite, Fe-hedenbergite and andradite or magnetite, which are all typical Fe^{3+}-bearing minerals. Lobato and Fyfe (1990) argued that formation of garnet and magnetite are the result of oxidation reactions in the range of -23 to -21 of oxygen fugacity. Therefore, the positive Eu* anomaly probably reflects the timing of ST crystallization and not the oxygen fugacity predominant during hydrothermal alteration. In addition, it is possible to conclude that Eu* in this titanite was not affected by alteration processes.

Ore-related, type-III titanite has contrasting behaviour. Titanite from sample POAB 05 has a distinctive negative Eu* anomaly, on the other hand, sample *BIAB 129* has a slightly positive Eu* value. Petrographical data shows that in sample POAB 05, uraninite is exsolved from titanite (Fig. 35D, E), this information coupled with the high U contents in titanite (618 ppm on average), uncommon for this mineral, shows that titanite precipitation is related to uranium mineralisation event and its chemistry probably represents the chemistry of the ore fluid. The europium anomaly in this case reflects oxidizing conditions, which is in agreement with the associated mineral assemblage composed of diopside, which usually contains noticeable Fe^{3+} contents. U-rich titanite may precipitated from this oxidized U-rich fluid and following this, uraninite exsolution was probably thermally activated. The process of uranium exsolution from titanite, or other silicate phases has never been described in the literature. However, the close relationship between uranium ore and veinlets in high-strain zones indicate that metamorphic heating or late decompression may have influenced the exsolution process.

In the sample BIAB 129, the timing of titanite growth in relation to uranium mineralization is ambiguous as uraninite occurs as inclusions in titanite or filling grain contacts (Fig. 35I) but if we consider the unusual high U contents of titanite (3000 ppm) in this sample as well as in the POAB 05, it is reasonable to conclude that this mineral is related to a uranium hydrothermal event. The europium anomaly indicates less oxidizing

to reducing conditions in relation to sample POAB 05, and, in this case, uraninite is associated with minerals that do not contain appreciable Fe^{3+}- (i.e. augite and biotite). Indicating that titanite precipitated from less oxidizing fluids.

However, in the studied samples the Ce anomaly has the opposite behaviour of the Eu anomaly in titanite, mainly in the type-I and type-II titanite, as type-III has no Ce anomaly. The contrasting behaviour may represent variations in oxygen fugacity through the hydrothermal processes.

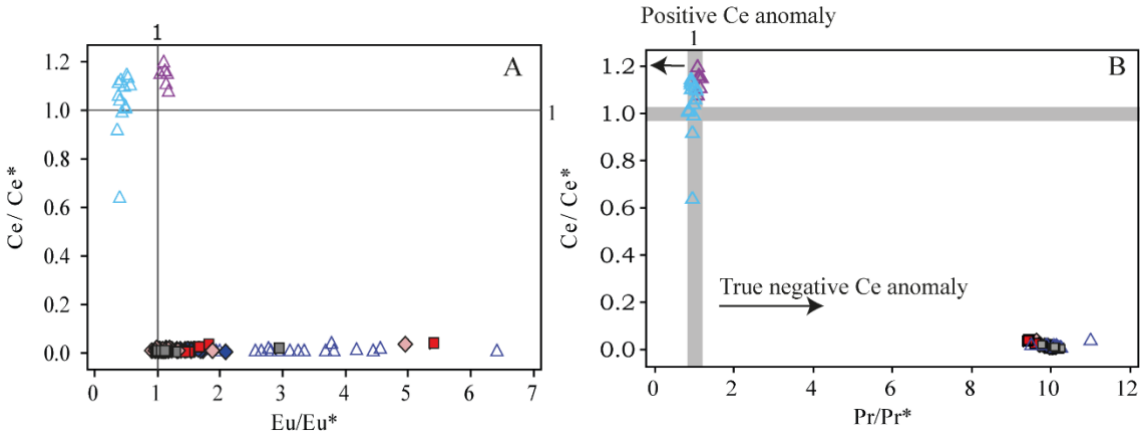

Fig. 40: Bivariant plots with europium and cerium anomaly. a) Europium vs. Cerium anomaly. b) Discriminative plot of $(Ce/Ce^*)_N$ versus $(Pr/Pr^*)_N$. Negative Ce anomaly as defined by (Bau and Dulski, 1996) as $(Ce/Ce^*)_N = Ce_N / [0.5 (Pr_N + La_N)] <1$ and $(Pr/Pr^*)_N = Pr_N/[0.5 (Ce_N + 0.5Nd_N)] > 1$

5.7.3 Origin of U-bearing titanite

Chaves (2013) described U-rich titanite (8-38 wt.% UO_2) related to uraninite in mineralized samples from the Cachoeira mine, which would indicate that titanite was a U-source mineral. However, our study records low U contents in titanite and a progressive U-decrease in titanite from magmatic to ore-related samples (Fig. 42D), and in some cases the ore-related samples have no detectable uranium content in titanite (i.e. sample ALB05) making them unsuitable for geochronology. On the other hand, some ore-related titanite do have high uranium contents but they are significantly lower (between 5 to 34470 ppm) than those reported in Chaves (2013). Therefore, our work attests the presence of U-rich titanite, however the presence of U as major element in titanite was not observed. In addition, U content itself is not a good parameter to characterize the titanite related to the U-mineralization as it was affected by processes that resulted in both U-decrease and U-upgrade. As mentioned above, the Th/U ratio looks more reliable in this case.

Titanite from the three uranium-ore-related samples, ALB 05, POAB 05 and BIAB 129, displays diverse chemical and petrographical characteristics. Chaves et al., (2009) showed five groups of high-U titanite chemical ages (around 1.7 Ga, 1.4 Ga, 1.2 Ga, 1.1 Ga and 978 Ma) which are coeval with tectonic events registered during the evolution of Paramirim Aulacogen. Authors argued that these ages resulted from uranium and lead mobilization during at least five hydrothermal events. Lobato et al. (2015) reported ages from a high U-titanite of around 960 Ma (U-Pb; LA-ICP-MS). The contrasting REE-signature, texture and, Ce* and Eu* anomalies observed in this work, may reflect the age variability, and consequently variable crystallization conditions, previously observed in titanite from Lagoa Real. This age variability also indicates multiple uranium precipitation events.

5.7.4 Formation temperature of titanite

The Zr content in titanite can be used as a geothermometer (Hayden et al., 2008), however, it is highly pressure dependent. For this reason, an independent means of determining the pressure was used. We applied the Al-in-amphibole geobarometer of Schmidt (1992) to amphibole in all of the samples (Appendix 2 – 2D). For the granite-gneiss rocks (samples GRA01 and 9-4), amphibole is magmatic indicating that the estimated pressure obtained should be appropriate for the type-I titanite. In samples 7-1B and GNA02, hastingsite is relict and in the mineralized albitite sample (ALB05), amphibole is texturally late, replacing diopside. This is also reflected in the results from Al-in-amphibole geobarometry with sample GRA01 giving pressures of 7–8 kbar (average of 7.25 kbar) and sample 9–4 giving 7.5–8.5 kbar (average of 7.7 kbar), whereas sample 7–1B gives 4–6 kbar (average of 5 kbar) and GNA02 gives 1.5–2.5 kbar (average of 2 kbar). Given this obvious textural relationship, we have used the maximum obtained pressure estimates for determining the Zr-in-titanite temperatures but also investigated the effect of using higher or lower values.

The results from the Zr-in-titanite geothermometer are given in Fig. 41 (also see Supplementary material). For the granite-gneiss sample, type-I titanite, the average temperatures obtained at 8 kbars are 670–690 ºC, similar to the P–T conditions obtained by Amorim (2012) of 700 °C and 7 kbar for deuteric alteration of the São Timóteo granite. The results from the albitite samples are generally more variable and higher T (although this may be a function of using a pressure value that is too high). This is particular apparent in the mineralized samples ALB 05 and POAB 05. The temperature variability

is a result of high dispersion of Zr contents in mineralized albitites as shown in Section 5.1.3. The Zr dispersion is related to mobility of this element during ore precipitation, evidenced by the precipitation of hydrothermal zircon associated with the ore assemblage, which resulted in Zr enrichment in titanite and makes the Zr-in-titanite geothermometer unreliable.

The type-II (magnetite-bearing albitite; GNA 02) shows the lowest Zr variability and gives quite similar results to those found in type-I titanite at 8 kbar, 670 ºC. At the pressure obtained using the Al-in-amphibole barometer for sample GNA 02 (2 kbar) the calculated Zr in titanite temperature is 620 ºC (average).

However, for the type-II titanite from the garnet-bearing albitite (7-1B), using 5 kbar gives temperatures of 680 ºC (average). Indicating that the temperatures obtained for titanite in the barren albitites is not very different from the magmatic samples. These temperatures may represent the temperature of the first hydrothermal alteration, as the garnet-bearing albitite is a transitional rock, and titanite is intergrown with andradite and is texturally different to the type-I corona-texture titanite. Such high temperatures are consistent with experimental temperatures (around 600 ºC) of hastingsite dehydration (Thomas, 1962) and K-feldspar replacement by albite (Hovelmann et al., 2010).

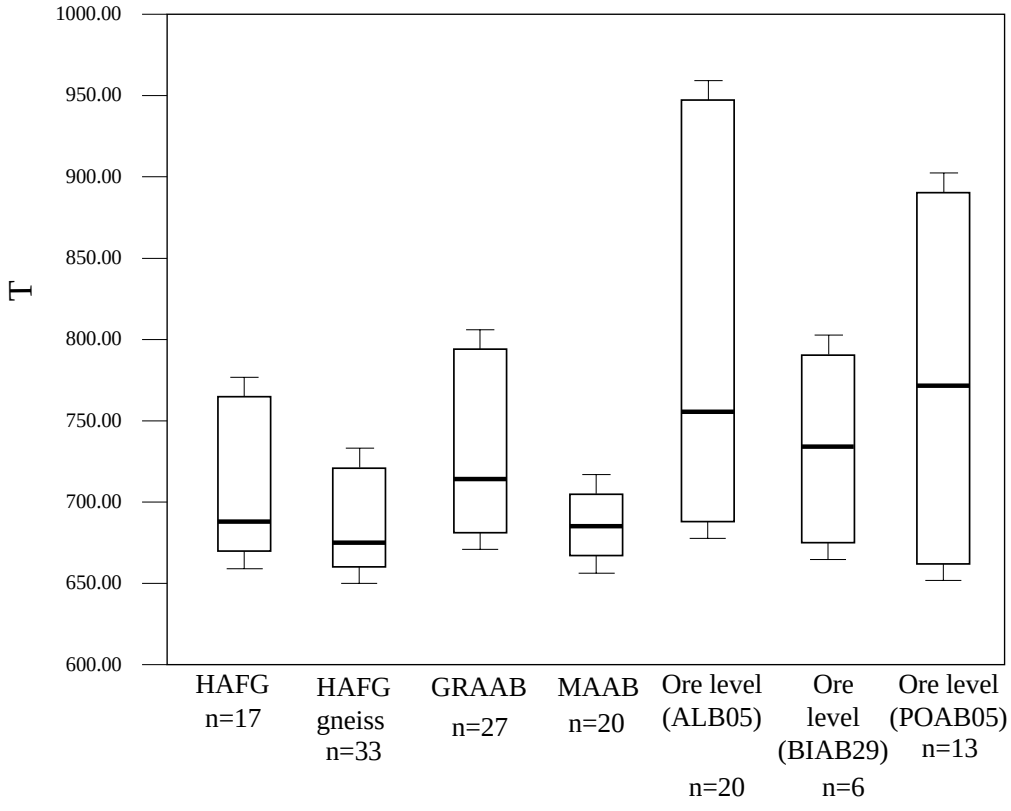

Fig. 41: Plot of the temperature results obtained from each sample using the Zr-in-titanite geothermometer (Hayden et al., 2008). The box indicates the range of values obtained for the sample using a pressure of 8 kbars, the thick black line in the box indicates the average temperature value obtained for a pressure of 8 kbar. The error bars surrounding the boxes indicate the lowest value obtained using a lower pressure (7 kbars) and the highest obtained value using a higher pressure (9 kbar). HAFG: hypersolvus alkali-feldspar granite, GRAAB: garnet-bearing albitite (sample 7-1B), MAAB: magnetite bearing albitite (sample GNA-02).

5.7.5 Vanadium

Previous studies using whole rock geochemical analyses have shown the positive relationship between V and U in the Lagoa Real deposits (Maruejol, 1988; Lobato and Fyfe, 1990) and in some other albitite-type uranium deposits such as Jacques's Lake in Canada, and Valhalla in Australia (Wilde, 2013). The uranium-related titanite chemistry presented here shows this same relationship and has the highest V contents as well (Fig. 41D).

Bernau and Franz (1987) reported that V^{5+} substitution on the Ti site occurs under highly oxidizing conditions above the hematite-magnetite buffer during calc-silicate alteration. This is consistent with the fact that V is more soluble and mobile under high fO_2 oxidizing conditions (Micko, 2010), which increases the oxidation state from V^{3+} to V^{5+} and facilitates V incorporation into the titanite structure.

Bernau and Franz (1987) showed that the main mechanism of V substitution in titanite is through coupled substitutions: Ti + O = V^{3+} + (OH, F); Ti = V^{4+}; and 2 Ti = V^{5+} + (Al, Fe)$^{3+}$. However, in our samples, V correlates positively with Ti (Fig. 11A) and has a negative linear correlation with Al + Fe (Fig. 11B) and Y (Fig. 11C), which means that none of the aforementioned reactions work in our case. In addition, the substituting relationship with elements in the 3+ oxidation state and similar ionic radii indicates that vanadium was incorporated in titanite in the reduced form, V^{3+}. The low Fe^{3+} content in the related titanite-ore can be the result of increasing vanadium replacement, as they both have similar charge and ionic radius (V^{3+}= 0.065A; Fe^{3+}=0.067A).

Similar to uranium, V mobility is controlled by redox conditions and high valence V (V^{5+}) is transported in oxidizing environments. Because of that, the close relationship between U and V is usual in uranium sandstone-hosted deposits, where V is generally hosted in uranium minerals, i.e. coffinite, uraninite, or vanadium alumino-silicates

(Thamm et al, 1981; Northrop et al, 1990). In this case, the V source likely is the dissolution of Fe-Ti oxides related to migration of brines that move upwards and mix with meteoric water (Breit and Goldhaber, 1996). Previous electron microprobe analyses in uraninite from Lagoa Real do not showed appreciable vanadium contents in uraninite or other uranium minerals (Maruejol, 1988; Avelar, 2008), therefore titanite, and probably other silicates, like amphibole and biotite, are the main V hosts in Lagoa Real. The consumption of ilmenite and magnetite may be a likely V source, which would explain the presence of V with +3 valence (Fig. 42B and C) as vanadium frequently occurs in the reduced form in primary minerals (Kelley et al, 2007).

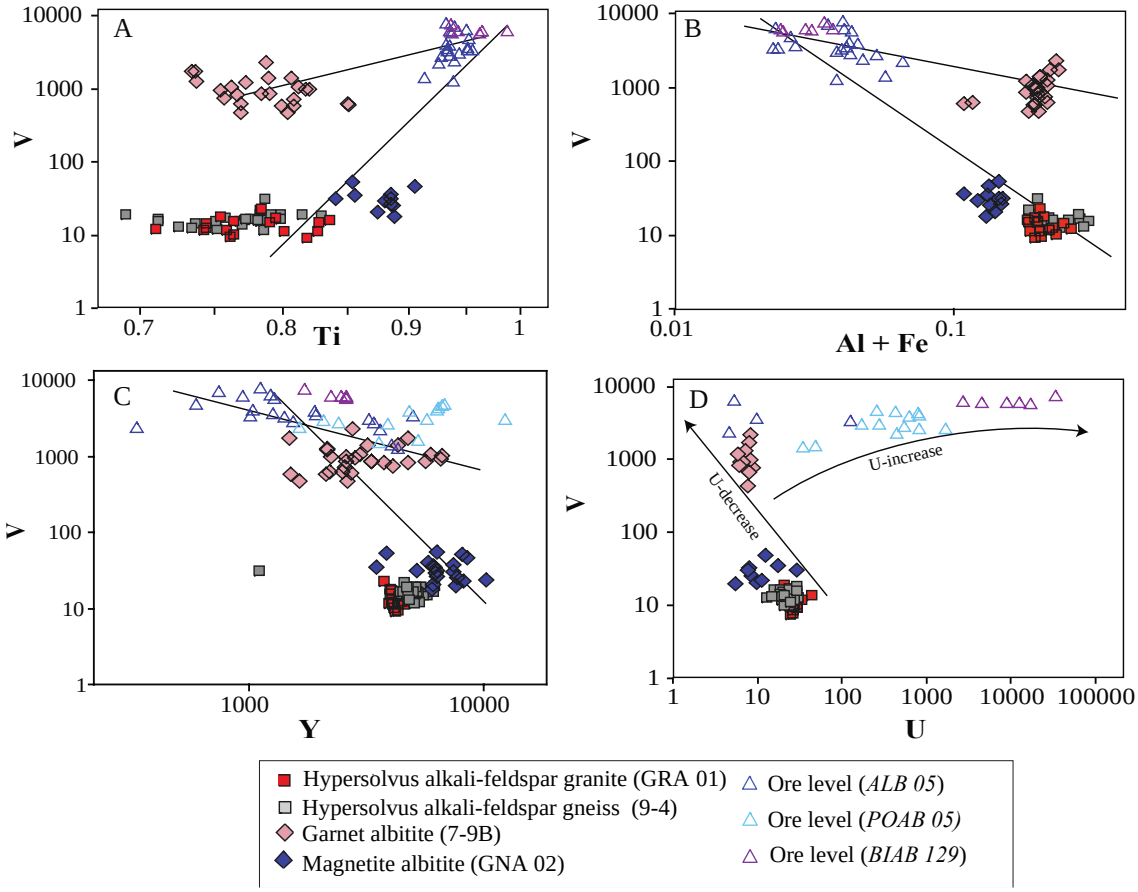

Fig. 42: Bivariant plots showing vanadium correlation with selected elements. a) V vs.Ti. b) V vs. Al + Fe. c) V vs. Y. d) V vs U.

5.7.6 Zirconium and Hafnium

The relationship of Zr and Hf was studied by Bau (1996), who put forward that elements with similar charge and radius, like Zr and Hf, have similar chondritic behavior and, hence, can be good indicators of interaction with aqueous fluids. Bau (1996) further stated that these geochemical twins may behave differently in an aqueous fluid. Our data show

that there is a decrease in the Hf contents in relation to Zr (Fig. 6A), which results in the increase of the Zr/Hf ratio. The Hf loss probably is related to the precipitation of zircon in mineralized rocks, as Hf is strongly partitioned into this mineral. Evidence for mobilization of Zr from zircon in Lagoa Real was recently observed by Marques et al. (2020a) who described porous, fractured zircon crystals surrounded by a rim of newly precipitated zircon, and the presence of tiny inclusions of zircon in titanite which shows that zircon experienced dissolution-reprecipitation processes during U mineralization.
Zirconium transport, the high Zr/Hf ratios, albitization and quartz dissolution previously observed in albitite rocks (Lobato and Fyfe, 1990) coherently indicate a high alkalinity for the fluid (Aja et al., 1995; Pouchon et al., 2001) responsible for the metasomatic alteration, and alkaline pH also favours elevated U solubilities as hydroxyl complexes (Romberger, 1984). Our data shows that titanite acted at least as one possible uranium source, as titanite with a magmatic signature shows progressive U-loss and uraninite was exsolved from titanite.

5.8 CONCLUSIONS

Rare-earth-element patterns of titanite and its V, Zr/Hf, HREE, Y, Fe, Al and Th/U contents are capable of tracking the genetic signature of titanite. The europium anomaly can be used as a redox tracer, suggesting that oxygen fugacity was variable during U precipitation in the Gameleira I uranium deposit. According to the Zr-in-titanite geothermometer, magmatic titanite crystallized at 670 – 690 ºC. Titanite in the magnetite-bearing albitite and garnet-bearing albitite, which represents the Ca-Fe-Mg alteration, was formed at 620 ºC and 680 ºC, respectively. The temperature obtained from titanite is similar to the magmatic samples, and is concordant with albitization and hastingsite dehydration. Zirconium mobility during U precipitation makes the geothermometer unreliable in the mineralized samples.

Our data suggest that the trace-element signature of titanite from host granitic rocks, through barren albitite, to mineralized albitite tracks an evolution from magmatic titanite, through its partial alteration during the albitite-forming process, to the new formation of hydrothermal titanite in U-mineralized albitite and that titanite acted as a possible uranium source. Variable REE-chondrite normalized patterns, contrasting Eu* and Ce* anomalies in the altered and hydrothermal titanite may reflect the different precipitation age already described in the literature

5.9 REFERENCES

Aleinikoff, J.N., Wintsch, R.P., Fanning, C.M., Dorais, M.J., 2002. U-Pb geochronology of zircon and polygenetic titanite from the Glastonbury Complex, Connecticut, USA: An integrated SEM, EMPA, TIMS, and SHRIMP study. Chem. Geol. 188, 125–147. https://doi.org/10.1016/S0009-2541(02)00076-1

Alkmim, F.F., Marshak, S., Pedrosa-Soares, A.C., Peres, G.G., Cruz, S.C.P., Whittington, A., Carlos Pedrosa-Soares, A., Gravina Peres, G., Cruz, S.C.P., Whittington, A., 2006. Kinematic evolution of the Araçuaí-West Congo orogen in Brazil and Africa: Nutcracker tectonics during the Neoproterozoic assembly of Gondwana. Precambrian Res. 149, 43–64. https://doi.org/10.1016/j.precamres.2006.06.007

Alkmim, F., Brito Neves, B.B, Alves, J.A.C., 1993. Arcabouço tectônico do Cráton do São Francisco: uma revisão, in: BA/SE, N. (Ed.), O Cráton Do São Francisco. Sociedade Brasileira de Geologia, Salvador, pp. 45–62.

Amorim, L.E.D., 2012. O granito São Timóteo no perfil Monsenhor Bastos, Província uranífera de Lagoa Real. Centro de Desenvolvimento da Tecnologia Nuclear.

Amorim, L.E.D., Rios, F. J., Freitas, M. E., Cutts, K., Geraldes, M. C., Diniz, A. C. D., Matos, E. C. 2020. Zircon U-Pb geochronology of Paleoproterozoic Statherian intraplate A-Type magmatic associations of the Lagoa Real Uranium Province, São Francisco Craton (Bahia, Brazil). Journal of South American Earth Sciences. submitted.

Anderson, J. L., & Smith, D. R., 1995. The effects of temperature and f O2 on the Al-in-hornblende barometer. *American Mineralogist*, *80*(5-6), 549-559.

Arcanjo, J., Marques-Martins, A., Loureiro, H.S., Varela, P.H., 2005. Projeto Vale do Paramirim, Bahia: geologia e recursos minerais. Companhia Baiana de Pesquisa Mineral (CBPM), Salvador.

Avelar, S. C. P.. Datação química U-Th-Pb de minerais dos albititos uraníferos da região de Lagoa Real (Ba) por microssonda eletrônica. 2005. CDTN-CNEN/BH. Dissertação (Mestrado). Centro de Desenvolvimento da Tecnologia Nuclear, Belo Horizonte.

Aja, S.U., Wood, S.A., Williams-Jones, A.E., 1995. The aqueous geochemistry of Zr and the solubility of some Zr-bearing minerals. Applied Geochemistry 10, 603–620

Babinski, M., Van Schmus, W.R., Chemale Jr, F., 1999. Pb–Pb dating and Pb isotope geochemistry of Neoproterozoic carbonate rocks from the São Francisco basin,

Brazil: implications for the mobility of Pb isotopes during tectonism and metamorphism. Chem. Geol. 160, 175–199.

Bastos-Leal, L.R., Teixeira, W., Cunha, J.C., Leal, A.B.M., Macambira, M.J.B., Rosa, M.L.S., 2000. Isotopic signatures of paleoproterozoica granitoids of the Gavião block and implications for the evolution of the São Francisco craton, Bahia, Brazil. Rev. Bras. Geociências 30, 66–69.

Bastos-Leal, L.R., Teixeira, W., Cunha, J.C., Macambira, M.J.B., 1998. Archean tonalitic- trondhjemitic and granitic plutonism in the Gavião block, São Francisco Craton, Bahia, Brazil: Geochemical and geochronology characteristics. Rev. Bras. Geociência 2, 209–220.

Bau, M., 1996. Controls on the fractionation of isovalent trace elements in magmatic and aqueous systems: evidence from Y/Ho, Zr/Hf, and lanthanide tetrad effect. Contrib. to Mineral. Petrol. 123, 323–333. https://doi.org/10.1007/s004100050159

Bau, M., Dulski, P., 1996. Distribution of yttrium and rare-earth elements in the Penge and Kuruman iron-formations, Transvaal Supergroup, South Africa. Precambrian Res. 79(1–2), 37–55.

Bernau, R., Franz, G., 1987. Crystal chemistry and genesis of Nb-, V-, and Al-rich metamorphic titanate form Egypt and Greece. Can. Mineral. 25, 695–705.

Breit, G.N., and Wanty, R.B., 1991, Vanadium accumulation in carbonaceous rocks—A review of geochemical controls during deposition and diagenesis: Chemical Geology, v. 91, no. 2, p. 83–97.

Bitencourt, C.N., Cruz, S.C.P., dos Anjos Cruz, V., Pedrosa-Soares, A.C., Paquette, J.L., Alkmim, A.R., Barbosa, J.S.F., 2019. Rifting events in the southern sector of the Paramirim Aulacogen, NE Brazil: New geochronological data and correlations for the São Francisco – Congo paleocontinent. Precambrian Res. 326, 417–446. https://doi.org/10.1016/j.precamres.2018.12.005

Brito, W., Raposo, C., Matos, E.C. De, 1984. Os albititos uraníferos de Lagoa Real. In: Anais do XXXIII Congresso Brasileiro de Geologia, Rio de Janeiro, vol. 3, pp. 1475 –1488.

Broska, I., Harlov, D., Tropper, P., Siman, P., 2007. Formation of magmatic titanite and titanite-ilmenite phase relations during granite alteration in the Tribeč Mountains, Western Carpathians, Slovakia. Lithos 95, 58–71. https://doi.org/10.1016/j.lithos.2006.07.012

Boynton, W. V. Geochemistry of the rare earth elements: meteorite studies. In: Henderson, P. (Ed.), Rare Earth Element Geochemistry. Elsevier, p. 63-114. 1984.

Carlier, G., Lorand, J.P., 2008. Zr-rich accessory minerals (titanite, perrierite, zirconolite, baddeleyite) record strong oxidation associated with magma mixing in the south Peruvian potassic province. Lithos 104, 54–70.

Cempírek, J., Houzar, S., Novák, M., 2008. Complexly zoned niobian titanite from hedenbergite skarn at Písek, Czech Republic, constrained by substitutions Al(Nb, Ta) Ti-2, Al(F, OH)(TiO)-1 and SnTi-1. Mineral. Mag. 72(6), 1293–1305.

Chaves, A. de O., 2013. New geological model of the Lagoa Real uraniferous albitites from Bahia (Brazil). Cent. Eur. J. Geosci. 5, 354–373. https://doi.org/10.2478/s13533-012-0134-7

Chaves, A. O., Tubrett, M., Avelar, S. C., Rios, F. J., Sgarbi, G. N., Neves, J. M., Alves, J. V., Fuzikawa, K., Matos, E. C., Prates, S. P. (2009). Electron microprobe chemical U-Th-Pb and La-ICP-MS U-Pb dating of multiple hydrothermal and metamorphic events recorded in minerals of the Lagoa Real uraniferous albitites (Brazil). Pesquisas em Geociências, 36(2), 181-201

Che, X.D., Linen, R.L., Wang, R.C., Groat, L.A., Br, A.A., 2013. Distribution of trace and rare earth elements in titanite from tungsten and molybdenum deposits in Yukon and British Columbia, Canada. Can. Mineral. 51, 415–438. https://doi.org/10.3749/canmin.51.3.415

Cherniak, D.J., 2006. Zr diffusion in titanite. Contrib. to Mineral. Petrol. 152, 639–647. https://doi.org/10.1007/s00410-006-0133-0

Cordani, U.G., Iyer, S.S., Taylor, P.N., Kawashita, K., Sato, K., McReath, I., 1992. Pb-Pb, Rb-Sr, and K-Ar systematics of the Lagoa real uranium province (south-central Bahia, Brazil) and the Espinhaço Cycle (ca. 1.5-1.0 Ga). J. South Am. Earth Sci. 5, 33–36.

Cordani, U.G., Sato, K., Marinho, M.M., 1985. The geologic evolution of the ancient granite-greenstone terrane of central-southern Bahia, Brazil. Precambrian Res. 27, 187–213.

Cruz, S.C.P., Alkmim, F.F., 2017. The Paramirim Aulacogen, in: Heilbron, M., Cordani, U.G., Alkmim, Fernando F. (Eds.), São Francisco Craton, Eastern Brazil: Tectonic Genealogy of a Miniature Continent, Regional Geology Reviews. Springer International Publishing, Cham, p. 326. https://doi.org/10.1007/978-3-319-01715-0

Cruz, S.C.P., Alkmim, F.F., 2007. A história de inversão do aulacógeno do Paramirim contada pela sinclinal de Ituaçu , extremo sul da Chapada Diamantina (BA). Rev. Bras. Geociências 37, 92–110.

Cruz, S.C.P., Barbosa, J.S.F., Santos Pinto, M., Peucat, J.J., Paquette, J.L., Souza, J.S., Martins, V.S., Chemale Júnior, F., Carneiro, M.A., 2016. The Siderian-Orosirian magmatism in the Gavião Paleoplate, Brazil: U-Pb geochronology, geochemistry and tectonic implications. J. S. Am. Earth Sci. 69, 43–79.

Cruz, S.C.P., Peucat, J.J., Teixeira, L., Carneiro, M.A., Marques Martins, A.A., Santana, J. dos S., De Souza, J.S., Barbosa, J.S.F., Leal, Â.B.M., Dantas, E., Pimentel, M., 2012. The Caraguataí syenitic suite, a ca. 2.7Ga-old alkaline magmatism (petrology, geochemistry and U-Pb zircon ages). Southern Gavião block (São Francisco Craton), Brazil. J. South Am. Earth Sci. 37, 95–112. https://doi.org/10.1016/j.jsames.2011.11.006

Cunha, J.C., Barbosa, J.S.F., Mascarenhas, J.F., 2012. Greenstones Belts e Sequências Similares, in: Geologia Da Bahia. Pesquisa e Atualização, CBPM Série Publicações Especiais. Salvador, pp. 203–325.

Cruz, S. C. P., Alkmim, F. F., Barbosa, J. S. F., Dussin, I., Gomes, L. C. C., 2015. Tectonic inversion of compressional structures in the Southern portion of the Paramirim Corridor, Bahia, Brazil. Brazilian Journal of Geology, 45(4), 541-567

Danderfer, A., Dardenne, M.A., 2002. Tectonoestratigrafia Da Bacia Espinhaço Na Porção Cen- Tro-Norte Do Cráton Do São Francisco : Registro De Uma Evolução Poliistórica Descontínua 32, 449–460.

Danderfer, A., De Waele, B., Pedreira, A.J., Nalini, H.A., 2009. New geochronological constraints on the geological evolution of Espinhaço basin within the São Francisco Craton—Brazil. Precambrian Res. 170, 116–128. https://doi.org/10.1016/j.precamres.2009.01.002

Danderfer Filho, A., Lana, C.C., Nalini Junior, H.A., Costa, A.F.O.O., Nalini Júnior, H.A., Costa, A.F.O.O., 2015. Constraints on the Statherian evolution of the intraplate rifting in a Paleo-Mesoproterozoic paleocontinent: New stratigraphic and geochronology record from the eastern São Francisco craton. Gondwana Res. 28, 668–688. https://doi.org/10.1016/j.gr.2014.06.012

Danderfer Filho, A., 2000. Geologia sedimentar e evolução tectônica do Espinhaço Setentrional, estado da Bahia. Universidade Federal de Brasília, Brasília. Unpublished Ph.D. thesis

Danderfer Filho, A., 1990. Análise estrutural descritiva e cinemática do Supergrupo Espinhaço na região da Chapada Diamantina (BA). Universidade Federal de Ouro Preto. Unpublished MsC thesis

Danderfer Filho, A., Lagoeiro, L.E., Alkmim, F.F., 1993. O sistema de dobramentos e empurrões da Chapada Diamantina (BA): registro da inversão do Aulacógeno do Espinhaço no decorrer do Evento Brasiliano, in: Simpósio Sobre o Cráton Do São Francisco. pp. 97–99.

Deer, W.A., Howie, R.A., Zussman, J., 1982. Rock-forming minerals: orthosilicates, Volume 1A. Geological Society of London.

Della Ventura, G., Bellatreccia, F., Williams, C., 1999. Zr- and LREE-rich titanite from Tre Croci, Vico volcanic complex (Latium, Italy). Mineral. Mag. 63, 123–130.

Deng, X., Li, J., Zhou, M., Zhao, X., Yan, D., 2015. In-situ LA-ICPMS trace elements and U – Pb analysis of titanite from the Mesozoic Ruanjiawan W – Cu – Mo skarn deposit , Daye district , China. Ore Geol. Rev. 65, 990–1004. https://doi.org/10.1016/j.oregeorev.2014.08.011

Franz, G., Spear, F.S., 1985. Aluminous titanite (sphene) from the Eclogite Zone, south-central Tauern Window, Austria. Chem. Geol. 50, 33–46. https://doi.org/10.1016/0009-2541(85)90110-X

Frost, B.R., Chamberlain, K.R., Schumacher, J.C., 2000. Sphene (titanite): phase relations and role as a geochronometer. Chem. Geol. 172, 131–148. https://doi.org/10.1016/S0009-2541(00)00240-0

Fu, Y., Sun, X., Zhou, H., Lin, H., Yang, T., 2016. In-situ LA-ICP-MS U-Pb geochronology and trace elements analysis of polygenetic titanite from the giant Beiya gold-polymetallic deposit in Yunnan Province, Southwest China. Ore Geol. Rev. 77, 43–56. https://doi.org/10.1016/j.oregeorev.2016.02.001

Gao, X.-Y., Zheng, Y.-F., Chen, Y.-X., Guo, J., 2012. Geochemical and U–Pb age constraints on the occurrence of polygenetic titanites in UHP metagranite in the Dabie orogen. Lithos 136, 93–108.

Geisel Sobrinho, E., Raposo, C., Alves, J. V, Brito, W.D., Vasconcelos, T.G., 1980. O distrito uranífero de Lagoa Real, Bahia. Congr. Bras. Geol. 31, 1499–1512.

Giannetti, B., Luhr, J.F., 1983. The white trachytic tuff of Roccamonfina Volcano (Roman Region, Italy). Contrib. to Mineral. Petrol. 84, 235–252.

Guillong, M., Meier, D.L., Allan, M.M., Heinrich, C.A., Yardley, B.W.D., 2008. Appendix A6: SILLS: A MATLAB-based program for the reduction of laser

ablation ICP-MS data of homogeneous materials and inclusions. Mineral. Assoc. Canada Short Course 40, 328–333.

Guimarães, J.T., Santos, R.A., Melo, R.C., 2008. Geologia da Chapada Diamantina (Projeto Ibitiara-Rio de Contas). CBPM, Série Arqu. ed. Salvador, BA.

Guo, J.-L., Gao, S., Wu, Y.-B., Hu, Z.-C., Xu, W.-L., Zong, K.-Q., Liu, Y.-S., Yuan, H.-L., 2014. Titanite evidence for Triassic thickened lower crust along southeastern margin of North China Craton. Lithos 206, 277–288.

Harlov, D., Tropper, P., Seifert, W., Nijland, T., Förster, H.-J., 2006. Formation of Al-rich titanite (CaTiSiO4O–CaAlSiO4OH) reaction rims on ilmenite in metamorphic rocks as a function of fH2O and fO2. Lithos 88, 72–84. https://doi.org/10.1016/j.lithos.2005.08.005

Hayden, L.A., Watson, E.B., Wark, D.A., 2008. A thermobarometer for sphene (titanite). Contrib. to Mineral. Petrol. 155, 529–540. https://doi.org/10.1007/s00410-007-0256-y

Henderson, P., 1980. Rare earth element partition between sphene, apatite and other coexisting minerals of the Kang-erdlugssuaq intrusion, E. Greenland. Contrib. to Mineral. Petrol. 72, 81–85.

Horie, K., Hidaka, H., Gauthier-Lafaye, F., 2008. Elemental distribution in apatite, titanite and zircon during hydrothermal alteration: Durability of immobilization mineral phases for actinides. Phys. Chem. Earth 33, 962–968. https://doi.org/10.1016/j.pce.2008.05.008

Hovelmann, J., Putnis, A., Geisler, T., Schmidt, B.C., Golla-Schindler, U., 2010. The replacement of plagioclase feldspars by albite: observations from hydrothermal experiments. Contrib. Mineral Petrol. 159, 43–59.

Kelley, K.D., Scott, C.T., Polyak, D.E., and Kimball, B.E., 2017, Vanadium, chap. U *of* Schulz, K.J., DeYoung, J.H., Jr., Seal, R.R., II, and Bradley, D.C., eds., Critical mineral resources of the United States—Economic and environmental geology and prospects for future supply: U.S. Geological Survey Professional Paper 1802, p. U1–U36, https://doi.org/ 10.3133/pp1802U.

King, P., Sham, T., Gordon, R., Dyar, M., 2013. Microbeam X-ray analysis ofCe3+/Ce4+ in Ti-rich minerals: a case study with titanite (sphene) with implications for multivalent trace element substitution in minerals. Am. Mineral. 98, 110–119.

Kohn, M.J., 2018. Titanite Petrochronology. Rev. Mineral. Geochemistry 83, 419–441. https://doi.org/10.2138/rmg.2017.83.13

Kowallis, B.J., Christiansen, E.H., Griffen, D.T., 1997. Composicional variations in titanite, in: Geological Society of America Abstracts with Programs. p. A-402, v.29.

Leake, B. E., Woolley, A. R., Birch, W. D., Burke, E. A., Ferraris, G., Grice, J. D., Hawthorne, F. C., Kisch, H. J., Krivovichev, V. G., Schumacher, J. C.; Stephenson, N. C. N., Whittaker, E. J. W. 2004. Nomenclature of amphiboles: additions and revisions to the International Mineralogical Association's amphibole nomenclature. *Mineralogical Magazine*, *68*(1), 209-215.

Deng, J.W., X.D., Zhou, M.F., Liu, Y.S., Zhao, X.F., Guo, J.L., 2010. Laser ablation ICP-MS titanite U-Th-Pb dating of hydrothermal ore deposits: A case study of the Tonglushan Cu-Fe-Au skarn deposit, SE Hubei Province, China. Chem. Geol. 270, 56–67. https://doi.org/10.1016/j.chemgeo.2009.11.005

Liu, Y., Fan, Y., Zhou, T., Zhang, L., White, N.C., Hong, H., Zhang, W., 2018. LA-ICP-MS titanite U-Pb dating and mineral chemistry of the Luohe magnetite-apatite (MA)-type deposit in the Lu-Zong volcanic basin, Eastern China. Ore Geol. Rev. 92, 284–296. https://doi.org/10.1016/j.oregeorev.2017.11.018

Lobato, L.M., Fyfe, W.S., 1990. Metamorphism, metasomatism, and mineralization at Lagoa Real, Bahia, Brazil. Econ. Geol. 85, 968–989. https://doi.org/10.2113/gsecongeo.85.5.968

Lobato, L.M., Pimentel, M.M., Cruz, S.C.P., Machado, N., Noce, C.M., Alkmim, F.F., 2015. U-Pb geochronology of the Lagoa Real uranium district, Brazil: Implications for the age of the uranium mineralization. J. South Am. Earth Sci. 58, 129–140. https://doi.org/10.1016/j.jsames.2014.12.005

Loureiro, H.S.C., Bahiense, I.C., Neves, J.P., Guimarães, J.T., Teixeira, L.R., Santos, R.A., Melo, R.C., 2009. Geologia e recursos minerais da parte norte do corredor de deformação do Paramirim (Projeto Barra – Oliveira dos Brejinhos)., Série Arqu. ed. Salvador, BA.

Machado, G. S. 2008. Geologia da porção sul do complexo Lagoa Real, Caetité, Bahia. Trabalho Final de Graduação, Instituto de Geociências, Universidade Federal da Bahia, Salvador.

Marinho, M.M., 1991. La séquence volcano-sédimentaire de Contendas-Mirante et la bordure occidentale du Bloc Jequié (Craton du São Francisco, Brésil): un exemple de transition Archéen-Proterozóïque.

Martin, H., Peucat, J.J., Sabaté, P., Cunha, J.C., 1991. Um segment de croûte continentale d'Age archéean ancien (3.5 millards d'années): lê massif de Sete Voltas (Bahia, Brésil). Les Comptes Rendus l'Académie des Sci. Paris 313, 531–538.

Maruejol, P., 1988. Métasomatose alcaline et minéralisations uranifères : les albitites du gisement de Lagoa Real (Bahia, Brésil) et exemples complémentaires de Xihuashan (SE Chine), Zheltorechensk (Ukraine) et Chhuling Khola (Népal central). Ph.D. thesis, Centre de Recherches sur la Geologie de l'Uranium, Nancy, France.

Maruéjol, P., Cuney, M., Fuzikawa, K., Netto, A.M., Poty, B., 198. The Lagoa Real subalkaline granitic complex (South Bahia, Brazil). Rev. Bras. Geociências 17, 578–594.

Matos, E.C., Villegas, R.A.S., 2010. Exploration and mining activities in the uranium province of Lagoa Real. In: Ozberk, E. (Ed.). Uranium 2010: The Future is U. Proceedings, The Canadian Institute of Mining, Metallurgy and Petroleum, vol. 1, pp. 153–159.

Matos, E.C., Silva, J.R.A., Rubini, L.A., 2003. A província uranífera de Lagoa Real - garantia de fornecimento de concentrado de urânio (DUA) para as necessidades brasileiras. Revista de Geolologia 16, 111–120.

Mazdab, F.., 2009. Characterization of flux-grown trace-element-doped titanite using high-mass-resolution ion microprobe (SHRIMP-RG). Can. Mineral. 47, 813–831.

McLeod, G., Dempster, T., Faithfull, J., 2010. Deciphering magma- mixing processes using zoned titanite from the Ross of Mull Gran- ite, Scotland. J. Petrol. 55–82.

Medeiros, E.L.M., Cruz, S.C.P., Barbosa, J.S.F., Paquette, J.L., Peucat, J., Jesus, S.S.G.P., Barbosa, R.G., Brito, R.S., Carneiro, M.A., 2017. The Santa Izabel complex, Gavião Block, Brazil: components, geocronology, regional correlations and tectonic implications. J. South Am. Earth Sci. 80, 66–94.

Menezes, R.C.L., Conceição, H., Rosa, M.D.L.D.S., Macambira, M.J.B., Galarza, M.A., Rios, D.C., 2012. Geoquímica e geocronologia de granitos anorogênicos Tonianos (ca. 914–899 Ma) da Faixa Araçuaí no sul do Estado da Bahia. Geonomos 20, 1–13.

Micko, J., 2010. The Geology and Genesis of the Central Zone alkalic Cu-Au porphyry deposit, Galore Creek District, Northwestern BC, Canada. The University of British Columbia, Vancouver, British Columbia.

Misi, A., Veizer, J., 1996. Chemostratigraphy of neoproterozoic carbonate sequences of the Una Group, Irecê Basin, Brazil, in: 39 Congresso Brasileiro de Geologia.

Morad, S., Geosciences, P., Dhabi, A., Box, P.O., Dhabi, A., 2009. Hydrothermal Alteration of Magmatic Titanite : Evidence From Proterozoic Granitic Rocks , Southeastern Sweden 47, 801–811.

Morimoto, N. 1988. Nomenclature of pyroxenes. Mineralogy and Petrology,39(1), 55-76.

Northrop, H.R., Goldhaber, M.B., Landis, G.P., Unruh, J.W., Reynolds, R.L., Campbell, J.A., Wanty, R.B., Grauch, R.I., Whitney, G., and Rye, R.O., 1990, Genesis of the tabular- type vanadium-uranium deposits of the Henry basin, Utah: Economic Geology, v. 85, p. 215–269.

Nutman, A.P., Cordani, U.G., 1993. SHRIMP U-Pb zircon geochronology of Archaean granitoids from the Contendas-Mirante area of the São Francisco Craton, Bahia, Brazil. Precambrian Res. 63, 179–188.

Oberti, R., Smith, D.C., Rossi, G. and Caucia, F. (1991) The crystal-chemistry of high-aluminium titanites. *European Journal of Mineralogy*, **3**, 777–792.

Pedrosa-Soares, A.C., Alkmim, F.F., Tack, L., Noce, C.M., Babinski, M., Silva, L.C. da, Martins-Neto, M.A., 2008. Similarities and differences between the Brazilian and African counterparts of the Neoproterozoic Araçuaí-West Congo Orogen. Geol. Soc. London, Spec. Publ. 294, 153–172.

Pedrosa-Soares, A.C., Noce, C.M., Alkmim, F.F. De, Carlos, L., Babinski, M., Cordani, U., Castañeda, C., 2007. Orógeno Araçuaí : Síntese Do Conhecimento 30 Anos Após Almeida 1977 15, 1–16.

Pedrosa-Soares, A.C., Noce, C.M., Wiedemann, C.M., Pinto, C.P., 2001. The Araçuaı-West-Congo Orogen in Brazil: an overview of a confined orogen formed during Gondwanaland assembly. Precambrian Res. 110, 307–323.

Pedrosa-Soares, A.C., Wiedemann-Leonardos, C.M., 2000. Evolution of the Araçuaí Belt and its connection to the Ribeira Belt, Eastern Brazil. Tecton. Evol. South Am. 31, 265–310.

Peucat, J.-J., Mascarenhas, J. de F., Barbosa, J.S.F., de Souza, S.L., Marinho, M.M., Fanning, C.M., Leite, C.M.M., 2002. 3.3 Ga SHRIMP U–Pb zircon age of a felsic metavolcanic rock from the Mundo Novo greenstone belt in the São Francisco craton, Bahia (NE Brazil). J. South Am. Earth Sci. 15, 363–373.

Piccoli, P., Candela, P., Rivers, M., 2000. Interpreting magmatic processes from accessory phases: titanite—a small-scale recorder of large- scale processes. Earth Env. Sci Trans R Soc Edinb 91, 257–267.

Pouchon, M.A., Curti, E., Degueldre, C., Tobler, L., 2001. The influence of carbonate complexes on the solubility of zirconia: new experimental data. Progress in Nuclear Energy 38, 443–446

Prowatke, S., Klemme, S., 2005. Effect of melt composition on the partitioning of trace elements between titanite and silicate melt. Geochim. Cosmochim. Acta 69, 695–709. https://doi.org/10.1016/j.gca.2004.06.037

Raposo, C., Matos, E.C. de, Brito, W., 1984. Zoneamento cálcico-sódico nas rochas da Província Uranífera de Lagoa Real, in: Anais do XXXIII Congresso Brasileiro de Geologia, Rio de Janeiro, 1984

Rosa, A.M.L.S., Conceição, H., Oberli, F., Meier, M., Martin, H., Macambira, M.B., Santos, E.B., Paim, M.M., Leahy, G.A.S., Bastos Leal, L.R., 2000. Geochronology (U-Pb/Pb- Pb) and isotopic signature (Rb-Sr/Sm-Nd) of the paleoproterozoic Guanambi Batholith, southWestern Bahia State (NE Brazil). Rev. Bras. Geociência 30, 062–06.

Romberger, S.B., 1984. Transport and deposition of uranium in hydrothermal systems at temperatures up to 300 °C: geological implications. In: DeVivo, B., Ippolito, F., Capaldi, G., Simpson, P.R. (Eds.), Uranium Geochemistry, Mineralogy, Geology, Exploration and Resources. Institution of Mining and Metallurgy, London, pp. 12–17

Santana, A.V., 2016. Análise estratigráfica em alta resolução em rampa carbonática dominada por microbiolitos, Formação Salitre, Bacia de Irecê, Bahia. Ph.D. Thesis. Universidade Federal de Brasília, Brasília.

Santos, C. M., Cabral, A. R., Rios, F., 2020. Whole-rock chemistry of the Gameleira I uranium deposit, Lagoa Real, Brazil. Chemie der Erde. In press.

Santos-Pinto, M.., Peucat, J.J., Martin, H., Sabaté, P., 1998. Recycling of the Archaean continental crust: the case study of the Gavião Block, Bahia, Brazil. J. South Am. Earth Sci. Am. Earth Sci. 11, 487–498.

Santos-Pinto, M., Peucat, J.-J., Martin, H., Barbosa, J.S.F., Fanning, C.M., Cocherie, A., Paquette, J.-L., 2012. Crustal evolution between 2.0 and 3.5 Ga in the southern Gavião block (Umburanas-Brumado-Aracatu region), São Francisco Craton,

Brazil: a 3.5–3.8 Ga proto-crust in the Gavião block? J. South Am. Earth Sci. 40, 129–142.

Schmidt, M.W., 1992. Amphibole composition in tonalite as a function of pressure: an experimental calibration of the Al-in-hornblende barometer. Contrib. to Mineral. Petrol. 110, 304–310. https://doi.org/10.1007/BF00310745

Schobbenhaus, C., 2017. As tafrogêneses superpostas Espinhaço e Santo Onofre, estado da Bahia: Revisão e novas propostas. Rev. Bras. Geociências 26, 265–276.

Silveira, E.M., Söderlund, U., Oliveira, E.P., Ernst, R.E., Leal Menezes, A.B., 2013. First precise U–Pb baddeleyite ages of 1500Ma mafic dykes from the São Francisco Craton, Brazil, and tectonic implications. Lithos 174, 144–156. https://doi.org/10.1016/j.lithos.2012.06.004

Smith, M.P., Storey, C.D., Jeffries, T.E., Ryan, C., 2009. In situ U-Pb and trace element analysis of accessory minerals in the Kiruna District, Norrbotten, Sweden: New constraints on the timing and origin of mineralization. J. Petrol. 50, 2063–2094. https://doi.org/10.1093/petrology/egp069

Storey, C.D., Jeffries, T.E., Smith, M., 2006. Common lead-corrected laser ablation ICP–MS U–Pb systematics and geochronology of titanite. Chem. Geol. 227, 37–52.

Teixeira, L.R., 2000. Programa de Levantamentos Geológicos Basicos do Brasil.

Thamm, J.K., Kovschak, A.A., Jr., and Adams, S.S., 1981, National uranium resource evaluation—Geology and recognition criteria for sandstone uranium deposits of the Salt Wash type, Colorado Plateau province—Final report: Grand Junction, Colo., U.S. Department of Energy Report no. GJBX-6(81), 135 p

Tiepolo, M., Oberti, R., Vannucci, R., 2002. Trace-element incorporation in titanite: Constraints from experimentally determined solid/liquid partition coefficients. Chem. Geol. 191, 105–119. https://doi.org/10.1016/S0009-2541(02)00151-1

Tindle, A.G., Webb, P.C., 1994. PROBE-AMPH a spreadsheet to classify microprobe-derived amphibole analyses. Computers and Geosciences 20, 1201-1228. https://doi.org/10.1016/0098-3004(94)90071-X.

Tischendorf, G., Gottesmann, B., Förster, H.-J. and Trumbull, R.B. 1997. On Li-bearing Micas: Estimating Li from Electron Microprobe Analyses and an Improved Diagram for Graphical Representation. *Mineralogical Magazine*, **61**, 809–834.

Thomas, W.M., 1982. Stability relations of the amphibole hastingsite. American Journal of Science 282, 136–164.

Turpin, L., Maruejol, P., Cuney, M., 1988. U-Pb, Rb-Sr and Sm-Nd chronology of granitic basement, hydrothermal albitites and uranium mineralization (Lagoa Real, South-Bahia, Brazil). Contrib. to Mineral. Petrol. 98, 139–147. https://doi.org/10.1007/BF00402107

Wilde, A., 2013. Towards a Model for Albitite-Type Uranium. Minerals 3, 36–48. https://doi.org/10.3390/min3010036

Xie, L., Wang, R.C., Chen, J., Zhu, J.C., 2010. Mineralogical evidence for magmatic and hydrothermal processes in the Qitianling oxidized tin-bearing granite (Hunan, South China): EMP and (MC)-LA-ICPMS investigations of three types of titanite. Chem. Geol. 276, 53–68. https://doi.org/10.1016/j.chemgeo.2010.05.020

Xu, L., Bi, X., Hu, R., Tang, Y., Wang, X., Xu, Y., 2015. LA-ICP-MS mineral chemistry of titanite and the geological implications for exploration of porphyry Cu deposits in the Jinshajiang – Red River alkaline igneous belt, SW China. Mineral. Petrol. 109, 181–200. https://doi.org/10.1007/s00710-014-0359-x

CAPÍTULO 6 – EVOLUTION OF THE NORTHWEST LAGOA REAL URANIUM DEPOSITS, BRAZIL: CONSTRAINTS FROM MAGMATIC TO HYDROTHERMAL ASSEMBLAGE

Camila Marques[a,b*], Francisco Javier Rios[c] Alexandre Raphael Cabral [c,d] Clemente Recio[b]

[a]Programa de Pós-Graduação em Ciência e Tecnologia das Radiações, Minerais e Materiais. Centro de Desenvolvimento da Tecnologia Nuclear (CDTN/CNEN-MG). Av. Antonio Carlos 6627 – Universidade Federal de Minas Gerais – Campus Pampulha, 30270-901, Belo Horizonte, Minas Gerais, Brazil – camisgeo@gmail.com

[b]Programa de Doctorado em Geología. Departamento de Geología, Facultad de Ciencias, Universidad de Salamanca, Plaza de los Caídos, s/n, 37008, Salamanca, España

[c]Centro de Desenvolvimento da Tecnologia Nuclear (CDTN/CNEN-MG). Av. Antonio Carlos 6627 – Universidade Federal de Minas Gerais – Campus Pampulha, 30270-901, Belo Horizonte, Minas Gerais, Brazil – javier@cdtn.br

[d]Centro de Pesquisas Professor Manoel Teixeira da Costa (CPMTC), Instituto de Geociências. Universidade Federal de Minas Gerais (UFMG), Av. Antonio Carlos 6627, 30270-901, Belo Horizonte, Minas Gerais, Brazil – arcabral@geol.igc.ufmg.br

Abstract

The Lagoa Real uranium (U) province, here referred to as Lagoa Real, hosts South America's only uranium mine currently in operation. Uranium orebodies are spatially associated with strongly deformed albite-rich rock, known as albitite, where uraninite occurs as fine-grained crystals. Albitite occurs as pods within granitic-gneissic rocks of the ca. 1.75 Ga Lagoa Real suite intrusive (LRSI). The studied deposits are located in the northwest of Lagoa Real where drill-holes intersect granite-gneiss wall rocks, barren albitite and U-mineralized albitite. Despite the importance of this deposit, the petrography and mineral chemistry of the host-rocks are currently poorly characterized. Here, we present new petrographical and mineral-chemical data of these deposits providing a detailed mineral characterization. Uraninite chemical dating via electron microprobe is also presented in order to understand the age of deposit. Granitic-gneissic wall rocks of LRIS is represented by the hypersolvus alkali-feldspar granite facies, which crystallized at around 900 ºC and below the FMQ buffer. Metasomatism and mineralization developed in two major stages, being the first developed prior Brasiliano orogeny and the second syn-to-post Brasiliano. The first stage is made up of the sodic-calcic (680–400 ºC) and iron-calcic-magnesian alteration. It records the complete conversion of the magmatic assemblage into albitite, which resulted in a mineral assemblage composed by albite and a series of Fe-Ca-Mg clinopyroxene, plus andradite, titanite and magnetite. This event probably occurred during the late-magmatic stage of LRIS crystallization, under variable oxygen fugacity as recorded in the clinopyroxene and titanite chemistry. U-enrichment in titanite is related to the reducing trend associated to Ca-Mg rocks. The second stage is represented by the K-Mg and late calcic alteration. Potassic-magnesian assemblage is made up of amphibole and biotite, whose developed under amphibolite-to greenschist facies at around 650–400 ºC and 3–0.9 kbar. This retrograde parageneses overprints the earlier stages and the composition of which seems to have been controlled by the clinopyroxene precursor. During the late calcic stage allanite, epidote and calcite precipitated under ductile-to-brittle regime and temperature below 300 ºC. Uraninite precipitated at around 580 Ma in a veinlet-style in the shear-zones during the Brasiliano syn-collisional stage. Uraninite chemical data attest for high temperature crystallization given its low U/Th ratio and high Y contents. During the late-to-post collisional Brasiliano orogeny (530–450 Ma) uraninite was redistributed as disseminations and was altered to U^{+6} species, i.e. uranophane. Mineral chemistry indicates that fluids circulated in the shear-zones collecting Cl from the early assemblage. This fluid is probably

meteoric in origin as indicated by low oxygen isotopic values, and this was responsible by the redistribution of early uranium mineralization.

Keywords: petrography, mineralogy, Lagoa Real uranium province, uranium deposit.

6.1 INTRODUCTION

The Lagoa Real U province (LRUP), referred as Lagoa Real, hosts the main U deposit of South America and the sixth largest uranium (U) resource in the world (OECD/NEA-IAEA, 2012). It is located on the eastern border of the northern Espinhaço fold thrust belt, in the intracontinental sector of the Araçuaí-West Congo Orogen. Lagoa Real has 38 uraniferous anomalies spread along approximately 35 km, structured in three semi-arched lineaments (Fig. 1) near the municipality of Caetité.

The hydrothermal formation of albitite is a well-known process in U deposits associated with Na-metasomatites, which involve the replacement of granitoid and metavolcanosedimentary magmatic assemblages by albite. This process has been described in U-deposits worldwide such as in the Ukraine (Central Ukrainian Uranium Province - CUUP; Cuney et al., 2012), Australia (Valhalla deposit, Mount Isa inlier; Polito et al., 2009) and in western Guyana (Aricheng South deposit; Alexandre, 2010), here the precipitation of albite is usually associated to quartz dissolution coupled with precipitation of other sodic-calcic phases (i.e., riebeckite, andradite, aegirine, epidote, calcite) and chlorite. The U-precipitation usually postdates albititzation in these deposits. Alteration and mineralization are usually the result of mixing between meteoric/basinal and magmatic fluids.

Sodium metasomatism and quartz dissolution are also described in Sn and Cu-Zn- Sn-W deposits worldwide (Costi et al., 2002; Cabellero, 1993; Tornos et al., 2000) and in the complex but well-defined group of rocks known fenites (Elliot et al., 2018). High temperature (>650 ºC) episyenite/albitite usually forms fenite- and skarn-like alteration, which includes Na-, Ca–Na, and Ca-amphiboles, commonly riebeckite or actinolite; and clinopyroxene, such as hedenbergite–aegirine or augite–aegirine. Whereas chloritization is by far the most common low temperature alteration (< 270 ºC).

Previous works (Maruejol, 1989; Lobato et al, 1983; Lobato and Fyfe, 1990; Cruz, 2004) describe the Lagoa Real albitite rocks as the result of sodium enrichment and quartz leaching along with calcic metasomatism and oxidizing reactions. Lobato et al, (1983) estimated the

temperature of hydrothermal alteration through oxygen isotopes to be around 500 ºC. The fluids were basinal brines and uranium deposition occurred in response to reduction of the fluid phase. While the timing of metasomatism and the driving mechanisms leading to the metasomatic alteration remain disputed, the preference of uranium mineralization to occur within the garnet-hedenbergite-bearing albitite seems to be unanimously acknowledged (Maruejol 1989; Lobato and Fyfe, 1990).

The mineral chemistry usually reflects variations in the physicochemical parameters such as temperature, pressure and redox conditions during magmatic and-/or hydrothermal processes. For this reason, systematic studies are of fundamental importance for the characterization of hydrothermal processes that led to ore deposition.

This contribution presents new mineral chemical data, hydrogen and oxygen stable isotope study from the magmatic and hydrothermal parageneses of three U-deposits located in the northwestern portion of the LRUP. The objective is to advance the understanding of the major mechanisms controlling the development of one of the most important uranium districts in the world associated with Na-metasomatism.

6.2 REGIONAL GEOLOGICAL CONTEXT

The Lagoa Real uranium province is located in northern part of the Neoproterozoic Araçuaí–West Congo orogenic system (AWCO), in a structure called the Paramirim aulacogen in the western sector of the São Francisco – Congo paleocontinent (Fig. 43; Alkmim et al., 2006; Pedrosa-Soares et al., 2007, 2008; Pedrosa-Soares and Wiedemann-Leonardos, 2000). The Paramirim aulacogen composes part of the intracontinental rift that preceded the AWCO and corresponds to a partially inverted rift-sag basin, filled by sediment cover that accumulated on the cratonic terrane from the Statherian (1775 ± 7 Ma; Danderfer Filho et al., 2015) through to the early-Ediacaran (675 Ma, Santana, 2016). Basin inversion occurred during the amalgamation of Gondwana in the Ediacaran-Cambrian Araçuai orogen (Cruz and Alkmim, 2007).

The basement of the Paramirim aulacogen (the Gavião block) is composed of: metagranitoids; orthogneiss rocks, often with Archean mafic and ultramafic migmatitic enclaves; greenstone belts; Paleoarchean, Neoarchean and Siderian–Rhyacian metavolcano-sedimentary sequences; and acidic, intrusive plutonic rocks of Siderian, Rhyacian and Orosirian ages (Cordani et al., 1985; Nutman and Cordani, 1993; Bastos-Leal et al., 1998,

2000; Cruz et al., 2012; Cruz et al., 2016; Cunha et al., 2012; Medeiros et al., 2017; Rosa et al., 2000; Santos-Pinto et al., 1998, 2012).

Anorogenic alkaline rocks in Lagoa Real, defined as the Lagoa Real intrusive suite (Arcanjo et al., 2005) and commonly known as the São Timóteo granite, crystallized at ca. 1750 Ma based on U-Pb in zircon (Lobato et al., 2015; Pimentel et al., 1994; Turpin et al., 1988, Amorim, 2020 - *submitted*). The São Timóteo granite consists of bodies of porphyritic and coarse-grained hastingsite-bearing syenite, syenogranite, and alkali granite. These are geochemically characterized as a reduced, ferroan A-type, metaluminous, high-K and Fe-rich calc-alkaline series (Maruejol et al., 1987; Teixeira, 2000, Amorim et al., 2020; Marques et al., 2020a). The Lagoa Real intrusive suite together with the Borrachudos and Catolé suites, and widespread meta-rhyolites and metamafic rocks in Espinhaço domains, make up a silicic large igneous province (SLIP) that erupted on the Sao Francisco paleocontinent from ca.1.79 Ga to 1.70 Ga (Magalhães et al., 2018 and references therein).

The metasedimentary cover units, the Espinhaço (Paleo-Mesoproterozoic) and São Francisco (Neoproterozoic) Supergroups outcrop in the Northern Espinhaço and Chapada Diamantina regions, these are also called the western and eastern basins respectively (Guimarães et al., 2012), and are separated by the Paramirim High (Cruz et al., 2012). The stratigraphic correlation of these Supergroups is still disputed despite decades of study (i.e. Derby, 1906; Schobbenhaus, 1996; Guimarães et al., 2012).

The Espinhaço Supergroup comprises a succession of siliciclastic rocks (metasandstones, metapelites, and metaconglomerates) with acidic, alkaline, and anorogenic subordinate metavolcanic rocks. The Supergroup has distinct facies in each basin and numerous works in the region have resulted in numerous names and stratigraphic correlations (see Cruz and Alkmim 2017). In the Northern Espinhaço Range, the Supergroup is subdivided into the Algodão Formation, and the Oliveira dos Brejinhos and São Marcos Groups. In the Chapada Diamantina basin, the Espinhaco Supergroup is comprised of the Serra da Gameleira Formation, and Rio dos Remédios, Paraguaçu and Chapada Diamantina Groups. Deposition of the Espinhaço Supergroup occurred from 1775 ± 26 Ma (U-Pb, LA-ICP-MS, zircon from volcanic rocks; Danderfer Filho et al., 2015) to around 1140 Ma (whole-rock Pb-Pb carbonate; Babinski et al., 1993).

The São Francisco Supergroup comprises the Santo Onofre group in the Northern Espinhaço basin, as well as the Bebedouro and Salitre Formations in the Chapada Diamantina basin. The Sao Francisco Supergroup is composed of siliciclastic rocks of

marine to alluvial origin, in addition to diamictites and carbonates that represent the Neoproterozoic Sturtian glacial event (ca. 715-650 Ma; Rooney et al 2017). The São Francisco Supergroup was deposited between ca. 850 Ma (U-Pb in detrital zircon; Bitencourt et al., 2019) to 675 Ma (U-Pb, SHRIMP, zircon; Santana, 2016).

Two groups of mafic sills and dikes intrude the Espinhaço Supergoup (Arcanjo et al., 2005; Menezes et al., 2012). These intrusions have tholeiitic compositions and continental intraplate affinity. The oldest group has ages of 1514 ± 22 Ma (Babinski et al., 1999), 1496 ± 3.2 Ma and 1492 ± 16 Ma (Guimarães et al., 2008; Loureiro et al., 2009) and 1507 ± 7 Ma (Silveira et al., 2013), and is located in the Chapada Diamantina basin. The youngest group has ages of 934 ± 14 Ma and 854 ± 23 Ma (respectively, Loureiro et al., 2009 and Danderfer et al., 2009), and occurs in both Northern Espinhaço and Chapada Diamantina basins. The latter are related to the early Tonian rifting event that resulted in the formation of a large Neoproterozoic intracratonic basin, known as the Macaubas Basin (Babinski et al., 2012; Moreira et al., 2020; Pedrosa-Soares et al., 2011a), the precursor for the Araçuaí orogen (Ediacaran to Cambrian).

The Paramirim aulacogen was partially inverted during the Ediacaran–Cambrian Araçuai orogen (Cruz and Alkmim, 2006; Danderfer Filho, 2000, 1990; Danderfer Filho et al., 1993; Guimarães et al., 2008; Loureiro et al., 2009) when the São Francisco and Congo cratons collided. The NNW-trending zone that concentrates most of the deformational structures is defined as the Paramirim corridor (Alkmim et al., 1993). Its tectonic framework comprises contractional and extensional families of structures related to rift nucleation, reactivation and inversion of the aulacogen.

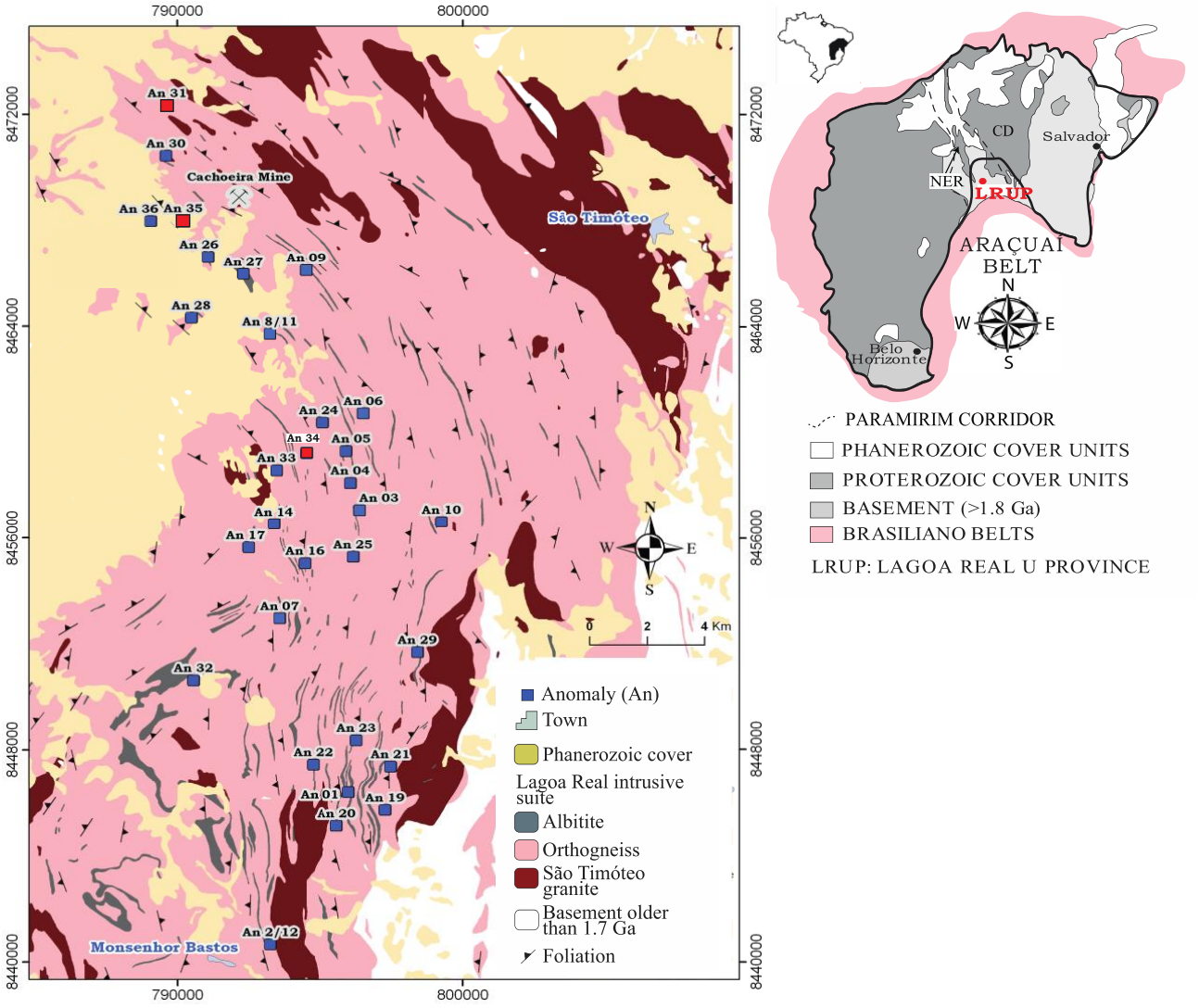

Fig. 43: Geological map of the Lagoa Real uranium province showing the distribution of uranium anomalies and the location of the Cachoeira mine (adapted from Costa et al., 1985). NER: Northern Espinhaço Range, CD: Chapada Diamantina.

6.4 THE LAGOA REAL URANIUM PROVINCE

The LRUP is located in the southern sector of the Paramirim corridor, where the Lagoa Real intrusive suite (LRIS) is exposed. The LRIS consists of A-type granitoids that enclose lens-shaped albite-rich rocks, henceforth referred to as albitite, the host rock of U deposits in LRUP. Other metasomatic bodies also occur associated with the LRIS. These include epidosites, oligoclasites and microclinites, found interlayered with amphibolite and diabase bodies (Costa, 1985; Cruz et al, 2007). Albitite bodies are discontinuous, massive or gneissified, fusiform, and variable in length, ranging from metric to hundreds of metres (<480 m; Ribeiro et al., 1984). Albitite is a sodium-enriched rock dominated by plagioclase

(albite ± oligoclase), and a variety of iron-calcic-silicate mineral assemblages that include garnet, clinopyroxene, amphibole, epidote and titanite. Albitite pods have gradational or abrupt contacts with the LRIS granitoid rocks and, in general, are interpreted as the product of metasomatic alteration of the granite–gneiss country rock by sodium enrichment and silica depletion (Maruejol, 1989; Lobato and Fyfe, 1990). However, Chaves (2013) favored a magmatic origin for the albitites, as intrusive Na-rich, quartz-free syenitic rocks. Such contrasting views exemplify the lack of consensus regarding the origin of the Lagoa Real albitites, despite numerous studies (Geisel Sobrinho et al., 1980; Lobato, 1985; Fuzikawa et al., 1988; Maruejol, 1989; Lobato and Fyfe, 1990; Chaves, 2013). Uranium mineralization is made up mainly of disseminated crystals of fine-grained uraninite (<5 μm), which is highly concentrated in the most mylonitized zones, but uranophane and pitchblende have also been described as uranium ore. Lobato and Fyfe (1990) and Maruejol (1989) reported the preferential occurrence of uranium minerals in Fe^{3+}-rich garnet–hedenbergite-bearing albitites.

The regional, concordant intercalation of LRIS rocks with the metasomatic bodies of albitite, microclinites and oligoclasites, as well as the features of albitization in LRIS rocks, are the primary observations suggesting a common origin for these rocks (Maruejol, 1989; Lobato and Fyfe, 1990; Cruz et al., 2007). However, the Brasiliano orogeny that resulted in the partial inversion of the aulacogen makes the reconstruction of this scenario challenging.

6.4 GEOLOGY OF GAMELEIRA I (AN35), BARRINHA (AN34) AND BARREIRO (AN31) DEPOSITS.

6.4.1 Main units

The Gameleira I, Barrinha and Barreiro deposits are in the northwest region of the Lagoa Real deposit. Dominant lithology is granite-gneisses of the LRIS, with albitite rocks. Cross-sections of the studied drill-holes are presented in Fig. 44.

The LRIS is represented by the hypersolvus alkali-feldspar granite, that corresponds to a grey colored, isotropic and coarse-grained rock composed by macrocrystals (~8 mm) of K-feldspar (60%) and quartz (30%) with interstitial clinopyroxene, amphibole, biotite, titanite, ilmenite, zircon and apatite. These rocks are variably converted into gneisses, varying from gneisses with discontinuous foliation and augen gneisses to striped gneisses with a continuous foliation. They are variable grey-to-pink in color, porphyritic and consist of the same mineral assemblage as the weakly deformed LRIS granite. Amphibolite is rare and

occurs only in the Barreiro deposit where it has abrupt but concordant contacts with the granite-gneiss of LRIS.

6.4.2 Hydrothermal alteration

Metasomatic bodies are represented by the albitites enclosed as lenses within the LRIS granite-gneiss, with abrupt or transitional contacts. Four main types of albitite are identified based on the characteristic rock-forming minerals present: (i) garnet albitite; (ii) magnetite albitite; (iii) pyroxene-to-amphibole albitite, (iv) and biotite albitite, but mixed components are also observed. Albitite is a medium-to coarse grained rock, massive, foliated or brecciated, with a pinkish to whitish color. Uranium mineralization is hosted within the foliated to augen-like albitite, occurring concordantly with the foliation, although it is invisible to the naked eye. Hydrothermal alteration developed under dominantly under a ductile regime as veins are rare.

The early stage of alteration is dominated by pervasive replacement of K-feldspar by albite. Albite accounts for 60–80 vol.% of these rocks and occurs mainly as chessboard albite in a porphyroclastic polygonal fabric. Polygonal matrix albite is either twinned or untwinned. The growth of sodic pyroxene and partial quartz dissolution are probably associated with this stage, although distinctive textures were not observed.

After the sodic stage, an iron-calcic-magnesian stage proceeds with the precipitation of clinopyroxene and titanite with variable composition (see Results). Initially, Fe-rich clinopyroxene, andradite, magnetite and titanite precipitated. Trace amounts of quartz and K-feldspar are observed. Later on the widespread replacement of the early minerals by Mg-clinopyroxene and titanite converts the rock into pyroxene albitite, which is the main host for the uranium ore. Uraninite occurs as fine-grained crystals (< 5 μm) intergrown with titanite and zircon as veinlets following a well-developed foliation.

Clinopyroxene is also observed in the biotite-rich rocks of the K-Mg stage, however the dark-green amphibole and biotite are largely produced during this phase as replacement products of the early clinopyroxene. Actinolite replaces the dark green amphibole, and both amphiboles are converted into biotite. Uraninite occurs in the biotite-rich rocks mainly disseminated in titanite, but also occurs in biotite and carbonate.

A late calcic stage occurs overprinting the early stages or as an infill stage. The mineral assemblage of this phase is represented by calcite, epidote, allanite, monazite, chlorite, K-

feldspar and apatite. Allanite and epidote occur as halos on the ore-shoots. The infill phase is marked mainly by calcite precipitation, along with disseminated chalcopyrite and pyrite.

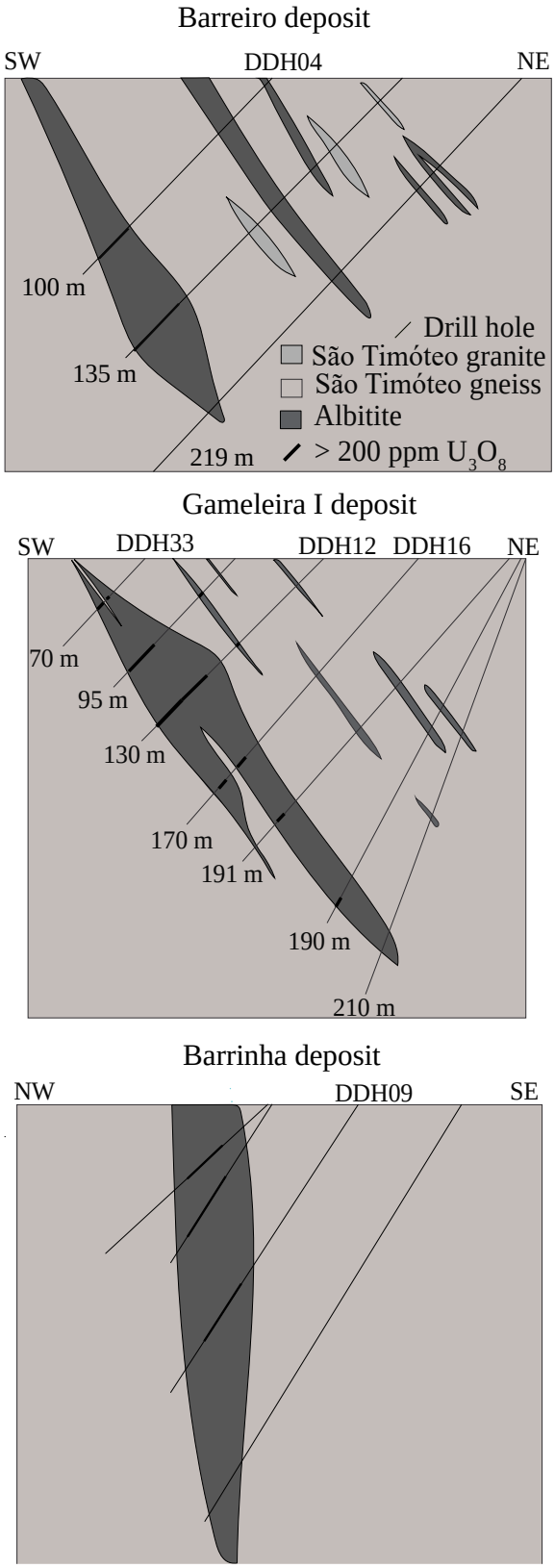

Fig. 44: Cross-sections of the studied deposits.

Fig. 45: Drill-core photographs of fresh to hydrothermally altered rocks at the Gameleira I, Barrinha and Barreiro deposits. **A.** Preserved unaltered and undeformed São Timóteo granite typically coarse-grained and grey in color. **B.** Weakly deformed São Timóteo granite with a discontinuous foliation showing signs of albitization represented by the pinkish color. **C.** São Timóteo gneiss showing augen-fabric and a pinkish color as a result of albitization. **D.** Striped São Timóteo gneiss with stretched crystals of feldspar and quartz. **E.** Massive pyroxene-andradite bearing albitite. Note the extreme pyroxene enrichment with no apparent fabric. **F.** Massive pyroxene-andradite bearing albitite, with garnet surrounded by pyroxene. **G.** Foliated pyroxene-andradite bearing albitite, where the modal volume of pyroxene is enhanced. **H.** Magnetite-rich albitite with low mafic content. Magnetite and titanite are

parallel to the foliation. **I.** Contact between a magnetite-bearing albitite with a low modal volume of clinopyroxene and a pyroxene-bearing albitite, where the modal volume of clinopyroxene (probably diopside) is abruptly enhanced. **J.** Diopside-rich albitite with a well-developed augen-like fabric. Note the development of biotite (black lines) along foliation. **K.** Levels of clinopyroxene enriched in titanite. **L.** Quartz and carbonate vein cutting the biotite albitite. Note that crystals of carbonate are deformed. **M.** Biotite-rich augen albitite showing porphyroblasts of albite. *Bt* Biotite, *Amp* amphibole, *Ttn* titanite, *Fsp* Feldspar, *Qz* quartz, *Grt* garnet, *Cb* carbonate, *Ab* albite.

6.6 MATERIALS AND METHODS

Ten - sixty cm long slabs of drill cores were collected from seven diamond drill holes from three anomalies; AN-35 (DDH-F10, DDH-F33, DDH-F12, DDH-F16), AN-31 (DDH-F11, DDH-F04) and AN-34 (DDH-F9). Polished thin sections were prepared for transmitted- and reflected-light microscopy. Electron-microprobe analyses were then performed on the polished thin sections at the Centro de Microscopia, Universidade Federal de Minas Gerais (UFMG), Brazil, using a JEOL JXA-8900RL. The instrument was operated at 15-kV acceleration voltage and 20-nA beam current. The electron beam size was 5 μm. Elements and reference materials were (in parentheses) as follows: Na (jadeite), K (sanidine), Mn (rhodonite), Mg (MgO), Ca ($Ca_2P_2O_7$), Fe (magnetite), Al (Al_2O_3), Si (quartz), F (fluorite), Cl (Cl-apatite). For the uranium minerals were used: Mg (MgO), As ($FeAs_2$), Ti (rutile), Ca ($CaWO_4$), Al (Al_2O_3), Fe ($FeAs_2$), Zr (ZrO_2), Si ($ThSiO_4$), V (V_2O_3), U (metallic), P and Y (YPO_4), Th ($ThSiO_4$), Pb (crocoite). *K*α X-ray lines of all elements were measured. Results are given in Appendix 3.

6.7 RESULTS

6.7.1 EPMA mineral chemistry

The chemical composition of major silicate minerals, determined by electron-microprobe analyses, is presented below.

Feldspars. Feldspar is the most widespread mineral that occurs in the Lagoa Real rocks. The compositional variability of feldspars is displayed in Fig. 46. K-feldspar occurs mainly in the wall-rocks of LRSI as perthitic alkali-feldspar (Fig. 47A). However, the latter shows albitization microstructures as micro-to-meso perthites, plagioclase patches (Fig. 47A) and

albite swapped rims (Fig. 47B). Perthitic K-feldspar composition varies in terms of the orthoclase end member from 86 to 98% – i.e., $Or_{86–98}$.

Plagioclase is associated with perthitic K-feldspar as patches in the weakly deformed and altered LRIS granite. Compositionally, it is in the albite–oligoclase range ($An_{2–23}$), whereas less altered sample (8-11) has a more oligoclase-rich composition ($An_{12–22}$). The plagioclase in the granite-gneiss rocks is also in the albite–oligoclase range (An_{2-16}).

In albitites, plagioclase accounts for 60-80 vol.% of these rocks and occurs as: i) medium- to coarse-grained porphyroclasts with chessboard microstructure or polysynthetic twinning. Kinking (Fig. 47C), growth twinning, core-and-mantle, undulose extinction and subgrain boundaries are the main microstructures observed in the porphyroclasts attesting to post-replacement high-temperature intracrystalline deformation. Chessboard microstructure is usually observed in the coarse-grained rocks (Fig. 47D); and, ii) fine-to medium-grained (200–250 µm) mostly untwined granoblastic crystals of polygonal shapes, which surround plagioclase porphyroclasts forming core-and-mantle textures. Feldspar shows variable decalcification alteration such as epidotization, fluoritization and carbonatation, as shown by Marques et al (2020a,b).

Independent of texture, plagioclase in the albitite is almost pure albite ($An_{0–2}$). Exception occurs in anomaly-34, which has An contents between 0 and 9%.

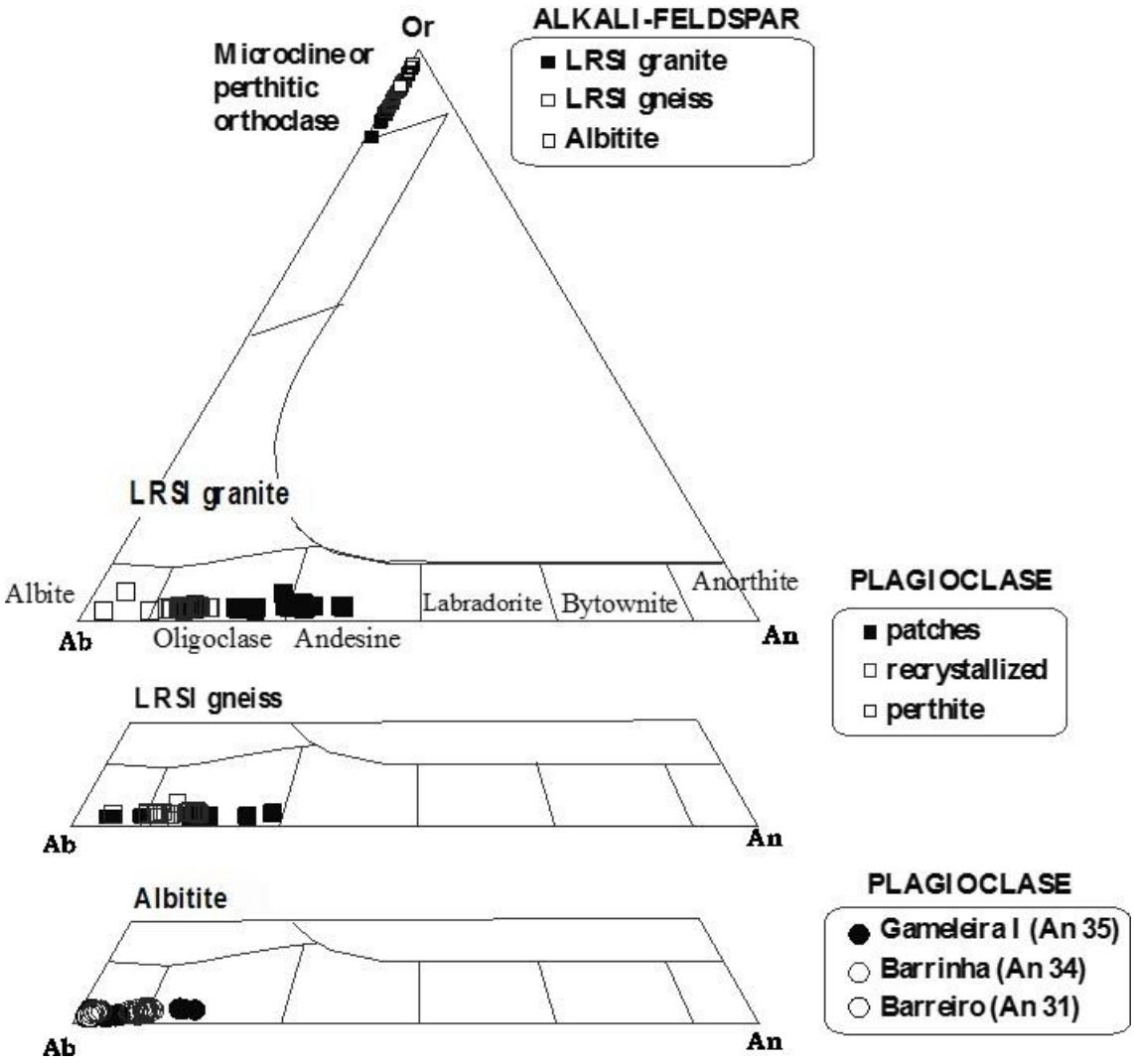

Fig. 46: Ternary diagrams of end-member orthoclase (Or) vs. albite (Ab) vs. anorthite (Na) for feldspar minerals in the São Timóteo granite, gneisses and albitites.

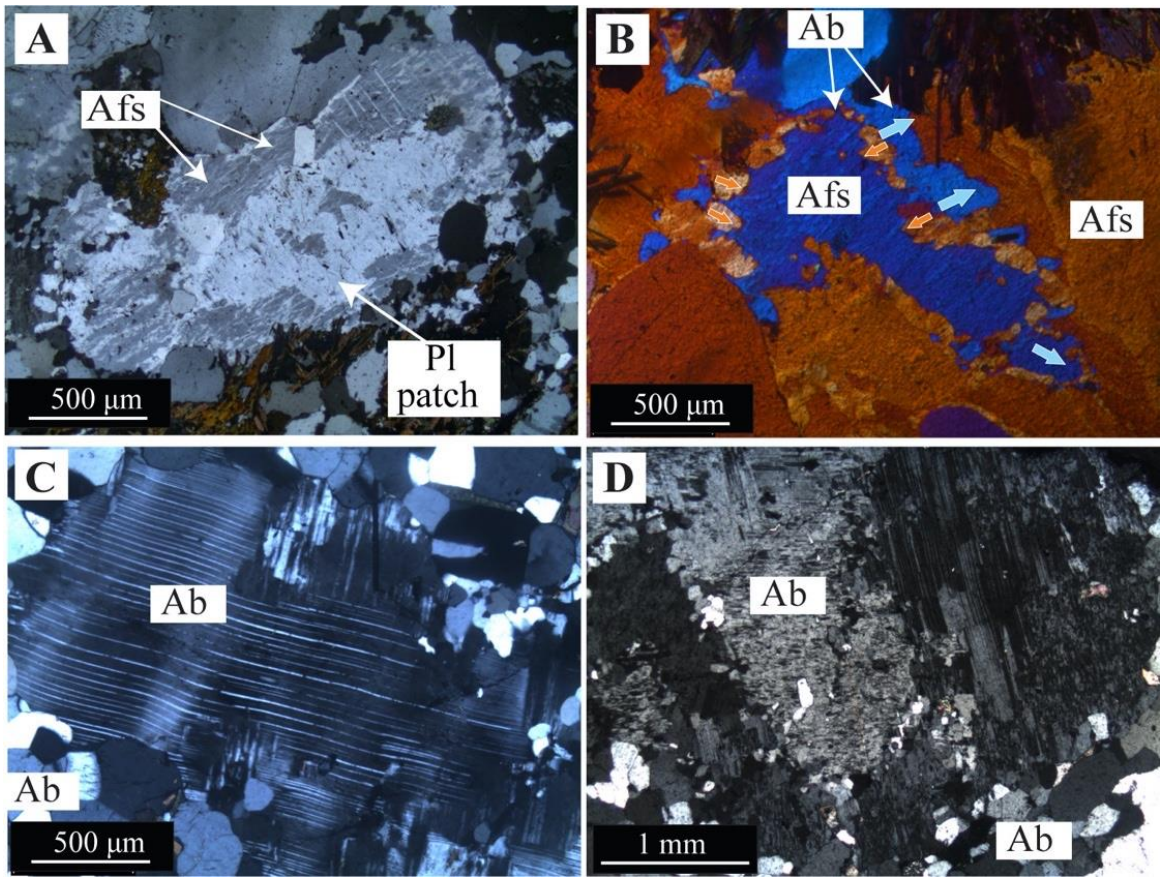

Fig. 47: Photomicrographs of feldspars in cross-polarized transmitted light (XPL). **A.** Megacrystal of perthitic alkali feldspar (rim) with domains of patch oligoclase perthites (core) in a slightly altered sample of São Timóteo granite. **B.** Albite rimming alkali feldspars in a swapped rims texture (arrows) in a slightly altered sample of São Timóteo granite – XPL with a gypsum plate. **C.** Twined and kinked albite porphyroclast, surrounded by untwined, granoblastic polygonal albite grains in an albitite. **D.** Megacrystal of chessboard albite surrounded by granoblastic polygonal untwined albite grains in an albitite.

Pyroxene. Pyroxene is the most widespread mineral phase in the Lagoa Real rocks after feldspars. It is present in the magmatic rocks of LRIS as well as in the albitites. In the albitites, clinopyroxene occurs through the early to late stages of alteration. The mineral is mostly Quadrilateral, Fe-Mg-rich, in composition and rarely plots in the Ca-Na field (Fig. 48A). Clinopyroxene is classified according to Morimoto (1988) and corresponds mostly to pyroxene of Ca-Fe-Mg series varying in composition from hedenbergite to augite (Fig. 48B), but also plots as aegirine-augite (Fig. 48C).

Clinopyroxene is rare in the São Timóteo granite, however it is occasionally observed as fine-grained crystals rimed by hastingsite (Fig. 49A) and it plots in the hedenbergite field

($Wo_{48–50}En_{8–9}Fs_{40–44}$; Fe/Mg = ~9). In albitites, there are three groups of clinopyroxene, they all have close associations with titanite. No obvious temporal relationships between clinopyroxenes are observed, but they are distinguishable based on composition, mineral association and depth, as follows: i) aegirine-augite, ii) hedenbergite-diopside and iii) augite. Yellowish green crystals of aegirine-augite composition ($Wo_{44–48}En_{27–35}Fs_{19–26}$; Na_2O = 4–6%; Fe/Mg = 2.5) with polygonal shapes occur as lenses concordant with the foliation and associated with andradite + magnetite, or as almost monomineralic clumps of aegirine-augite + titanite (Fig. 49B). Aegirine-augite was only observed in the Gameleira I deposit, in the contact zone between granite-gneisses of LRIS and albitite. Light-to-dark green polygonal crystals with hedenbergite to diopside composition ($Wo_{47–55}En_{1.5–37}Fs_{13–44}$; Fe/Mg = 1 to 200) associated with the iron-calcic assemblage, andradite and magnetite (Fig. 49C), occur in albitites with transitional contacts with the granite-gneisses of LRIS, in a similar fashion to the aegirine-augite. Hedenbergite seems to replace andradite (Fig. 49D) and magnetite, and varies between an Fe-rich to Mg-rich composition. However, it is noticeable that sodic-calcic and iron-calcic pyroxene were not observed in the same anomaly. Hedenbergite predominates in distal zones (DDHF10) of the Gameleira I deposit and in the Barrinha deposit. In addition, in the shallower zones near the LRIS granite contacts, pyroxene is mostly Fe-Mg hedenbergite or aegirine-augite in composition, and in the central zones it is diopside (Fig. 49E). Augite ($Wo_{23–26}En_{54–60}Fs_{15–22}$; Fe/Mg = 0.25 – 30) occurs in the deepest portions of the Gameleira I deposit, mainly associated with biotite and carbonate as a foliation-forming mineral (Fig. 49F) A schematic figure showing the main occurrence of clinopyroxene at depth is given in Fig. 49G.

Clinopyroxenes are somewhat rich in an Mn (0.2 to 2% of MnO) component independent of rock or type.

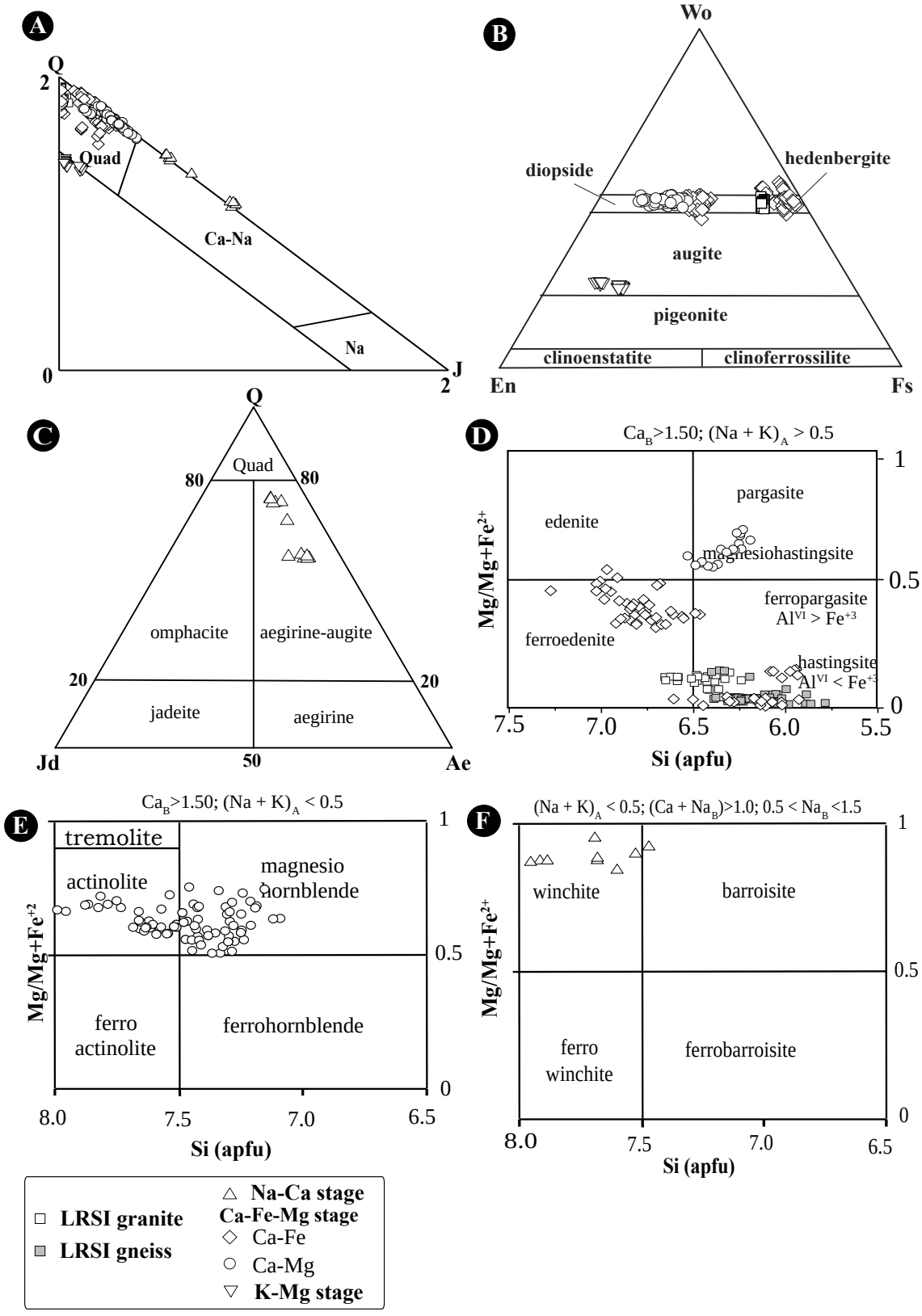

Fig. 48: Compositional classification of clinopyroxene and amphibole generations. **A.** *Q–J* diagram, clinopyroxenes from most samples plot in the Quad area, Q = Ca + Mg + Fe^{2+} and J = 2Na ± R+(R: Al, Fe^{3+}, Cr^{3+}, Sc^{3+}). Clinopyroxene from some albitite samples plot in the

Ca-Na are (Morimoto et al. 1988). **B–C**. Pyroxene classification diagrams of Morimoto (1988). Wo–En–Fs diagram shows that the clinopyroxenes are mainly diopside–hedenbergite–augite series. **D–F**. Amphibole classification diagrams of Leake et al. (2004). See text for details.

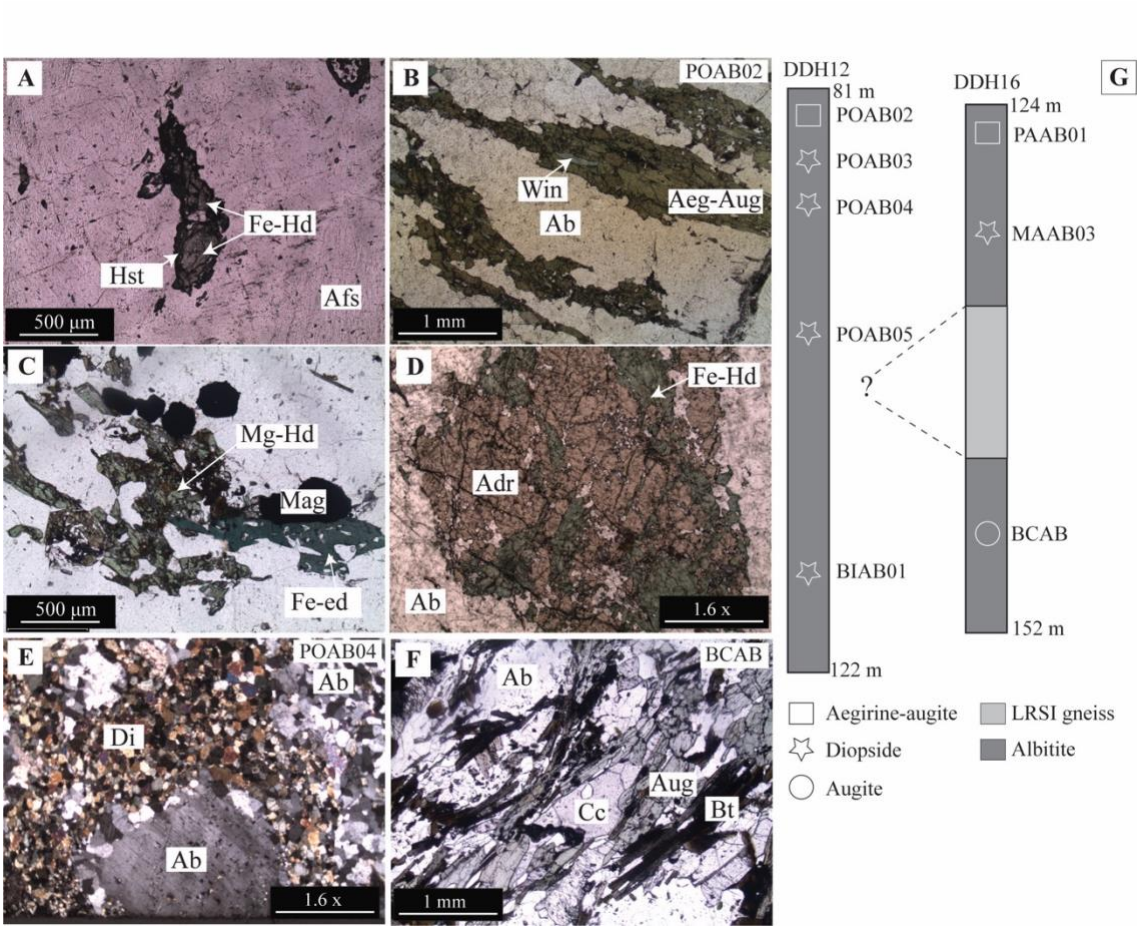

Fig. 49: Photomicrographs of clinopyroxene from the studied rocks in cross-polarized transmitted light (XPL) and plane polarized transmitted light (PPL), and sketch of selected drill-holes. **A.** Aggregate of Fe-hedenbergite (Fe-Hd) and hastingsite (Hst), as core and rim, respectively, included in alkali feldspar of a São Timóteo granite sample – PPL. **B.** Layers of aegirine-augite intercalated with albite in an albitite– PPL. **C.** Mg-hedenbergite (Mg-Hd) coexisting with Fe-edenite (Fe-ed) and magnetite in albitite – PPL. **D.** Andradite (Adr) and Fe-hedenbergite in a garnet-rich albitite. Note that Fe-hedenbergite apparently fills andradite fractures – PPL. **E.** Diopside-rich albitite with albite porphyroclasts and a matrix of granoblastic polygonal diopside – XPL. **F.** Biotite, augite and carbonate as foliation-forming minerals in a biotite albitite– PPL. **G.** Sketch of DDH-12 and DDH-16 drill cores of Gameleira I deposit showing the distribution of clinopyroxene composition. In shallow

zones, clinopyroxene is sodic-calcic (aegirine-augite), in the middle zones diopside predominates and at depth clinopyroxene is augite.

Amphibole. Amphibole is present in both unaltered and altered rocks. Amphiboles were classified according to IMA-04 (Leake et al., 2004). Amphibole is mostly calcic irrespective of rock type, and has a wide compositional spectrum in calcic fields from Fe-rich to Mg-rich compositions (Fig. 48D, E), but rarely is also sodic-calcic, being classified as winchite (Fig. 48F).

In the São Timóteo granite amphibole is dark-green, and forms interstitial aggregates of tabular habit, symplectic microstructure (Fig. 50A), or envelops clinopyroxene (Fig. 49A). In the granite-gneiss amphibole has a similar texture to the low strain rocks but defines the foliation, together with biotite and titanite. Undeformed and deformed rocks of LRIS have amphibole compositions between hastingsite and ferroedenite [Ca_B> 1.50; $(Na+K)_A$> 0.5]. Amphibole is compositionally homogeneous with Fe/Fe+Mg ratio between 0.87 and 0.99, independently of its occurrence in granite-gneisses of LRSI. The magmatic hastingsite is also preserved in some albitites that make contacts with LRIS rocks.

In the albitites there are three main groups of amphibole: i) rare light-bluish-green amphibole plots in the winchite field [0.5 < Na_B < 1.5; $(Na+Ca)_B$>1; Fe/Fe+Mg = 0.26–0.37] and probably replaces aegirine-augite (Fig. 50B). The rims of these crystals are pale green, reflecting differences in chemical composition, mainly Na and Fe^{3+} loss (Fig. 50C); ii) dark-green amphibole replaces clinopyroxene on grain boundaries or along cleavage planes (Fig. 50D it has Fe-edenite composition (Fe/Fe+Mg = 0.58–0.72) and is associated with the iron-calcic assemblage (hedenbergite + andradite + magnetite); iii) light-pale-green amphibole, occurs with the Ca-Mg assemblage and substitutes mainly for diopside (Fig. 50E, F), but also for winchite (Fig. 50B). This amphibole has an Mg-hornblende to actinolite composition [Ca_B >1.50; Ca_A < 0.5; $(Na + K)_A$ <0.5; Fe/Fe+Mg = 0.31–0.48], and in some zones their replacement is ubiquitous forming actinolite albitite (Fig. 50F) . Diopside is also replaced by a dark-green amphibole with an Mg-hastingsite composition (Fe/Fe+Mg = 0.46–0.57). Substitution textures between actinolite and Mg-hastingsite were not observed, but it seems that actinolite tends to occur in distal and-or shallower zones.

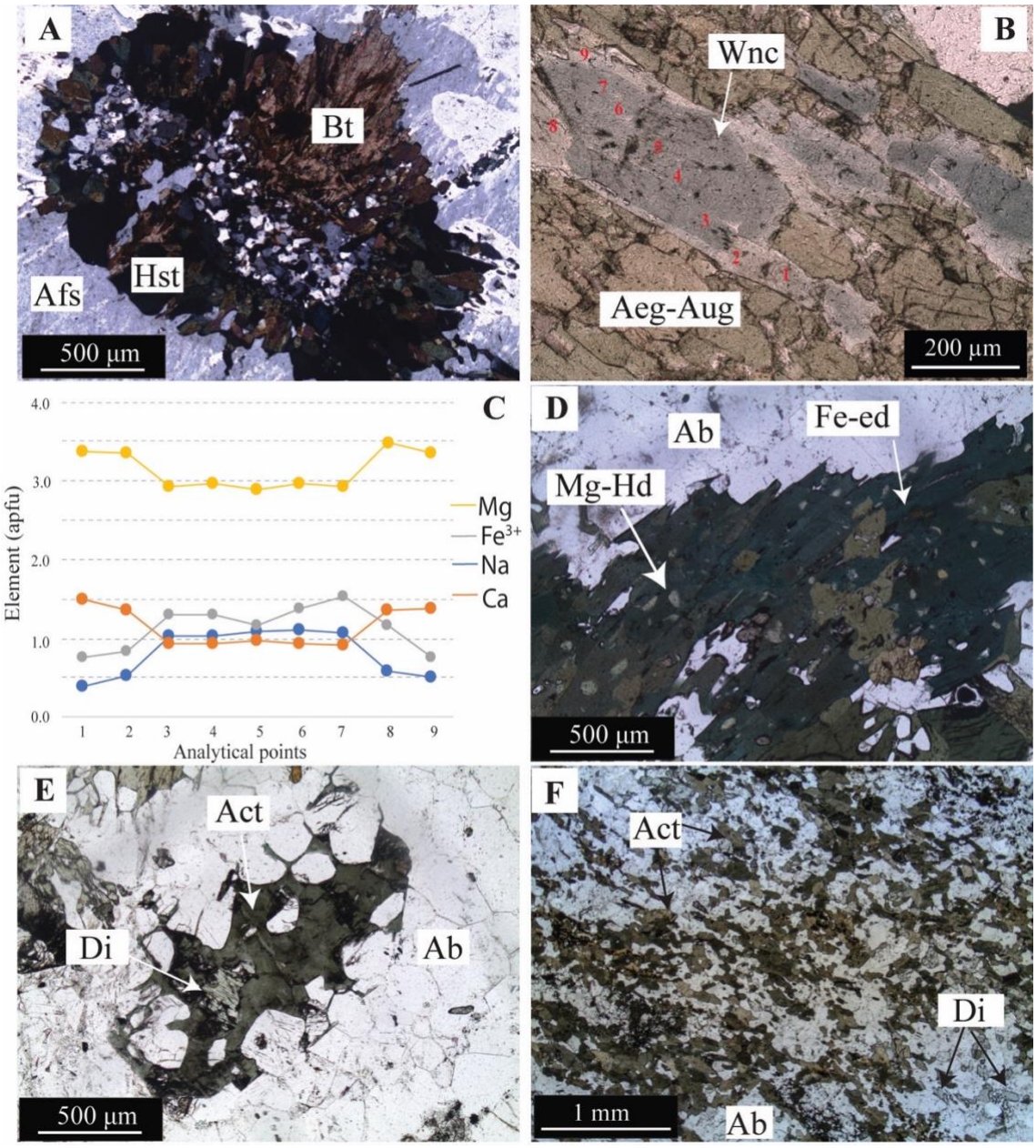

Fig. 50: Photomicrographs of amphibole in the studied rocks. **A.** Symplectic hastingsite (Hst) associated with biotite (Bt) in the São Timóteo granite sample – XPL. **B.** Zoned winchite (Wnc) replacing aegirine-augite (Aeg-Aug) crystals. Numbers refer to analyses in C. **C.** Major element distribution across the winchite crystal in part B. The crystal rim shows a gain in Ca and Mg as a consequence of replacement of winchite by actinolite. **D.** Dark-green crystals of Fe-edenite (Fe-ed) in the pyroxene-rich albitite, replacing Mg-hedenbergite, showed as light-green spots –PPL. **E.** Diopside replacement by actinolite – PPL. **F.** In the zones where the actinolite replacement is ubiquitous the rock is an actinolite albitite –PPL.

Biotite. Biotite is often a product of amphibole and/or clinopyroxene hydration and occurs either as green or brown aggregates.

Mica recalculation, end-member names, molecular fractions, as well as estimation of ferric and ferrous iron on the basis of stoichiometric constraints, were carried out using the $Mica^{+}$ program of Yavuz (2003).

Mica compositions are plotted on the mgli-(Mg–Li)-vs.-feal-(Fe_{tot}+Mg+Ti–Al^{VI}) diagram of Tischendorf *et al* (1997), which provides a simple means to classify mica in terms of chemical composition and site occupancy Fig. 51A.

In the São Timóteo granite-gneiss rocks biotite is part of the magmatic assemblage and occurs as interstitial mafic patches, brown in color, together with hastingsite and titanite. In gneissic rocks it defines foliation along with hastingsite and titanite. Biotite, in these rocks, plots in the lepidomelane field.

In the albitites, biotite is a result of the K-Mg stage which forms the biotite albitite rocks. Biotite replaces diopside or augite directly (Fig. 52A), but also is observed in the Fe-Ca-Mg assemblage replacing clinopyroxene and amphibole (Fig. 52B) and spatially associated with magnetite and titanite (Fig. 52C). In these cases, biotite is classified as Mg-biotite and has some variability in Mg content. Near the ore shoot, biotite is rich in inclusions of a metamict mineral (Fig. 52D). It is associated with the ore assemblage and also host uraninite crystals.

In the distal drill-hole, DDH-F10, biotite is often green (Fig. 52B, C, E), but in the proximal zones, biotite is mostly brown, despite the fact that in both scenarios it replaces the same mineral assemblage. Biotite also fills lithological contacts between albitite and the wall rocks parallel to the foliation (Fig. 52E). In this case, biotite is the main rock-forming mineral along with zircon and titanite, and has both green and brown color. However, the differences in color do not reflect chemical differences as both are classified as Fe-biotite. Biotite also fills veinlets associated with carbonate (Fig. 52F).

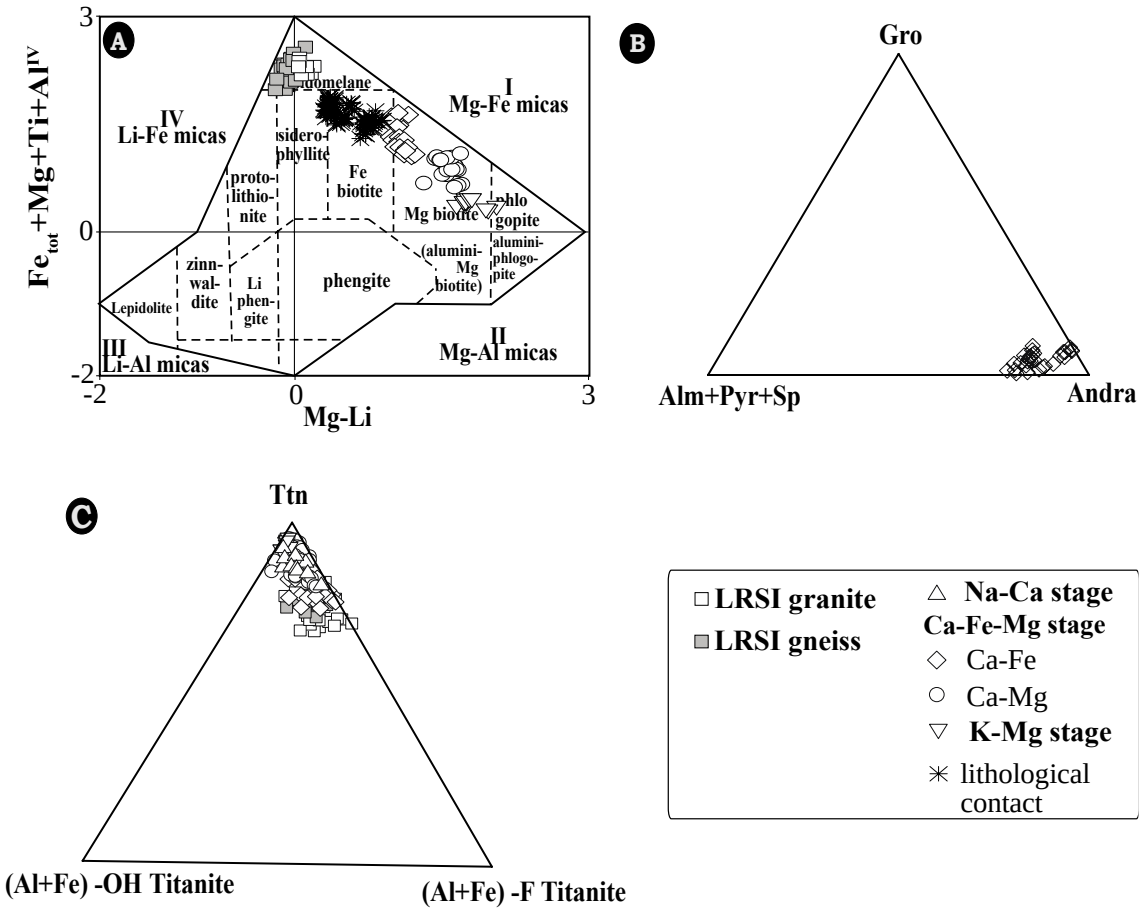

Fig. 51: Compositional classification of biotite, titanite and garnet. **A.** Chemical compositions of biotite plotted on the (Mg–Li)-vs.-(Fe_{tot} +Mg + Ti–Al^{VI}) classification diagram of Tischendorf et al. (1997). **B.** Chemical composition of garnet from the albitite. **C.** Ternary diagram with titanite (Ttn)–Al–F titanite (Al+Fe^{3+}–F Ttn)– Al–OH titanite (Al, Fe^{3+}–OH Ttn) illustrating the extent of the Al-bearing titanite components in the solid solution from Harlov et al., (2006). Note that titanite from the albitite samples are near the Ttn composition.

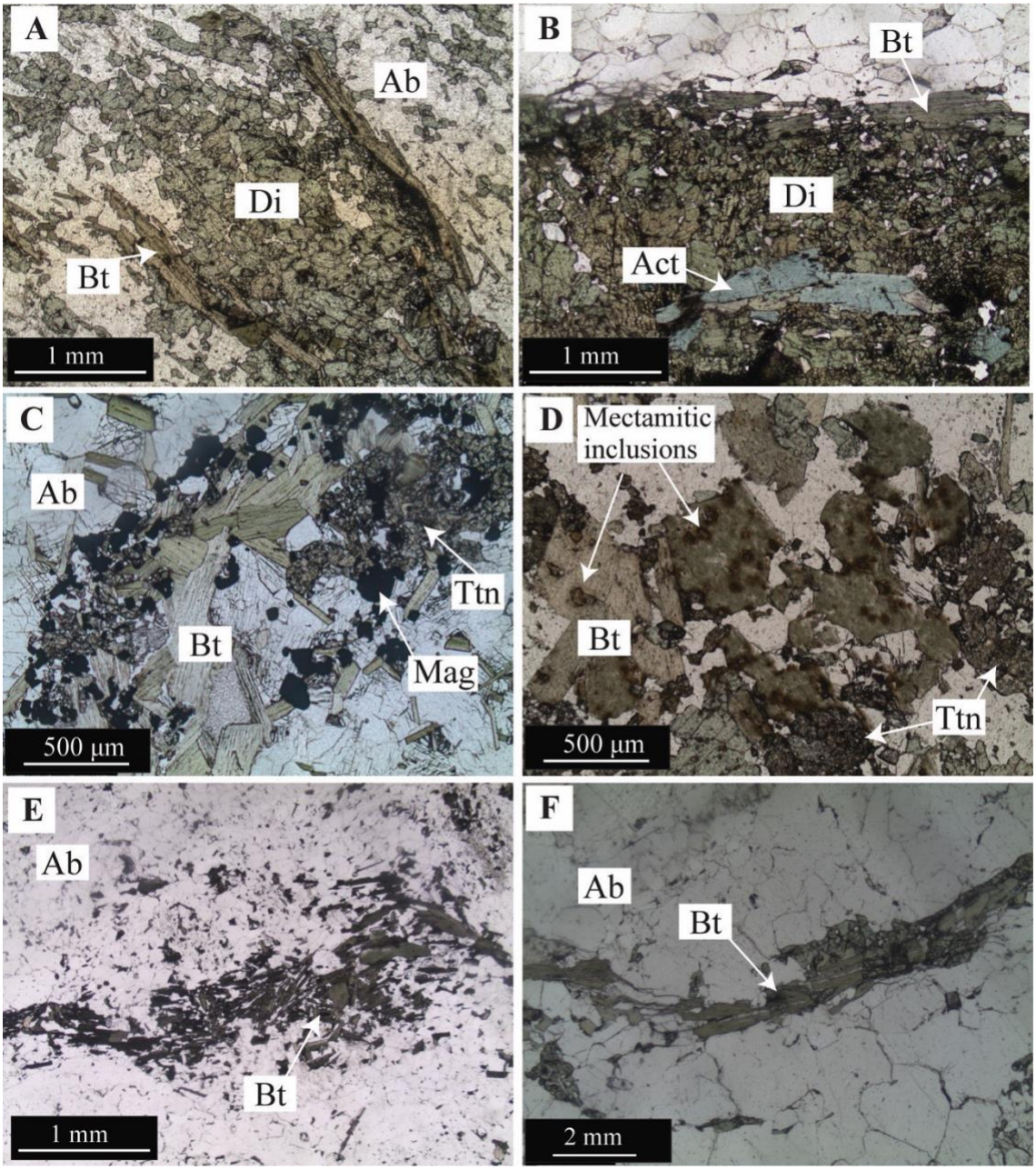

Fig. 52: Photomicrographs of biotite in albitite samples in plane-polarized transmitted light. **A.** Biotite replacing diopside in the absence of amphibole. The sample shown is that of Fig. 45J. **B.** Diopside (Di), actinolite (Act) and Mg-biotite (Bt) forming a mafic layer in an albitite. **C.** Green biotite associated with titanite (Ttn) and magnetite (Mag). **D.** Green biotite rich in metamict inclusions (allanite?) near the ore-shoot. **E.** Fine-grained green biotite near the lithologic contact between the albitite and LRIS. **F.** Green biotite filling veinlets.

Garnet. Garnet recalculation, end-member names, molecular fractions, as well as estimation of ferric and ferrous iron on the basis of stoichiometric constraints, were carried out using the spreadsheet of Locock (2008). The results are presented in (Fig. 49D), respectively, and

is classified as andradite Fig. 51B. The EPMA analyses of garnet show that andradite is the major component, with most grains having between 73 – 85 (mol%) andradite. Andradite associated with aegirine-augite is zoned and the core analyses have low totals (~90%), probably as consequence of hydration and the presence of Y. The latter was observed in EDS analyses. The main differences between core and rim compositions are in relation to Ca, Na and Mg contents. The core is Na and Mg-enriched (~0.2% and ~1%, respectively) and Ca-poor (~24%) and rim is Ca-enriched (~30%), Na and Mg-poor (around 0% for both).

Titanite Titanite occurs associated with both unaltered and altered rocks. In magmatic rocks, this mineral is interstitial to the magmatic assemblage, occurring as coronas riming ilmenite and is light brown in color (Fig. 53A). The proportion of titanite in such corona-like texture is enhanced from the undeformed granites to the granite-gneisses of LRIS (Fig. 53B). In the albitites, titanite texture is variable. It may occur as corona-like with ilmenite like in the granite-gneiss. This type of occurrence is more evident in the transitional zones, mainly associated with magnetite and albite in the iron-calcic assemblage (Fig. 52C). However, in the albitites, titanite is mostly euhedral-to subhedral colorless or with a brownish tint (Fig. 53C) with the typical bipyramidal habit. It is intergrown with andradite or enclosed in clinopyroxene forming aggregates orientated parallel to the foliation (Fig. 53D). Titanite also forms part of the ore assemblage, in this case titanite is brown to reddish in color (Fig. 53E), in general with strong pleochroism.

Calcium and silica contents are regular in titanite and they are between 24 and 35% for CaO and 22 and 32% for SiO_2. Calculation of OH, and consequently H_2O, allows for estimation of the amount of the $(Al+Fe^{3+})$–OH titanite component. Samples from LRIS granites and gneisses and the Ca-Fe stage are enriched in the (Al+Fe3+)–F component (10 to 20%) and samples from the following stages tend to be progressively poor in both $(Al+Fe^{3+})$–F and $(Al+Fe^{3+})$–OH components reaching 0% for each Fig. 51C.

Epidote. Epidote is the main mineral associated with the late calcic stage together with allanite. Epidote occurs as light green fine-grained subhedral crystals and develops mainly as halos in the ore-shoots. In this case it replaces the early minerals (Fig. 53F), mainly titanite and allanite (Fig. 53G). Epidote is also associated with K-feldspar and galena precipitation. Based on the calculated atomic abundance of Al, Fe, Mn per formula unit, analyses were of true epidote. Calculation of mineral compositions is carried out on the basis of 12.5 oxygens and total cations equal to 8.0. Epidote has around 22% of CaO, 13% of FeO, 21% of Al_2O_3 and 37% of SiO_2.

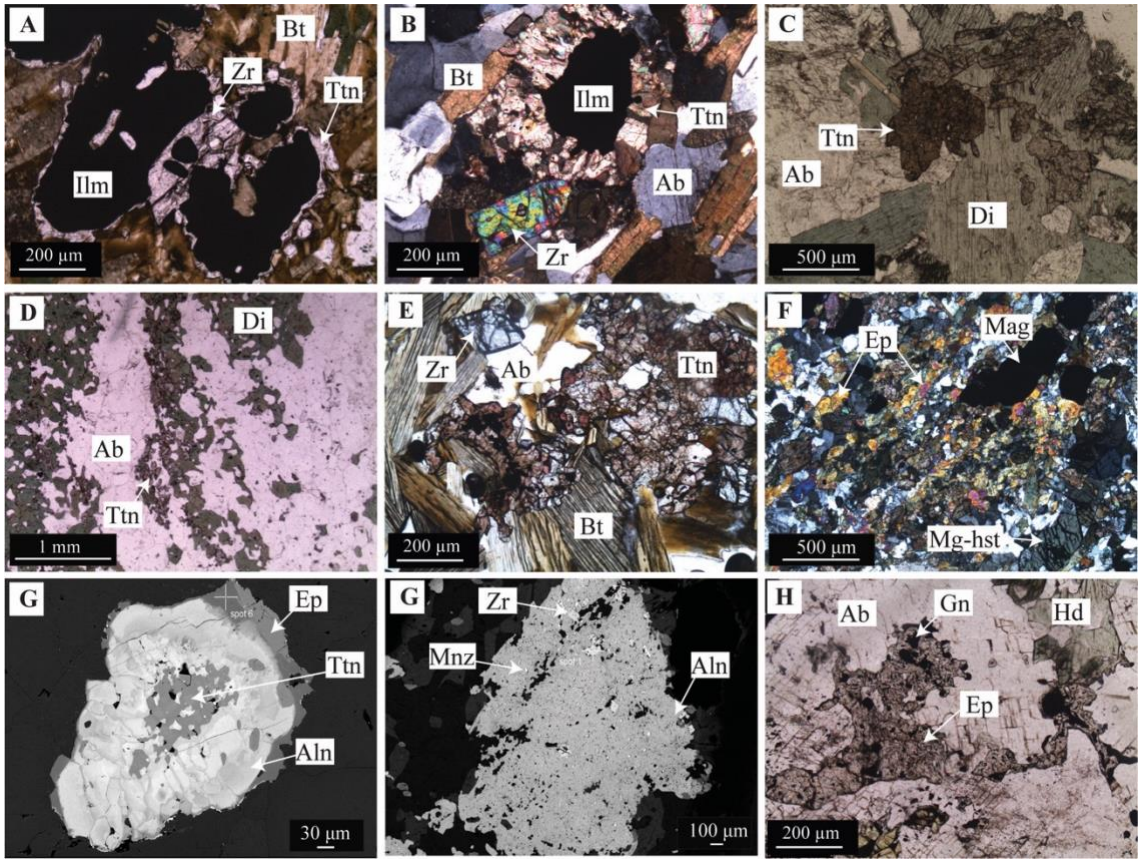

Fig. 53: Photomicrographs and backscattered-electron image (BSE) of titanite from the studied samples. **A.** Ilmenite–titanite corona-like microstructure, associated with zircon in the São Timóteo granite – PPL. **B.** Ilmenite–titanite corona-like microstructure from a São Timóteo gneiss sample – XPL. Note that titanite is more developed in comparison to A. **C.** Euhedral brown coloured titanite in albite – PPL. **D.** Titanite aggregates in clinopyroxene albitite – PPL. **E.** Pleochroic reddish titanite associated with biotite and zircon in an ore-shoot in the biotite albitite –PPL. **F.** Widespread epidote (Ep) replacement over Mg-hastingsite (Mg–Hst) along the foliation in the vicinity of ore-shoots – XPL. **G.** BSE image of titanite–allanite–epidote corona-like microstructure from core to rim, respectively. Note that epidote is in the outermost region. **H.** BSE image of allanite with inclusions of fine-grained BSE bright crystals of monazite and zircon. **I.** Epidote spatially associated with galena (Gn) in the pyroxene albitite – PPL.

Uranium minerals. Representative samples of uraninite and other uranium minerals were analysed for major elements and are displayed in Appendix 3 – 3I.

The uranium ore is mostly represented by uraninite, but also uranophane and a few other secondary uranium minerals. Uraninite is dominantly present in millimetric veinlets hosted by diopside-bearing albitites of the ferric-calcic stage (Fig. 54A). The veinlets are concordant with the foliation and the ore assemblage is composed of fine-grained uraninite (<5 μm) crystals intergrown with titanite and zircon. The relationship between titanite and uraninite is particular apparent in zones of lower strain, where the distribution of uraninite is completely driven by the presence of titanite (Fig. 54B).). In this case, uraninite is homogeneously distributed within titanite crystals without any preferential orientation (Fig. 54c). Therefore, it seems pertinent to conclude that uraninite was exsolved from titanite. Presence of hydrothermal zircon is a remarkable feature in the uranium-ore-veinlet assemblage. Zircon occurs as fine-grained rounded crystals (<5 μm) (Fig. 54D or as fractured, porous crystals with overgrowth rims (Fig. 54E).

Uraninite is also hosted in rocks of the potassic-magnesian stage, as coarser grains (<10 μm) than those in the veinlets. In this case, uraninite is disseminated in biotite (Fig. 54F) and carbonate but also shows a strong preference by titanite similar to the veinlet occurence.

Uraninite from the veinlets and also disseminated occurances were analysed and both have similar PbO contents (4.8 – 6.8%). Uraninite from the Barrinha (An 34) deposit has higher ThO_2 contents (0.8 – 1.5%) in relation to those from the Gameleira I (An 35) deposit (0 – 0.6%). The main differences in uraninite style is related to uranium and some minor elements contents. Uraninite related to the veinlet-style occurrence is characterized by the lowest UO_2 values of 67 – 82% and low totals (80 – 94%). They also have a large range of CaO (0.3 – 6.7%) and Y_2O_3 (0.9 – 9%) concentrations. Uraninite from the disseminated occurrence has the highest UO_2 contents of 78 – 91% and high totals (90 – 100%). The calcium and yttrium contents of these grains have smaller ranges (0.3 – 3.1% of CaO and Y_2O_3 <1%), except for sample 34BALB04, which reaches ~3% of Y_2O_3.

Alteration phases are represented by uranophane, coffinite and brannerite. Uranophane is the most typical alteration phase and is observed as fibrous crystals of anomalous interference color, which fills cleavages, fractures and interstitial spaces (Fig. 54G). Uranophane, coffinite, and brannerite also mimetize uraninite as rounded, fine-grained crystals included in titanite, zircon, allanite and albite, or fracture infilling crystals (Fig. 54H). The chemical compositions of uranophane and U-Ti-Ca species are displayed in Appendix 3 – 3J.

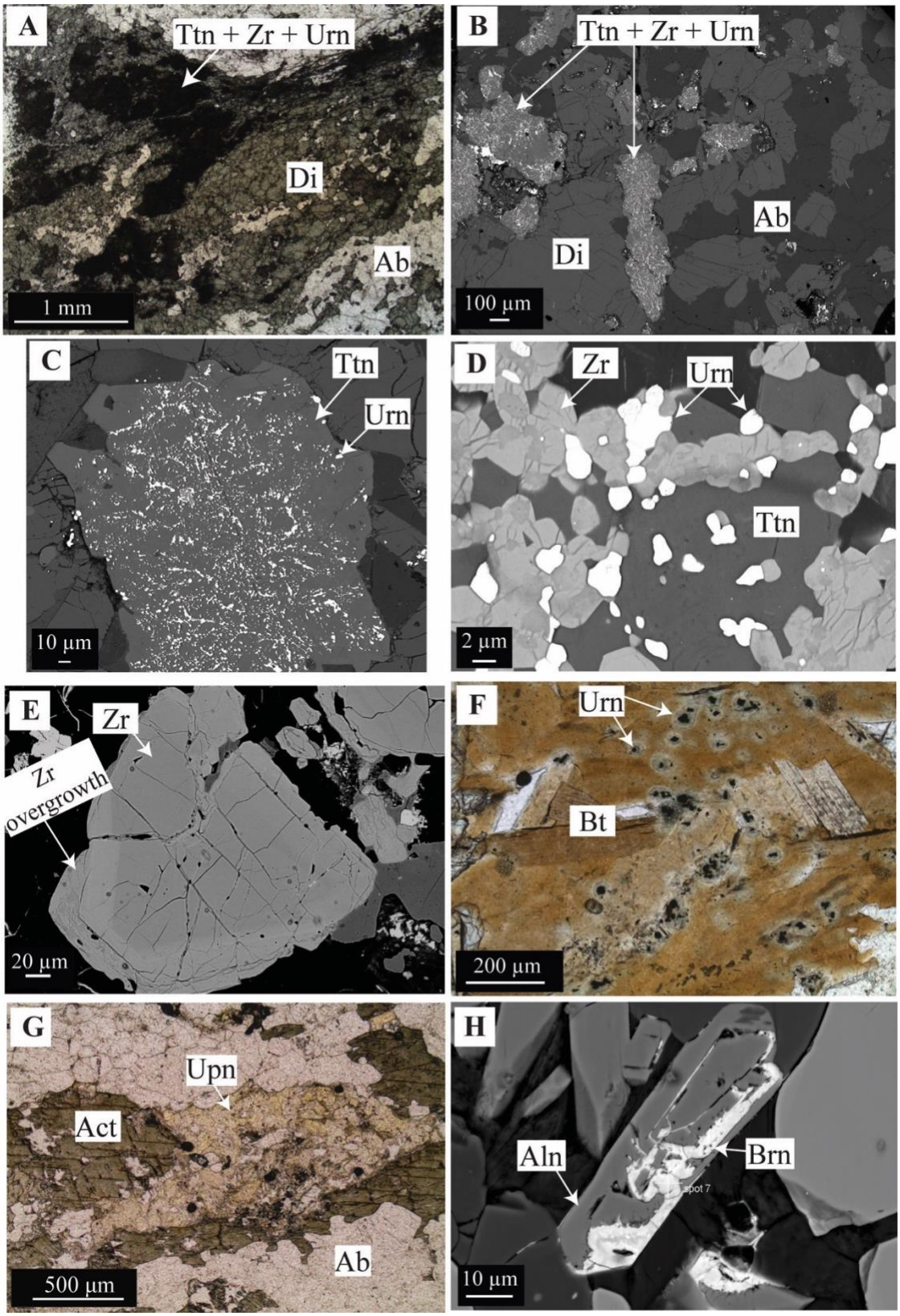

Fig. 54: Photomicrographs and backscattered-electron image of the uranium minerals. **A.** Typical occurrence of the ore assemblage as veinlets composed of uraninite, titanite and zircon, aligned concordantly with the foliation and spatially associated with diopside (Di).

B. Outside the veinlets in less foliated portions of the rock, titanite is rich in rounded uraninite crystals. Note the strong preference of uraninite by titanite crystals (bright spotted regions) – BSE image. **C.** BSE image of a closer view of B, which shows uraninite occurring as inclusions in titanite without orientation suggestive of exsolution. **D.** Detailed BSE image of the ore assemblage present in the veinlets reveals the strong association of fine-grained uraninite and rounded hydrothermal zircon. **E.** Fractured porous zircon, overgrown by new zircon rims, which is indicative of dissolution-reprecipitation process. **F.** Crystals of metamictic uraninite associated with biotite clots in biotite albitite – PPL. Note that this generation is coarser than those in veinlets as shown in A. **G.** Uranophane (Upn) associated to actinolite (Act) in shallow regions of the Gameleira I deposit – PPL. **H.** Allanite (Aln) being replaced by brannerite (Brn) along fractures – BSE image.

6.7.2 Uraninite chemical dating

U-Th-total Pb chemical dating via electron microprobe is a non-destructive technique with a high spatial resolution such that small grains can be targeted. This makes it an ideal technique for preliminary studies, although it does not generate as precise and accurate ages for uraninite mineralization as the isotopic dating techniques such LA-ICP-MS, ID-TIMS and SIMS. The reliability of uraninite chemical calculated ages relies on two assumptions: 1) the total uraninite Pb budget is a product of the radioactive decay of U and Th, and therefore, initial Pb content is negligible (Bowles, 1990); and 2) the system remained closed, meaning that loss or gain of parent/daughter material has not taken place since the uraninite crystallized (Bowles, 1990; Kempe, 2003). The first assumption cannot be fully confirmed because there is currently no established method to calculate the common Pb content. However, as U and Pb have a good positive correlation (Fig. 55A), a normal behavior resulting from uranium decay, it is reasonable to assume that all lead is a result of U decay. The second assumption means that alteration processes do not cause U, Th or Pb gains/losses during fluid-assisted secondary alteration affecting the age calculations. Usually, uraninite alteration shows increases in Ca, Si and Fe, replacing radiogenic Pb in the uraninite structure, leading to a decrease in the calculated age. Except for sample POAB05, which shows the highest Ca, Fe, Si and Y contents, uraninite from Lagoa Real samples does not show linear correlation between minor elements (i.e., Ca, Fe, Si, Y) with U, Pb or age, and therefore, it can be assumed that the uraninite was not altered (Fig. 55B and C).

Keeping the above in mind, the chemical U-Th-total Pb age was calculated using the equation (1) for the radioactive decay of U and Th (i.e., Hurtado et al., 2007). The Pb contents in ppm (C_{Pb}) after time (t) is ruled by the equation:

$$C_{Pb} = C_{Th}[0.897(e^{\lambda 232\, t} - 1)] + C_U\,[0.859(e^{\lambda 238\, t} - 1) + 0.006(e^{\lambda 235\, t} - 1)] \quad (1)$$

where C_{Pb}, C_{Th}, and C_U are concentrations (in ppm) of Pb, Th and U, respectively; λ_{232} λ_{238}, and λ_{235} are the decay constants (in yr^{-1}) for ^{232}Th, ^{238}U, and ^{235}U, respectively; and t is age in years. The coefficient preceding the first exponential term is the mass ratio of ^{208}Pb to ^{232}Th – i.e., $208/232 \approx 0.897$; the coefficients preceding the second and third exponential terms are the ratios of the abundance fractions of the respective U isotopes to the mean atomic mass of U – i.e., $0.9928/238.04 \approx 0.859$ for ^{238}U.

Excluding the outlier values, the age obtained is between 600 and 460 Ma (530 Ma on average) – See Appendix 3 – 3I. The uraninite occurring in veinlets has a slight tendency to record older ages than the disseminated uraninite (Fig. 55C).

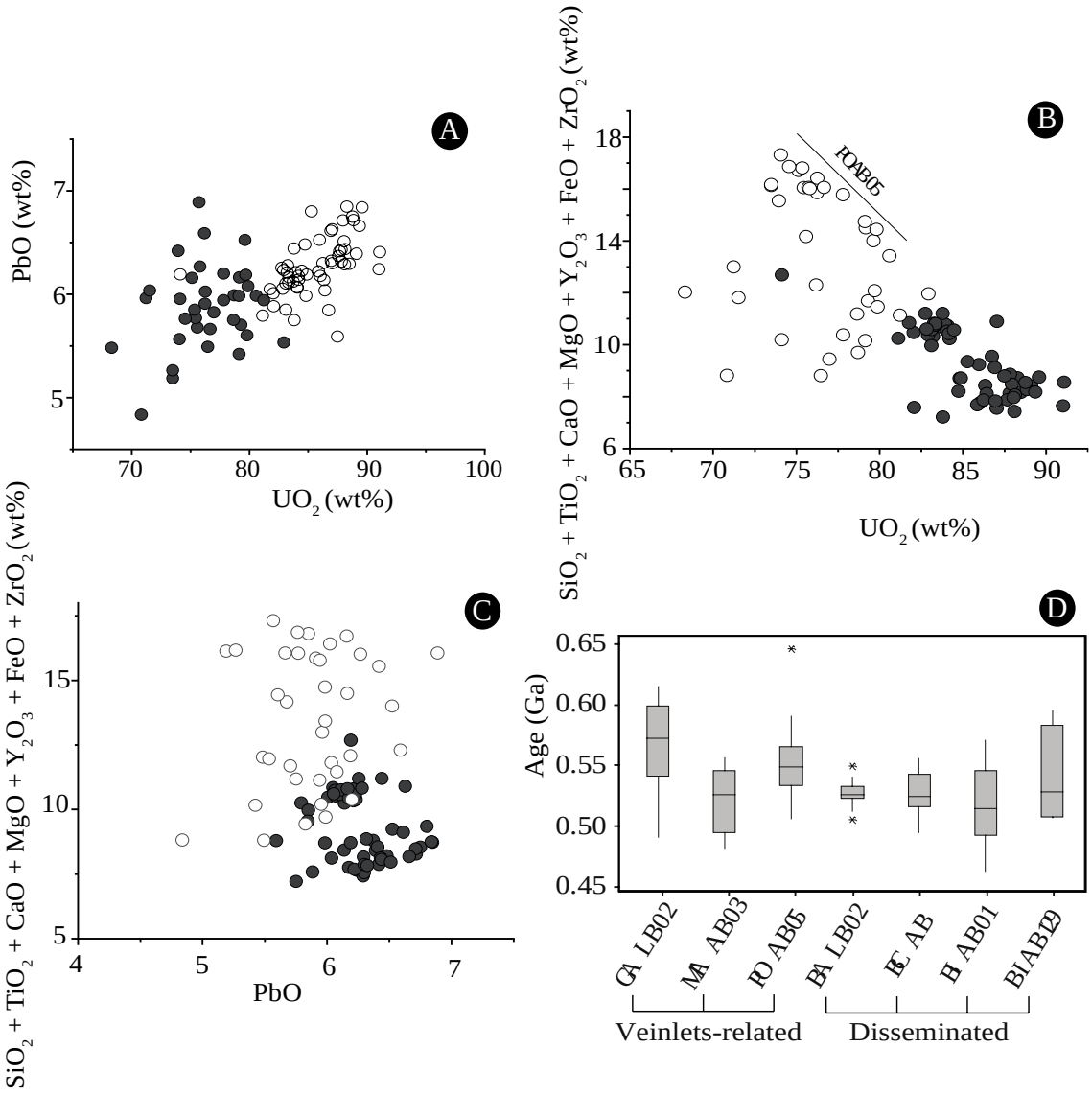

Fig. 55: Biplot of the main chemical trends in uraninite and a boxplot of the ages. Black circle is the veintlet-related uraninite and the white circle represents uraninite as dissemination. **A.** UO_2 *versus* PbO showing a positive correlation indicative no gain or loss in relation to these elements (closed system behavior). **B.** Sum of concentrations of various elements in uraninite plotted *versus* UO_2 concentrations showing that the sum of impurities do not show correlation with UO_2 contents, except for sample POAB05. **C.** Sum of concentrations of various elements in uraninite plotted *versus* PbO. Note that there is no correlation between PbO, UO_2 and the other elements showing that uraninite was not submitted to U or Pb loss. The two different groups are differentiated by Y_2O_3 contents. See text for more information. **D.** Boxplot of calculated chemical ages in uraninite.

6.7.3 Geothermobarometry

Compositional variation among amphibole, amphibole-plagioclase pairs, garnet-clinopyroxene pairs and feldspars, in addition to the zircon and P_2O_5 saturation, can be used to place constraints on the T-P-fO_2 conditions of crystallization from the magmatic and hydrothermal events. These parameters are fundamental to understand the history of the magmatic and hydrothermal systems.

São Timóteo granite intensive parameters: temperature, pressure, and oxygen fugacity

Factors such as oxygen fugacity, temperature and pressure are important to understand the conditions of crystallization of magmatic rocks. These conditions can be constrained through mineral chemistry and geochemistry of selected elements. A synthesis of the main applicable geobarometers and geothermometers in the studied Lagoa Real suite intrusive rocks is given in Table 3.

The zircon and P_2O_5 saturation is related to temperature and the SiO_2 content in the melt as demonstrated by Watson and Harrison, (1983) and Harrison and Watson, (1984). Based on geochemical data produced by Marques et al., (2020a), we used these elements to constrain early liquidus temperature information. Despite of the metamorphic overprint, unaltered to minorly altered granitic-gneiss samples show similar results. The zircon saturation thermometer provided initial temperatures of between 867 and 910 ºC for the hypersolvus alkali-feldspar granite (HAFG) and 875 and 906 ºC for its gneissified correspondent rock (HAFG gneiss). Apatite saturation overlaps this data and shows temperatures between 813 and 916 ºC (HAFG) and 820 and 930 ºC for the gneisses.

Several studies use amphibole composition to infer pressure (e.g., Schmidt 1992; Mutch et al, 2016), temperature (e.g., Holland and Blundy, 1994; Putirka, 2016), and oxygen fugacity (e.g., Anderson and Smith, 1995) conditions of the magma upon crystallization. Recently, Ridolfi et al. (2010) and Ridolfi and Renzulli (2012) reviewed thermobarometric equations available in the literature and presented calibration models to estimate temperature using the concentrations of the main oxides in amphibole. The geothermometer of Ridolfi et al., (2010) applied to the studied amphiboles indicates temperatures between 765 to 877 °C and 821 to 916 ºC, for the HAFG and HAFG gneiss rocks, respectively, overlapping with the results obtained through zircon and P_2O_5 saturation.

The Al content in calcic amphiboles is known to be sensitive in relation to pressure changes (Hammarstron and Zen, 1986; Hollister et al, 1987). We employed the

geobarometers of Hammarstron and Zen (1986), Anderson and Smith (1995), and Schmidt (1992) to infer pressure. Considering all calibrations, the pressures obtained from magmatic amphiboles range from 4 to 8 kbar in the granitic rocks, corresponding to high pressure amphiboles. The gneiss samples show slightly higher ranges (6 to 10 kbar), indicating that the amphibole composition was probably modified by later processes, so the underfomed samples are the best estimate.

Dominant oxygen fugacity during crystallization has a strong chemical control over major mafic phases in igneous rocks (Anderson and Smith, 1995) and iron-titanium oxide minerals (Ishihara, 1981). According Anderson and Smith (1995), fugacity can be estimated using Fe/(Fe + Mg) in amphibole and biotite and the nature of iron-titanium oxide minerals. The studied amphibole and biotite show Fe/(Fe + Mg) ratios up to 0.8 indicating low oxygen fugacity conditions (Anderson and Smith, 1995).

Table 3: Estimate of pressure and temperature of crystallization for the hypersolvus facies of São Timóteo granite.

	HAFG	HAFG gneiss
Temperature (ºC)		
Zr saturation	867–910	875–906
Zr (ppm)	456–701	491–696
P_2O_5 (wt%)	0.03–0.14	0.03–0.14
P_2O_5 saturation	813–916	820–930
Ridolfi et al (2010)	765–877	821–916
Pressure (Kbar)		
Anderson and Smith (1995)	4.1–8.0	5.9–10.0
Hammarstrom & Zen (1986)	3.8–7.3	6.2–9.2
Schmidt (1992)	4.2–7.7	6.5–9.4
Al total	1.5–2.2	2–2.6

Two-feldspar geothermometer. The two-feldspar thermometer was used in order to obtain temperatures of the early albitization stage, petrographically observed by the presence of oligoclase patches and swapped rims in the K-feldspars. Temperature estimates were obtained using the equation 27b of Putirka (2008). In order to constrain the minimum temperature of plagioclase exsolution as patch perthites in the granitic rocks of LRIS, only unaltered and minorly deformed samples where plagioclase occurs as patches in K-feldspar

(8-11 and GRA01) were used in the calculations. Application of the feldspar geothermometer within these patch perthites, using an average pressure estimated by the Al-in-amphibole barometer (Table 3) of 6 kbar, yields temperatures between 400 and 500 °C (Table 4).

Table 4: Calculated temperatures (°C) for the Lagoa Real uranium deposits by geothermometric methods.

	Plagioclase		K-feldspar		
	Xan	Xab	Xan	Xab	T (ºC)
F11-811- C1-1	0.13	0.86	0.00	0.09	432.07
F11-8-11-C3-1	0.22	0.77	0.00	0.08	466.27
F11-8-11-C3-2	0.22	0.76	0.00	0.05	464.29
F11-8-11-C3-3	0.22	0.77	0.00	0.10	451.34
F11 - 811- C6 - 1	0.18	0.81	0.00	0.13	506.78
F11 - 811- C7 - 1	0.15	0.81	0.00	0.07	438.82
F11 - 811- C7 - 2	0.16	0.82	0.00	0.09	444.46
F11 - 811- C7 - 3	0.16	0.82	0.00	0.09	474.92
AM35F10-GRA01-C3-4	0.08	0.90	0.00	0.11	436.18
AM35F10-GRA01-C3-6	0.07	0.92	0.00	0.05	411.14
AM35F10-GRA01-C4-5	0.14	0.86	0.00	0.06	444.48
AM35F10-GRA01-C4-6	0.14	0.85	0.00	0.06	451.66
AM35F10-GRA01-C4-10	0.06	0.93	0.00	0.06	417.20
AM35F10-GRA01-C5-5	0.17	0.82	0.00	0.07	486.31
AM35F10-GRA01-C5-6	0.09	0.90	0.00	0.09	458.03

Garnet-hedenbergite geothermometer. Variations in garnet and clinopyroxene compositions in LRUP were used to determine P–T variations and conditions during the sodic-calcic to early iron-calcic stage. According to Nakamura and Hirajima, (2005), the Grt–Cpx pair can be used as a thermometer based on Fe–Mg exchange based on the following reaction:

$Fe_3Al_2Si_3O_{12}$(garnet) + $3CaMgSi_2O_6$(pyroxene) = $Mg_3Al_2Si_3O_{12}$(garnet) + $3CaFeSi_2O_6$(pyroxene).

Garnet–clinopyroxene thermometry utilizes the partitioning of Fe^{2+} and Mg between these two minerals (Raheim and Green 1974). To determine the formation temperature of pair garnet and pyroxene minerals, three important methods of Raheim and Green, (1974), Powell (1985), Krough (1988) were implemented. Results are given in Table 5.

Considering the average crystallization pressure of 6 kbar estimated for São Timoteo granite emplacement, we applied different pressures around those of São Timóteo granite (3, 5 and 7 kbar) in order to test the dependence of the calculations on pressure. Results are in the range of 300 and 550 ºC for all three geothermometers. Any differences were observed between samples whose garnet is associated with aegirine-augite (PAAB01 sample) or hedenbergite (7-1B, 7-2B and GALB04 samples).

Table 5: Calculated temperatures (°C) of the garnet-bearing albitites representing sodic-calcic and iron-calcic stage of the Lagoa Real uranium deposits by geothermometric methods. Asterisks indicate discarded outlier values.

	Raheim and Green (1974)			Powell (1985)			Krough (1988)		
Pressure (Kbar)	3	5	7	3	5	7	3	5	7
F10-7-1B-C4-1	509.7	521.4	533.1	398.4	401.2	404.0	320.6	323.9	327.1
F10-7-1B-C4-2	427.0	437.5	448.0	336.6	339.2	341.8	274.6	277.6	280.5
F10-7-1B-C4-3	464.0	475.0	486.1	364.7	367.4	370.0	295.7	298.8	301.9
F10-7-1B-C1-4	514.9	526.7	538.5	405.2	408.0	410.8	322.2	325.4	328.6
F10-7-1B-C1-5	489.7	501.1	512.5	382.2	384.9	387.6	310.5	313.6	316.8
F10-7-1B-C1-6	440.0	450.7	461.4	347.1	349.8	352.4	282.0	285.0	288.0
LR35-F10-7-2B-C2-1	542.8	555.0	567.3	412.3	415.2	418.1	341.9	345.2	348.6
LR35-F10-7-2B-C2-2	*	*	*	*	*	*	*	*	*
LR35-F10-7-2B-C2-3	537.8	550.0	562.1	410.3	413.2	416.1	338.7	342.0	345.3
LR35-F10-7-2B-C2-4	537.8	550.0	562.1	415.3	418.1	421.0	336.8	340.1	343.4
LR35-F10-7-2B-C2-5	*	*	*	*	*	*	*	*	*
LR35-F10-7-2B-C2-6	460.2	471.2	482.2	359.8	362.5	365.2	294.2	297.3	300.3
F10-7-2B-C2-7	*	*	*	*	*	*	*	*	*
F10-7-2B-C2-8	502.7	514.4	526.0	386.4	389.2	391.9	319.4	322.6	325.8
3409GALB04-C1-1	411.3	421.5	431.8	323.7	330.1	328.8	265.5	272.7	271.3
3409GALB04-C9-22	*	*	*	*	*	*	*	*	*
3409GALB04-C9-24	542.7	573.3	567.2	407.0	414.2	412.7	343.6	351.9	350.2
3516-PAAB01-C1-38	461.2	472.3	483.3	354.4	357.1	359.8	296.5	299.5	302.6
3516-PAAB01-C1-39	499.5	511.1	522.6	397.8	400.6	403.3	312.3	315.5	318.7

Plagioclase-amphibole geothermometer. The thermal conditions for amphibole-after clinopyroxene formation were estimated with the plagioclase-amphibole geothermometer of Holland and Blundy, (1994). Despite all hydrothermal amphibole being dependent on the earlier clinopyroxene composition (see discussion) we chose amphibole after diopside to apply the geothermometer. This was because this amphibole is related to the mineralization, and despite being compositionally related to the earlier diopside, these amphiboles show some chemical variability, indicating that their composition may also be influenced by fluid.

Plagioclase-amphibole thermometry was tested using the edenite-richterite calibration, which is quartz independent. Pressure values were estimated based on Ridolfi et al, (2010), which use the concentration of the main oxides in amphibole to calculate pressure. Despite, this barometer is only valid for calc-alkaline volcanic samples, owing to the polybaric history experienced by many amphiboles, the pressures calculated via Ridolfi et al, (2010) method are used in the Holland and Blundy (1994) calculation. The plagioclase composition was fixed at X_{An} = 0.01 and X_{Ab} = 0.98, which corresponds of average values calculated in the studied deposits. The data and respective results are shown in Table 6.

Calculated pressures are in the range of 2 to 4 kbar for Mg-hastingsite, 0.4 to 0.8 for Mg-hornblende and 0.2 to 0.5 kbar for actinolite. In terms of temperature, Mg-hastingsite has the highest average values, which are between 530 and 680 ºC, whereas Mg-hornblende and actinolite are in the similar range (486 – 450 ºC).

Table 6: Calculated temperatures (°C) of the amphibole after-clinopyroxene of the Lagoa Real uranium deposits using Holland and Blundy (1994) geothermometer.

Sample	Amphibole composition	T ºC (average)	Pressure (Kbar)
3516-MAAB03	Mg-hastingsite	682.03	4–6
POAB05	Mg-hastingsite	582.91	6
3104BIAB	Mg-hastingsite	530.67	3–5
3409BALBO02	Mg-hornblende	475.84	0.1–0.9
ALBGNA01	Mg-hornblende	486.69	0.10
AM31F11ALB02	Mg-hornblende	465.73	0.6–0.7
PAB03	actinolite	418.04	0.20
ALB 04	actinolite	454.16	0.40
ALB05	actinolite	454.16	0.40

6.7.4 Oxygen and hydrogen isotopes

The $\delta^{18}O$ and δD values for feldspar, titanite and biotite of LRIS granite-gneisses, barren and mineralized albitites are presented in Table 7.

The fractionation factor from Zheng (1993a) was used for fluid-mineral equilibrium for feldspar and titanite. The fractionation factor for fluid-mineral equilibrium in biotite is from Suzouki and Epstein (1976) for hydrogen, and Zheng (1993a) for oxygen.

The $\delta^{18}O$ results for LRIS granite-gneiss range from +5.7 to +8.5‰ for K-feldspar, +2.6 to +7.7‰ for titanite and 2.4 to 4.9‰ for biotite. The δD values range from -108.3 to -118.9‰ for biotite. In barren albitites, $\delta^{18}O$ is lower than in the LRIS samples, between +0.8 and +3.3‰ for albite and -1.4 to +0.6‰ to titanite. Similarly to barren albitites, mineralized albitites have $\delta^{18}O$ values from 0.3 to 3.5‰ for albite, -1 to -0.84‰ for titanite. The $\delta^{18}O$ obtained for biotite in albitite rocks unrelated and related to uranium mineralization are -1 and +3.1‰ and 0.0 to -1.9‰, respectively.

Fluid composition. To estimate fluid composition in equilibrium with analyzed rocks we considered the calculated temperature from Marques et al (2020c) for titanite crystallization in LRIS granite-gneissic rocks based on Zr-in-titanite thermometer, which gives average of 680 ºC. This value was used for feldspar, titanite and biotite of LRIS gneiss. We assumed the temperature interval between 600 and 400ºC for the albitites, as this interval agrees with calculated two-feldspar thermometer for feldspar alteration, but also overlaps i) the experimental temperature of 600 ºC calculated for albitization from Hovelmann et al., (2010), and ii) the experimental temperature of hastingsite dehydration to form hedenbergite + andradite (Thomas, 1982). Fuzikawa et al., (1988) estimated temperature of aquosaline fluids in a calcite vein between 100 to 300ºC. Because biotite can occur either in shear zones or breccias zones, the temperature of 300ºC was assumed for biotite albitite samples, as it probably represents the temperature transition between ductile to brittle regime in Lagoa Real and temperature of the final stages of the hydrothermal system.

The calculated $\delta^{18}O$ of fluid in equilibrium is shown in Table 7.. Feldspar, titanite and biotite are +8.0‰, 8.4–10.4‰, 7.4–7.8‰, respectively in LRSI gneiss. In albitized sample, values are slightly lower: +5.5‰, 5.2‰ and 4.9‰ for feldspar, titanite and biotite, respectively. Albitites have even lower values independently of presence of mineralization. Feldspar is between -2.1 to +2.9‰. Fluid in equilibrium with titanite is between 0.9 and 3.3‰. The $\delta^{18}O$ fluid in equilibrium with biotite is between -0.8 and 4.2‰.

Table 7: Isotopic data on feldspar, titanite and biotite.

Paragenesis	sample	rock	$d^{18}O_{min}$	$d^{18}O_{fluido}$	$d^{18}O_{min}$	$d^{18}O_{fluido}$	$d^{18}O_{min}$	$d^{18}O_{fluido}$	dD_{min}
			feldspar	feldspar	titanite	titanite	biotite	biotite	biotite
hast+bt+ttn+ilm+mgn+kfd+qz	3516 am01t	LRSI gneiss	-	-	7.7	10.4	4.9	7.4	-108.30
hast+bt+ttn+ilm	35 12 AM19	LRSI gneiss	8.5	8.0	5.7	8.4	5.3	7.8	-118.90
hast+bt+ttn+ilm+mgn+abchess	35 12 AM06	LRSI gneiss	5.7	5.5	2.6	5.23	2.4	4.9	-115.10
andrad+hedemb+ttn+ab	35 10 GRAAB	Ca-Fe stage	3.3	0.9–2.7	0.6	2.9–3.3	-		-
andrad+hedemb+ttn+ab	34 09 GRABA	Ca-Fe stage	1.7	-0,7–1.1	-0.9	1.4–1.8	-		-
andrad+hedemb+ttn+ab	34 09 AM 14A	Ca-Fe stage	0.80	-1.6–0.2	-1.4	0.9–1.3	-		-
biot+ab+carb+qz	3516 am13b	biotite-carbonate breccia	-	-	-	-	3.1	4.2	-
biot+ab+zr+ttn	3510 am06b	K-Mg stage	-	-	-	-	-1.0	0.1	-
diop+ttn+urn	3512 AM12A	Ca-Mg stage	0.28	-2.1–(-0.3)	-0.84	1.4–1.8	-		-
diop+act+mgn+urn	3510 am11a	Ca-Mg stage	3.50	1.1–2.9	-0.64	1,6–2	-		-
diop+act+bt+urn	3512 AM 16A	Ca-Mg stage	2.58	0.2–2	-0.99	1.3–1.7	0.0	1.1	-
biot+ab+carb+urn	3516 am10b	K-Mg stage	-	-	-	-	-1.9	-0.8	-

Isotopic relationship. Temperature of a hydrothermal fluid is calculated from isotopic measurements of two coexisting minerals in equilibrium with that fluid. However, in LRSI we do not have clear petrographical evidence of mineral pairs in equilibrium for each hydrothermal stage. In the absence of evidences for coeval precipitation, we tested the $\delta^{18}O$ equilibrium of feldspar and titanite, which are common minerals in all rocks of the LRSI.

A number of papers have explored the use of δi vs. δj diagrams for determining the extent of isotope disequilibrium and open system fluid exchange (Gregory and Criss 1986, Gregory and Taylor 1986a,b; Criss et al. 1987, Gregory et al. 1989). At equilibrium, the isotopic compositions of the two minerals, $\delta^{18}O_1$ and $\delta^{18}O_2$, plots as a single point on a straight line with a slope of 45° and intercept $\Delta_{1\text{-}2}$ that is an isotherm and represents the isotopic temperature of formation. $\Delta_{1\text{-}2}$ is the difference in individual δ values, which are related to temperature of equilibrium by the isotopic fractionation factor, α according to the equation $\alpha_{1\text{-}2} = (1000+\delta_1) / (1000+\delta_2)$ and it can be shown that $10^3 \ln\alpha_{1\text{-}2} \approx \delta_1 - \delta_2 = \Delta_{1\text{-}2}$.

Because different rocks or minerals would exchange with infiltrating fluids at different rates, the slopes of the trends on $\delta^{18}O_1$–$\delta^{18}O_2$ plots can be used as a semiquantitative index of the duration and physical conditions of the infiltration event (Criss et al., 1987; Gregory et al., 1989). Accordingly, shallow, low temperature and short-lived hydrothermal systems, such as occur in epizonal environments, characteristically exhibit steep trends on $\delta^{18}O_1$–$\delta^{18}O_2$ plots, indicative of pronounced isotopic disequilibrium (Criss and Taylor, 1983; 1986).

In contrast, high temperature, deep and long-lived hydrothermal systems, such as occur in mesozonal and catazonal environments, characteristically exhibit unit-sloped trends on $\delta^{18}O_1$-$\delta^{18}O_2$ plots, indicating that a new state of equilibrium has been approached during infiltration. According to that, in $\delta^{18}O_{feldspar}$–$\delta^{18}O_{titanite}$ plot for studied rocks we observe two trends: 1) a unit-slope 45° defined by LRSI granite-gneisses and non-mineralized albitites, which cross the isotherm $\Delta_{Fsp\text{-}Ttn}$ at 675 ºC. Represented by the red line; and 2) a steep vertical-sloped non-equilibrium array defined by mineralized rocks. Represented by the black line.

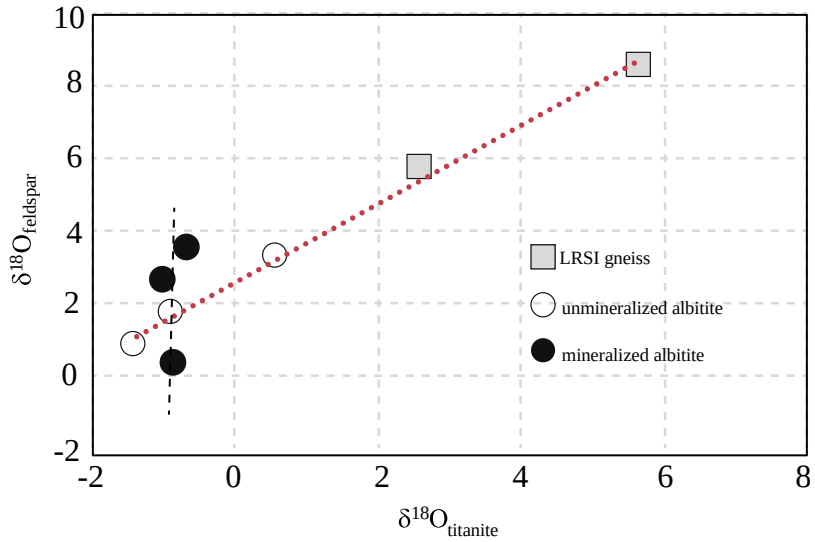

Fig. 56: Biplot for $\delta^{18}O_1$–$\delta^{18}O_2$ for feldspar and titanite.

6.8 DISCUSSION

6.8.1 Crystallization parameters of São Timóteo granite.

The ca. 1.75 Lagoa Real intrusive suite (after Arcanjo et al., 2005), known as the São Timóteo granite, covers a substantial area of the Lagoa Real uranium province, but its boundaries extrapolate the limits of the LRUP covering an area of 200 km in length. São Timóteo granite is geochemically characterized as a reduced, ferroan A-type, A2 series, metaluminous, high-K and Fe-rich calc-alkaline series (Teixeira, 2000; Marques et al., 2020a; Amorim et al., 2020). Despite the geochemical characterization, the intensive crystallization parameters of this rocks are poor or unknown. First discussions are in Maruejol et al., (1987), which based on petrographical criteria assumed crystallization conditions at high temperature, low O_2 fugacity and low water pressure.

Temperatures based on zircon and apatite saturation thermometers are quite similar to each other and give values between 800 and 900 ºC. Zircon and apatite are early crystallized minerals as they are included in the magmatic paragenesis and therefore this range should represent the liquidus temperature. These data are concordant with the high early-temperature crystallization of A-type granites (> 800 °C; e.g. Collins et al., 1982; Clemens et al., 1986; King et al., 1997). The amphibole thermometer of Ridolfi et al (2010) (see Table 3) produced a slightly lower temperature range (765–877 °C), this interval is above the solidus temperature estimated in the literature for granitic systems with moderate water and not enriched in fluorine, boron and lithium (Dall'Agnol et al., 1999b; Naney, 1983) and probably represents near-liquidus temperature. Clinopyroxene relicts included in amphibole are locally present, but clinopyroxene is extremely rare. This finding suggests that the stability field of clinopyroxene was rarely reached and that, if it was stable in the early magmatic stage, it should have reacted completely during cooling.

The dominant low oxygen fugacity during LRSI crystallization is indicated by the high Fe/(Fe + Mg) ratio for biotite and amphibole (this work) and whole-rock $Fe_t/(Fe_t + Mg)$ ratio (up to 0.8) from Marques et al. (2020a). As a rule, ilmenite is the only iron-titanium oxide and is enveloped by corona of titanite, what indicates conditions below the FMQ buffer. The presence of the ilmenite + titanite paragenesis in the São Timóteo granite reinforces the hypothesis of crystallization under reducing conditions in the sense of Ishihara (1981). In addition, the corona texture titanite shows positive Eu/Eu* anomaly (Marques et al. 2020c) in agreement with this finding.

The estimation of emplacement pressure for São Timóteo granite is a difficult task considering their reduced character that contrasts with the oxidized nature of the rocks for which the Al-in-hornblende geobarometer was originally defined (Blundy and Holland, 1990; Hammarstron and Zen, 1986; Hollister et al., 1987; Johnson and Rutherford, 1989; Schmidt, 1992). However, in the absence of another tools, pressure was tested by available thermometers and results are between 4 and 8 kbar.

Literature shows that in granitic systems calcic amphibole crystallization is dependent on the H_2O and CaO content in magma. In addition, the water content is pressure sensitive as a minimum water content of 4 wt% at 200–400 MPa is needed to stabilize amphibole at magmatic temperatures (Naney, 1983; Dall'Agnol et al., 1999; Klimm et al., 2003; Bogaerts et al., 2006), but it is larger at higher pressures and 5 wt% water at 400 MPa or 7–9 wt% of water at 960 MPa is required for the amphibole to be the silicic liquidus phase and to prevent

pyroxene formation (Naney, 1983; Prouteau and Scaillet, 2003; Oliveira et al., 2010). In the absence of safe pressure estimative we can conclude that the hypersolvus facies of São Timóteo granite derived from magmas containing at least 4 wt% H_2O and, depending of the assumed pressure of crystallization, possibly even more than 7 wt% H_2O, as indicated by the rarity or absence of pyroxene in the granites.

Marques et al., (2020c) described temperatures between 660 and 690 ºC based on Zr-in-titanite geothermometer which is related to the late magmatic stage, as titanite rims ilmenite and has crystallized after hastingsite.

6.8.2 Albitization process

The albitization process is a common hydrothermal alteration recognized in a wide variety of ore deposits (i.e, IOCG, carbonatite-related, greisen-related) and is a diagnostic feature of U deposits hosted by albitite rocks. Albitization is not restricted to ore deposits and it is also documented from a number of igneous-metamorphic terranes including the Bamble Sector, Norway (Engvik et al., 2008) and the Cloncurry District, Queensland, Australia (e.g., Oliver et al., 2004). The feldspar alteration results in variable textures which are recognized from nano-to mesoscale, and it is a process that could occurs by isochemical subsolidus re-equilibration during slow cooling of igneous rocks (Parsons et al., 2015), a process known as deuteric coarsening (Brown and Parsons, 1984), or by non-isochemical replacement of feldspar by albite that generally occurs through coupled dissolution- precipitation mechanisms (Putnis, 2002).

Chessboard texture, swapped albite rims and patch perthites are the main albitization textures observed in Lagoa Real rocks. Patch perthite manifests itself as oligoclase-to-albite patches in the core of K-feldspar grains and is a remarkable feature in the less altered rocks. Patches are interconnected with micro-to-mesoperthites and show intense decalcification alteration (i.e, saussuritization, fluoritization, carbonatation). Literature shows that the patch perthite intergrowth forms through deuteric coarsening (Brown and Parsons, 1984), which involves circulation of a deuteric fluid (post-magmatic, internally exsolved), and results in the formation of highly porous, strain-free regions of albite- and orthoclase-rich subgrains within perthitic feldspars (Lee and Parsons, 1997). The high porosity is reflected by the plagioclase reddish color which results from the hematite precipitation in the pore space, as experimentally observed by Putnis et al., (2007). Two-feldspar thermometry result is

between 400 to 500 ºC, which marks the onset of deuteric coarsening, and shows that albitization started in a late-magmatic stage.

The chessboard texture is well developed in coarse-grained rocks, and in those that fine-grained it is preserved as porphyroclasts, showing that albitization proceded in a pre-kinematic stage, and the metamorphic event converted albite in fine-grained untwinned albite. Isotopic data of albite results in low $\delta^{18}O$ values (< 5‰) which show that magmatic fluids interacted with surficial fluids, which probably resulted in pervasive albitization and widespread formation of the chessboard albite texture with composition of almost pure albite.

6.8.3 Hydrothermal history of the Gameleira I, Barrinha and Barreiro deposits

Constrains on the metasomatic events occurred at LRUP in association with its tectono-thermal history provided by petrographic analysis is summarized in Fig. 57. Petrographic and mineral chemistry data indicate a sequence that can be grouped in two major stages, which mostly developed under a ductile regime, and reflect different timing and chemical trends.

The first corresponds to the sodic–calcic and iron-calcic-magnesian stages, which was accompanied by partial to total quartz dissolution and likely uranium enrichment. The uraninite in veinlets-style is spatially related to the final stages of iron-calcic-magnesian stage, as the assemblage titanite + uraninite is usually hosted by the most magnesian clinopyroxenes, diopside and augite.

The second stage is represented by the potassic-magnesian and the late calcic stage, which corresponds to a retrograde assemblage and evolved under ductil-brittle regime. The uranium crystallization/redistribution is spatially and temporally related to this stage, as uraninite is associated with titanite but also is disseminated in biotite, albite and carbonate. An infill stage is represented mainly by carbonate veins.

The mode of occurrence of the LRSI-derived albitites as pod-like bodies (Fig. 44) along shear zones is analogous to albitites elsewhere (see Suikkanen and Rämö, 2019a for a list). Quartz depletion and neoformation of alkaline feldspar are usual in albitites, which makes they also be called epysienites (Lacroix, 1920). However, Lagoa Real albitites lack the vuggy texture that is a common feature of episyenites (e.g. Costi et al, 2002). The widespread presence of hydrothermal clinopyroxene is a striking feature in Lagoa Real, although not usual in albitites worldwide, it is usual in metasomatic rocks of high temperature (> 450 ºC;

Caballero, 1993; Cuney et al, 2012; Suikkanen and Rämö, 2019b). Hydrothermal stages in Lagoa Real is similar to the major U-albitite hosted deposits documented, such as the Kirovograd–Krivoi Rog district, Ukraine (Cuney et al., 2012), but in the Lagoa Real deposits, chloritization was not efficient and the system evolved mostly under ductile regime.

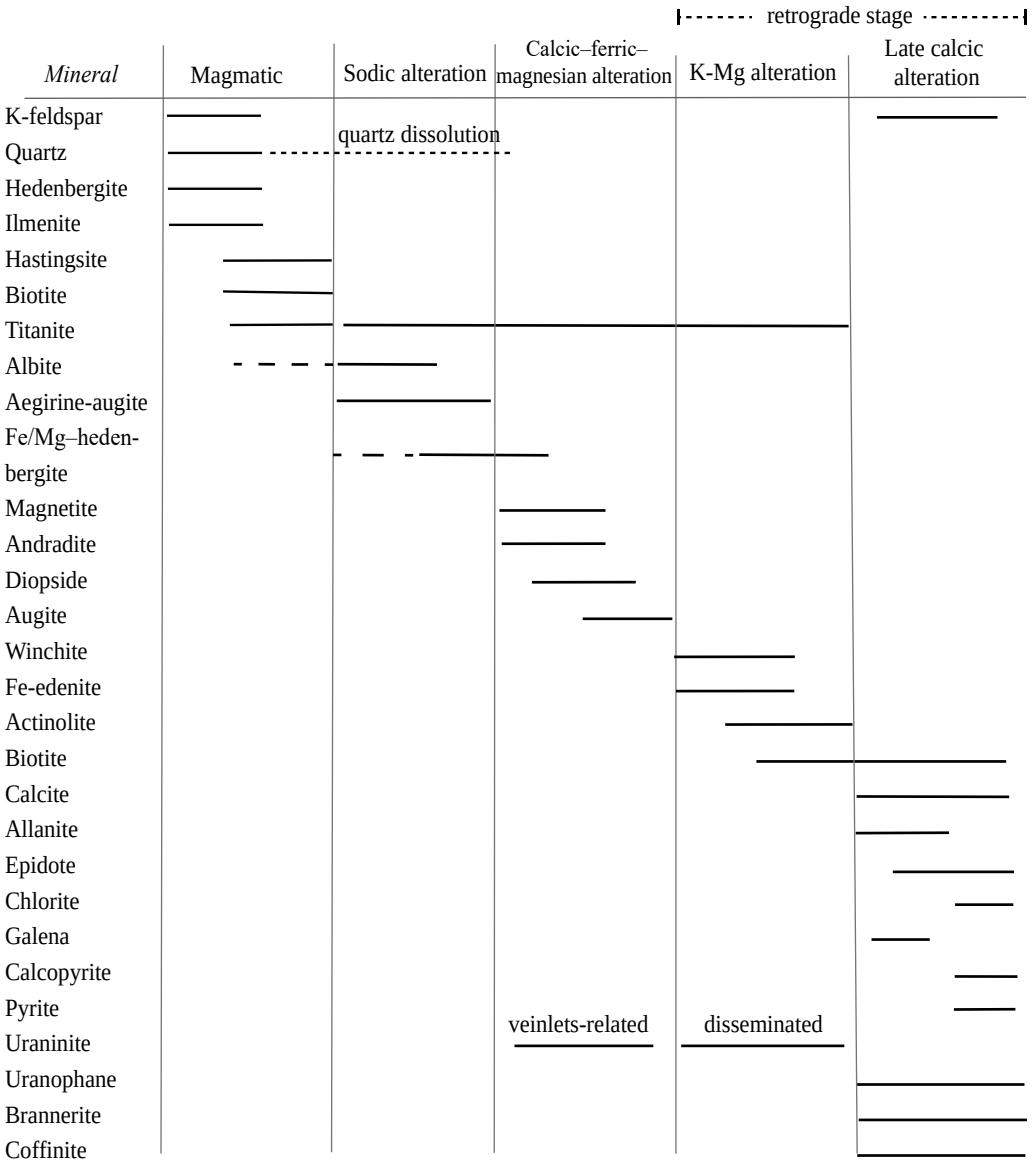

Fig. 57: Mineral parageneses in the host Lagoa Real suite intrusive rocks and albitites.

6.8.4 Thermal and temporal constrains

Early hydrothermal transformation is represented by the albite replacement over K-feldspar. Felspars show textural features common in tardi-magmatic alteration, such as the development of patch perthites, and occurred at temperatures between 400 and 500 ºC. A

high temperature range is given by the assemblage aegirine-augite + andradite and hedenbergite + andradite (300–550ºC). However, Zr-in-titanite geothermometer calculated for titanite intergrown with andradite gives temperatures around 650 ºC Marques et al., (2020c). Calculated temperatures indicate that from sodic-calcic to the early stage of the iron-calcic-magnesian alteration temperatures are between 400–650 ºC. Estimated pressure for garnet-bearing and magnetite-bearing paragenesis has different results of 6 kbar and 2 kbar, respectively. Due to the intense recrystallization, the timing of quartz-depletion is not easily constrained. Absence of vuggy texture does not permit ascertaining if quartz was initially removed at all, only that if so, quartz dissolution was not complete at this stage. The temperature of the magnesian albitites (diopside- and augite-bearing) is not possible calculate, as suitable assemblage for temperature calculations is lack.

Amphibole and biotite precipitation represent the retrograde potassic-magnesian stage. However, in the diopside-bearing albitites, amphibole either has Mg-hastingsite or Mg-hornblende/actinolite composition, which reflects differences in pressure and temperature conditions. According to calculations, Mg-hastingsite reflects temperature between 680 to 530 ºC and pressure range between 3 and 6 kbar. The Mg-hornblende/actinolite precipitation represents fall in temperature and pressure which are between 470 and 450 ºC and 0.1–0.9 kbar, respectively.

Next, biotite precipitated followed by the calcite and epidote precipitation in the late calcic stage, whose both temperatures were not possible to calculate. Fluid inclusion data in vein-filling carbonate from Fuzikawa et al, (1988) gave temperature between 300 and 100 ºC, which indicates that biotite precipitation and late calcic stage temperature are between 450 and 300 ºC.

The Paramirim aulacogen has a long geodynamic history that span more than 1 billion years. The first rift phase started at around 1.75 Ga, which covers the emplacement of Lagoa Real intrusive suite, and ended at around 580Ma when the aulacogen was inverted. This wide lifetime interval and the final Brasiliano metamorphic overprint that affected Lagoa Real rocks make it difficult to recognize the textural features of the early hydrothermal paragenesis and it is also difficult to connect the input of hydrothermal alteration to some specific event, causing a plethora of models (i.e., Maruejol, 1988; Lobato and Fyfe, 1990; Chaves, 2013). Recent geochronological work by Marques et al., (2020b) points out to a multi-stage model for mineralization that probably occurred episodically over 1 Ga of Paramirim aulacogen evolution with distinct peaks, but ended in the Brasiliano–Pan African orogeny. Accordingly, uranium accumulation is suggested to have had took place between

1.7 Ga and 580 Ma, indicated by the multiage U-related titanite (i.e., 1.7 Ga, 1.5 Ga, 1.1 Ga Ga, 960 Ma; Chaves et al., 2009; Lobato et al., 2015; Marques et al., 2020b). Uraninite crystallization, in turn, occurred between 580 to 520 Ma (U–Pb–SIMS uraninite; uraninite chemical dating), motivated by the Brasiliano-Pan African orogeny.

Considering the abovementioned model and the data of the present work, we can address that the high temperature Na-Ca and Fe-Ca-Mg alteration stages probably started in the late magmatic stage or well after the ca. 1.75 Ga São Timóteo granite emplacement. This event provided albite, clinopyroxene, titanite and andradite precipitation. Although there is no distinctive feature to connect temporally this first hydrothermal event with the São Timóteo emplacement itself, albitization and desquartzification of granitic rocks usually occur in the late-magmatic stage in albitite-hosted U deposits worlwide (Cuney et al., 2012; Alexandre, 2010) and in epysienite-related deposits elsewhere (Recio et al., 1997; Costi et al., 2002; Suikkanen and Rämö, 2019). In addition, the preservation of coarser grained pyroxene-bearing albitites as massive-to weak foliated rocks and the presence of pyroxene with intracrystalline deformation, suggest that early assemblage precipitated prior to deformation, as opposed to those albitites with retrograde assemblage, which are well-developed as foliated augen-like rocks. According that, we believe that this high temperature alteration occurred well after the 1.75 Ga São Timóteo crystallization, however, we should also consider the 1.5 Ga age proposed by Maruejol (1989) and Cordani et al., (1992). These two ages correspond to rift events in Paramirim aulacogen with associated vulcanism (i.e., Danderfer Filho et al., 2009; 2015; Santos et al., 2020), which should also have contributed to the circulation of high-temperature hydrothermal fluids.

Temporally disconnected to this event is, however, the retrograde stages, represented by the K-Mg and late calcic alteration, which occurred during the Brasiliano-Pan African orogeny. The thermometric calculations describe a trajectory from medium-amphibolite to greenschist facies (680–530 ºC; 3–6 Kbar (Mg-hastingsite precipitation) → 470–450 ºC; 0.1–0.9 Kbar (Mg-hornblende/actinolite precipitation) → 450–300 ºC (biotite and carbonate precipitation). This temperature interval is concordant with the calculated temperature from Peixoto et al., (2018) in Rio Pardo Salient (RPS), south of the studied area, which gave temperature and pressure of 650 ºC and 8.5 kbar → 650–530 ºC and 3–5.5 kbar, related to the syn-collisional (575–565 Ma) and orogenetic collapse stages (530 Ma), respectively. The authors also found an age of 530–490 Ma, which is related to the cooling and hydrothermal activity widespread in the Araçuaí orogen, also studied by other authors (Scholz et al., 2012; Cabral et al., 2013; Cabral and Zeh, 2015; Gonçalves et al., 2019).

The wide time interval between first and second hydrothermal events also led to titanite recrystallization and uranium endowment (see Marques et al., 2020b for a discussion) in the following stages of the aulacogen opening causing the multiple intermediate U-Pb ages.

The main textural relationship in the veinlet-related uraninite, interpreted as primary ore, is the close association between uraninite, zircon and titanite. Uraninite looks to be disposed as inclusions in the titanite. However, a closer view in the less intensely sheared zones, in which uraninite + titanite are not so sheared, indicates that uraninite is disposed randomly through the titanite crystals showing an exsolution texture. Zircon and titanite are intergrown as well, and it is noticed that in more intensely sheared regions, both, uraninite and zircon, are more abundant. This relationship and the complete absence of uraninite outside of micro-shear zones points out to a syn-metamorphic uraninite precipitation, otherwise, there is no reason to not have any uraninite crystal associated to other matrix minerals, i.e., clinopyroxene, if ore deposition was occurred in a pre-metamorphic event. This observation is confirmed by the calculated uraninite chemical ages which results in ages between 600 and 450 Ma, which is coincident with the precise Pb-Pb SIMS age of 580 Ma of uraninite (Marques et al., 2020b) and overlap the syn-to post collisional stage (580–490 Ma) of Brasiliano orogeny. The thermodynamic condition for uraninite precipitation is unknown and it is not trivial to constrain, as this relationship was never described before and exsolution may occurs as consequence of multiple factors such as rapid cooling, tectonic stress, slow cooling, anomalous mixtures (Ramdohr, 1969).

Marques et al., (2020c) described U, Hf and REE+Y loss in titanite from São Timóteo granite rocks towards the ore shoot. In addition, chemical analyses of uraninite showed high Y (+REE?) contents. This behavior indicates that titanite probably acted as source of some elements, including uranium, to precipitate uraninite. Shearing concentrated U-rich titanite and magmatic-to-hydrothermal zircon in the shear zones causing the exsolution-texture uraninite in the veinlets-related mineralization during the Brasiliano metamorphic event. Post-to-late collisional event was responsible to redistribute uraninite as disseminations and U^{+6} specimens.

6.8.6 Chemical trends

Where two or more cations have a similar affinity for specific crystal sites within the same mineral, they will compete for them, and substitute for, one another. Certain factors such as temperature and fugacity, together with the activity of aqueous species, will determine how

much of each element may be incorporated. Because of that, chemical trends in mineral assemblage can provide important information about geological processes.

Clinopyroxene and titanite. The early stage of alteration formed the albitites with pyroxene of variable composition. Pyroxene is the main hydrothermal mineral forming at this stage and its composition reflects the evolution from the Na-Ca stage, recorded by aegirine-augite replacement, through Ca-Fe to Ca-Mg stage with hedenbergite, diopside and augite replacement.

Oxygen fugacity trends can be deduced from Fe^{3+} incorporation into the pyroxene structure. Schweitzer et al., (1974) constructed a diagram to evaluate if Fe^{3+} incorporation reflects charge balance through a plot of charge deficiency site (Y axis) *vs.* charge excess site (X axis). If Fe^{3+} incorporation is the result of charge compensation it should plot in the $Fe^{3+} = 0$ line. According to this diagram (Fig. 58A), the Lagoa Real pyroxenes show two trends: 1) One plotting above the $Fe^{3+} = 0$ line that includes the hydrothermal Na-Ca and Ca-Fe pyroxenes (aegirine-augite, Fe-to-Mg-hedenbergite and diopside), which indicates high oxygen fugacity. That $ƒO_2$ was high is reinforced by the association of those pyroxenes with another Fe^{3+}-bearing minerals (andradite and magnetite); and 2) A second trend plots below the $Fe^{3+} = 0$ line, composed of magmatic hedenbergite of São Timóteo granite and Ca-Mg pyroxene of augite composition, indicating low oxygen fugacity conditions. Therefore, a Fe^{3+} *vs*. Fe^{2+} diagram (Fig. 58B) should define a trajectory towards higher oxygen fugacity from São Timóteo granite to Na-Ca stage, and lower oxygen fugacity from Na-Ca to Fe-Ca-Mg stage.

Accordingly, titanite, also a common mineral of the early stage of alteration, may provide oxygen fugacity information as it is an important Fe^{3+} carrier mineral. The chemical composition of titanite exhibits two well-defined trends in the Fe-*vs*-Al diagram (Fig. 58C) defined by: 1) a negative correlation towards $ƒO_2^+$ increases, and therefore high oxygen fugacity, from the São Timóteo granite and its gneissic rocks through the Ca-Fe and Na-Ca stages, where the peak of high $ƒO_2$ was reached; and 2) a positive correlation towards the lowest Al and Fe^{3+} values, which represents low $ƒO_2$. The lowest $ƒO_2$ is represented by the augite-bearing albitite. The Al and Fe decrease is counterbalanced by an increase in Ti, that attains its highest values in the ore-hosted titanite. The negative linear correlation of (Al + Fe) vs. Ti in titanite (Fig. 58D) represents the coupled substitution $(Al,Fe^{3+}) + (F,OH)^- = Ti^{4+} + O^{2-}$, the most common substitution in natural titanite (Franz and Spear, 1985; Troitzsch and Ellis, 2002; Tropper et al., 2002). It is noticeable that uraninite-related titanite

is correlated with the reducing trends (low Al and Fe contents) and the high Ti contents (Fig. 58E, F).

Therefore, clinopyroxene and titanite have a similar trend in relation to Fe^{3+} incorporation that reflects oxygen fugacity during hydrothermal system evolution. This finding shows the potential of titanite in the Lagoa Real context not only as geochronometer, as it is well known in the literature, but also as a good redox tracer.

It seems pertinent to point out the spatial coincidence between diopside, augite and Ti-Fe^{3+}-poor titanite of the orebody. Lobato and Fyfe (1990) indicated that the U mineralization is spatially associated with an Fe^{+3}-rich mineral assemblage, which would represent the peak of oxidizing conditions, but our data show that uraninite is close to Mg-rich and Fe^{3+}-poor minerals represented by diopside, augite and titanite, and therefore the

less oxidizing-to-reducing conditions.

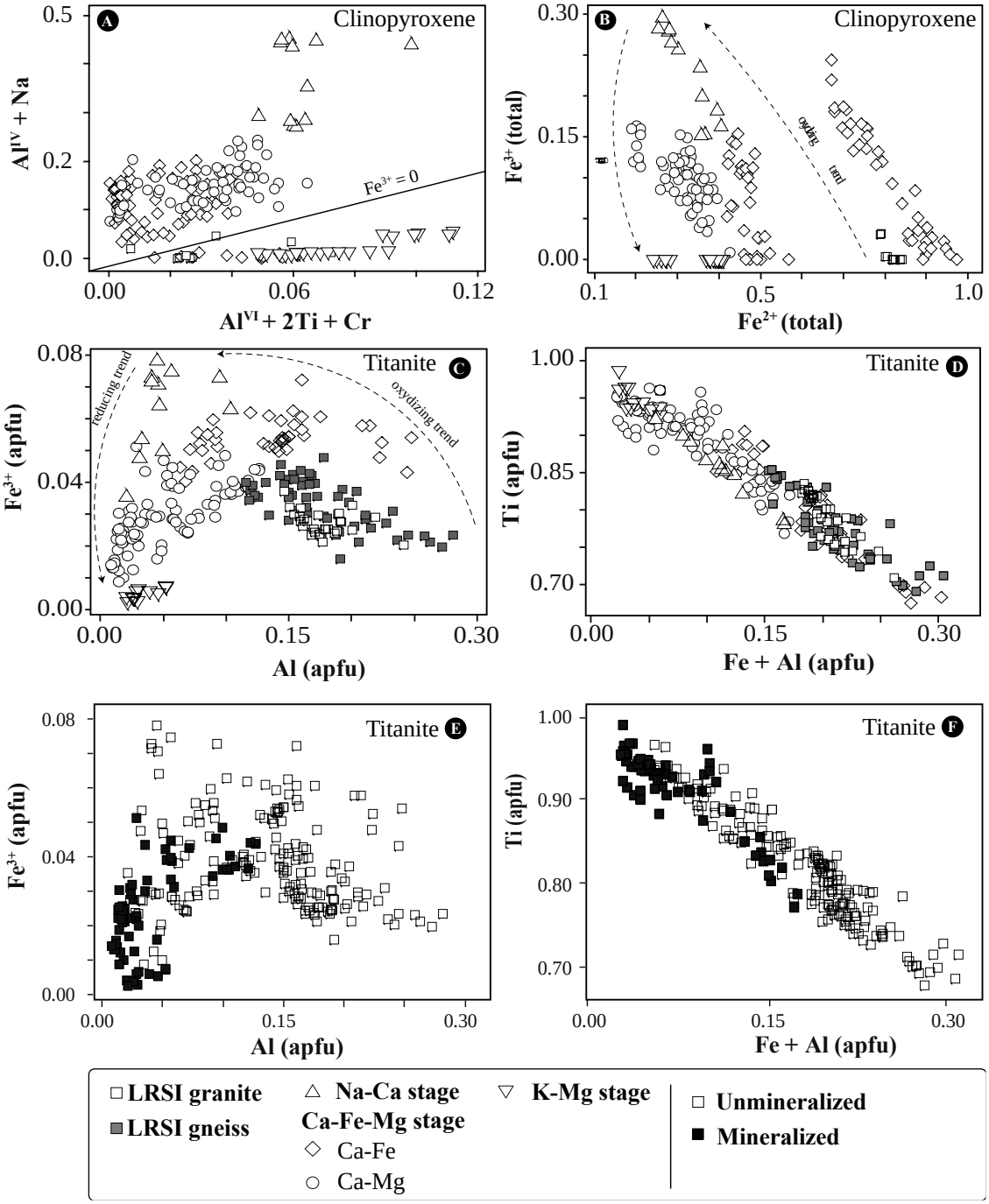

Fig. 58: Biplots showing the main trends in clinopyroxene and titanite. A. Position of pyroxenes in the Na + Al^{VI} vs Al^{VI} +2Ti + Cr diagram (Schweitzer et al. 1974). B. Fe^{+3} incorporation trend in clinopyroxene. C. Compositional variations of titanite in atoms per formula unit (apfu). Aluminium vs. Fe, showing similar trend for Fe incorporation as in clinopyroxene in B. D. Aluminium + Fe vs. Ti in titanite. E. Compositional variations of titanite comparing unmineralized and mineralized samples.

Amphibole and biotite. Amphibole and biotite are widespread in the augen and foliated albitites; however, their composition reflects that of their clinopyroxene precursor as already stated by Maruejol (1989), Lobato and Fyfe (1990) and Cruz (2004). This finding is showed in the Fe vs Fe/(Fe + Mg) diagram (Fig. 59A, B, C), and shows that apparently, the fluid played a less decisive role in the amphibole and biotite composition.

The positive correlation between Cl and (Fe/Fe + Mg) (Fig. 60A, B) in biotite and amphibole indicates that Mg-Cl avoidance mechanisms (Ramberg, 1952; Munoz & Swenson., 1981; Volfinger et al., 1985) controlled the incorporation of this halogen in the mineral structure as the substitution of Cl is likely where Cl-bearing anion sites are enlarged. The implication of this correlation was addressed by Kullerud (1995), who pointed out that it is not possible to decide whether the concentration of one component is dependent on the concentration of another (e.g. Cl is dependent on Fe, or Fe is dependent on Cl) from the correlation itself, or whether the concentrations of the components are dependent on an external factor such as temperature, pressure or chemical potentials. However, since amphibole and biotite follow the clinopyroxene composition, as shown, it seems reasonable to suppose that halogen substitution was dependent on Fe/Mg ratio.

On the other hand, the absence of correlation between F and (Fe/Fe+Mg) for entire samples contrasts with the Fe-F avoidance (Fig. 60C, D). The low F^- in biotite from K-Mg stage is not correlated with Mg contents, which shows that probably the absence of fluorine incorporation was influenced by fluid composition in this case, which in turn means that fluid was devoid of F^-.

Samples of São Timóteo granite and its gneisses, and those of K-Mg stage show a linear trend of Cl decrease and OH increase in the diagram (Fig. 60E). This behavior indicates that the latter fluid flow probably was mainly composed by OH^- and it was responsible by OH^- incorporation and Cl^- scavenging from the early precipitated minerals through the shear zones, as Cl^- is strongly partitioned into the fluid phase (Oberti, 1993).

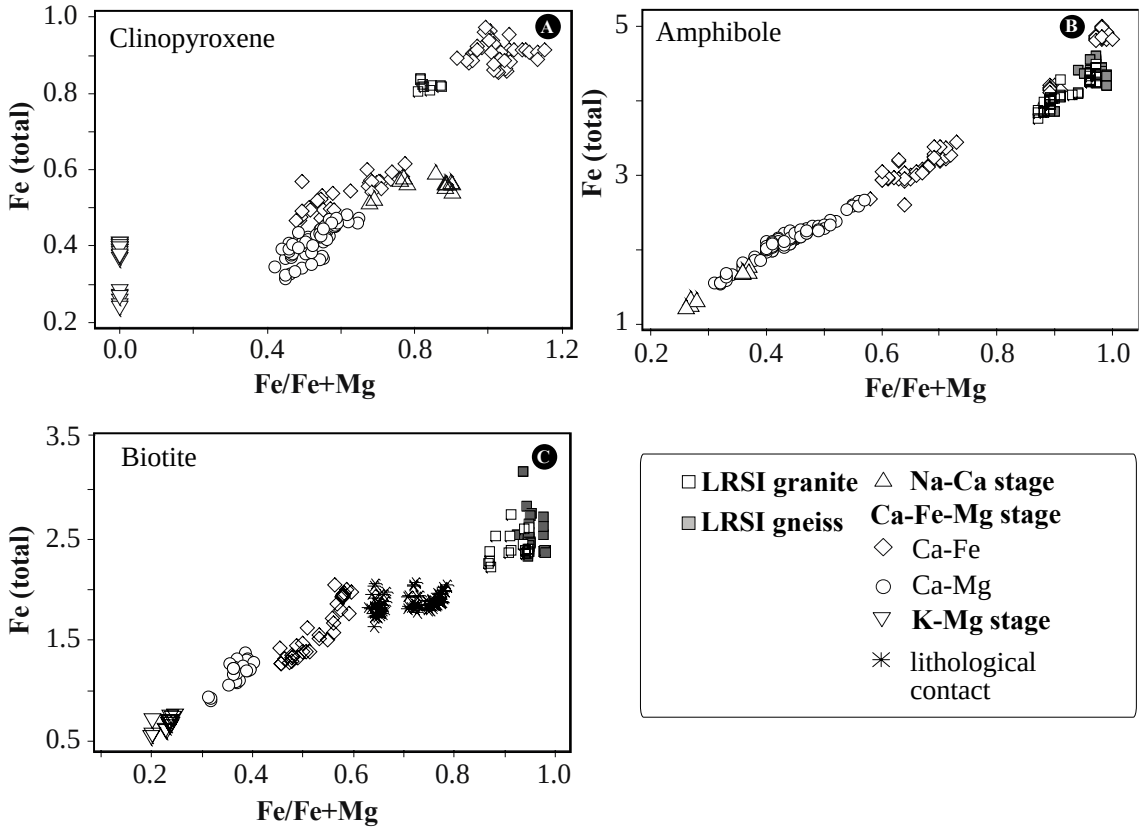

Fig. 59: Biplots showing the main trends in relation to Fe and Mg in A. clinopyroxene, B. amphibole and C. biotite.

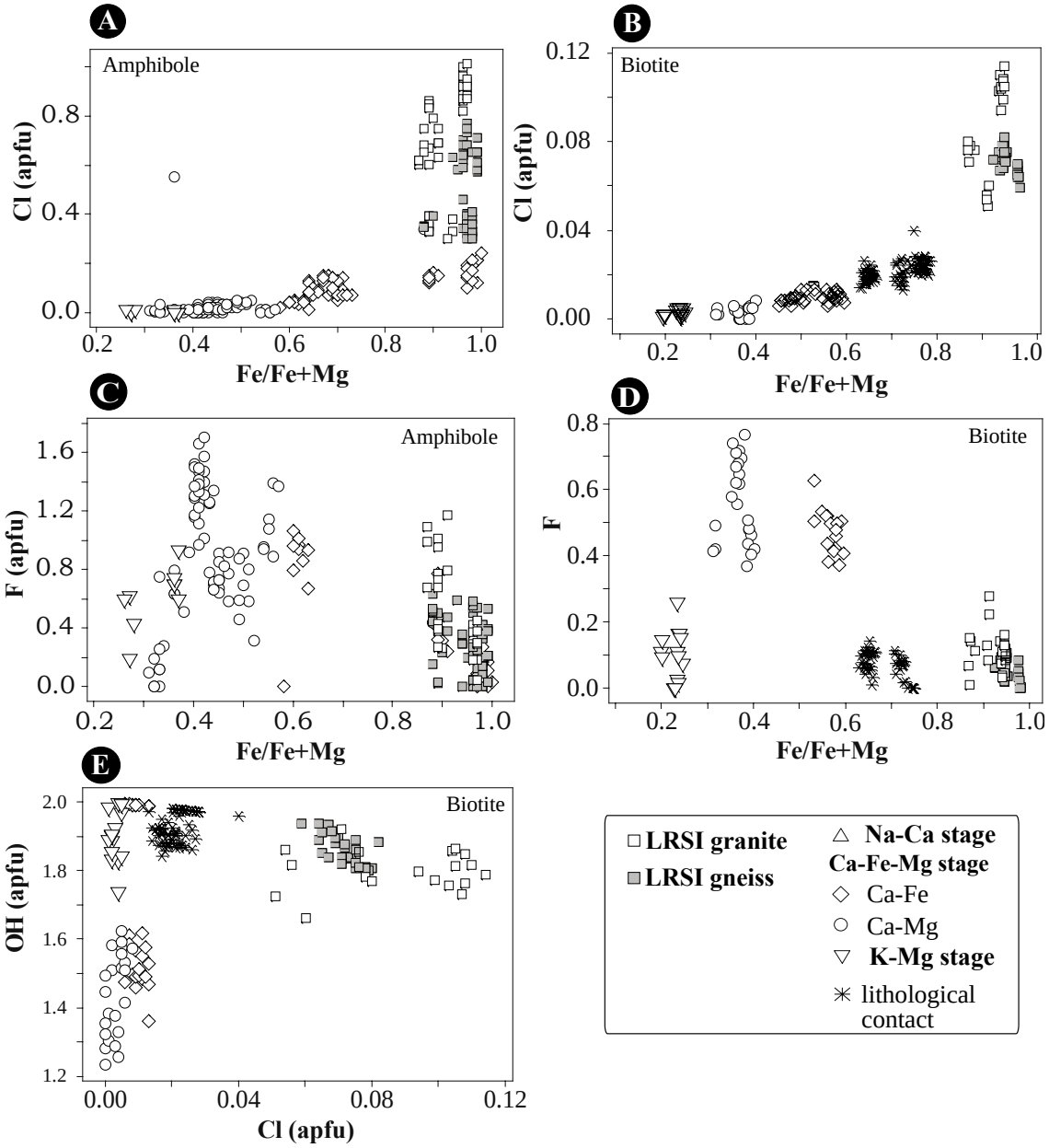

Fig. 60: Biplots showing the main halogen trends in amphibole and biotite.

Uraninite. Recent and non-so recent studies of uraninite chemistry have shown that this mineral is a good tool to obtain useful information about precipitation temperature and is a potential track of the uranium deposit type. In this sense, uraninite REE+Y contents, REE-normalized pattern and Th/U ratio are the tools main used (Fryer and Taylor, 1987; Mercadier et al, 2011; Eglinger, et al 2013). Frimmel et al, (2014) assumes the U/Th ratio of 10^3 as a boundary to discriminate between high and low temperature uraninite. Low temperature uraninite has U/Th ratio up to 10^3 and high temperature uraninite (> 450 ±50 ºC) is usually below this value. In addition, U/Th ratio < 10^2 indicates even high temperature

of crystallization (i.e. magmatic or amphibolite facies). Analyzed samples of Lagoa Real are in general in the boundary or below 10^3 indicating moderately-to-high temperature conditions of crystallization (Fig. 61A). Samples from Barrinha deposit (An 34) have U/Th around or less than 10^2 showing its even higher temperature of formation compared to the other anomalies.

The high temperature of uraninite formation is also constrained by its Y contents, and by extension the REE contents, as they are physicochemically similar elements as a result of their trivalent character, similar electronegativity and ionic radii, and therefore they are usually correlated in geological systems. Cuney, (2010) and Mercadier et al., (2011) showed that incorporation of REE into the crystallographic structure of uranium oxide is a function of both their atomic radii and temperature, however, because of charge balance, at low temperature, REE incorporation requires a coupled substitution. At high temperature, REE+Y is easily incorporated in uraninite through the dilatational nature of this mineral. Therefore, the uncommon high Y_2O_3 contents (around 2% and maximum 9% in one sample) coupled with the low U/Th ($<10^3$ ratio) mainly in the veinlets-related uraninite (Fig. 61A) of Gameleira I deposit, even if the lacking REE analyses, confirms its high temperature crystallization (> 450 ±50 ºC). In addition, the high Y contents, coupled with the low totals in uraninite probably indicates presence of rare-earth elements, which were not analyzed.

In comparison with uranium deposits of Lufilian belt which shows well constrained temperature trajectory manifested by their uraninite REE+Y contents (Eglinger et al., 2013), uraninite from Lagoa Real shows Y(+REE?) contents similar to those crystallized under upper greenschist to upper amphibolite facies (350–550ºC; 0.5% >Y_2O_3 < 2.5%). In addition, in Gameleira I deposit, veinlets-related uraninite shows higher Y_2O_3 (>1%) in relation to those retrograde-related (Y_2O_3 <1%), which probably reflects high and low relative temperature, respectively. In the Barrinha deposit uraninite groups are in a similar range as both have high Y_2O_3 contents (2–3%). The anomalous high Y contents in uraninite probably reveals not only high temperature but also high REE+Y availability during uraninite crystallization. The positive correlation between Y_2O_3 and P_2O_5 (Fig. 61B) shows that PO^{3-}_4 complexes played an important role in the REE+Y transport or deposition. This relation is also confirmed by the usual presence of monazite inclusions in allanite, mainly in the Barrinha deposit (Fig. 53G).

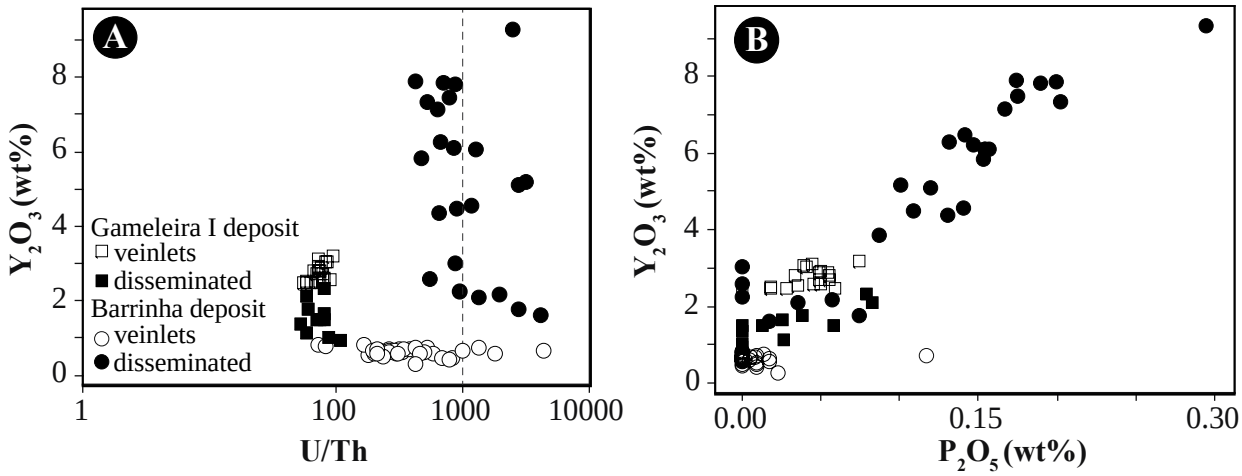

Fig. 61: Biplots for uraninite generations. A. U/Th *versus* Y_2O_3 diagram showing that samples have U/Th ratio around 10^3, the estimated boundary between low and high temperature established by Frimmel et al., (2014). Samples from Barrinha deposit (AN 34) are near 10^2. B. The plots in the Y_2O_3 *versus* P_2O_5 diagram shows positive correlation.

6.8.6 Nature and source of hydrothermal fluids

Except for the 3512 AM06 sample, which shows albitization evidences, i.e., chessboard texture, analyzed LRIS granite-gneisses do not show evidences of hydrothermal alteration. Therefore, magmatic $\delta^{18}O$ values are to be expected for the minerals. Typical $\delta^{18}O$ values in granitic rocks are between +7 to +15‰ for feldspar (Taylor and Sheppard, 1986) and 4 to 7‰ for titanite (King et al., 2001 and references therein). The 3512 AM06 sample is the only one that is out of this typical magmatic range showing the lowest values ($\delta^{18}O$ = 5.7 and 2.6 for feldspar and titanite, respectively). The albitite samples show low $\delta^{18}O$ values (2 to -2‰). The nature of this fluid could be meteoric or metamorphic water. Meteoric or surface-derived waters are very low in $\delta^{18}O$ (e.g. in meteoric water, $\delta^{18}O$ is between 0 and -10‰; Sheppard, 1986) and would thus cause depletion of $\delta^{18}O$ in minerals, whereas metamorphic fluid is heavier ($\delta^{18}O$ = +3 – +10‰; Sheppard, 1986) and probably is not able to decrease oxygen values as observed in the samples.

The isotopic equilibrium between unaltered LRIS gneissic rocks and hydrothermal albitite shown in Fig. 56 defined by the unit-slope 45° trend have two interpretations: a) albitization occurred by hot fluids at temperatures high enough to isotopically homogenize both, feldspars and titanite, in mesozonal or catazonal long-lived hydrothermal conditions or b) the unit-slope is a re-equilibrium produced by a high temperature post-hydrothermal event, i.e. during Brasiliano amphibolite facies metamorphic event. The second slope

indicates that albite-titanite pair is strongly out of isotopic equilibrium. A low temperature event explains this disequilibrium and has affected mainly mineralized rocks below titanite closure temperature as the $\delta^{18}O$ of albite was reequilibrated in this new condition and $\delta^{18}O$ of titanite remained constant. This low temperature event probably is related to greenschist facies metamorphic event during Brasiliano orogeny which affected the rocks.

6.7 CONCLUSIONS

(1) Crystallization of São Timóteo granite occurred at around ca. 1.75 Ga at near liquidus high temperature of 900 ºC, reducing conditions below the FMQ buffer and high-water contents of ~4 wt%.

(2) Temperatures of around 680 and 400 ºC was reached during the late magmatic stage (Zr-in-titanite geothermometry and two feldspar thermometry), when albite and probably clinopyroxene replacement occurred. This process probably started under oxidizing conditions, but ended at reducing oxygen fugacity. The close association between uranium mineralization and clinopyroxene of diopside and augite composition indicates that a U-enriched titanite was coprecipitated with clinopyroxene at high temperature and low oxygen fugacity conditions. Probably this process represents the starting point of U endowment in rocks.

(3) A new fluid circulation occurred during the Brasiliano orogeny causing precipitation of retrograde assemblage, mainly amphibole and biotite, and late calcic assemblage at medium amphibolite to greenschist facies (650 to 450 ºC; 3–6 to 0.1–0.9 kbar). Meteoric water probably was responsible for this process. High temperature OH- and PO^{3-}_4 -rich fluids played a role in uraninite crystallization and resulted in Y(REE?)-rich uraninite.

Considering this model, we can address that the Brasiliano metamorphic event was associated with uraninite crystallization, however the uranium itself was previously enriched in the titanite structure. Firstly, uraninite was exsolved from titanite structure and they both were concentrated as veinlets in albitite during the Brasiliano-Pan African orogeny. Later, uraninite was remobilized and redistribuited as disseminations in biotite, calcite and albite during the final stages of retrometamorphic event.

6.8 REFERENCES

Alexandre, P. (2010). Mineralogy and geochemistry of the sodium metasomatism-related uranium occurrence of Aricheng South, Guyana. *Mineralium Deposita, 45*(4), 351-367.

Alkmim, F.F., Marshak, S., Pedrosa-Soares, A.C., Peres, G.G., Cruz, S.C.P., Whittington, A., Carlos Pedrosa-Soares, A., Gravina Peres, G., Cruz, S.C.P., Whittington, A., 2006. Kinematic evolution of the Araçuaí-West Congo orogen in Brazil and Africa: Nutcracker tectonics during the Neoproterozoic assembly of Gondwana. Precambrian Research 149, 43–64. https://doi.org/10.1016/j.precamres.2006.06.007

Alkmim, F.F., Brito Neves, B.B. de, Alves, J.A.C., 1993. Arcabouço tectônico do Cráton do São Francisco: uma revisão, in: Dominguez, J.M., Misi, A. (Eds.), O Cráton Do São Francisco. Sociedade Brasileira de Geologia, Salvador, pp. 45–62.

Amorim, L.E.D., Rios, F. J., Freitas, M. E., Cutts, K., Geraldes, M. C., Diniz, A. C. D., Matos, E. C. 2020. Zircon U-Pb geochronology of Paleoproterozoic Stratherian intraplate A-Type magmatic associations of the Lagoa Real Uranium Province, São Francisco Craton (Bahia, Brazil). Journal of South American Earth Sciences. *submitted.*

Anderson, J. L., & Smith, D. R. (1995). The effects of temperature and fO_2 on the Al-in-hornblende barometer. *American Mineralogist, 80*(5-6), 549-559.

Arcanjo, J.B.A., Martins, A.M., Loureiro, H.C., Delgado, I.M., Souza, J.D., Neves, J.P., Oliveira, J.E., Teixeira, L.R., Varela, P.H., Gomes, R.D., 2005. Vale do Paramirim, Bahia: Geologia e recursos minerais. Série Arq. Abertos 22.

Babinski, M., Pedrosa-Soares, A.C., Trindade, R.I.F., Martins, M., Noce, C.M., Liu, D., 2012. Neoproterozoic glacial deposits from the Araçuaí orogen, Brazil: Age, provenance and correlations with the São Francisco craton and West Congo belt. Gondwana Res. 21, 451–465. https://doi.org/10.1016/j.gr.2011.04.008

Babinski, M., Van Schmus, W.R., Chemale Jr, F., 1999. Pb–Pb dating and Pb isotope geochemistry of Neoproterozoic carbonate rocks from the São Francisco basin, Brazil: implications for the mobility of Pb isotopes during tectonism and metamorphism. Chem. Geol. 160, 175–199.

Babinski, M., Van Schmus, W.R., Chemale Jr., F., Brito Neves, B.B., Rocha, A.J.D. 1993. Idade isocrônica Pb/Pb em rochas carbonáticas da Formação Caboclo em Morro do

Chapéu. In: Pedreira, A.J., Misi, A., Dominguez, J.M.L. (eds.), II Simpósio sobre o Craton do São Francisco. Brazilian Geological Society, Salvador, p. 160–16

Bastos-Leal, L.R., Teixeira, W., Cunha, J.C., Leal, A.B.M., Macambira, M.J.B., Rosa, M.L.S., 2000. Isotopic signatures of paleoproterozoica granitoids of the Gavião block and implications for the evolution of the São Francisco craton, Bahia, Brazil. Rev. Bras. Geociências 30, 66–69.

Bastos-Leal, L.R., Teixeira, W., Cunha, J.C., Macambira, M.J.B., 1998. Archean tonalitic-trondhjemitic and granitic plutonism in the Gavião block, São Francisco Craton, Bahia, Brazil: Geochemical and geochronology characteristics. Rev. Bras. Geociências 2, 209–220.

Bitencourt, C.N., Cruz, S.C.P., dos Anjos Cruz, V., Pedrosa-Soares, A.C., Paquette, J.L., Alkmim, A.R., Barbosa, J.S.F., 2019. Rifting events in the southern sector of the Paramirim Aulacogen, NE Brazil: New geochronological data and correlations for the São Francisco–Congo paleocontinent. Precambrian Res. 326, 417–446. https://doi.org/10.1016/j.precamres.2018.12.005

Bogaerts, M., Scaillet, B., Vander Auwera, J., 2006. Phase equilibria of the Lyngdal granodiorite (Norway): implications for the origin of metaluminous ferroan granitoids. J. Petrology 47, 2405–2431

Bowles, J. F. (1990). Age dating of individual grains of uraninite in rocks from electron microprobe analyses. *Chemical Geology*, *83*(1-2), 47-53.

Brown, W. L., & Parsons, I. (1984). The nature of potassium feldspar, exsolution microtextures and development of dislocations as a function of composition in perthitic alkali feldspars. *Contributions to Mineralogy and Petrology*, *86*(4), 335-341.

Caballero, J. M. (1993). Las Episienitas de la Sierra de Guadarama: Un Caso Singular de Alteración Hidrothermal de Edad Post-hercínica. Thesis (Doctorado). Madrid: Universidad Complutense de Madrid. 313 p.

Chaves, A. de O., 2013. New geological model of the Lagoa Real uraniferous albitites from Bahia (Brazil). Cent. Eur. J. Geosci. 5, 354–373. https://doi.org/10.2478/s13533-012-0134-7

Clemens, J. D., Holloway, J. R., & White, A. J. R. (1986). Origin of an A-type granite; experimental constraints. *American Mineralogist*, *71*(3-4), 317-324

Collins, W. J., Beams, S. D., White, A. J. R., & Chappell, B. W. (1982). Nature and origin of A-type granites with particular reference to southeastern Australia. *Contributions to mineralogy and petrology*, *80*(2), 189-200.

Cordani, U.G., Sato, K., Marinho, M.M., 1985. The geologic evolution of the ancient granite-greenstone terrane of central-southern Bahia, Brazil. Precambrian Res. 27, 187–213.

Costa, P.H.O., Andrade, A.R.F., Lopes, G.A., Souza, S.L., 1985. Projeto Lagoa Real: mapeamento geológico 1:25000, textos e mapas. Companhia Baiana de Pesquisa Mineral-CBPM/ Empresas Nucleares Brasileiras (NUCLEBRAS), Salvador.

Cruz, S.C.P, 2004. A interação tectônica entre o Paramirim Aulacogen e o Orógeno Araçuaí. Tese (Ph. D. Thesis), Departamento de Geologia, Universidade Federal de Ouro Preto - UFOP, Minas Gerais, 503p.

Cruz, S.C.P., Alkmim, F.F., 2017. The Paramirim Aulacogen, in: Heilbron, M., Cordani, U.G., Alkmim, Fernando F. (Eds.), São Francisco Craton, Eastern Brazil: Tectonic Genealogy of a Miniature Continent, Regional Geology Reviews. Springer International Publishing, Cham, p. 326. https://doi.org/10.1007/978-3-319-01715-0

Cruz, S.C.P., Alkmim, F.F., 2007. A história de inversão do aulacógeno do Paramirim contada pela sinclinal de Ituaçu, extremo sul da Chapada Diamantina (BA). Revista Brasileira de Geociências. 37, 92–110.

Cruz, S. C. P., Alkmim, F. F. D., Leite, C. M. M., Evangelista, H. J., Cunha, J. C., Matos, E. C., Noce, C. M., Marinho, M. M., 2007. Geologia e arcabouço estrutural do Complexo Lagoa Real, Vale do Paramirim, Centro-Oeste da Bahia. Revista Brasileira de Geociências. 37, 128–146.

Cruz, S.C.P., Alkmim, F.F., 2006. The tectonic interaction between the Paramirim aulacogen and the Araçuaí belt, São Francisco craton region, Eastern Brazil. An. Acad. Bras. Cienc. 78, 151–173. https://doi.org//S0001-37652006000100014

Cruz, S. C. P, Alkmim, F.F., Pedreira, A., Teixeira, L., Pedrosa-Soares, A.C., Gomes, L.C.C., Souza, J.S., Leal, A.B.M., 2012. O Orógeno Araçuaí, in: Geologia Da Bahia. Pesquisa e Atualização de Dados. CBPM Salvador, pp. 131–178.

Cruz, S.C.P., Barbosa, J.S.F., Santos Pinto, M., Peucat, J.J., Paquette, J.L., Souza, J.S., Martins, V.S., Chemale Júnior, F., Carneiro, M.A., 2016. The Siderian-Orosirian magmatism in the Gavião Paleoplate, Brazil: U-Pb geochronology, geochemistry and tectonic implications. J. S. Am. Earth Sci. 69, 43–79.

Criss, R. E., & Taylor Jr, H. P. (1983). An 18O/16O and D/H study of Tertiary hydrothermal systems in the southern half of the Idaho batholith. *Geological Society of America Bulletin*, *94*(5), 640-663

Criss RE, Taylor HP Jr (1986) Stable isotope geochemistry of metamorphic rocks. Rev Mineral 16:373-424

Criss RE, Gregory RT, Taylor HP (1987) Kinetic theory of oxygen isotopic exchange between minerals and water. Geochim Cosmochim Acta 51:1099-1108

Cuney, M., 2010. Evolution of uranium fractionation processes through time: driving the secular variation of uranium deposit types. Econ. Geol. 105, 553–569.

Cuney, M., Emetz, A., Mercadier, J., Mykchaylov, V., Shunko, V., & Yuslenko, A. (2012). Uranium deposits associated with Na-metasomatism from central Ukraine: A review of some of the major deposits and genetic constraints. *Ore Geology Reviews, 44*, 82-106.

Cunha, J.C., Barbosa, J.S.F., Mascarenhas, J.F., 2012. Greenstones Belts e Sequências Similares, in: Geologia da Bahia. Pesquisa e Atualização, CBPM Série Publicações Especiais. Salvador, pp. 203–325.

Costi, H. T., Dall'Agnol, R., Borges, R. M. K., Minuzzi, O. R. R., & Teixeira, J. T. (2002). Tin-bearing sodic episyenites associated with the Proterozoic, A-type Água Boa granite, Pitinga mine, Amazonian Craton, Brazil. *Gondwana Research*, *5*(2), 435-451.

Dall'Agnol, R., Scaillet, B., Pichavant, M., 1999. An experimental study of a lower Proterozoic A-type granite from the eastern Amazonian craton, Brazil. J. Petrology 40, 1673–1698.

Danderfer, A., de Waele, B., Pedreira, A.J., Nalini, H.A., 2009. New geochronological constraints on the geological evolution of Espinhaço basin within the São Francisco Craton-Brazil. Precambr. Res. 170, 116–128.

Danderfer Filho, A., 2000. Geologia sedimentar e evolução tectônica do Espinhaço Setentrional, estado da Bahia. Unpubl. Ph.D. Thesis. Univ. Fed. de Brasília, UnB.

Danderfer Filho, A., 1990. Análise descritiva e cinemática do Supergrupo Espinhaço na região da Chapada Diamantina, BA. Unpubl. MsC Thesis, Univ. Fed. Ouro Preto, UFOP.

Danderfer Filho, A., Lagoeiro, L.E., Alkmim, F.F., 1993. O Sistema de dobramentos e empurrões da Chapada Diamantina (BA): Registro da inversão do Aulacógeno do

Espinhaço no decorrer do Evento Brasiliano. SBG, II Simpósio sobre o Crát. São Fr. Tectônica e Met. An. 197–199.

Danderfer Filho, A., Lana, C.C., Nalini Júnior, H.A., Costa, A.F.O., 2015. Constraints on the Statherian evolution of the intraplate rifting in a Paleo-Mesoproterozoic paleocontinent: New stratigraphic and geochronology record from the eastern São Francisco craton. Gondwana Res. 28, 668–688. https://doi.org/10.1016/j.gr.2014.06.012

Derby, O. A. (1906). The Serra do Espinhaço, Brazil. *The Journal of Geology*, *14*(5), 374-401.

Elliott, H. A.L., Wall, F., Chakhmouradian, A. R., Siegfried, P. R., Dahlgren, S., Weatherley, S., Finch, A. A., Marks, M. A.W., Dowman, E., Deady, E. (2018). Fenites associated with carbonatite complexes: A review. *Ore Geology Reviews*, *93*, 38-59

Eglinger, A., André-Mayer, A. S., Vanderhaeghe, O., Mercadier, J., Cuney, M., Decrée, S., Feybesse, J., Milesi, J. P., 2013. Geochemical signatures of uranium oxides in the Lufilian belt: From unconformity-related to syn-metamorphic uranium deposits during the Pan-African orogenic cycle. Ore Geology Reviews, 54, 197-213.

Engvik, A. K., Putnis, A., Gerald, J. D. F., & Austrheim, H. (2008). Albitization of granitic rocks: the mechanism of replacement of oligoclase by albite. *The Canadian Mineralogist*, *46*(6), 1401-1415

Frimmel, H. E., Schedel, S., & Brätz, H., 2014. Uraninite chemistry as forensic tool for provenance analysis. Applied Geochemistry, 48, 104-121.

Franz, G., & Spear, F. S. (1985). Aluminous titanite (sphene) from the eclogite zone, south-central Tauern Window, Austria. Chemical Geology, 50(1-3), 33-46

Fryer, B. J., & Taylor, R. P. (1987). Rare-earth element distributions in uraninites: implications for ore genesis. *Chemical Geology*, *63*(1-2), 101-108.

Fuzikawa, K., Alves, J., Maruejol, P., Cuney, M., Kostonlayl, C., Poty, B., 1988. The Lagoa Real Uranium Province, Bahia state, Brazil: some petrographic aspects and fluid inclusion studies. Geochim. Bras. 2, 109–118.

Gregory RT, Criss RE, Taylor HP (1989) Oxygen isotope exchange kinetics of mineral pairs in closed and open systems: Applications to problems of hydrothermal alteration of igneous rocks and Precambrian iron formations. Chem Geol 75:1-42

Gregory, R.T., Criss, R.E., 1986. Isotopic exchange in open and closed systems. Rev. Mineral. 16, 91–127.

Gregory RT, Taylor HP (1986a) Possible non-equilibrium oxygen isotope effects in mantle nodules, an alternative to the Kyser-O'Neil-Carmichael 18O/16O geothermometer. Contrib Mineral Petrol 93: 114-119

Gregory RT, Taylor HP (1986b) Non-equilibrium, metasomatic 18O/16O effects in upper mantle mineral assemblages. Contrib Mineral Petrol 93:124-135

Guimarães, J.T., Alkmim, F.F., Cruz, S.C.P., 2012. Supergrupos Espinhaço e São Francisco. Geol. da Bahia. Pesqui. e atualização dados 2, 33–86.

Guimarães, J.T., Santos, R.A., Melo, R.C., 2008. Geologia da Chapada Diamantina (Projeto Ibitiara-Rio de Contas). CBPM, Série Arqu. ed. Salvador, BA.

Harrison, T.M., Watson, E.B., 1984. The behavior of apatite during crustal anatexis: equilibrium and kinetic considerations. Geochim. Cosmochim. Acta 48, 1467e1477.

Hammarstrom, J. M., & Zen, E. A. (1986). Aluminum in hornblende: an empirical igneous geobarometer. *American mineralogist*, *71*(11-12), 1297-1313.

Holland, T., & Blundy, J. (1994). Non-ideal interactions in calcic amphiboles and their bearing on amphibole-plagioclase thermometry. *Contributions to mineralogy and petrology*, *116*(4), 433-447.

Hollister, L. S., Grissom, G. C., Peters, E. K., Stowell, H. H., & Sisson, V. B. (1987). Confirmation of the empirical correlation of Al in hornblende with pressure of solidification of calc-alkaline plutons. *American Mineralogist*, *72*(3-4), 231-239

Hurtado, J., Chatterjee, N., Ramezani, J., Hodges, K., & Bowring, S. (2007). Electron microprobe chemical dating of uraninite as a reconnaissance tool for leucogranite geochronology. *Nature Precedings*, 1-1

Ishihara, S., 1981. The granitoid series and mineralization. Economic Geology 75th Anniversary volume, 458–484

Kempe, U. (2003). Precise electron microprobe age determination in altered uraninite: consequences on the intrusion age and the metallogenic significance of the Kirchberg granite (Erzgebirge, Germany). *Contributions to Mineralogy and Petrology*, *145*(1), 107-118.

King, P. L., White, A. J. R., Chappell, B. W., & Allen, C. M. (1997). Characterization and origin of aluminous A-type granites from the Lachlan Fold Belt, southeastern Australia. *Journal of petrology*, *38*(3), 371-391

King, E. M., Valley, J. W., Davis, D. W., & Kowallis, B. J. (2001). Empirical determination of oxygen isotope fractionation factors for titanite with respect to zircon and quartz. *Geochimica et Cosmochimica Acta*, *65*(18), 3165-3175

Klimm, K., Holtz, F., Johannes, W., King, P.L., 2003. Fractionation of metaluminous A-type granites: an experimental study of the Wangrah suite, Lachlan Fold Belt, Australia. Precambrian Res. 124, 327–341.

Krough, E.J., (1988). The garnet-clinopyroxene Fe-Mg geothermometer—a reintrepration of existing experimental data. Mineral Petrol 99:44–48

Kullerud, K. (1995). Chlorine, titanium and barium-rich biotites: factors controlling biotite composition and the implications for garnet-biotite geothermometry. *Contributions to Mineralogy and Petrology*, *120*(1), 42-59.

Lacroix, M. A. (1920). Les roches éruptives du Crétacé pyrénéen et la nomenclature des roches éruptives modifiées. *Comptes Rendues Acad Sci France*, *170*, 685-690

Leake, B. E., Woolley, A. R., Birch, W. D., Burke, E. A., Ferraris, G., Grice, J. D., Hawthorne, F. C., Kisch, H. J., Krivovichev, V. G., Schumacher, J. C., Stephenson, N. C. N., Whittaker, E. J. W. (2004). Nomenclature of amphiboles: additions and revisions to the International Mineralogical Association's amphibole nomenclature. *Mineralogical Magazine*, *68*(1), 209-215

Lee, M. R., Waldron, K. A., Parsons, I., & Brown, W. L. (1997). Feldspar–fluid interactions in braid microperthites: pleated rims and vein microperthites. *Contributions to Mineralogy and Petrology*, *127*(3), 291-304

Lobato, L. M., Forman, J. M., Fuzikawa, K., Fyfe, W. S., & Kerrich, R. (1983). Uranium in overthrust Archean basement, Bahia, Brazil. *The Canadian Mineralogist*, *21*(4), 647-654.

Lobato, L.M., Fyfe, W.S., 1990. Metamorphism, metasomatism, and mineralization at Lagoa Real, Bahia, Brazil. Econ. Geol. 85, 968–989. https://doi.org/10.2113/gsecongeo.85.5.968

Lobato, L.M., Pimentel, M.M., Cruz, S.C.P., Machado, N., Noce, C.M., Alkmim, F.F., 2015. U-Pb geochronology of the Lagoa Real uranium district, Brazil: Implications for the age of the uranium mineralization. J. South Am. Earth Sci. 58, 129–140. https://doi.org/10.1016/j.jsames.2014.12.005

Locock, A. J. (2008). An Excel spreadsheet to recast analyses of garnet into end-member components, and a synopsis of the crystal chemistry of natural silicate garnets. *Computers & Geosciences*, *34*(12), 1769-1780.

Loureiro, H.S.C., Bahiense, I.C., Neves, J.P., Guimarães, J.T., Teixeira, L.R., Santos, R.A., Melo, R.C., 2009. Geologia e recursos minerais da parte norte do corredor de

deformação do Paramirim (Projeto Barra – Oliveira dos Brejinhos)., Série Arqu. ed. Salvador, BA.

Marques, C., Cabral, A. R., Rios, F., 2020a. Whole-rock chemistry of the Gameleira I uranium deposit, Lagoa Real, Brazil. Chemie der Erde. In press.

Marques, C. M., Cutts, K., Rocholl, A., Wiedenbeck, M., Cabral, A. R., Rios, F., 2020b. The Lagoa Real uranium province: a case of "étagement temporel". *submitted*

Maruejol, P., Cuney, M., Poty, B., Fuzikawa, K., & Neto, A. M. (1987). The Lagoa Real subalkaline granitic complex (South Bahia, Brazil): a source for uranium mineralizations associated with Na-Ca metasomatism. *Revista Brasileira de Geociências, 17*(4), 578-594.

Maruejol, P., 1989. Métasomatose alcaline et minéralisations uranifères: les albitites du gisement de Lagoa Real (Bahia, Brésil) et exemples complémentaires de Xihuashan (SE Chine), Zheltorechensk (Ukraine) et Chhuling Khola (Népal central). Unp. Ph.D. thesis.

Medeiros, E.L.M., Cruz, S.C.P., Barbosa, J.S.F., Paquette, J.L., Peucat, J., Jesus, S.S.G.P., Barbosa, R.G., Brito, R.S., Carneiro, M.A., 2017. The Santa Izabel complex, Gavião Block, Brazil: components, geocronology, regional correlations and tectonic implications. J. South Am. Earth Sci. 80, 66–94.

Menezes, R.C.L., Conceição, H., Rosa, M.D.L.D.S., Macambira, M.J.B., Galarza, M.A., Rios, D.C., 2012. Geoquímica e geocronologia de granitos anorogênicos Tonianos (ca. 914–899 Ma) da Faixa Araçuaí no sul do Estado da Bahia. Geonomos 20, 1–13.

Mercadier, J., Cuney, M., Lach, P., Boiron, M. C., Bonhoure, J., Richard, A., Leisen, M., Kister, P., 2011. Origin of uranium deposits revealed by their rare earth element signature. Terra Nova, 23(4), 264-269.

Moreira, H.F., Danderfer, A., Costa, A.F.O., Bersan, S.M., Lana, C.C., Queiroga, G.N., 2020. Record of Early Tonian mafic magmatism in the central Espinhaço (Brazil): New insights for break-up of the Neoproterozoic landmass ancestor of São Francisco-Congo paleocontinent. Geosci. Front. https://doi.org/10.1016/j.gsf.2020.02.007

Morimoto, N., Fabries, J., & Ferguson, A. K. (1988). Pyroxene nomenclature. *Mineral. Petrol, 39*, 55-76.

Munoz, J. L., & Swenson, A. (1981). Chloride-hydroxyl exchange in biotite and estimation of relative HCl/HF activities in hydrothermal fluids. *Economic Geology*, *76*(8), 2212-2221.

Mutch, E. J. F., Blundy, J. D., Tattitch, B. C., Cooper, F. J., & Brooker, R. A. (2016). An experimental study of amphibole stability in low-pressure granitic magmas and a revised Al-in-hornblende geobarometer. *Contributions to Mineralogy and Petrology*, *171*(10), 85.

Nakamura D, Hirajima T (2005) Experimental evaluation of garnet clinopyroxene geothermometry as applied to eclogites. Contrib Mineral Petrol 150:581–588. doi:10.1007/s00410-005-0023-x

Naney, M.T., 1983. Phase equilibria of rock-forming ferromagnesian silicates in granitc systems. Am. Mineralogist 65, 639–653.

Nutman, A.P., Cordani, U.G., 1993. SHRIMP U-Pb zircon geochronology of Archaean granitoids from the Contendas-Mirante area of the São Francisco Craton, Bahia, Brazil. Precambrian Res. 63, 179–188.

Oberti, R., Ungaretti, L., Cannillo, E. and Hawthorne, F.C. (1993) The mechanism of Cl incorporation in amphibole. *American Mineralogist*, 78, 746–752. Mineralogical Society of America

OECD/NEA-IAEA, 2012. Uranium 2011: resources, production and demand. A Joint Report by the OECD Nuclear Energy Agency and the IAEA. OECD, Paris.

Oliveira, D.C., Santos, P.J.L., Gabriel, E.O., Rodrigues, D.S., Faresin, A.C., Silva, M.L.T., Sousa, S.D., Santos, R.V., Silva, A.C., Souza, M.C., Santos, R.D., Macambira, M.J.B., 2010a. Aspectos geológicos e geocronológicos das rochas magmáticas e metamórficas da região entre os municípios de ?Agua Azul do Norte e Canaã dos Carajás e Província Mineral de Carajás. Congr. Bras. Geol. 45. Belém. CD-rom (in Portuguese).

Oliver, N. H., Cleverley, J. S., Mark, G., Pollard, P. J., Fu, B., Marshall, L. J., ... & Baker, T. (2004). Modeling the role of sodic alteration in the genesis of iron oxide-copper-gold deposits, Eastern Mount Isa block, Australia. *Economic Geology*, *99*(6), 1145-1176.

Parsons, I., Gerald, J. D. F., & Lee, M. R. (2015). Routine characterization and interpretation of complex alkali feldspar intergrowths. *American Mineralogist*, *100*(5-6), 1277-1303

Pedrosa-Soares, A.C., Alkmim, F.F., Tack, L., Noce, C.M., Babinski, M., Silva, L.C. da, Martins-Neto, M.A., 2008. Similarities and differences between the Brazilian and African counterparts of the Neoproterozoic Araçuaí-West Congo Orogen. Geol. Soc. London, Spec. Publ. 294, 153–172.

Pedrosa-Soares, A.C., Babinski, M., Noce, C., Martins, M., Queiroga, G., Vilela, F., 2011a. The Neoproterozoic Macaúbas Group, Araçuaí orogen, SE Brazil. Geol. Soc. London, Mem. 36, 523–534.

Pedrosa-Soares, A.C., Noce, C.M., Alkmim, F.F. De, Carlos, L., Babinski, M., Cordani, U., Castañeda, C., 2007. Orógeno Araçuaí: síntese do conhecimento 30 anos após Almeida 1977 15, 1–16.

Pedrosa-Soares, A.C., Wiedemann-Leonardos, C.M., 2000. Evolution of the Araçuaí belt and its connection to the Ribeira Belt, Eastern Brazil, in: Tectonic Evolution of South America. Sociedade Brasileira de Geologia São Paulo, pp. 265–310.

Pimentel, M. M., Machado, N., & Lobato, L. M., 1994. Geocronologia U/Pb de rochas graníticas e gnáissicas da região de Lagoa Real, Bahia, e implicações para a idade da mineralização de urânio. In SBG, Congresso Brasileiro de Geologia (Vol. 38, pp. 389-390)

Polito, P. A., Kyser, T. K., & Stanley, C. (2009). The Proterozoic, albitite-hosted, Valhalla uranium deposit, Queensland, Australia: a description of the alteration assemblage associated with uranium mineralisation in diamond drill hole V39. *Mineralium Deposita*, *44*(1), 11-40.

Powell, R. (1985). Regression diagnostics and robust regression in geothermometer/geobarometer calibration: the garnet-clinopyroxene geothermometer revisited. Journal of Metamorphic Geol 3:231–243

Putirka, K. (2016). Amphibole thermometers and barometers for igneous systems and some implications for eruption mechanisms of felsic magmas at arc volcanoes. *American Mineralogist*, *101*(4), 841-858

Putnis, A. (2002). Mineral replacement reactions: from macroscopic observations to microscopic mechanisms. *Mineralogical Magazine*, *66*(5), 689–708

Putnis, A., Hinrichs, R., Putnis, C. V., Golla-Schindler, U., & Collins, L. G. (2007). Hematite in porous red-clouded feldspars: evidence of large-scale crustal fluid–rock interaction. *Lithos*, *95*(1-2), 10-18.

Raheim A, Green DH (1974) Experimental determination of the temper- ature and pressure dependence ofthe Fe-Mg partition coefficient for coexisting garnet and clinopyroxene. Mineral Petrol 48:279–203

Ramdohr, P. (1969). The ore minerals and their intergrowths. Elsevier.

Ramberg, H. (1952): Chemical bonds and the distribution of cations in silicates. J. Geol. 60. 33 l-355

Raposo, C., Matos, E.C. de, Brito, W., 1984. Zoneamento cálcico-sódico nas rochas da Província Uranífera de Lagoa Real, in: Anais do XXXIII Congresso Brasileiro de Geologia, Rio de Janeiro, 1984

Ribeiro, C. I., Carvalho Filho, C. D., & Hashizume, S., 1984. As jazidas de urânio de Lagoa Real. In: Anais do XXXIII Congresso Brasileiro de Geologia, Rio de Janeiro, vol. 3, pp. 1463–1474.

Ridolfi, F., Renzulli, A., & Puerini, M. (2010). Stability and chemical equilibrium of amphibole in calc-alkaline magmas: an overview, new thermobarometric formulations and application to subduction-related volcanoes. *Contributions to Mineralogy and Petrology*, *160*(1), 45-66

Ridolfi, F., & Renzulli, A. (2012). Calcic amphiboles in calc-alkaline and alkaline magmas: thermobarometric and chemometric empirical equations valid up to 1,130° C and 2.2 GPa. *Contributions to Mineralogy and Petrology*, *163*(5), 877-895.

Recio, C., Fallick, A. E., Ugidos, J. M., & Stephens, W. E. (1997). Characterization of multiple fluid-granite interaction processes in the episyenites of Avila-Béjar, Central Iberian Massif, Spain. *Chemical Geology*, *143*(3-4), 127-144

Rooney, A. D.; *Strauss*, J. V.; Brandon, A. D.; Macdonald, F. A., 2017. A Cryogenian chronology: Two long-lasting synchronous Neoproterozoic glaciations. Geology. **43** (5): 459–462. *doi*:*10.1130/G36511.1*

Rosa, A.M.L.S., Conceição, H., Oberli, F., Meier, M., Martin, H., Macambira, M.B., Santos, E.B., Paim, M.M., Leahy, G.A.S., Bastos Leal, L.R., 2000. Geochronology (U-Pb/Pb-Pb) and isotopic signature (Rb-Sr/Sm-Nd) of the paleoproterozoic Guanambi Batholith, southwestern Bahia State (NE Brazil). Rev. Bras. Geociência 30, 062–06.

Santana, A.V., 2016. Análise estratigráfica em alta resolução em rampa carbonática dominada por microbiolitos, Formação Salitre, Bacia de Irecê, Bahia. Unp. Ph.D. Thesis. Universidade Federal de Brasília, Brasília.

Santos-Pinto, M.., Peucat, J.J., Martin, H., Sabaté, P., 1998. Recycling of the Archaean continental crust: the case study of the Gavião Block, Bahia, Brazil. J. South Am. Earth Sci. Am. Earth Sci. 11, 487–498.

Santos-Pinto, M., Peucat, J.-J., Martin, H., Barbosa, J.S.F., Fanning, C.M., Cocherie, A., Paquette, J.-L., 2012. Crustal evolution between 2.0 and 3.5 Ga in the southern Gavião block (Umburanas-Brumado-Aracatu region), São Francisco Craton, Brazil: a 3.5–3.8 Ga proto-crust in the Gavião block? J. South Am. Earth Sci. 40, 129–142.

Schweitzer EL, Papike JJ, Bence AE (1974) Statistical analysis of clinopyroxenes from deep-sea basalts. Am Mineral 64:501–513

Schobbenhaus, C. (1996). As tafrogêneses superpostas Espinhaço e Santo Onofre, estado da Bahia: Revisão e novas propostas. *Revista Brasileira de Geociências*, *26*(4), 265-276.

Schmidt, M. W. (1992). Amphibole composition in tonalite as a function of pressure: an experimental calibration of the Al-in-hornblende barometer. *Contributions to mineralogy and petrology*, *110*(2-3), 304-310.

Sheppard, S. M. (1986). Characterization and isotope variations in natural waters. *Rev. Miner.*, *16*, 165-183

Silveira, E.M., Söderlund, U., Oliveira, E.P., Ernst, R.E., Leal Menezes, A.B., 2013. First precise U–Pb baddeleyite ages of 1500Ma mafic dykes from the São Francisco Craton, Brazil, and tectonic implications. Lithos 174, 144–156. https://doi.org/10.1016/j.lithos.2012.06.004

Suikkanen, E., & Rämö, O. T. (2019a). Episyenites—Characteristics, Genetic Constraints, and Mineral Potential. *Mining, metallurgy & exploration*, 1-18.

Suikkanen, E., Rämö, O. T., Ahtola, T., & Lintinen, P. (2019). Clinopyroxene episyenites in a Proterozoic rapakivi granite, SE Finland—recrystallization textures, mass transfer and implications for the petrology of A-type granite complexes. *Mineralogy and Petrology*, *113*(6), 727-743.

Suzuoki, T., Epstein, S., 1976. Hydrogen isotope fractionation between OH-bearing minerals and water. Geochim. Cosmochim. Acta 40, 1229–1240.

Taylor, H.P Jr., Sheppard, S.M.F., (1986) Igneous rocks: I. Processes of isotopic fractionation and isotopic systematics. Rev Mineral 16:227-272

Tischendorf, G., Gottesmann, B., Förster, H. J., & Trumbull, R. B. (1997). On Li-bearing micas: estimating Li from electron microprobe analyses and an improved diagram for graphical representation. *Mineralogical Magazine*, *61*(409), 809-834.

Teixeira, L.R., 2000. Relatório temático de litogeoquímica. Projeto Vale do Paramirim. Companhia Baiana de Pesquisa Mineral–CBPM/Companhia de Pesquisa de Recursos Minerais – CPRM. Salvador, Bahia, Brasil.

Thomas, W. M. (1982). Stability relations of the amphibole hastingsite. *American Journal of Science*, *282*(2), 136-164

Tornos, F., Delgado, A., Casquet, C., Galindo, C. (2000). 300 Million years of episodic hydrothermal activity: stable isotope evidence from hydrothermal rocks of the Eastern Iberian Central System. Mineralium Deposita, 35(6), 551- 569. https://doi.org/10.1007/s001260050261

Troitzsch, U., & Ellis, D. J. (2002). Thermodynamic properties and stability of AlF-bearing titanite CaTiOSiO 4–CaAlFSiO 4. *Contributions to Mineralogy and Petrology*, *142*(5), 543-563.

Tropper, P., & Manning, C. E. (2008). The current status of titanite–rutile thermobarometry in ultrahigh-pressure metamorphic rocks: the influence of titanite activity models on phase equilibrium calculations. *Chemical Geology*, *254*(3-4), 123-132.

Turpin, L., Maruejol, P., Cuney, M., 1988. U-Pb, Rb-Sr and Sm-Nd chronology of granitic basement, hydrothermal albitites and uranium mineralization (Lagoa Real, South-Bahia, Brazil). Contrib. To Mineral. Petrol. 98, 139–147. https://doi.org/10.1007/BF00402107

Volfinger, M., Robert, J. L., Vielzeuf, D., & Neiva, A. M. R. (1985). Structural control of the chlorine content of OH-bearing silicates (micas and amphiboles). *Geochimica et Cosmochimica Acta*, *49*(1), 37-48

Watson, E.B., Harrison, T.M., 1983. Zircon saturation revisited: temperature and composition effects in a variety of crustal magma types. Earth Planet. Sci. Lett. 64, 295–304.

Yavuz, F. (2003). Evaluating micas in petrologic and metallogenic aspect: Part II—Applications using the computer program Mica+. *Computers & geosciences*, *29*(10), 1215-1228.

Zheng, Y.F., 1993a. Calculation of oxygen isotope fractionation in hydroxyl–bearing silicates. Earth Planet. Sci. Lett. 120, 247–263.

CAPÍTULO 7 – CONCLUSÕES

Os dados coletados nos depósitos Gameleira I (AN 35), Barreiro (AN 31) e Barrinha (AN 34) localizados na região noroeste da PULR e discutidos nos capítulos anteriores da tese permitiram definir as conclusões:

Suíte Intrusiva Lagoa Real: Nos depósitos estudados a ocorrência da Suíte Intrusiva Lagoa Real se dá através da facies *hipersolvus* álcali-feldspato granito. Este granito se caracteriza por conter álcali-feldspato pertítico, hedenbergita, hastingsita, biotita e titanita como assembléia mineral principal. Estas rochas são geoquímicamente caracterizadas pelo seu caráter metaluminoso, alcalino, reduzido, ferroan e mostram características de granitos do tipo-A, intraplaca e A2, nos diagramas de discriminação geotectônica.

Os parâmetros de cristalização dessas rochas mostram que a temperatura do *liquidus* esteve entre 800 e 900 ºC, enquanto a temperatura de esfriamento tardi-magmático esteve entre 660 and 690 ºC, baseado no geotermômetro *Zr-in-titanite*. A baixa fugacidade de oxigênio também é refletida na alta razão Fe/(Fe + Mg), geralmente maior que 0,8 tanto nos minerais ferro-magnesianos quanto na geoquímica de rocha total, e devem indicar fugacidade abaixo do FMQ *buffer*. A estimativa de pressão de cristalização é dificultosa, devido a ausência de paragênese ideal para aplicação nos geobarômetros disponíveis, mas resultam entre 4 e 8 kbar.

Origem dos albititos: Foram observados dois estágios de alteração principais que ocorreram majoritariamente em regime dúctil. O primeiro é pré-metamórfico em relação à orogênse Brasiliana e corresponde às alterações sódico-cálcica e ferro-cálcico-magnesiana. A sódico-cálcica foi responsável principalmente pela albitização dos granitos e é observada através das texturas como as *patch phertites*, *albite chessboard* e *swapped rims* que refletem a substituição *subsolidus* de K-feldspato por albita. Há também precipitação de clinopiroxênio sódico-cálcico (aegirina-augita) e titanita. Porém a intensa precipitação de clinopiroxênio e titanita é marca da alteração ferro-cálcico-magnesiana que ocorre precipitando clinopiroxênio de variada composição química (hedembergita-diopsídio-augita). O primeiro estágio de alteração também é marcado pela dessilicificação, porém a ausência de texturas distintivas dificulta a localização temporal desse processo, mas os indícios são bem marcados na geoquímica. Clinopiroxênio e titanita são bons marcadores de fugacidade de oxigênio durante este primeiro estágio de alteração e refletem uma trajetória que se inicia em caráter redutor assim como no estágio tardi-magmático, alcança picos de oxidação no estágio sódico-cálcico e termina novamente com característica redutora no final

do estágio ferro-calcico-magnesiano. Embora não haja evidência direta do momento que se deu o primeiro estágio de alteração, é possível que tenha ocorrido ainda no estágio tardi-magmático e de alta temperatura (650–400 ºC) entre 6 e 2 kbar, já que a titanita de alguns albititos mostra padrão de ETR idêntico aos granitos e gnaisses da SILR. Além disso, as texturas de albitização observadas e a desquartzificação são também processos comuns em granitos alterados em estágio tardi-magmático ocorridos em outros lugares do mundo. É possível ainda que o *input* de alteração hidrotermal possa ter sido o rifteamento de 1.5 Ga conforme discutido por autores anteriores.

O segundo estágio de alteração está desconectado temporalmente do primeiro e é sin a tardi-tectônico. Este estágio é responsável pela substituição da paragênese anterior por anfibólio e biotita principalmente representando uma alteração potássica-magnesiana, além de uma assembleia cálcica tardia representada por epidoto, allanita e calcita. Este segundo estágio sob condições de fácies anfibolito a xisto verde no intervalo de temperatura entre 680 e 450 ºC e pressão entre 6 e 0.1 kbar no estágio K-Mg. A precipitação da assembleia cálcica deve ter se dado em temperatura máxima de 300 ºC.

Estilo de mineralização: A mineralização de U manifesta-se através da uraninita principalmente, e subordinadamente, por uranofana, coffinita e U-Ti-Ca espécies. A uraninita está majoritariamente associada à titanita e zircão e é observada como *veinlets* ou disseminações. Os *veinlets* possuem espessura milimétrica e estão via de regra hospedados em albititos com diopsídio concordantes à foliação, enquanto as disseminações ocorrem em albititos ricos em assembleia retrógrada (biotita ou anfibólio albititos). Nos *veinlets* a uraninita é fina (< 5 µm) e ocorre intercrescida com titanita e zircão hidrotermal, nas disseminações a uraninita é mais grossa (< 10 µm) e ocorre inclusa na maioria dos minerais, mas ainda mostra alguma preferência pela titanita. A uranofana ocorre preferencialmente preenchendo fraturas e clivagens dos outros minerais, mas assim como outros minerais de U pode mimetizar a uraninita como finos cristais arredondados. Embora a literatura da área ressalte que a mineralização é fortemente associada com a paragênese granada+hedembergita, o presente trabalho não constatou tal preferência.

Gênese da mineralização de U: Os dados geocronológicos U-Pb obtidos em zircão (LA-ICP-MS e SIMS) nos albititos revelam a idade do protólito (~1.75 Ga) coincidente com a idade de cristalização do Granito São Timóteo. Idade U-Pb (LA-ICP-MS e SIMS) em zircão e titanita associados à uraninita resultaram em 1179 ± 27 Ma, 1165 ± 21 Ma, respectivamente. Idades químicas obtidas por microssonda eletrônica para uraninita

resultaram no intervalo entre 600 e 450 Ma e uma idade precisa (U-Pb; SIMS) resultou em 582 ± 5 Ma.

Os dados do presente trabalho, juntamente com os trabalhos anteriores mostram que os as idades obtidas para minerais relacionados à mineralização abrangem um amplo espectro de idade que varia entre 1,5 Ga e 0,48 Ga ou 1,7 e 0,48 Ga quando consideradas idades químicas calculadas. Entretanto, conforme discutido no Capítulo 4 esta variabilidade não representa um artefato analítico, mas é coincidente com múltiplos eventos tectônicos que ocorreram no Aulacógeno do Paramirim e foram detectados por diversos autores. Esta coincidência reflete o caráter multi-estágio da mineralização de urânio em Lagoa Real definida pelo conceito de *"étagement temporel"* (superposição temporal) proposto por Routhier (1967). Sob esta perspectiva, os metais são concentrados em uma área em diferentes momentos e por diferentes processos geológicos. Desta forma, não é possível afirmar se um dos eventos foi o principal ou se o urânio foi concentrado progressivamente através do tempo geológico, alcançando seu máximo durante a orogênese Brasiliana. O estilo de mineralização e a idade da uraninita (~580 Ma) indicam que o processo de mineralização teve seu fim durante o Brasiliano. A idade química da uraninita (600–450 Ma) abrange ainda os estágios sin- a pós-colisionais amplamente identificados no Orógeno Araçuaí. Desta maneira, o estágio sin-colisional seria responsável por encaixar a titanita e a uraninita nas estruturas sob a forma de *veinlets*, e nos estágios tardi a pós-colisionais motivados pelo colapso orogenético a uraninita passaria por uma remobilização e alteração final para as espécies U^{+6} (ex. uranofana, branerita).

Provável fonte do U e V: O enriquecimento em U é acompanhado por enriquecimento em V, Nb, Ta, Zr/Hf, Mg e Na; perda de SiO_2, K_2O, Rb e Ba. A razão Th/U dos granitos e gnaisses São Timóteo (1,9–6,1) é próximo ou acima do Clarke (3,9) o que sugere que o U pode ter sido lixiviado destas rochas, especialmente dos minerais acessórios como zircão e titanita. A forte associação entre a mineralização de U e zircão com sinais de dissolução e reprecipitação é um forte argumento em favor disso. Além disso, os dados de elementos traço em titanita mostram que este mineral passou por processos que levaram a perda de Y+ETRP (elementos terras-raras pesados) e Hf, e em alguns casos de U. Urânio, Y e ETRP, por outro lado, são elementos enriquecidos na uraninita. Estes dados indicam que a titanita pode ter servido de fonte desses elementos para precipitar uraninita. O comportamento do U nas amostras distais (Furo 10) é inverso às proximais no depósito Gameleira. Nas amostras distais há perda progressiva de U enquanto as proximais do mesmo depósito mostram forte enriquecimento neste elemento. Este fato pode ser indicativo de que a lixiviação de U na

titanita pode ter se dado das porções mais externas para as mais internas e a titanita teria atuado como fonte de U também. O V é fortemente enriquecido na titanita dos albititos (> 500 ppm) e este mineral deve ser o principal portador desse elemento, já que não foi detectado V na uraninita nas análises por microssonda.

A associação geral entre U, V, Nb e Ta pode indicar influencia de rochas máficas também, já que são rochas comumente portadoras desses elementos.

Fluidos: Os dados de isótopos de oxigênio e de hidrogênio mostram que os fluidos foram inicialmente enriquecidos em $\delta^{18}O_{smow}$ provavelmente de natureza magmática e tornaram-se empobrecidos em $\delta^{18}O_{smow}$, o que denota a influencia de água meteórica. O equilíbrio isotópico entre feldspato e titanita nas rochas não mineralizadas pode indicar que a alteração hidrotermal ocorreu por fluidos quentes em temperatura alta o suficiente para rehomogeneizá-los isotopicamente em profundidades catazonais ou mesozonais. Esse equilíbrio pode ainda ser resultado do metamorfismo de facies anfibolito durante a orogenia Brasiliana. As rochas mineralizadas mostram desequilibrio isotópico entre titanita e albita indicando um evento de baixa temperatura durante provavelmente relacionado ao metamorfismo de facies xisto verde no final da orogenia Brasiliana.

ANEXOS (APPENDICES)

Anexo 1 (Appendix 1) – Geochronological results

1A - Zircon U–Pb data of barren samples (3409 and 3510) obtained via LA–ICP–MS

1B – Zircon U–Pb data of mineralized albitite (MAAB03) obtained through SIMS.

Number of analyses refers to grains in Fig. 27.

1C – Titanite U–Pb data of mineralized sample (TAR2) obtained via LA–ICP–MS.

1D – Electron-microprobe results for uraninite and calculated chemical ages.

1E – Analytical methods

Anexo 2 (Appendix 2) – Titanite chemistry

2A: LA-ICP-MS analyses of titanite

2B: Results of statistics calculation for the detection limit of trace elements obtained by LA-ICP-MS during analyses of titanite.

2C: Microprobe analyses of titanite and recalculated formula on the basis of 8 oxygens

2D: Zr-in-titanite geothermometry

Anexo 3 (Appendix 3) – Mineral chemistry analyses

3A: K-feldspar

3B: Plagioclase

3C: Pyroxene

3D: Amphibole

3E: Biotite

3F: Garnet

3G: Titanite

3H: Epidote

3I: Uraninite

3J: Other uranium minerals

Abreviation

HAFG hypersolvus alkali-feldspar granite
HAFGg hypersolvus alkali-feldspar gneiss
AB or alb albitite
PAT patches
POL polygonal
Alb albitite
Hd1 Fe-hedenbergite granite-related
Hd2 Fe-hedenbergite albitite-related
Hd3 Mg-hedenbergite albitite-related
AA aegirine-augite
Dp diopside
Ag augite
Hst hastingsite
Fed Fe-edenite
Mhrn Mg-hornblende
Wnc winchite
Act actinolite

Anexo 4 (Appendix 4) – Lista de amostras coletadas

4A– Anomalia 35 – Depósito Gameleira I

4B– Anomalia 34 – Depósito Barrinha

4C–Anomalia 31 Depósito Barreiro

APPENDIX 1 – Geochronological results

1A: Zircon U–Pb data of barren samples (3409 and 3510) obtained via LA–ICP–MS

Analyses name	^{207}Pb (cps)	^{206}Pb (cps)	U (µg g-1) a	Th U	^{206}Pb ^{204}Pb	^{207}Pb ^{206}Pb	1*s*	^{206}Pb ^{238}U	1 *s*	^{207}Pb ^{235}U	1 *s*	^{208}Pb ^{232}Th	1 *s*	^{207}Pb ^{206}Pb	2*s* (%)	^{207}Pb ^{235}U	2*s* (%)	^{206}Pb ^{238}U	2*s* (%)	Rho	^{208}Pb ^{232}Th	2*s* (%)	^{207}Pb ^{206}Pb	2*s* abs	^{206}Pb ^{238}U	2*s* abs	^{207}Pb ^{235}U	2*s* abs	^{208}Pb ^{232}Th	2*s* abs	% conc
Sample 3409																															
SMPABC007	966689	10246 4	294.46	0.15	170.2	0.11	0	0.31	0	4.50	0	0.09	0	0.11	1.07	4.50	1.91	0.31	1.58	0.83	0.09	2.19	173 2	20	173 0	24	173 1	16	178 6	37	100
SMPABC008	155142	16107	50.66	0.22	460.2	0.10	0	0.29	0	4.11	0	0.07	0	0.10	1.13	4.11	1.96	0.29	1.60	0.82	0.07	1.84	169 4	21	162 7	23	165 6	16	146 1	26	98
SMPABC009	853708	91438	261.14	0.14	110.2	0.11	0	0.31	0	4.53	0	0.09	0	0.11	1.10	4.53	1.92	0.31	1.58	0.82	0.09	2.07	175 1	20	172 4	24	173 6	16	177 7	35	99
SMPABC010	344292	35745	112.89	0.30	218.0	0.10	0	0.29	0	4.09	0	0.06	0	0.10	2.17	4.09	2.77	0.29	1.72	0.62	0.06	1.42	169 4	40	162 1	25	165 3	23	116 2	16	98
SMPABC011	230667	24557	69.55	0.36	24557	0.11	0	0.31	0	4.56	0	0.08	0	0.11	1.10	4.56	1.93	0.31	1.59	0.82	0.08	1.94	174 0	20	174 6	24	174 3	16	162 3	30	100
SMPABC012	339304	35943	103.04	0.39	169.5	0.11	0	0.31	0	4.51	0	0.08	0	0.11	1.06	4.51	1.89	0.31	1.57	0.83	0.08	1.74	173 1	19	173 5	24	173 3	16	160 4	27	100
SMPABC013	174308	18576	52.68	0.25	18576	0.11	0	0.31	0	4.56	0	0.07	0	0.11	1.14	4.56	1.97	0.31	1.61	0.81	0.07	2.03	174 2	21	174 2	25	174 2	17	140 5	28	100
SMPABC014	854631	90044	257.56	0.38	90044	0.11	0	0.31	0	4.52	0	0.08	0	0.11	1.08	4.52	1.91	0.31	1.55	0.84	0.08	1.83	172 1	19	174 6	24	173 5	16	162 9	29	101
SMPABC015	153024	16219	46.28	0.23	141.0	0.11	0	0.31	0	4.53	0	0.08	0	0.11	1.10	4.53	1.94	0.31	1.60	0.82	0.08	1.88	173 2	20	174 1	24	173 7	16	164 8	30	100
SMPABC016	513550	54554	155.85	0.26	108.2	0.11	0	0.31	0	4.53	0	0.08	0	0.11	1.08	4.53	1.91	0.31	1.57	0.83	0.08	1.68	173 6	19	173 6	24	173 6	16	154 9	25	100
SMPABC017	568744	60716	172.21	0.24	60.6	0.11	0	0.31	0	4.56	0	0.09	0	0.11	1.07	4.56	1.91	0.31	1.58	0.83	0.09	2.01	174 5	20	173 9	24	174 2	16	167 6	32	100
SMPABC018	103928 1	11057 2	315.40	0.18	254.2	0.11	0	0.31	0	4.53	0	0.08	0	0.11	1.08	4.53	1.91	0.31	1.57	0.83	0.08	1.81	173 9	19	173 6	24	173 7	16	156 7	28	100
SMPABC019	635982	66961	191.68	0.25	1860. 0	0.11	0	0.31	0	4.52	0	0.08	0	0.11	2.15	4.52	2.77	0.31	1.69	0.61	0.08	1.78	171 9	40	174 6	26	173 4	23	159 3	27	101
SMPABC020	350553	37453	85.24	0.53	28.7	0.11	0	0.39	0	5.71	0	0.05	0	0.11	1.30	5.68	2.05	0.39	1.58	0.77	0.05	1.44	174 6	24	210 2	28	192 8	18	959	14	109
SMPABC027	144501 9	15378 0	438.89	0.27	470.3	0.11	0	0.31	0	4.53	0	0.08	0	0.11	1.08	4.53	1.91	0.31	1.56	0.84	0.08	1.91	173 4	19	173 4	24	173 6	16	147 2	27	100
SMPABC028	595691	62964	181.35	0.17	38.3	0.11	0	0.31	0	4.50	0	0.06	0	0.11	1.11	4.49	1.92	0.31	1.57	0.82	0.06	1.41	172 7	20	173 1	24	172 9	16	116 6	16	100

SMPABC029	754327	80318	227.96	0.41	185.9	0.11	0	0.31	0	4.56	0	0.07	0	0.11	1.07	4.56	1.92	0.31	1.59	0.83	0.07	1.99	1740	20	1742	24	1741	16	1411	27	100
SMPABC030	981898	103754	299.55	0.35	196.1	0.11	0	0.31	0	4.48	0	0.08	0	0.11	1.04	4.48	1.88	0.31	1.57	0.83	0.08	1.87	1726	19	1728	24	1727	16	1483	27	100
SMPABC031	1112437	117624	335.05	0.15	333.2	0.11	0	0.31	0	4.54	0	0.08	0	0.11	2.16	4.54	2.75	0.31	1.71	0.62	0.08	2.13	1727	40	1747	26	1738	23	1550	32	101
SMPABC032	746109	78957	226.39	0.27	192.6	0.11	0	0.31	0	4.51	0	0.07	0	0.11	2.17	4.51	2.78	0.31	1.73	0.62	0.07	2.20	1729	40	1736	26	1733	23	1418	30	100
SMPABC033	770883	81961	235.94	0.31	132.0	0.11	0	0.31	0	4.49	0	0.07	0	0.11	1.04	4.49	1.90	0.31	1.59	0.84	0.07	2.06	1737	19	1723	24	1729	16	1383	27	100
SMPABC034	419025	44690	126.83	0.23	971.5	0.11	0	0.31	0	4.55	0	0.08	0	0.11	2.14	4.56	2.73	0.31	1.70	0.62	0.08	1.94	1743	39	1740	26	1741	23	1487	28	100
SMPABC035	999749	99943	353.87	0.15	113.8	0.10	0	0.26	0	3.66	0	0.07	0	0.10	1.02	3.65	1.87	0.26	1.57	0.74	0.07	1.77	1623	19	1515	21	1561	15	1277	23	97
SMPABC036	708734	73900	230.12	0.32	73900	0.10	0	0.29	0	4.15	0	0.08	0	0.10	1.15	4.15	1.96	0.29	1.59	1.08	0.08	2.99	1701	21	1635	23	1665	16	1475	43	98
SMPABC037	883184	92329	257.30	0.28	160.6	0.10	0	0.32	0	4.64	0	0.07	0	0.10	1.02	4.64	1.87	0.32	1.57	0.74	0.07	1.92	1706	19	1799	25	1756	16	1424	26	102
SMPABC038	680530	71560	204.73	0.33	144.6	0.11	0	0.31	0	4.52	0	0.07	0	0.11	1.02	4.52	1.87	0.31	1.57	0.74	0.07	1.94	1717	19	1749	24	1734	16	1347	25	101
SMPABC039	768500	80823	243.18	0.25	1719.6	0.10	0	0.30	0	4.29	0	0.07	0	0.11	2.18	4.30	2.78	0.30	1.73	0.62	0.07	2.24	1717	40	1673	26	1693	23	1326	29	99
SMPABC040	1720817	162557	692.05	0.14	92.9	0.09	0	0.23	0	3.04	0	0.05	0	0.09	1.03	3.04	1.88	0.23	1.57	0.74	0.05	1.95	1517	19	1351	19	1417	14	993	19	95
Sample 3510																															
SMPABC047	418941	43348	124.58	0.45	119.7	0.10	0	0.32	0	4.50	0	0.07	0	0.10	1.11	4.50	1.94	0.32	1.59	0.82	0.07	2.29	1687	20	1767	25	1729	16	1429	32	102
SMPABC048	391226	41183	118.11	0.40	86.2	0.11	0	0.31	0	4.52	0	0.07	0	0.11	1.13	4.51	1.96	0.31	1.60	0.82	0.07	2.15	1719	21	1744	24	1732	16	1417	29	101
SMPABC049	295909	31571	90.25	0.26	48.6	0.11	0	0.31	0	4.52	0	0.07	0	0.11	1.11	4.52	1.95	0.31	1.60	0.82	0.07	2.49	1744	20	1728	24	1735	16	1454	35	100
SMPABC050	552086	58024	166.00	0.16	2231.7	0.11	0	0.31	0	4.52	0	0.08	0	0.11	2.20	4.52	2.78	0.31	1.71	0.61	0.08	2.61	1716	40	1750	26	1734	23	1495	38	101
SMPABC051	945974	97175	278.95	0.17	284.1	0.10	0	0.32	0	4.50	0	0.08	0	0.10	1.21	4.50	2.00	0.32	1.60	0.80	0.08	3.41	1670	22	1780	25	1729	17	1539	51	103
SMPABC052	1025282	107029	306.56	0.14	#####	0.10	0	0.31	0	4.51	0	0.08	0	0.10	1.04	4.51	1.90	0.31	1.58	0.83	0.08	2.40	1704	19	1758	24	1733	16	1480	34	101
SMPABC053	647301	66866	192.71	0.30	66866	0.10	0	0.31	0	4.49	0	0.08	0	0.10	1.22	4.49	2.02	0.31	1.60	0.80	0.08	3.38	1684	23	1765	25	1728	17	1477	48	102
SMPABC054	419136	43951	126.05	0.34	43951	0.10	0	0.31	0	4.51	0	0.07	0	0.10	1.07	4.51	1.92	0.31	1.59	0.83	0.07	2.29	1712	20	1749	24	1732	16	1412	31	101
SMPABC055	313586	30327	123.56	0.17	278.2	0.10	0	0.24	0	3.17	0	0.07	0	0.10	2.34	3.17	2.96	0.24	1.81	0.61	0.07	2.30	1562	44	1376	22	1451	23	1426	32	95
SMPABC056	790516	78783	288.74	0.22	78783	0.10	0	0.26	0	3.53	0	0.07	0	0.10	1.05	3.53	1.91	0.26	1.59	0.83	0.07	2.36	1618	20	1473	21	1533	15	1356	31	96

SMPABC057	335413	32837	127.31	0.26	185.5	0.10	0	0.25	0	3.33	0	0.04	0	0.10	1.05	3.33	1.93	0.25	1.62	0.84	0.04	1.84	1585	20	1423	21	1489	15	755	13	96
SMPABC058	1566904	16631	477.47	0.10	11087	0.11	0	0.31	0	4.50	0	0.08	0	0.11	1.13	4.50	1.95	0.31	1.59	0.82	0.08	3.00	1734	21	1729	24	1732	16	969	43	100
SMPABC059	1285572	12864	464.06	0.06	224.5	0.10	0	0.26	0	3.59	0	0.07	0	0.10	1.01	3.58	1.88	0.26	1.58	0.84	0.07	1.94	1625	19	1489	21	1566	15	334	25	96
SMPABC060	949703	100049	287.93	0.18	342.6	0.11	0	0.31	0	4.49	0	0.08	0	0.11	1.19	4.49	2.00	0.31	1.60	0.80	0.08	3.25	1720	22	1737	24	1720	17	474	46	100
SMPABC067	615129	65048	188.49	0.14	148.2	0.11	0	0.31	0	4.47	0	0.09	0	0.11	1.11	4.46	1.95	0.31	1.61	0.82	0.09	2.58	1727	20	1721	24	1724	16	657	41	100
SMPABC068	595803	63240	181.23	0.42	710.6	0.11	0	0.31	0	4.51	0	0.08	0	0.11	1.43	4.51	2.19	0.31	1.66	0.76	0.08	4.68	1734	26	1732	25	1733	18	481	67	100
SMPABC069	1032163	10636	305.70	0.19	#####	0.10	0	0.32	0	4.50	0	0.07	0	0.10	1.09	4.50	1.93	0.32	1.60	0.83	0.07	2.73	1680	20	1773	25	1731	16	379	37	102
SMPABC070	1102953	11382	372.90	0.09	161.2	0.10	0	0.28	0	3.95	0	0.07	0	0.10	1.07	3.95	1.92	0.28	1.60	0.83	0.07	2.42	1682	20	1578	22	1623	16	327	32	97
SMPABC071	510553	51530	180.60	0.19	97.2	0.10	0	0.27	0	3.69	0	0.07	0	0.10	1.09	3.69	1.94	0.27	1.63	0.83	0.07	2.55	1641	20	1516	22	1569	16	364	34	97
SMPABC072	627456	45177	409.50	0.04	45177	0.07	0	0.14	0	1.43	0	0.04	0	0.07	0.97	1.43	1.86	0.14	1.59	0.85	0.04	1.82	986	20	865	13	900	11	764	14	96
SMPABC073	1136212	11950	341.60	0.09	#####	0.11	0	0.31	0	4.52	0	0.07	0	0.11	1.21	4.52	2.02	0.31	1.62	0.80	0.07	3.42	1717	22	1750	25	1735	17	404	47	101
SMPABC074	365625	38475	110.02	0.33	38475	0.11	0	0.31	0	4.52	0	0.07	0	0.11	1.55	4.52	2.30	0.31	1.70	0.74	0.07	5.13	1718	28	1749	26	1735	19	845	72	101
SMPABC075	849676	90000	265.49	0.33	203	0.11	0	0.30	0	4.39	0	0.07	0	0.11	1.79	4.38	2.49	0.30	1.73	0.70	0.07	6.33	1730	33	1692	26	1709	21	1393	85	99
SMPABC076	671967	68765	230.24	0.22	695	0.10	0	0.27	0	3.86	0	0.07	0	0.10	1.11	3.86	1.96	0.27	1.62	0.83	0.07	2.70	1663	20	1559	22	1606	16	317	34	97
SMPABC077	275933	29238	84.40	0.41	29238	0.11	0	0.31	0	4.48	0	0.06	0	0.11	1.12	4.48	1.97	0.31	1.62	0.82	0.06	2.61	1731	21	1724	25	1727	17	1262	32	100
SMPABC078	410733	43640	127.47	0.37	428	0.11	0	0.30	0	4.43	0	0.07	0	0.11	1.68	4.43	2.41	0.30	1.72	0.71	0.07	5.74	1736	31	1702	26	1717	20	1415	78	99
SMPABC079	491860	39659	252.61	0.10	3966	0.08	0	0.18	0	2.03	0	0.04	0	0.08	0.98	2.03	1.87	0.18	1.59	0.85	0.04	1.85	1212	19	1081	16	1126	13	834	15	96

1B: Zircon U–Pb data of mineralized albitite (MAAB03) obtained through SIMS. Number of analyses refers to grains in Fig. 27.

	Analyses	Sample/ spot #	^{238}U ppm	$^{90}Zr^{216}O$ *cps*	$\frac{^{90}Zr^{216}}{O}$ ^{238}U	[U] ppm	[Th] ppm	[Pb] ppm	$\frac{^{207}Pb}{^{235}U}$	±s %	$\frac{^{206}Pb}{^{238}U}$	±s %	r	$\frac{^{208}Pb}{^{232}Th}$	$\frac{^{207}Pb}{^{206}Pb}$	±s	$\frac{^{207}Pb}{^{235}U}$	±s	$\frac{^{206}Pb}{^{238}U}$	±s	$\frac{^{208}Pb}{^{232}Th}$	±s	% conc
					cps/cps	86	31	18															
	standart	91500@1				83	31	18	1.891	4.139	0.181	1.210	0.292	0.052	1085	77	1078	28	1075	12	1034	82	100
	standart	91500@2				65	19	14	2.022	3.806	0.181	1.486	0.390	0.054	1218	67	1123	26	1074	15	1068	87	96
	standart	91500@3				84	30	18	1.864	4.605	0.180	1.214	0.264	0.060	1071	87	1068	31	1067	12	1186	100	100
	standart	91500@4				818	74	147	1.832	4.463	0.178	1.210	0.271	0.051	1060	84	1057	30	1056	12	1012	85	100
Prismatic	9	area5-24@1	818	966	1.90	13306	44	3901	1.824	3.652	0.159	3.137	0.859	0.080	1275	36	1054	24	951	28	1552	210	90
Prismatic	8	Area5-20@1	13306	711	0.31	4470	22	965	2.673	1.306	0.274	1.210	0.927	0.044	953	10	1321	10	1559	17	874	1121	118
Agglomerates	1	Area4-4@1	4470	978	0.40	414	89	185	2.181	1.852	0.199	1.229	0.664	0.102	1179	27	1175	13	1173	13	1958	547	100
Prismatic	11	Area7-2@1	414	1036	3.87	1088	143	371	5.026	1.998	0.390	1.522	0.762	0.087	1496	24	1824	17	2124	28	1681	126	116
Prismatic	10	xx-5@1	1088	1010	1.55	444	54	104	4.238	1.401	0.298	1.221	0.871	0.090	1680	13	1681	12	1683	18	1741	124	100
Prismatic	10	xx-5@2	444	858	4.28	6486	188	683	2.548	1.998	0.206	1.271	0.636	0.078	1418	29	1286	15	1208	14	1525	108	94
Prismatic	4	Area5-5@1	6486	856	0.72	1382	42	301	0.979	5.336	0.098	5.226	0.979	0.016	1003	22	693	27	601	30	327	50	87
Prismatic	4	Area5-5@2	1382	966	1.27	784	395	259	2.562	2.743	0.197	2.586	0.943	0.061	1511	17	1290	20	1161	28	1191	188	90
Prismatic	4	Area5-5@3	784	853	1.63	2416	374	650	3.792	2.728	0.263	2.580	0.946	0.079	1707	16	1591	22	1505	35	1536	85	95
Agglomerates	4	Area5-5@4	2416	803	0.67	29911	149	3104	3.112	5.183	0.237	5.015	0.967	0.061	1531	24	1436	41	1372	62	1194	151	96
Prismatic	5	Area5-7@1	29911	528	0.11	597	71	123	0.905	3.075	0.097	2.738	0.890	0.023	856	29	654	15	597	16	458	76	91
Prismatic	4	Area5-5@5	597	875	2.66	401	203	115	2.471	2.967	0.181	2.539	0.856	0.069	1610	28	1264	22	1070	25	1353	110	85
Agglomerates	2	AXX10@1	401	776	3.26	11254	152	1061	3.048	4.234	0.220	3.694	0.872	0.090	1630	38	1420	33	1284	43	1735	162	90
Prismatic	3	AXX9@1	11254	784	0.38	1232	537	504	0.760	4.356	0.088	4.177	0.959	0.029	686	26	574	19	546	22	576	129	95
Prismatic	7	Area5-20@1	1232	504	0.99	2060	148	495	4.853	2.773	0.330	2.649	0.955	0.101	1742	15	1794	24	1839	43	1942	107	103
Prismatic	6	Area5-13@1	2060	645	1.03	#####	9219	65368	2.481	3.624	0.217	2.937	0.811	0.066	1264	41	1267	27	1268	34	1288	128	100
uraninite	6	Area5-13-U@1	1153715	394	0.02	1054	312	288	0.438	5.258	0.053	5.254	0.999	0.007	582	5	369	16	336	17	144	13	91

Agglomerates	12	XX-7@1	1054	754	1.44	1732	98	288	2.936	2.876	0.226	2.562	0.891	0.088	1510	25	1391	22	1315	31	1705	138	95
Agglomerates	12	XX-7@2	1732	829	0.74	71	22	15	1.639	2.796	0.149	2.570	0.919	0.094	1190	22	985	18	896	22	1818	144	91
	standart	91500@5				81	30	17	1.804	4.412	0.177	1.234	0.280	0.058	1036	83	1047	29	1052	12	1149	99	101
	standart	91500@6				89	33	19	1.947	3.652	0.181	1.210	0.331	0.051	1146	67	1097	25	1073	12	1008	79	98
	standart	91500@7				87	33	18	1.852	3.696	0.177	1.258	0.340	0.051	1096	68	1064	25	1048	12	1005	79	99
	standart	91500@8				90	34	19	1.902	3.637	0.178	1.210	0.333	0.055	1137	67	1082	24	1054	12	1075	86	97
	standart	91500@9							1.817	4.040	0.179	1.212	0.300	0.052	1027	76	1051	27	1063	12	1025	80	101

1C: Titanite U–Pb data of mineralized sample (TAR2) obtained via LA–ICP–MS.

grain	^{207}Pba (cps)	Ub (ppm)	Pbb (ppm)	U/Pb	Thb / U	^{206}Pbcc (%)	^{206}Pbd / ^{238}U	±2s (%)	^{207}Pbd / 235U	±2s (%)	rhoe	^{207}Pbd / ^{206}Pb	±2s (%)	^{206}Pb / ^{238}U	±2s (Ma)	^{207}Pb / ^{235}U	±2s (Ma)	^{207}Pb / ^{206}Pb	±2s (Ma)	**disc (%)**
BRL standard	19267	382	76	5.01	0.02	1.5	0.2	0.6	1.8304	1.9	0.30	0.0748	1.8	1053	6	1056	13	1063	37	**99**
BRL standard	19232	403	79	5.10	0.02	0.9	0.2	0.6	1.8170	1.2	0.50	0.0750	1.0	1043	6	1052	8	1069	21	**98**
BRL standard	17733	379	74	5.09	0.02	1.0	0.2	0.5	1.8144	1.3	0.43	0.0744	1.1	1050	5	1051	8	1052	23	**100**
Khan standard	16821	1099	103	10.65	0.02	0.0	0.1	0.7	0.6676	0.8	0.84	0.0578	0.4	519	3	519	3	521	10	**99**
Khan standard	15927	1035	97	10.67	0.02	0.2	0.1	2.3	0.6663	2.4	0.97	0.0577	0.5	518	12	518	10	520	12	**100**
Khan standard	16691	1085	101	10.69	0.02	0.1	0.1	1.9	0.6651	2.0	0.97	0.0578	0.5	517	9	518	8	522	11	**99**
Khan standard	16605	1083	101	10.68	0.02	0.2	0.1	0.8	0.6647	1.0	0.81	0.0577	0.6	517	4	517	4	520	13	**100**
Run number: 17	27764	296	51	5.80	0.00	0.8	0.2	15.0	1.9147	15.1	1.00	0.0787	1.3	1048	147	1086	106	1163	27	**90**
Run number: 15	8235	26	7	3.80	0.00	3.7	0.2	13.8	2.0327	14.1	0.98	0.0818	2.7	1068	138	1127	101	1241	54	**86**
Run number: 22	11746	111	34	3.30	0.00	0.0	0.3	0.7	4.8862	0.9	0.79	0.1211	0.6	1655	10	1800	8	1973	10	**84**
Run number: 27	7117	67	29	2.31	0.00	0.0	0.4	1.8	14.8765	1.9	0.91	0.2978	0.8	1993	30	2807	19	3459	13	**58**
Run number: 12	9632	25	30	0.82	0.00	0.2	1.3	6.2	12.9920	6.2	1.00	0.0736	0.6	5315	229	2679	61	1030	12	**516**
Run number: 11	18281	167	189	0.88	0.00	0.8	1.2	3.5	12.3542	4.5	0.79	0.0738	2.7	5124	126	2632	43	1036	55	**495**
Run number: 25	15194	78	72	1.09	0.00	0.0	1.0	4.3	9.3642	4.4	0.99	0.0704	0.6	4352	139	2374	41	941	12	**462**
Run number: 29	9052	51	22	2.38	0.00	3.0	0.4	1.2	5.4556	2.5	0.46	0.0980	2.2	2187	22	1894	22	1586	42	**138**
Run number: 26	16304	42	53	0.79	0.00	0.0	1.1	1.1	44.2047	1.2	0.92	0.2986	0.5	4702	38	3870	12	3463	7	**136**
Run number: 24	14594	33	57	0.59	0.00	0.0	1.3	1.5	80.0566	1.6	0.95	0.4427	0.5	5402	54	4463	16	4061	7	**133**
Run number: 16	2948	7	8	0.93	0.00	0.0	0.9	3.4	33.5404	3.4	0.98	0.2647	0.7	4202	105	3597	34	3275	11	**128**
Run number: 28	13027	189	46	4.15	0.00	0.5	0.2	0.7	3.1263	1.0	0.73	0.0917	0.7	1424	9	1439	8	1461	13	**97**

Run number: 20	6802	42	17	2.46	0.00	1.8	0.4	0.9	6.4520	1.6	0.58	0.1279	1.3	2010	16	2039	14	2069	23	**97**
Run number: 18	6762	34	16	2.13	0.00	0.0	0.4	1.3	8.1447	1.6	0.85	0.1413	0.8	2251	26	2247	14	2244	14	**100**
Run number: 30	8484	105	23	4.59	0.00	5.1	0.2	1.0	2.3035	4.0	0.24	0.0794	3.9	1231	11	1213	29	1182	77	**104**
Run number: 21	14600	340	64	5.28	0.00	0.3	0.2	1.5	2.1198	1.6	0.92	0.0785	0.6	1153	16	1155	11	1160	13	**99**
Run number: 13	8898	115	24	4.86	0.00	2.7	0.2	3.5	2.1957	4.4	0.79	0.0808	2.7	1160	37	1180	31	1216	53	**95**
Run number: 23	8439	68	13	5.03	0.00	2.7	0.2	3.6	2.0309	4.4	0.82	0.0787	2.5	1107	37	1126	30	1163	50	**95**
Run number: 14	4306	52	11	4.85	0.00	5.3	0.2	0.9	2.1032	3.8	0.23	0.0809	3.7	1114	9	1150	27	1219	73	**91**

1D: Electron-microprobe results for uraninite and calculated chemical ages.

Sample	MAAB03							BCAB																						
SiO2	0.49	0.29	0.07	0.11	0.07	0.38	0.25	0.06	0.10	0.04	0.09	0.08	0.46	0.21	0.09	0.23	0.04	0.09	0.09	0.06	0.04	0.02	0.07	0.16	0.06	0.13	0.09	0.09	0.12
TiO2	0.11	0.39	0.15	0.07	0.01	0.27	b.d.	b.d.	b.d.	0.10	0.13	0.10	0.19	0.14	b.d.	b.d.	0.04	0.04	b.d.	b.d.	0.09	0.04	0.04	b.d.	b.d.	0.06	0.00	0.02	b.d.
CaO	2.93	3.41	2.15	2.61	2.52	3.22	2.92	0.52	0.65	0.50	0.55	0.50	0.57	0.41	0.42	0.95	0.62	0.79	0.49	0.43	0.49	0.47	0.34	0.59	0.49	0.46	0.85	0.35	0.39
Al2O3	0.02	0.01	b.d.	b.d.	b.d.	0.01	b.d.	b.d.	b.d.	b.d.	0.01	0.01	0.31	0.02	b.d.	0.01	b.d.	b.d.	b.d.	0.01	b.d.	b.d.	b.d.	b.d.	b.d.	0.02	0.05	b.d.	0.02
MgO	b.d.	b.d.	b.d.	0.06	0.04	0.03	0.06	0.01	0.03	0.03	b.d.	b.d.	0.19	0.09	0.03	0.02	0.04	0.01	0.00	0.02	0.01	0.00	0.02	0.03	0.03	0.01	0.02	0.03	0.03
Y2O3	1.62	2.16	2.23	3.00	2.57	1.75	2.09	0.43	0.49	0.57	0.72	0.61	0.70	0.59	0.65	0.67	0.60	0.67	0.66	0.64	0.60	0.82	0.80	0.65	0.58	0.58	0.57	0.58	0.52
FeO	0.03	b.d.	0.34	0.16	0.14	b.d.	0.06	0.23	0.36	0.41	0.17	0.45	0.27	0.22	0.28	0.03	0.12	0.02	0.37	0.42	0.45	0.06	0.20	0.25	0.27	0.18	0.17	0.49	0.55
ZrO2	0.01	0.14	0.07	0.11	0.07	0.23	0.11	0.01	b.d.	b.d.	0.04	b.d.	0.06	0.03	0.03	b.d.	b.d.	0.03	0.02	b.d.	b.d.	b.d.	0.02	b.d.	0.03	b.d.	0.07	b.d.	b.d.
V2O3	b.d.	b.d.	b.d.	0.01	b.d.	b.d.	b.d.	b.d.	0.05	b.d.	0.04	0.02	0.08	0.04	0.00	0.09	0.04	b.d.	b.d.	0.01	b.d.	b.d.	0.01	0.03	0.05	b.d.	b.d.	0.01	0.03
P2O5	0.02	0.06	b.d.	b.d.	b.d.	0.07	0.04	b.d.	b.d.	b.d.	b.d.	b.d.	b.d.	b.d.	b.d.	b.d.	b.d.	0.01	0.01	b.d.	b.d.	b.d.	b.d.	b.d.	b.d.	b.d.	b.d.	b.d.	0.01
UO2	81.21	82.92	79.13	79.29	79.88	79.69	78.65	88.09	86.02	87.03	84.73	85.87	84.87	82.07	83.80	86.42	88.84	88.28	87.80	87.66	86.23	87.82	88.76	87.94	89.35	88.11	89.57	88.04	86.95
ThO2	0.02	0.04	0.08	0.09	0.14	0.03	0.06	0.12	0.36	0.05	0.19	0.17	0.25	0.30	0.28	0.22	0.26	0.27	0.44	0.33	0.36	1.20	0.53	0.38	0.36	0.39	0.29	0.43	0.47
PbO	5.94	5.53	5.42	5.70	6.08	6.19	5.75	6.29	6.18	6.30	6.48	6.22	6.19	5.88	5.75	6.04	6.72	6.85	6.43	6.42	6.30	6.32	6.75	6.71	6.66	6.44	6.84	6.51	6.32
Total	92.39	94.94	89.64	91.20	91.51	91.87	89.97	95.78	94.28	95.03	93.17	94.06	94.13	90.01	91.38	94.80	97.33	97.04	96.34	95.99	94.57	96.75	97.59	96.76	97.87	96.38	98.52	96.54	95.41
Formula based on 1 cation (apfu)																													
Si	0.02	0.01	0.00	0.01	0.00	0.02	0.01	0.00	0.00	0.00	0.00	0.00	0.02	0.01	0.00	0.01	0.00	0.00	0.00	0.00	0.00	0.00	0.00	0.01	0.00	0.01	0.00	0.00	0.01
Ti	0.00	0.02	0.01	0.00	0.00	0.01	0.00	0.00	0.00	0.00	0.01	0.00	0.01	0.01	0.00	0.00	0.00	0.00	0.00	0.00	0.00	0.00	0.00	0.00	0.00	0.00	0.00	0.00	0.00
Ca	0.07	0.08	0.06	0.07	0.06	0.08	0.07	0.01	0.02	0.01	0.01	0.01	0.01	0.01	0.01	0.02	0.02	0.02	0.01	0.01	0.01	0.01	0.01	0.01	0.01	0.01	0.02	0.01	0.01
Al	0.00	0.00	0.00	0.00	0.00	0.00	0.00	0.00	0.00	0.00	0.00	0.00	0.01	0.00	0.00	0.00	0.00	0.00	0.00	0.00	0.00	0.00	0.00	0.00	0.00	0.00	0.00	0.00	0.00
Mg	0.00	0.00	0.00	0.00	0.00	0.00	0.00	0.00	0.00	0.00	0.00	0.00	0.01	0.00	0.00	0.00	0.00	0.00	0.00	0.00	0.00	0.00	0.00	0.00	0.00	0.00	0.00	0.00	0.00
Y	0.03	0.04	0.04	0.06	0.05	0.03	0.04	0.01	0.01	0.01	0.01	0.01	0.01	0.01	0.01	0.01	0.01	0.01	0.01	0.01	0.01	0.02	0.01	0.01	0.01	0.01	0.01	0.01	0.01
Fe	0.00	0.00	0.01	0.00	0.00	0.00	0.00	0.00	0.01	0.01	0.00	0.01	0.01	0.00	0.01	0.00	0.00	0.00	0.01	0.01	0.01	0.00	0.00	0.00	0.01	0.00	0.00	0.01	0.01
Zr	0.00	0.00	0.00	0.00	0.00	0.01	0.00	0.00	0.00	0.00	0.00	0.00	0.00	0.00	0.00	0.00	0.00	0.00	0.00	0.00	0.00	0.00	0.00	0.00	0.00	0.00	0.00	0.00	0.00

V	0.00	0.00	0.00	0.00	0.00	0.00	0.00	0.00	0.00	0.00	0.00	0.00	0.00	0.00	0.00	0.00	0.00	0.00	0.00	0.00	0.00	0.00	0.00	0.00	0.00	0.00	0.00	0.00	0.00	0.00
P	0.00	0.00	0.00	0.00	0.00	0.00	0.00	0.00	0.00	0.00	0.00	0.00	0.00	0.00	0.00	0.00	0.00	0.00	0.00	0.00	0.00	0.00	0.00	0.00	0.00	0.00	0.00	0.00	0.00	0.00
U	0.83	0.81	0.85	0.83	0.84	0.81	0.83	0.93	0.92	0.92	0.91	0.91	0.87	0.91	0.92	0.91	0.92	0.91	0.92	0.92	0.92	0.92	0.92	0.91	0.92	0.92	0.91	0.92	0.91	0.91
Th	0.00	0.00	0.00	0.00	0.00	0.00	0.00	0.00	0.00	0.00	0.00	0.00	0.00	0.00	0.00	0.00	0.00	0.00	0.00	0.00	0.00	0.00	0.01	0.01	0.00	0.00	0.00	0.00	0.00	0.01
Pb	0.04	0.03	0.04	0.04	0.04	0.04	0.04	0.04	0.04	0.04	0.04	0.04	0.04	0.04	0.04	0.04	0.04	0.04	0.04	0.04	0.04	0.04	0.04	0.04	0.04	0.04	0.04	0.04	0.04	0.04
Age (Ga)	0.53	0.48	0.49	0.52	0.55	0.56	0.53	0.51	0.52	0.52	0.55	0.52	0.52	0.52	0.49	0.50	0.54	0.56	0.53	0.53	0.52	0.52	0.54	0.55	0.53	0.52	0.55	0.53	0.52	

1E – Analytical Methods

U–Pb dating by LA–ICP–MS

Zircon and titanite grains were handpicked from heavy-mineral separates of crushed and panned samples. Subsequently, the grains were mounted in 25-mm-diameter circular epoxy mounts and polished to expose their cores. Prior to analysis, zircon grains were imaged with cathodoluminescence imaging (CL) and, both zircon and titanite, with backscattered-electron imaging (BSE) using a JEOL 6510 Scanning Electron Microscope (SEM), equipped with a Centaurus CL detector, at the Geology Department of the Universidade Federal de Ouro Preto (UFOP, Brazil). This was conducted in order to obtain information on their internal structures. Zircon U–Pb isotope analyses were performed by LA–ICP–MS at UFOP using a Thermo-Fisher Element II sector field ICP–MS, coupled to a CETAC LSX-213 G2+ (λ = 213 nm) Nd:YAG laser. A detailed description of the method is given by (Gerdes and Zeh, 2006, 2009). Ablation was carried out in a low-volume cell with helium as the carrier gas; laser-beam parameters were a spot size of 20 µm, a repetition rate of 10 Hz, and a fluence of ~3 J cm^{-2}. Time-resolved raw data were corrected offline for background signal, common Pb, laser-induced elemental fractionation, instrumental mass discrimination, and time-dependent elemental fractionation of Pb–U using the GLITTER software package (Van Actherbergh et al., 2001). The common Pb correction was applied using the interference- and background-corrected ^{204}Pb signal and a model Pb composition (Stacey and Kramers, 1975). Laser-induced elemental fractionation and instrumental mass discrimination were corrected by normalization to the reference zircon GJ-1 (Jackson et al., 2004), which was routinely measured within each analytical session. The drift in inter-elemental fractionation (Pb–U) during 30 s of sample ablation was corrected individually before normalization to GJ-1. Reported uncertainties (2σ) were propagated by quadratic addition of the external reproducibility, obtained from the reference zircon GJ-1 during the analytical session (2σ in %) and the within-run precision of each analysis (standard error in %). In order to test the validity of the applied methods and the reproducibility of the zircon data, multiple analyses of the reference zircon Plešovice (Sláma et al., 2008) were performed. The latter gave a concordia age of 339 ± 2 Ma (n = 10, MSWD = 1.12). This is in agreement, within uncertainty, with the accepted ID-TIMS age reported for Plešovice (337.3 ± 0.4 Ma, 2σ, Sláma et al., 2008). In addition, several analyses of the in-house reference zircon BB

(Santos et al., 2017) were conducted, yielding a concordia age of 569 ± 3 Ma (n = 10, MSWD = 0.79), which is consistent with the reported LA–SF–ICP–MS age of this reference material (562 ± 9 Ma, 2σ, Santos et al., 2017). Data were plotted using Isoplot v. 4.15 (Ludwig, 2011). For titanite analyses, the titanite reference material BLR was used (TIMS normalization data $^{207}Pb/^{235}U$ = 1048.0 ± 0.7 Ma; $^{207}Pb/^{206}Pb$ = 1049.9 ± 1.3 Ma and $^{206}Pb/^{238}U$ = 1047.1 ± 0.4 Ma; Aleinikoff et al., 2007; Mazdab, 2009) for external corrections, inter-element fractionation and instrumental mass discrimination. The primary reference materials were analyzed under exactly the same conditions as the samples. A drift correction was applied by interpolation over a sequence of 12 – 20 reference materials (for 30 – 50 unknowns). Accuracy was checked using the Khan titanite as a secondary reference material (ca. 520 Ma; Heaman, 2009; Kinny et al., 1994). Over the duration of the study, the average normalized ages for Khan were 518 ± 2.3 Ma (n = 3) and 1049 ± 3 Ma (n = 5) for BRL.

Zircon U–Pb dating by SIMS

Determination for U–Pb isotopes by SIMS were conducted by means of a CAMECA 1280-HR instrument, housed at the Helmholtz Zentrum Potsdam in Germany. The SIMS analytical method followed that of Glynn et al. (2017), where it is described in detail. SIMS analyses were conducted in situ on a polished thin section in order to analyze only grains inside the microshear zone. SIMS analyses employed a 150-pA, $^{16}O_2^-$ primary ion beam, operated in Köhler mode, resulting in a beam diameter of approximately 5 µm on the sample surface. Positive secondary ions were extracted using a +10-kV potential as applied to the sample holder. Each analysis was preceded by a 150-pA, pre-sputtering lasting 150 seconds and employed a 15 µm raster. Oxygen flooding was used to enhance Pb sensitivity. The mass resolution of the instrument was set at approximately $M/\Delta M \approx 5400$. Data were acquired using an ETP electron multiplier operating in mono-collection mode. A single analysis consisted of 20 cycles of the peak stepping sequence: $^{90}Zr_2\ ^{16}O$ (1 second integration time per cycle), $^{92}Zr_2\ ^{16}O$ (1s), 200.5 (4s), $^{94}Zr_2\ ^{16}O$ (1s), ^{204}Pb (6s), ^{206}Pb (4s), ^{207}Pb (6s), ^{208}Pb (2s), $^{177}Hf\ ^{16}O_2$ (1s), ^{232}Th (2s), ^{238}U (2s), $^{232}Th\ ^{16}O$ (2s), $^{238}U\ ^{16}O$ (2s) and $^{238}U\ ^{16}O_2$ (2s). Thus, including pre-sputtering and waiting times, a single analysis lasted approximately 20 minutes.

The U–Pb inter-element calibration for this analytical series was based on the zircon reference material (RM) 91500 ($^{206}Pb/^{238}U$ age: 1062.4 ± 0.4 Ma; $^{207}Pb/^{206}Pb$ age: 1065.4 ±

0.3; Wiedenbeck et al., 1995), and the Temora 2 RM ($^{206}Pb/^{238}U$ age: 416.78 ± 0.33 Ma; Black et al., 2004), which was used as a quality-control material to evaluate the accuracy and stability of the U–Pb calibration measurements. Data collection employed a series of regularly interspersed analyses of these RMs between multiple analyses, typically 4, of the "unknown" sample grains. Data reduction used the Excel-based program "NordAge" (M. Whitehouse, NORDSIM facility, Stockholm), which established the U–Pb inter-element fractionation against which the unknowns were calibrated by way of a Pb/UO-vs.-UO_2/UO calibration. The software package Isoplot (Ludwig, 2012) was used to plot the data employing the decay constants recommended by the IUGS sub-commission on geochronology (Steiger and Jäger, 1977). The individual $^{207}Pb/^{206}Pb$ ratios and ages reported in the tables have an analytical uncertainty of one standard deviation, whereas the error ellipses on the concordia plots are at the two-standard-deviation level. A correction for common Pb was based on the observed ^{204}Pb counts in conjunction with the modern common Pb compositions from the model of Stacey and Kramers (1975). Eleven determinations of RM 91500 and RM Temora 2 yielded concordia ages of 1063 ± 15 Ma (2sd) and 417.4 ± 7.4 Ma (2sd), respectively. Based both on the repeatability of the U–Pb calibration on our primary RM 91500, as well as the results from our quality control RM Temora 2, we conclude that our U–Pb results are reliable to better than ± 2 % (2sd).

Electron-microprobe chemical age determination

Electron-microprobe analyses were performed on polished thin sections at the Centro de Microscopia, Universidade Federal de Minas Gerais (UFMG), Brazil, using a JEOL JXA-8900RL. The instrument was operated with a 15-kV acceleration voltage and a 20-nA beam current. The electron beam size was 5 μm. Elements and their X-ray lines, and RMs were as follows: Mg – MgO, As – $FeAs_2$, Ti – rutile, Ca – $CaWO_4$, Al – Al_2O_3, Fe – $FeAs_2$, Zr – ZrO_2, Si – $ThSiO_4$, V – V_2O_3, U – metallic, P and Y – YPO_4, Th – $ThSiO_4$, Pb – crocoite.

Assuming that the total Pb in uraninite is radiogenic, resulting from the decay of Th and U, and there was no Pb loss, the Pb contents in ppm (C_{Pb}) after time (t) are ruled by the equation (1) in Hurtado et al. (2007):

$$C_{Pb} = C_{Th}[0.897(e^{\lambda_{232}t} - 1)] + C_U [0.859(e^{\lambda_{238}t} -1) + 0.006(e^{\lambda_{235}t} -1)] \quad (1)$$

where C_{Pb}, C_{Th}, and C_U are concentrations (in ppm) of Pb, Th and U, respectively; λ_{232} λ_{238}, and λ_{235} are the decay constants (in yr^{-1}) for ^{232}Th, ^{238}U, and ^{235}U, respectively; and t is

age in years. The coefficient preceding the first exponential term is the mass ratio of ^{208}Pb to ^{232}Th – i.e., 208/232 ≈ 0.897; the coefficients preceding the second and third exponential terms are the ratios of the abundance fractions of the respective U isotopes to the mean atomic mass of U – i.e., 0.9928/238.04 ≈ 0.859 for ^{238}U.

References

Aleinikoff, J.N., Wintsch, R.P., Tollo, R.P., Unruh, D.M., Fanning, C.M., Schmitz, M.D., 2007. Ages and origins of rocks of the Killingworth dome, south-central Connecticut: Implications for the tectonic evolution of southern New England. Am. J. Sci. 307, 63–118.

Black, L.P., Kamo, S.L., Allen, C.M., Davis, D.W., Aleinikoff, J.N., Valley, J.W., Mundil, R., Campbell, I.H., Korsch, R.J., Williams, I.S., 2004. Improved 206Pb/238U microprobe geochronology by the monitoring of a trace-element-related matrix effect; SHRIMP, ID–TIMS, ELA–ICP–MS and oxygen isotope documentation for a series of zircon standards. Chem. Geol. 205, 115–140.

Gerdes, A., Zeh, A., 2009. Zircon formation versus zircon alteration—new insights from combined U–Pb and Lu–Hf in-situ LA-ICP-MS analyses, and consequences for the interpretation of Archean zircon from the Central Zone of the Limpopo Belt. Chem. Geol. 261, 230–243.

Gerdes, A., Zeh, A., 2006. Combined U–Pb and Hf isotope LA-(MC-) ICP-MS analyses of detrital zircons: comparison with SHRIMP and new constraints for the provenance and age of an Armorican metasediment in Central Germany. Earth Planet. Sci. Lett. 249, 47–61.

Glynn, S.M., Master, S., Wiedenbeck, M., Davis, D.W., Kramers, J.D., Belyanin, G.A., Frei, D., Oberthür, T., 2017. The Proterozoic Choma-Kalomo Block, SE Zambia: exotic terrane or a reworked segment of the Zimbabwe Craton? Precambrian Res. 298, 421–438.

Heaman, L.M., 2007. The application of U–Pb geochronology to mafic, ultramafic and alkaline rocks: an evaluation of three mineral standards. Chem. Geol. 261, 43–52.

Jackson, S.E., Pearson, N.J., Griffin, W.L., Belousova, E.A., 2004. The application of laser ablation-inductively coupled plasma-mass spectrometry to in situ U–Pb zircon geochronology. Chem. Geol. 211, 47–69.

Hurtado, J., Chatterjee, N., Ramezani, J., Hodges, K., & Bowring, S. (2007). Electron microprobe chemical dating of uraninite as a reconnaissance tool for leucogranite geochronology. *Nature Precedings*, 1-1

Kinny, P.D., Mcnaughton, N., Fanning, C.M., Maas, R., 1994. 518 Ma sphene (titanite) from the Khan pegmatite, Namibia, southwest Africa: A potential ionmicroprobe standard, in: 518 Ma Sphene (Titanite) from the Khan Pegmatite, Namibia, Southwest Africa: A Potential Ionmicroprobe Standard. US Geological Survey, p. 171.

Ludwig, K.R., 2012. A geochronological toolkit for Microsoft Excel Berkeley Geochronology Center Sp.

Ludwig, K.R., 2011. User's manual for Isoplot 4.15: A geochronological toolkit for Microsoft Excel. Berkeley Geochronology Center, Berkeley, California, USA concentrations: Loess and the upper continental crust. Geochemistry, Geophys. Geosystems 2.

Mazdab, F., 2009. Characterization of flux-grown trace-element-doped titanite using high-mass-resolution ion microprobe (SHRIMP-RG). Can. Mineral. 47, 813–831.

Santos, M.M., Lana, C., Scholz, R., Buick, I., Schmitz, M.D., Kamo, S.L., Gerdes, A., Corfu, F., Tapster, S., Lancaster, P., 2017. A new appraisal of Sri Lankan BB zircon as a reference material for LA-ICP-MS U-Pb geochronology and Lu-Hf isotope tracing. Geostand. Geoanalytical Res. 41, 335–358.

Sláma, J., Košler, J., Condon, D.J., Crowley, J.L., Gerdes, A., Hanchar, J.M., Horstwood, M.S.A., Morris, G.A., Nasdala, L., Norberg, N., 2008. Plešovice zircon—a new natural reference material for U–Pb and Hf isotopic microanalysis. Chem. Geol. 249, 1–35.

Stacey, J.S., Kramers, J.D., 1975. Approximation of terrestrial lead isotope evolution by a two-stage model. Earth Planet. Sci. Lett. 26, 207–221.

Steiger, R.H., Jäger, E., 1977. Subcommission on geochronology: convention on the use of decay constants in geo-and cosmochronology. Earth Planet. Sci. Lett. 36, 359–362.

Van Actherbergh, E., Ryan, C.., Jackson, S.., Griffin, W., 2001. Data reduction software for LA-ICP-MS, in: Laser Ablation-ICP-Mass Spectrometry in the Earth Sciences: Principles and Applications. Mineralogical Associates, pp. 239–243.

Wiedenbeck, M., Alle, P., Corfu, F., Griffin, W.L., Meier, M., Oberli, F. v, Quadt, A. von, Roddick, J.C., Spiegel, W., 1995. Three natural zircon standards for U–Th–Pb, Lu–Hf, trace element and REE analyses. Geostand. Newsl. 19, 1–23.

Anexo 2 (Appendix 2) – Titanite chemistry
2A: LA-ICP-MS results of titanite

CLASSIFICATION	Unaltered																
LITHOTYPE	São Timóteo granite																
SAMPLES	GRA01 1	GRA01 2	GRA01 3,xl	GRA01 4,xl	GRA01 5,xl	GRA01 6,xl	GRA01 7,xl	GRA01 8,xl	GRA01 9,xl	GRA01 10,xl	GRA01 11,xl	GRA01 12,xl	GRA01 13,xl	GRA01 14,xl	GRA01 15,xl	GRA01 16,xl	GRA01 17,xl
V51	15.60	11.77	11.27	17.09	22.64	17.75	10.36	12.08	15.16	9.47	11.70	12.50	14.35	11.14	9.15	15.21	16.24
Zn66	100.47	79.75	85.25	424.88	61.21	59.69	b.d.l.	b.d.l.	172.48	60.26	78575.16	2041.89	814.05	59.48	245.85	653.25	157.80
Ga69	8.68	8.47	7.16	6.77	7.27	8.81	7.53	7.50	16.20	7.79	9.81	22.82	8.63	8.38	6.50	6.56	30.58
Ge72	17.36	14.83	14.96	18.26	13.31	12.86	17.12	b.d.l.	19.43	12.90	16.06	14.17	b.d.l.	14.69	13.12	15.99	52.15
Rb85	b.d.l.	b.d.l.	b.d.l.	b.d.l.	8.67	26.88	b.d.l.	b.d.l.	136.24	b.d.l.	b.d.l.	214.72	b.d.l.	b.d.l.	1.93	2.46	13.70
Sr88	14.18	16.28	15.65	14.46	14.20	15.53	14.33	11.91	14.41	14.40	15.91	12.45	13.01	14.70	18.34	28.72	291.02
Y89	4012.24	3933.04	4114.10	4063.48	3737.12	3968.85	4137.01	4027.71	4549.03	4322.97	4283.12	4779.23	4357.40	4587.97	4187.96	4438.85	4936.97
Zr90	95.72	77.84	83.81	81.34	451.04	68.29	82.58	72.51	72.22	82.55	204.95	84.59	72.06	74.42	78.90	86.01	230.59
Nb93	2967.88	2811.79	2721.73	3371.20	2983.84	3107.28	2436.95	2507.08	2876.36	2489.34	2348.60	2712.86	4545.18	2520.74	2564.10	3197.95	2676.59
Ba135	b.d.l.	b.d.l.	b.d.l.	b.d.l.	b.d.l.	26.54	b.d.l.	b.d.l.	129.95	b.d.l.	b.d.l.	222.11	b.d.l.	b.d.l.	19.72	22.95	119.68
La139	46.33	53.78	62.12	52.70	36.06	40.17	57.85	54.45	68.18	66.87	64.20	58.44	56.97	60.94	54.14	53.25	207.39
Ce140	3.40	4.51	4.40	5.09	2.01	2.48	6.27	9.23	7.05	7.12	15.79	6.75	7.40	7.03	49.04	96.96	1753.90
Pr141	357.34	382.32	392.75	392.18	274.45	278.99	369.80	338.89	349.48	405.36	394.64	318.74	377.07	368.28	569.25	845.44	12880.78
Nd146	343.04	367.02	376.98	376.49	263.48	267.84	354.97	325.30	335.48	389.08	378.78	305.93	361.97	353.46	546.10	810.93	12142.17
Sm152	825.93	847.85	878.67	850.29	622.39	647.86	789.58	716.72	751.81	872.98	823.02	687.81	783.86	758.97	819.35	924.23	5417.92
Eu151	108.47	117.45	125.16	112.13	87.57	90.25	107.17	103.79	101.26	117.79	112.06	90.75	104.42	107.44	131.46	151.26	1414.81
Gd155	65.32	67.30	75.28	70.51	51.84	51.71	77.32	68.02	86.15	79.35	75.61	77.92	67.46	72.46	70.81	69.96	117.76
Tb159	831.58	839.16	872.68	811.14	636.29	719.67	785.25	709.47	815.11	775.28	771.97	741.37	742.45	781.64	729.53	746.87	1209.67
Dy163	807.47	824.64	837.59	839.82	638.39	703.78	780.57	717.25	812.42	812.56	764.93	773.25	750.63	805.26	721.99	699.77	1190.76
Ho165	195.92	203.28	205.50	205.77	166.45	183.09	190.66	171.27	208.90	187.61	186.08	186.43	173.68	189.38	172.27	176.94	229.21
Er167	1324.82	1363.99	1395.94	1341.21	1207.30	1274.07	1278.37	1196.04	1410.19	1259.89	1290.04	1318.89	1196.59	1329.82	1180.44	1222.80	1463.61
Tm169	290.71	303.72	303.82	297.35	266.37	283.93	295.69	270.71	309.20	279.85	277.94	291.09	264.16	279.12	260.82	271.50	309.86
Yb172	804.67	852.13	824.72	823.04	786.27	823.58	834.58	793.13	883.22	790.76	796.02	864.62	769.75	811.09	772.39	741.63	865.04
Lu175	128.79	132.52	132.12	135.63	119.77	132.00	134.15	124.60	147.04	125.36	123.64	136.91	117.02	127.33	123.78	122.71	139.76
Hf178	716.45	748.50	759.01	752.86	715.00	746.77	751.79	712.13	849.75	717.29	703.33	786.37	677.38	740.19	711.54	689.77	757.35
Ta181	4.44	3.73	3.53	3.20	4.42	3.66	3.37	b.d.l.	2.92	4.42	50.12	5.28	b.d.l.	3.75	8.74	13.27	133.62
Pb208	421.28	374.18	297.47	322.87	470.62	455.90	365.51	336.38	461.88	321.06	298.90	419.20	390.41	334.33	401.74	450.34	508.16
Th232	452.14	401.58	319.25	346.51	505.09	489.29	392.28	361.02	495.71	344.58	320.79	449.90	419.00	358.82	431.16	483.32	545.37
U238	24.78	26.86	29.16	28.55	20.68	24.67	25.61	26.32	29.23	26.26	23.81	28.96	33.18	28.38	24.47	27.15	43.40
U/Pb	0.06	0.07	0.10	0.09	0.04	0.05	0.07	0.08	0.06	0.08	0.08	0.07	0.08	0.08	0.06	0.06	0.09

U/Th	0.05	0.07	0.09	0.08	0.04	0.05	0.07	0.07	0.06	0.08	0.07	0.06	0.08	0.08	0.06	0.06	0.08
ΣETR	6133.78	6359.66	6487.72	6313.35	5158.64	5499.43	6062.22	5598.88	6285.49	6169.87	6074.73	5858.90	5773.42	6052.21	6201.37	6934.24	39342.65
Zr/Hf	0.13	0.10	0.11	0.11	0.63	0.09	0.11	0.10	0.08	0.12	0.29	0.11	0.11	0.10	0.11	0.12	0.30
Th/U	18.24	14.95	10.95	12.14	24.42	19.83	15.32	13.71	16.96	13.12	13.47	15.54	12.63	12.64	17.62	17.80	12.57
REEY	10146.02	10292.70	10601.81	10376.83	8895.76	9468.28	10199.23	9626.59	10834.52	10492.83	10357.86	10638.13	10130.82	10640.18	10389.32	11373.09	44279.63
HREEY	8461.51	8519.77	8761.75	8587.94	7609.81	8140.69	8513.59	8078.20	9221.26	8633.63	8569.36	9169.71	8439.13	8984.06	8219.99	8491.04	10462.66
Eu/Eu*	1.43	1.50	1.49	1.40	1.49	1.51	1.33	1.44	1.22	1.37	1.37	1.20	1.39	1.40	1.67	1.82	5.42
Ce/Ce*	0.0	0.0	0.0	0.0	0.0	0.0	0.0	0.0	0.0	0.0	0.0	0.0	0.0	0.0	0.0	0.0	0.0
Gd/Gd*	0.03	0.03	0.03	0.03	0.03	0.02	0.03	0.03	0.04	0.03	0.03	0.04	0.03	0.03	0.03	0.03	0.02
La/Yb	0.04	0.04	0.05	0.04	0.03	0.03	0.05	0.05	0.05	0.06	0.05	0.05	0.05	0.05	0.05	0.05	0.16
La/Sm	0.04	0.04	0.04	0.04	0.04	0.04	0.05	0.05	0.06	0.05	0.05	0.05	0.05	0.05	0.04	0.04	0.02
Gd/Yb	0.07	0.06	0.07	0.07	0.05	0.05	0.07	0.07	0.08	0.08	0.08	0.07	0.07	0.07	0.07	0.08	0.11
Pr/Pr*	10.17	10.15	10.16	10.14	10.19	10.18	10.11	10.04	10.09	10.11	9.94	10.08	10.09	10.10	9.61	9.42	9.42

continuação

CLASSIFICATION	Unaltered																		
LITHOTYPE	São Timóteo gneiss																		
SAMPLES	GNA 1,xl	GNA 2,xl	GNA 3,xl	GNA 4,xl	GNA 5,xl	GNA 6,xl	GNA 7,xl	GNA 8,xl	GNA 9,xl	GNA 10,xl	GNA 11,xl	GNA 12,xl	GNA 13,xl	GNA 14,xl	GNA 15,xl	GNA 16,xl	GNA 17,xl	GNA 18,xl	GNA 19,xl
V51	18.94	13.24	15.52	16.41	15.92	21.74	16.70	19.17	16.83	14.12	18.89	15.46	16.78	18.34	15.96	15.89	19.20	31.25	11.91
Zn66	b.d.l.	b.d.l.	b.d.l.	102.34	b.d.l.	b.d.l.	b.d.l.	b.d.l.	b.d.l.	b.d.l.	b.d.l.	b.d.l.	b.d.l.	217.73	b.d.l.	b.d.l.	b.d.l.	1946.69	b.d.l.
Ga69	12.71	16.28	11.16	15.83	b.d.l.	b.d.l.	b.d.l.	12.57	b.d.l.	11.96	13.25	11.97	b.d.l.	17.52	b.d.l.	b.d.l.	b.d.l.	176.01	10.27
Ge72	b.d.l.	b.d.l.	b.d.l.	b.d.l.	b.d.l.	b.d.l.	b.d.l.	b.d.l.	b.d.l.	b.d.l.	b.d.l.	b.d.l.	b.d.l.	b.d.l.	b.d.l.	b.d.l.	b.d.l.	b.d.l.	b.d.l.
Rb85	b.d.l.	b.d.l.	b.d.l.	b.d.l.	b.d.l.	b.d.l.	b.d.l.	b.d.l.	b.d.l.	b.d.l.	b.d.l.	b.d.l.	12.95	24.44	7.83	b.d.l.	b.d.l.	1911.57	b.d.l.
Sr88	11.72	14.21	16.03	13.15	13.93	14.89	14.52	13.29	16.17	14.92	10.86	16.53	10.09	10.38	15.38	13.89	12.69	138.53	11.45
Y89	4700.25	4800.35	4772.87	4511.98	4670.70	4549.71	4391.97	4742.07	4998.78	4741.36	5107.27	4446.26	5188.23	5114.50	4869.84	5271.38	5348.25	1094.16	5049.47
Zr90	64.13	56.76	61.57	66.76	58.06	50.38	60.45	62.73	57.96	70.46	57.78	72.32	57.91	54.73	64.45	58.67	55.23	4782.29	184.00
Nb93	2735.31	2441.50	2395.16	2281.46	2522.33	2770.42	2293.25	2868.19	2825.58	2541.57	2792.49	2171.56	2655.14	2814.57	2456.76	2712.07	2830.57	166.93	2662.91
Ba135	b.d.l.	b.d.l.	b.d.l.	b.d.l.	b.d.l.	b.d.l.	b.d.l.	b.d.l.	b.d.l.	b.d.l.	b.d.l.	b.d.l.	b.d.l.	37.77	b.d.l.	b.d.l.	b.d.l.	2016.53	b.d.l.
La139	63.28	57.43	64.42	57.47	51.59	44.42	44.69	54.65	64.23	71.00	54.41	64.03	56.18	52.85	55.89	57.58	45.78	34.27	34.69
Ce140	6.10	4.88	6.44	7.92	5.07	5.07	5.02	5.08	5.22	7.55	4.64	5.48	6.54	5.14	5.73	4.78	3.72	70.72	b.d.l.
Pr141	279.61	252.81	301.05	322.95	245.98	230.95	242.85	251.02	275.01	339.54	255.19	339.89	236.02	216.29	277.03	244.09	222.93	1070.57	215.84
Nd146	268.44	242.71	289.01	310.02	236.15	221.72	233.14	240.98	264.02	325.94	244.98	326.28	226.57	207.63	265.94	234.31	214.00	1026.79	207.18
Sm152	597.82	541.05	608.49	629.00	536.36	465.37	498.48	534.42	606.39	717.95	553.66	731.61	534.84	499.32	613.30	542.97	486.07	593.91	421.67
Eu151	83.65	71.89	86.86	88.67	72.12	67.43	66.72	71.24	77.94	94.76	72.44	92.22	67.40	70.39	79.96	69.93	66.00	131.72	56.22
Gd155	87.43	79.21	88.94	89.21	79.59	71.80	74.19	76.00	92.53	94.40	82.77	89.19	84.01	76.83	80.14	78.98	77.47	31.75	63.56
Tb159	682.97	634.71	703.06	683.71	636.87	584.71	572.56	629.20	675.08	731.18	615.01	703.47	638.56	628.25	676.64	662.01	613.67	185.23	546.12
Dy163	675.94	620.76	703.70	687.03	647.10	561.43	573.57	622.16	738.24	723.81	635.19	717.21	671.35	619.70	646.66	638.04	621.90	219.32	559.25
Ho165	170.33	155.07	173.28	158.48	155.17	143.47	142.27	154.62	166.45	163.43	156.74	160.98	153.54	154.38	162.04	160.07	153.32	35.16	146.02
Er167	1239.78	1191.26	1228.79	1182.32	1181.38	b.d.l.	1063.92	1197.43	1215.54	1168.85	1193.27	1093.63	1199.61	1182.00	1176.36	1212.47	1187.83	220.86	1156.02
Tm169	264.97	257.28	267.61	253.90	255.26	233.25	225.68	265.29	270.70	242.37	258.33	224.05	256.18	261.53	246.65	264.87	258.90	39.31	244.72
Yb172	778.10	788.54	780.88	746.02	762.17	700.07	680.63	796.04	852.28	730.41	757.01	706.75	801.95	806.16	753.79	803.37	801.26	117.22	746.31
Lu175	128.98	132.69	127.60	117.59	121.74	119.81	113.97	127.54	131.84	116.19	132.17	105.99	125.37	128.70	115.85	127.29	128.30	18.98	121.33
Hf178	790.71	811.19	754.48	711.81	768.45	763.39	696.44	748.66	b.d.l.	678.34	799.25	633.50	805.25	795.70	702.91	770.32	754.39	102.97	724.06
Ta181	b.d.l.	b.d.l.	b.d.l.	b.d.l.	b.d.l.	b.d.l.	5.16	b.d.l.	b.d.l.	b.d.l.	b.d.l.	13.19	b.d.l.	b.d.l.	b.d.l.	b.d.l.	b.d.l.	27.93	b.d.l.
Pb208	313.33	196.56	133.86	140.36	256.41	225.14	172.36	290.93	237.26	231.14	263.09	140.02	287.29	344.68	187.09	310.73	285.62	b.d.l.	337.10
Th232	336.28	210.96	143.66	150.64	275.19	241.63	184.98	312.24	254.64	248.07	282.36	150.28	308.34	369.92	200.79	333.49	306.54	b.d.l.	361.79
U238	28.88	23.91	14.41	20.63	19.24	28.73	18.61	23.79	24.48	26.40	25.61	26.80	24.02	19.78	21.41	21.73	18.52	b.d.l.	20.28
U/Pb	0.09	0.12	0.11	0.15	0.08	0.13	0.11	0.08	0.10	0.11	0.10	0.19	0.08	0.06	0.11	0.07	0.06	0.00	0.06
U/Th	0.09	0.11	0.10	0.14	0.07	0.12	0.10	0.08	0.10	0.11	0.09	0.18	0.08	0.05	0.11	0.07	0.06	0.00	0.06
ΣETR	5327.39	5030.28	5430.14	5334.28	4986.54	4549.50	4537.69	5025.67	5435.45	5527.37	5015.82	5360.79	5058.12	4909.17	5155.99	5100.77	4881.14	3795.80	4518.94

Zr/Hf	0.08	0.07	0.08	0.09	0.08	0.07	0.09	0.08	0.07	0.10	0.07	0.11	0.07	0.07	0.09	0.08	0.07	46.45	0.25
Th/U	11.64	8.82	9.97	7.30	14.31	8.41	9.94	13.13	10.40	9.40	11.03	5.61	12.84	18.71	9.38	15.35	16.55	0.00	17.84
REEY	10027.64	9830.63	10203.01	9846.25	9657.24	9099.21	8929.66	9767.74	10434.23	10268.73	10123.08	9807.05	10246.35	10023.67	10025.83	#######	10229.40	4889.97	9568.42
HREEY	8728.74	8659.86	8846.72	8430.24	8509.97	8064.26	7838.76	8610.34	9141.43	8711.99	8937.75	8247.54	9118.80	8972.05	8727.97	9218.48	9190.91	1961.99	8632.82
Eu/Eu*	1.12	1.06	1.14	1.14	1.07	1.13	1.06	1.08	1.01	1.11	1.03	1.10	0.97	1.10	1.10	1.03	1.04	2.93	1.05
Ce/Ce*	0.0	0.0	0.0	0.0	0.0	0.0	0.0	0.0	0.0	0.0	0.0	0.0	0.0	0.0	0.0	0.0	0.0	0.0	0.0
Gd/Gd*	0.04	0.04	0.04	0.04	0.04	0.04	0.04	0.04	0.05	0.04	0.05	0.04	0.05	0.04	0.04	0.04	0.04	0.04	0.04
La/Yb	0.05	0.05	0.06	0.05	0.05	0.04	0.04	0.05	0.05	0.07	0.05	0.06	0.05	0.04	0.05	0.05	0.04	0.20	0.03
La/Sm	0.07	0.07	0.07	0.06	0.06	0.06	0.06	0.06	0.07	0.06	0.06	0.06	0.07	0.07	0.06	0.07	0.06	0.04	0.05
Gd/Yb	0.09	0.08	0.09	0.10	0.08	0.08	0.09	0.08	0.09	0.10	0.09	0.10	0.08	0.08	0.09	0.08	0.08	0.22	0.07
Pr/Pr*	10.08	10.09	10.08	10.06	10.08	10.07	10.08	10.09	10.10	10.07	10.10	10.12	10.03	10.06	10.09	10.09	10.12	9.76	10.25

continuação

CLASSIFICATION																Partially altered			
LITHOTYPE																Garnet albitite			
SAMPLES	GNA 20,xl	GNA 21,xl	GNA 22,xl	GNA 23,xl	GNA 24,xl	GNA 25,xl	GNA 26,xl	GNA 27,xl	GNA 28,xl	GNA 29,xl	GNA 30,xl	GNA 31,xl	GNA 32,xl	GNA 33,xl	GNA 34,xl	GRAAB 1,xl	GRAAB 2,xl	GRAAB 3,xl	GRAAB 4,xl
V51	15.73	12.70	17.12	b.d.l.	15.34	14.26	19.32	12.14	15.04	18.90	b.d.l.	19.97	16.82	15.21	17.82	963.79	826.62	1222.96	609.32
Zn66	b.d.l.	b.d.l.	b.d.l.	b.d.l.	b.d.l.	b.d.l.	b.d.l.	b.d.l.	b.d.l.	b.d.l.	182.11	b.d.l.	b.d.l.	b.d.l.	b.d.l.	b.d.l.	b.d.l.	b.d.l.	67.39
Ga69	11.77	10.57	b.d.l.	b.d.l.	14.12	11.70	11.73	b.d.l.	b.d.l.	b.d.l.	b.d.l.	10.16	b.d.l.	b.d.l.	13.24	b.d.l.	b.d.l.	5.55	9.93
Ge72	b.d.l.	b.d.l.	b.d.l.	b.d.l.	b.d.l.	b.d.l.	b.d.l.	b.d.l.	b.d.l.	b.d.l.	b.d.l.	b.d.l.	b.d.l.	b.d.l.	b.d.l.	18.19	b.d.l.	15.16	b.d.l.
Rb85	29.92	b.d.l.	b.d.l.	b.d.l.	b.d.l.	b.d.l.	b.d.l.	b.d.l.	b.d.l.	59.08	b.d.l.	b.d.l.	b.d.l.	b.d.l.	16.94	b.d.l.	b.d.l.	b.d.l.	b.d.l.
Sr88	13.03	11.47	12.92	16.75	14.34	13.45	12.72	14.90	15.85	20.06	14.29	16.56	8.98	14.10	13.57	66.92	76.08	78.32	73.03
Y89	5112.48	4867.48	5060.45	4982.34	4913.80	4761.46	4999.75	5288.34	5497.96	5384.11	5829.91	6182.01	6082.65	5709.43	5954.83	2818.40	3746.03	2135.32	2726.03
Zr90	116.44	198.62	97.57	64.45	77.53	64.52	69.05	56.06	56.08	198.65	160.71	103.38	83.00	77.33	60.13	123.63	187.13	144.05	140.73
Nb93	2531.47	2261.34	2615.31	2412.18	2386.81	2130.20	2345.21	2475.47	2614.03	2828.46	2968.18	2924.33	2703.76	2385.62	2968.55	2619.20	2441.84	2285.88	2386.28
Ba135	b.d.l.	b.d.l.	b.d.l.	b.d.l.	b.d.l.	b.d.l.	b.d.l.	b.d.l.	b.d.l.	b.d.l.	b.d.l.	b.d.l.	b.d.l.	b.d.l.	b.d.l.	b.d.l.	b.d.l.	23.63	19.07
La139	52.87	56.57	58.37	63.86	59.93	59.64	54.70	51.24	51.26	46.34	43.68	75.75	71.18	59.93	55.03	88.69	104.22	62.44	109.84
Ce140	6.56	5.91	5.49	5.63	6.82	b.d.l.	b.d.l.	b.d.l.	b.d.l.	b.d.l.	b.d.l.	b.d.l.	b.d.l.	3.11	3.24	4.86	10.11	16.33	20.13
Pr141	287.54	388.24	291.60	310.31	316.57	263.64	269.93	239.29	263.58	192.73	240.22	335.16	308.77	525.12	327.66	204.59	336.28	228.05	386.46
Nd146	276.00	372.64	279.90	297.85	303.86	253.05	259.09	229.69	253.00	185.00	230.57	321.68	296.35	503.92	314.44	196.39	322.78	218.91	370.92
Sm152	599.71	719.63	639.66	707.70	690.59	595.67	595.64	596.29	647.60	458.83	528.16	724.00	734.53	796.81	599.42	565.36	757.64	478.16	750.38
Eu151	76.97	96.71	84.67	89.44	88.87	77.73	77.72	77.92	73.71	60.82	73.65	94.95	88.41	112.98	76.70	66.41	97.16	58.68	101.08
Gd155	83.72	87.97	83.67	88.71	87.26	72.05	80.67	76.92	83.97	74.60	75.30	92.15	90.28	90.78	96.39	78.65	93.00	70.56	93.87
Tb159	700.61	690.92	699.24	711.71	697.46	598.58	656.91	651.57	656.23	564.10	669.14	794.42	734.94	732.44	708.37	618.75	663.33	530.59	604.69
Dy163	687.84	687.97	728.45	688.73	726.51	670.97	676.29	665.34	677.60	572.74	702.08	811.21	779.28	769.10	731.06	639.59	705.68	553.41	636.51
Ho165	158.19	158.16	157.87	155.42	162.17	144.83	151.36	157.88	161.45	144.73	155.33	184.17	179.10	170.45	177.78	109.99	125.54	88.76	110.24
Er167	1187.19	1151.09	1170.29	1150.78	1118.50	1052.44	1121.43	1219.24	1229.77	1146.05	1194.56	1352.20	1336.77	1270.14	1354.78	628.63	822.65	487.77	628.48
Tm169	246.73	236.74	244.40	237.55	236.40	233.23	233.32	264.21	255.38	253.47	255.63	284.09	275.33	259.47	288.15	100.61	142.24	70.80	98.64
Yb172	754.93	700.76	753.82	710.17	673.33	690.13	714.13	838.32	818.07	824.05	755.96	863.21	824.17	767.75	864.28	227.96	387.58	155.47	233.05
Lu175	119.87	110.32	108.92	110.81	102.54	107.02	109.09	122.42	121.38	126.30	126.61	127.92	123.06	121.16	136.61	25.69	46.31	18.71	27.00
Hf178	709.32	656.93	666.87	680.74	636.15	616.53	656.10	751.23	752.21	723.20	708.67	791.97	758.32	708.95	811.04	144.38	256.05	102.92	133.83
Ta181	10.96	b.d.l.	5.33	b.d.l.	b.d.l.	b.d.l.	b.d.l.	b.d.l.	b.d.l.	b.d.l.	8.72	b.d.l.	b.d.l.	b.d.l.	10.05	14.24	19.79	9.50	8.77
Pb208	281.57	156.27	208.11	189.11	141.95	191.88	243.97	221.93	248.47	305.66	250.59	272.58	170.46	144.78	458.28	117.34	117.78	88.99	125.70
Th232	302.19	167.71	223.35	202.96	152.35	205.93	261.83	238.19	266.67	328.04	268.95	292.55	182.94	155.39	491.84	125.93	126.41	95.51	134.91
U238	22.77	22.97	18.48	20.74	29.56	19.11	15.46	23.29	12.83	20.08	26.24	23.00	24.95	22.81	21.99	b.d.l.	b.d.l.	5.74	b.d.l.

U/Pb	0.08	0.15	0.09	0.11	0.21	0.10	0.06	0.10	0.05	0.07	0.10	0.08	0.15	0.16	0.05	0.00	0.00	0.06	0.00
U/Th	0.08	0.14	0.08	0.10	0.19	0.09	0.06	0.10	0.05	0.06	0.10	0.08	0.14	0.15	0.04	0.00	0.00	0.06	0.00
ΣETR	5238.74	5463.63	5306.33	5328.67	5270.82	4818.99	5000.28	5190.34	5293.02	4649.76	5050.89	6060.93	5842.17	6183.17	5733.90	3556.16	4614.51	3038.64	4171.30
Zr/Hf	0.16	0.30	0.15	0.09	0.12	0.10	0.11	0.07	0.07	0.27	0.23	0.13	0.11	0.11	0.07	0.86	0.73	1.40	1.05
Th/U	13.27	7.30	12.09	9.79	5.15	10.77	16.94	10.23	20.78	16.33	10.25	12.72	7.33	6.81	22.37	0.00	0.00	16.63	0.00
REEY	10351.21	10331.11	10366.78	10311.01	10184.62	9580.45	10000.03	10478.68	10790.98	10033.87	10880.79	12242.94	11924.82	11892.61	11688.73	6374.57	8360.53	5173.95	6897.33
HREEY	9051.56	8691.41	9007.10	8836.23	8717.98	8330.72	8742.95	9284.26	9501.82	9090.15	9764.52	10691.39	10425.58	9890.73	10312.24	5248.28	6732.35	4111.39	5158.52
Eu/Eu*	1.05	1.18	1.12	1.09	1.11	1.15	1.08	1.11	0.97	1.01	1.13	1.12	1.05	1.28	0.98	0.96	1.12	0.98	1.16
Ce/Ce*	0.0	0.0	0.0	0.0	0.0	0.0	0.0	0.0	0.0	0.0	0.0	0.0	0.0	0.0	0.0	0.0	0.0	0.0	0.0
Gd/Gd*	0.04	0.04	0.04	0.04	0.04	0.04	0.04	0.04	0.04	0.05	0.04	0.04	0.04	0.04	0.05	0.04	0.05	0.05	0.05
La/Yb	0.05	0.05	0.05	0.06	0.06	0.06	0.05	0.04	0.04	0.04	0.04	0.06	0.06	0.05	0.04	0.26	0.18	0.27	0.32
La/Sm	0.06	0.05	0.06	0.06	0.05	0.06	0.06	0.05	0.05	0.06	0.05	0.07	0.06	0.05	0.06	0.10	0.09	0.08	0.09
Gd/Yb	0.09	0.10	0.09	0.10	0.10	0.08	0.09	0.07	0.08	0.07	0.08	0.09	0.09	0.10	0.09	0.28	0.19	0.37	0.33
Pr/Pr*	10.07	10.13	10.10	10.11	10.08	10.25	10.25	10.25	10.25	10.25	10.25	10.25	10.25	10.20	10.17	10.06	10.01	9.71	9.85

continuação

CLASSIFICATION LITHOTYPE SAMPLES	GRAA B 5,xl	GRAA B 6,xl	GRAA B 7,xl	GRAA B 8,xl	GRAA B 9,xl	GRAA B 10,xl	GRAA B 11,xl	GRAA B 12,xl	GRAA B 13,xl	GRAA B 14,xl	GRAA B 15,xl	GRAA B 16,xl	GRAAB 17,xl	GRAA B 18,xl	GRAA B 19,xl	GRAA B 20,xl	GRAA B 21,xl	GRAA B 22,xl	GRAA B 23,xl
V51	627.42	867.90	982.26	477.70	1051.35	714.17	592.31	1399.95	590.58	854.91	971.10	735.33	1059.05	1273.86	626.98	1760.67	1428.34	1705.61	474.20
Zn66	b.d.l.	69.95	115.68	b.d.l.	110.04	467.61	597.65	b.d.l.	b.d.l.	68.96	b.d.l.	88.46	76.50	b.d.l.	b.d.l.	88.03	b.d.l.	b.d.l.	75.01
Ga69	8.62	8.35	6.26	b.d.l.	9.07	12.00	16.94	6.94	8.87	5.23	8.33	5.99	7.10	b.d.l.	b.d.l.	7.16	b.d.l.	b.d.l.	b.d.l.
Ge72	b.d.l.	b.d.l.	16.23	b.d.l.	b.d.l.	18.97	19.78	b.d.l.	b.d.l.	b.d.l.	13.46	17.15	21.87	22.82	b.d.l.	18.64	20.81	b.d.l.	18.64
Rb85	b.d.l.	11.00	2.74	b.d.l.	b.d.l.	3.30	b.d.l.	b.d.l.	5.27	b.d.l.	2.60	2.75	3.03	3.13	b.d.l.	b.d.l.	3.51	b.d.l.	3.06
Sr88	70.52	90.09	72.41	69.19	67.54	79.30	82.40	84.82	65.88	69.40	66.72	72.75	62.45	70.82	65.44	67.50	98.13	96.40	128.24
Y89	2205.70	2588.97	2228.56	1643.49	2978.36	2558.20	1502.44	4303.15	2116.49	3333.54	2596.02	4101.59	5940.02	2159.30	2487.39	1486.57	3206.70	4757.86	2618.51
Zr90	140.00	164.62	150.82	3994.52	131.40	122.56	87.24	216.84	122.68	184.94	117.39	756.98	216.32	135.15	129.25	154.45	######	575.54	113.54
Nb93	2287.19	2429.79	2266.63	2193.43	2048.00	987.99	583.11	2443.72	2169.70	2164.66	2151.67	2078.42	2355.31	2078.83	2269.30	2522.75	2536.96	2892.23	1943.66
Ba135	b.d.l.	343.81	19.07	b.d.l.	17.63	40.03	b.d.l.	21.74	95.85	77.39	31.09	16.94	20.08	b.d.l.	b.d.l.	20.69	56.48	233.06	b.d.l.
La139	98.98	78.51	69.93	80.59	91.68	65.42	31.36	92.54	99.06	119.19	75.07	132.44	146.45	52.00	105.54	46.79	296.89	145.54	73.58
Ce140	10.34	28.16	12.01	4.48	12.08	10.96	7.17	7.05	9.44	12.28	4.87	14.40	24.64	5.65	9.78	2.17	17.44	15.91	8.42
Pr141	289.84	395.78	213.34	148.27	280.37	232.15	140.63	232.84	280.55	324.56	188.60	415.34	554.95	164.53	290.34	119.42	452.08	856.87	329.45
Nd146	278.21	379.87	204.79	142.33	269.12	222.79	134.98	223.52	269.28	311.53	181.04	398.61	532.55	157.94	278.69	114.65	433.88	822.09	316.21
Sm152	643.74	618.96	505.45	360.85	620.10	471.87	276.82	586.25	639.81	706.09	526.66	929.88	1212.82	458.27	647.48	304.12	750.65	1660.72	770.46
Eu151	81.24	81.74	59.60	43.16	76.12	62.20	35.64	72.02	81.28	94.31	62.95	118.49	158.33	57.59	81.02	37.66	102.71	238.02	101.70
Gd155	76.34	70.29	62.87	59.20	74.86	57.18	33.24	72.45	75.80	85.55	69.43	116.60	140.02	54.84	83.36	42.59	75.24	91.22	74.43
Tb159	525.62	537.16	474.34	445.15	522.86	407.02	240.76	572.50	519.51	615.26	496.21	775.55	965.78	406.66	578.64	334.51	537.52	767.13	516.00
Dy163	528.54	558.52	487.69	439.00	555.79	388.01	236.29	559.13	573.27	649.62	444.01	815.67	1013.81	429.59	588.37	318.86	578.46	777.91	519.55
Ho165	88.95	90.75	81.52	68.36	98.40	72.98	45.23	107.70	90.15	113.53	82.04	144.27	201.78	71.81	98.29	52.25	101.06	130.60	86.56
Er167	487.23	534.50	495.17	388.44	636.12	467.46	289.18	835.19	502.61	676.92	538.01	856.47	1230.22	431.31	559.64	311.15	700.82	849.28	565.19
Tm169	75.89	80.26	77.37	57.09	111.42	82.71	55.70	169.62	74.69	111.33	88.95	149.64	208.02	79.00	91.16	52.94	122.14	159.34	92.59
Yb172	187.78	224.87	199.21	148.21	289.77	228.07	142.42	548.81	184.38	307.27	262.87	356.82	567.85	233.04	203.71	166.11	354.63	480.31	239.26
Lu175	23.64	25.56	25.14	16.55	37.26	25.26	16.70	81.73	21.72	37.39	34.02	40.81	66.52	31.99	25.49	20.90	50.82	63.66	29.10
Hf178	118.85	114.42	133.28	85.76	173.23	124.20	89.94	508.49	105.82	201.04	183.39	203.81	307.51	178.58	125.02	129.87	319.71	382.29	140.48
Ta181	11.10	106.40	27.89	6.31	10.46	17.28	16.54	31.38	5.58	39.71	8.43	7.59	17.84	11.11	9.19	8.88	67.44	293.66	10.82
Pb208	108.29	111.99	103.56	117.77	82.74	50.66	33.77	124.10	105.67	111.32	110.97	126.78	112.81	124.78	122.07	97.58	137.86	132.08	187.80
Th232	116.23	120.19	111.15	126.39	88.80	54.37	36.24	133.19	113.41	119.48	119.10	136.07	121.07	133.92	131.01	104.73	147.96	141.76	201.56
U238	b.d.l.	5.91	6.65	b.d.l.	b.d.l.	7.77	b.d.l.	7.01	b.d.l.	b.d.l.	6.10	7.64	8.06	b.d.l.	b.d.l.	7.85	b.d.l.	b.d.l.	7.63
U/Pb	0.00	0.05	0.06	0.00	0.00	0.15	0.00	0.06	0.00	0.00	0.05	0.06	0.07	0.00	0.00	0.08	0.00	0.00	0.04
U/Th	0.00	0.05	0.06	0.00	0.00	0.14	0.00	0.05	0.00	0.00	0.05	0.06	0.07	0.00	0.00	0.07	0.00	0.00	0.04

ΣETR	3396.35	3704.91	2968.42	2401.68	3675.95	2794.09	1686.13	4161.34	3421.54	4164.84	3054.73	5264.99	7023.73	2634.22	3641.52	1924.14	4574.34	7058.60	3722.50
Zr/Hf	1.18	1.44	1.13	46.58	0.76	0.99	0.97	0.43	1.16	0.92	0.64	3.71	0.70	0.76	1.03	1.19	69.71	1.51	0.81
Th/U	0.00	20.33	16.71	0.00	0.00	7.00	0.00	19.01	0.00	0.00	19.52	17.80	15.02	0.00	0.00	13.34	0.00	0.00	26.42
REEY	5602.05	6293.88	5196.98	4045.17	6654.32	5352.29	3188.57	8464.49	5538.03	7498.37	5650.75	9366.58	12963.75	4793.52	6128.91	3410.71	7781.03	######	6341.01
HREEY	4199.69	4710.87	4131.86	3265.49	5304.85	4286.89	2561.97	7250.28	4158.61	5930.42	4611.56	7357.42	10334.01	3897.55	4716.05	2785.90	5727.40	8077.31	4741.18
Eu/Eu*	1.12	1.20	1.02	0.90	1.08	1.16	1.14	1.07	1.13	1.17	1.01	1.10	1.17	1.11	1.07	1.01	1.32	1.87	1.30
Ce/Ce*	0.0	0.0	0.0	0.0	0.0	0.0	0.0	0.0	0.0	0.0	0.0	0.0	0.0	0.0	0.0	0.0	0.0	0.0	0.0
Gd/Gd*	0.05	0.04	0.04	0.05	0.05	0.05	0.05	0.04	0.05	0.05	0.05	0.05	0.05	0.05	0.05	0.04	0.05	0.04	0.05
La/Yb	0.36	0.24	0.24	0.37	0.21	0.19	0.15	0.11	0.36	0.26	0.19	0.25	0.17	0.15	0.35	0.19	0.56	0.20	0.21
La/Sm	0.10	0.08	0.09	0.14	0.09	0.09	0.07	0.10	0.10	0.11	0.09	0.09	0.08	0.07	0.10	0.10	0.25	0.06	0.06
Gd/Yb	0.33	0.25	0.25	0.32	0.21	0.20	0.19	0.11	0.33	0.22	0.21	0.26	0.20	0.19	0.33	0.21	0.17	0.15	0.25
Pr/Pr*	9.97	9.71	9.82	10.01	9.92	9.89	9.86	10.01	9.99	9.96	10.05	9.98	9.91	9.98	9.99	10.10	9.95	10.11	10.05

continuação

CLASSIFICATION							Partially altered									
LITHOTYPE							Magnetite albitite									
SAMPLES	GRAAB 24,xl	GRAAB 25,xl	GRAAB 26,xl	GRAAB 27,xl	GRAAB 28,xl	GRAAB 29,xl	GNA02 1,xl	GNA02 2,xl	GNA02 3,xl	GNA02 4,xl	GNA02 5,xl	GNA02 6,xl	GNA02 7,xl	GNA02 8,xl	GNA02 9,xl	GNA02 10,xl
V51	2280.10	828.81	867.35	906.66	1015.53	861.40	25.79	20.27	18.12	26.67	46.38	31.91	35.05	29.75	35.81	53.37
Zn66	79.07	85.65	b.d.l.	b.d.l.	73.81	79.17	b.d.l.	b.d.l.	b.d.l.	b.d.l.	b.d.l.	b.d.l.	b.d.l.	b.d.l.	b.d.l.	b.d.l.
Ga69	6.85	11.65	13.79	b.d.l.	6.53	27.64	8.68	b.d.l.	b.d.l.	b.d.l.	b.d.l.	b.d.l.	5.75	6.93	b.d.l.	b.d.l.
Ge72	b.d.l.	20.51	b.d.l.	24.36	23.16	56.48	22.97	29.82	26.53	23.52	22.92	b.d.l.	20.40	25.06	17.79	21.07
Rb85	b.d.l.	30.87	16.21	b.d.l.	2.75	7.09	b.d.l.	b.d.l.	b.d.l.	b.d.l.	3.75	12.43	3.91	5.83	3.35	b.d.l.
Sr88	54.46	89.64	65.87	53.49	56.76	638.86	79.70	76.89	82.02	88.74	80.83	123.62	77.31	92.20	61.44	64.58
Y89	2758.48	4757.89	5623.35	6594.55	6615.20	3322.04	7668.5	6072.5	6032.4	6321.9	8557.0	5163.6	6130.1	6224.7	6107.2	3865.9
Zr90	281.03	154.60	172.70	169.56	182.85	157.27	98.39	100.29	93.45	98.49	65.16	89.98	108.17	112.65	79.63	49.13
Nb93	3215.59	2325.41	2344.68	1995.44	2165.30	2063.14	3669.7	2286.8	1790.0	2453.7	2814.4	1769.1	2732.4	2806.2	2411.3	1679.9
Ba135	22.18	659.85	508.98	b.d.l.	75.55	417.86	b.d.l.	b.d.l.	b.d.l.	b.d.l.	b.d.l.	19.09	b.d.l.	20.62	b.d.l.	b.d.l.
La139	60.16	116.60	144.39	171.64	160.37	196.38	68.40	50.11	43.49	59.28	37.25	47.59	80.26	73.83	59.76	29.44
Ce140	7.46	16.03	20.81	27.65	30.52	1785.40	57.30	41.54	39.46	45.45	30.62	37.91	62.26	57.01	37.72	20.33
Pr141	180.64	376.12	487.43	565.63	565.28	16562.7	1392.2	1319.2	1328.0	1475.6	736.5	1008.6	1432.8	1378.1	1027.8	533.4
Nd146	173.39	361.03	467.81	542.82	542.47	15597.7	1335.5	1265.4	1273.6	1415.4	706.6	967.6	1374.3	1321.9	986.1	511.9
Sm152	425.24	802.71	968.85	1075.16	1035.41	7128.2	2465.4	2059.3	2200.4	2243.0	1353.4	1381.8	2039.8	2020.7	1540.4	868.5
Eu151	59.97	106.40	128.23	156.77	148.67	1869.41	376.20	310.65	307.98	357.13	191.65	231.21	321.86	321.63	241.62	132.95
Gd155	56.47	100.05	128.85	124.94	134.07	186.94	198.70	154.32	171.14	178.46	234.64	166.81	200.71	205.61	192.59	111.46
Tb159	393.28	740.94	885.42	979.81	933.63	1072.7	1617.2	1270.5	1358.5	1402.0	1394.2	859.7	1157.3	1129.8	1044.4	621.4
Dy163	406.27	698.48	916.60	956.70	900.85	1085.6	1651.3	1257.7	1320.1	1355.4	1313.0	821.3	1111.6	1146.5	999.3	599.6
Ho165	81.00	134.26	174.13	196.94	176.49	148.27	279.33	207.74	237.24	236.74	248.21	153.24	207.53	209.31	188.55	111.71
Er167	525.94	933.04	1128.95	1364.02	1234.56	803.39	1901.1	1351.2	1467.8	1615.5	1846.3	1095.7	1357.3	1358.9	1265.0	799.5
Tm169	98.41	158.79	207.03	248.59	226.69	122.46	337.80	244.82	261.28	285.41	309.95	204.70	261.34	260.11	245.83	147.48
Yb172	297.87	459.22	544.64	690.87	661.66	284.41	989.28	721.26	776.61	754.89	892.97	582.78	729.06	774.00	718.31	428.34
Lu175	38.74	56.19	68.72	77.58	83.93	36.04	123.12	89.36	92.62	94.28	124.34	83.05	98.64	104.10	96.67	57.30
Hf178	197.73	261.33	319.62	353.92	369.23	150.79	665.47	525.35	609.04	557.56	779.62	475.73	558.93	605.97	595.68	353.08
Ta181	8.72	6.80	7.56	7.33	8.41	145.12	14.94	18.93	14.80	17.59	11.93	12.17	20.62	18.57	14.50	11.88
Pb208	69.56	160.37	147.30	149.40	136.28	113.26	225.45	129.34	93.27	124.91	134.75	65.41	100.98	114.55	80.90	61.63
Th232	74.66	172.12	158.09	160.34	146.26	121.56	241.96	138.81	100.11	134.06	144.62	70.20	108.38	122.94	86.82	66.14
U238	8.09	8.65	b.d.l.	b.d.l.	7.32	7.81	10.92	b.d.l.	b.d.l.	b.d.l.	b.d.l.	b.d.l.	7.61	b.d.l.	b.d.l.	b.d.l.
U/Pb	0.12	0.05	0.00	0.00	0.05	0.07	0.05	0.00	0.00	0.00	0.00	0.00	0.08	0.00	0.00	0.00
U/Th	0.11	0.05	0.00	0.00	0.05	0.06	0.05	0.00	0.00	0.00	0.00	0.00	0.07	0.00	0.00	0.00
ΣETR	2804.8	5059.9	6271.9	7179.1	6834.6	46879.6	12792.8	10343.2	10878.2	11518.6	9419.7	7642.1	10434.7	10361.6	8644.1	4973.2

Zr/Hf	1.42	0.59	0.54	0.48	0.50	1.04	0.15	0.19	0.15	0.18	0.08	0.19	0.19	0.19	0.13	0.14
Th/U	9.23	19.90	0.00	0.00	19.99	15.56	22.15	0.00	0.00	0.00	0.00	0.00	14.24	0.00	0.00	0.00
REEY	5563.3	9817.7	11895.2	13773.7	13449.8	50201.6	20461.2	16415.7	16910.6	17840.4	17976.7	12805.7	16564.8	16586.3	14751.3	8839.1
HREEY	4656.5	8038.9	9677.7	11234.0	10967.1	7061.8	14766.3	11369.5	11717.7	12244.6	14920.6	9131.0	11253.6	11413.0	10857.9	6742.6
Eu/Eu*	1.18	1.15	1.11	1.31	1.22	4.95	1.64	1.68	1.53	1.73	1.04	1.47	1.54	1.53	1.36	1.31
Ce/Ce*	0.0	0.0	0.0	0.0	0.0	0.0	0.0	0.0	0.0	0.0	0.0	0.0	0.0	0.0	0.0	0.0
Gd/Gd*	0.05	0.05	0.05	0.04	0.05	0.03	0.04	0.04	0.04	0.04	0.06	0.06	0.05	0.06	0.06	0.06
La/Yb	0.14	0.17	0.18	0.17	0.16	0.47	0.05	0.05	0.04	0.05	0.03	0.06	0.07	0.06	0.06	0.05
La/Sm	0.09	0.09	0.09	0.10	0.10	0.02	0.02	0.02	0.01	0.02	0.02	0.02	0.02	0.02	0.02	0.02
Gd/Yb	0.15	0.18	0.19	0.15	0.16	0.53	0.16	0.17	0.18	0.19	0.21	0.23	0.22	0.21	0.22	0.21
Pr/Pr*	9.93	9.92	9.92	9.88	9.84	9.63	9.94	10.01	10.03	10.02	9.93	9.96	9.92	9.94	9.97	9.96

continuação

CLASSIFICATION								Partially altered											
LITHOTYPE								Magnetite albitite mineralized											
SAMPLES	GNA0214,xl	GNA0215,xl	GNA0216,xl	GNA0217,xl	GNA0218,xl	GNA0219,xl	GNA0220,xl	ALB 05 1,xl	ALB 05 2,xl	ALB 05 3,xl	ALB 05 4,xl	ALB 05 5,xl	ALB 05 6,xl	ALB 05 7,xl	ALB 05 8,xl	ALB 05 9,xl	ALB 05 10,xl	ALB 05 11,xl	ALB 05 12,xl
V51	40.72	35.49	23.84	52.24	23.18	29.96	19.69	1361.39	1209.87	2323.78	3216.43	4598.06	3245.88	3526.07	7677.07	6159.63	3718.64	2178.27	5878.51
Zn66	b.d.l.	b.d.l.	b.d.l.	b.d.l.	b.d.l.	b.d.l.	b.d.l.	b.d.l.	b.d.l.	b.d.l.	b.d.l.	b.d.l.	372.31	b.d.l.	b.d.l.	b.d.l.	b.d.l.	b.d.l.	b.d.l.
Ga69	6.46	b.d.l.	b.d.l.	8.81	b.d.l.	b.d.l.	b.d.l.	b.d.l.	b.d.l.	b.d.l.	5.93	b.d.l.	44.08	12.64	b.d.l.	b.d.l.	9.68	b.d.l.	b.d.l.
Ge72	31.19	15.04	b.d.l.	b.d.l.	b.d.l.	25.88	27.50	20.53	18.97	b.d.l.	17.30	25.01	50.98	25.48	b.d.l.	b.d.l.	23.36	19.52	18.59
Rb85	b.d.l.	b.d.l.	b.d.l.	54.36	b.d.l.	b.d.l.	3.96	b.d.l.	b.d.l.	1.87	2.59	b.d.l.	9.74	b.d.l.	b.d.l.	b.d.l.	14.58	b.d.l.	b.d.l.
Sr88	79.70	80.73	65.40	53.62	67.84	78.15	73.40	81.55	80.94	46.57	127.11	94.30	1135.90	101.06	91.48	79.83	207.66	102.72	69.29
Y89	5766.2	3496.7	10223.9	8053.2	8150.2	7376.5	7631.1	4043.0	4284.2	331.9	1005.7	592.9	4984.0	1257.7	1118.0	1229.9	1894.4	3607.0	938.1
Zr90	94.98	63.97	86.31	143.93	89.84	99.48	109.33	102.32	100.06	197.09	1049.1	613.2	7492.6	595.4	923.1	1282.1	925.5	110.5	289.1
Nb93	2443.9	1717.0	3373.7	3542.2	3672.2	3423.4	3613.0	3647.7	3297.7	2602.8	2760.5	2603.0	3631.4	2814.3	2075.2	2107.0	3692.0	3443.9	2363.2
Ba135	b.d.l.	b.d.l.	b.d.l.	60.08	b.d.l.	b.d.l.	b.d.l.	b.d.l.	b.d.l.	b.d.l.	323.62	44.65	4096.36	42.90	22.22	18.25	307.98	b.d.l.	27.51
La139	65.97	34.53	40.73	46.21	62.94	55.13	62.97	191.68	190.55	13.63	7306.76	438.42	b.d.l.	1315.29	148.14	825.73	8411.15	146.44	563.22
Ce140	46.17	21.17	46.53	22.48	52.94	52.66	55.24	19.78	22.08	b.d.l.	222.46	7.47	6598.09	23.74	22.37	47.71	140.46	22.05	19.29
Pr141	1273.5	705.2	884.5	1758.3	1252.5	1331.5	1424.3	788.3	880.0	289.1	2125.6	3252.7	56105.8	1247.1	1424.0	1031.8	4742.7	1247.4	1092.7
Nd146	1221.6	676.7	848.5	1685.9	1201.4	1277.2	1366.1	756.5	844.4	277.6	2037.6	3116.0	45321.7	1196.2	1365.6	989.7	4530.6	1196.5	1048.3
Sm152	1836.2	935.2	2003.5	2089.1	2053.0	1961.5	2139.6	1466.4	1554.5	225.1	1381.9	1810.6	4631.9	1026.4	1242.7	946.2	2465.3	2019.9	896.4
Eu151	297.22	156.55	245.58	387.20	305.85	312.00	337.88	213.27	233.58	48.49	321.71	454.16	1194.06	215.54	271.15	177.28	593.09	298.54	188.00
Gd155	177.54	105.47	215.92	153.87	174.28	172.37	179.28	106.28	113.88	8.74	33.88	25.80	202.80	40.15	38.16	40.28	76.47	148.18	27.11
Tb159	997.81	566.87	2039.88	1388.47	1537.68	1516.41	1545.69	751.03	781.60	45.95	209.75	167.85	1255.38	240.22	211.16	221.73	496.88	898.72	160.14
Dy163	969.30	559.04	2035.13	1285.53	1597.83	1450.80	1479.25	703.91	791.28	49.42	202.87	152.06	1219.06	251.27	234.37	222.24	505.89	943.44	148.79
Ho165	178.00	101.60	363.35	255.28	312.23	268.28	277.89	121.90	131.30	8.67	34.48	21.21	218.68	38.21	30.70	36.27	81.11	138.52	26.02
Er167	1197.32	669.01	2673.07	1759.84	1976.77	1776.85	1888.64	778.04	800.95	49.97	212.71	128.26	1405.35	240.39	201.86	228.23	507.74	847.53	162.37
Tm169	223.68	133.94	433.32	308.46	363.04	318.43	332.00	127.32	135.99	9.65	36.36	21.68	234.50	40.61	37.85	40.98	73.72	127.75	27.35
Yb172	659.96	390.59	1173.14	927.33	1032.22	958.38	934.74	359.04	397.00	33.19	107.03	61.41	627.75	112.31	112.75	107.69	202.64	327.88	84.16
Lu175	88.44	52.20	175.24	128.79	127.77	122.80	120.36	51.64	58.40	4.89	16.05	9.58	83.89	15.40	18.05	18.22	30.95	43.96	15.30
Hf178	561.01	312.95	849.55	748.87	730.20	686.28	634.13	303.13	337.59	34.31	110.95	60.82	464.20	98.52	109.18	124.95	150.90	244.47	108.60
Ta181	16.41	14.28	11.53	9.39	16.96	19.96	18.68	12.14	11.97	8.66	92.04	26.39	1060.9	22.67	19.70	27.56	208.81	18.63	16.75
Pb208	90.21	50.65	280.23	153.46	194.31	190.38	234.29	232.22	183.70	46.95	170.75	207.64	328.95	147.47	148.67	123.88	255.46	222.24	106.98
Th232	96.82	54.35	300.75	164.70	208.54	204.33	251.45	249.23	197.15	50.39	183.26	222.85	353.04	158.27	159.56	132.95	274.17	238.52	114.82
U238	17.36	28.47	9.64	b.d.l.	5.42	8.27	b.d.l.	b.d.l.	b.d.l.	4.49	b.d.l.	b.d.l.	123.56	9.48	b.d.l.	5.19	b.d.l.	b.d.l.	b.d.l.
U/Pb	0.19	0.56	0.03	0.00	0.03	0.04	0.00	0.00	0.00	0.10	0.00	0.00	0.38	0.06	0.00	0.04	0.00	0.00	0.00

U/Th	0.18	0.52	0.03	0.00	0.03	0.04	0.00	0.00	0.00	0.09	0.00	0.00	0.35	0.06	0.00	0.04	0.00	0.00	0.00
ΣETR	9232.7	5108.2	13178.4	12196.8	12050.5	11574.4	12143.9	6435.1	6935.6	1064.5	14249.2	9667.3	119098.9	6002.8	5358.9	4934.1	22858.7	8406.8	4459.2
Zr/Hf	0.17	0.20	0.10	0.19	0.12	0.14	0.17	0.34	0.30	5.74	9.46	10.08	16.14	6.04	8.45	10.26	6.13	0.45	2.66
Th/U	5.58	1.91	31.20	0.00	38.47	24.70	0.00	0.00	0.00	11.22	0.00	0.00	2.86	0.00	0.00	25.64	0.00	0.00	0.00
REEY	14998.9	8604.9	23402.3	20249.9	20200.7	18950.9	19775.1	10478.1	11219.8	1396.4	15254.9	10260.2	124082.9	7260.6	6476.8	6164.0	24753.2	12013.8	5397.3
HREEY	10258.2	6075.5	19332.9	14260.7	15272.0	13960.8	14389.0	7042.2	7494.6	542.4	1858.9	1180.8	10231.4	2236.3	2002.9	2145.5	3869.8	7083.0	1589.4
Eu/Eu*	1.59	1.52	1.14	2.09	1.56	1.64	1.67	1.65	1.70	3.34	4.55	6.42	3.77	3.25	3.81	2.78	4.18	1.67	3.69
Ce/Ce*	0.0	0.0	0.0	0.0	0.0	0.0	0.0	0.0	0.0	0.0	0.0	0.0	0.0	0.0	0.0	0.0	0.0	0.0	0.0
Gd/Gd*	0.05	0.06	0.04	0.03	0.04	0.04	0.04	0.04	0.04	0.04	0.03	0.02	0.04	0.04	0.04	0.04	0.03	0.05	0.04
La/Yb	0.07	0.06	0.02	0.03	0.04	0.04	0.05	0.36	0.32	0.28	46.03	4.81	0.00	7.90	0.89	5.17	27.98	0.30	4.51
La/Sm	0.02	0.02	0.01	0.01	0.02	0.02	0.02	0.08	0.08	0.04	3.33	0.15	0.00	0.81	0.07	0.55	2.15	0.05	0.40
Gd/Yb	0.22	0.22	0.15	0.13	0.14	0.15	0.15	0.24	0.23	0.21	0.26	0.34	0.26	0.29	0.27	0.30	0.30	0.36	0.26
Pr/Pr*	9.97	10.02	9.85	10.16	9.93	9.95	9.96	10.05	10.06	10.25	9.49	10.25	10.99	10.11	10.13	9.90	10.06	10.12	10.12

continuação

CLASSIFICATION									Hydrothermal					
LITHOTYPE									Biotite albitite mineralized					
SAMPLES	ALB 05 13,xl	ALB 05 14,xl	ALB 05 15,xl	ALB 05 16,xl	ALB 05 17,xl	ALB 05 18,xl	ALB 05 19,xl	ALB 05 20,xl	BIAB129 01	BIAB129 02	BIAB129 03	BIAB129 04	BIAB129 05	BIAB129 06
V51	2899.1	3137.7	3844.5	3374.4	6849.3	2633.9	5538.3	2716.5	6010.4	5849.2	5865.7	5825.9	5534.9	7225.3
Zn66	b.d.l.	b.d.l.	b.d.l.	b.d.l.	b.d.l.	b.d.l.	b.d.l.	b.d.l.	20.69	12.16	22.25	20.58	19.63	22.11
Ga69	b.d.l.	b.d.l.	b.d.l.	b.d.l.	b.d.l.	b.d.l.	14.35	b.d.l.	5.34	5.43	7.37	3.97	9.20	7.64
Ge72	21.10	24.24	b.d.l.	b.d.l.	27.09	b.d.l.	b.d.l.	b.d.l.	29.04	19.69	25.49	20.34	25.72	20.30
Rb85	b.d.l.	b.d.l.	b.d.l.	b.d.l.	b.d.l.	b.d.l.	b.d.l.	b.d.l.	0.91	0.77	3.87	0.39	1.44	3.34
Sr88	100.69	76.45	78.68	69.59	72.86	83.77	101.45	103.82	90.16	90.08	107.43	85.65	132.83	143.45
Y89	3229.0	1411.9	1028.6	1913.7	742.3	3418.1	1281.2	1532.9	2593.6	2238.0	2450.1	2584.8	2596.1	1722.5
Zr90	211.4	321.1	330.4	224.2	235.5	120.3	217.3	246.1	226.5	716.0	467.3	133.2	289.2	75.5
Nb93	3174.4	2674.0	2118.3	2776.7	2560.4	3083.4	2109.0	2874.6	6212.2	4850.2	4157.5	4299.8	4323.1	3148.2
Ba135	b.d.l.	b.d.l.	b.d.l.	b.d.l.	18.91	b.d.l.	b.d.l.	b.d.l.	73.70	166.20	296.84	54.71	403.31	425.50
La139	588.96	828.83	403.65	246.21	474.17	189.40	269.31	306.22	850.39	719.33	809.22	615.15	841.10	662.61
Ce140	22.78	9.50	10.28	17.47	11.90	17.93	13.57	16.28	4099.77	3200.80	3707.02	2773.58	3479.34	2363.52
Pr141	1270.49	1245.12	1001.41	1638.61	1963.31	1121.56	1316.93	1141.25	746.03	554.49	618.12	517.25	584.80	403.88
Nd146	1218.9	1194.4	960.8	1571.4	1882.4	1076.0	1263.3	1095.1	3318.5	2614.4	2910.9	2407.9	2586.3	1921.7
Sm152	1934.5	1352.4	1127.2	1655.4	1498.4	1594.8	1368.0	1071.6	688.9	547.5	660.5	543.2	579.8	459.1
Eu151	307.54	253.09	219.26	299.45	340.78	271.18	265.15	200.24	218.30	185.58	225.70	197.39	211.00	170.54
Gd155	122.40	56.03	41.40	77.47	36.87	108.58	56.49	49.44	601.41	465.77	595.43	528.94	541.07	425.93
Tb159	762.30	363.62	256.79	418.68	184.59	699.54	312.18	315.31	78.64	66.25	84.25	72.61	76.20	55.17
Dy163	759.17	366.87	276.74	431.79	190.13	604.46	315.62	299.36	447.75	437.35	484.98	428.10	450.65	292.88
Ho165	117.19	55.47	39.17	64.99	24.13	113.67	41.73	46.41	81.02	80.35	87.26	74.65	79.19	49.75
Er167	679.19	312.89	220.27	391.03	144.87	694.19	257.45	306.24	216.36	215.68	219.54	198.17	207.63	123.61
Tm169	110.94	53.99	34.60	63.52	23.16	112.25	42.58	52.57	29.26	27.71	29.05	27.17	27.70	15.69
Yb172	292.27	134.26	89.20	167.46	58.90	345.45	117.83	147.11	178.32	162.87	171.98	151.31	167.26	83.58
Lu175	38.40	17.75	12.53	22.42	8.86	43.24	16.61	17.85	19.63	17.06	19.07	16.42	18.64	8.65
Hf178	242.31	99.58	80.65	128.34	55.21	278.25	108.62	114.44	9.77	15.33	11.01	7.95	11.28	3.62
Ta181	27.39	32.69	40.93	14.53	33.97	12.56	18.25	13.91	344.47	276.14	261.99	203.08	255.45	279.14
Pb208	183.61	125.61	127.51	124.76	102.76	108.81	96.20	206.66	247.91	376.77	714.19	246.68	959.52	1014.18
Th232	197.06	134.81	136.85	133.90	110.29	116.78	103.24	221.80	26.48	65.32	123.40	19.88	170.87	256.43
U238	b.d.l.	b.d.l.	b.d.l.	b.d.l.	b.d.l.	b.d.l.	b.d.l.	b.d.l.	2697.4	9016.5	12729.3	4642.5	17476.8	34470.4
U/Pb	0.00	0.00	0.00	0.00	0.00	0.00	0.00	0.00	10.88	23.93	17.82	18.82	18.21	33.99
U/Th	0.00	0.00	0.00	0.00	0.00	0.00	0.00	0.00	101.88	138.03	103.16	233.53	102.28	134.43
ΣETR	8225.0	6244.2	4693.3	7065.9	6842.4	6992.2	5656.7	5065.0	11574.3	9295.2	10623.0	8551.9	9850.6	7036.6

Zr/Hf	0.87	3.22	4.10	1.75	4.27	0.43	2.00	2.15	23.18	46.69	42.44	16.76	25.64	20.86
Th/U	0.00	0.00	0.00	0.00	0.00	0.00	0.00	0.00	b.d.l.	b.d.l.	b.d.l.	b.d.l.	b.d.l.	b.d.l.
REEY	11454.0	7656.1	5721.9	8979.6	7584.7	10410.3	6937.9	6597.9	14167.9	11533.1	13073.1	11136.7	12446.7	8759.1
HREEY	6110.9	2772.8	1999.3	3551.1	1413.8	6139.5	2441.6	2767.2	4246.0	3711.0	4141.7	4082.2	4164.5	2777.8
Eu/Eu*	1.93	2.81	3.10	2.56	4.43	1.99	2.92	2.66	1.04	1.12	1.10	1.13	1.15	1.18
Ce/Ce*	0.0	0.0	0.0	0.0	0.0	0.0	0.0	0.0	1.1	1.2	1.2	1.1	1.1	1.1
Gd/Gd*	0.05	0.04	0.04	0.05	0.03	0.05	0.04	0.04	1.00	0.92	0.95	0.97	0.93	0.94
La/Yb	1.36	4.16	3.05	0.99	5.43	0.37	1.54	1.40	3.22	2.98	3.17	2.74	3.39	5.35
La/Sm	0.19	0.39	0.23	0.09	0.20	0.07	0.12	0.18	0.78	0.83	0.77	0.71	0.91	0.91
Gd/Yb	0.34	0.34	0.37	0.37	0.51	0.25	0.39	0.27	2.72	2.31	2.79	2.82	2.61	4.11
Pr/Pr*	10.11	10.19	10.17	10.17	10.21	10.13	10.17	10.14	1.15	1.09	1.07	1.14	1.11	1.08

continuação

CLASSIFICATION	Hydrothermal												
LITHOTYPE	Pyroxene albitite mineralized												
SAMPLES	POAB 05 01	POAB 05 02	POAB 05 03	POAB 05 04	POAB 05 05	POAB 05 06	POAB 05 07	POAB 05 08	POAB 05 09	POAB 05 10	POAB 05 11	POAB 05 12	POAB 05 13
V51	2799.79	2261.64	1462.44	2920.90	4589.02	4189.71	4424.02	3734.99	3886.07	1546.56	2979.13	2601.59	2592.82
Zn66	18.05	18.12	14.49	15.35	17.48	17.52	17.35	15.58	15.09	15.44	12.10	32.49	14.92
Ga69	1.74	1.24	3.17	7.25	2.59	2.70	2.62	2.64	3.00	2.46	5.81	3.08	3.35
Ge72	7.58	6.77	3.23	7.90	18.82	19.45	19.12	15.52	19.65	2.82	14.97	7.28	6.62
Rb85	0.75	0.63	b.d.l.	0.85	1.11	b.d.l.	0.79	0.64	0.84	0.71	0.85	0.48	0.56
Sr88	147.04	95.59	77.42	112.11	112.22	111.76	111.76	143.44	182.15	37.52	141.51	142.41	168.56
Y89	2079.16	1636.24	3551.05	12273.56	6825.11	6395.87	6645.20	4824.43	6280.39	5250.69	5743.07	2412.08	3905.49
Zr90	511.09	387.61	57.47	265.98	356.73	269.68	326.61	2457.45	3440.60	127.49	1294.03	697.77	744.34
Nb93	3489.04	4746.50	4962.64	4395.97	3785.75	3440.22	3673.61	3470.79	4539.08	2906.60	5492.87	3143.01	2917.88
Ba135	24.56	9.95	1.75	16.78	11.43	14.44	12.49	37.03	53.97	1.12	62.03	28.64	30.83
La139	128.96	74.27	4.82	124.27	1845.76	1591.97	1760.20	1123.57	1599.01	15.73	864.34	153.59	142.71
Ce140	390.36	239.51	61.20	437.30	4446.00	3684.90	4188.06	2112.93	3032.76	55.23	2059.37	362.44	390.59
Pr141	56.93	39.12	27.30	95.93	452.34	384.48	428.83	193.37	278.43	8.84	215.38	50.64	57.58
Nd146	258.61	207.34	244.81	673.79	1601.48	1393.18	1529.08	679.89	951.40	45.67	774.74	239.49	287.02
Sm152	103.82	120.68	279.20	640.37	447.03	391.31	429.56	197.34	273.21	45.55	235.86	112.34	165.41
Eu151	21.43	18.14	51.52	116.53	97.23	94.99	96.17	43.90	59.81	13.13	43.95	21.24	31.25
Gd155	190.27	189.12	590.28	1559.61	750.68	688.94	724.68	386.28	526.70	242.60	435.66	209.63	361.09
Tb159	38.72	41.98	116.88	290.86	147.15	134.14	141.97	77.34	105.59	82.25	104.01	45.01	78.14
Dy163	278.40	302.98	665.46	1848.77	1058.34	932.31	1010.42	618.51	838.02	757.51	806.29	340.87	563.01
Ho165	57.85	60.50	106.28	354.36	222.30	186.97	209.05	138.40	184.87	162.09	163.37	71.66	119.55
Er167	174.15	165.18	260.25	970.29	610.13	540.48	583.67	419.87	541.37	432.00	478.22	211.99	334.81
Tm169	23.81	22.20	33.08	119.94	79.11	71.01	76.13	61.58	77.82	49.74	65.11	31.05	42.73
Yb172	158.55	138.34	195.72	721.19	448.23	428.42	441.27	399.67	496.06	260.77	419.80	206.81	264.80
Lu175	19.18	15.36	22.32	87.89	52.63	49.79	51.53	44.76	54.90	25.82	50.78	26.02	32.65
Hf178	3.06	2.51	2.17	5.20	3.68	2.59	3.27	23.56	34.07	3.60	18.51	3.51	5.05
Ta181	18.00	21.64	112.25	95.04	41.27	33.38	38.64	64.83	89.05	134.96	152.37	16.27	44.66
Pb208	6.72	9.64	5.64	14.45	11.78	11.68	11.61	18.60	25.72	4.49	31.87	12.75	9.61
Th232	0.17	0.13	0.25	8.03	2.97	1.65	2.49	0.46	0.58	0.11	0.64	0.39	0.96
U238	544.06	447.55	33.72	272.94	258.73	784.54	436.98	618.65	819.78	47.97	169.35	821.71	1694.62
U/Pb	81.02	46.44	5.98	18.89	21.96	67.18	37.63	33.26	31.88	10.68	5.31	64.43	176.28
U/Th	3110.31	3436.82	133.43	33.98	87.03	474.82	175.50	1353.00	1412.38	440.93	264.45	2086.96	1766.20

ΣETR	1901.03	1634.68	2659.11	8041.09	12258.40	10572.90	11670.62	6497.43	9019.94	2196.93	6716.88	2082.77	2871.35
Zr/Hf	167.26	154.16	26.44	51.17	96.98	104.08	99.80	104.30	100.99	35.40	69.91	198.94	147.32
Th/U	b.d.l.	b.d.l.	b.d.l.	0.03	0.01	b.d.l.	b.d.l.	b.d.l.	b.d.l.	b.d.l.	b.d.l.	b.d.l.	b.d.l.
REEY	3980.19	3270.92	6210.16	20314.65	19083.51	16968.77	18315.82	11321.86	15300.33	7447.62	12459.95	4494.85	6776.84
HREEY	3020.09	2571.88	5541.30	18226.46	10193.68	9427.94	9883.92	6970.85	9105.71	7263.47	8266.31	3555.11	5702.28
Eu/Eu*	0.47	0.37	0.39	0.36	0.51	0.56	0.53	0.49	0.48	0.38	0.42	0.42	0.39
Ce/Ce*	1.1	1.1	0.6	0.9	1.1	1.1	1.1	1.0	1.0	1.1	1.1	1.0	1.0
Gd/Gd*	1.33	1.29	1.44	1.56	1.31	1.29	1.30	1.34	1.34	0.98	1.20	1.31	1.34
La/Yb	0.55	0.36	0.02	0.12	2.78	2.51	2.69	1.90	2.17	0.04	1.39	0.50	0.36
La/Sm	0.78	0.39	0.01	0.12	2.60	2.56	2.58	3.58	3.68	0.22	2.31	0.86	0.54
Gd/Yb	0.97	1.10	2.43	1.75	1.35	1.30	1.33	0.78	0.86	0.75	0.84	0.82	1.10
Pr/Pr*	1.02	1.00	0.93	0.94	0.91	0.92	0.91	0.85	0.85	1.00	0.92	0.98	0.98

2B: Results of statistics calculation for the detection limit of trace elements obtained by LA-ICP-MS during analyses of titanite.

Sample	GRA 01			9-4			GNA02			7-1B			ALB05			BIAB 129			POAB 05		
	n=17			n=34			n=29			n=20			n=20			n=6			n=13		
	median	media	s	median	media	s	median	media	s	median	media	s	median	media	s	median	media	s	median	media	s
Sc45	7.07	7.38	1.40	12.74	13.67	3.50	9.28	9.33	1.02	8.30	8.55	1.01	8.47	9.14	1.64	0.26	0.30	0.11	0.24	0.28	0.11
V51	4.37	4.64	1.11	8.96	9.27	2.44	6.06	6.00	0.68	5.72	5.63	0.75	5.62	5.86	1.08	0.64	0.73	0.25	0.73	0.87	0.34
Cr52	13.99	14.62	2.84	26.80	28.53	7.63	17.75	18.10	1.86	17.58	17.67	1.87	17.79	19.25	3.50	1.20	1.34	0.46	1.13	1.31	0.47
Cu63	6.83	7.39	1.99	14.88	15.78	4.07	9.53	9.93	1.55	9.81	10.12	1.27	9.23	9.89	2.21	0.78	0.89	0.30	0.74	0.90	0.38
Zn66	48.91	52.70	13.31	108.05	111.44	28.27	69.95	71.56	9.16	76.38	79.25	9.64	68.96	73.12	19.23	3.01	3.51	1.31	3.03	3.51	1.39
Ga69	4.20	4.55	1.17	9.42	9.79	2.30	5.91	6.06	0.82	5.96	6.08	0.70	5.67	6.10	1.45	0.16	0.20	0.11	0.17	0.20	0.09
Ge72	11.10	12.13	2.74	24.09	25.78	6.90	15.91	15.94	2.22	16.81	16.82	2.38	14.95	15.69	3.07	1.62	1.90	0.71	1.53	1.82	0.69
Rb85	1.81	1.93	0.45	3.96	4.14	1.03	2.68	2.69	0.38	2.65	2.66	0.32	2.56	2.58	0.66	0.17	0.20	0.10	0.17	0.20	0.08
Sr88	1.39	1.48	0.34	3.16	3.21	0.65	2.07	2.09	0.39	2.09	2.10	0.33	2.04	2.07	0.49	0.10	0.15	0.11	0.10	0.12	0.06
Y89	0.67	0.72	0.21	1.96	2.04	0.49	1.81	1.76	0.24	1.66	1.71	0.22	1.66	1.76	0.36	0.11	0.10	0.04	0.08	0.14	0.13
Zr90	2.36	2.54	0.61	5.29	5.39	1.23	3.37	3.42	0.50	3.46	3.54	0.48	3.32	3.51	0.86	0.57	0.66	0.32	0.58	0.64	0.31
Nb93	1.11	1.17	0.29	2.68	2.84	0.78	2.10	2.09	0.28	2.08	2.09	0.23	1.94	2.05	0.43	0.12	0.12	0.05	0.09	0.19	0.23
Ba135	15.20	16.77	3.85	34.66	36.62	9.33	17.63	17.99	2.43	18.33	18.69	2.17	17.12	18.37	4.30	0.78	0.94	0.47	0.74	0.81	0.28
La139	1.32	1.44	0.32	2.96	3.14	0.75	1.98	2.00	0.28	1.86	1.96	0.29	1.91	1.98	0.44	0.09	0.11	0.06	0.09	0.10	0.05
Ce140	1.26	1.33	0.32	2.84	2.97	0.67	1.81	1.86	0.21	1.73	1.80	0.23	1.72	1.84	0.32	0.11	0.11	0.05	0.08	0.10	0.07
Pr141	0.90	0.95	0.20	2.05	2.12	0.52	1.40	1.36	0.19	1.38	1.38	0.17	1.25	1.33	0.30	0.08	0.09	0.05	0.07	0.09	0.05
Nd146	1.09	1.15	0.24	2.45	2.55	0.63	1.68	1.63	0.23	1.66	1.65	0.22	1.49	1.59	0.37	0.56	0.61	0.27	0.59	0.72	0.29
Sm152	5.61	5.99	1.33	12.66	13.15	2.98	8.64	9.02	1.61	8.12	8.54	1.18	7.97	8.61	2.32	0.13	0.14	0.05	0.11	0.13	0.06
Eu151	0.95	1.03	0.29	2.12	2.26	0.59	1.15	1.16	0.17	1.12	1.14	0.16	1.02	1.13	0.29	0.56	0.67	0.30	0.51	0.54	0.30
Gd155	1.97	2.15	0.48	4.53	4.74	1.11	2.32	2.40	0.34	2.35	2.37	0.28	2.26	2.36	0.54	0.42	0.43	0.14	0.35	0.43	0.21
Tb159	5.97	6.37	1.19	13.71	14.54	3.92	7.84	7.71	1.25	7.31	7.45	0.96	7.19	7.51	1.60	0.06	0.07	0.03	0.06	0.06	0.03
Dy163	5.59	6.08	1.38	12.86	13.62	3.27	8.63	8.97	1.58	8.43	8.73	1.21	8.46	9.22	2.14	0.35	0.44	0.18	0.32	0.39	0.20
Ho165	0.97	1.02	0.22	2.07	2.20	0.55	1.41	1.42	0.19	1.39	1.39	0.18	1.28	1.40	0.35	0.06	0.07	0.03	0.07	0.08	0.03
Er167	3.77	4.00	0.87	8.64	8.99	2.28	5.96	6.13	0.91	6.07	6.01	0.80	5.64	5.96	1.65	0.17	0.21	0.11	0.19	0.20	0.06
Tm169	0.92	1.02	0.24	2.17	2.28	0.56	1.18	1.17	0.15	1.12	1.15	0.15	1.06	1.12	0.26	0.07	0.08	0.03	0.06	0.07	0.03
Yb172	4.00	4.19	1.07	9.50	9.80	2.40	6.42	6.61	1.05	6.38	6.34	0.76	6.05	6.43	1.37	0.35	0.39	0.15	0.34	0.39	0.19

Lu175	0.97	1.08	0.25	2.25	2.36	0.50	1.21	1.20	0.18	1.17	1.17	0.16	1.09	1.16	0.24	0.06	0.08	0.05	0.05	0.06	0.04
Hf178	4.17	4.51	0.99	9.70	10.00	2.34	6.27	6.58	0.92	6.32	6.34	0.73	5.99	6.39	1.38	0.28	0.31	0.18	0.22	0.26	0.16
Ta181	2.46	2.62	0.61	5.11	5.41	1.48	3.50	3.52	0.52	3.58	3.52	0.55	3.37	3.55	0.83	0.09	0.11	0.05	0.08	0.09	0.04
Pb208	0.95	1.02	0.25	2.19	2.23	0.46	1.39	1.42	0.24	1.39	1.40	0.18	1.35	1.39	0.30	0.38	0.44	0.20	0.30	0.37	0.16
Th232	1.02	1.10	0.27	2.35	2.39	0.50	1.49	1.53	0.26	1.50	1.50	0.19	1.45	1.50	0.32	0.02	0.03	0.03	0.02	0.03	0.02
U238	4.41	4.76	1.04	10.20	10.62	2.49	6.52	6.66	1.01	6.62	6.58	0.83	6.19	6.42	1.58	0.05	0.08	0.08	0.02	0.05	0.07

2C: Microprobe analyses of titanite and recalculated formula on the basis of 8 oxygens.

SiO_2	TiO_2	Al_2O_3	Fe_2O_3	CaO	F	TOTAL	Si	Al	Ti	Fe	Ca	F
Sample GRA 01												
31.34	31.56	4.61	1.32	28.51	1.69	97.41	1.01	0.17	0.76	0.02	0.98	0.17
31.75	31.04	5.10	1.57	28.40	1.95	95.69	1.01	0.19	0.74	0.03	0.97	0.20
30.63	32.90	4.55	1.64	28.03	1.33	94.93	0.99	0.17	0.80	0.03	0.97	0.14
31.11	32.69	4.47	1.40	28.06	1.36	96.64	1.00	0.17	0.79	0.03	0.97	0.14
30.38	31.61	4.60	1.37	28.27	1.20	96.27	1.00	0.18	0.78	0.03	1.00	0.13
30.90	30.26	4.78	1.29	28.57	1.03	97.20	1.02	0.19	0.75	0.02	1.01	0.11
29.64	29.91	5.01	1.73	27.53	0.94	98.54	1.01	0.20	0.76	0.03	1.00	0.10
31.42	29.50	6.42	1.13	28.92	1.84	97.71	1.00	0.24	0.71	0.02	0.99	0.19
30.26	31.89	4.57	1.16	27.91	1.39	97.19	1.00	0.18	0.79	0.02	0.98	0.15
30.69	31.32	4.72	1.39	28.22	2.05	96.30	0.99	0.18	0.76	0.03	0.98	0.21
31.26	31.03	5.00	1.51	28.12	1.35	97.85	1.02	0.19	0.76	0.03	0.98	0.14
31.00	30.77	5.29	1.40	28.49	1.90	98.46	1.00	0.20	0.74	0.03	0.98	0.19
31.10	30.84	5.79	1.63	28.75	1.50	96.86	1.00	0.22	0.74	0.03	0.99	0.15
Sample 9-4												
31.21	32.35	4.61	1.26	29.23	0.77	95.79	1.01	0.18	0.79	0.02	1.02	0.08
31.23	30.80	5.61	1.59	29.09	1.67	96.73	1.00	0.21	0.74	0.03	1.00	0.17
32.03	32.92	5.21	0.91	29.54	1.65	96.47	1.00	0.19	0.77	0.02	0.99	0.16
30.53	31.46	5.29	1.44	28.28	1.48	94.98	0.99	0.20	0.77	0.03	0.98	0.15
30.99	30.57	6.07	1.53	28.77	1.88	96.10	0.99	0.23	0.73	0.03	0.98	0.19
31.64	30.67	5.76	1.44	29.17	1.66	96.05	1.00	0.22	0.73	0.03	0.99	0.17
31.26	31.41	5.10	1.39	29.28	2.18	95.70	0.99	0.19	0.75	0.02	0.99	0.22
31.33	32.26	4.59	2.01	29.09	1.44	95.84	1.00	0.17	0.77	0.04	0.99	0.15
31.35	31.60	5.52	1.19	29.48	1.71	94.93	0.99	0.21	0.75	0.02	1.00	0.17
30.82	31.48	4.71	1.64	29.00	2.03	96.01	0.99	0.18	0.76	0.03	0.99	0.21
30.78	33.06	5.02	1.31	28.44	1.69	96.39	0.98	0.19	0.79	0.02	0.97	0.17
31.10	32.00	5.03	1.38	28.44	1.59	95.07	1.00	0.19	0.77	0.02	0.97	0.16
Sample 7-9B												
29.85	33.74	3.82	2.94	28.97	1.48	96.99	0.96	0.15	0.82	0.05	1.00	0.15
30.70	33.60	3.58	2.89	28.91	1.61	96.84	0.98	0.13	0.80	0.05	0.98	0.16
30.72	33.66	3.71	2.85	28.61	1.39	95.61	0.98	0.14	0.81	0.05	0.98	0.14
29.65	32.81	3.77	2.91	29.07	1.17	96.46	0.97	0.15	0.81	0.05	1.02	0.12
29.70	32.73	3.69	2.91	29.10	1.12	95.75	0.97	0.14	0.81	0.05	1.02	0.12
30.34	32.93	3.90	3.00	29.09	0.89	96.56	0.99	0.15	0.81	0.05	1.01	0.09
29.92	33.01	3.76	2.77	29.39	1.73	95.63	0.96	0.14	0.80	0.05	1.01	0.18
30.22	32.66	3.81	3.30	29.05	1.66	94.95	0.97	0.14	0.79	0.06	1.00	0.17
28.75	33.47	3.78	2.97	29.06	1.71	95.94	0.94	0.14	0.82	0.05	1.01	0.18
Sample GNA02												
28.84	35.72	2.27	2.49	28.57	0.98	96.05	0.95	0.09	0.89	0.05	1.01	0.10

29.13	35.81	2.24	3.03	28.59	1.51	98.02	0.95	0.09	0.87	0.05	0.99	0.16
28.85	35.74	2.07	2.71	28.55	1.03	95.01	0.95	0.08	0.89	0.05	1.01	0.11
28.31	34.67	2.32	2.94	28.16	0.58	97.65	0.96	0.09	0.88	0.06	1.02	0.06
28.60	36.26	1.97	3.00	28.41	0.80	96.66	0.95	0.08	0.90	0.06	1.01	0.08
28.89	35.47	2.29	3.22	28.05	0.75	97.21	0.96	0.09	0.88	0.06	1.00	0.08
30.72	35.47	2.10	2.92	27.09	1.77	96.11	0.99	0.08	0.86	0.05	0.93	0.18
30.53	35.70	1.85	2.76	26.91	1.01	94.06	1.00	0.07	0.88	0.05	0.94	0.10
30.64	36.29	1.66	2.47	26.78	1.48	96.58	0.99	0.06	0.88	0.04	0.93	0.15
30.80	34.84	2.38	2.94	26.71	1.26	95.37	1.00	0.09	0.85	0.05	0.93	0.13
30.65	34.26	2.42	2.82	27.07	1.43	95.52	1.00	0.09	0.84	0.05	0.95	0.15
Sample ALB 05												
30.77	35.71	0.62	1.67	27.20	n.m.	96.05	1.05	0.02	0.91	0.03	0.99	0.00
30.79	37.07	0.43	1.12	27.28	n.m.	98.02	1.04	0.02	0.94	0.02	0.98	0.00
30.87	37.40	0.63	1.19	27.46	n.m.	95.01	1.03	0.02	0.94	0.02	0.98	0.00
31.29	38.38	0.22	0.76	28.34	n.m.	97.65	1.03	0.01	0.95	0.01	1.00	0.00
30.60	37.69	0.28	0.78	27.67	n.m.	97.21	1.03	0.01	0.95	0.01	1.00	0.00
31.12	38.60	0.27	0.70	28.43	n.m.	96.11	1.02	0.01	0.96	0.01	1.00	0.00
31.04	38.38	0.30	0.84	28.43	n.m.	94.06	1.02	0.01	0.95	0.02	1.00	0.00
30.85	37.03	0.37	1.35	28.05	n.m.	96.58	1.03	0.015	0.932	0.025	1.006	0.000
30.61	37.78	0.25	0.70	28.28	n.m.	95.37	1.02	0.010	0.949	0.013	1.013	0.000
30.42	36.66	0.36	1.61	27.47	n.m.	95.17	1.03	0.015	0.935	0.030	0.998	0.000
30.73	36.82	0.91	1.60	27.73	n.m.	95.02	1.03	0.036	0.925	0.030	0.993	0.000
30.73	37.16	0.42	1.28	28.03	n.m.	94.87	1.03	0.02	0.94	0.02	1.00	0.00
30.74	37.81	0.34	1.32	28.51	n.m.	94.72	1.02	0.01	0.94	0.02	1.01	0.00
31.31	37.63	0.47	1.15	28.46	n.m.	94.58	1.03	0.02	0.93	0.02	1.01	0.00
31.06	37.27	0.49	1.23	28.21	n.m.	94.43	1.03	0.02	0.93	0.02	1.00	0.00
31.09	37.36	0.44	1.28	28.09	n.m.	94.28	1.03	0.02	0.93	0.02	1.00	0.00
30.62	37.01	0.33	1.17	27.57	n.m.	94.13	1.03	0.01	0.94	0.02	1.00	0.00
30.37	36.52	0.64	1.45	27.84	n.m.	93.98	1.03	0.03	0.93	0.03	1.01	0.00
31.08	37.61	0.47	1.34	28.16	n.m.	93.84	1.03	0.02	0.94	0.02	1.00	0.00
31.21	37.84	0.43	1.40	28.67	n.m.	93.69	1.03	0.02	0.93	0.03	1.01	0.00
31.18	37.94	0.39	1.32	28.20	n.m.	93.54	1.03	0.02	0.94	0.02	1.00	0.00
Sample POAB 05												
30.94	35.27	0.55	0.90	28.34	0.27	96,200	1.05	0.02	0.90	0.02	1.03	0.03
30.39	37.29	0.37	0.64	28.34	0.06	97,100	1.02	0.01	0.94	0.01	1.02	0.01
31.31	36.38	1.16	0.86	28.08	0.45	98,098	1.03	0.04	0.90	0.02	0.99	0.05
31.47	36.57	0.68	0.68	28.67	0.32	98,295	1.04	0.03	0.91	0.01	1.01	0.03
30.45	34.88	0.34	0.97	27.88	0.21	94,686	1.05	0.01	0.90	0.02	1.03	0.02
31.49	37.04	0.38	0.47	28.91	0.25	98,442	1.04	0.01	0.92	0.01	1.02	0.03
31.47	37.10	0.47	0.54	28.93	0.63	98,908	1.03	0.02	0.91	0.01	1.01	0.06
Sample BIAB 129												
29.40	39.13	0.54	0.13	28.33	n.m.	97.56	0.99	0.02	0.99	0.00	1.02	0.00
29.84	38.14	0.65	0.20	28.47	n.m.	97.46	1.00	0.03	0.96	0.00	1.02	0.00

30.26	37.34	0.77	0.34	28.61	n.m.	97.35	1.02	0.03	0.94	0.01	1.03	0.00
30.43	36.96	0.68	0.20	28.55	n.m.	96.83	1.03	0.03	0.94	0.00	1.03	0.00
30.37	38.49	0.52	0.21	28.73	n.m.	98.34	1.01	0.02	0.96	0.00	1.02	0.00
30.82	37.33	0.72	0.31	28.62	n.m.	97.82	1.03	0.03	0.94	0.01	1.02	0.00
30.16	38.58	0.75	0.15	28.66	n.m.	98.31	1.00	0.03	0.96	0.00	1.02	0.00

2D: Zr-in-titanite geothermometry

			PRESSURE (Gpa)								
	Sample	Zr90	0.1	0.2	0.3	0.4	0.5	0.6	0.7	0.8	0.9
HAFG	GRA-01	95.72	609.80	620.66	631.52	642.38	653.24	664.10	674.96	685.82	696.68
HAFG	GRA-01	77.84	600.92	611.67	622.42	633.17	643.92	654.67	665.43	676.18	686.93
HAFG	GRA-01	83.81	604.08	614.87	625.66	636.45	647.24	658.03	668.82	679.60	690.39
HAFG	GRA-01	81.34	602.80	613.57	624.35	635.12	645.89	656.67	667.44	678.21	688.99
HAFG	GRA-01	451.04	682.57	694.33	706.08	717.84	729.59	741.35	753.10	764.86	776.61
HAFG	GRA-01	68.29	595.40	606.08	616.76	627.44	638.13	648.81	659.49	670.17	680.86
HAFG	GRA-01	82.58	603.44	614.23	625.01	635.79	646.57	657.35	668.13	678.91	689.70
HAFG	GRA-01	72.51	597.92	608.64	619.35	630.06	640.78	651.49	662.20	672.92	683.63
HAFG	GRA-01	72.22	597.75	608.46	619.17	629.89	640.60	651.31	662.02	672.73	683.44
HAFG	GRA-01	82.55	603.43	614.21	624.99	635.77	646.55	657.34	668.12	678.90	689.68
HAFG	GRA-01	204.95	644.10	655.39	666.67	677.95	689.23	700.51	711.79	723.08	734.36
HAFG	GRA-01	84.59	604.48	615.27	626.06	636.86	647.65	658.45	669.24	680.04	690.83
HAFG	GRA-01	72.06	597.66	608.37	619.08	629.79	640.50	651.21	661.92	672.63	683.34
HAFG	GRA-01	74.42	599.02	609.75	620.47	631.20	641.93	652.66	663.38	674.11	684.84
HAFG	GRA-01	78.90	601.50	612.26	623.02	633.77	644.53	655.29	666.05	676.80	687.56
HAFG	GRA-01	86.01	605.19	615.99	626.79	637.59	648.40	659.20	670.00	680.81	691.61
HAFG	GRA-01	230.59	649.66	661.01	672.36	683.71	695.06	706.41	717.76	729.11	740.46
HAFG GNEISS	9-4	64.13	592.77	603.42	614.07	624.72	635.37	646.02	656.67	667.32	677.97
HAFG GNEISS	9-4	56.76	587.71	598.29	608.88	619.47	630.06	640.65	651.23	661.82	672.41
HAFG GNEISS	9-4	61.57	591.07	601.70	612.33	622.96	633.59	644.21	654.84	665.47	676.10
HAFG GNEISS	9-4	66.76	594.45	605.12	615.79	626.46	637.13	647.80	658.47	669.14	679.81
HAFG GNEISS	9-4	58.06	588.64	599.24	609.83	620.43	631.03	641.63	652.23	662.83	673.43
HAFG GNEISS	9-4	50.38	582.81	593.34	603.87	614.40	624.93	635.45	645.98	656.51	667.04
HAFG GNEISS	9-4	60.45	590.31	600.93	611.55	622.17	632.79	643.41	654.03	664.65	675.27
HAFG GNEISS	9-4	62.73	591.85	602.49	613.13	623.77	634.40	645.04	655.68	666.32	676.96
HAFG GNEISS	9-4	57.96	588.57	599.17	609.77	620.37	630.97	641.56	652.16	662.76	673.36
HAFG GNEISS	9-4	70.46	596.71	607.41	618.11	628.81	639.51	650.20	660.90	671.60	682.30
HAFG GNEISS	9-4	57.78	588.44	599.04	609.63	620.23	630.83	641.42	652.02	662.62	673.21
HAFG GNEISS	9-4	72.32	597.81	608.52	619.23	629.95	640.66	651.37	662.08	672.79	683.51
HAFG GNEISS	9-4	57.91	588.53	599.13	609.73	620.33	630.92	641.52	652.12	662.72	673.32
HAFG GNEISS	9-4	54.73	586.20	596.77	607.34	617.91	628.48	639.05	649.62	660.19	670.76
HAFG GNEISS	9-4	64.45	592.97	603.63	614.28	624.93	635.58	646.24	656.89	667.54	678.19
HAFG GNEISS	9-4	58.67	589.07	599.68	610.28	620.89	631.49	642.10	652.70	663.31	673.91
HAFG GNEISS	9-4	55.23	586.58	597.15	607.73	618.30	628.88	639.45	650.02	660.60	671.17
HAFG GNEISS	9-4	184.00	639.09	650.31	661.53	672.75	683.97	695.19	706.41	717.63	728.85
HAFG GNEISS	9-4	116.44	618.38	629.35	640.31	651.28	662.24	673.21	684.17	695.14	706.10
HAFG GNEISS	9-4	198.62	642.64	653.90	665.17	676.43	687.69	698.96	710.22	721.48	732.75
HAFG GNEISS	9-4	97.57	610.64	621.51	632.38	643.25	654.12	664.99	675.86	686.73	697.60
HAFG GNEISS	9-4	64.45	592.97	603.63	614.28	624.93	635.58	646.24	656.89	667.54	678.19
HAFG GNEISS	9-4	77.53	600.75	611.50	622.25	633.00	643.75	654.50	665.24	675.99	686.74
HAFG GNEISS	9-4	64.52	593.02	603.67	614.32	624.98	635.63	646.28	656.94	667.59	678.24
HAFG GNEISS	9-4	69.05	595.86	606.55	617.24	627.93	638.62	649.31	659.99	670.68	681.37

HAFG GNEISS	9-4	56.06	587.20	597.78	608.36	618.94	629.52	640.10	650.69	661.27	671.85
HAFG GNEISS	9-4	56.08	587.21	597.79	608.37	618.96	629.54	640.12	650.70	661.28	671.87
HAFG GNEISS	9-4	198.65	642.65	653.91	665.17	676.44	687.70	698.96	710.23	721.49	732.76
HAFG GNEISS	9-4	160.71	632.86	644.01	655.15	666.29	677.44	688.58	699.72	710.87	722.01
HAFG GNEISS	9-4	103.38	613.15	624.05	634.95	645.86	656.76	667.66	678.56	689.46	700.36
HAFG GNEISS	9-4	83.00	603.66	614.44	625.23	636.01	646.80	657.58	668.36	679.15	689.93
HAFG GNEISS	9-4	77.33	600.65	611.39	622.14	632.89	643.64	654.38	665.13	675.88	686.62
HAFG GNEISS	9-4	60.13	590.09	600.71	611.32	621.94	632.56	643.17	653.79	664.41	675.03
GRAAB	7-1B	123.63	621.04	632.04	643.04	654.03	665.03	676.03	687.03	698.03	709.02
GRAAB	7-1B	187.13	639.87	651.10	662.33	673.56	684.79	696.02	707.24	718.47	729.70
GRAAB	7-1B	144.05	627.89	638.97	650.06	661.14	672.22	683.30	694.39	705.47	716.55
GRAAB	7-1B	140.73	626.84	637.91	648.98	660.05	671.12	682.19	693.26	704.33	715.39
GRAAB	7-1B	140.00	626.61	637.67	648.74	659.81	670.87	681.94	693.00	704.07	715.14
GRAAB	7-1B	164.62	633.96	645.12	656.28	667.43	678.59	689.75	700.90	712.06	723.22
GRAAB	7-1B	150.82	629.97	641.08	652.19	663.29	674.40	685.51	696.62	707.73	718.83
GRAAB	7-1B	131.40	623.76	634.79	645.82	656.85	667.88	678.92	689.95	700.98	712.01
GRAAB	7-1B	122.56	620.65	631.65	642.64	653.63	664.63	675.62	686.61	697.61	708.60
GRAAB	7-1B	87.24	605.80	616.61	627.42	638.23	649.04	659.85	670.66	681.47	692.28
GRAAB	7-1B	216.84	646.75	658.07	669.38	680.69	692.01	703.32	714.64	725.95	737.27
GRAAB	7-1B	122.68	620.70	631.69	642.68	653.68	664.67	675.67	686.66	697.65	708.65
GRAAB	7-1B	184.94	639.32	650.55	661.77	672.99	684.21	695.44	706.66	717.88	729.11
GRAAB	7-1B	117.39	618.74	629.71	640.68	651.65	662.62	673.59	684.56	695.53	706.50
GRAAB	7-1B	756.98	709.63	721.72	733.81	745.89	757.98	770.07	782.16	794.24	806.33
GRAAB	7-1B	216.32	646.64	657.95	669.26	680.58	691.89	703.20	714.52	725.83	737.14
GRAAB	7-1B	135.15	625.02	636.07	647.12	658.16	669.21	680.26	691.30	702.35	713.40
GRAAB	7-1B	129.25	623.02	634.04	645.07	656.09	667.11	678.13	689.16	700.18	711.20
GRAAB	7-1B	154.45	631.05	642.17	653.29	664.41	675.54	686.66	697.78	708.90	720.02
GRAAB	7-1B	575.54	695.12	707.03	718.94	730.85	742.76	754.67	766.58	778.49	790.40
GRAAB	7-1B	113.54	617.27	628.22	639.17	650.12	661.08	672.03	682.98	693.93	704.88
GRAAB	7-1B	281.03	659.12	670.59	682.06	693.52	704.99	716.46	727.92	739.39	750.86
GRAAB	7-1B	154.60	631.10	642.22	653.34	664.46	675.58	686.71	697.83	708.95	720.07
GRAAB	7-1B	172.70	636.16	647.34	658.53	669.71	680.90	692.08	703.26	714.45	725.63
GRAAB	7-1B	169.56	635.32	646.49	657.67	668.84	680.01	691.19	702.36	713.53	724.71
GRAAB	7-1B	182.85	638.80	650.01	661.23	672.44	683.66	694.88	706.09	717.31	728.53
GRAAB	7-1B	157.27	631.88	643.01	654.14	665.27	676.40	687.53	698.66	709.79	720.93
MAAB	GNA02	98.39	611.00	621.87	632.74	643.62	654.49	665.37	676.24	687.12	697.99
MAAB	GNA02	100.29	611.83	622.71	633.60	644.48	655.37	666.25	677.14	688.02	698.91
MAAB	GNA02	93.45	608.76	619.61	630.46	641.31	652.15	663.00	673.85	684.69	695.54
MAAB	GNA02	98.49	611.04	621.92	632.79	643.67	654.54	665.42	676.29	687.17	698.04
MAAB	GNA02	65.16	593.43	604.09	614.75	625.41	636.06	646.72	657.38	668.04	678.70
MAAB	GNA02	89.98	607.13	617.96	628.78	639.61	650.44	661.26	672.09	682.92	693.74
MAAB	GNA02	108.17	615.14	626.06	636.99	647.91	658.84	669.77	680.69	691.62	702.54
MAAB	GNA02	112.65	616.92	627.87	638.82	649.77	660.71	671.66	682.61	693.55	704.50
MAAB	GNA02	79.63	601.89	612.66	623.42	634.18	644.94	655.70	666.47	677.23	687.99
MAAB	GNA02	49.13	581.80	592.31	602.83	613.34	623.86	634.37	644.89	655.40	665.92
MAAB	GNA02	109.45	615.65	626.59	637.52	648.45	659.38	670.31	681.24	692.18	703.11

MAAB	GNA02	100.79	612.04	622.93	633.82	644.71	655.59	666.48	677.37	688.26	699.14
MAAB	GNA02	121.42	620.24	631.23	642.21	653.20	664.19	675.18	686.17	697.16	708.14
MAAB	GNA02	94.98	609.47	620.32	631.18	642.03	652.89	663.74	674.60	685.45	696.31
MAAB	GNA02	63.97	592.67	603.31	613.96	624.61	635.26	645.91	656.56	667.21	677.86
MAAB	GNA02	86.31	605.34	616.14	626.95	637.75	648.56	659.36	670.17	680.97	691.78
MAAB	GNA02	143.93	627.86	638.94	650.02	661.10	672.18	683.27	694.35	705.43	716.51
MAAB	GNA02	89.84	607.06	617.89	628.71	639.54	650.37	661.19	672.02	682.84	693.67
MAAB	GNA02	99.48	611.48	622.36	633.24	644.12	655.00	665.88	676.76	687.64	698.52
MAAB	GNA02	109.33	615.60	626.54	637.47	648.40	659.33	670.26	681.19	692.12	703.05
MINERALIZADO	ALB05	102.32	612.71	623.60	634.50	645.39	656.29	667.18	678.08	688.97	699.87
MINERALIZADO	ALB05	100.06	611.73	622.61	633.50	644.38	655.26	666.15	677.03	687.91	698.80
MINERALIZADO	ALB05	197.09	642.28	653.54	664.80	676.06	687.32	698.58	709.83	721.09	732.35
MINERALIZADO	ALB05	1049.08	727.48	739.79	752.10	764.41	776.71	789.02	801.33	813.64	825.94
MINERALIZADO	ALB05	613.17	698.44	710.39	722.34	734.29	746.24	758.19	770.14	782.09	794.04
MINERALIZADO	ALB05	7492.58	850.46	864.28	878.10	891.92	905.74	919.56	933.38	947.20	961.02
MINERALIZADO	ALB05	595.40	696.90	708.83	720.76	732.69	744.62	756.55	768.48	780.41	792.34
MINERALIZADO	ALB05	923.12	720.41	732.63	744.85	757.07	769.29	781.51	793.73	805.95	818.17
MINERALIZADO	ALB05	1282.15	738.79	751.23	763.68	776.13	788.57	801.02	813.46	825.91	838.36
MINERALIZADO	ALB05	925.48	720.55	732.77	744.99	757.22	769.44	781.66	793.88	806.10	818.33
MINERALIZADO	ALB05	110.53	616.09	627.02	637.96	648.90	659.84	670.77	681.71	692.65	703.58
MINERALIZADO	ALB05	289.07	660.49	671.97	683.46	694.94	706.42	717.91	729.39	740.87	752.35
MINERALIZADO	ALB05	211.39	645.56	656.86	668.16	679.46	690.75	702.05	713.35	724.65	735.95
MINERALIZADO	ALB05	321.10	665.61	677.16	688.71	700.25	711.80	723.35	734.89	746.44	757.98
MINERALIZADO	ALB05	330.40	667.02	678.58	690.14	701.71	713.27	724.83	736.40	747.96	759.52
MINERALIZADO	ALB05	224.20	648.33	659.66	670.99	682.33	693.66	704.99	716.33	727.66	738.99
MINERALIZADO	ALB05	235.53	650.66	662.02	673.39	684.75	696.11	707.47	718.84	730.20	741.56
MINERALIZADO	ALB05	120.30	619.83	630.81	641.79	652.78	663.76	674.74	685.73	696.71	707.69
MINERALIZADO	ALB05	217.32	646.86	658.17	669.49	680.80	692.12	703.43	714.75	726.06	737.38
MINERALIZADO	ALB05	246.15	652.76	664.15	675.54	686.92	698.31	709.70	721.09	732.48	743.87
MINERALIZADO	BIAB129	226.52	648.81	660.15	671.49	682.83	694.17	705.51	716.85	728.19	739.53
MINERALIZADO	BIAB129	716.00	706.65	718.70	730.75	742.80	754.85	766.90	778.96	791.01	803.06
MINERALIZADO	BIAB129	467.26	684.37	696.15	707.93	719.70	731.48	743.26	755.04	766.81	778.59
MINERALIZADO	BIAB129	133.20	624.37	635.41	646.45	657.49	668.52	679.56	690.60	701.64	712.68
MINERALIZADO	BIAB129	289.16	660.51	671.99	683.47	694.96	706.44	717.92	729.41	740.89	752.37
MINERALIZADO	BIAB129	75.54	599.65	610.38	621.12	631.85	642.59	653.32	664.06	674.79	685.53
MINERALIZADO	poab05	511.09	688.97	700.80	712.64	724.47	736.30	748.14	759.97	771.80	783.64
MINERALIZADO	poab05	387.61	674.93	686.60	698.26	709.92	721.58	733.24	744.90	756.56	768.22
MINERALIZADO	poab05	57.47	588.22	598.81	609.41	620.00	630.59	641.19	651.78	662.38	672.97
MINERALIZADO	poab05	265.98	656.47	667.90	679.34	690.77	702.20	713.64	725.07	736.51	747.94
MINERALIZADO	poab05	356.73	670.80	682.41	694.02	705.63	717.24	728.85	740.46	752.07	763.68
MINERALIZADO	poab05	269.68	657.14	668.58	680.02	691.46	702.90	714.35	725.79	737.23	748.67
MINERALIZADO	poab05	326.61	666.45	678.00	689.56	701.12	712.67	724.23	735.79	747.34	758.90
MINERALIZADO	poab05	2457.45	777.26	790.18	803.10	816.02	828.94	841.86	854.78	867.70	880.62
MINERALIZADO	poab05	3440.60	798.33	811.51	824.69	837.87	851.05	864.23	877.40	890.58	903.76
MINERALIZADO	poab05	127.49	622.41	633.43	644.44	655.45	666.47	677.48	688.50	699.51	710.53
MINERALIZADO	poab05	1294.03	739.31	751.76	764.22	776.67	789.12	801.58	814.03	826.48	838.93

MINERALIZADO	poab05	697.77	705.27	717.31	729.34	741.38	753.41	765.44	777.48	789.51	801.55
MINERALIZADO	poab05	744.34	708.73	720.80	732.88	744.96	757.03	769.11	781.19	793.26	805.34

Anexo 3 (Appendix 3) – Mineral chemistry analyses
3A: Microprobe analyses of K-feldspar and recalculated formula on the basis of 16 oxygens.

Sample	Rock	SiO2	Al2O3	CaO	Na2O	K2O	TOTAL	Si	Al	Ca	Na	K	Total	An	Ab	Or
8_11	HAFG	64.19	19.42	0.01	1.06	15.75	100.4	5.91	2.11	0.00	0.19	1.85	10.06	0.03	9.24	90.73
8_11	HAFG	64.69	19.55	0.00	1.13	15.71	101.1	5.91	2.11	0.00	0.20	1.83	10.05	0.00	9.84	90.16
8_11	HAFG	64.75	19.53	0.00	0.88	15.76	100.9	5.92	2.11	0.00	0.16	1.84	10.02	0.00	7.82	92.18
8_11	HAFG	63.14	19.62	0.00	1.23	15.15	99.1	5.88	2.15	0.00	0.22	1.80	10.05	0.00	10.98	89.02
8_11	HAFG	64.41	19.39	0.01	0.94	15.89	100.6	5.92	2.10	0.00	0.17	1.86	10.05	0.05	8.24	91.71
8_11	HAFG	64.23	19.26	0.02	0.58	16.11	100.2	5.93	2.10	0.00	0.10	1.90	10.02	0.07	5.15	94.77
8_11	HAFG	63.88	19.27	0.01	1.09	15.69	99.9	5.91	2.10	0.00	0.20	1.85	10.06	0.03	9.57	90.40
8_11	HAFG	64.81	19.21	0.02	1.52	14.85	100.4	5.94	2.08	0.00	0.27	1.74	10.02	0.08	13.47	86.46
8_11	HAFG	64.40	19.19	0.01	0.80	15.91	100.3	5.93	2.08	0.00	0.14	1.87	10.03	0.04	7.11	92.85
8_11	HAFG	64.77	19.33	0.01	1.04	15.76	100.9	5.93	2.09	0.00	0.18	1.84	10.04	0.03	9.12	90.84
8_11	HAFG	64.19	19.30	0.01	1.03	15.65	100.2	5.92	2.10	0.00	0.18	1.84	10.04	0.07	9.05	90.88
GRA01	HAFG	64.15	19.31	0.01	1.27	15.37	100.1	5.92	2.10	0.00	0.23	1.81	10.05	0.03	11.15	88.82
GRA01	HAFG	64.43	19.28	0.03	1.08	15.35	100.2	5.93	2.09	0.00	0.19	1.80	10.02	0.16	9.64	90.20
GRA01	HAFG	65.02	19.26	0.01	0.61	16.29	101.2	5.94	2.07	0.00	0.11	1.90	10.02	0.04	5.34	94.62
GRA01	HAFG	65.30	19.41	0.00	0.62	16.03	101.4	5.95	2.08	0.00	0.11	1.86	10.00	0.00	5.59	94.41
GRA01	HAFG	64.21	19.10	0.01	0.61	15.89	99.8	5.94	2.08	0.00	0.11	1.88	10.01	0.06	5.52	94.42
GRA01	HAFG	64.65	19.34	0.01	0.69	16.03	100.7	5.93	2.09	0.00	0.12	1.88	10.02	0.07	6.15	93.78
GRA01	HAFG	64.67	19.33	0.01	0.65	15.95	100.6	5.94	2.09	0.00	0.12	1.87	10.01	0.04	5.85	94.11
GRA01	HAFG	64.50	19.10	0.00	0.65	15.94	100.2	5.95	2.08	0.00	0.12	1.87	10.01	0.00	5.82	94.18
GRA01	HAFG	65.15	19.39	0.02	0.82	16.16	101.5	5.93	2.08	0.00	0.14	1.88	10.04	0.11	7.15	92.74
GRA01	HAFG	64.85	19.50	0.01	1.02	15.66	101.0	5.92	2.10	0.00	0.18	1.83	10.03	0.07	8.99	90.95
GRA01	HAFG	63.42	19.17	0.02	0.87	15.30	98.8	5.92	2.11	0.00	0.16	1.82	10.01	0.11	7.96	91.93
GRA01	HAFG	64.47	19.30	0.00	0.88	15.80	100.5	5.93	2.09	0.00	0.16	1.85	10.03	0.00	7.77	92.23
GRA01	HAFG	64.84	19.23	0.02	0.90	16.03	101.0	5.94	2.07	0.00	0.16	1.87	10.04	0.10	7.89	92.01
GRA01	HAFG	64.51	19.47	0.00	0.37	16.38	100.7	5.92	2.11	0.00	0.07	1.92	10.01	0.00	3.30	96.70
GRA01	HAFG	63.49	19.55	0.00	0.23	16.10	99.4	5.91	2.14	0.00	0.04	1.91	10.00	0.00	2.09	97.91
GRA01	HAFG	64.11	19.28	0.01	0.49	16.11	100.0	5.93	2.10	0.00	0.09	1.90	10.02	0.03	4.41	95.56
GRA01	HAFG	65.01	19.18	0.01	0.81	15.87	100.9	5.95	2.07	0.00	0.14	1.85	10.01	0.02	7.21	92.77
GRA01	HAFG	63.86	19.15	0.02	0.39	16.36	99.8	6.03	2.09	0.00	0.07	1.94	10.03	0.07	3.53	96.40
GRA01	HAFG	64.99	18.17	0.02	0.36	16.16	99.7	6.02	1.98	0.00	0.06	1.91	9.98	0.11	3.28	96.61
GRA01	HAFG	65.99	18.50	0.02	0.57	15.68	100.9	5.95	1.99	0.00	0.10	1.83	9.95	0.11	5.19	94.71
GRA01	HAFG	64.89	19.43	0.03	0.64	16.10	101.1	5.96	2.09	0.00	0.11	1.88	10.02	0.16	5.71	94.14
GRA01	HAFG	64.23	18.71	0.00	0.83	15.78	99.6	6	2.05	0.00	0.15	1.87	10.02	0.00	7.43	92.57

9-4	HAFGg	66.36	18.47	0.00	0.51	15.38	100.7	6.04	1.98	0.00	0.09	1.79	9.90	0.00	4.84	95.16
9-4	HAFGg	64.16	19.38	0.00	1.09	15.71	100.3	5.91	2.10	0.00	0.19	1.85	10.06	0.00	9.55	90.45
9-4	HAFGg	64.73	19.26	0.01	1.00	15.88	100.9	5.93	2.08	0.00	0.18	1.86	10.04	0.03	8.71	91.26
9-4	HAFGg	65.15	19.63	0.41	3.31	12.20	100.7	5.91	2.10	0.04	0.58	1.41	10.04	1.96	28.62	69.42
9-4	HAFGg	63.33	19.24	0.01	0.82	15.86	99.3	5.91	2.11	0.00	0.15	1.89	10.05	0.04	7.25	92.71
9-4	HAFGg	63.75	19.44	0.00	0.82	15.98	100.0	5.90	2.12	0.00	0.15	1.89	10.05	0.00	7.21	92.79
9-4	HAFGg	64.17	19.44	0.01	0.79	15.83	100.2	5.92	2.11	0.00	0.14	1.86	10.03	0.05	7.06	92.89
9-4	HAFGg	64.70	19.39	0.01	0.72	15.92	100.7	5.93	2.09	0.00	0.13	1.86	10.02	0.02	6.43	93.54
9-4	HAFGg	64.06	19.20	0.00	0.83	15.65	99.7	5.93	2.09	0.00	0.15	1.85	10.02	0.00	7.45	92.55
9-4	HAFGg	64.25	19.45	0.01	0.82	16.25	100.8	5.91	2.11	0.00	0.15	1.91	10.07	0.03	7.08	92.88
9-4	HAFGg	64.23	19.39	0.02	0.51	16.16	100.3	5.92	2.11	0.00	0.09	1.90	10.02	0.08	4.54	95.38
9-4	HAFGg	64.51	19.26	0.00	0.58	16.31	100.7	5.93	2.09	0.00	0.10	1.91	10.03	0.00	5.09	94.91
ALB-01	AB	64.76	18.22	0.01	0.26	15.95	99.2	6.02	2.00	0.00	0.05	1.89	9.95	0.06	2.40	97.55
ALB-01	AB	62.95	19.22	0.01	0.36	16.38	98.9	5.90	2.12	0.00	0.06	1.96	10.05	0.05	3.21	96.75
ALB-01	AB	61.95	19.37	0.00	0.22	16.69	98.2	5.86	2.16	0.00	0.04	2.02	10.08	0.01	1.97	98.01
ALB-01	AB	62.41	19.34	0.01	0.35	16.43	98.5	5.88	2.15	0.00	0.06	1.97	10.07	0.02	3.14	96.84
ALB-01	AB	63.60	19.12	0.01	0.28	16.44	99.5	5.92	2.10	0.00	0.05	1.95	10.03	0.05	2.50	97.45
ALB-01	AB	63.16	19.13	0.00	0.39	16.43	99.1	5.91	2.11	0.00	0.07	1.96	10.05	0.00	3.49	96.51
ALB-01	AB	63.01	18.95	0.00	0.36	16.56	98.9	5.91	2.10	0.00	0.07	1.98	10.06	0.00	3.23	96.77
GNA04	AB	61.02	19.03	0.01	0.91	15.85	96.8	5.86	2.15	0.00	0.17	1.94	10.12	0.05	8.04	91.91
GNA04	AB	64.03	18.89	0.01	0.93	15.69	99.5	5.94	2.07	0.00	0.17	1.86	10.04	0.04	8.23	91.73
GNA04	AB	63.52	19.01	0.01	0.56	16.08	99.2	5.93	2.09	0.00	0.10	1.91	10.03	0.04	5.04	94.92
GNA04	AB	62.69	19.19	0.00	0.63	15.73	98.2	5.90	2.13	0.00	0.12	1.89	10.04	0.01	5.76	94.24
GNA04	AB	64.51	18.93	0.01	0.66	15.94	100.1	5.96	2.06	0.00	0.12	1.88	10.01	0.06	5.91	94.03
GNA04	AB	64.44	18.84	0.01	0.71	15.87	99.9	5.96	2.05	0.00	0.13	1.87	10.01	0.04	6.35	93.61

3B: EPMA analyses of plagioclase. Recalculated formula on the basis of 16 oxygens.

Type	Sample	An	ROCK	SiO2	Al2O3	CaO	Na2O	K2O	TOTAL	Si	Al	Ca	Na	K	An	Ab	Or
PAT	8_11	31	HAFG	63.35	22.97	4.20	8.18	0.25	99.0	5.63	2.41	0.40	1.41	0.03	21.8	76.7	1.5
PAT	8_11	31	HAFG	63.44	23.12	4.23	8.03	0.23	99.1	5.63	2.42	0.40	1.38	0.03	22.2	76.3	1.4
PAT	8_11	31	HAFG	63.74	22.95	4.30	8.19	0.20	99.4	5.64	2.39	0.41	1.41	0.02	22.2	76.6	1.2
PAT	8_11	31	HAFG	62.49	24.44	4.17	10.21	0.19	101.5	5.47	2.52	0.39	1.73	0.02	18.2	80.8	1.0
PAT	8_11	31	HAFG	62.49	24.69	4.06	9.85	0.24	101.3	5.47	2.55	0.38	1.67	0.03	18.3	80.4	1.3
PAT	8_11	31	HAFG	63.32	24.63	4.17	9.83	0.26	102.2	5.50	2.52	0.39	1.65	0.03	18.7	79.9	1.4
PAT	8_11	31	HAFG	63.37	24.10	3.36	9.69	0.70	101.2	5.55	2.49	0.31	1.65	0.08	15.4	80.7	3.9
PAT	8_11	31	HAFG	63.33	23.76	3.57	10.02	0.30	101.0	5.56	2.46	0.34	1.70	0.03	16.2	82.2	1.6
PAT	8_11	31	HAFG	61.88	24.02	3.73	10.39	0.31	100.3	5.49	2.51	0.35	1.79	0.03	16.3	82.1	1.6
PAT	8_11	31	HAFG	60.75	23.94	3.78	10.37	0.30	99.1	5.46	2.54	0.36	1.81	0.03	16.5	81.9	1.5
PAT	8_11	31	HAFG	64.21	23.40	3.00	11.08	0.20	101.9	5.59	2.40	0.28	1.87	0.02	12.9	86.1	1.0
PAT	8_11	31	HAFG	61.74	24.03	4.08	10.26	0.34	100.5	5.47	2.51	0.39	1.76	0.04	17.7	80.5	1.7
PAT	8_11	31	HAFG	64.19	23.90	3.70	10.04	0.24	102.1	5.57	2.44	0.34	1.69	0.03	16.7	82.0	1.3
PAT	8_11	31	HAFG	63.45	23.92	3.90	10.30	0.25	101.8	5.53	2.46	0.36	1.74	0.03	17.1	81.6	1.3
PHT	8_11	31	HAFG	65.09	21.81	1.49	11.64	0.16	100.2	5.73	2.26	0.14	1.99	0.02	6.6	92.6	0.8
PHT	8_11	31	HAFG	67.89	21.34	0.30	11.81	0.08	101.4	5.86	2.17	0.03	1.98	0.01	1.4	98.2	0.4
PHT	8_11	31	HAFG	64.38	21.71	1.16	12.53	0.11	99.9	5.70	2.27	0.11	2.15	0.01	4.8	94.6	0.5
PHT	8_11	31	HAFG	63.39	23.89	3.60	10.37	0.18	101.4	5.54	2.46	0.34	1.76	0.02	15.9	83.1	0.9
PAT	8_11	31	HAFG	62.03	24.28	4.15	10.18	0.22	100.9	5.47	2.52	0.39	1.74	0.02	18.2	80.7	1.2
PAT	8_11	31	HAFG	63.39	23.96	4.07	9.38	0.28	101.1	5.55	2.47	0.38	1.59	0.03	19.0	79.4	1.6
PAT	8_11	31	HAFG	63.27	23.97	4.13	9.53	0.29	101.2	5.54	2.47	0.39	1.62	0.03	19.0	79.4	1.6
PAT	8_11	31	HAFG	62.88	24.41	4.36	10.27	0.30	102.2	5.48	2.51	0.41	1.73	0.03	18.7	79.8	1.5
PAT	8_11	31	HAFG	62.92	24.34	4.15	9.77	0.29	101.5	5.50	2.51	0.39	1.66	0.03	18.7	79.8	1.5
PAT	8_11	31	HAFG	61.42	24.38	4.00	10.50	0.26	100.6	5.44	2.55	0.38	1.80	0.03	17.2	81.5	1.3
PAT	8_11	31	HAFG	59.42	24.52	4.17	10.31	0.40	98.8	5.37	2.61	0.40	1.81	0.05	17.9	80.1	2.0
PAT	8_11	31	HAFG	64.03	23.75	3.81	9.79	0.30	101.7	5.57	2.44	0.35	1.65	0.03	17.4	81.0	1.6
PAT	35F10-GRA01-C3-4	35	HAFG	64.98	21.85	1.80	10.93	0.27	101.7	5.74	2.27	0.17	1.87	0.03	8.2	90.3	1.5
PAT	35F10-GRA01-C3-5	35	HAFG	63.42	21.13	1.59	11.44	0.22	101.7	5.73	2.25	0.15	2.00	0.03	7.0	91.8	1.2
PAT	35F10-GRA01-C3-6	35	HAFG	61.85	21.26	1.74	11.88	0.19	101.7	5.66	2.29	0.17	2.11	0.02	7.4	91.6	1.0
POL	35F10-GRA01-C4-04	35	HAFG	63.61	22.98	2.63	9.57	0.13	101.7	5.65	2.41	0.25	1.65	0.01	13.1	86.1	0.8
POL	35F10-GRA01-C4-5	35	HAFG	64.44	22.82	2.69	9.29	0.11	101.7	5.69	2.37	0.25	1.59	0.01	13.7	85.6	0.6
POL	35F10-GRA01-C4-6	35	HAFG	63.79	23.25	3.15	10.81	0.21	101.7	5.59	2.40	0.30	1.84	0.02	13.7	85.2	1.1
POL	35F10-GRA01-C4-13	35	HAFG	66.52	22.22	1.86	11.10	0.18	101.7	5.75	2.26	0.17	1.86	0.02	8.4	90.6	1.0
POL	35F10-GRA01-C4-14	35	HAFG	64.11	22.72	2.67	10.93	0.21	101.7	5.64	2.35	0.25	1.86	0.02	11.7	87.1	1.1
POL	35F10-GRA01-C4-15	35	HAFG	63.93	23.59	3.30	9.11	1.53	101.7	5.59	2.43	0.31	1.55	0.17	15.3	76.3	8.4
POL	35F10-GRA01-C5-4	35	HAFG	60.77	23.46	3.50	9.90	0.45	101.7	5.50	2.50	0.34	1.74	0.05	15.9	81.6	2.4
POL	35F10-GRA01-C5-5	35	HAFG	63.49	24.25	3.86	10.06	0.23	101.7	5.52	2.49	0.36	1.70	0.03	17.3	81.5	1.2
PAT	35F10-GRA01-C5-6	35	HAFG	65.54	22.55	1.89	10.14	0.14	101.7	5.73	2.33	0.18	1.72	0.02	9.2	90.0	0.8
PAT	35F10-GRA01-C5-7	35	HAFG	65.41	23.04	2.64	10.56	0.18	101.7	5.67	2.35	0.24	1.77	0.02	12.0	87.0	1.0
PAT	35F10-GRA01-C3-7	35	HAFG	65.67	21.87	1.83	11.03	0.24	101.7	5.75	2.26	0.17	1.87	0.03	8.3	90.4	1.3
POL	35F10-GRA01-C3-8	35	HAFG	65.68	21.79	1.91	11.07	0.27	101.7	5.75	2.25	0.18	1.88	0.03	8.6	90.0	1.4
POL	35F10-GRA01-C3-9	35	HAFG	65.64	21.65	1.79	11.23	0.23	101.7	5.75	2.24	0.17	1.91	0.03	8.0	90.8	1.2
POL	35F10-GRA01-C3-10	35	HAFG	65.63	21.74	1.94	11.03	0.19	101.7	5.75	2.25	0.18	1.87	0.02	8.7	90.2	1.0
PAT	35F10-GRA01-C3-11	35	HAFG	65.99	21.79	1.66	11.23	0.11	101.7	5.76	2.24	0.16	1.90	0.01	7.5	91.9	0.6
PAT	35F10-GRA01-C3-12	35	HAFG	66.04	22.03	1.85	10.93	0.23	101.7	5.75	2.26	0.17	1.84	0.03	8.5	90.3	1.2
PAT	35F10-GRA01-C3-13	35	HAFG	66.71	22.34	2.06	10.82	0.20	101.7	5.75	2.27	0.19	1.81	0.02	9.4	89.5	1.1
PAT	35F10-GRA01-C3-14	35	HAFG	66.39	22.32	2.05	10.48	0.18	101.7	5.75	2.28	0.19	1.76	0.02	9.7	89.3	1.0
PAT	35F10-GRA01-C4-10	35	HAFG	64.15	21.42	1.51	12.02	0.18	101.7	5.72	2.25	0.14	2.08	0.02	6.4	92.7	0.9
PAT	35F10-GRA01-C4-11	35	HAFG	66.96	22.25	1.63	10.67	0.22	101.7	5.78	2.26	0.15	1.78	0.02	7.7	91.1	1.2
PAT	35F10-GRA01-C4-12	35	HAFG	67.03	20.63	0.50	11.24	0.14	101.7	5.89	2.14	0.05	1.91	0.02	2.4	96.8	0.8

Type	Sample	An	ROCK	SiO2	Al2O3	CaO	Na2O	K2O	TOTAL	Si	Al	Ca	Na	K	An	Ab	Or
POL	35F10-GRA01-C1-01	35	HAFG	67.15	22.25	1.62	10.96	0.17	101.7	5.77	2.25	0.15	1.83	0.02	7.5	91.6	0.9
POL	35F10-GRA01-C1-2	35	HAFG	66.81	21.81	1.55	11.03	0.19	101.7	5.79	2.23	0.14	1.85	0.02	7.2	91.8	1.0
POL	35F10-GRA01-C1-3	35	HAFG	66.34	22.01	1.65	10.79	0.16	101.7	5.77	2.26	0.15	1.82	0.02	7.7	91.4	0.9
POL	35F10-GRA01-C1-4	35	HAFG	84.06	21.11	1.55	6.12	0.09	101.7	6.31	1.87	0.12	0.89	0.01	12.2	87.0	0.8
POL	35F10-GRA01-C1-5	35	HAFG	67.07	22.30	1.67	11.31	0.22	101.7	5.76	2.26	0.15	1.88	0.02	7.4	91.4	1.2
POL	35F10-GRA01-C1-6	35	HAFG	66.60	21.61	1.39	11.16	0.15	101.7	5.80	2.22	0.13	1.88	0.02	6.4	92.8	0.8
POL	35F10-GRA01-C1-7	35	HAFG	66.92	21.89	1.54	11.10	0.14	101.7	5.79	2.23	0.14	1.86	0.02	7.1	92.1	0.8
POL	35F10-GRA01-C1-8	35	HAFG	66.73	21.87	1.50	10.86	0.22	101.7	5.79	2.24	0.14	1.83	0.02	7.0	91.8	1.2
POL	35F10-GRA01-C1-9	35	HAFG	67.08	22.05	1.60	11.07	0.19	101.7	5.78	2.24	0.15	1.85	0.02	7.3	91.6	1.0
POL	35F10-GRA01-C1-10	35	HAFG	66.20	20.00	1.36	11.55	0.18	101.7	5.87	2.09	0.13	1.98	0.02	6.1	93.0	0.9
POL	F10-5-8A-C2-1	35	HAFGg	68.07	20.30	0.94	10.00	0.11	101.7	5.96	2.09	0.09	1.70	0.01	4.9	94.4	0.7
POL	F10-5-8A-C2-2	35	HAFGg	68.60	20.13	0.44	10.18	0.09	101.7	5.99	2.07	0.04	1.72	0.01	2.3	97.1	0.6
POL	F10-5-8A-C2-3	35	HAFGg	68.60	20.21	0.57	10.13	0.09	101.7	5.98	2.08	0.05	1.71	0.01	3.0	96.5	0.6
POL	F10-5-8A-C4-1	35	HAFGg	67.39	20.82	1.36	9.57	0.17	101.7	5.91	2.15	0.13	1.63	0.02	7.2	91.7	1.1
POL	F10-5-8A-C4-2	35	HAFGg	67.63	20.73	1.36	9.50	0.17	101.7	5.92	2.14	0.13	1.61	0.02	7.3	91.6	1.1
POL	F10-5-8A-C4-3	35	HAFGg	67.76	20.60	1.22	9.62	0.22	101.7	5.93	2.13	0.11	1.63	0.02	6.4	92.2	1.4
POL	F10-5-8A-C4-4	35	HAFGg	68.49	21.10	1.02	9.76	0.20	101.7	5.92	2.15	0.09	1.64	0.02	5.4	93.4	1.3
POL	F10-5-8A-C4-5	35	HAFGg	67.42	20.43	1.18	9.71	0.18	101.7	5.94	2.12	0.11	1.66	0.02	6.2	92.6	1.2
POL	F10-5-8A-C4-6	35	HAFGg	67.44	20.59	1.15	9.71	0.17	101.7	5.93	2.13	0.11	1.65	0.02	6.1	92.9	1.0
POL	F10-5-8A-C4-7	35	HAFGg	68.31	19.83	0.51	10.04	0.16	101.7	6.00	2.05	0.05	1.71	0.02	2.7	96.3	1.0
POL	F10-5-8A-C4-8	35	HAFGg	67.76	20.60	1.13	9.65	0.16	101.7	5.94	2.13	0.11	1.64	0.02	6.0	93.0	1.0
POL	F10-5-8A-C4-9	35	HAFGg	67.71	20.43	1.03	9.72	0.15	101.7	5.95	2.12	0.10	1.66	0.02	5.5	93.6	1.0
POL	F10-9-4-C3-1	35	HAFGg	65.81	22.48	2.06	11.49	0.24	101.7	5.70	2.29	0.19	1.93	0.03	8.9	89.8	1.2
POL	F10-9-4-C3-2	35	HAFGg	66.14	22.29	2.07	10.94	0.28	101.7	5.73	2.28	0.19	1.84	0.03	9.3	89.2	1.5
POL	F10-9-4-C3-3	35	HAFGg	64.64	22.58	2.04	11.58	0.24	101.7	5.66	2.33	0.19	1.97	0.03	8.8	90.0	1.2
POL	F10-9-4-C3-4	35	HAFGg	60.81	22.45	2.02	11.88	0.23	101.7	5.56	2.42	0.20	2.10	0.03	8.5	90.4	1.1
POL	F10-9-4-C3-5	35	HAFGg	64.01	22.32	1.65	11.18	0.55	101.7	5.68	2.33	0.16	1.92	0.06	7.3	89.8	2.9
POL	F10-9-4-C3-6	35	HAFGg	66.03	22.09	1.57	11.72	0.21	101.7	5.73	2.26	0.15	1.97	0.02	6.8	92.1	1.1
POL	F10-9-4-C3-7	35	HAFGg	65.31	22.31	2.07	11.11	0.25	101.7	5.70	2.30	0.19	1.88	0.03	9.2	89.5	1.3
POL	F10-9-4-C3-8	35	HAFGg	65.50	22.47	2.12	11.26	0.23	101.7	5.69	2.30	0.20	1.90	0.03	9.3	89.5	1.2
POL	F10-9-4-C3-9	35	HAFGg	65.75	22.03	2.06	11.03	0.26	101.7	5.73	2.26	0.19	1.87	0.03	9.2	89.4	1.4
POL	F10-9-4-C3-10	35	HAFGg	66.19	22.07	1.95	10.98	0.28	101.7	5.75	2.26	0.18	1.85	0.03	8.8	89.7	1.5
POL	GNA 05 - C1 - 1	35	HAFGg	67.18	18.90	0.99	11.20	0.17	101.7	5.98	1.98	0.09	1.93	0.02	4.6	94.5	0.9
POL	GNA 05 - C1 - 2	35	HAFGg	69.96	19.60	0.35	11.86	0.18	101.7	6.00	1.98	0.03	1.97	0.02	1.6	97.5	0.9
POL	GNA 05 - C1 - 3	35	HAFGg	70.88	19.25	0.38	11.51	0.20	101.7	6.05	1.94	0.04	1.90	0.02	1.8	97.1	1.1
POL	GNA 05 - C1 - 4	35	HAFGg	71.11	20.50	0.58	11.32	0.20	101.7	5.98	2.03	0.05	1.85	0.02	2.7	96.2	1.1
POL	GNA 05 - C1 - 5	35	HAFGg	70.35	19.36	0.69	11.64	0.20	101.7	6.02	1.95	0.06	1.93	0.02	3.1	95.8	1.1
POL	GNA 05 - C1 - 6	35	HAFGg	69.26	19.72	0.98	11.47	0.21	101.7	5.97	2.00	0.09	1.92	0.02	4.4	94.4	1.1
POL	GNA 05 - C1 - 7	35	HAFGg	71.75	19.72	0.29	11.69	0.17	101.7	6.04	1.96	0.03	1.91	0.02	1.4	97.7	0.9
POL	GNA 05 - C1 - 8	35	HAFGg	70.28	19.66	0.50	11.09	0.21	101.7	6.02	1.99	0.05	1.84	0.02	2.4	96.4	1.2
POL	GNA 05 - C1 - 9	35	HAFGg	70.65	19.56	0.23	11.81	0.17	101.7	6.02	1.97	0.02	1.95	0.02	1.0	98.0	0.9
POL	GNA 05 - C1 - 10	35	HAFGg	69.22	19.60	0.26	11.41	0.11	101.7	6.00	2.00	0.02	1.92	0.01	1.2	98.1	0.6
POL	GNA 05 - C3 - 1	35	HAFGg	69.31	19.34	0.58	11.88	0.19	101.7	5.99	1.97	0.05	1.99	0.02	2.6	96.4	1.0
POL	GNA 05 - C3 - 3	35	HAFGg	65.77	19.23	0.72	11.07	0.11	101.7	5.94	2.05	0.07	1.94	0.01	3.4	95.9	0.6
POL	GNA 05 - C3 - 4	35	HAFGg	69.60	19.75	0.40	11.79	0.17	101.7	5.98	2.00	0.04	1.97	0.02	1.8	97.3	0.9
POL	GNA 05 - C3 - 6	35	HAFGg	68.80	19.48	0.51	11.66	0.20	101.7	5.98	2.00	0.05	1.97	0.02	2.3	96.6	1.1
POL	GNA 05 - C7 - 7	35	HAFGg	66.17	19.77	1.24	10.31	0.15	101.7	5.92	2.09	0.12	1.79	0.02	6.2	92.9	0.9
POL	GNA 05 - C7 - 8	35	HAFGg	66.59	19.43	1.30	10.55	0.24	101.7	5.94	2.04	0.12	1.83	0.03	6.3	92.3	1.4
POL	GNA 05 - C7 - 9	35	HAFGg	67.78	20.00	1.37	10.63	0.19	101.7	5.93	2.06	0.13	1.80	0.02	6.6	92.3	1.1
POL	GNA 05 - C7 - 10	35	HAFGg	67.32	19.48	0.97	10.79	0.18	101.7	5.96	2.03	0.09	1.85	0.02	4.7	94.3	1.0
POL	GNA 05 - C7 - 11	35	HAFGg	69.42	20.27	1.02	10.87	0.18	101.7	5.96	2.05	0.09	1.81	0.02	4.9	94.1	1.0
POL	GNA 05 - C7 - 12	35	HAFGg	69.32	19.75	0.68	10.94	0.17	101.7	6.00	2.01	0.06	1.83	0.02	3.3	95.7	1.0

Type	Sample	An	ROCK	SiO2	Al2O3	CaO	Na2O	K2O	TOTAL	Si	Al	Ca	Na	K	An	Ab	Or
POL	GNA 05 - C8 - 1	35	HAFGg	69.31	19.90	0.53	11.99	0.17	101.7	5.96	2.02	0.05	2.00	0.02	2.4	96.7	0.9
POL	GNA 05 - C8 - 2	35	HAFGg	69.28	19.71	0.59	11.48	0.18	101.7	5.98	2.01	0.05	1.92	0.02	2.7	96.3	1.0
POL	GNA 05 - C8 - 3	35	HAFGg	67.48	19.39	0.68	11.03	0.17	101.7	5.97	2.02	0.06	1.89	0.02	3.3	95.8	1.0
POL	GNA 05 - C8 - 4	35	HAFGg	66.22	19.53	1.06	10.42	0.15	101.7	5.94	2.07	0.10	1.81	0.02	5.3	93.9	0.9
POL	3409GNA01-C1-59	34	HAFGg	64.68	23.11	2.91	9.18	0.28	100.3	5.67	2.39	0.27	1.56	0.03	14.7	83.7	1.7
POL	3409GNA01-C1-61	34	HAFGg	64.80	23.10	3.07	9.36	0.26	100.7	5.67	2.38	0.29	1.59	0.03	15.1	83.4	1.5
POL	F11-9-9A-C1-1	31	HAFGg	66.98	21.28	1.77	9.78	0.09	100.0	5.86	2.19	0.17	1.66	0.01	9.0	90.4	0.6
POL	F11-9-9A-C1-2	31	HAFGg	65.75	22.28	2.75	9.22	0.12	100.2	5.75	2.30	0.26	1.56	0.01	14.0	85.2	0.7
POL	F11-9-9A-C1-3	31	HAFGg	66.89	21.16	1.83	9.76	0.11	99.8	5.86	2.18	0.17	1.66	0.01	9.3	90.0	0.7
POL	F11-9-9A-C7-1	31	HAFGg	66.96	21.04	1.86	9.61	0.19	99.7	5.87	2.17	0.17	1.63	0.02	9.5	89.3	1.1
POL	F11-9-9A-C7-2	31	HAFGg	66.82	21.39	1.85	9.56	0.17	99.9	5.85	2.21	0.17	1.62	0.02	9.6	89.4	1.0
POL	F11-9-9A-C7-3	31	HAFGg	66.77	20.52	1.24	9.91	0.08	98.5	5.91	2.14	0.12	1.70	0.01	6.4	93.1	0.5
POL	F11-9-9A-C7-4	31	HAFGg	67.05	21.07	1.74	9.48	0.11	99.5	5.88	2.18	0.16	1.61	0.01	9.1	90.2	0.7
POL	F11-9-9A-C7-6	31	HAFGg	64.43	22.23	3.10	8.70	0.20	98.8	5.73	2.33	0.30	1.50	0.02	16.3	82.5	1.2
POL	35 F10 - GNA 04 - C5 - 1	35	Alb	67.60	20.48	0.39	11.80	0.12	100.4	5.90	2.11	0.04	2.00	0.01	1.8	97.6	0.7
POL	35 F10 - GNA 04 - C5 - 2	35	Alb	65.65	21.10	0.63	12.85	0.08	100.3	5.78	2.19	0.06	2.19	0.01	2.6	97.0	0.4
POL	35 F10 - GNA 04 - C5 - 3	35	Alb	66.88	20.93	0.41	12.30	0.11	100.6	5.84	2.15	0.04	2.08	0.01	1.8	97.6	0.6
POL	F10-7-1B-C3-4	35	Alb	69.29	19.89	0.15	10.37	0.10	99.9	6.02	2.04	0.01	1.75	0.01	0.8	98.6	0.6
POL	F10-7-1B-C3-5	35	Alb	69.90	19.81	0.18	10.57	0.09	100.5	6.04	2.02	0.02	1.77	0.01	0.9	98.6	0.5
POL	F10-7-1B-C3-6	35	Alb	69.82	19.32	0.12	10.49	0.10	100.0	6.07	1.98	0.01	1.77	0.01	0.6	98.8	0.6
POL	F10-7-1B-C6-1	35	Alb	68.56	19.77	0.27	10.47	0.18	99.3	6.01	2.04	0.03	1.78	0.02	1.4	97.5	1.1
POL	31 - F10 -ALB01 -C2 - 7	31	Alb	67.70	20.56	0.29	12.04	0.11	100.7	5.89	2.11	0.03	2.03	0.01	1.3	98.1	0.6
POL	31 - F10 -ALB01 -C2 - 8	31	Alb	67.92	20.52	0.19	12.39	0.10	101.1	5.89	2.10	0.02	2.08	0.01	0.8	98.6	0.5
POL	31 - F10 -ALB01 -C2 - 9	31	Alb	68.22	20.44	0.16	12.47	0.10	101.4	5.90	2.08	0.01	2.09	0.01	0.7	98.8	0.5
POL	31 - F10 -ALB01 -C2 - 10	31	Alb	68.19	20.69	0.29	12.68	0.12	102.0	5.88	2.10	0.03	2.12	0.01	1.2	98.1	0.6
POL	31 - F10 -ALB01 -C3 - 1	31	Alb	66.84	20.76	0.19	12.71	0.13	100.6	5.84	2.14	0.02	2.15	0.01	0.8	98.5	0.7
POL	31 - F10 -ALB01 -C3 - 2	31	Alb	66.94	20.95	0.19	12.60	0.12	100.8	5.84	2.15	0.02	2.13	0.01	0.8	98.6	0.6
POL	31 - F10 -ALB01 -C3 - 3	31	Alb	66.57	21.18	0.19	12.95	0.12	101.0	5.81	2.18	0.02	2.19	0.01	0.8	98.6	0.6
POL	31 - F10 -ALB01 -C4 - 1	31	Alb	67.32	20.78	0.26	12.69	0.14	101.2	5.85	2.13	0.02	2.14	0.02	1.1	98.2	0.7
POL	31 - F10 -ALB01 -C4 - 2	31	Alb	67.73	20.70	0.27	12.54	0.14	101.4	5.87	2.11	0.02	2.11	0.02	1.2	98.1	0.7
POL	31 - F10 -ALB01 -C4 - 3	31	Alb	66.73	20.92	0.27	12.65	0.12	100.7	5.83	2.16	0.03	2.14	0.01	1.2	98.2	0.6
POL	31 - F10 -ALB01 -C4 - 4	31	Alb	64.69	21.02	0.28	12.97	0.14	99.1	5.77	2.21	0.03	2.24	0.02	1.2	98.2	0.7
POL	31 - F10 -ALB01 -C4 - 5	31	Alb	68.38	20.81	0.21	12.04	0.09	101.5	5.90	2.12	0.02	2.01	0.01	0.9	98.6	0.5
POL	31 - F10 -ALB01 -C5- 11	31	Alb	68.10	21.00	0.23	12.56	0.10	102.0	5.86	2.13	0.02	2.10	0.01	1.0	98.5	0.5
POL	31 - F10 -ALB01 -C5- 12	31	Alb	66.90	20.48	0.28	11.30	0.11	99.1	5.90	2.13	0.03	1.93	0.01	1.4	98.0	0.7
POL	31 - F10 -ALB01 -C5- 13	31	Alb	67.66	20.34	0.25	10.35	0.08	98.7	5.96	2.11	0.02	1.77	0.01	1.3	98.2	0.5
POL	35 F10 - GNA 04 - C2 - 1	35	Alb	65.63	20.81	0.19	12.61	0.08	99.3	5.82	2.17	0.02	2.17	0.01	0.8	98.8	0.4
POL	35 F10 - GNA 04 - C2 - 2	35	Alb	64.89	20.63	0.21	12.50	0.11	98.4	5.81	2.18	0.02	2.17	0.01	0.9	98.5	0.6
POL	35 F10 - GNA 04 - C2 - 3	35	Alb	65.40	20.63	0.20	12.62	0.13	99.0	5.82	2.16	0.02	2.18	0.01	0.8	98.5	0.6
POL	35 F10 - GNA 04 - C1 - 1	35	Alb	67.41	20.52	0.20	13.08	0.07	101.3	5.86	2.10	0.02	2.20	0.01	0.8	98.8	0.3
POL	35 F10 - GNA 04 - C1 - 2	35	Alb	67.57	20.41	0.25	12.68	0.08	101.0	5.88	2.09	0.02	2.14	0.01	1.1	98.5	0.4
POL	F10-7-1B-C6-2	35	Alb	69.46	20.46	0.29	10.21	0.22	100.8	5.99	2.08	0.03	1.71	0.02	1.5	97.1	1.4
POL	F10-7-1B-C6-3	35	Alb	69.08	19.64	0.26	10.15	0.21	99.5	6.04	2.02	0.02	1.72	0.02	1.4	97.3	1.3
POL	F10-7-1B-C4-1	35	Alb	70.01	19.91	0.17	10.53	0.10	100.8	6.03	2.02	0.02	1.76	0.01	0.9	98.5	0.6
POL	31 - F10 -ALB01 -C5- 1	31	Alb	68.45	20.48	0.08	12.31	0.11	101.4	5.91	2.09	0.01	2.06	0.01	0.4	99.0	0.6
POL	31 - F10 -ALB01 -C5- 2	31	Alb	67.75	20.69	0.08	12.64	0.08	101.2	5.88	2.11	0.01	2.13	0.01	0.4	99.3	0.4
POL	31 - F10 -ALB01 -C5- 3	31	Alb	67.03	20.82	0.17	12.80	0.07	100.9	5.84	2.14	0.02	2.16	0.01	0.7	98.9	0.4

POL	35 F10 - GNA 04 - C3-2	35	Alb	64.21	20.74	0.41	13.04	0.18	98.6	5.76	2.19	0.04	2.27	0.02	1.7	97.4	0.9
POL	35 F10 - GNA 04 - C3-7	35	Alb	66.84	20.54	0.38	12.19	0.13	100.1	5.87	2.12	0.04	2.07	0.01	1.7	97.6	0.7
POL	35 F10 - GNA 04 - C3-9	35	Alb	67.38	21.10	0.47	12.40	0.16	101.5	5.84	2.15	0.04	2.08	0.02	2.0	97.1	0.8
POL	35 F10 - GNA 04 - C3-10	35	Alb	66.85	21.12	0.68	12.30	0.12	101.1	5.82	2.17	0.06	2.08	0.01	2.9	96.4	0.6
POL	35 F10 - GNA 04 - C2 - 4	35	Alb	67.96	20.21	0.18	12.23	0.11	100.7	5.92	2.07	0.02	2.06	0.01	0.8	98.6	0.6
POL	35 F10 - GNA 04 - C2 - 5	35	Alb	65.71	20.63	0.28	12.36	0.20	99.2	5.83	2.16	0.03	2.13	0.02	1.2	97.7	1.0
POL	35 F10 - GNA 04 - C2 - 6	35	Alb	66.65	20.50	0.33	11.87	0.22	99.6	5.87	2.13	0.03	2.03	0.02	1.5	97.3	1.2
POL	35 F10 - GNA 04 - C1 - 4	35	Alb	68.11	20.46	0.30	11.94	0.18	101.0	5.91	2.09	0.03	2.01	0.02	1.3	97.7	1.0
POL	35 F10 - GNA 04 - C1 - 5	35	Alb	67.64	20.43	0.28	12.17	0.19	100.7	5.89	2.10	0.03	2.06	0.02	1.3	97.8	1.0
POL	35 F10 - GNA 04 - C1 - 6	35	Alb	67.97	20.53	0.26	12.14	0.20	101.1	5.90	2.10	0.02	2.04	0.02	1.2	97.8	1.0
POL	35 F10 - GNA 04 - C1 - 7	35	Alb	65.09	20.77	0.29	13.03	0.18	99.4	5.79	2.18	0.03	2.25	0.02	1.2	97.9	0.9
POL	35 F10 - GNA 04 - C1 - 8	35	Alb	65.75	20.85	0.37	12.96	0.22	100.2	5.80	2.17	0.03	2.22	0.03	1.5	97.4	1.1
POL	35 F10 - GNA 04 - C1 - 9	35	Alb	64.57	20.85	0.30	12.77	0.18	98.7	5.78	2.20	0.03	2.22	0.02	1.2	97.8	0.9
POL	35 F10 - GNA 04 - C1 - 10	35	Alb	66.78	20.39	0.29	11.44	0.20	99.1	5.90	2.12	0.03	1.96	0.02	1.4	97.5	1.1
POL	35 F10 - GNA 04 - C1 - 11	35	Alb	66.95	20.69	0.28	11.48	0.22	99.6	5.88	2.14	0.03	1.96	0.02	1.3	97.5	1.2
POL	F10-7-1B-C4-2	35	Alb	69.55	19.87	0.19	10.58	0.08	100.3	6.02	2.03	0.02	1.78	0.01	1.0	98.5	0.5
POL	F10-7-1B-C4-3	35	Alb	69.91	19.91	0.18	10.58	0.09	100.8	6.03	2.02	0.02	1.77	0.01	0.9	98.5	0.6
POL	F10-7-1B-C5-1	35	Alb	69.34	19.71	0.33	10.34	0.22	100.1	6.03	2.02	0.03	1.74	0.02	1.7	96.9	1.4
POL	F10-7-1B-C5-2	35	Alb	69.43	19.82	0.30	10.52	0.20	100.5	6.02	2.03	0.03	1.77	0.02	1.5	97.3	1.2
POL	F10-7-1B-C5-3	35	Alb	68.63	19.45	0.23	10.22	0.19	99.3	6.04	2.02	0.02	1.74	0.02	1.2	97.6	1.2
POL	F10-7-1B-C2-1	35	Alb	69.52	19.77	0.19	10.48	0.17	100.2	6.03	2.02	0.02	1.76	0.02	1.0	98.0	1.0
POL	F10-7-1B-C2-2	35	Alb	69.48	19.63	0.26	10.59	0.17	100.2	6.03	2.01	0.02	1.78	0.02	1.3	97.6	1.1
POL	F10-7-1B-C2-3	35	Alb	69.67	19.76	0.32	10.30	0.21	100.4	6.03	2.02	0.03	1.73	0.02	1.6	97.1	1.3
POL	31 - F10 -ALB01 C1- 7	31	Alb	67.45	20.72	0.33	12.21	0.19	100.9	5.87	2.13	0.03	2.06	0.02	1.5	97.6	1.0
POL	31 - F10 -ALB01 C1- 8	31	Alb	67.84	20.75	0.18	12.06	0.16	101.0	5.89	2.12	0.02	2.03	0.02	0.8	98.4	0.8
POL	31 - F10 -ALB01 C1- 9	31	Alb	67.06	20.95	0.37	12.53	0.21	101.1	5.84	2.15	0.03	2.11	0.02	1.6	97.3	1.1
POL	31 - F10 -ALB01 C1- 10	31	Alb	66.66	20.87	0.35	12.15	0.17	100.2	5.84	2.16	0.03	2.07	0.02	1.5	97.6	0.9
POL	31 - F10 -ALB01 C1- 11	31	Alb	65.69	20.79	0.28	13.31	0.17	100.2	5.79	2.16	0.03	2.28	0.02	1.1	98.0	0.8
POL	31 - F10 -ALB01 C1- 12	31	Alb	64.75	21.21	0.34	12.73	0.14	99.2	5.76	2.22	0.03	2.20	0.02	1.5	97.8	0.7
POL	31 - F10 -ALB01 -C3 - 4	31	Alb	67.07	20.98	0.26	12.61	0.13	101.0	5.84	2.15	0.02	2.13	0.01	1.1	98.2	0.7
POL	31 - F10 -ALB01 -C3-5	31	Alb	66.68	20.31	0.22	11.61	0.13	99.0	5.90	2.12	0.02	1.99	0.01	1.0	98.3	0.7
POL	31 - F10 -ALB01 -C3-6	31	Alb	68.02	20.62	0.24	12.17	0.12	101.2	5.90	2.11	0.02	2.04	0.01	1.1	98.3	0.6
POL	31 - F10 -ALB01 -C3-7	31	Alb	67.92	20.79	0.32	11.93	0.15	101.1	5.89	2.12	0.03	2.00	0.02	1.4	97.7	0.8
POL	31 - F10 -ALB01 -C3-8	31	Alb	67.96	20.61	0.22	12.07	0.13	101.0	5.90	2.11	0.02	2.03	0.01	1.0	98.3	0.7
POL	31 - F10 -ALB01 -C3-9	31	Alb	67.83	20.53	0.27	11.63	0.11	100.4	5.91	2.11	0.03	1.97	0.01	1.2	98.1	0.6
POL	31 - F10 -ALB01 -C3-10	31	Alb	67.77	20.88	0.38	12.25	0.15	101.4	5.87	2.13	0.04	2.06	0.02	1.7	97.5	0.8
POL	31 - F10 -ALB01 -C3-11	31	Alb	67.94	20.84	0.33	12.24	0.17	101.5	5.87	2.12	0.03	2.05	0.02	1.4	97.6	0.9
POL	31 - F10 -ALB01 -C3-12	31	Alb	67.86	20.74	0.33	12.34	0.21	101.5	5.87	2.12	0.03	2.07	0.02	1.4	97.5	1.1
POL	31 - F10 -ALB01 -C5- 4	31	Alb	65.55	21.01	0.39	12.41	0.21	99.6	5.80	2.19	0.04	2.13	0.02	1.7	97.2	1.1
POL	31 - F10 -ALB01 -C5- 5	31	Alb	65.82	20.85	0.34	12.51	0.20	99.7	5.81	2.17	0.03	2.14	0.02	1.5	97.5	1.0
POL	31 - F10 -ALB01 -C5- 6	31	Alb	66.38	21.39	0.40	12.51	0.17	100.8	5.80	2.20	0.04	2.12	0.02	1.7	97.4	0.9
POL	31 - F10 -ALB01 -C5- 7	31	Alb	65.73	20.83	0.38	12.42	0.19	99.5	5.81	2.17	0.04	2.13	0.02	1.6	97.4	1.0
POL	31 - F10 -ALB01 -C5- 8	31	Alb	66.90	20.73	0.29	12.08	0.21	100.2	5.86	2.14	0.03	2.05	0.02	1.3	97.6	1.1
POL	31 - F10 -ALB01 -C5- 9	31	Alb	67.17	20.67	0.31	12.03	0.23	100.4	5.87	2.13	0.03	2.04	0.03	1.4	97.4	1.2
POL	31 - F10 -ALB01 -C5-10	31	Alb	68.30	20.75	0.26	12.40	0.11	101.8	5.89	2.11	0.02	2.07	0.01	1.1	98.3	0.6
POL	ALB05 - C6 - 1	35	Alb	66.24	20.80	0.29	12.44	0.20	100.0	5.83	2.16	0.03	2.12	0.02	1.3	97.7	1.0
POL	ALB05 - C6 - 2	35	Alb	66.43	20.53	0.24	12.65	0.24	100.1	5.85	2.13	0.02	2.16	0.03	1.0	97.8	1.2
POL	ALB05 - C6 - 3	35	Alb	66.66	20.68	0.23	12.47	0.26	100.3	5.85	2.14	0.02	2.12	0.03	1.0	97.7	1.4

POL	ALB05 - C6 - 4	35	Alb	66.12	20.53	0.29	12.52	0.22	99.7	5.84	2.14	0.03	2.14	0.02	1.2	97.6	1.1
POL	ALB05 - C6 - 5	35	Alb	66.88	20.51	0.25	12.22	0.19	100.1	5.87	2.12	0.02	2.08	0.02	1.1	97.9	1.0
POL	ALB05 - C6 - 6	35	Alb	67.21	20.43	0.28	12.23	0.23	100.4	5.88	2.11	0.03	2.08	0.03	1.2	97.6	1.2
POL	ALB05 - C6 - 7	35	Alb	67.28	20.58	0.24	12.12	0.22	100.4	5.88	2.12	0.02	2.05	0.02	1.1	97.8	1.1
POL	ALB05 - C6 - 8	35	Alb	67.00	20.42	0.23	12.02	0.21	99.9	5.89	2.11	0.02	2.05	0.02	1.1	97.8	1.1
POL	ALB05 - C6 - 9	35	Alb	66.72	20.62	0.25	12.06	0.22	99.9	5.87	2.14	0.02	2.06	0.02	1.1	97.7	1.2
POL	ALB05 - C6 - 10	35	Alb	67.14	20.86	0.24	12.56	0.21	101.0	5.85	2.14	0.02	2.12	0.02	1.0	97.9	1.1
POL	ALB05 - C5-1	35	Alb	67.45	20.05	0.17	12.16	0.10	99.9	5.92	2.07	0.02	2.07	0.01	0.8	98.7	0.5
POL	ALB05 - C5-2	35	Alb	66.78	20.59	0.19	12.66	0.09	100.3	5.85	2.13	0.02	2.15	0.01	0.8	98.7	0.5
POL	ALB05 - C5-6	35	Alb	66.10	20.88	0.24	12.56	0.21	100.0	5.82	2.17	0.02	2.14	0.02	1.0	97.9	1.1
POL	ALB05 - C5-7	35	Alb	66.28	20.65	0.26	12.60	0.26	100.0	5.84	2.14	0.02	2.15	0.03	1.1	97.5	1.3
POL	ALB05 - C5-8	35	Alb	66.30	20.54	0.27	12.53	0.20	99.8	5.85	2.13	0.03	2.14	0.02	1.1	97.8	1.0
POL	ALB05 - C5-9	35	Alb	66.30	20.98	0.26	11.98	0.25	99.8	5.84	2.18	0.02	2.04	0.03	1.2	97.5	1.3
POL	35F10-BAB129-1-C3-1	35	Alb	67.85	20.80	0.29	11.36	0.08	100.4	5.90	2.13	0.03	1.92	0.01	1.4	98.1	0.5
POL	35F10-BAB129-1-C3-2	35	Alb	67.48	20.78	0.26	11.51	0.08	100.1	5.89	2.14	0.02	1.95	0.01	1.2	98.3	0.4
POL	35F10-BAB129-1-C3-3	35	Alb	67.16	20.62	0.15	11.76	0.07	99.8	5.89	2.13	0.01	2.00	0.01	0.7	98.9	0.4
POL	35F10-BAB129-1-C4-1	35	Alb	68.94	20.99	0.24	12.45	0.06	102.7	5.89	2.11	0.02	2.06	0.01	1.1	98.6	0.3
POL	35F10-BAB129-1-C4-2	35	Alb	69.10	20.92	0.29	12.35	0.10	102.8	5.90	2.10	0.03	2.04	0.01	1.3	98.2	0.5
POL	35F10-BAB129-1-C4-3	35	Alb	67.88	20.97	0.24	13.07	0.05	102.2	5.85	2.13	0.02	2.18	0.01	1.0	98.7	0.3
POL	35F10-BAB129-1-C5-1	35	Alb	65.96	21.14	0.26	12.92	0.10	100.4	5.79	2.19	0.02	2.20	0.01	1.1	98.4	0.5
POL	35F10-BAB129-1-C5-2	35	Alb	67.53	20.66	0.24	12.46	0.11	101.0	5.87	2.12	0.02	2.10	0.01	1.1	98.4	0.6
POL	35F10-BAB129-1-C5-3	35	Alb	68.75	21.01	0.24	12.17	0.10	102.3	5.89	2.12	0.02	2.02	0.01	1.1	98.4	0.5
POL	35F10-BAB129-1-C5-6	35	Alb	67.74	21.29	0.26	12.46	0.07	101.8	5.84	2.16	0.02	2.08	0.01	1.1	98.5	0.3
POL	35F10-BAB129-1-C5-7	35	Alb	68.44	21.16	0.32	12.39	0.10	102.4	5.86	2.14	0.03	2.06	0.01	1.4	98.1	0.5
POL	35F10-BAB129-1-C6-4	35	Alb	67.43	20.78	0.28	12.53	0.09	101.1	5.86	2.13	0.03	2.11	0.01	1.2	98.3	0.5
POL	35F10-BAB129-1-C6-5	35	Alb	64.09	21.06	0.22	13.11	0.09	98.6	5.75	2.23	0.02	2.28	0.01	0.9	98.6	0.4
POL	35F10-BAB129-1-C6-6	35	Alb	67.11	21.28	0.19	12.65	0.08	101.3	5.82	2.18	0.02	2.13	0.01	0.8	98.8	0.4
POL	35F10-BAB129-1-C6-7	35	Alb	64.33	21.06	0.17	12.97	0.09	98.6	5.76	2.22	0.02	2.25	0.01	0.7	98.8	0.5
POL	35F10-BAB129-1-C6-8	35	Alb	68.85	21.08	0.18	12.41	0.08	102.6	5.88	2.12	0.02	2.06	0.01	0.8	98.8	0.4
POL	35F10-BAB129-1-C2-4	35	Alb	65.86	21.34	0.54	12.60	0.11	100.4	5.78	2.21	0.05	2.14	0.01	2.3	97.2	0.5
POL	35F10-BAB129-1-C2-5	35	Alb	65.43	21.11	0.47	12.51	0.09	99.6	5.79	2.20	0.04	2.15	0.01	2.0	97.5	0.4
POL	31 - F10 -ALB01 -C5- 1	31	Alb	68.45	20.48	0.08	12.31	0.11	101.4	5.91	2.09	0.01	2.06	0.01	0.4	99.0	0.6
POL	31 - F10 -ALB01 -C5- 2	31	Alb	67.75	20.69	0.08	12.64	0.08	101.2	5.88	2.11	0.01	2.13	0.01	0.4	99.3	0.4
POL	31 - F10 -ALB01 -C5- 3	31	Alb	67.03	20.82	0.17	12.80	0.07	100.9	5.84	2.14	0.02	2.16	0.01	0.7	98.9	0.4
POL	35F10-BAB129-1-C4-5	35	Alb	67.32	20.88	0.10	12.96	0.07	101.3	5.85	2.14	0.01	2.18	0.01	0.4	99.2	0.3
POL	35F10-BAB129-1-C4-6	35	Alb	68.50	21.00	0.33	12.29	0.20	102.3	5.88	2.12	0.03	2.04	0.02	1.4	97.5	1.0
POL	35F10-BAB129-1-C4-10	35	Alb	68.47	20.88	0.12	11.91	0.10	101.5	5.90	2.12	0.01	1.99	0.01	0.6	98.9	0.5
POL	35F10-BAB129-1-C4-11	35	Alb	68.30	20.66	0.14	12.15	0.09	101.3	5.90	2.10	0.01	2.04	0.01	0.6	98.9	0.5
POL	35F10-BAB129-1-C6-1	35	Alb	67.48	20.97	0.14	12.42	0.11	101.1	5.86	2.15	0.01	2.09	0.01	0.6	98.8	0.6
POL	35F10-BAB129-1-C6-2	35	Alb	68.48	21.03	0.10	12.29	0.07	102.0	5.88	2.13	0.01	2.05	0.01	0.5	99.2	0.4
POL	35F10-BAB129-1-C6-3	35	Alb	66.98	21.28	0.29	12.61	0.07	101.2	5.82	2.18	0.03	2.12	0.01	1.2	98.4	0.4
POL	35F10-BAB129-1-C8-1	35	Alb	67.93	21.08	0.17	12.64	0.08	101.9	5.86	2.14	0.02	2.11	0.01	0.7	98.9	0.4
POL	35F10-BAB129-1-C8-2	35	Alb	67.71	21.15	0.32	12.80	0.11	102.1	5.84	2.15	0.03	2.14	0.01	1.4	98.1	0.5
POL	35F10-BAB129-1-C8-3	35	Alb	69.46	21.19	0.22	12.03	0.08	103.0	5.90	2.12	0.02	1.98	0.01	1.0	98.6	0.5
POL	35F10-BAB129-1-C8-4	35	Alb	69.67	20.73	0.22	11.90	0.06	102.6	5.94	2.08	0.02	1.97	0.01	1.0	98.6	0.3
POL	35F10-BAB129-1-C8-5	35	Alb	66.98	21.11	0.24	12.59	0.07	101.0	5.83	2.17	0.02	2.12	0.01	1.0	98.6	0.4
POL	35F10-BAB129-1-C2-1	35	Alb	67.52	20.62	0.06	12.16	0.04	100.4	5.89	2.12	0.01	2.06	0.00	0.3	99.5	0.2
POL	35F10-BAB129-1-C2-2	35	Alb	64.92	20.83	0.20	12.57	0.07	98.6	5.80	2.19	0.02	2.18	0.01	0.8	98.8	0.4
POL	35F10-BAB129-1-C2-3	35	Alb	65.51	20.84	0.20	12.63	0.07	99.3	5.81	2.18	0.02	2.17	0.01	0.9	98.7	0.4
POL	31 - F10 -ALB01 C1- 7	31	Alb	67.45	20.72	0.33	12.21	0.19	100.9	5.87	2.13	0.03	2.06	0.02	1.5	97.6	1.0
POL	31 - F10 -ALB01 C1- 8	31	Alb	67.84	20.75	0.18	12.06	0.16	101.0	5.89	2.12	0.02	2.03	0.02	0.8	98.4	0.8
POL	31 - F10 -ALB01 C1- 9	31	Alb	67.06	20.95	0.37	12.53	0.21	101.1	5.84	2.15	0.03	2.11	0.02	1.6	97.3	1.1
POL	31 - F10 -ALB01 C1- 10	31	Alb	66.66	20.87	0.35	12.15	0.17	100.2	5.84	2.16	0.03	2.07	0.02	1.5	97.6	0.9

POL	31 - F10 -ALB01 C1- 11	31	Alb	65.69	20.79	0.28	13.31	0.17	100.2	5.79	2.16	0.03	2.28	0.02	1.1	98.0	0.8
POL	31 - F10 -ALB01 C1- 12	31	Alb	64.75	21.21	0.34	12.73	0.14	99.2	5.76	2.22	0.03	2.20	0.02	1.5	97.8	0.7
POL	31 - F10 -ALB01 -C3 - 4	31	Alb	67.07	20.98	0.26	12.61	0.13	101.0	5.84	2.15	0.02	2.13	0.01	1.1	98.2	0.7
POL	31 - F10 -ALB01 -C3-5	31	Alb	66.68	20.31	0.22	11.61	0.13	99.0	5.90	2.12	0.02	1.99	0.01	1.0	98.3	0.7
POL	31 - F10 -ALB01 -C3-6	31	Alb	68.02	20.62	0.24	12.17	0.12	101.2	5.90	2.11	0.02	2.04	0.01	1.1	98.3	0.6
POL	31 - F10 -ALB01 -C3-7	31	Alb	67.92	20.79	0.32	11.93	0.15	101.1	5.89	2.12	0.03	2.00	0.02	1.4	97.7	0.8
POL	31 - F10 -ALB01 -C3-8	31	Alb	67.96	20.61	0.22	12.07	0.13	101.0	5.90	2.11	0.02	2.03	0.01	1.0	98.3	0.7
POL	31 - F10 -ALB01 -C3-9	31	Alb	67.83	20.53	0.27	11.63	0.11	100.4	5.91	2.11	0.03	1.97	0.01	1.2	98.1	0.6
POL	31 - F10 -ALB01 -C3-10	31	Alb	67.77	20.88	0.38	12.25	0.15	101.4	5.87	2.13	0.04	2.06	0.02	1.7	97.5	0.8
POL	31 - F10 -ALB01 -C3-11	31	Alb	67.94	20.84	0.33	12.24	0.17	101.5	5.87	2.12	0.03	2.05	0.02	1.4	97.6	0.9
POL	31 - F10 -ALB01 -C3-12	31	Alb	67.86	20.74	0.33	12.34	0.21	101.5	5.87	2.12	0.03	2.07	0.02	1.4	97.5	1.1
POL	31 - F10 -ALB01 -C5- 4	31	Alb	65.55	21.01	0.39	12.41	0.21	99.6	5.80	2.19	0.04	2.13	0.02	1.7	97.2	1.1
POL	31 - F10 -ALB01 -C5- 5	31	Alb	65.82	20.85	0.34	12.51	0.20	99.7	5.81	2.17	0.03	2.14	0.02	1.5	97.5	1.0
POL	31 - F10 -ALB01 -C5- 6	31	Alb	66.38	21.39	0.40	12.51	0.17	100.8	5.80	2.20	0.04	2.12	0.02	1.7	97.4	0.9
POL	31 - F10 -ALB01 -C5- 7	31	Alb	65.73	20.83	0.38	12.42	0.19	99.5	5.81	2.17	0.04	2.13	0.02	1.6	97.4	1.0
POL	31 - F10 -ALB01 -C5- 8	31	Alb	66.90	20.73	0.29	12.08	0.21	100.2	5.86	2.14	0.03	2.05	0.02	1.3	97.6	1.1
POL	31 - F10 -ALB01 -C5- 9	31	Alb	67.17	20.67	0.31	12.03	0.23	100.4	5.87	2.13	0.03	2.04	0.03	1.4	97.4	1.2
POL	31 - F10 -ALB01 -C5- 10	31	Alb	68.30	20.75	0.26	12.40	0.11	101.8	5.89	2.11	0.02	2.07	0.01	1.1	98.3	0.6
POL	35F10-BAB129-1-C4-7	35	Alb	66.45	20.69	0.08	12.02	0.09	99.3	5.87	2.15	0.01	2.06	0.01	0.3	99.2	0.5
POL	35F10-BAB129-1-C4-8	35	Alb	69.01	20.73	0.23	12.47	0.19	102.6	5.90	2.09	0.02	2.07	0.02	1.0	98.0	1.0
POL	35F10-BAB129-1-C4-9	35	Alb	68.61	20.84	0.12	12.21	0.08	101.8	5.90	2.11	0.01	2.04	0.01	0.5	99.1	0.4
POL	35F10-BAB129-1-C8-6	35	Alb	68.51	21.09	0.34	12.04	0.24	102.2	5.88	2.13	0.03	2.00	0.03	1.5	97.2	1.3
POL	35F10-BAB129-1-C8-7	35	Alb	67.74	21.13	0.37	12.19	0.17	101.6	5.85	2.15	0.03	2.04	0.02	1.7	97.4	0.9
POL	35F10-BAB129-1-C8-8	35	Alb	67.72	21.12	0.37	12.32	0.18	101.7	5.85	2.15	0.03	2.06	0.02	1.6	97.5	0.9
POL	35F10-BAB129-1-C8-9	35	Alb	67.94	20.63	0.32	11.65	0.22	100.8	5.90	2.11	0.03	1.96	0.02	1.5	97.3	1.2
POL	35F10-BAB129-1-C8-11	35	Alb	64.73	21.06	0.35	12.72	0.18	99.0	5.77	2.21	0.03	2.20	0.02	1.5	97.6	0.9
POL	35F10-BAB129-1-C8-12	35	Alb	65.76	20.96	0.35	12.50	0.11	99.7	5.81	2.18	0.03	2.14	0.01	1.5	98.0	0.5
POL	35F10-BAB129-1-C8-13	35	Alb	64.32	20.91	0.31	12.58	0.19	98.3	5.77	2.21	0.03	2.19	0.02	1.3	97.7	1.0
POL	35F10-BAB129-1-C8-14	35	Alb	68.17	20.87	0.36	11.90	0.19	101.5	5.89	2.12	0.03	1.99	0.02	1.6	97.3	1.0
POL	35F10-BAB129-1-C8-15	35	Alb	66.41	21.30	0.40	12.35	0.16	100.6	5.81	2.20	0.04	2.09	0.02	1.8	97.4	0.8
POL	35F10-BAB129-1-C1-2	35	Alb	66.88	20.87	0.34	12.09	0.20	100.4	5.85	2.15	0.03	2.05	0.02	1.5	97.4	1.1
POL	35F10-BAB129-1-C1-3	35	Alb	67.28	21.07	0.37	11.99	0.18	100.9	5.85	2.16	0.03	2.02	0.02	1.7	97.4	1.0
POL	35F10-BAB129-1-C1-4	35	Alb	67.43	20.78	0.34	12.39	0.16	101.1	5.86	2.13	0.03	2.09	0.02	1.5	97.7	0.9
POL	35F10-BAB129-1-C1-5	35	Alb	67.44	21.10	0.33	12.17	0.17	101.2	5.85	2.16	0.03	2.05	0.02	1.5	97.6	0.9
POL	35F10-BAB129-1-C1-6	35	Alb	67.28	20.87	0.33	12.24	0.19	100.9	5.86	2.14	0.03	2.07	0.02	1.5	97.5	1.0
POL	35F10-BAB129-1-C1-7	35	Alb	68.10	20.96	0.35	11.54	0.18	101.1	5.89	2.14	0.03	1.94	0.02	1.6	97.4	1.0
POL	35F10-BAB129-1-C1-8	35	Alb	67.83	20.95	0.32	11.96	0.17	101.2	5.87	2.14	0.03	2.01	0.02	1.5	97.6	0.9
POL	35F10-BAB129-1-C1-9	35	Alb	68.05	20.73	0.41	11.33	0.22	100.7	5.91	2.12	0.04	1.91	0.02	1.9	96.8	1.2
POL	35F10-BAB129-1-C1-10	35	Alb	67.93	20.87	0.41	11.73	0.20	101.1	5.88	2.13	0.04	1.97	0.02	1.9	97.1	1.1
POL	35F10-BAB129-1-C1-11	35	Alb	68.34	20.72	0.35	11.37	0.20	101.0	5.92	2.11	0.03	1.91	0.02	1.7	97.2	1.1
POL	35F10-BAB129-1-C1-12	35	Alb	67.94	20.72	0.39	11.53	0.16	100.7	5.90	2.12	0.04	1.94	0.02	1.8	97.3	0.9
POL	35F10-BAB129-1-C1-13	35	Alb	66.66	21.00	0.36	12.42	0.18	100.6	5.83	2.16	0.03	2.11	0.02	1.6	97.5	0.9
POL	35F10-BAB129-1-C1-14	35	Alb	66.13	21.02	0.28	12.46	0.19	100.1	5.82	2.18	0.03	2.12	0.02	1.2	97.8	1.0
POL	35F10-BAB129-1-C1-15	35	Alb	65.41	21.04	0.32	12.42	0.19	99.4	5.80	2.20	0.03	2.13	0.02	1.4	97.6	1.0
POL	35F10-BAB129-1-C1-16	35	Alb	66.36	21.18	0.34	12.33	0.16	100.4	5.82	2.19	0.03	2.10	0.02	1.5	97.7	0.9
POL	35F10-BAB129-1-C1-17	35	Alb	65.55	21.05	0.29	12.64	0.19	99.7	5.79	2.19	0.03	2.17	0.02	1.3	97.8	1.0
POL	35F10-BAB129-1-C1-18	35	Alb	64.61	20.98	0.26	12.78	0.18	98.8	5.77	2.21	0.02	2.21	0.02	1.1	98.0	0.9
POL	3512-POAB02-C1-3	35	Alb	74.58	20.41	0.02	6.89	0.06	102.0	6.22	2.01	0.00	1.11	0.01	0.1	99.3	0.6
POL	3512-POAB02-C1-4	35	Alb	70.88	19.44	0.05	10.06	0.19	100.8	6.10	1.97	0.00	1.68	0.02	0.3	98.5	1.2
POL	3512-POAB02-C1-2	35	Alb	70.00	19.39	0.03	10.35	0.21	100.4	6.07	1.98	0.00	1.74	0.02	0.2	98.5	1.3
POL	3512-POAB02-C1-3	35	Alb	69.20	19.19	0.03	10.21	0.22	99.2	6.07	1.98	0.00	1.74	0.02	0.2	98.4	1.4
POL	3512-POAB02-C1-4	35	Alb	69.46	18.94	0.05	10.20	0.19	99.2	6.09	1.96	0.00	1.73	0.02	0.3	98.5	1.2
POL	3512-POAB02-C1-5	35	Alb	69.95	19.46	0.04	10.50	0.20	100.3	6.06	1.99	0.00	1.76	0.02	0.2	98.6	1.2

POL	3512-POAB02-C1-6	35	Alb	69.83	19.59	0.06	10.56	0.20	100.5	6.05	2.00	0.01	1.77	0.02	0.3	98.5	1.2
POL	3512-POAB02-C1-7	35	Alb	69.96	19.42	0.04	10.23	0.23	100.2	6.07	1.99	0.00	1.72	0.03	0.2	98.3	1.5
POL	3516-BCAB-C1-5	35	Alb	68.17	20.09	0.79	9.94	0.08	99.1	5.98	2.08	0.07	1.69	0.01	4.2	95.3	0.5
POL	3516-BCAB-C1-6	35	Alb	68.90	20.46	0.87	10.17	0.12	100.6	5.96	2.09	0.08	1.71	0.01	4.5	94.8	0.8
POL	3516-BCAB-C2-11	35	Alb	68.29	20.84	0.94	10.12	0.09	100.3	5.93	2.13	0.09	1.70	0.01	4.9	94.6	0.5
POL	3516-BCAB-C2-12	35	Alb	69.26	20.35	0.62	10.00	0.06	100.5	5.99	2.08	0.06	1.68	0.01	3.3	96.3	0.4
POL	3516-PAAB01-C4-54	35	Alb	69.02	19.77	0.17	10.10	0.23	99.6	6.03	2.04	0.02	1.71	0.03	0.9	97.7	1.4
POL	3516-PAAB01-C4-55	35	Alb	69.49	19.80	0.30	10.07	0.21	100.0	6.04	2.03	0.03	1.70	0.02	1.6	97.1	1.3
POL	3516-PAAB01-C4-56	35	Alb	70.12	19.93	0.21	9.91	0.19	100.7	6.05	2.03	0.02	1.66	0.02	1.1	97.6	1.3
POL	3516-PAAB01-C4-57	35	Alb	70.53	20.95	0.13	10.29	0.15	102.2	5.99	2.10	0.01	1.70	0.02	0.7	98.4	0.9
POL	3516-PAAB01-C4-58	35	Alb	71.13	20.17	0.15	10.24	0.21	102.3	6.05	2.02	0.01	1.69	0.02	0.8	97.9	1.3
POL	3516-MAAB03-C2-21	35	Alb	65.73	22.02	2.38	8.99	0.26	99.4	5.78	2.28	0.22	1.53	0.03	12.6	85.8	1.6
POL	3516-MAAB03-C2-22	35	Alb	64.80	22.42	2.51	9.11	0.25	99.4	5.73	2.34	0.24	1.56	0.03	13.0	85.4	1.5
POL	3516-MAAB03-C2-23	35	Alb	66.03	22.17	2.81	8.86	0.22	100.2	5.77	2.28	0.26	1.50	0.02	14.7	83.9	1.4
POL	3516-MAAB03-C2-24	35	Alb	67.38	22.20	2.40	9.19	0.26	101.7	5.81	2.25	0.22	1.53	0.03	12.4	86.0	1.6
POL	3409GALB04-C2-31	34	Alb	65.96	22.36	1.31	9.76	0.24	99.9	5.78	2.31	0.12	1.66	0.03	6.8	91.7	1.5
POL	3409GALB04-C2-35	34	Alb	65.11	22.53	1.07	9.51	0.19	98.5	5.77	2.35	0.10	1.63	0.02	5.8	93.0	1.2
POL	3409BALBO02-C2-96	34	Alb	68.71	20.37	0.21	11.22	0.19	100.9	5.95	2.08	0.02	1.89	0.02	1.0	97.9	1.1
POL	3409BALBO02-C2-97	34	Alb	68.13	20.44	0.16	11.40	0.22	100.6	5.93	2.10	0.01	1.92	0.02	0.8	98.0	1.2
POL	3409BALBO02-C2-98	34	Alb	69.45	20.96	0.29	11.09	0.18	102.1	5.94	2.11	0.03	1.84	0.02	1.4	97.5	1.0
POL	3409BALBO02-C2-99	34	Alb	69.69	20.94	0.29	11.36	0.23	102.6	5.94	2.10	0.03	1.88	0.02	1.4	97.3	1.3
POL	3409BALBO02-C2-100	34	Alb	67.90	20.95	0.39	11.04	0.24	100.7	5.90	2.15	0.04	1.86	0.03	1.9	96.7	1.4
POL	3409BALBO02-C2-101	34	Alb	68.44	21.01	0.13	11.38	0.16	101.3	5.91	2.14	0.01	1.91	0.02	0.6	98.5	0.9
POL	3409MALB12-C1-123	34	Alb	67.11	20.88	1.68	10.30	0.19	100.4	5.87	2.15	0.16	1.75	0.02	8.2	90.7	1.1
POL	3409MALB12-C1-124	34	Alb	66.28	20.79	1.56	10.16	0.20	99.1	5.86	2.17	0.15	1.74	0.02	7.7	91.1	1.2
POL	3409MALB12-C1-125	34	Alb	67.20	22.13	1.65	10.14	0.19	101.5	5.80	2.25	0.15	1.70	0.02	8.2	90.7	1.1
POL	3409MALB12-C1-126	34	Alb	66.02	21.00	1.69	10.33	0.22	99.5	5.83	2.19	0.16	1.77	0.02	8.2	90.5	1.3
POL	3409MALB12-C1-127	34	Alb	66.54	20.75	1.47	10.02	0.28	99.4	5.87	2.16	0.14	1.72	0.03	7.4	91.0	1.7
POL	3409MALB12-C1-128	34	Alb	67.12	20.38	1.19	10.37	0.14	99.3	5.91	2.12	0.11	1.77	0.02	5.9	93.3	0.8
POL	AN34-C5-2	34	Alb	67.16	20.99	1.65	9.51	0.18	99.6	5.89	2.17	0.16	1.62	0.02	8.7	90.2	1.1
POL	AN34-C5-3	34	Alb	67.25	20.73	1.50	9.58	0.24	99.4	5.91	2.15	0.14	1.63	0.03	7.8	90.7	1.5
POL	AN34-C5-4	34	Alb	67.32	20.74	1.35	9.74	0.16	99.5	5.91	2.15	0.13	1.66	0.02	7.1	92.0	1.0
POL	AN34-C5-5	34	Alb	65.98	22.33	1.49	9.07	0.18	99.2	5.80	2.31	0.14	1.55	0.02	8.2	90.6	1.2
POL	AN34-C5-6	34	Alb	67.54	20.48	1.22	9.87	0.17	99.4	5.93	2.12	0.11	1.68	0.02	6.3	92.7	1.0
POL	AN34-C4-4	34	Alb	67.29	20.68	1.38	9.76	0.10	99.3	5.91	2.14	0.13	1.66	0.01	7.2	92.2	0.6
POL	AN34-C4-5	34	Alb	66.93	20.74	1.51	9.43	0.28	99.0	5.90	2.16	0.14	1.61	0.03	8.0	90.3	1.7
POL	AN34-C4-6	34	Alb	67.24	20.58	1.51	9.48	0.18	99.0	5.92	2.14	0.14	1.62	0.02	8.0	90.9	1.1
POL	AN34-C1-1	34	Alb	67.09	20.96	1.50	9.66	0.21	99.6	5.89	2.17	0.14	1.64	0.02	7.8	90.9	1.3
POL	AN34-C1-2	34	Alb	67.54	20.95	1.55	9.44	0.24	99.9	5.90	2.16	0.15	1.60	0.03	8.2	90.3	1.5
POL	AN34-C1-3	34	Alb	66.93	20.81	1.73	9.50	0.23	99.4	5.89	2.16	0.16	1.62	0.03	9.0	89.6	1.4
POL	AN34-C1-4	34	Alb	66.92	20.97	1.65	9.57	0.28	99.5	5.88	2.17	0.16	1.63	0.03	8.5	89.7	1.7
POL	AN34-C1-5	34	Alb	66.79	20.95	1.59	9.67	0.22	99.2	5.88	2.17	0.15	1.65	0.03	8.2	90.4	1.4
POL	AN34-C1-6	34	Alb	67.27	20.79	1.67	9.54	0.17	99.5	5.90	2.15	0.16	1.62	0.02	8.7	90.2	1.1

3C: EPMA analyses of clinopyroxene. Recalculated formula on the basis of 8 oxygens.

Analysis	1	2	3	4	5	6	7	8	9	10	11	12	13	14	15
Sample	8_11	8_11	8_11	8_11	8_11	8_11	8_11	8_11	8_11	POAB02	POAB02	POAB02	POAB02	POAB02	POAB02
Pyroxene Name]	Hd1	Hd1	Hd1	Hd1	Hd1	Hd1	Hd1	Hd1	Hd1	AA	AA	AA	AA	AA	AA
Alteration	Mag	Mag	Mag	Mag	Mag	Mag	Mag	Mag	Mag	Na-Ca	Na-Ca	Na-Ca	Na-Ca	Na-Ca	Na-Ca
SiO2	49.98	49.38	50.30	49.16	50.11	50.78	51.23	51.02	51.15	52.43	52.70	53.97	53.88	54.26	54.45
TiO2	0.06	0.09	0.09	0.04	0.16	0.04	0.68	0.03	0.08	0.10	0.07	0.07	0.02	0.10	0.07
Al2O3	0.51	0.45	0.46	1.34	1.38	0.42	0.77	0.45	0.46	1.36	2.10	1.18	1.31	1.21	1.18
FeO	24.15	24.40	24.23	24.51	24.29	23.60	24.83	23.87	23.57	16.68	17.23	17.89	17.75	18.04	17.98
MnO	0.59	0.64	0.70	0.53	0.66	0.65	0.69	0.63	0.65	2.12	1.86	1.71	2.15	1.88	1.76
MgO	2.62	2.60	2.53	2.64	3.11	3.07	3.03	2.93	2.94	6.49	6.52	6.95	6.48	6.77	7.00
CaO	22.60	22.74	22.69	21.64	20.89	21.87	21.75	22.58	22.49	12.02	11.62	12.10	11.94	11.88	12.07
Na2O	0.03	0.00	0.01	0.18	0.25	0.00	0.10	0.02	0.00	5.98	5.94	6.20	5.95	6.23	6.16
K2O	0.46	0.46	0.40	0.53	0.58	0.43	0.48	0.41	0.45	0.03	0.05	0.01	0.03	0.00	0.00
Total	101.0	100.8	101.4	100.6	101.4	100.9	103.6	101.9	101.8	97.2	98.1	100.1	99.5	100.4	100.7
[Si (T)	2.00	1.98	2.00	1.97	1.99	2.03	2.00	2.02	2.02	2.02	2.01	2.01	2.03	2.02	2.02
Al (T)	0.00	0.02	0.00	0.03	0.01	0.00	0.00	0.00	0.00	0.00	0.00	0.00	0.00	0.00	0.00
Fe3+ (T)	0.00	0.00	0.00	0.00	0.00	0.00	0.00	0.00	0.00	0.00	0.00	0.00	0.00	0.00	0.00
Total (T)]	2.00	2.00	2.00	2.00	2.00	2.03	2.00	2.02	2.02	2.02	2.01	2.01	2.03	2.02	2.02
[Al (M1)	0.02	0.00	0.02	0.03	0.05	0.02	0.03	0.02	0.02	0.06	0.09	0.05	0.06	0.05	0.05
Fe3+ (M1)	0.00	0.03	0.00	0.03	0.00	0.00	0.00	0.00	0.00	0.28	0.26	0.29	0.26	0.28	0.28
Ti (M1)	0.00	0.00	0.00	0.00	0.00	0.00	0.02	0.00	0.00	0.00	0.00	0.00	0.00	0.00	0.00
Mg (M1)	0.16	0.16	0.15	0.16	0.18	0.18	0.18	0.17	0.17	0.37	0.37	0.39	0.36	0.38	0.39
Fe2+ (M1)	0.80	0.79	0.82	0.78	0.76	0.80	0.77	0.81	0.80	0.25	0.27	0.26	0.30	0.28	0.28
Mn (M1)	0.01	0.02	0.01	0.00	0.00	0.00	0.00	0.00	0.00	0.03	0.00	0.00	0.02	0.01	0.00
Total (M1)]	1.00	1.00	1.00	1.00	1.00	1.00	1.00	1.00	1.00	1.00	1.00	1.00	1.00	1.00	1.00
[Mg (M2)	0.00	0.00	0.00	0.00	0.00	0.00	0.00	0.00	0.00	0.00	0.00	0.00	0.00	0.00	0.00
Fe2+ (M2)	0.00	0.00	0.00	0.01	0.04	0.04	0.07	0.01	0.02	0.00	0.02	0.00	0.00	0.00	0.00
Mn (M2)	0.01	0.00	0.02	0.02	0.02	0.02	0.02	0.02	0.02	0.04	0.06	0.05	0.05	0.05	0.05
Ca (M2)	0.97	0.98	0.97	0.93	0.89	0.94	0.91	0.96	0.95	0.50	0.47	0.48	0.48	0.47	0.48
Na (M2)	0.00	0.00	0.00	0.01	0.02	0.00	0.01	0.00	0.00	0.45	0.44	0.45	0.43	0.45	0.44
K (M2)	0.02	0.02	0.02	0.03	0.03	0.02	0.02	0.02	0.02	0.00	0.00	0.00	0.00	0.00	0.00
Total (M2)]	1.00	1.00	1.01	1.00	1.00	1.02	1.03	1.01	1.02	0.98	0.99	0.99	0.97	0.98	0.98
Wo	50.19	50.88	49.97	49.49	47.38	47.89	47.18	49.13	48.88	44.14	42.01	42.67	41.94	41.92	41.86
En	8.10	8.09	7.75	8.40	9.81	9.35	9.15	8.87	8.89	33.16	32.80	34.10	31.67	33.24	33.78
Fs	41.72	41.03	42.28	42.11	42.81	42.76	43.67	42.00	42.23	22.69	25.20	23.23	26.39	24.84	24.36
Fe/Fe+Mg	0.84	0.87	0.85	0.87	0.81	0.81	0.81	0.82	0.82	0.90	0.88	0.90	0.88	0.90	0.89
Q	1.93	1.92	1.94	1.88	1.87	1.95	1.93	1.95	1.95	1.12	1.13	1.13	1.15	1.13	1.15
J	0.00	0.00	0.00	0.03	0.04	0.00	0.02	0.00	0.00	0.89	0.88	0.90	0.87	0.90	0.89
Group	Ca-Mg-Fe	Ca-Mg-Fe	Ca-Mg-Fe	Ca-Mg-Fe	Ca-Mg-Fe	Ca-Mg-Fe	Ca-Mg-Fe	Ca-Mg-Fe	Ca-Mg-Fe	Ca-Na	Ca-Na	Ca-Na	Ca-Na	Ca-Na	Ca-Na
Na+AlIV	0.00	0.02	0.00	0.04	0.03	0.00	0.01	0.00	0.00	0.45	0.44	0.45	0.43	0.45	0.44
AlVI + 2Ti + Cr	0.03	0.01	0.03	0.03	0.06	0.02	0.07	0.02	0.03	0.07	0.10	0.06	0.06	0.06	0.06

Analysis	16	17	18	19	20	21	22	23	24	25	26	27	28
Sample	PAA B01	PAA B01	PAA B01	PAA B01	PAA B01	PAA B01	34GAL B04	34GAL B04	34GAL B04	34GAL B04	34GAL B04	34GAL B04	34GAL B04
Pyroxene Name]	AA	AA	AA	AA	AA	AA	Hd2	Hd2	Hd2	Hd2	Hd2	Hd2	Hd2
Alteration	Na-Ca	Na-Ca	Na-Ca	Na-Ca	Na-Ca	Na-Ca	Ca-Fe	Ca-Fe	Ca-Fe	Ca-Fe	Ca-Fe	Ca-Fe	Ca-Fe
SiO2	52.67	51.67	53.37	52.78	53.51	53.74	47.47	46.95	47.33	47.71	46.44	48.30	48.83
TiO2	0.00	0.03	0.08	0.13	0.05	0.03	0.00	0.09	0.03	0.03	0.06	0.05	0.05
Al2O3	1.34	1.34	1.33	1.64	1.31	1.32	1.18	1.06	1.07	1.00	1.16	1.24	1.27
FeO	18.16	17.42	18.01	18.73	16.19	16.54	26.16	25.39	25.40	25.38	26.02	26.23	25.48
MnO	0.40	0.28	0.45	0.24	0.42	0.31	0.61	0.59	0.63	0.60	0.59	0.59	0.53
MgO	7.05	7.14	6.90	6.60	8.12	7.94	1.71	1.81	1.91	1.85	1.72	1.80	1.78
CaO	16.54	16.90	16.70	15.80	16.90	17.06	20.26	20.03	20.79	20.91	20.34	19.25	19.66
Na2O	3.81	3.73	3.88	4.61	3.69	3.74	1.26	0.97	1.14	1.23	1.28	1.58	1.56
K2O	0.00	0.01	0.01	0.01	0.01	0.00	0.61	0.59	0.63	0.60	0.59	0.59	0.53
Total	100.0	98.5	100.7	100.5	100.2	100.7	99.3	97.5	98.9	99.3	98.2	99.6	99.7
[Si (T)	2.00	1.99	2.01	1.98	2.01	2.01	1.92	1.94	1.92	1.93	1.90	1.94	1.96
Al (T)	0.00	0.01	0.00	0.02	0.00	0.00	0.06	0.05	0.05	0.05	0.06	0.06	0.04
Fe3+ (T)	0.00	0.00	0.00	0.00	0.00	0.00	0.02	0.01	0.03	0.02	0.04	0.00	0.00
Total (T)]	2.00	2.00	2.01	2.00	2.01	2.01	2.00	2.00	2.00	2.00	2.00	2.00	2.00
[Al (M1)	0.06	0.05	0.06	0.06	0.06	0.06	0.00	0.00	0.00	0.00	0.00	0.00	0.02
Fe3+ (M1)	0.18	0.20	0.16	0.23	0.15	0.15	0.17	0.13	0.16	0.16	0.18	0.17	0.13
Ti (M1)	0.00	0.00	0.00	0.00	0.00	0.00	0.00	0.00	0.00	0.00	0.00	0.00	0.00
Mg (M1)	0.40	0.41	0.39	0.37	0.46	0.44	0.10	0.11	0.12	0.11	0.11	0.11	0.11
Fe2+ (M1)	0.36	0.34	0.39	0.34	0.33	0.35	0.70	0.74	0.68	0.68	0.67	0.72	0.72
Mn (M1)	0.00	0.00	0.00	0.00	0.00	0.00	0.02	0.02	0.02	0.02	0.02	0.00	0.01
Total (M1)]	1.00	1.00	1.00	1.00	1.00	1.00	0.99	1.00	0.97	0.97	0.98	1.00	1.00
[Mg (M2)	0.00	0.00	0.00	0.00	0.00	0.00	0.00	0.00	0.00	0.00	0.00	0.00	0.00
Fe2+ (M2)	0.03	0.02	0.02	0.02	0.02	0.02	0.00	0.00	0.00	0.00	0.00	0.00	0.00
Mn (M2)	0.01	0.01	0.01	0.01	0.01	0.01	0.00	0.00	0.00	0.00	0.00	0.02	0.00
Ca (M2)	0.67	0.70	0.67	0.64	0.68	0.68	0.88	0.89	0.90	0.91	0.89	0.83	0.85
Na (M2)	0.28	0.28	0.28	0.34	0.27	0.27	0.10	0.08	0.09	0.10	0.10	0.12	0.12
K (M2)	0.00	0.00	0.00	0.00	0.00	0.00	0.03	0.03	0.03	0.03	0.03	0.03	0.03
Total (M2)]	1.00	1.00	0.99	1.00	0.99	0.99	1.01	1.00	1.03	1.03	1.02	1.00	1.00
Wo	45.88	47.48	45.96	46.76	45.57	45.83	52.26	51.11	53.28	53.45	53.49	50.16	50.48
En	27.21	27.91	26.42	27.18	30.46	29.68	6.14	6.43	6.81	6.58	6.29	6.53	6.36
Fs	26.91	24.60	27.61	26.06	23.97	24.50	41.60	42.47	39.91	39.98	40.21	43.31	43.16
Fe/Fe+Mg	0.77	0.78	0.76	0.86	0.68	0.69	1.04	1.01	1.02	1.02	1.03	1.06	1.03
Q	1.47	1.47	1.47	1.36	1.49	1.49	1.68	1.74	1.70	1.69	1.67	1.66	1.68
J	0.56	0.56	0.57	0.67	0.54	0.54	0.20	0.16	0.18	0.19	0.20	0.25	0.24
Group	Ca-Na	Ca-Na	Ca-Na	Ca-Na	Ca-Na	Ca-Na	Ca-Mg-Fe	Ca-Mg-Fe	Ca-Mg-Fe	Ca-Mg-Fe	Ca-Mg-Fe	Ca-Mg-Fe	Ca-Mg-Fe
Na+AlIV	0.28	0.29	0.28	0.35	0.27	0.27	0.16	0.13	0.14	0.14	0.16	0.18	0.16
AlVI + 2Ti + Cr	0.06	0.05	0.06	0.06	0.06	0.06	0.00	0.01	0.00	0.00	0.00	0.01	0.03

Analysis	29	30	31	32	33	34	35	36	37	38	39	40	41
Sample	34GALB04	34GALB04	7_1b	7_1b	7_1b	7_1b	7_1b	7_1b	7_1b	7_1b	7_2b	7_2b	7_2b
Name	Hd2	Hd2	Hd2	Hd2	Hd2	Hd2	Hd2	Hd2	Hd2	Hd2	Hd2	Hd2	Hd2
Alteration	Ca-Fe	Ca-Fe	Ca-Fe	Ca-Fe	Ca-Fe	Ca-Fe	Ca-Fe	Ca-Fe	Ca-Fe	Ca-Fe	Ca-Fe	Ca-Fe	Ca-Fe
SiO2	48.65	48.55	49.74	49.96	49.55	49.71	49.64	49.46	48.98	49.28	51.00	50.21	50.22
TiO2	0.00	0.09	0.05	0.07	0.02	0.01	0.01	0.05	0.07	0.01	0.08	0.05	0.01
Al2O3	1.19	1.11	0.75	0.91	0.86	0.15	1.26	1.00	0.93	0.49	1.10	1.11	1.04
FeO	25.76	25.64	27.14	27.77	27.12	27.25	26.88	26.64	27.14	28.42	26.70	26.42	26.51
MnO	0.64	0.77	0.49	0.52	0.49	0.61	0.56	0.51	0.39	0.58	0.51	0.58	0.48
MgO	1.82	1.80	1.01	1.07	1.02	1.12	1.33	1.66	1.09	0.51	1.34	1.32	1.25
CaO	19.87	20.12	20.41	19.99	19.87	21.95	19.22	18.99	19.72	20.78	19.15	19.32	20.10
Na2O	1.45	1.35	1.38	1.90	1.66	0.59	1.95	2.08	1.75	1.17	0.02	0.11	0.00
K2O	0.64	0.77	0.00	0.01	0.01	0.00	0.03	0.01	0.03	0.00	2.20	2.05	2.04
Total	100.0	100.2	101.0	102.2	100.6	101.4	100.9	100.4	100.1	101.2	102.1	101.2	101.7
[Si (T)	1.95	1.94	1.99	1.97	1.99	2.00	1.98	1.97	1.97	1.98	2.03	2.02	2.01
Al (T)	0.05	0.05	0.01	0.03	0.01	0.00	0.02	0.03	0.03	0.02	0.00	0.00	0.00
Fe3+ (T)	0.00	0.00	0.00	0.00	0.00	0.00	0.00	0.00	0.00	0.00	0.00	0.00	0.00
Total (T)]	2.00	2.00	2.00	2.00	2.00	2.00	2.00	2.00	2.00	2.00	2.03	2.02	2.01
[Al (M1)	0.01	0.00	0.03	0.01	0.03	0.00	0.04	0.02	0.02	0.01	0.05	0.05	0.05
Fe3+ (M1)	0.15	0.16	0.07	0.13	0.09	0.04	0.12	0.14	0.12	0.08	0.00	0.02	0.03
Ti (M1)	0.00	0.00	0.00	0.00	0.00	0.00	0.00	0.00	0.00	0.00	0.00	0.00	0.00
Mg (M1)	0.11	0.11	0.06	0.06	0.06	0.07	0.08	0.10	0.07	0.03	0.08	0.08	0.07
Fe2+ (M1)	0.71	0.70	0.84	0.78	0.82	0.88	0.77	0.74	0.79	0.87	0.87	0.84	0.84
Mn (M1)	0.02	0.03	0.00	0.01	0.00	0.01	0.00	0.00	0.00	0.01	0.00	0.00	0.00
Total (M1)]	1.00	0.99	1.00	1.00	1.00	1.00	1.00	1.00	1.00	1.00	1.00	1.00	1.00
[Mg (M2)	0.00	0.00	0.00	0.00	0.00	0.00	0.00	0.00	0.00	0.00	0.00	0.00	0.00
Fe2+ (M2)	0.00	0.00	0.00	0.00	0.00	0.00	0.01	0.01	0.00	0.00	0.03	0.02	0.01
Mn (M2)	0.00	0.00	0.02	0.01	0.02	0.01	0.02	0.02	0.01	0.01	0.02	0.02	0.02
Ca (M2)	0.85	0.86	0.88	0.84	0.85	0.95	0.82	0.81	0.85	0.90	0.82	0.83	0.86
Na (M2)	0.11	0.10	0.11	0.15	0.13	0.05	0.15	0.16	0.14	0.09	0.00	0.01	0.00
K (M2)	0.03	0.04	0.00	0.00	0.00	0.00	0.00	0.00	0.00	0.00	0.11	0.11	0.10
Total (M2)]	1.00	1.01	1.00	1.00	1.00	1.00	1.00	1.00	1.00	1.00	0.97	0.98	0.99
Wo	51.06	51.75	49.29	49.92	49.31	49.94	48.85	48.78	49.74	49.81	45.67	46.82	48.09
En	6.51	6.44	3.39	3.72	3.52	3.55	4.70	5.93	3.83	1.70	4.45	4.45	4.16
Fs	42.43	41.80	47.32	46.36	47.17	46.52	46.45	45.29	46.44	48.49	49.88	48.73	47.74
Fe/Fe+Mg	1.05	1.05	1.01	1.07	1.03	0.97	1.04	1.04	1.06	1.05	0.92	0.94	0.95
Q	1.67	1.67	1.78	1.69	1.73	1.89	1.68	1.66	1.71	1.80	1.79	1.77	1.79
J	0.23	0.21	0.21	0.29	0.26	0.09	0.30	0.32	0.27	0.18	0.00	0.02	0.00
Group	Ca-Mg-Fe	Ca-Mg-Fe	Ca-Mg-Fe	Ca-Mg-Fe	Ca-Mg-Fe	Ca-Mg-Fe	Ca-Mg-Fe	Ca-Mg-Fe	Ca-Mg-Fe	Ca-Mg-Fe	Ca-Mg-Fe	Ca-Mg-Fe	Ca-Mg-Fe
Na+AlIV	0.16	0.16	0.11	0.18	0.14	0.05	0.17	0.19	0.16	0.11	0.00	0.01	0.00
AlVI+2Ti+Cr	0.01	0.01	0.03	0.02	0.03	0.01	0.04	0.02	0.02	0.01	0.06	0.06	0.05

Analysis	42	43	44	45	46	47	48	49	50	51	52	53
Sample	7_2b	7_2b	7_2b	7_2b	7_2b	7_2b	7_2b	7-9b	7-9b	7-9b	7-9b	7-9b
Name	Hd2	Hd2	Hd2	Hd2	Hd2	Hd2	Hd2	Hd2	Hd2	Hd2	Hd2	Hd2
Alteration	Ca-Fe	Ca-Fe	Ca-Fe	Ca-Fe	Ca-Fe	Ca-Fe	Ca-Fe	Ca-Fe	Ca-Fe	Ca-Fe	Ca-Fe	Ca-Fe
SiO2	50.85	49.65	50.09	49.53	49.77	49.82	49.79	50.84	50.16	49.11	49.53	50.17
TiO2	0.07	0.06	0.00	0.04	0.07	0.02	0.00	0.00	0.01	0.02	0.02	0.00
Al2O3	0.98	0.49	0.49	0.83	0.72	0.88	0.31	0.37	0.29	0.24	0.16	0.08
FeO	26.50	27.27	27.02	27.90	27.81	27.39	26.83	28.07	28.57	27.54	27.81	28.67
MnO	0.56	0.35	0.52	0.50	0.59	0.50	0.59	0.75	0.80	0.59	0.76	0.85
MgO	1.23	0.71	0.86	0.63	0.63	0.65	0.79	0.14	0.27	0.63	0.28	0.30
CaO	19.67	21.25	21.33	20.53	21.08	20.94	22.42	21.39	21.25	21.95	22.48	22.14
Na2O	0.03	0.01	0.03	0.01	0.02	0.02	0.02	0.67	0.62	0.57	0.50	0.43
K2O	2.33	1.22	1.27	1.56	1.57	1.44	0.68	0.01	0.07	0.01	0.00	0.01
Total	102.2	101.0	101.6	101.5	102.3	101.7	101.4	102.2	102.0	100.7	101.5	102.7
[Si (T)	2.02	2.01	2.01	2.00	1.99	2.00	2.01	2.04	2.02	1.99	2.00	2.01
Al (T)	0.00	0.00	0.00	0.00	0.01	0.00	0.00	0.00	0.00	0.01	0.00	0.00
Fe3+ (T)	0.00	0.00	0.00	0.00	0.00	0.00	0.00	0.00	0.00	0.00	0.00	0.00
Total (T)]	2.02	2.01	2.01	2.00	2.00	2.00	2.01	2.04	2.02	2.00	2.00	2.01
[Al (M1)	0.05	0.02	0.02	0.04	0.02	0.04	0.01	0.02	0.01	0.01	0.01	0.00
Fe3+ (M1)	0.02	0.01	0.01	0.04	0.05	0.02	0.01	0.00	0.01	0.04	0.03	0.01
Ti (M1)	0.00	0.00	0.00	0.00	0.00	0.00	0.00	0.00	0.00	0.00	0.00	0.00
Mg (M1)	0.07	0.04	0.05	0.04	0.04	0.04	0.05	0.01	0.02	0.04	0.02	0.02
Fe2+ (M1)	0.86	0.91	0.89	0.89	0.88	0.90	0.90	0.97	0.95	0.90	0.91	0.95
Mn (M1)	0.00	0.01	0.02	0.00	0.01	0.00	0.02	0.00	0.01	0.02	0.03	0.02
Total (M1)]	1.00	1.00	1.00	1.00	1.00	1.00	0.99	1.00	1.00	1.00	0.99	1.00
[Mg (M2)	0.00	0.00	0.00	0.00	0.00	0.00	0.00	0.00	0.00	0.00	0.00	0.00
Fe2+ (M2)	0.00	0.00	0.00	0.02	0.00	0.00	0.00	0.00	0.00	0.00	0.00	0.00
Mn (M2)	0.02	0.00	0.00	0.02	0.01	0.02	0.00	0.02	0.02	0.00	0.00	0.01
Ca (M2)	0.84	0.92	0.92	0.89	0.90	0.90	0.97	0.92	0.91	0.95	0.97	0.95
Na (M2)	0.00	0.00	0.00	0.00	0.00	0.00	0.00	0.05	0.05	0.04	0.04	0.03
K (M2)	0.12	0.06	0.07	0.08	0.08	0.07	0.04	0.00	0.00	0.00	0.00	0.00
Total (M2)]	0.98	0.99	0.99	1.00	1.00	1.00	1.01	1.00	0.98	1.00	1.01	0.99
Wo	47.37	49.16	49.29	48.54	49.63	49.02	50.57	48.33	48.51	50.49	51.14	49.60
En	4.12	2.29	2.77	2.07	2.06	2.12	2.48	0.44	0.86	2.02	0.89	0.94
Fs	48.50	48.55	47.95	49.38	48.30	48.86	46.95	51.23	50.63	47.49	47.97	49.46
Fe/Fe+Mg	0.95	0.97	0.96	1.00	1.01	0.98	0.96	0.99	0.99	1.00	1.01	0.99
Q	1.77	1.88	1.86	1.83	1.82	1.84	1.92	1.90	1.89	1.89	1.90	1.91
J	0.00	0.00	0.00	0.00	0.00	0.00	0.00	0.10	0.10	0.09	0.08	0.07
Group	Ca-Mg-Fe	Ca-Mg-Fe	Ca-Mg-Fe	Ca-Mg-Fe	Ca-Mg-Fe	Ca-Mg-Fe	Ca-Mg-Fe	Ca-Mg-Fe	Ca-Mg-Fe	Ca-Mg-Fe	Ca-Mg-Fe	Ca-Mg-Fe
Na+AlIV	0.00	0.00	0.00	0.00	0.01	0.00	0.00	0.05	0.05	0.05	0.04	0.03
AlVI+2Ti+Cr	0.05	0.03	0.02	0.04	0.03	0.04	0.01	0.02	0.01	0.01	0.01	0.00

Analysis	54	55	56	57	58	59	60	61	62	63	64
Sample	7-9b	34MALB02	34MALB02	34MALB02	34MALB02	34MALB02	34MALB02	ALB/GNA01	ALB/GNA01	ALB/GNA01	ALB/GNA01
Name	Hd2	Hd3	Hd3	Hd3	Hd3	Hd3	Hd3	Hd3	Hd3	Hd3	Hd3
Alteration	Ca-Fe	Ca-Fe	Ca-Fe	Ca-Fe	Ca-Fe	Ca-Fe	Ca-Fe	Ca-Fe	Ca-Fe	Ca-Fe	Ca-Fe
SiO2	50.37	47.90	50.00	49.58	48.21	48.67	48.80	51.76	52.63	51.90	51.94
TiO2	0.00	0.08	0.04	0.12	0.05	0.12	0.03	0.03	0.03	0.02	0.07
Al2O3	0.26	1.06	0.34	1.32	0.57	0.55	0.36	0.81	0.92	0.87	0.95
FeO	28.97	27.41	27.08	27.51	26.81	27.29	27.27	18.50	17.03	17.17	18.25
MnO	0.83	2.00	2.00	1.00	2.00	2.00	2.00	1.13	1.05	1.01	0.97
MgO	0.26	0.41	0.39	0.45	0.38	0.41	0.43	6.35	7.48	7.10	6.35
CaO	21.91	19.88	20.64	19.83	20.30	20.30	20.45	20.01	19.59	19.86	20.00
Na2O	0.56	1.24	1.23	1.31	0.67	0.67	0.70	2.05	2.35	2.27	2.45
K2O	0.02	1.63	1.53	1.37	1.66	1.63	1.53	0.02	0.01	0.02	0.01
Total	103.2	101.6	103.3	102.5	100.7	101.6	101.6	100.7	101.1	100.2	101.0
[Si (T)	2.00	1.91	1.96	1.96	1.95	1.95	1.96	1.99	1.99	1.99	1.98
Al (T)	0.00	0.05	0.02	0.04	0.03	0.03	0.02	0.01	0.01	0.01	0.02
Fe3+ (T)	0.00	0.04	0.02	0.00	0.02	0.02	0.02	0.00	0.00	0.00	0.00
Total (T)]	2.00	2.00	2.00	2.00	2.00	2.00	2.00	2.00	2.00	2.00	2.00
[Al (M1)	0.01	0.00	0.00	0.02	0.00	0.00	0.00	0.03	0.04	0.03	0.02
Fe3+ (M1)	0.02	0.21	0.16	0.15	0.15	0.14	0.14	0.11	0.12	0.13	0.14
Ti (M1)	0.00	0.00	0.00	0.00	0.00	0.00	0.00	0.00	0.00	0.00	0.00
Mg (M1)	0.02	0.02	0.02	0.03	0.02	0.02	0.03	0.36	0.42	0.41	0.36
Fe2+ (M1)	0.94	0.67	0.71	0.76	0.74	0.76	0.76	0.48	0.42	0.42	0.44
Mn (M1)	0.01	0.07	0.07	0.03	0.07	0.07	0.07	0.01	0.00	0.02	0.03
Total (M1)]	1.00	0.97	0.96	0.99	0.98	0.99	0.99	1.00	1.00	1.00	1.00
[Mg (M2)	0.00	0.00	0.00	0.00	0.00	0.00	0.00	0.00	0.00	0.00	0.00
Fe2+ (M2)	0.00	0.00	0.00	0.00	0.00	0.00	0.00	0.00	0.00	0.00	0.00
Mn (M2)	0.02	0.00	0.00	0.00	0.00	0.00	0.00	0.02	0.03	0.02	0.00
Ca (M2)	0.93	0.85	0.87	0.84	0.88	0.87	0.88	0.82	0.80	0.81	0.82
Na (M2)	0.04	0.10	0.09	0.10	0.05	0.05	0.05	0.15	0.17	0.17	0.18
K (M2)	0.00	0.08	0.08	0.07	0.09	0.08	0.08	0.00	0.00	0.00	0.00
Total (M2)]	1.00	1.03	1.04	1.01	1.02	1.01	1.01	1.00	1.00	1.00	1.00
Wo	49.37	55.02	54.34	51.71	53.54	52.81	52.94	49.34	48.49	49.58	50.48
En	0.82	1.58	1.43	1.63	1.39	1.48	1.55	21.79	25.76	24.66	22.30
Fs	49.82	43.40	44.23	46.66	45.07	45.71	45.51	28.87	25.75	25.76	27.22
Fe/Fe+Mg	1.01	1.15	1.13	1.13	1.11	1.10	1.09	0.74	0.68	0.71	0.77
Q	1.89	1.55	1.60	1.62	1.65	1.65	1.66	1.67	1.64	1.64	1.62
J	0.09	0.19	0.19	0.20	0.11	0.10	0.11	0.31	0.35	0.34	0.36
Group	Ca-Mg-Fe	Ca-Mg-Fe	Ca-Mg-Fe	Ca-Mg-Fe	Ca-Mg-Fe	Ca-Mg-Fe	Ca-Mg-Fe	Ca-Mg-Fe	Ca-Mg-Fe	Ca-Mg-Fe	Ca-Mg-Fe
Na+AlIV	0.04	0.15	0.11	0.14	0.08	0.08	0.07	0.16	0.18	0.18	0.20
AlVI+2Ti+Cr	0.01	0.00	0.00	0.03	0.00	0.01	0.00	0.03	0.04	0.03	0.03

Analysis	65	66	67	68	69	70	71	72	73	74	75
Sample	ALB/GN A01	ALB/GN A01	ALB/GN A01	ALB/GN A01	ALB/GN A01	ALB/GN A01	F11AL B01	F11AL B01	F11AL B01	F11AL B01	F11AL B01
Name	Hd3	Hd3	Hd3	Hd3	Hd3	Hd3	Hd3	Hd3	Hd3	Hd3	Hd3
Alteration	Ca-Fe	Ca-Fe	Ca-Fe	Ca-Fe	Ca-Fe	Ca-Fe	Ca-Fe	Ca-Fe	Ca-Fe	Ca-Fe	Ca-Fe
SiO2	51.17	50.77	50.60	51.08	52.65	52.33	50.63	49.97	49.68	49.24	49.79
TiO2	0.02	0.06	0.08	0.04	0.04	0.04	0.04	0.06	0.06	0.00	0.01
Al2O3	0.97	0.91	0.83	1.00	0.89	0.99	0.55	0.68	1.03	0.93	0.68
FeO	17.56	17.73	18.86	17.67	17.96	17.73	15.12	16.90	17.30	17.01	17.33
MnO	1.11	1.19	1.35	1.13	1.16	1.04	0.74	0.72	0.90	0.76	0.76
MgO	7.00	6.50	5.97	6.17	6.85	6.77	8.13	7.17	6.78	6.90	7.09
CaO	19.68	20.00	20.12	19.59	19.84	19.88	22.45	21.41	21.22	21.16	21.25
Na2O	1.83	2.15	1.88	2.21	2.18	2.24	0.84	1.26	1.33	1.26	1.19
K2O	0.02	0.02	0.01	0.03	0.02	0.01	0.00	0.00	0.01	0.00	0.00
Total	99.4	99.3	99.7	98.9	101.6	101.0	98.5	98.2	98.3	97.3	98.1
[Si (T)	1.99	1.97	1.97	1.99	2.00	1.99	1.98	1.97	1.96	1.96	1.96
Al (T)	0.01	0.03	0.03	0.01	0.00	0.01	0.02	0.03	0.04	0.04	0.03
Fe3+ (T)	0.00	0.00	0.00	0.00	0.00	0.00	0.00	0.00	0.00	0.00	0.00
Total (T)]	2.00	2.00	2.00	2.00	2.00	2.00	2.00	2.00	2.00	2.00	2.00
[Al (M1)	0.03	0.01	0.01	0.04	0.04	0.04	0.00	0.00	0.00	0.00	0.00
Fe3+ (M1)	0.10	0.14	0.13	0.11	0.10	0.11	0.07	0.10	0.11	0.11	0.10
Ti (M1)	0.00	0.00	0.00	0.00	0.00	0.00	0.00	0.00	0.00	0.00	0.00
Mg (M1)	0.41	0.38	0.35	0.36	0.39	0.38	0.47	0.42	0.40	0.41	0.42
Fe2+ (M1)	0.46	0.43	0.49	0.47	0.47	0.46	0.43	0.45	0.46	0.45	0.46
Mn (M1)	0.00	0.03	0.03	0.02	0.00	0.01	0.02	0.02	0.03	0.02	0.01
Total (M1)]	1.00	1.00	1.00	1.00	1.00	1.00	1.00	1.00	1.00	1.00	1.00
[Mg (M2)	0.00	0.00	0.00	0.00	0.00	0.00	0.00	0.00	0.00	0.00	0.00
Fe2+ (M2)	0.01	0.00	0.00	0.00	0.00	0.00	0.00	0.00	0.00	0.00	0.00
Mn (M2)	0.04	0.01	0.02	0.01	0.03	0.02	0.00	0.00	0.00	0.00	0.01
Ca (M2)	0.82	0.83	0.84	0.82	0.81	0.81	0.94	0.90	0.90	0.90	0.90
Na (M2)	0.14	0.16	0.14	0.17	0.16	0.17	0.06	0.10	0.10	0.10	0.09
K (M2)	0.00	0.00	0.00	0.00	0.00	0.00	0.00	0.00	0.00	0.00	0.00
Total (M2)]	1.00	1.00	1.00	1.00	1.00	1.00	1.00	1.00	1.00	1.00	1.00
Wo	48.31	50.74	50.23	49.84	48.56	49.11	51.04	50.88	51.20	51.15	50.46
En	23.91	22.95	20.74	21.84	23.33	23.27	25.72	23.71	22.76	23.21	23.43
Fs	27.77	26.31	29.03	28.32	28.11	27.63	23.24	25.42	26.03	25.64	26.11
Fe/Fe+Mg	0.68	0.76	0.77	0.74	0.70	0.71	0.58	0.67	0.71	0.70	0.68
Q	1.69	1.64	1.67	1.64	1.66	1.65	1.84	1.77	1.75	1.76	1.78
J	0.28	0.32	0.28	0.33	0.32	0.33	0.13	0.19	0.20	0.19	0.18
Group	Ca-Mg-Fe	Ca-Mg-Fe	Ca-Mg-Fe	Ca-Mg-Fe	Ca-Mg-Fe	Ca-Mg-Fe	Ca-Mg-Fe	Ca-Mg-Fe	Ca-Mg-Fe	Ca-Mg-Fe	Ca-Mg-Fe
Na+AlIV	0.15	0.19	0.17	0.17	0.16	0.17	0.09	0.13	0.15	0.14	0.12
AlVI+2Ti+Cr	0.03	0.02	0.01	0.04	0.04	0.04	0.01	0.00	0.01	0.00	0.00

Analysis	76	77	78	79	80	81	82	83	84	85	86
Sample	F11ALB01	F11ALB01	F11ALB01	F11ALB01	F11ALB01	F11ALB01	F11ALB01	F11ALB01	F11ALB01	F11ALB01	F11ALB01
Name	Hd3	Hd3	Hd3	Hd3	Hd3	Hd3	Hd3	Hd3	Hd3	Hd3	Hd3
Alteration	Ca-Fe	Ca-Fe	Ca-Fe	Ca-Fe	Ca-Fe	Ca-Fe	Ca-Fe	Ca-Fe	Ca-Fe	Ca-Fe	Ca-Fe
SiO2	51.83	49.17	51.65	51.88	52.00	50.94	52.83	53.05	52.16	52.41	51.94
TiO2	0.03	0.04	0.04	0.03	0.00	0.09	0.00	0.07	0.00	0.00	0.01
Al2O3	0.71	0.68	0.37	0.79	0.58	0.56	0.56	0.62	0.49	0.23	0.13
FeO	16.49	18.16	15.97	14.23	14.21	15.28	16.27	14.83	15.24	14.68	15.32
MnO	0.51	0.74	0.70	0.59	0.58	0.64	0.56	0.64	0.62	0.91	1.07
MgO	7.48	7.32	8.47	8.30	8.73	8.35	8.44	8.64	8.18	8.18	8.13
CaO	20.14	20.93	20.03	20.30	20.54	21.70	20.93	21.21	21.69	22.09	22.85
Na2O	1.48	1.23	0.60	1.20	1.18	1.01	1.18	1.17	0.92	0.71	0.68
K2O	0.00	0.01	0.02	0.01	0.00	0.02	0.00	0.00	0.00	0.01	0.03
Total	98.7	98.3	97.9	97.3	97.8	98.6	100.8	100.2	99.3	99.2	100.2
[Si (T)	2.02	1.94	2.04	2.04	2.03	1.98	2.02	2.03	2.02	2.04	2.00
Al (T)	0.00	0.03	0.00	0.00	0.00	0.02	0.00	0.00	0.00	0.00	0.00
Fe3+ (T)	0.00	0.03	0.00	0.00	0.00	0.00	0.00	0.00	0.00	0.00	0.00
Total (T)]	2.02	2.00	2.04	2.04	2.03	2.00	2.02	2.03	2.02	2.04	2.00
[Al (M1)	0.03	0.00	0.02	0.04	0.03	0.01	0.03	0.03	0.02	0.01	0.01
Fe3+ (M1)	0.03	0.12	0.00	0.00	0.00	0.06	0.03	0.00	0.00	0.00	0.03
Ti (M1)	0.00	0.00	0.00	0.00	0.00	0.00	0.00	0.00	0.00	0.00	0.00
Mg (M1)	0.44	0.43	0.50	0.49	0.51	0.49	0.48	0.49	0.47	0.47	0.47
Fe2+ (M1)	0.50	0.44	0.48	0.48	0.46	0.43	0.47	0.47	0.49	0.50	0.46
Mn (M1)	0.00	0.00	0.00	0.00	0.00	0.00	0.00	0.00	0.01	0.02	0.03
Total (M1)]	1.00	1.00	1.00	1.00	1.00	1.00	1.00	1.00	1.00	1.00	1.00
[Mg (M2)	0.00	0.00	0.00	0.00	0.00	0.00	0.00	0.00	0.00	0.00	0.00
Fe2+ (M2)	0.01	0.00	0.09	0.02	0.00	0.00	0.02	0.00	0.00	0.00	0.00
Mn (M2)	0.02	0.02	0.02	0.02	0.02	0.02	0.02	0.02	0.01	0.01	0.00
Ca (M2)	0.84	0.88	0.85	0.86	0.86	0.91	0.86	0.87	0.90	0.92	0.94
Na (M2)	0.11	0.09	0.05	0.09	0.09	0.08	0.09	0.09	0.07	0.05	0.05
K (M2)	0.00	0.00	0.00	0.00	0.00	0.00	0.00	0.00	0.00	0.00	0.00
Total (M2)]	0.98	1.00	1.00	0.98	0.97	1.00	0.98	0.97	0.98	0.99	1.00
Wo	47.09	50.24	44.25	46.66	46.89	49.64	46.80	47.32	48.33	48.56	50.47
En	24.33	24.45	26.03	26.55	27.73	26.58	26.26	26.82	25.36	25.02	24.98
Fs	28.57	25.30	29.72	26.79	25.37	23.79	26.95	25.86	26.31	26.42	24.55
Fe/Fe+Mg	0.58	0.67	0.49	0.49	0.48	0.57	0.53	0.49	0.51	0.51	0.55
Q	1.79	1.76	1.91	1.83	1.83	1.82	1.83	1.84	1.86	1.89	1.87
J	0.22	0.19	0.09	0.18	0.18	0.15	0.17	0.17	0.14	0.11	0.10
Group	Ca-Mg-Fe	Ca-Mg-Fe	Ca-Mg-Fe	Ca-Mg-Fe	Ca-Mg-Fe	Ca-Mg-Fe	Ca-Mg-Fe	Ca-Mg-Fe	Ca-Mg-Fe	Ca-Mg-Fe	Ca-Mg-Fe
Na+AlIV	0.11	0.13	0.05	0.09	0.09	0.09	0.09	0.09	0.07	0.05	0.05
AlVI+2Ti+Cr	0.03	0.00	0.02	0.04	0.03	0.02	0.03	0.03	0.02	0.01	0.01

Analysis	87	88	89	90	91	92	93	94	95	96	97
Sample	F11ALB01	F11ALB01	F11ALB01	F11ALB01	F11ALB01	F11ALB01	AN34	AN34	AN34	AN34	AN34
Name	Hd3	Hd3	Hd3	Hd3	Hd3	Hd3	Dp	Dp	Dp	Dp	Dp
Alteration	Ca-Fe	Ca-Fe	Ca-Fe	Ca-Fe	Ca-Fe	Ca-Fe	Ca-Mg	Ca-Mg	Ca-Mg	Ca-Mg	Ca-Mg
SiO2	51.65	52.72	52.90	52.67	51.23	50.55	52.96	52.32	53.34	51.36	53.36
TiO2	0.03	0.04	0.00	0.00	0.00	0.04	0.06	0.03	0.03	0.00	0.02
Al2O3	0.92	0.60	0.58	0.53	0.55	0.79	1.20	1.22	0.99	1.25	1.00
FeO	16.89	16.32	16.53	14.56	14.56	17.28	14.08	14.48	12.89	14.61	12.65
MnO	0.68	0.62	0.45	0.66	0.66	0.67	0.41	0.37	0.24	0.37	0.28
MgO	7.50	8.18	7.84	8.78	8.48	6.87	8.74	8.65	10.27	8.27	10.19
CaO	20.93	20.84	21.00	21.65	22.74	21.52	21.30	21.26	21.86	21.32	21.91
Na2O	1.42	1.22	1.21	0.99	0.80	1.27	1.90	1.79	1.83	1.62	1.60
K2O	0.01	0.04	0.01	0.00	0.00	0.02	0.00	0.01	0.01	0.01	0.00
Total	100.0	100.6	100.5	99.8	99.0	99.0	100.7	100.1	101.5	98.8	101.0
[Si (T)	1.99	2.02	2.03	2.02	1.99	1.98	2.00	1.99	1.98	1.98	1.99
Al (T)	0.01	0.00	0.00	0.00	0.01	0.02	0.00	0.01	0.02	0.02	0.01
Fe3+ (T)	0.00	0.00	0.00	0.00	0.00	0.00	0.00	0.00	0.00	0.00	0.00
Total (T)]	2.00	2.02	2.03	2.02	2.00	2.00	2.00	2.00	2.00	2.00	2.00
[Al (M1)	0.03	0.03	0.03	0.02	0.01	0.01	0.05	0.04	0.02	0.04	0.04
Fe3+ (M1)	0.07	0.02	0.01	0.01	0.05	0.09	0.07	0.09	0.11	0.08	0.07
Ti (M1)	0.00	0.00	0.00	0.00	0.00	0.00	0.00	0.00	0.00	0.00	0.00
Mg (M1)	0.43	0.47	0.45	0.50	0.49	0.40	0.49	0.49	0.57	0.48	0.57
Fe2+ (M1)	0.47	0.48	0.52	0.46	0.42	0.48	0.37	0.37	0.29	0.39	0.32
Mn (M1)	0.00	0.00	0.00	0.01	0.02	0.02	0.01	0.01	0.01	0.01	0.00
Total (M1)]	1.00	1.00	1.00	1.00	1.00	1.00	1.00	1.00	1.00	1.00	1.00
[Mg (M2)	0.00	0.00	0.00	0.00	0.00	0.00	0.00	0.00	0.00	0.00	0.00
Fe2+ (M2)	0.01	0.02	0.00	0.00	0.00	0.00	0.00	0.00	0.00	0.00	0.00
Mn (M2)	0.02	0.02	0.01	0.02	0.00	0.00	0.00	0.00	0.00	0.00	0.01
Ca (M2)	0.86	0.85	0.86	0.89	0.94	0.90	0.86	0.86	0.87	0.88	0.88
Na (M2)	0.11	0.09	0.09	0.07	0.06	0.10	0.14	0.13	0.13	0.12	0.12
K (M2)	0.00	0.00	0.00	0.00	0.00	0.00	0.00	0.00	0.00	0.00	0.00
Total (M2)]	1.00	0.98	0.97	0.98	1.00	1.00	1.00	1.00	1.00	1.00	1.00
Wo	48.81	46.98	47.03	48.02	50.92	50.66	49.94	50.02	50.21	50.54	49.60
En	24.34	25.66	24.43	27.10	26.42	22.50	28.51	28.32	32.82	27.28	32.09
Fs	26.85	27.36	28.53	24.88	22.65	26.83	21.54	21.66	16.97	22.19	18.31
Fe/Fe+Mg	0.63	0.55	0.55	0.49	0.54	0.68	0.55	0.57	0.52	0.59	0.48
Q	1.77	1.82	1.83	1.85	1.86	1.78	1.72	1.73	1.73	1.74	1.77
J	0.21	0.18	0.18	0.15	0.12	0.19	0.28	0.26	0.26	0.24	0.23
Group	Ca-Mg-Fe	Ca-Mg-Fe	Ca-Mg-Fe	Ca-Mg-Fe	Ca-Mg-Fe	Ca-Mg-Fe	Ca-Mg-Fe	Ca-Mg-Fe	Ca-Mg-Fe	Ca-Mg-Fe	Ca-Mg-Fe
Na+AlIV	0.12	0.09	0.09	0.07	0.07	0.12	0.14	0.15	0.15	0.14	0.12
AlVI+2Ti+Cr	0.03	0.03	0.03	0.02	0.01	0.02	0.05	0.04	0.02	0.04	0.04

Analysis	98	99	100	101	102	103	104	105	106	107	108
Sample	AN34	AN34	AN34	AN34	AN34	AN34	AN34	AN34	AN34	AN34	ALB/GNA01 DP
Name	Dp	Dp	Dp	Dp	Dp	Dp	Dp	Dp	Dp	Dp	Dp
Alteration	Ca-Mg	Ca-Mg	Ca-Mg	Ca-Mg	Ca-Mg	Ca-Mg	Ca-Mg	Ca-Mg	Ca-Mg	Ca-Mg	Ca-Mg
SiO2	52.27	51.99	52.89	53.31	52.58	52.66	52.53	53.00	52.98	53.55	53.38
TiO2	0.02	0.03	0.06	0.00	0.04	0.03	0.04	0.04	0.01	0.02	0.03
Al2O3	1.14	1.17	1.01	1.21	1.35	1.36	1.16	1.40	1.22	0.91	0.65
FeO	14.56	13.52	13.75	14.89	15.26	13.65	13.50	14.46	13.04	12.93	13.24
MnO	0.27	0.31	0.49	0.36	0.30	0.42	0.30	0.35	0.31	0.38	1.09
MgO	9.02	9.66	9.33	9.04	8.25	9.26	8.43	8.65	9.50	9.98	9.55
CaO	21.28	22.29	21.74	21.22	21.03	21.60	21.66	21.25	21.83	22.32	21.68
Na2O	1.85	1.39	1.69	1.95	2.06	1.65	1.42	2.07	1.62	1.31	1.56
K2O	0.00	0.03	0.01	0.00	0.00	0.00	0.00	0.00	0.00	0.00	0.02
Total	100.4	100.4	101.0	102.0	100.9	100.6	99.0	101.2	100.5	101.4	101.2
[Si (T)	1.97	1.96	1.99	1.98	1.98	1.98	2.02	1.99	1.99	2.00	2.00
Al (T)	0.03	0.04	0.01	0.02	0.02	0.02	0.00	0.01	0.01	0.00	0.00
Fe3+ (T)	0.00	0.00	0.00	0.00	0.00	0.00	0.00	0.00	0.00	0.00	0.00
Total (T)]	2.00	2.00	2.00	2.00	2.00	2.00	2.02	2.00	2.00	2.00	2.00
[Al (M1)	0.03	0.01	0.03	0.04	0.04	0.04	0.05	0.05	0.05	0.04	0.03
Fe3+ (M1)	0.11	0.10	0.09	0.10	0.10	0.08	0.01	0.09	0.06	0.04	0.07
Ti (M1)	0.00	0.00	0.00	0.00	0.00	0.00	0.00	0.00	0.00	0.00	0.00
Mg (M1)	0.51	0.54	0.52	0.50	0.46	0.52	0.48	0.48	0.53	0.56	0.53
Fe2+ (M1)	0.35	0.32	0.35	0.36	0.38	0.35	0.43	0.36	0.35	0.36	0.35
Mn (M1)	0.01	0.01	0.01	0.00	0.01	0.01	0.01	0.01	0.01	0.00	0.02
Total (M1)]	1.00	1.00	1.00	1.00	1.00	1.00	0.98	1.00	1.00	1.00	1.00
[Mg (M2)	0.00	0.00	0.00	0.00	0.00	0.00	0.00	0.00	0.00	0.00	0.00
Fe2+ (M2)	0.00	0.00	0.00	0.00	0.00	0.00	0.00	0.00	0.00	0.00	0.00
Mn (M2)	0.00	0.00	0.00	0.01	0.00	0.01	0.00	0.00	0.00	0.01	0.01
Ca (M2)	0.86	0.90	0.87	0.85	0.85	0.87	0.89	0.85	0.88	0.89	0.87
Na (M2)	0.14	0.10	0.12	0.14	0.15	0.12	0.11	0.15	0.12	0.09	0.11
K (M2)	0.00	0.00	0.00	0.00	0.00	0.00	0.00	0.00	0.00	0.00	0.00
Total (M2)]	1.00	1.00	1.00	1.00	1.00	1.00	1.00	1.00	1.00	1.00	1.00
Wo	50.10	50.96	50.18	49.42	50.15	49.93	49.54	50.33	49.99	49.40	49.69
En	29.55	30.73	29.96	29.29	27.37	29.78	26.83	28.50	30.27	30.73	30.45
Fs	20.35	18.31	19.86	21.29	22.48	20.29	23.63	21.17	19.74	19.87	19.86
Fe/Fe+Mg	0.59	0.55	0.54	0.58	0.62	0.53	0.48	0.58	0.50	0.47	0.51
Q	1.72	1.77	1.74	1.71	1.69	1.75	1.80	1.70	1.76	1.81	1.75
J	0.27	0.20	0.25	0.28	0.30	0.24	0.21	0.30	0.24	0.19	0.23
Group	Ca-Mg-Fe	Ca-Mg-Fe	Ca-Mg-Fe	Ca-Mg-Fe	Ca-Mg-Fe	Ca-Mg-Fe	Ca-Mg-Fe	Ca-Mg-Fe	Ca-Mg-Fe	Ca-Mg-Fe	Ca-Mg-Fe
Na+AlIV	0.16	0.14	0.14	0.16	0.17	0.14	0.11	0.16	0.12	0.10	0.11
AlVI+2Ti+Cr	0.03	0.02	0.03	0.04	0.05	0.05	0.06	0.05	0.05	0.04	0.03

Analysis	109	110	111	112	113	114	115	116	117	118
Sample	ALB/GNA01 DP	ALB/GNA01 DP	ALB/GNA01 DP	ALB/GNA01 DP	ALB/GNA01 DP	ALB05	ALB05	ALB05	ALB05	ALB05
Name	Dp	Dp	Dp	Dp	Dp	Dp	Dp	Dp	Dp	Dp
Alteration	Ca-Mg	Ca-Mg	Ca-Mg	Ca-Mg	Ca-Mg	Ca-Mg	Ca-Mg	Ca-Mg	Ca-Mg	Ca-Mg
SiO2	53.25	52.97	52.36	53.34	53.39	54.16	54.19	54.10	53.98	53.49
TiO2	0.06	0.02	0.03	0.02	0.02	0.01	0.02	0.01	0.02	0.02
Al2O3	0.65	0.53	0.88	0.92	0.66	0.65	0.60	0.71	0.54	0.42
FeO	13.36	12.19	14.16	14.88	13.40	12.59	13.21	12.58	12.39	12.05
MnO	1.08	1.07	1.05	1.01	1.03	0.34	0.37	0.37	0.46	0.44
MgO	9.88	10.42	8.73	8.69	9.45	10.54	10.34	10.49	10.39	10.42
CaO	21.00	21.31	20.62	19.93	20.60	21.53	21.89	21.60	22.22	22.16
Na2O	2.07	1.90	1.97	2.09	2.04	1.64	1.65	1.47	1.46	1.56
K2O	0.01	0.01	0.02	0.01	0.01	0.01	0.01	0.01	0.01	0.01
Total	101.4	100.4	99.8	100.9	100.6	101.5	102.3	101.3	101.5	100.6
[Si (T)	1.98	1.98	1.99	2.01	2.01	2.01	2.00	2.01	2.01	2.00
Al (T)	0.02	0.02	0.01	0.00	0.00	0.00	0.00	0.00	0.00	0.00
Fe3+ (T)	0.00	0.00	0.00	0.00	0.00	0.00	0.00	0.00	0.00	0.00
Total (T)]	2.00	2.00	2.00	2.01	2.01	2.01	2.00	2.01	2.01	2.00
[Al (M1)	0.01	0.01	0.03	0.04	0.03	0.03	0.03	0.03	0.02	0.02
Fe3+ (M1)	0.12	0.12	0.10	0.07	0.09	0.06	0.07	0.04	0.05	0.07
Ti (M1)	0.00	0.00	0.00	0.00	0.00	0.00	0.00	0.00	0.00	0.00
Mg (M1)	0.55	0.58	0.50	0.49	0.53	0.58	0.57	0.58	0.58	0.58
Fe2+ (M1)	0.29	0.26	0.35	0.39	0.34	0.33	0.33	0.35	0.33	0.31
Mn (M1)	0.02	0.03	0.02	0.00	0.02	0.00	0.00	0.00	0.01	0.01
Total (M1)]	1.00	1.00	1.00	1.00	1.00	1.00	1.00	1.00	1.00	0.99
[Mg (M2)	0.00	0.00	0.00	0.00	0.00	0.00	0.00	0.00	0.00	0.00
Fe2+ (M2)	0.00	0.00	0.00	0.00	0.00	0.00	0.00	0.01	0.00	0.00
Mn (M2)	0.01	0.01	0.01	0.03	0.01	0.01	0.01	0.01	0.00	0.00
Ca (M2)	0.84	0.86	0.84	0.80	0.83	0.86	0.87	0.86	0.89	0.89
Na (M2)	0.15	0.14	0.15	0.15	0.15	0.12	0.12	0.11	0.11	0.11
K (M2)	0.00	0.00	0.00	0.00	0.00	0.00	0.00	0.00	0.00	0.00
Total (M2)]	1.00	1.00	1.00	0.99	0.99	0.99	1.00	0.99	0.99	1.00
Wo	49.94	50.32	49.81	47.68	48.96	48.25	48.97	47.94	49.38	50.03
En	32.69	34.24	29.34	28.93	31.25	32.87	32.19	32.39	32.12	32.73
Fs	17.36	15.44	20.85	23.39	19.79	18.88	18.84	19.67	18.50	17.23
Fe/Fe+Mg	0.56	0.52	0.58	0.57	0.53	0.46	0.49	0.44	0.46	0.47
Q	1.68	1.70	1.69	1.69	1.69	1.78	1.77	1.80	1.79	1.78
J	0.30	0.28	0.29	0.31	0.30	0.24	0.24	0.21	0.21	0.23
Group	Ca-Mg-Fe	Ca-Mg-Fe	Ca-Mg-Fe	Ca-Mg-Fe	Ca-Mg-Fe	Ca-Mg-Fe	Ca-Mg-Fe	Ca-Mg-Fe	Ca-Mg-Fe	Ca-Mg-Fe
Na+AlIV	0.17	0.15	0.15	0.15	0.15	0.12	0.12	0.11	0.11	0.11
AlVI+2Ti+Cr	0.02	0.01	0.03	0.04	0.03	0.03	0.03	0.03	0.02	0.02

Analysis	119	120	121	122	123	124	125	126	127	128
Sample	ALB05	ALB05	ALB05	ALB05	ALB05	ALB05	ALB05	ALB05	ALB05	MAAB03
Name	Dp	Dp	Dp	Dp	Dp	Dp	Dp	Dp	Dp	Dp
Alteration	Ca-Mg	Ca-Mg	Ca-Mg	Ca-Mg	Ca-Mg	Ca-Mg	Ca-Mg	Ca-Mg	Ca-Mg	Ca-Mg
SiO2	52.83	51.48	52.82	52.92	53.23	53.48	52.91	53.06	52.44	53.30
TiO2	0.02	0.04	0.00	0.00	0.02	0.03	0.00	0.07	0.00	0.04
Al2O3	0.73	2.21	0.58	0.70	0.48	0.82	0.51	0.68	0.63	1.64
FeO	13.40	12.54	12.69	13.42	13.42	13.43	12.69	14.17	13.89	12.07
MnO	0.36	0.49	0.47	0.43	0.32	0.41	0.38	0.51	0.32	0.31
MgO	9.88	9.55	10.13	9.78	9.74	9.66	9.73	9.73	9.91	10.64
CaO	21.52	21.03	21.70	20.94	20.55	21.21	21.59	21.86	21.43	20.98
Na2O	1.54	1.59	1.69	2.08	2.16	1.62	1.39	1.63	1.72	1.89
K2O	0.02	0.03	0.02	0.02	0.06	0.01	0.01	0.00	0.02	0.00
Total	100.3	99.0	100.1	100.3	100.0	100.7	99.2	101.7	100.4	100.9
[Si (T)	1.99	1.96	1.99	1.99	2.01	2.01	2.02	1.98	1.98	1.98
Al (T)	0.01	0.04	0.01	0.01	0.00	0.00	0.00	0.02	0.02	0.02
Fe3+ (T)	0.00	0.00	0.00	0.00	0.00	0.00	0.00	0.00	0.00	0.00
Total (T)]	2.00	2.00	2.00	2.00	2.01	2.01	2.02	2.00	2.00	2.00
[Al (M1)	0.03	0.06	0.02	0.02	0.02	0.04	0.02	0.01	0.00	0.05
Fe3+ (M1)	0.08	0.08	0.10	0.12	0.10	0.05	0.03	0.11	0.12	0.08
Ti (M1)	0.00	0.00	0.00	0.00	0.00	0.00	0.00	0.00	0.00	0.00
Mg (M1)	0.56	0.54	0.57	0.55	0.55	0.54	0.55	0.54	0.56	0.59
Fe2+ (M1)	0.34	0.32	0.30	0.30	0.32	0.37	0.37	0.34	0.32	0.27
Mn (M1)	0.00	0.00	0.02	0.01	0.01	0.00	0.01	0.01	0.00	0.00
Total (M1)]	1.00	1.00	1.00	1.00	1.00	1.00	0.99	1.00	1.00	1.00
[Mg (M2)	0.00	0.00	0.00	0.00	0.00	0.00	0.00	0.00	0.00	0.00
Fe2+ (M2)	0.00	0.01	0.00	0.00	0.00	0.00	0.00	0.00	0.00	0.02
Mn (M2)	0.01	0.02	0.00	0.00	0.00	0.01	0.00	0.01	0.01	0.01
Ca (M2)	0.87	0.86	0.88	0.84	0.83	0.85	0.88	0.87	0.87	0.84
Na (M2)	0.11	0.12	0.12	0.15	0.16	0.12	0.10	0.12	0.13	0.14
K (M2)	0.00	0.00	0.00	0.00	0.00	0.00	0.00	0.00	0.00	0.00
Total (M2)]	1.00	1.00	1.00	1.00	0.99	0.99	0.99	1.00	1.00	1.00
Wo	49.11	49.77	50.14	49.74	48.90	48.24	48.85	49.88	49.76	48.65
En	31.37	31.45	32.57	32.32	32.25	30.57	30.63	30.89	32.02	34.33
Fs	19.51	18.78	17.29	17.94	18.85	21.19	20.52	19.24	18.22	17.02
Fe/Fe+Mg	0.51	0.50	0.51	0.56	0.54	0.49	0.46	0.56	0.56	0.46
Q	1.77	1.73	1.75	1.70	1.70	1.77	1.81	1.75	1.74	1.72
J	0.23	0.24	0.25	0.30	0.32	0.24	0.21	0.24	0.25	0.27
Group	Ca-Mg-Fe	Ca-Mg-Fe	Ca-Mg-Fe	Ca-Mg-Fe	Ca-Mg-Fe	Ca-Mg-Fe	Ca-Mg-Fe	Ca-Mg-Fe	Ca-Mg-Fe	Ca-Mg-Fe
Na+AlIV	0.12	0.15	0.13	0.16	0.16	0.12	0.10	0.14	0.15	0.16
AlVI+2Ti+Cr	0.03	0.06	0.02	0.02	0.02	0.04	0.02	0.01	0.00	0.06

Analysis	129	130	131	132	133	134	135	136	137	138
Sample	MAAB03	MAAB03	MAAB03	MAAB03	POAB05	POAB05	POAB05	POAB05	POAB05	POAB05
Name	Dp	Dp	Dp	Dp	Dp	Dp	Dp	Dp	Dp	Dp
Alteration	Ca-Mg	Ca-Mg	Ca-Mg	Ca-Mg	Ca-Mg	Ca-Mg	Ca-Mg	Ca-Mg	Ca-Mg	Ca-Mg
SiO2	53.44	54.00	53.05	52.84	51.92	52.18	52.98	52.45	51.94	52.56
TiO2	0.07	0.02	0.04	0.04	0.01	0.08	0.04	0.06	0.03	0.00
Al2O3	1.64	1.32	1.34	1.74	1.58	1.36	1.55	2.06	2.15	2.04
FeO	12.00	11.24	11.71	12.19	10.46	11.22	10.40	11.69	11.80	11.77
MnO	0.19	0.17	0.23	0.22	0.24	0.28	0.29	0.23	0.26	0.33
MgO	11.11	11.71	11.07	10.59	11.19	11.34	11.60	10.61	10.55	10.72
CaO	21.01	21.28	20.96	20.64	20.85	21.57	20.86	20.15	19.58	19.96
Na2O	1.92	1.81	1.80	2.14	2.05	2.02	2.08	2.59	2.67	2.69
K2O	0.00	0.00	0.01	0.00	0.01	0.00	0.03	0.01	0.00	0.00
Total	101.4	101.6	100.2	100.4	98.3	100.0	99.8	99.9	99.0	100.1
[Si (T)	1.97	1.98	1.98	1.97	1.96	1.94	1.97	1.95	1.95	1.95
Al (T)	0.03	0.02	0.02	0.03	0.04	0.06	0.03	0.05	0.05	0.05
Fe3+ (T)	0.00	0.00	0.00	0.00	0.00	0.00	0.00	0.00	0.00	0.00
Total (T)]	2.00	2.00	2.00	2.00	2.00	2.00	2.00	2.00	2.00	2.00
[Al (M1)	0.04	0.04	0.04	0.05	0.03	0.00	0.04	0.05	0.05	0.04
Fe3+ (M1)	0.10	0.09	0.09	0.11	0.12	0.16	0.11	0.15	0.16	0.16
Ti (M1)	0.00	0.00	0.00	0.00	0.00	0.00	0.00	0.00	0.00	0.00
Mg (M1)	0.61	0.64	0.62	0.59	0.63	0.63	0.64	0.59	0.59	0.59
Fe2+ (M1)	0.25	0.23	0.25	0.25	0.21	0.19	0.20	0.21	0.20	0.20
Mn (M1)	0.00	0.00	0.00	0.00	0.00	0.01	0.00	0.00	0.00	0.00
Total (M1)]	1.00	1.00	1.00	1.00	1.00	0.99	1.00	1.00	1.00	1.00
[Mg (M2)	0.00	0.00	0.00	0.00	0.00	0.00	0.00	0.00	0.00	0.00
Fe2+ (M2)	0.03	0.03	0.02	0.01	0.00	0.00	0.01	0.00	0.01	0.00
Mn (M2)	0.01	0.01	0.01	0.01	0.00	0.00	0.01	0.01	0.01	0.01
Ca (M2)	0.83	0.84	0.84	0.82	0.85	0.86	0.83	0.80	0.79	0.79
Na (M2)	0.14	0.13	0.13	0.15	0.15	0.15	0.15	0.19	0.19	0.19
K (M2)	0.00	0.00	0.00	0.00	0.00	0.00	0.00	0.00	0.00	0.00
Total (M2)]	1.00	1.00	1.00	1.00	1.00	1.01	1.00	1.00	1.00	1.00
Wo	48.46	48.16	48.42	49.10	50.23	51.22	49.35	50.08	49.55	49.95
En	35.66	36.88	35.58	35.05	37.50	37.47	38.19	36.70	37.16	37.33
Fs	15.88	14.96	16.00	15.85	12.27	11.31	12.46	13.22	13.28	12.71
Fe/Fe+Mg	0.46	0.42	0.45	0.50	0.47	0.52	0.45	0.54	0.55	0.55
Q	1.71	1.74	1.73	1.68	1.68	1.68	1.69	1.61	1.59	1.59
J	0.27	0.26	0.26	0.31	0.30	0.29	0.30	0.37	0.39	0.39
Group	Ca-Mg-Fe	Ca-Mg-Fe	Ca-Mg-Fe	Ca-Mg-Fe	Ca-Mg-Fe	Ca-Mg-Fe	Ca-Mg-Fe	Ca-Mg-Fe	Ca-Mg-Fe	Ca-Mg-Fe
Na+AlIV	0.17	0.15	0.15	0.19	0.19	0.20	0.18	0.23	0.24	0.24
AlVI+2Ti+Cr	0.05	0.04	0.04	0.05	0.04	0.01	0.04	0.05	0.05	0.04

Analysis	139	140	141	142	143	144	145	146	147	148
Sample	POAB05	POAB05	POAB05	31BIAB	31BIAB	31BIAB	31BIAB	31BIAB	31BIAB	F11ALB02
Name	Dp	Dp	Dp	Dp	Dp	Dp	Dp	Dp	Dp	Dp
Alteration	Ca-Mg	Ca-Mg	Ca-Mg	Ca-Mg	Ca-Mg	Ca-Mg	Ca-Mg	Ca-Mg	Ca-Mg	Ca-Mg
SiO2	52.13	52.25	52.57	52.23	51.30	51.77	51.44	52.23	51.78	51.60
TiO2	0.04	0.01	0.03	0.03	0.09	0.07	0.15	0.04	0.04	0.05
Al2O3	1.77	1.59	1.65	1.38	1.78	1.30	1.80	1.39	1.89	0.67
FeO	10.80	9.95	10.36	14.23	14.47	13.41	14.48	13.01	14.97	13.70
MnO	0.18	0.31	0.23	0.63	0.66	0.62	0.47	0.51	0.59	0.69
MgO	11.11	11.49	11.36	9.18	8.67	9.58	8.68	9.67	8.68	9.54
CaO	20.25	20.28	20.81	20.08	19.32	20.38	19.94	20.86	20.09	21.51
Na2O	2.37	2.23	2.14	2.17	2.40	2.04	2.48	2.04	2.36	1.07
K2O	0.00	0.01	0.01	0.00	0.00	0.00	0.01	0.00	0.00	0.69
Total	98.7	98.1	99.2	99.9	98.7	99.2	99.5	99.7	100.4	99.5
[Si (T)	1.96	1.97	1.97	1.98	1.97	1.97	1.95	1.97	1.95	1.97
Al (T)	0.04	0.03	0.03	0.02	0.03	0.03	0.05	0.03	0.05	0.03
Fe3+ (T)	0.00	0.00	0.00	0.00	0.00	0.00	0.00	0.00	0.00	0.00
Total (T)]	2.00	2.00	2.00	2.00	2.00	2.00	2.00	2.00	2.00	2.00
[Al (M1)	0.04	0.04	0.04	0.04	0.05	0.03	0.03	0.03	0.04	0.00
Fe3+ (M1)	0.14	0.12	0.12	0.12	0.13	0.12	0.15	0.12	0.15	0.11
Ti (M1)	0.00	0.00	0.00	0.00	0.00	0.00	0.00	0.00	0.00	0.00
Mg (M1)	0.62	0.65	0.63	0.52	0.50	0.54	0.49	0.54	0.49	0.54
Fe2+ (M1)	0.20	0.19	0.21	0.33	0.32	0.30	0.31	0.30	0.32	0.33
Mn (M1)	0.00	0.00	0.00	0.00	0.00	0.00	0.01	0.01	0.00	0.02
Total (M1)]	1.00	1.00	1.00	1.00	1.00	1.00	1.00	1.00	1.00	1.00
[Mg (M2)	0.00	0.00	0.00	0.00	0.00	0.00	0.00	0.00	0.00	0.00
Fe2+ (M2)	0.00	0.01	0.00	0.01	0.01	0.00	0.00	0.00	0.00	0.00
Mn (M2)	0.01	0.01	0.01	0.02	0.02	0.02	0.01	0.01	0.02	0.01
Ca (M2)	0.82	0.82	0.84	0.81	0.79	0.83	0.81	0.84	0.81	0.88
Na (M2)	0.17	0.16	0.16	0.16	0.18	0.15	0.18	0.15	0.17	0.08
K (M2)	0.00	0.00	0.00	0.00	0.00	0.00	0.00	0.00	0.00	0.03
Total (M2)]	1.00	1.00	1.00	1.00	1.00	1.00	1.00	1.00	1.00	1.00
Wo	49.76	49.36	49.81	48.94	48.99	49.52	50.39	50.12	50.03	50.35
En	37.99	38.93	37.83	31.13	30.59	32.40	30.52	32.32	30.06	31.07
Fs	12.25	11.71	12.36	19.93	20.42	18.09	19.09	17.56	19.91	18.58
Fe/Fe+Mg	0.49	0.45	0.46	0.58	0.62	0.57	0.64	0.55	0.65	0.56
Q	1.64	1.66	1.68	1.66	1.62	1.68	1.61	1.68	1.62	1.75
J	0.35	0.33	0.31	0.32	0.36	0.30	0.37	0.30	0.35	0.16
Group	Ca-Mg-Fe	Ca-Mg-Fe	Ca-Mg-Fe	Ca-Mg-Fe	Ca-Mg-Fe	Ca-Mg-Fe	Ca-Mg-Fe	Ca-Mg-Fe	Ca-Mg-Fe	Ca-Mg-Fe
Na+AlIV	0.21	0.19	0.19	0.18	0.21	0.18	0.23	0.18	0.22	0.11
AlVI+2Ti+Cr	0.04	0.04	0.04	0.04	0.05	0.03	0.04	0.04	0.04	0.00

Analysis	149	150	151	152	153	154	155	156	157	158
Sample	F11ALB02	F11ALB02	F11ALB02	F11ALB02	F11ALB02	F11ALB02	F11ALB02	BCAB	BCAB	BCAB
Name	Dp	Dp	Dp	Dp	Dp	Dp	Dp	Ag	Ag	Ag
Alteration	Ca-Mg	Ca-Mg	Ca-Mg	Ca-Mg	Ca-Mg	Ca-Mg	Ca-Mg	K-Mg	K-Mg	K-Mg
SiO2	51.09	50.95	52.09	51.98	52.49	51.78	52.04	55.14	55.64	55.19
TiO2	0.06	0.04	0.00	0.04	0.06	0.06	0.05	0.17	0.09	0.02
Al2O3	0.51	0.57	0.45	0.68	0.63	0.59	0.54	2.34	2.17	2.02
FeO	13.37	13.95	14.04	14.04	14.08	14.48	13.94	6.02	5.20	5.36
MnO	0.65	0.67	0.72	0.53	0.67	0.69	0.65	0.24	0.16	0.30
MgO	9.52	9.56	9.46	9.65	9.68	9.35	9.53	20.82	20.71	21.16
CaO	21.72	21.51	22.48	22.00	22.36	22.37	22.62	12.01	12.36	12.29
Na2O	0.99	1.00	0.77	1.09	1.06	0.90	0.82	0.69	0.68	0.69
K2O	0.65	0.67	0.72	0.53	0.67	0.69	0.65	0.27	0.20	0.24
Total	98.6	98.9	100.7	100.5	101.7	100.9	100.8	97.7	97.2	97.3
[Si (T)	1.97	1.96	1.97	1.97	1.96	1.96	1.97	2.03	2.05	2.03
Al (T)	0.02	0.03	0.02	0.03	0.03	0.03	0.02	0.00	0.00	0.00
Fe3+ (T)	0.01	0.01	0.01	0.00	0.01	0.02	0.01	0.00	0.00	0.00
Total (T)]	2.00	2.00	2.00	2.00	2.00	2.00	2.00	2.03	2.05	2.03
[Al (M1)	0.00	0.00	0.00	0.00	0.00	0.00	0.00	0.10	0.09	0.09
Fe3+ (M1)	0.11	0.12	0.10	0.11	0.12	0.11	0.10	0.00	0.00	0.00
Ti (M1)	0.00	0.00	0.00	0.00	0.00	0.00	0.00	0.00	0.00	0.00
Mg (M1)	0.55	0.55	0.53	0.54	0.54	0.53	0.54	0.89	0.90	0.91
Fe2+ (M1)	0.32	0.32	0.34	0.33	0.32	0.33	0.33	0.00	0.00	0.00
Mn (M1)	0.02	0.02	0.02	0.01	0.02	0.02	0.02	0.00	0.00	0.00
Total (M1)]	1.00	1.00	1.00	1.00	0.99	0.99	0.99	1.00	1.00	1.00
[Mg (M2)	0.00	0.00	0.00	0.00	0.00	0.00	0.00	0.25	0.24	0.25
Fe2+ (M2)	0.00	0.00	0.00	0.00	0.00	0.00	0.00	0.27	0.28	0.24
Mn (M2)	0.00	0.01	0.00	0.00	0.00	0.00	0.00	0.01	0.01	0.01
Ca (M2)	0.90	0.89	0.91	0.89	0.90	0.91	0.92	0.47	0.49	0.48
Na (M2)	0.07	0.07	0.06	0.08	0.08	0.07	0.06	0.05	0.05	0.05
K (M2)	0.03	0.03	0.03	0.03	0.03	0.03	0.03	0.01	0.01	0.01
Total (M2)]	1.00	1.00	1.00	1.00	1.01	1.01	1.01	1.06	1.07	1.05
Wo	50.91	50.58	51.00	50.54	51.13	51.32	51.25	25.10	25.56	25.68
En	31.05	31.28	29.86	30.85	30.80	29.84	30.04	60.55	59.60	61.53
Fs	18.05	18.14	19.15	18.61	18.08	18.84	18.71	14.35	14.84	12.79
Fe/Fe+Mg	0.54	0.55	0.55	0.56	0.56	0.56	0.54	0.00	0.00	0.00
Q	1.76	1.75	1.79	1.76	1.75	1.77	1.79	1.88	1.91	1.89
J	0.15	0.15	0.11	0.16	0.15	0.13	0.12	0.10	0.10	0.10
Group	Ca-Mg-Fe	Ca-Mg-Fe	Ca-Mg-Fe	Ca-Mg-Fe	Ca-Mg-Fe	Ca-Mg-Fe	Ca-Mg-Fe	Ca-Mg-Fe	Ca-Mg-Fe	Ca-Mg-Fe
Na+AlIV	0.10	0.10	0.08	0.11	0.10	0.09	0.08	0.05	0.05	0.05
AlVI+2Ti+Cr	0.00	0.00	0.00	0.00	0.00	0.00	0.00	0.11	0.10	0.09

Analysis	159	160	161	162	163	164	165	166	167	168
Sample	BCAB	BCAB	BCAB	BIAB129	BIAB129	BIAB129	BIAB129	BIAB129	BIAB129	BIAB129
Name	Ag	Ag	Ag	Ag	Ag	Ag	Ag	Ag	Ag	Ag
Alteration	K-Mg	K-Mg	K-Mg	K-Mg	K-Mg	K-Mg	K-Mg	K-Mg	K-Mg	K-Mg
SiO2	54.81	56.05	56.34	57.54	57.60	57.55	57.31	57.31	57.50	58.18
TiO2	0.12	0.08	0.06	0.05	0.10	0.08	0.12	0.12	0.10	0.07
Al2O3	2.42	2.25	2.08	1.05	1.05	1.30	1.57	1.50	1.40	1.20
FeO	5.66	5.62	5.43	6.04	6.14	6.27	6.14	6.42	6.24	6.14
MnO	0.17	0.20	0.25	0.30	0.28	0.29	0.14	0.21	0.23	0.21
MgO	20.67	20.95	21.15	20.55	20.31	20.09	20.12	20.46	20.41	20.54
CaO	12.18	12.57	12.64	12.76	12.35	12.27	12.37	12.17	12.74	12.77
Na2O	0.77	0.74	0.65	0.17	0.14	0.17	0.19	0.20	0.18	0.14
K2O	0.31	0.28	0.20	0.42	0.63	0.62	0.43	0.68	0.42	0.42
Total	97.1	98.7	98.8	98.9	98.6	98.6	98.4	99.1	99.2	99.7
[Si (T)	2.02	2.04	2.05	2.11	2.12	2.11	2.11	2.09	2.10	2.11
Al (T)	0.00	0.00	0.00	0.00	0.00	0.00	0.00	0.00	0.00	0.00
Fe3+ (T)	0.00	0.00	0.00	0.00	0.00	0.00	0.00	0.00	0.00	0.00
Total (T)]	2.02	2.04	2.05	2.11	2.12	2.11	2.11	2.09	2.10	2.11
[Al (M1)	0.11	0.10	0.09	0.05	0.05	0.06	0.07	0.06	0.06	0.05
Fe3+ (M1)	0.00	0.00	0.00	0.00	0.00	0.00	0.00	0.00	0.00	0.00
Ti (M1)	0.00	0.00	0.00	0.00	0.00	0.00	0.00	0.00	0.00	0.00
Mg (M1)	0.89	0.90	0.91	0.95	0.95	0.94	0.93	0.93	0.94	0.95
Fe2+ (M1)	0.00	0.00	0.00	0.00	0.00	0.00	0.00	0.00	0.00	0.00
Mn (M1)	0.00	0.00	0.00	0.00	0.00	0.00	0.00	0.00	0.00	0.00
Total (M1)]	1.00	1.00	1.00	1.00	1.00	1.00	1.00	1.00	1.00	1.00
[Mg (M2)	0.25	0.23	0.24	0.17	0.16	0.16	0.18	0.18	0.17	0.17
Fe2+ (M2)	0.25	0.26	0.27	0.38	0.40	0.40	0.41	0.38	0.39	0.40
Mn (M2)	0.01	0.01	0.01	0.01	0.01	0.01	0.00	0.01	0.01	0.01
Ca (M2)	0.48	0.49	0.49	0.50	0.49	0.48	0.49	0.48	0.50	0.50
Na (M2)	0.06	0.05	0.05	0.01	0.01	0.01	0.01	0.01	0.01	0.01
K (M2)	0.01	0.01	0.01	0.02	0.03	0.03	0.02	0.03	0.02	0.02
Total (M2)]	1.05	1.05	1.06	1.09	1.09	1.10	1.11	1.09	1.10	1.10
Wo	25.79	25.96	25.75	25.01	24.37	24.30	24.36	24.22	24.97	24.70
En	60.90	60.19	59.96	56.05	55.77	55.35	55.14	56.66	55.67	55.27
Fs	13.31	13.85	14.29	18.93	19.86	20.36	20.50	19.12	19.36	20.03
Fe/Fe+Mg	0.00	0.00	0.00	0.00	0.00	0.00	0.00	0.00	0.00	0.00
Q	1.87	1.88	1.91	2.00	1.99	1.99	2.00	1.97	1.99	2.01
J	0.11	0.10	0.09	0.02	0.02	0.02	0.03	0.03	0.03	0.02
Group	Ca-Mg-Fe	Ca-Mg-Fe	Ca-Mg-Fe	Ca-Mg-Fe	Ca-Mg-Fe	Ca-Mg-Fe	Ca-Mg-Fe	Ca-Mg-Fe	Ca-Mg-Fe	Ca-Mg-Fe
Na+AlIV	0.06	0.05	0.05	0.01	0.01	0.01	0.01	0.01	0.01	0.01
AlVI+2Ti+Cr	0.11	0.10	0.09	0.05	0.05	0.06	0.07	0.07	0.07	0.06

Analysis	169	170	171	172	173	174	175	176	177	178	179	180
Sample	BIAB129	BIAB129	BIAB129	BIAB129	BIAB129	BIAB129	BIAB129	BIAB129	BIAB129	BIAB129	BIAB129	BIAB129
Name	Ag	Ag	Ag	Ag	Ag	Ag	Ag	Ag	Ag	Ag	Ag	Ag
Alteration	K-Mg	K-Mg	K-Mg	K-Mg	K-Mg	K-Mg	K-Mg	K-Mg	K-Mg	K-Mg	K-Mg	K-Mg
SiO2	57.65	57.62	58.33	57.17	57.45	58.15	57.18	57.91	57.24	57.22	57.87	57.50
TiO2	0.11	0.08	0.09	0.08	0.08	0.11	0.10	0.10	0.14	0.10	0.10	0.04
Al2O3	1.23	1.04	1.02	1.35	1.31	1.28	1.45	1.70	1.78	1.99	1.30	1.27
FeO	6.12	6.09	6.15	5.85	5.93	6.04	6.29	6.71	6.42	6.48	6.15	5.84
MnO	0.34	0.31	0.35	0.26	0.19	0.29	0.23	0.33	0.15	0.27	0.31	0.27
MgO	20.63	20.67	20.71	20.28	20.48	20.42	20.21	20.30	20.05	20.08	20.35	20.64
CaO	12.12	12.26	12.36	12.31	12.18	12.48	12.18	12.19	12.23	12.37	12.20	12.14
Na2O	0.10	0.13	0.12	0.15	0.15	0.17	0.15	0.20	0.22	0.22	0.15	0.11
K2O	0.57	0.52	0.45	0.56	0.44	0.54	0.59	0.67	0.61	0.79	0.55	0.57
Total	98.9	98.7	99.6	98.0	98.2	99.5	98.4	100.1	98.8	99.5	99.0	98.4
[Si (T)	2.11	2.11	2.12	2.11	2.12	2.12	2.11	2.10	2.10	2.08	2.12	2.11
Al (T)	0.00	0.00	0.00	0.00	0.00	0.00	0.00	0.00	0.00	0.00	0.00	0.00
Fe3+ (T)	0.00	0.00	0.00	0.00	0.00	0.00	0.00	0.00	0.00	0.00	0.00	0.00
Total (T)]	2.11	2.11	2.12	2.11	2.12	2.12	2.11	2.10	2.10	2.08	2.12	2.11
[Al (M1)	0.05	0.04	0.04	0.06	0.06	0.05	0.06	0.07	0.08	0.09	0.06	0.06
Fe3+ (M1)	0.00	0.00	0.00	0.00	0.00	0.00	0.00	0.00	0.00	0.00	0.00	0.00
Ti (M1)	0.00	0.00	0.00	0.00	0.00	0.00	0.00	0.00	0.00	0.00	0.00	0.00
Mg (M1)	0.94	0.95	0.95	0.94	0.94	0.94	0.93	0.92	0.92	0.91	0.94	0.94
Fe2+ (M1)	0.00	0.00	0.00	0.00	0.00	0.00	0.00	0.00	0.00	0.00	0.00	0.00
Mn (M1)	0.00	0.00	0.00	0.00	0.00	0.00	0.00	0.00	0.00	0.00	0.00	0.00
Total (M1)]	1.00	1.00	1.00	1.00	1.00	1.00	1.00	1.00	1.00	1.00	1.00	1.00
[Mg (M2)	0.18	0.18	0.17	0.18	0.18	0.17	0.18	0.17	0.18	0.18	0.17	0.19
Fe2+ (M2)	0.40	0.39	0.41	0.39	0.41	0.40	0.40	0.40	0.40	0.37	0.41	0.39
Mn (M2)	0.01	0.01	0.01	0.01	0.01	0.01	0.01	0.01	0.00	0.01	0.01	0.01
Ca (M2)	0.48	0.48	0.48	0.49	0.48	0.49	0.48	0.47	0.48	0.48	0.48	0.48
Na (M2)	0.01	0.01	0.01	0.01	0.01	0.01	0.01	0.01	0.02	0.02	0.01	0.01
K (M2)	0.03	0.02	0.02	0.03	0.02	0.03	0.03	0.03	0.03	0.04	0.03	0.03
Total (M2)]	1.10	1.09	1.10	1.10	1.11	1.10	1.10	1.10	1.10	1.09	1.10	1.10
Wo	23.79	24.06	23.90	24.42	23.91	24.36	24.17	24.06	24.34	24.84	23.92	23.91
En	56.33	56.43	55.71	55.99	55.93	55.45	55.80	55.76	55.52	56.11	55.53	56.55
Fs	19.88	19.51	20.39	19.59	20.17	20.19	20.03	20.17	20.15	19.04	20.55	19.54
Fe/Fe+Mg	0.00	0.00	0.00	0.00	0.00	0.00	0.00	0.00	0.00	0.00	0.00	0.00
Q	2.00	2.00	2.02	1.99	2.01	2.00	1.99	1.97	1.97	1.94	2.00	2.00
J	0.01	0.02	0.02	0.02	0.02	0.02	0.02	0.03	0.03	0.03	0.02	0.02
Group	Ca-Mg-Fe	Ca-Mg-Fe	Ca-Mg-Fe	Ca-Mg-Fe	Ca-Mg-Fe	Ca-Mg-Fe	Ca-Mg-Fe	Ca-Mg-Fe	Ca-Mg-Fe	Ca-Mg-Fe	Ca-Mg-Fe	Ca-Mg-Fe
Na+AlIV	0.01	0.01	0.01	0.01	0.01	0.01	0.01	0.01	0.02	0.02	0.01	0.01
AlVI+2Ti+Cr	0.06	0.05	0.05	0.06	0.06	0.06	0.07	0.08	0.08	0.09	0.06	0.06

3D: EPMA analyses of amphibole. Recalculated formula on the basis of 23 oxygens.

	1	2	3	4	5	6	7	8	9	10	11	12
Sample	GRA01	GRA01	GRA01	GRA01	GRA01	GRA01	GRA01	GRA01	GRA01	GRA01	GRA01	GRA01
Rock	HAFG	HAFG	HAFG	HAFG	HAFG	HAFG	HAFG	HAFG	HAFG	HAFG	HAFG	HAFG
Alteration	Mag	Mag	Mag	Mag	Mag	Mag	Mag	Mag	Mag	Mag	Mag	Mag
Name	Hst	Hst	Hst	Hst	Hst	Hst	Hst	Hst	Hst	Hst	Hst	Hst
SiO2	37.99	38.19	37.31	38.73	39.18	39.44	39.46	39.42	39.45	39.12	39.25	38.96
TiO2	0.90	0.82	0.79	0.91	0.81	0.80	0.89	0.66	0.85	0.68	0.76	0.95
Al2O3	11.10	10.95	10.98	11.21	11.96	11.37	11.34	11.36	11.48	11.69	11.69	11.05
FeO(Total)	32.64	32.74	32.77	32.31	31.80	32.05	32.55	31.59	32.01	31.74	31.85	32.48
MnO	0.00	0.00	0.00	0.00	0.00	0.00	0.00	0.00	0.00	0.00	0.00	0.00
MgO	0.64	0.60	0.64	0.59	0.63	0.67	0.71	0.74	0.71	0.66	0.65	0.69
CaO	10.63	10.81	10.98	11.05	11.32	10.78	10.96	11.24	11.26	11.09	11.08	11.09
Na2O	1.56	1.57	1.35	1.42	1.41	1.72	1.53	1.53	1.34	1.49	1.69	1.37
K2O	2.24	2.23	2.15	2.25	2.28	2.15	2.17	2.21	2.08	2.34	2.27	2.21
F	0.30	0.29	0.04	0.45	0.38	0.58	0.27	0.29	0.37	0.42	0.04	0.18
Cl	0.92	0.87	0.95	0.88	1.01	0.92	0.82	0.87	0.92	0.96	0.93	0.90
O=F,Cl	0.33	0.32	0.23	0.39	0.39	0.45	0.30	0.32	0.36	0.39	0.23	0.28
Total	98.59	98.75	97.73	99.41	100.39	100.03	100.40	99.59	100.11	99.80	99.98	99.60
[Si	6.17	6.21	6.12	6.25	6.26	6.31	6.27	6.34	6.30	6.28	6.28	6.26
Al(IV)	1.83	1.79	1.88	1.75	1.74	1.69	1.73	1.66	1.70	1.72	1.72	1.74
Ti	0.00	0.00	0.00	0.00	0.00	0.00	0.00	0.00	0.00	0.00	0.00	0.00
Al(VI)	0.30	0.30	0.25	0.39	0.51	0.46	0.40	0.49	0.46	0.50	0.49	0.35
Ti	0.11	0.10	0.10	0.11	0.10	0.10	0.11	0.08	0.10	0.08	0.09	0.11
Fe3+	0.65	0.57	0.69	0.41	0.27	0.37	0.47	0.20	0.35	0.30	0.26	0.46
Mg	0.16	0.15	0.16	0.14	0.15	0.16	0.17	0.18	0.17	0.16	0.16	0.17
Fe2+	3.79	3.88	3.81	3.95	3.98	3.92	3.86	4.05	3.92	3.97	4.01	3.91
Mn	0.00	0.00	0.00	0.00	0.00	0.00	0.00	0.00	0.00	0.00	0.00	0.00
[Mn	0.00	0.00	0.00	0.00	0.00	0.00	0.00	0.00	0.00	0.00	0.00	0.00
Fe2+	0.00	0.00	0.00	0.00	0.00	0.00	0.00	0.00	0.00	0.00	0.00	0.00
Mg	0.00	0.00	0.00	0.00	0.00	0.00	0.00	0.00	0.00	0.00	0.00	0.00
Fe3+	0.00	0.00	0.00	0.00	0.00	0.00	0.00	0.00	0.00	0.00	0.00	0.00
Ca	1.85	1.88	1.93	1.91	1.94	1.85	1.87	1.94	1.93	1.91	1.90	1.91
Na	0.15	0.12	0.07	0.09	0.06	0.15	0.13	0.06	0.07	0.09	0.10	0.09
Na	0.34	0.38	0.36	0.36	0.37	0.38	0.34	0.41	0.34	0.37	0.43	0.34
Ca	0.00	0.00	0.00	0.00	0.00	0.00	0.00	0.00	0.00	0.00	0.00	0.00
K	0.46	0.46	0.45	0.46	0.46	0.44	0.44	0.45	0.42	0.48	0.46	0.45
F	0.16	0.15	0.02	0.23	0.19	0.30	0.14	0.15	0.19	0.21	0.02	0.09
Cl	0.26	0.24	0.27	0.24	0.27	0.25	0.22	0.24	0.25	0.26	0.25	0.25
OH	1.59	1.61	1.71	1.53	1.53	1.45	1.64	1.61	1.56	1.52	1.73	1.66
Fe/Fe+Mg	0.97	0.97	0.97	0.97	0.97	0.96	0.96	0.96	0.96	0.96	0.96	0.96

	13	14	15	16	17	18	19	20	21	22	23	24
Sample	GRA01	GRA01	GRA01	GRA01	8_11	8_11	8_11	8_11	8_11	8_11	8_11	8_11
Rock	HAFG	HAFG	HAFG	HAFG	HAFG	HAFG	HAFG	HAFG	HAFG	HAFG	HAFG	HAFG
Alteration	Mag	Mag	Mag	Mag	Mag	Mag	Mag	Mag	Mag	Mag	Mag	Mag
Name	Hst	Hst	Hst	Hst	Hst	Hst	Hst	Hst	Hst	Hst	Hst	Hst
SiO2	38.45	39.03	38.99	38.59	40.18	39.51	38.78	39.40	40.11	38.54	36.98	39.47
TiO2	0.86	0.89	0.78	0.74	0.52	0.46	0.52	0.48	0.63	0.41	0.37	0.35
Al2O3	11.68	11.25	11.21	11.58	10.91	11.07	11.38	11.55	11.02	11.38	11.07	10.87
FeO(Total)	31.55	32.56	32.28	32.22	27.85	28.69	28.24	28.50	28.72	28.09	28.36	29.16
MnO	0.00	0.00	0.00	0.00	0.50	0.34	0.45	0.42	0.37	0.47	0.25	0.50
MgO	0.67	0.69	0.65	0.63	2.28	2.34	2.27	2.16	2.18	2.01	1.87	1.98
CaO	11.06	10.88	11.02	11.09	11.30	11.09	10.92	11.41	11.21	11.68	11.49	11.54
Na2O	1.44	1.66	1.53	1.49	1.42	1.26	1.39	1.15	1.50	1.43	1.44	1.41
K2O	2.43	2.20	2.25	2.21	2.09	2.18	2.13	2.40	2.20	2.25	2.17	2.30
F	0.32	0.55	0.25	0.18	1.09	0.99	0.68	0.53	0.52	0.03	0.39	0.43
Cl	1.00	0.86	0.91	0.94	0.62	0.62	0.60	0.65	0.75	0.83	0.85	0.86
O=F,Cl	0.36	0.43	0.31	0.29	0.60	0.56	0.42	0.37	0.39	0.20	0.36	0.38
Total	99.10	100.14	99.56	99.38	98.16	97.99	96.94	98.28	98.82	96.92	94.88	98.49
[Si	6.23	6.25	6.28	6.22	6.49	6.37	6.30	6.34	6.43	6.33	6.24	6.39
Al(IV)	1.77	1.75	1.72	1.78	1.51	1.63	1.70	1.66	1.57	1.67	1.76	1.61
Ti	0.00	0.00	0.00	0.00	0.00	0.00	0.00	0.00	0.00	0.00	0.00	0.00
Al(VI)	0.46	0.37	0.40	0.42	0.56	0.47	0.48	0.53	0.51	0.53	0.44	0.46
Ti	0.10	0.11	0.09	0.09	0.06	0.06	0.06	0.06	0.08	0.05	0.05	0.04
Fe3+	0.31	0.47	0.39	0.44	0.04	0.38	0.40	0.23	0.15	0.00	0.13	0.14
Mg	0.16	0.16	0.16	0.15	0.55	0.56	0.55	0.52	0.52	0.49	0.47	0.48
Fe2+	3.97	3.89	3.96	3.91	3.71	3.49	3.44	3.61	3.69	3.86	3.88	3.81
Mn	0.00	0.00	0.00	0.00	0.07	0.05	0.06	0.06	0.05	0.07	0.04	0.07
[Mn	0.00	0.00	0.00	0.00	0.00	0.00	0.00	0.00	0.00	0.00	0.00	0.00
Fe2+	0.00	0.00	0.00	0.00	0.00	0.00	0.00	0.00	0.00	0.00	0.00	0.00
Mg	0.00	0.00	0.00	0.00	0.00	0.00	0.00	0.00	0.00	0.00	0.00	0.00
Fe3+	0.00	0.00	0.00	0.00	0.00	0.00	0.00	0.00	0.00	0.00	0.00	0.00
Ca	1.92	1.87	1.90	1.91	1.95	1.91	1.90	1.97	1.92	2.00	2.00	2.00
Na	0.08	0.13	0.10	0.09	0.05	0.09	0.10	0.03	0.08	0.00	0.00	0.00
Na	0.37	0.38	0.38	0.38	0.40	0.31	0.34	0.33	0.39	0.46	0.47	0.44
Ca	0.00	0.00	0.00	0.00	0.00	0.00	0.00	0.00	0.00	0.06	0.08	0.00
K	0.50	0.45	0.46	0.45	0.43	0.45	0.44	0.49	0.45	0.47	0.47	0.47
F	0.17	0.28	0.13	0.09	0.56	0.51	0.35	0.27	0.26	0.02	0.21	0.22
Cl	0.28	0.24	0.25	0.26	0.17	0.17	0.17	0.18	0.20	0.23	0.24	0.24
OH	1.56	1.48	1.62	1.65	1.27	1.32	1.48	1.55	1.53	1.75	1.55	1.54
Fe/Fe+Mg	0.96	0.96	0.97	0.97	0.87	0.87	0.87	0.88	0.88	0.89	0.89	0.89

	25	26	27	28	29	30	31	32	33	34	35	36	37
Sample	8_11	8_11	8_11	8_11	8_11	8_11	8_11	8_11	8_11	8_11	8_11	8_11	8_11
Rock	HAFG	HAFG	HAFG	HAFG	HAFG	HAFG	HAFG	HAFG	HAFG	HAFG	HAFG	HAFG	HAFG
Alteration	Mag	Mag	Mag	Mag	Mag	Mag	Mag	Mag	Mag	Mag	Mag	Mag	Mag
Name	Hst	Hst	Hst	Hst	Hst	Hst	Hst	Hst	Hst	Hst	Hst	Hst	Hst
SiO2	39.94	39.28	39.62	39.61	39.06	40.41	40.77	41.27	41.58	39.44	40.17	40.86	39.56
TiO2	0.40	0.89	0.98	0.99	1.31	1.10	1.22	1.15	0.98	0.31	0.37	0.28	0.57
Al2O3	10.96	7.67	10.27	9.95	9.25	9.71	9.16	8.63	8.83	10.51	10.17	10.10	11.24
FeO(Total)	29.49	30.55	30.25	30.01	29.13	30.14	29.34	29.55	30.13	29.58	30.20	30.47	30.36
MnO	0.45	0.56	0.46	0.40	0.50	0.57	0.48	0.38	0.51	0.56	0.53	0.53	0.46
MgO	2.04	1.68	1.69	1.74	1.77	1.68	2.07	2.19	2.18	2.09	1.99	2.08	1.21
CaO	11.55	10.10	10.36	10.56	10.29	10.66	10.52	10.79	10.85	10.76	11.04	10.83	10.53
Na2O	1.31	1.30	1.65	1.64	1.69	1.60	1.53	1.67	1.58	1.41	1.53	1.60	1.69
K2O	2.18	1.59	2.03	1.94	1.74	1.93	1.77	1.77	1.80	2.06	2.00	1.95	2.01
F	0.27	0.47	1.17	0.38	0.26	0.79	1.01	0.51	0.68	0.50	0.02	0.38	0.59
Cl	0.84	0.69	0.63	0.75	0.79	0.69	0.60	0.68	0.67	0.39	0.39	0.33	0.30
O=F,Cl	0.30	0.35	0.63	0.33	0.29	0.49	0.56	0.37	0.44	0.30	0.10	0.23	0.32
Total	99.13	94.43	98.48	97.64	95.50	98.79	97.91	98.22	99.35	97.31	98.31	99.18	98.20
[Si	6.39	6.59	6.38	6.43	6.48	6.50	6.58	6.66	6.62	6.38	6.44	6.48	6.36
Al(IV)	1.61	1.41	1.62	1.57	1.52	1.50	1.42	1.34	1.38	1.62	1.56	1.52	1.64
Ti	0.00	0.00	0.00	0.00	0.00	0.00	0.00	0.00	0.00	0.00	0.00	0.00	0.00
Al(VI)	0.46	0.10	0.34	0.33	0.29	0.34	0.33	0.30	0.28	0.38	0.36	0.36	0.49
Ti	0.05	0.11	0.12	0.12	0.16	0.13	0.15	0.14	0.12	0.04	0.04	0.03	0.07
Fe3+	0.24	0.69	0.53	0.41	0.34	0.34	0.31	0.15	0.30	0.57	0.44	0.53	0.44
Mg	0.49	0.42	0.41	0.42	0.44	0.40	0.50	0.53	0.52	0.50	0.48	0.49	0.29
Fe2+	3.70	3.59	3.55	3.66	3.70	3.71	3.65	3.83	3.71	3.43	3.61	3.51	3.65
Mn	0.06	0.08	0.06	0.05	0.07	0.08	0.07	0.05	0.07	0.08	0.07	0.07	0.06
[Mn	0.00	0.00	0.00	0.00	0.00	0.00	0.00	0.00	0.00	0.00	0.00	0.00	0.00
Fe2+	0.00	0.00	0.00	0.00	0.00	0.00	0.00	0.00	0.00	0.00	0.00	0.00	0.00
Mg	0.00	0.00	0.00	0.00	0.00	0.00	0.00	0.00	0.00	0.00	0.00	0.00	0.00
Fe3+	0.00	0.00	0.00	0.00	0.00	0.00	0.00	0.00	0.00	0.00	0.00	0.00	0.00
Ca	1.98	1.81	1.79	1.84	1.83	1.84	1.82	1.86	1.85	1.86	1.90	1.84	1.81
Na	0.02	0.19	0.21	0.16	0.17	0.16	0.18	0.14	0.15	0.14	0.10	0.16	0.19
Na	0.39	0.24	0.30	0.35	0.37	0.33	0.30	0.39	0.34	0.31	0.37	0.33	0.34
Ca	0.00	0.00	0.00	0.00	0.00	0.00	0.00	0.00	0.00	0.00	0.00	0.00	0.00
K	0.45	0.34	0.42	0.40	0.37	0.40	0.36	0.36	0.37	0.42	0.41	0.39	0.41
F	0.14	0.25	0.60	0.20	0.14	0.40	0.52	0.26	0.34	0.26	0.01	0.19	0.30
Cl	0.23	0.20	0.17	0.21	0.22	0.19	0.17	0.19	0.18	0.11	0.11	0.09	0.08
OH	1.63	1.55	1.22	1.60	1.64	1.41	1.32	1.55	1.47	1.63	1.88	1.72	1.61
Fe/Fe+Mg	0.89	0.91	0.91	0.91	0.90	0.91	0.89	0.88	0.89	0.89	0.89	0.89	0.54

	38	39	40	41	42	43	44	45	46	47	48	49	50	51
Sample	8_11	8_11	8_11	8_11	8_11	34GNA01	34GNA01	34GNA01	34GNA01	34GNA01	34GNA01	34GNA01	34MALB	34MALB
Rock	HAFG	HAFG	HAFG	HAFG	HAFG	HAFGg	HAFGg	HAFGg	HAFGg	HAFGg	HAFGg	HAFGg	HAFGg	HAFGg
Alteration	Mag	Mag	Mag	Mag	Mag	Mag	Mag	Mag	Mag	Mag	Mag	Mag	Mag	Mag
Name	Hst	Hst	Hst	Hst	Hst	Hst	Hst	Hst	Hst	Hst	Hst	Hst	Hst	Hst
SiO2	39.95	39.95	40.91	41.05	40.62	35.07	34.33	36.75	38.01	38.07	37.47	34.91	37.11	37.79
TiO2	0.61	0.61	0.38	0.39	0.39	0.75	0.91	0.58	0.91	0.82	0.80	0.72	0.46	0.24
Al2O3	10.93	10.50	10.01	9.82	10.27	12.84	12.56	13.65	13.00	12.89	13.12	13.17	11.11	11.96
FeO(Total)	30.43	30.63	28.90	28.59	29.47	30.78	30.47	30.81	31.52	31.23	31.25	31.76	32.17	32.39
MnO	0.54	0.80	0.60	0.58	0.61	0.57	0.54	0.54	0.62	0.63	0.63	0.57	1.03	1.04
MgO	1.17	1.17	2.05	1.95	1.96	0.25	0.23	0.22	0.24	0.26	0.26	0.28	0.35	0.35
CaO	10.44	10.24	10.61	11.15	10.91	10.38	10.11	10.62	10.32	10.07	10.44	10.88	10.10	10.43
Na2O	1.70	1.61	1.49	1.46	1.50	1.48	1.39	1.12	1.65	1.68	1.62	1.28	1.44	1.39
K2O	1.98	1.97	1.82	1.97	2.01	2.21	2.19	2.21	2.22	2.20	2.23	2.22	2.13	2.21
F	0.36	0.00	0.73	0.77	0.95	0.21	0.38	0.03	0.21	0.39	0.53	0.42	0.14	0.09
Cl	0.33	0.38	0.33	0.36	0.35	0.65	0.61	0.71	0.58	0.57	0.65	0.65	0.36	0.41
O=F,Cl	0.23	0.09	0.38	0.41	0.48	0.24	0.30	0.17	0.22	0.29	0.37	0.32	0.14	0.13
Total	98.21	97.77	97.45	97.68	98.56	94.95	93.42	97.07	99.06	98.52	98.63	96.54	96.26	98.17
[Si	6.42	6.43	6.59	6.65	6.51	5.89	5.86	5.98	6.08	6.12	6.04	5.79	6.12	6.10
Al(IV)	1.58	1.57	1.41	1.35	1.49	2.11	2.14	2.02	1.92	1.88	1.96	2.21	1.88	1.90
Ti	0.00	0.00	0.00	0.00	0.00	0.00	0.00	0.00	0.00	0.00	0.00	0.00	0.00	0.00
Al(VI)	0.49	0.42	0.49	0.53	0.45	0.44	0.39	0.60	0.53	0.56	0.54	0.36	0.28	0.37
Ti	0.07	0.07	0.05	0.05	0.05	0.09	0.12	0.07	0.11	0.10	0.10	0.09	0.06	0.03
Fe3+	0.42	0.57	0.33	-0.01	0.32	0.79	0.87	0.75	0.67	0.69	0.65	0.93	1.01	0.97
Mg	0.28	0.28	0.49	0.47	0.47	0.06	0.06	0.05	0.06	0.06	0.06	0.07	0.09	0.08
Fe2+	3.66	3.55	3.56	3.89	3.63	3.54	3.48	3.45	3.55	3.51	3.57	3.47	3.42	3.40
Mn	0.07	0.11	0.08	0.08	0.08	0.08	0.08	0.07	0.08	0.09	0.09	0.08	0.14	0.14
[Mn	0.00	0.00	0.00	0.00	0.00	0.00	0.00	0.00	0.00	0.00	0.00	0.00	0.00	0.00
Fe2+	0.00	0.00	0.00	0.00	0.00	0.00	0.00	0.00	0.00	0.00	0.00	0.00	0.00	0.00
Mg	0.00	0.00	0.00	0.00	0.00	0.00	0.00	0.00	0.00	0.00	0.00	0.00	0.00	0.00
Fe3+	0.00	0.00	0.00	0.00	0.00	0.00	0.00	0.00	0.00	0.00	0.00	0.00	0.00	0.00
Ca	1.80	1.76	1.83	1.94	1.87	1.87	1.85	1.85	1.77	1.73	1.80	1.93	1.78	1.80
Na	0.20	0.24	0.17	0.06	0.13	0.13	0.15	0.15	0.23	0.27	0.20	0.07	0.22	0.20
Na	0.33	0.27	0.30	0.39	0.34	0.35	0.31	0.21	0.28	0.26	0.31	0.34	0.24	0.24
Ca	0.00	0.00	0.00	0.00	0.00	0.00	0.00	0.00	0.00	0.00	0.00	0.00	0.00	0.00
K	0.41	0.40	0.37	0.41	0.41	0.47	0.48	0.46	0.45	0.45	0.46	0.47	0.45	0.45
F	0.18	0.00	0.37	0.39	0.48	0.11	0.21	0.02	0.11	0.20	0.27	0.22	0.07	0.05
Cl	0.09	0.10	0.09	0.10	0.10	0.19	0.18	0.20	0.16	0.16	0.18	0.19	0.10	0.11
OH	1.72	1.90	1.53	1.51	1.42	1.70	1.61	1.79	1.73	1.64	1.55	1.59	1.82	1.84
Fe/Fe+Mg	0.55	0.55	0.55	0.56	0.54	0.99	0.99	0.99	0.99	0.99	0.99	0.98	0.98	0.98

	52	53	54	55	56	57	58	59	60	61	62	63	64
Sample	34MALB	34MALB	34MALB	34MALB	9_4	9_4	9_4	9_4	9_4	9_4	9_4	9_4	9_4
Rock	HAFGg	HAFGg	HAFGg	HAFGg	HAFGg	HAFGg	HAFGg	HAFGg	HAFGg	HAFGg	HAFGg	HAFGg	HAFGg
Alteration	Mag	Mag	Mag	Mag	Mag	Mag	Mag	Mag	Mag	Mag	Mag	Mag	Mag
Name	Hst	Hst	Hst	Hst	Hst	Hst	Hst	Hst	Hst	Hst	Hst	Hst	Hst
SiO2	37.05	39.41	39.04	38.92	38.96	38.70	37.94	39.18	39.14	38.52	37.29	37.21	36.75
TiO2	0.44	0.69	0.81	0.73	0.72	0.93	0.68	0.44	0.69	0.91	0.36	0.72	0.79
Al2O3	11.32	10.82	10.55	11.06	11.69	12.04	11.24	12.16	12.10	12.07	12.13	11.86	11.79
FeO(Total)	32.38	33.03	32.05	32.67	33.20	32.65	31.16	32.81	32.21	33.20	31.70	32.08	31.73
MnO	0.99	0.97	1.03	0.94	0.00	0.00	0.00	0.00	0.00	0.00	0.00	0.00	0.00
MgO	0.41	0.38	0.41	0.38	0.62	0.65	0.64	0.57	0.57	0.68	0.75	0.72	0.85
CaO	10.08	10.38	10.23	10.31	11.04	11.13	11.08	10.95	11.42	11.05	10.85	10.80	10.85
Na2O	1.50	1.64	1.60	1.66	1.71	1.60	1.81	1.52	1.42	1.78	1.58	1.67	1.67
K2O	2.15	2.03	2.05	2.06	2.23	2.24	2.11	2.23	2.29	2.13	2.13	2.21	2.25
F	0.20	0.36	0.33	0.17	0.54	0.12	0.38	0.44	0.26	0.22	0.04	0.21	0.20
Cl	0.38	0.30	0.33	0.33	0.68	0.75	0.68	0.73	0.77	0.64	0.59	0.62	0.58
O=F,Cl	0.17	0.22	0.21	0.15	0.38	0.22	0.31	0.35	0.28	0.24	0.15	0.23	0.22
Total	96.73	99.79	98.22	99.08	101.01	100.59	97.41	100.68	100.59	100.96	97.27	97.87	97.24
[Si	6.08	6.27	6.31	6.23	6.18	6.15	6.27	6.20	6.23	6.09	6.10	6.07	6.04
Al(IV)	1.92	1.73	1.69	1.77	1.82	1.85	1.73	1.80	1.77	1.91	1.90	1.93	1.96
Ti	0.00	0.00	0.00	0.00	0.00	0.00	0.00	0.00	0.00	0.00	0.00	0.00	0.00
Al(VI)	0.27	0.30	0.33	0.32	0.36	0.40	0.45	0.47	0.50	0.34	0.44	0.36	0.33
Ti	0.05	0.08	0.10	0.09	0.09	0.11	0.08	0.05	0.08	0.11	0.04	0.09	0.10
Fe3+	1.08	0.80	0.69	0.80	0.56	0.50	0.17	0.59	0.31	0.63	0.63	0.62	0.60
Mg	0.10	0.09	0.10	0.09	0.15	0.15	0.16	0.13	0.14	0.16	0.18	0.18	0.21
Fe2+	3.36	3.59	3.64	3.58	3.85	3.84	4.14	3.75	3.97	3.76	3.71	3.75	3.76
Mn	0.14	0.13	0.14	0.13	0.00	0.00	0.00	0.00	0.00	0.00	0.00	0.00	0.00
[Mn	0.00	0.00	0.00	0.00	0.00	0.00	0.00	0.00	0.00	0.00	0.00	0.00	0.00
Fe2+	0.00	0.00	0.00	0.00	0.00	0.00	0.00	0.00	0.00	0.00	0.00	0.00	0.00
Mg	0.00	0.00	0.00	0.00	0.00	0.00	0.00	0.00	0.00	0.00	0.00	0.00	0.00
Fe3+	0.00	0.00	0.00	0.00	0.00	0.00	0.00	0.00	0.00	0.00	0.00	0.00	0.00
Ca	1.77	1.77	1.77	1.77	1.88	1.89	1.96	1.86	1.95	1.87	1.90	1.89	1.91
Na	0.23	0.23	0.23	0.23	0.12	0.11	0.04	0.14	0.05	0.13	0.10	0.11	0.09
Na	0.25	0.28	0.27	0.28	0.40	0.39	0.54	0.32	0.38	0.42	0.40	0.42	0.44
Ca	0.00	0.00	0.00	0.00	0.00	0.00	0.00	0.00	0.00	0.00	0.00	0.00	0.00
K	0.45	0.41	0.42	0.42	0.45	0.45	0.44	0.45	0.46	0.43	0.44	0.46	0.47
F	0.11	0.18	0.17	0.09	0.27	0.06	0.20	0.22	0.13	0.11	0.02	0.11	0.11
Cl	0.11	0.08	0.09	0.09	0.19	0.20	0.19	0.20	0.21	0.17	0.17	0.17	0.16
OH	1.79	1.73	1.74	1.82	1.54	1.74	1.61	1.58	1.66	1.71	1.81	1.72	1.73
Fe/Fe+Mg	0.98	0.98	0.98	0.98	0.97	0.97	0.96	0.97	0.97	0.96	0.96	0.96	0.95

	65	66	67	68	69	70	71	72	73	74	75	76	77
Sample	9_4	9_4	9_4	9_4	9_4	GNA05	GNA05	GNA05	GNA05	GNA05	GNA05	GNA05	GNA05
Rock	HAFGg	HAFGg	HAFGg	HAFGg	HAFGg	HAFGg	HAFGg	HAFGg	HAFGg	HAFGg	HAFGg	HAFGg	HAFGg
Alteration	Mag	Mag	Mag	Mag	Mag	Mag	Mag	Mag	Mag	Mag	Mag	Mag	Mag
Name	Hst	Hst	Hst	Hst	Hst	Hst	Hst	Hst	Hst	Hst	Hst	Hst	Hst
SiO2	37.19	39.02	37.71	36.82	37.91	39.51	36.61	39.53	39.21	37.75	37.12	37.60	36.78
TiO2	0.64	0.87	0.79	0.57	0.71	0.93	0.66	0.98	0.97	0.83	0.71	0.89	1.10
Al2O3	11.86	11.98	11.86	12.21	11.98	11.08	10.59	10.97	11.35	10.44	11.54	10.54	10.06
FeO(Total)	32.05	33.31	33.23	34.06	33.01	31.38	33.06	31.54	32.21	32.59	33.48	33.27	32.05
MnO	0.00	0.00	0.00	0.00	0.00	0.00	0.00	0.00	0.00	0.00	0.00	0.00	0.00
MgO	0.81	0.87	1.12	0.78	0.83	0.59	0.64	0.66	0.58	0.57	0.59	0.58	0.54
CaO	10.25	10.84	10.72	11.00	10.90	10.43	10.66	10.31	10.19	10.53	10.71	10.38	10.07
Na2O	1.77	2.15	1.50	1.06	1.09	1.48	1.54	1.56	1.57	1.59	1.43	1.50	1.64
K2O	2.17	1.84	2.04	2.13	2.10	2.11	2.10	1.99	2.10	2.06	2.24	2.07	2.14
F	0.54	0.50	0.29	0.54	0.30	0.00	0.00	0.00	0.00	0.00	0.00	0.00	0.00
Cl	0.66	0.46	0.63	0.64	0.70	0.34	0.36	0.34	0.35	0.39	0.30	0.40	0.36
O=F,Cl	0.38	0.31	0.26	0.37	0.28	0.08	0.08	0.08	0.08	0.09	0.07	0.09	0.08
Total	97.56	101.53	99.63	99.44	99.25	97.77	96.14	97.80	98.45	96.66	98.05	97.14	94.66
[Si	6.07	6.12	6.00	5.89	6.05	6.39	6.09	6.38	6.28	6.23	6.02	6.16	6.20
Al(IV)	1.93	1.88	2.00	2.11	1.95	1.61	1.91	1.62	1.72	1.77	1.98	1.84	1.80
Ti	0.00	0.00	0.00	0.00	0.00	0.00	0.00	0.00	0.00	0.00	0.00	0.00	0.00
Al(VI)	0.35	0.33	0.22	0.19	0.31	0.50	0.16	0.47	0.43	0.26	0.23	0.19	0.20
Ti	0.08	0.10	0.09	0.07	0.09	0.11	0.08	0.12	0.12	0.10	0.09	0.11	0.14
Fe3+	0.83	0.69	1.06	1.25	0.97	0.37	0.85	0.45	0.64	0.64	0.94	0.88	0.68
Mg	0.20	0.20	0.27	0.19	0.20	0.14	0.16	0.16	0.14	0.14	0.14	0.14	0.14
Fe2+	3.55	3.68	3.36	3.30	3.44	3.87	3.75	3.80	3.68	3.86	3.60	3.68	3.84
Mn	0.00	0.00	0.00	0.00	0.00	0.00	0.00	0.00	0.00	0.00	0.00	0.00	0.00
[Mn	0.00	0.00	0.00	0.00	0.00	0.00	0.00	0.00	0.00	0.00	0.00	0.00	0.00
Fe2+	0.00	0.00	0.00	0.00	0.00	0.00	0.00	0.00	0.00	0.00	0.00	0.00	0.00
Mg	0.00	0.00	0.00	0.00	0.00	0.00	0.00	0.00	0.00	0.00	0.00	0.00	0.00
Fe3+	0.00	0.00	0.00	0.00	0.00	0.00	0.00	0.00	0.00	0.00	0.00	0.00	0.00
Ca	1.79	1.82	1.83	1.88	1.86	1.81	1.90	1.78	1.75	1.86	1.86	1.82	1.82
Na	0.21	0.18	0.17	0.12	0.14	0.19	0.10	0.22	0.25	0.14	0.14	0.18	0.18
Na	0.35	0.47	0.29	0.21	0.20	0.27	0.40	0.27	0.24	0.37	0.31	0.30	0.36
Ca	0.00	0.00	0.00	0.00	0.00	0.00	0.00	0.00	0.00	0.00	0.00	0.00	0.00
K	0.45	0.37	0.41	0.43	0.43	0.44	0.45	0.41	0.43	0.43	0.46	0.43	0.46
F	0.28	0.25	0.15	0.28	0.15	0.00	0.00	0.00	0.00	0.00	0.00	0.00	0.00
Cl	0.19	0.12	0.17	0.18	0.19	0.09	0.10	0.09	0.10	0.11	0.08	0.11	0.10
OH	1.53	1.62	1.68	1.54	1.65	1.91	1.90	1.91	1.90	1.89	1.92	1.89	1.90
Fe/Fe+Mg	0.96	0.96	0.94	0.96	0.96	0.97	0.97	0.96	0.97	0.97	0.97	0.97	0.97

	78	79	80	81	82	83	84	85	86	87	88	89	90
Sample	GNA05	GNA05	GNA05	GNA05	GNA05	GNA05	7_9B	7_9B	7_9B	7_9B	7_9B	7_9B	7_9B
Rock	HAFGg	HAFGg	HAFGg	HAFGg	HAFGg	HAFGg	Ab	Ab	Ab	Ab	Ab	Ab	Ab
Alteration	Mag	Mag	Mag	Mag	Mag	Mag	Mag	Mag	Mag	Mag	Mag	Mag	Mag
Name	Hst	Hst	Hst	Hst	Hst	Hst	Hst	Hst	Hst	Hst	Hst	Hst	Hst
SiO2	37.81	37.52	39.51	38.45	38.77	37.93	38.05	39.80	39.55	37.84	40.78	36.41	37.88
TiO2	0.64	0.61	0.84	0.85	0.99	0.70	0.25	0.16	0.25	0.29	0.19	0.16	0.18
Al2O3	10.37	11.87	10.91	10.89	10.97	11.13	10.59	9.47	10.48	10.72	9.02	10.12	8.03
FeO(Total)	32.42	31.80	32.73	33.00	32.88	31.96	35.98	36.81	37.30	36.40	37.49	36.67	35.91
MnO	0.00	0.00	0.00	0.00	0.00	0.00	0.00	0.00	0.00	0.00	0.00	0.00	0.00
MgO	0.62	0.46	0.62	0.59	0.54	0.45	0.10	0.34	0.57	0.35	0.67	0.48	0.40
CaO	10.15	10.34	10.10	10.29	10.26	10.33	10.95	10.84	10.78	10.70	10.46	10.77	10.83
Na2O	1.48	1.49	1.89	1.71	1.78	1.46	0.98	0.86	1.15	1.54	1.12	1.48	1.27
K2O	1.95	2.24	1.96	2.07	2.05	2.15	2.00	1.70	1.62	2.11	1.70	1.91	1.55
F	0.00	0.00	0.00	0.00	0.00	0.00	0.03	0.27	0.07	0.18	0.24	0.20	0.03
Cl	0.32	0.36	0.40	0.36	0.38	0.31	0.24	0.17	0.15	0.21	0.18	0.19	0.13
O=F,Cl	0.07	0.08	0.09	0.08	0.09	0.07	0.07	0.15	0.06	0.12	0.14	0.13	0.04
Total	95.69	96.61	98.87	98.13	98.53	96.35	99.10	100.27	101.86	100.22	101.71	98.26	96.17
[Si	6.26	6.15	6.32	6.22	6.24	6.24	6.11	6.28	6.11	6.02	6.32	5.93	6.30
Al(IV)	1.74	1.85	1.68	1.78	1.76	1.76	1.89	1.72	1.89	1.98	1.65	1.94	1.58
Ti	0.00	0.00	0.00	0.00	0.00	0.00	0.00	0.00	0.00	0.00	0.02	0.02	0.02
Al(VI)	0.28	0.45	0.37	0.29	0.32	0.40	0.11	0.04	0.02	0.04	0.00	0.00	0.00
Ti	0.08	0.08	0.10	0.10	0.12	0.09	0.03	0.02	0.03	0.03	0.00	0.00	0.00
Fe3+	0.82	0.67	0.66	0.76	0.68	0.62	1.23	1.37	1.58	1.32	1.53	1.54	1.17
Mg	0.15	0.11	0.15	0.14	0.13	0.11	0.02	0.08	0.13	0.08	0.15	0.12	0.10
Fe2+	3.67	3.69	3.72	3.71	3.75	3.78	3.60	3.49	3.24	3.53	3.32	3.34	3.73
Mn	0.00	0.00	0.00	0.00	0.00	0.00	0.00	0.00	0.00	0.00	0.00	0.00	0.00
[Mn	0.00	0.00	0.00	0.00	0.00	0.00	0.00	0.00	0.00	0.00	0.00	0.00	0.00
Fe2+	0.00	0.00	0.00	0.00	0.00	0.00	0.00	0.00	0.00	0.00	0.01	0.11	0.10
Mg	0.00	0.00	0.00	0.00	0.00	0.00	0.00	0.00	0.00	0.00	0.00	0.00	0.00
Fe3+	0.00	0.00	0.00	0.00	0.00	0.00	0.00	0.00	0.00	0.00	0.00	0.00	0.00
Ca	1.80	1.82	1.73	1.78	1.77	1.82	1.88	1.83	1.78	1.83	1.74	1.88	1.90
Na	0.20	0.18	0.27	0.22	0.23	0.18	0.12	0.17	0.22	0.17	0.25	0.01	0.00
Na	0.27	0.29	0.32	0.32	0.33	0.29	0.19	0.10	0.13	0.30	0.09	0.46	0.41
Ca	0.00	0.00	0.00	0.00	0.00	0.00	0.00	0.00	0.00	0.00	0.00	0.00	0.03
K	0.41	0.47	0.40	0.43	0.42	0.45	0.41	0.34	0.32	0.43	0.34	0.40	0.33
F	0.00	0.00	0.00	0.00	0.00	0.00	0.02	0.14	0.04	0.09	0.12	0.11	0.02
Cl	0.09	0.10	0.11	0.10	0.11	0.09	0.07	0.05	0.04	0.06	0.05	0.05	0.04
OH	1.91	1.90	1.89	1.90	1.89	1.91	1.92	1.81	1.92	1.85	1.83	1.84	1.95
Fe/Fe+Mg	0.97	0.97	0.97	0.97	0.97	0.98	1.00	0.98	0.97	0.98	0.97	0.98	0.98

	91	92	93	94	95	96	97	98	99	100	101	102
Sample	7_9B	7_9B	7_9B	7_9B	7_9B	7_9B	7_9B	7_9B	GNA02 AB	GNA02 AB	GNA02 AB	GNA02 AB
Rock	Ab	Ab	Ab	Ab	Ab	Ab	Ab	Ab	Ab	Ab	Ab	Ab
Alteration	Mag	Mag	Mag	Mag	Mag	Mag	Mag	Mag	Mag	Mag	Mag	Mag
Name	Hst	Hst	Hst	Hst	Hst	Hst	Hst	Hst	Fed	Fed	Fed	Fed
SiO2	41.41	38.60	40.59	40.99	37.16	37.43	38.85	39.09	46.04	44.08	44.55	46.75
TiO2	0.27	0.53	0.16	0.18	0.28	0.28	0.23	0.29	0.29	0.66	0.50	0.37
Al2O3	8.06	9.51	8.35	7.19	10.37	9.62	10.54	10.34	5.31	6.53	6.63	5.92
FeO(Total)	36.91	36.10	37.14	36.15	36.34	36.61	36.55	36.81	24.24	25.31	25.34	23.45
MnO	0.00	0.00	0.00	0.00	0.00	0.00	0.00	0.00	0.00	0.00	0.00	0.00
MgO	0.54	0.60	0.15	0.54	0.17	0.35	0.18	0.40	9.25	8.27	8.41	8.80
CaO	10.32	10.83	10.56	10.61	11.03	10.91	10.81	10.85	10.27	10.14	10.62	10.26
Na2O	1.76	1.49	0.97	0.48	0.73	1.25	1.34	1.50	2.08	1.85	1.74	1.41
K2O	1.53	1.81	1.54	1.35	2.13	1.91	2.14	2.05	1.18	1.35	1.38	1.19
F	0.09	0.00	0.11	0.00	0.00	0.17	0.17	0.22	0.96	0.67	0.93	1.06
Cl	0.14	0.19	0.12	0.10	0.21	0.20	0.21	0.19	0.04	0.04	0.05	0.04
O=F,Cl	0.07	0.04	0.07	0.02	0.05	0.12	0.12	0.14	0.41	0.29	0.40	0.46
Total	100.96	99.62	99.62	97.57	98.37	98.61	100.90	101.60	99.25	98.61	99.75	98.79
[Si	6.50	6.17	6.45	6.61	6.02	6.07	6.14	6.13	6.91	6.68	6.70	7.01
Al(IV)	1.49	1.79	1.55	1.37	1.98	1.84	1.86	1.87	0.94	1.17	1.17	0.99
Ti	0.01	0.03	0.00	0.02	0.00	0.03	0.00	0.00	0.03	0.08	0.06	0.00
Al(VI)	0.00	0.00	0.01	0.00	0.00	0.00	0.10	0.04	0.00	0.00	0.00	0.05
Ti	0.03	0.03	0.02	0.00	0.03	0.00	0.03	0.03	0.00	0.00	0.00	0.04
Fe3+	1.12	1.19	1.30	1.28	1.41	1.36	1.20	1.24	1.03	1.22	1.12	0.92
Mg	0.13	0.14	0.04	0.13	0.04	0.08	0.04	0.09	2.07	1.87	1.88	1.97
Fe2+	3.72	3.64	3.64	3.59	3.51	3.55	3.62	3.59	1.90	1.91	1.99	2.01
Mn	0.00	0.00	0.00	0.00	0.00	0.00	0.00	0.00	0.00	0.00	0.00	0.00
[Mn	0.00	0.00	0.00	0.00	0.00	0.00	0.00	0.00	0.00	0.00	0.00	0.00
Fe2+	0.00	0.00	0.00	0.00	0.00	0.05	0.00	0.00	0.11	0.08	0.07	0.00
Mg	0.00	0.00	0.00	0.00	0.00	0.00	0.00	0.00	0.00	0.00	0.00	0.00
Fe3+	0.00	0.00	0.00	0.00	0.00	0.00	0.00	0.00	0.00	0.00	0.00	0.00
Ca	1.74	1.86	1.80	1.83	1.91	1.90	1.83	1.82	1.65	1.65	1.71	1.65
Na	0.26	0.14	0.20	0.15	0.09	0.05	0.17	0.18	0.23	0.28	0.22	0.35
Na	0.27	0.32	0.10	0.00	0.14	0.34	0.24	0.28	0.37	0.27	0.29	0.06
Ca	0.00	0.00	0.00	0.00	0.00	0.00	0.00	0.00	0.00	0.00	0.00	0.00
K	0.31	0.37	0.31	0.28	0.44	0.40	0.43	0.41	0.23	0.26	0.26	0.23
F	0.05	0.00	0.06	0.00	0.00	0.09	0.09	0.11	0.47	0.33	0.45	0.51
Cl	0.04	0.05	0.03	0.03	0.06	0.06	0.06	0.05	0.01	0.01	0.01	0.01
OH	1.92	1.95	1.91	1.97	1.94	1.85	1.86	1.84	1.52	1.66	1.53	1.48
Fe/Fe+Mg	0.97	0.97	0.99	0.97	0.99	0.98	0.99	0.98	0.60	0.63	0.63	0.60

	103	104	105	106	107	108	109	110	111	112	113	114	115
Sample	GNA02 AB	GNA02 AB	GNA02 AB	GNA02 AB	GNA02 AB	GNA02	GNA02	GNA02	GNA02	GNA02	34GALB	34GALB	34GALB
Rock	Ab	Ab	Ab	Ab	Ab	Ab	Ab	Ab	Ab	Ab	Ab	Ab	Ab
Alteration	Mag	Mag	Mag	Mag	Mag	Mag	Mag	Mag	Mag	Mag	Mag	Mag	Mag
Name	Fed	Fed	Fed	Fed	Fed	Hst	Hst	Hst	Hst	Hst	Hst	Hst	Hst
SiO2	45.96	46.25	46.19	46.73	46.53	40.33	40.64	40.93	40.77	39.17	37.86	37.80	35.72
TiO2	0.30	0.14	0.30	0.28	0.29	0.63	0.72	0.55	0.79	0.30	0.27	0.26	0.31
Al2O3	6.54	6.13	6.15	6.46	6.40	11.05	10.92	10.98	10.84	12.46	11.70	11.55	11.62
FeO(Total)	23.51	23.21	23.22	23.73	23.48	30.20	29.58	29.43	30.14	29.15	30.56	30.99	29.96
MnO	0.00	0.00	0.00	0.00	0.00	1.08	1.14	1.16	1.16	1.16	0.35	0.30	0.25
MgO	8.34	8.44	8.77	8.50	8.15	2.25	2.24	2.17	2.27	1.85	2.15	2.15	2.16
CaO	10.38	10.02	9.18	10.57	10.30	10.51	10.53	10.69	10.90	11.03	10.71	10.64	10.51
Na2O	1.87	1.38	1.07	1.57	1.40	1.00	1.00	1.00	1.00	1.00	1.41	1.47	1.31
K2O	1.34	1.23	1.96	1.22	1.19	2.20	2.20	2.02	2.11	2.35	2.06	2.06	2.11
F	1.01	0.94	0.79	0.97	0.86	0.44	0.44	0.15	0.63	0.23	0.47	0.77	0.47
Cl	0.04	0.05	0.04	0.04	0.03	0.34	0.35	0.35	0.35	0.39	0.14	0.13	0.15
O=F,Cl	0.43	0.41	0.34	0.42	0.37	0.26	0.27	0.14	0.35	0.19	0.23	0.35	0.23
Total	98.86	97.38	97.33	99.65	98.26	99.77	99.48	99.27	100.61	98.91	97.45	97.77	94.34
[Si	6.95	7.03	6.97	6.98	7.03	6.29	6.36	6.40	6.33	6.19	6.08	6.07	5.94
Al(IV)	1.05	0.97	1.03	1.02	0.97	1.71	1.64	1.60	1.67	1.81	1.92	1.93	2.06
Ti	0.00	0.00	0.00	0.00	0.00	0.00	0.00	0.00	0.00	0.00	0.00	0.00	0.00
Al(VI)	0.11	0.12	0.06	0.11	0.17	0.32	0.37	0.43	0.32	0.52	0.30	0.25	0.22
Ti	0.03	0.02	0.03	0.03	0.03	0.07	0.08	0.07	0.09	0.04	0.03	0.03	0.04
Fe3+	0.70	0.91	1.24	0.78	0.77	0.99	0.83	0.75	0.82	0.70	1.00	1.08	1.14
Mg	1.88	1.91	1.97	1.89	1.83	0.52	0.52	0.51	0.52	0.44	0.51	0.51	0.54
Fe2+	2.27	2.04	1.69	2.19	2.20	2.95	3.04	3.10	3.10	3.16	3.10	3.08	3.03
Mn	0.00	0.00	0.00	0.00	0.00	0.14	0.15	0.15	0.15	0.15	0.05	0.04	0.04
[Mn	0.00	0.00	0.00	0.00	0.00	0.00	0.00	0.00	0.00	0.00	0.00	0.00	0.00
Fe2+	0.00	0.00	0.00	0.00	0.00	0.00	0.00	0.00	0.00	0.00	0.00	0.00	0.00
Mg	0.00	0.00	0.00	0.00	0.00	0.00	0.00	0.00	0.00	0.00	0.00	0.00	0.00
Fe3+	0.00	0.00	0.00	0.00	0.00	0.00	0.00	0.00	0.00	0.00	0.00	0.00	0.00
Ca	1.68	1.63	1.48	1.69	1.67	1.76	1.76	1.79	1.81	1.87	1.84	1.83	1.87
Na	0.32	0.37	0.31	0.31	0.33	0.24	0.24	0.21	0.19	0.13	0.16	0.17	0.13
Na	0.23	0.04	0.00	0.15	0.08	0.06	0.07	0.09	0.12	0.17	0.28	0.29	0.30
Ca	0.00	0.00	0.00	0.00	0.00	0.00	0.00	0.00	0.00	0.00	0.00	0.00	0.00
K	0.26	0.24	0.38	0.23	0.23	0.44	0.44	0.40	0.42	0.47	0.42	0.42	0.45
F	0.49	0.46	0.39	0.47	0.42	0.22	0.22	0.08	0.32	0.12	0.24	0.40	0.25
Cl	0.01	0.01	0.01	0.01	0.01	0.09	0.09	0.09	0.09	0.11	0.04	0.04	0.04
OH	1.50	1.53	1.60	1.52	1.57	1.69	1.68	1.83	1.59	1.77	1.72	1.56	1.70
Fe/Fe+Mg	0.61	0.61	0.60	0.61	0.62	0.88	0.88	0.88	0.88	0.90	0.89	0.89	0.89

	116	117	118	119	120	121	122	123	124	125	126	127	128
Sample	34GALB	34GALB	34GALB	34GALB	ABGNAed	ABGNAed	ABGNAed	ABGNAed	ABGNAed	ABGNAed	ABGNAed	ABGNAed	ABGNAed
Rock	Ab	Ab	Ab	Ab	Ab	Ab	Ab	Ab	Ab	Ab	Ab	Ab	Ab
Alteration	Mag	Mag	Mag	Mag	Mag	Mag	Mag	Mag	Mag	Mag	Mag	Mag	Mag
Name	Hst	Hst	Hst	Hst	Fed	Fed	Fed	Fed	Fed	Fed	Fed	Fed	Fed
SiO2	36.23	34.91	37.18	35.52	43.31	50.60	43.29	44.89	44.28	44.14	43.64	43.86	44.44
TiO2	0.31	0.26	0.28	0.14	0.34	0.00	0.28	0.38	0.37	0.38	0.31	0.35	0.28
Al2O3	11.62	11.43	12.12	11.88	8.59	0.69	8.72	7.52	7.58	7.86	8.02	8.09	7.47
FeO(Total)	30.57	28.95	30.60	30.04	25.29	18.20	25.21	25.20	25.23	24.98	25.06	25.42	24.14
MnO	0.23	0.22	0.42	0.30	1.11	1.14	1.11	1.31	1.27	1.27	1.07	0.92	1.03
MgO	2.14	1.99	1.78	1.87	5.50	5.82	5.72	6.10	5.95	5.77	6.12	6.29	6.40
CaO	10.48	10.09	10.86	10.67	10.54	20.77	10.74	10.75	10.75	10.55	10.93	10.68	10.82
Na2O	1.39	1.34	1.45	1.40	2.09	1.63	2.02	1.89	2.03	1.96	1.88	2.14	1.86
K2O	2.10	2.07	2.16	2.13	1.70	0.01	1.72	1.50	1.46	1.60	1.63	1.58	1.51
F	0.32	0.40	0.24	0.31	0.00	0.00	0.00	0.00	0.00	0.00	0.00	0.00	0.00
Cl	0.13	0.12	0.15	0.16	0.07	0.01	0.07	0.07	0.07	0.09	0.08	0.08	0.07
O=F,Cl	0.16	0.20	0.13	0.17	0.02	0.00	0.02	0.02	0.02	0.02	0.02	0.02	0.02
Total	95.36	91.58	97.11	94.25	98.52	98.87	98.86	99.59	98.97	98.58	98.72	99.39	98.00
[Si	5.95	5.98	6.02	5.94	6.70	8.62	6.67	6.84	6.81	6.81	6.73	6.70	6.87
Al(IV)	2.05	2.02	1.98	2.06	1.30	0.00	1.33	1.16	1.19	1.19	1.27	1.30	1.13
Ti	0.00	0.00	0.00	0.00	0.00	0.00	0.00	0.00	0.00	0.00	0.00	0.00	0.00
Al(VI)	0.20	0.28	0.33	0.28	0.27	0.14	0.26	0.19	0.18	0.24	0.19	0.16	0.23
Ti	0.04	0.03	0.03	0.02	0.04	0.00	0.03	0.04	0.04	0.04	0.04	0.04	0.03
Fe3+	1.19	1.08	0.91	1.02	0.49	-5.51	0.51	0.52	0.49	0.47	0.52	0.62	0.39
Mg	0.52	0.51	0.43	0.47	1.27	1.48	1.31	1.39	1.36	1.33	1.41	1.43	1.48
Fe2+	3.01	3.07	3.24	3.17	2.79	8.11	2.74	2.69	2.76	2.75	2.71	2.63	2.74
Mn	0.03	0.03	0.06	0.04	0.15	0.16	0.14	0.17	0.17	0.17	0.14	0.12	0.13
[Mn	0.00	0.00	0.00	0.00	0.00	0.00	0.00	0.00	0.00	0.00	0.00	0.00	0.00
Fe2+	0.00	0.00	0.00	0.00	0.00	0.00	0.00	0.00	0.00	0.00	0.00	0.00	0.00
Mg	0.00	0.00	0.00	0.00	0.00	0.00	0.00	0.00	0.00	0.00	0.00	0.00	0.00
Fe3+	0.00	0.00	0.00	0.00	0.00	0.00	0.00	0.00	0.00	0.00	0.00	0.00	0.00
Ca	1.85	1.85	1.88	1.91	1.75	2.00	1.77	1.76	1.77	1.74	1.81	1.75	1.79
Na	0.15	0.15	0.12	0.09	0.25	0.00	0.23	0.24	0.23	0.26	0.19	0.25	0.21
Na	0.29	0.30	0.34	0.36	0.38	0.54	0.38	0.31	0.38	0.33	0.37	0.38	0.35
Ca	0.00	0.00	0.00	0.00	0.00	1.79	0.00	0.00	0.00	0.00	0.00	0.00	0.00
K	0.44	0.45	0.45	0.45	0.34	0.00	0.34	0.29	0.29	0.31	0.32	0.31	0.30
F	0.17	0.22	0.13	0.17	0.00	0.00	0.00	0.00	0.00	0.00	0.00	0.00	0.00
Cl	0.04	0.04	0.04	0.05	0.02	0.00	0.02	0.02	0.02	0.02	0.02	0.02	0.02
OH	1.79	1.74	1.83	1.79	1.98	2.00	1.98	1.98	1.98	1.98	1.98	1.98	1.98
Fe/Fe+Mg	0.89	0.89	0.91	0.90	0.72	0.64	0.71	0.70	0.70	0.71	0.70	0.69	0.68

	129	130	131	132	133	134	135	136	137	138	139	140	141
Sample	ABGNAed	ABGNAed	ABGNAed	34BALB	34BALB	34BALB	34BALB	34BALB	34BALB	POAB02	POAB02	POAB02	POAB02
Rock	Ab	Ab	Ab	Ab	Ab	Ab	Ab	Ab	Ab	Ab	Ab	Ab	Ab
Alteration	Mag	Mag	Mag	Ret	Ret	Ret	Ret	Ret	Ret	Ret	Ret	Ret	Ret
Name	Fed	Fed	Fed	Mhrn	Mhrn	Mhrn	Mhrn	Mhrn	Mhrn	Wnc	Wnc	Wnc	Wnc
SiO2	42.45	45.24	44.17	50.70	50.26	50.99	50.27	51.63	51.69	56.29	56.36	54.35	54.18
TiO2	0.29	0.37	0.39	0.36	0.14	0.31	0.20	0.38	0.40	0.04	0.02	0.16	0.09
Al2O3	7.73	7.43	6.53	3.52	2.43	3.32	3.07	4.19	4.21	0.81	1.12	2.46	2.50
FeO(Total)	26.35	24.90	25.17	15.07	13.58	14.02	14.22	15.39	15.44	10.31	11.15	14.35	14.09
MnO	1.10	0.95	1.12	0.13	0.16	0.15	0.19	0.28	0.22	3.81	3.00	2.78	2.64
MgO	5.52	6.09	6.13	14.90	15.50	13.95	13.98	13.74	13.88	16.25	16.25	14.02	14.17
CaO	10.59	10.68	10.33	10.33	11.06	9.59	9.75	9.65	10.32	10.01	9.20	6.15	6.17
Na2O	1.76	1.96	1.93	2.06	1.36	2.15	1.55	2.29	2.02	1.45	1.99	3.82	3.81
K2O	1.63	1.51	1.40	0.55	0.44	1.22	0.49	0.59	0.58	0.28	0.42	0.64	0.62
F	0.00	0.00	0.00	0.79	0.75	0.63	0.63	0.92	0.51	0.60	0.43	0.74	0.70
Cl	0.07	0.08	0.05	0.01	0.03	0.55	0.01	0.01	0.01	0.01	0.01	0.00	0.01
O=F,Cl	0.02	0.02	0.01	0.33	0.32	0.39	0.27	0.39	0.22	0.25	0.18	0.31	0.30
Total	97.47	99.19	97.21	98.09	95.39	96.49	94.09	98.68	99.06	99.61	99.77	99.16	98.68
[Si	6.65	6.92	6.89	7.32	7.44	7.55	7.52	7.42	7.41	7.84	7.81	7.63	7.63
Al(IV)	1.35	1.08	1.11	0.60	0.42	0.45	0.48	0.58	0.59	0.13	0.18	0.37	0.37
Ti	0.00	0.00	0.00	0.04	0.02	0.00	0.00	0.00	0.00	0.00	0.00	0.00	0.00
Al(VI)	0.08	0.26	0.09	0.00	0.00	0.13	0.06	0.13	0.12	0.00	0.00	0.03	0.04
Ti	0.03	0.04	0.05	0.00	0.00	0.03	0.02	0.04	0.04	0.00	0.00	0.02	0.01
Fe3+	0.79	0.36	0.60	0.81	0.69	0.36	0.71	0.65	0.56	0.75	0.85	1.30	1.30
Mg	1.29	1.39	1.43	3.21	3.42	3.08	3.12	2.94	2.96	3.37	3.36	2.93	2.97
Fe2+	2.67	2.83	2.68	0.98	0.89	1.38	1.07	1.20	1.29	0.45	0.45	0.38	0.36
Mn	0.15	0.12	0.15	0.00	0.00	0.02	0.02	0.03	0.03	0.43	0.35	0.33	0.31
[Mn	0.00	0.00	0.00	0.02	0.02	0.00	0.00	0.00	0.00	0.02	0.00	0.00	0.00
Fe2+	0.00	0.00	0.00	0.03	0.10	0.00	0.00	0.00	0.00	0.00	0.00	0.00	0.00
Mg	0.00	0.00	0.00	0.00	0.00	0.00	0.00	0.00	0.00	0.00	0.00	0.00	0.00
Fe3+	0.00	0.00	0.00	0.00	0.00	0.00	0.00	0.00	0.00	0.00	0.00	0.00	0.00
Ca	1.78	1.75	1.73	1.60	1.75	1.52	1.56	1.49	1.58	1.49	1.37	0.92	0.93
Na	0.22	0.25	0.27	0.36	0.12	0.48	0.44	0.51	0.42	0.39	0.53	1.04	1.04
Na	0.31	0.33	0.31	0.22	0.27	0.14	0.01	0.12	0.15	0.00	0.00	0.00	0.00
Ca	0.00	0.00	0.00	0.00	0.00	0.00	0.00	0.00	0.00	0.00	0.00	0.00	0.00
K	0.33	0.29	0.28	0.10	0.08	0.23	0.09	0.11	0.11	0.05	0.07	0.11	0.11
F	0.00	0.00	0.00	0.37	0.36	0.30	0.30	0.42	0.23	0.27	0.19	0.34	0.32
Cl	0.02	0.02	0.01	0.00	0.01	0.14	0.00	0.00	0.00	0.00	0.00	0.00	0.00
OH	1.98	1.98	1.99	1.63	1.64	1.56	1.69	1.57	1.76	1.73	1.81	1.66	1.68
Fe/Fe+Mg	0.73	0.70	0.70	0.36	0.33	0.36	0.36	0.39	0.38	0.26	0.28	0.36	0.36

	142	143	144	145	146	147	148	149	150	151	152	153	154
Sample	POAB02	POAB02	POAB02	POAB02	POAB02	PAB 3.00	PAB 3.00	PAB 3.00	PAB 3.00	PAB 3.00	PAB 3.00	PAB 3.00	PAB 3.00
Rock	Ab	Ab	Ab	Ab	Ab	Ab	Ab	Ab	Ab	Ab	Ab	Ab	Ab
Alteration	Ret	Ret	Ret	Ret	Ret	Ret	Ret	Ret	Ret	Ret	Ret	Ret	Ret
Name	Wnc	Wnc	Wnc	Wnc	Wnc	Act	Act	Act	Act	Act	Act	Act	Act
SiO2	53.64	56.81	52.26	53.04	53.28	55.48	56.15	56.01	55.42	55.99	55.51	56.49	54.82
TiO2	0.01	0.04	0.13	0.16	0.15	0.10	0.01	0.03	0.02	0.00	0.02	0.02	0.23
Al2O3	1.15	0.92	3.13	3.23	3.26	2.03	1.47	1.56	1.69	1.23	1.17	0.96	2.60
FeO(Total)	11.00	10.65	13.90	14.20	14.98	13.84	13.25	13.46	13.75	13.02	13.20	12.96	13.99
MnO	3.12	3.20	2.63	2.70	2.78	0.20	0.25	0.30	0.20	0.14	0.32	0.14	0.15
MgO	16.41	16.27	13.43	14.06	14.09	15.53	15.99	15.60	15.56	15.60	16.33	15.79	15.09
CaO	8.87	9.31	6.27	6.14	6.12	12.22	12.51	12.13	12.46	12.54	12.50	12.51	12.01
Na2O	2.11	1.87	3.90	4.04	3.97	0.43	0.39	0.43	0.43	0.30	0.30	0.26	0.58
K2O	0.42	0.34	0.64	0.67	0.68	0.18	0.16	0.16	0.16	0.11	0.10	0.09	0.23
F	0.62	0.19	0.60	0.70	0.93	0.25	0.00	0.11	0.12	0.19	0.09	0.00	0.28
Cl	0.00	0.00	0.00	0.00	0.00	0.00	0.01	0.00	0.01	0.00	0.01	0.00	0.00
O=F,Cl	0.26	0.08	0.25	0.29	0.39	0.11	0.00	0.05	0.05	0.08	0.04	0.00	0.12
Total	97.09	99.52	96.64	98.65	99.85	100.16	100.19	99.75	99.76	99.03	99.51	99.21	99.86
[Si	7.64	7.87	7.56	7.49	7.44	7.77	7.85	7.86	7.81	7.94	7.80	7.97	7.71
Al(IV)	0.19	0.13	0.44	0.51	0.54	0.23	0.15	0.14	0.19	0.06	0.19	0.03	0.29
Ti	0.00	0.00	0.00	0.00	0.02	0.00	0.00	0.00	0.00	0.00	0.00	0.00	0.00
Al(VI)	0.00	0.02	0.09	0.02	0.00	0.10	0.09	0.12	0.09	0.14	0.00	0.13	0.15
Ti	0.00	0.00	0.01	0.02	0.00	0.01	0.00	0.00	0.00	0.00	0.00	0.00	0.02
Fe3+	1.17	0.77	1.17	1.37	1.53	0.29	0.18	0.22	0.20	0.01	0.35	0.02	0.27
Mg	3.48	3.36	2.89	2.96	2.93	3.24	3.33	3.26	3.27	3.30	3.42	3.32	3.17
Fe2+	0.14	0.47	0.51	0.31	0.22	1.33	1.37	1.36	1.42	1.53	1.20	1.51	1.38
Mn	0.21	0.38	0.32	0.32	0.32	0.02	0.03	0.04	0.02	0.02	0.03	0.02	0.02
[Mn	0.17	0.00	0.00	0.00	0.01	0.00	0.00	0.00	0.00	0.00	0.01	0.00	0.00
Fe2+	0.00	0.00	0.00	0.00	0.00	0.00	0.00	0.00	0.00	0.00	0.00	0.00	0.00
Mg	0.00	0.00	0.00	0.00	0.00	0.00	0.00	0.00	0.00	0.00	0.00	0.00	0.00
Fe3+	0.00	0.00	0.00	0.00	0.00	0.00	0.00	0.00	0.00	0.00	0.00	0.00	0.00
Ca	1.35	1.38	0.97	0.93	0.92	1.83	1.87	1.82	1.88	1.90	1.88	1.89	1.81
Na	0.48	0.50	1.03	1.07	1.07	0.12	0.11	0.12	0.12	0.08	0.08	0.07	0.16
Na	0.10	0.00	0.06	0.03	0.00	0.00	0.00	0.00	0.00	0.00	0.00	0.00	0.00
Ca	0.00	0.00	0.00	0.00	0.00	0.00	0.00	0.00	0.00	0.00	0.00	0.00	0.00
K	0.08	0.06	0.12	0.12	0.12	0.03	0.03	0.03	0.03	0.02	0.02	0.02	0.04
F	0.29	0.08	0.28	0.32	0.42	0.11	0.00	0.05	0.05	0.08	0.04	0.00	0.12
Cl	0.00	0.00	0.00	0.00	0.00	0.00	0.00	0.00	0.00	0.00	0.00	0.00	0.00
OH	1.71	1.92	1.72	1.68	1.58	1.89	2.00	1.95	1.95	1.92	1.96	2.00	1.87
Fe/Fe+Mg	0.27	0.27	0.37	0.36	0.37	0.33	0.32	0.33	0.33	0.32	0.31	0.32	0.34

	155	156	157	158	159	160	161	162	163	164	165	166
Sample	PAB 3.00	MAAB03	MAAB03	MAAB03	MAAB03	MAAB03	MAAB03	MAAB03	POAB05	POAB05	POAB05	POAB05
Rock	Ab	Ab	Ab	Ab	Ab	Ab	Ab	Ab	Ab	Ab	Ab	Ab
Alteration	Ret	Ret	Ret	Ret	Ret	Ret	Ret	Ret	Ret	Ret	Ret	Ret
Name	Act	Mhst	Mhst	Mhst	Mhst	Mhst	Mhst	Mhst	Mhst	Mhst	Mhst	Mhst
SiO2	55.26	41.49	41.56	42.00	41.96	42.70	41.48	42.56	41.57	41.56	41.31	41.87
TiO2	0.15	0.25	0.43	0.46	0.38	0.49	0.37	0.43	0.45	0.41	0.38	0.48
Al2O3	1.77	11.67	11.79	11.84	11.66	10.90	10.92	11.37	10.69	10.78	10.93	10.95
FeO(Total)	13.97	17.79	18.21	18.74	18.17	18.67	18.85	19.03	18.35	17.81	17.45	17.18
MnO	0.26	0.18	0.27	0.14	0.15	0.29	0.35	0.23	0.26	0.21	0.16	0.25
MgO	15.79	10.45	10.60	10.19	10.32	10.34	9.99	10.01	10.88	11.18	11.24	11.37
CaO	12.31	11.09	11.06	11.06	11.19	10.87	10.68	10.93	10.54	10.65	10.43	10.66
Na2O	0.45	1.89	2.05	2.01	2.03	2.16	2.16	1.98	2.51	2.58	2.65	2.69
K2O	0.17	1.95	1.96	1.96	1.96	1.88	1.90	1.92	1.78	1.77	1.74	1.76
F	0.00	0.87	0.59	0.80	0.91	0.69	0.58	0.31	0.46	0.58	0.92	0.82
Cl	0.01	0.05	0.04	0.04	0.03	0.04	0.03	0.05	0.02	0.03	0.02	0.01
O=F,Cl	0.00	0.38	0.26	0.35	0.39	0.30	0.25	0.14	0.20	0.25	0.39	0.35
Total	100.13	97.30	98.30	98.89	98.37	98.73	97.06	98.68	97.31	97.31	96.84	97.69
[Si	7.73	6.27	6.21	6.26	6.29	6.37	6.30	6.34	6.26	6.26	6.25	6.28
Al(IV)	0.27	1.73	1.79	1.74	1.71	1.63	1.70	1.66	1.74	1.74	1.75	1.72
Ti	0.00	0.00	0.00	0.00	0.00	0.00	0.00	0.00	0.00	0.00	0.00	0.00
Al(VI)	0.02	0.35	0.28	0.33	0.35	0.28	0.26	0.33	0.16	0.17	0.20	0.22
Ti	0.02	0.03	0.05	0.05	0.04	0.05	0.04	0.05	0.05	0.05	0.04	0.05
Fe3+	0.37	0.81	0.91	0.82	0.71	0.79	0.88	0.81	1.00	0.94	0.98	0.85
Mg	3.29	2.35	2.36	2.26	2.31	2.30	2.26	2.22	2.44	2.51	2.53	2.54
Fe2+	1.26	1.44	1.37	1.51	1.57	1.54	1.52	1.56	1.31	1.30	1.23	1.31
Mn	0.03	0.02	0.03	0.02	0.02	0.04	0.05	0.03	0.03	0.03	0.02	0.03
[Mn	0.00	0.00	0.00	0.00	0.00	0.00	0.00	0.00	0.00	0.00	0.00	0.00
Fe2+	0.00	0.00	0.00	0.00	0.00	0.00	0.00	0.00	0.00	0.00	0.00	0.00
Mg	0.00	0.00	0.00	0.00	0.00	0.00	0.00	0.00	0.00	0.00	0.00	0.00
Fe3+	0.00	0.00	0.00	0.00	0.00	0.00	0.00	0.00	0.00	0.00	0.00	0.00
Ca	1.84	1.80	1.77	1.76	1.80	1.74	1.74	1.74	1.70	1.72	1.69	1.71
Na	0.12	0.20	0.23	0.24	0.20	0.26	0.26	0.26	0.30	0.28	0.31	0.29
Na	0.00	0.35	0.36	0.35	0.39	0.36	0.37	0.32	0.43	0.47	0.47	0.50
Ca	0.00	0.00	0.00	0.00	0.00	0.00	0.00	0.00	0.00	0.00	0.00	0.00
K	0.03	0.38	0.37	0.37	0.37	0.36	0.37	0.36	0.34	0.34	0.34	0.34
F	0.00	0.42	0.28	0.38	0.44	0.33	0.28	0.15	0.22	0.28	0.45	0.40
Cl	0.00	0.01	0.01	0.01	0.01	0.01	0.01	0.01	0.01	0.01	0.01	0.00
OH	2.00	1.56	1.71	1.61	1.55	1.66	1.71	1.84	1.77	1.71	1.55	1.60
Fe/Fe+Mg	0.33	0.49	0.49	0.51	0.50	0.50	0.51	0.52	0.49	0.47	0.47	0.46

	167	168	169	170	171	172	173	174	175	176	177	178
Sample	AL04	AL04	AL04	AL04	AL04	AL04	AL04	AL04	AL04	AL04	AL04	AL04
Rock	Ab	Ab	Ab	Ab	Ab	Ab	Ab	Ab	Ab	Ab	Ab	Ab
Alteration	Ret	Ret	Ret	Ret	Ret	Ret	Ret	Ret	Ret	Ret	Ret	Ret
Name	Act	Act	Act	Act	Act	Act	Act	Act	Act	Act	Act	Act
SiO2	51.78	51.77	51.69	50.57	52.19	51.34	52.92	53.01	52.22	52.75	49.81	51.03
TiO2	0.21	0.27	0.23	0.34	0.31	0.30	0.31	0.24	0.29	0.32	0.44	0.37
Al2O3	2.79	3.46	3.44	3.45	3.18	3.58	2.86	2.65	3.29	3.12	3.83	3.32
FeO(Total)	17.10	18.64	18.28	17.49	16.94	17.98	17.65	17.40	18.07	17.74	18.62	17.99
MnO	0.07	0.10	0.08	0.09	0.01	0.11	0.11	0.11	0.14	0.11	0.18	0.06
MgO	12.73	12.08	12.37	12.53	12.72	12.20	12.53	12.94	12.27	12.61	11.45	11.98
CaO	9.93	9.53	9.81	10.43	10.65	9.98	10.62	10.34	10.10	10.21	10.31	10.63
Na2O	1.77	2.17	2.03	1.42	1.46	1.90	1.26	1.48	1.79	1.57	1.72	1.34
K2O	0.37	0.48	0.50	0.50	0.48	0.51	0.41	0.38	0.46	0.43	0.56	0.49
F	0.00	0.00	0.00	0.00	0.00	0.00	0.00	0.00	0.00	0.00	0.00	0.00
Cl	0.02	0.01	0.01	0.02	0.01	0.02	0.01	0.02	0.01	0.01	0.02	0.00
O=F,Cl	0.00	0.00	0.00	0.00	0.00	0.00	0.00	0.00	0.00	0.00	0.00	0.00
Total	96.77	98.51	98.44	96.84	97.95	97.92	98.68	98.57	98.64	98.87	96.94	97.21
[Si	7.60	7.50	7.49	7.45	7.60	7.49	7.64	7.64	7.56	7.59	7.40	7.52
Al(IV)	0.40	0.50	0.51	0.55	0.40	0.51	0.36	0.36	0.44	0.41	0.60	0.48
Ti	0.00	0.00	0.00	0.00	0.00	0.00	0.00	0.00	0.00	0.00	0.00	0.00
Al(VI)	0.08	0.09	0.08	0.05	0.14	0.11	0.13	0.09	0.12	0.11	0.08	0.10
Ti	0.02	0.03	0.03	0.04	0.03	0.03	0.03	0.03	0.03	0.03	0.05	0.04
Fe3+	0.57	0.69	0.67	0.64	0.37	0.58	0.45	0.55	0.54	0.57	0.53	0.46
Mg	2.79	2.61	2.67	2.75	2.76	2.65	2.70	2.78	2.65	2.70	2.54	2.63
Fe2+	1.53	1.57	1.54	1.51	1.69	1.61	1.68	1.54	1.64	1.57	1.78	1.76
Mn	0.01	0.01	0.01	0.01	0.00	0.01	0.01	0.01	0.02	0.01	0.02	0.01
[Mn	0.00	0.00	0.00	0.00	0.00	0.00	0.00	0.00	0.00	0.00	0.00	0.00
Fe2+	0.00	0.00	0.00	0.00	0.00	0.00	0.00	0.00	0.00	0.00	0.00	0.00
Mg	0.00	0.00	0.00	0.00	0.00	0.00	0.00	0.00	0.00	0.00	0.00	0.00
Fe3+	0.00	0.00	0.00	0.00	0.00	0.00	0.00	0.00	0.00	0.00	0.00	0.00
Ca	1.56	1.48	1.52	1.65	1.66	1.56	1.64	1.60	1.57	1.57	1.64	1.68
Na	0.44	0.52	0.48	0.35	0.34	0.44	0.35	0.40	0.43	0.43	0.36	0.32
Na	0.07	0.09	0.09	0.05	0.07	0.10	0.00	0.01	0.07	0.01	0.14	0.06
Ca	0.00	0.00	0.00	0.00	0.00	0.00	0.00	0.00	0.00	0.00	0.00	0.00
K	0.07	0.09	0.09	0.09	0.09	0.09	0.08	0.07	0.08	0.08	0.11	0.09
F	0.00	0.00	0.00	0.00	0.00	0.00	0.00	0.00	0.00	0.00	0.00	0.00
Cl	0.01	0.00	0.00	0.01	0.00	0.01	0.00	0.00	0.00	0.00	0.01	0.00
OH	1.99	2.00	2.00	1.99	2.00	1.99	2.00	2.00	2.00	2.00	1.99	2.00
Fe/Fe+Mg	0.43	0.46	0.45	0.44	0.43	0.45	0.44	0.43	0.45	0.44	0.48	0.46

	179	180	181	182	183	184	185	186	187	188	189	190	191
Sample	AL04	AL04	AL04	AL04	AL04	ABGNAC	ABGNAC	ABGNAC	ABGNAC	ABGNAC	ABGNAC	ABGNAC	ABGNAC
Rock	Ab	Ab	Ab	Ab	Ab	Ab	Ab	Ab	Ab	Ab	Ab	Ab	Ab
Alteration	Ret	Ret	Ret	Ret	Ret	Ret	Ret	Ret	Ret	Ret	Ret	Ret	Ret
Name	Act	Act	Act	Act	Act	Mhrn	Mhrn	Mhrn	Mhrn	Mhrn	Mhrn	Mhrn	Mhrn
SiO2	50.82	51.97	51.56	52.99	49.84	49.00	49.68	49.58	49.49	49.56	48.33	49.12	49.11
TiO2	0.45	0.33	0.33	0.27	0.53	0.05	0.15	0.00	0.19	0.05	0.00	0.04	0.13
Al2O3	4.12	3.52	3.50	2.89	4.33	3.83	3.95	4.03	3.98	4.32	4.37	3.79	4.06
FeO(Total)	18.67	18.05	18.32	17.99	18.49	16.67	16.40	16.58	16.94	17.19	17.10	16.43	16.10
MnO	0.09	0.14	0.16	0.12	0.08	0.00	0.00	0.00	0.00	0.00	0.00	0.00	0.00
MgO	11.36	11.84	11.83	12.51	11.73	13.47	13.78	13.55	13.46	13.51	13.61	13.39	13.78
CaO	9.90	9.99	10.18	10.74	10.11	11.48	11.16	10.76	10.30	9.66	9.89	14.53	13.77
Na2O	2.04	1.81	1.70	1.39	2.09	1.84	1.62	1.45	1.57	1.83	1.77	1.79	1.78
K2O	0.66	0.50	0.52	0.42	0.62	0.86	0.87	0.80	0.73	0.77	0.74	0.98	1.01
F	0.00	0.00	0.00	0.00	0.00	0.97	1.37	1.49	1.38	1.70	1.22	1.33	1.17
Cl	0.03	0.03	0.03	0.02	0.02	0.01	0.00	0.01	0.02	0.01	0.00	0.00	0.00
O=F,Cl	0.01	0.01	0.01	0.00	0.00	0.41	0.58	0.63	0.59	0.72	0.51	0.56	0.49
Total	98.13	98.17	98.12	99.34	97.84	97.77	98.40	97.62	97.47	97.88	96.52	100.84	100.42
[Si	7.45	7.57	7.53	7.62	7.33	7.27	7.28	7.29	7.27	7.22	7.13	7.31	7.25
Al(IV)	0.55	0.43	0.47	0.38	0.67	0.67	0.68	0.70	0.69	0.74	0.76	0.67	0.71
Ti	0.00	0.00	0.00	0.00	0.00	0.01	0.02	0.00	0.02	0.01	0.00	0.00	0.01
Al(VI)	0.17	0.18	0.13	0.11	0.08	0.00	0.00	0.00	0.00	0.00	0.00	0.00	0.00
Ti	0.05	0.04	0.04	0.03	0.06	0.00	0.00	0.00	0.00	0.00	0.00	0.00	0.00
Fe3+	0.47	0.46	0.50	0.44	0.57	0.43	0.60	0.76	0.92	1.13	1.20	-0.64	-0.30
Mg	2.48	2.57	2.58	2.68	2.57	2.98	3.01	2.97	2.95	2.94	2.99	2.97	3.03
Fe2+	1.82	1.74	1.73	1.73	1.71	1.59	1.39	1.27	1.14	0.94	0.81	2.67	2.27
Mn	0.01	0.02	0.02	0.01	0.01	0.00	0.00	0.00	0.00	0.00	0.00	0.00	0.00
[Mn	0.00	0.00	0.00	0.00	0.00	0.00	0.00	0.00	0.00	0.00	0.00	0.00	0.00
Fe2+	0.00	0.00	0.00	0.00	0.00	0.05	0.02	0.01	0.03	0.03	0.11	0.02	0.02
Mg	0.00	0.00	0.00	0.00	0.00	0.00	0.00	0.00	0.00	0.00	0.00	0.00	0.00
Fe3+	0.00	0.00	0.00	0.00	0.00	0.00	0.00	0.00	0.00	0.00	0.00	0.00	0.00
Ca	1.56	1.56	1.59	1.65	1.59	1.83	1.75	1.70	1.62	1.51	1.56	1.98	1.98
Na	0.44	0.44	0.41	0.35	0.41	0.12	0.23	0.29	0.35	0.46	0.33	0.00	0.00
Na	0.14	0.07	0.07	0.04	0.19	0.41	0.23	0.12	0.09	0.06	0.18	0.52	0.51
Ca	0.00	0.00	0.00	0.00	0.00	0.00	0.00	0.00	0.00	0.00	0.00	0.34	0.20
K	0.12	0.09	0.10	0.08	0.12	0.16	0.16	0.15	0.14	0.14	0.14	0.19	0.19
F	0.00	0.00	0.00	0.00	0.00	0.46	0.64	0.70	0.65	0.80	0.58	0.62	0.54
Cl	0.01	0.01	0.01	0.00	0.01	0.00	0.00	0.00	0.01	0.00	0.00	0.00	0.00
OH	1.99	1.99	1.99	2.00	1.99	1.54	1.36	1.29	1.34	1.19	1.42	1.38	1.46
Fe/Fe+Mg	0.48	0.46	0.46	0.45	0.47	0.41	0.40	0.41	0.41	0.42	0.41	0.41	0.40

	192	193	194	195	196	197	198	199	200	201	202	203	204
Sample	ABGNAAC	ABGNAAC	ABGNAAC	ABGNAAC	ABGNAAC	ABGNAAC	ABGNAAC	ABGNAAC	ABGNAAC	ABGNAAC	ABGNAAC	ABGNAAC	ABGNAAC
Rock	Ab	Ab	Ab	Ab	Ab	Ab	Ab	Ab	Ab	Ab	Ab	Ab	Ab
Alteration	Ret	Ret	Ret	Ret	Ret	Ret	Ret	Ret	Ret	Ret	Ret	Ret	Ret
Name	Mhrn	Mhrn	Mhrn	Mhrn	Mhrn	Mhrn	Mhrn	Mhrn	Mhrn	Mhrn	Mhrn	Mhrn	Mhrn
SiO2	48.78	49.77	49.29	49.10	48.96	49.55	49.84	50.48	48.73	51.86	50.88	50.87	52.38
TiO2	0.22	0.03	0.01	0.01	0.13	0.17	0.06	0.07	0.00	0.00	0.00	0.18	0.08
Al2O3	4.28	4.01	3.92	3.98	4.12	3.68	3.76	3.23	3.29	2.96	3.39	3.87	3.49
FeO(Total)	16.50	16.56	16.78	16.60	16.51	16.49	16.84	16.21	17.10	17.38	17.11	18.89	17.55
MnO	0.00	0.00	0.00	0.00	0.00	0.00	0.00	0.00	0.00	0.00	0.00	0.00	0.00
MgO	13.07	13.57	13.46	13.43	13.73	13.86	13.28	13.73	14.21	14.24	13.52	13.50	13.44
CaO	14.01	13.80	13.20	12.52	13.91	14.05	14.81	15.15	11.04	10.70	11.06	10.84	10.84
Na2O	1.69	1.99	1.93	2.04	1.86	1.91	1.58	1.20	1.68	1.76	1.67	1.87	1.85
K2O	1.09	1.03	1.02	0.97	0.46	0.42	0.42	0.41	0.93	0.88	0.92	1.04	0.89
F	1.11	1.36	1.66	1.41	1.50	1.16	1.01	1.52	1.30	1.47	1.31	1.34	1.47
Cl	0.01	0.00	0.00	0.01	0.01	0.00	0.00	0.00	0.00	0.01	0.01	0.02	0.00
O=F,Cl	0.47	0.57	0.70	0.60	0.63	0.49	0.43	0.64	0.55	0.62	0.55	0.57	0.62
Total	100.29	101.55	100.57	99.47	100.56	100.80	101.17	101.36	97.73	100.64	99.32	101.85	101.37
[Si	7.27	7.30	7.28	7.28	7.22	7.28	7.35	7.43	7.19	7.40	7.40	7.23	7.46
Al(IV)	0.73	0.69	0.68	0.70	0.72	0.64	0.65	0.56	0.57	0.50	0.58	0.65	0.54
Ti	0.00	0.00	0.00	0.00	0.01	0.02	0.00	0.01	0.00	0.00	0.00	0.02	0.00
Al(VI)	0.02	0.00	0.00	0.00	0.00	0.00	0.00	0.00	0.00	0.00	0.00	0.00	0.05
Ti	0.02	0.00	0.00	0.00	0.00	0.00	0.01	0.00	0.00	0.00	0.00	0.00	0.01
Fe3+	-0.50	-0.40	-0.17	0.00	-0.19	-0.28	-0.57	-0.62	0.90	0.78	0.52	0.85	0.49
Mg	2.90	2.97	2.96	2.97	3.02	3.04	2.92	3.01	3.13	3.03	2.93	2.86	2.85
Fe2+	2.56	2.44	2.20	2.03	2.17	2.25	2.64	2.61	0.98	1.19	1.55	1.29	1.60
Mn	0.00	0.00	0.00	0.00	0.00	0.00	0.00	0.00	0.00	0.00	0.00	0.00	0.00
[Mn	0.00	0.00	0.00	0.00	0.00	0.00	0.00	0.00	0.00	0.00	0.00	0.00	0.00
Fe2+	0.00	0.00	0.04	0.03	0.05	0.06	0.00	0.01	0.24	0.10	0.01	0.10	0.00
Mg	0.00	0.00	0.00	0.00	0.00	0.00	0.00	0.00	0.00	0.00	0.00	0.00	0.00
Fe3+	0.00	0.00	0.00	0.00	0.00	0.00	0.00	0.00	0.00	0.00	0.00	0.00	0.00
Ca	2.00	2.00	1.96	1.97	1.95	1.94	2.00	1.99	1.75	1.64	1.72	1.65	1.65
Na	0.00	0.00	0.00	0.00	0.00	0.00	0.00	0.00	0.02	0.26	0.26	0.25	0.35
Na	0.49	0.57	0.55	0.59	0.53	0.54	0.45	0.34	0.46	0.23	0.21	0.27	0.17
Ca	0.24	0.17	0.13	0.01	0.25	0.27	0.34	0.39	0.00	0.00	0.00	0.00	0.00
K	0.21	0.19	0.19	0.18	0.09	0.08	0.08	0.08	0.18	0.16	0.17	0.19	0.16
F	0.52	0.63	0.77	0.66	0.70	0.54	0.47	0.70	0.62	0.67	0.61	0.61	0.67
Cl	0.00	0.00	0.00	0.00	0.00	0.00	0.00	0.00	0.00	0.00	0.00	0.00	0.00
OH	1.48	1.37	1.23	1.34	1.30	1.46	1.53	1.30	1.38	1.32	1.39	1.38	1.33
Fe/Fe+Mg	0.41	0.41	0.41	0.41	0.40	0.40	0.42	0.40	0.40	0.41	0.42	0.44	0.42

	205	206	207	208	209	210	211	212	213	214	215	216	217
Sample	ABGNAAC	ABGNAAC	ABGNAAC	ABGNAAC	ABGNAAC	F11ALB01	F11ALB01	F11ALB01	F11ALB01	F11ALB01	F11ALB01	F11ALB01	F11ALB01
Rock	Ab	Ab	Ab	Ab	Ab	Ab	Ab	Ab	Ab	Ab	Ab	Ab	Ab
Alteration	Ret	Ret	Ret	Ret	Ret	Ret	Ret	Ret	Ret	Ret	Ret	Ret	Ret
Name	Mhrn	Mhrn	Mhrn	Mhrn	Mhrn	Fed	Fed	Fed	Fed	Fed	Fed	Fed	Fed
SiO2	52.62	50.05	50.09	49.37	48.74	42.29	44.69	44.13	43.97	44.21	44.00	39.26	40.22
TiO2	0.02	0.00	0.00	0.06	0.04	0.79	0.56	0.76	0.65	0.54	0.87	0.74	0.63
Al2O3	3.08	3.99	3.83	3.91	3.93	8.90	7.61	8.14	8.44	7.91	8.28	7.65	7.94
FeO(Total)	16.96	17.48	17.73	18.21	17.80	24.86	22.95	23.48	23.33	23.70	23.71	24.54	25.07
MnO	0.00	0.00	0.00	0.00	0.00	0.50	0.53	0.55	0.52	0.50	0.36	0.54	0.49
MgO	14.20	13.37	13.47	13.62	13.46	6.16	7.34	6.52	6.85	6.98	6.65	6.12	6.12
CaO	10.79	10.44	10.59	10.47	10.54	10.74	10.82	10.75	11.29	10.66	10.14	10.57	10.56
Na2O	1.90	2.08	1.86	2.03	1.92	1.83	1.63	1.75	1.48	1.76	2.31	2.07	1.88
K2O	0.90	1.03	1.03	1.04	1.05	1.41	1.13	1.20	1.21	1.22	1.26	1.21	1.24
F	1.29	1.57	1.40	1.26	1.25	0.00	0.00	0.00	0.00	0.00	0.00	0.00	0.00
Cl	0.01	0.00	0.01	0.02	0.02	0.10	0.08	0.14	0.08	0.09	0.15	0.14	0.13
O=F,Cl	0.55	0.66	0.59	0.54	0.53	0.02	0.02	0.03	0.02	0.02	0.03	0.03	0.03
Total	101.22	99.35	99.42	99.45	98.22	97.56	97.32	97.39	97.80	97.55	97.70	92.81	94.25
[Si	7.47	7.29	7.27	7.17	7.17	6.56	6.86	6.82	6.76	6.79	6.77	6.47	6.49
Al(IV)	0.52	0.68	0.66	0.67	0.68	1.44	1.14	1.18	1.24	1.21	1.23	1.48	1.51
Ti	0.00	0.00	0.00	0.01	0.00	0.00	0.00	0.00	0.00	0.00	0.00	0.05	0.00
Al(VI)	0.00	0.00	0.00	0.00	0.00	0.19	0.24	0.30	0.29	0.23	0.27	0.00	0.00
Ti	0.00	0.00	0.00	0.00	0.00	0.09	0.06	0.09	0.08	0.06	0.10	0.04	0.08
Fe3+	0.58	0.71	0.78	0.96	0.90	0.66	0.50	0.38	0.41	0.58	0.47	0.75	0.86
Mg	3.00	2.90	2.92	2.95	2.95	1.43	1.68	1.50	1.57	1.60	1.53	1.50	1.47
Fe2+	1.41	1.39	1.30	1.09	1.15	2.57	2.44	2.66	2.59	2.47	2.58	2.62	2.52
Mn	0.00	0.00	0.00	0.00	0.00	0.07	0.07	0.07	0.07	0.07	0.05	0.08	0.07
[Mn	0.00	0.00	0.00	0.00	0.00	0.00	0.00	0.00	0.00	0.00	0.00	0.00	0.00
Fe2+	0.02	0.03	0.07	0.16	0.14	0.00	0.00	0.00	0.00	0.00	0.00	0.00	0.00
Mg	0.00	0.00	0.00	0.00	0.00	0.00	0.00	0.00	0.00	0.00	0.00	0.00	0.00
Fe3+	0.00	0.00	0.00	0.00	0.00	0.00	0.00	0.00	0.00	0.00	0.00	0.00	0.00
Ca	1.64	1.63	1.65	1.63	1.66	1.79	1.78	1.78	1.86	1.76	1.67	1.87	1.83
Na	0.34	0.34	0.28	0.21	0.20	0.21	0.22	0.22	0.14	0.24	0.33	0.13	0.17
Na	0.18	0.24	0.24	0.36	0.35	0.34	0.27	0.30	0.30	0.28	0.36	0.53	0.41
Ca	0.00	0.00	0.00	0.00	0.00	0.00	0.00	0.00	0.00	0.00	0.00	0.00	0.00
K	0.16	0.19	0.19	0.19	0.20	0.28	0.22	0.24	0.24	0.24	0.25	0.25	0.26
F	0.59	0.73	0.65	0.59	0.59	0.00	0.00	0.00	0.00	0.00	0.00	0.00	0.00
Cl	0.00	0.00	0.00	0.01	0.01	0.03	0.02	0.04	0.02	0.02	0.04	0.04	0.04
OH	1.41	1.27	1.34	1.40	1.40	1.97	1.98	1.96	1.98	1.98	1.96	1.96	1.96
Fe/Fe+Mg	0.40	0.42	0.42	0.43	0.43	0.69	0.64	0.67	0.66	0.66	0.67	0.69	0.70

	218	219	220	221	222	223	224	225	226	227	228	229
Sample	F11ALB01	F11ALB01	F11ALB01	F11ALB01	F11ALB01	F11ALB01	F11ALB01	F11ALB01	F11ALB01	F11ALB01	F11ALB01	F11ALB01
Rock	Ab	Ab	Ab	Ab	Ab	Ab	Ab	Ab	Ab	Ab	Ab	Ab
Alteration	Ret	Ret	Ret	Ret	Ret	Ret	Ret	Ret	Ret	Ret	Ret	Ret
Name	Fed	Fed	Fed	Fed	Fed	Fed	Fed	Fed	Fed	Fed	Fed	Fed
SiO2	41.46	42.16	43.94	46.01	48.67	44.26	45.45	43.84	44.75	42.90	44.53	44.64
TiO2	0.77	0.85	0.75	0.14	0.10	0.53	0.11	0.36	0.36	0.79	0.67	0.63
Al2O3	7.99	8.46	8.33	7.02	5.78	8.30	7.16	8.45	7.79	9.18	8.09	8.10
FeO(Total)	24.63	25.87	24.19	23.24	21.37	22.84	23.88	23.29	23.59	23.80	22.77	23.57
MnO	0.36	0.51	0.38	0.52	0.45	0.45	0.55	0.45	0.49	0.43	0.49	0.43
MgO	6.15	5.89	6.44	7.63	8.83	6.81	7.50	7.12	7.31	6.45	7.15	7.36
CaO	10.08	10.14	10.22	10.97	11.24	10.64	11.03	10.79	10.78	10.07	10.56	10.56
Na2O	2.17	2.20	2.21	1.38	1.14	1.54	1.35	1.78	1.78	2.26	1.92	1.68
K2O	1.22	1.41	1.23	0.92	0.78	1.24	1.24	1.30	1.21	1.35	1.22	1.17
F	0.00	0.00	0.00	0.00	0.00	0.00	0.00	0.00	0.00	0.00	0.00	0.00
Cl	0.14	0.14	0.15	0.05	0.02	0.07	0.06	0.10	0.08	0.13	0.12	0.13
O=F,Cl	0.03	0.03	0.03	0.01	0.00	0.02	0.01	0.02	0.02	0.03	0.03	0.03
Total	94.94	97.60	97.81	97.87	98.38	96.66	98.32	97.46	98.12	97.33	97.49	98.24
[Si	6.61	6.55	6.76	6.98	7.27	6.84	6.90	6.74	6.82	6.62	6.84	6.77
Al(IV)	1.39	1.45	1.24	1.02	0.73	1.16	1.10	1.26	1.18	1.38	1.16	1.23
Ti	0.00	0.00	0.00	0.00	0.00	0.00	0.00	0.00	0.00	0.00	0.00	0.00
Al(VI)	0.11	0.10	0.27	0.24	0.29	0.36	0.19	0.27	0.22	0.29	0.30	0.22
Ti	0.09	0.10	0.09	0.02	0.01	0.06	0.01	0.04	0.04	0.09	0.08	0.07
Fe3+	0.73	0.82	0.52	0.59	0.33	0.45	0.66	0.56	0.58	0.62	0.43	0.71
Mg	1.46	1.37	1.48	1.73	1.97	1.57	1.70	1.63	1.66	1.48	1.64	1.66
Fe2+	2.56	2.54	2.59	2.36	2.34	2.51	2.37	2.43	2.43	2.45	2.50	2.28
Mn	0.05	0.07	0.05	0.07	0.06	0.06	0.07	0.06	0.06	0.06	0.06	0.06
[Mn	0.00	0.00	0.00	0.00	0.00	0.00	0.00	0.00	0.00	0.00	0.00	0.00
Fe2+	0.00	0.00	0.00	0.00	0.00	0.00	0.00	0.00	0.00	0.00	0.00	0.00
Mg	0.00	0.00	0.00	0.00	0.00	0.00	0.00	0.00	0.00	0.00	0.00	0.00
Fe3+	0.00	0.00	0.00	0.00	0.00	0.00	0.00	0.00	0.00	0.00	0.00	0.00
Ca	1.72	1.69	1.69	1.78	1.80	1.76	1.79	1.78	1.76	1.67	1.74	1.72
Na	0.28	0.31	0.31	0.22	0.20	0.24	0.21	0.22	0.24	0.33	0.26	0.28
Na	0.39	0.35	0.34	0.19	0.13	0.22	0.19	0.31	0.29	0.34	0.31	0.21
Ca	0.00	0.00	0.00	0.00	0.00	0.00	0.00	0.00	0.00	0.00	0.00	0.00
K	0.25	0.28	0.24	0.18	0.15	0.24	0.24	0.26	0.24	0.27	0.24	0.23
F	0.00	0.00	0.00	0.00	0.00	0.00	0.00	0.00	0.00	0.00	0.00	0.00
Cl	0.04	0.04	0.04	0.01	0.01	0.02	0.02	0.03	0.02	0.03	0.03	0.03
OH	1.96	1.96	1.96	1.99	1.99	1.98	1.98	1.97	1.98	1.97	1.97	1.97
Fe/Fe+Mg	0.69	0.71	0.68	0.63	0.58	0.65	0.64	0.65	0.64	0.67	0.64	0.64

	230	231	232	233	234	235	236	237	238	239	240
Sample	F11ALB02	F11ALB02	F11ALB02	F11ALB02	F11ALB02	F11ALB02	F11ALB02	F11ALB02	F11ALB02	F11ALB02	F11ALB02
Rock	Ab	Ab	Ab	Ab	Ab	Ab	Ab	Ab	Ab	Ab	Ab
Alteration	Ret	Ret	Ret	Ret	Ret	Ret	Ret	Ret	Ret	Ret	Ret
Name	Mhrn	Mhrn	Mhrn	Mhrn	Mhrn	Mhrn	Mhrn	Mhrn	Mhrn	Mhrn	Mhrn
SiO2	49.12	49.88	49.76	49.45	47.15	50.29	49.63	48.99	46.81	49.06	49.12
TiO2	0.30	0.34	0.30	0.39	0.30	0.35	0.43	0.38	0.31	0.31	0.30
Al2O3	5.37	4.67	4.81	5.13	5.28	4.73	4.89	5.21	5.14	5.65	5.37
FeO(Total)	17.46	16.80	17.36	17.50	17.21	16.54	17.15	17.44	17.22	18.06	17.46
MnO	0.43	0.52	0.50	0.53	0.52	0.60	0.44	0.52	0.47	0.51	0.43
MgO	11.86	12.04	12.14	12.13	12.25	12.26	12.37	12.17	11.95	11.65	11.86
CaO	11.32	11.50	11.51	11.36	10.94	11.30	11.05	10.92	10.82	11.12	11.32
Na2O	1.40	1.32	1.26	1.49	1.67	1.28	1.51	1.69	1.34	1.55	1.40
K2O	0.74	0.68	0.63	0.74	0.71	0.71	0.76	0.77	0.75	0.83	0.74
F	0.73	0.66	0.64	0.85	0.71	0.78	0.70	0.67	0.91	0.77	0.73
Cl	0.02	0.02	0.00	0.01	0.02	0.03	0.02	0.02	0.03	0.03	0.02
O=F,Cl	0.31	0.28	0.27	0.36	0.30	0.34	0.30	0.29	0.39	0.33	0.31
Total	98.44	98.15	98.64	99.22	96.46	98.53	98.65	98.49	95.36	99.21	98.44
[Si	7.23	7.36	7.29	7.23	7.07	7.37	7.26	7.19	7.10	7.18	7.23
Al(IV)	0.77	0.64	0.71	0.77	0.93	0.63	0.74	0.81	0.90	0.82	0.77
Ti	0.00	0.00	0.00	0.00	0.00	0.00	0.00	0.00	0.00	0.00	0.00
Al(VI)	0.16	0.17	0.12	0.11	0.00	0.18	0.10	0.09	0.02	0.15	0.16
Ti	0.03	0.04	0.03	0.04	0.03	0.04	0.05	0.04	0.04	0.03	0.03
Fe3+	0.43	0.25	0.43	0.46	0.72	0.33	0.51	0.58	0.76	0.52	0.43
Mg	2.60	2.65	2.65	2.64	2.74	2.68	2.70	2.66	2.70	2.54	2.60
Fe2+	1.72	1.83	1.70	1.68	1.44	1.70	1.59	1.56	1.43	1.69	1.72
Mn	0.05	0.07	0.06	0.07	0.07	0.07	0.05	0.06	0.06	0.06	0.05
[Mn	0.00	0.00	0.00	0.00	0.00	0.00	0.00	0.00	0.00	0.00	0.00
Fe2+	0.00	0.00	0.00	0.00	0.00	0.00	0.00	0.00	0.00	0.00	0.00
Mg	0.00	0.00	0.00	0.00	0.00	0.00	0.00	0.00	0.00	0.00	0.00
Fe3+	0.00	0.00	0.00	0.00	0.00	0.00	0.00	0.00	0.00	0.00	0.00
Ca	1.79	1.82	1.81	1.78	1.76	1.77	1.73	1.72	1.76	1.74	1.79
Na	0.21	0.18	0.19	0.22	0.24	0.23	0.27	0.28	0.24	0.26	0.21
Na	0.18	0.20	0.17	0.20	0.24	0.14	0.16	0.20	0.15	0.18	0.18
Ca	0.00	0.00	0.00	0.00	0.00	0.00	0.00	0.00	0.00	0.00	0.00
K	0.14	0.13	0.12	0.14	0.14	0.13	0.14	0.14	0.15	0.15	0.14
F	0.34	0.31	0.30	0.40	0.34	0.36	0.33	0.31	0.44	0.36	0.34
Cl	0.01	0.01	0.00	0.00	0.01	0.01	0.01	0.01	0.01	0.01	0.01
OH	1.65	1.69	1.70	1.60	1.65	1.63	1.67	1.68	1.55	1.63	1.65
Fe/Fe+Mg	0.45	0.44	0.45	0.45	0.44	0.43	0.44	0.45	0.45	0.47	0.45

	241	242	243	244	245	246	247	248	249	250	251	252
Sample	F11ALB02	31BIAB	31BIAB	31BIAB	31BIAB	31BIAB	31BIAB	31BIAB	ALB05	ALB05	ALB05	ALB05
Rock	Ab	Ab	Ab	Ab	Ab	Ab	Ab	Ab	Ab	Ab	Ab	Ab
Alteration	Ret	Ret	Ret	Ret	Ret	Ret	Ret	Ret	Ret	Ret	Ret	Ret
Name	Mhrn	Mhst	Mhst	Mhst	Mhst	Mhst	Mhst	Mhst	Act	Act	Act	Act
SiO2	49.88	41.90	42.29	43.21	41.98	42.54	42.52	42.36	50.32	52.60	52.85	52.78
TiO2	0.34	0.31	0.28	0.19	0.30	0.17	0.12	0.24	0.18	0.16	0.11	0.07
Al2O3	4.67	10.20	9.84	9.23	10.11	10.05	9.62	9.65	4.29	3.04	2.35	1.89
FeO(Total)	16.80	20.87	20.17	19.99	20.22	20.90	20.46	19.55	17.73	17.54	16.24	15.65
MnO	0.52	0.41	0.55	0.59	0.63	0.45	0.47	0.59	0.39	0.36	0.41	0.56
MgO	12.04	8.97	9.07	9.62	9.10	9.09	9.37	9.32	11.67	12.92	13.60	14.19
CaO	11.50	10.47	10.46	10.35	10.84	10.84	10.83	10.93	11.11	11.26	11.55	11.64
Na2O	1.32	2.12	2.06	2.23	2.21	1.99	1.95	1.99	1.52	1.28	0.99	0.89
K2O	0.68	1.79	1.59	1.43	1.72	1.72	1.65	1.61	0.66	0.47	0.33	0.26
F	0.66	1.37	0.89	0.94	1.08	1.39	1.14	0.95	0.00	0.00	0.00	0.00
Cl	0.02	0.01	0.00	0.00	0.01	0.00	0.01	0.01	0.02	0.04	0.01	0.00
O=F,Cl	0.28	0.58	0.37	0.40	0.46	0.59	0.48	0.40	0.00	0.01	0.00	0.00
Total	98.15	97.84	96.83	97.38	97.74	98.55	97.66	96.80	97.89	99.66	98.44	97.93
[Si	7.36	6.38	6.47	6.55	6.41	6.44	6.47	6.50	7.43	7.55	7.64	7.64
Al(IV)	0.64	1.62	1.53	1.45	1.59	1.56	1.53	1.50	0.57	0.45	0.36	0.32
Ti	0.00	0.00	0.00	0.00	0.00	0.00	0.00	0.00	0.00	0.00	0.00	0.01
Al(VI)	0.17	0.22	0.25	0.20	0.23	0.23	0.20	0.25	0.17	0.07	0.04	0.00
Ti	0.04	0.04	0.03	0.02	0.03	0.02	0.01	0.03	0.02	0.02	0.01	0.00
Fe3+	0.25	0.94	0.87	0.92	0.75	0.87	0.88	0.68	0.28	0.44	0.37	0.47
Mg	2.65	2.04	2.07	2.17	2.07	2.05	2.13	2.13	2.57	2.77	2.93	3.06
Fe2+	1.83	1.72	1.71	1.61	1.83	1.78	1.73	1.83	1.90	1.67	1.59	1.43
Mn	0.07	0.05	0.07	0.08	0.08	0.06	0.06	0.08	0.05	0.04	0.05	0.04
[Mn	0.00	0.00	0.00	0.00	0.00	0.00	0.00	0.00	0.00	0.00	0.00	0.03
Fe2+	0.00	0.00	0.00	0.00	0.00	0.00	0.00	0.00	0.00	0.00	0.00	0.00
Mg	0.00	0.00	0.00	0.00	0.00	0.00	0.00	0.00	0.00	0.00	0.00	0.00
Fe3+	0.00	0.00	0.00	0.00	0.00	0.00	0.00	0.00	0.00	0.00	0.00	0.00
Ca	1.82	1.71	1.71	1.68	1.77	1.76	1.77	1.80	1.76	1.73	1.79	1.81
Na	0.18	0.29	0.29	0.32	0.23	0.24	0.23	0.20	0.24	0.27	0.21	0.17
Na	0.20	0.34	0.33	0.34	0.43	0.34	0.34	0.39	0.19	0.09	0.07	0.08
Ca	0.00	0.00	0.00	0.00	0.00	0.00	0.00	0.00	0.00	0.00	0.00	0.00
K	0.13	0.35	0.31	0.28	0.34	0.33	0.32	0.32	0.12	0.09	0.06	0.05
F	0.31	0.67	0.44	0.46	0.53	0.68	0.56	0.47	0.00	0.00	0.00	0.00
Cl	0.01	0.00	0.00	0.00	0.00	0.00	0.00	0.00	0.01	0.01	0.00	0.00
OH	1.69	1.32	1.56	1.54	1.47	1.32	1.44	1.53	1.99	1.99	2.00	2.00
Fe/Fe+Mg	0.44	0.57	0.56	0.54	0.55	0.56	0.55	0.54	0.46	0.43	0.40	0.38

	253	254	255	256	257	258	259	260
Sample	ALB05	ALB05	ALB05	ALB05	ALB05	ALB05	ALB05	ALB05
Rock	Ab	Ab	Ab	Ab	Ab	Ab	Ab	Ab
Alteration	Ret	Ret	Ret	Ret	Ret	Ret	Ret	Ret
Name	Act	Act	Act	Act	Act	Act	Act	Act
SiO2	52.59	52.76	48.99	51.79	51.09	50.41	50.53	49.62
TiO2	0.08	0.17	0.25	0.14	0.12	0.25	0.25	0.35
Al2O3	2.75	2.78	3.99	3.09	3.46	3.80	4.02	4.75
FeO(Total)	16.23	16.69	17.58	16.00	17.12	17.65	17.23	17.41
MnO	0.34	0.37	0.35	0.40	0.32	0.37	0.38	0.30
MgO	13.04	13.20	11.54	12.85	12.55	12.26	12.33	11.39
CaO	11.32	11.64	11.22	11.08	10.97	10.86	10.44	10.95
Na2O	1.09	1.02	1.37	1.33	1.33	1.53	1.76	1.81
K2O	0.40	0.45	0.60	0.49	0.47	0.61	0.59	0.73
F	0.00	0.00	0.00	0.00	0.00	0.00	0.00	0.00
Cl	0.03	0.00	0.01	0.01	0.00	0.04	0.04	0.03
O=F,Cl	0.01	0.00	0.00	0.00	0.00	0.01	0.01	0.01
Total	97.86	99.08	95.90	97.18	97.43	97.77	97.56	97.33
[Si	7.67	7.61	7.40	7.62	7.50	7.41	7.42	7.39
Al(IV)	0.33	0.39	0.60	0.38	0.50	0.59	0.58	0.61
Ti	0.00	0.00	0.00	0.00	0.00	0.00	0.00	0.00
Al(VI)	0.14	0.08	0.11	0.15	0.10	0.07	0.11	0.22
Ti	0.01	0.02	0.03	0.02	0.01	0.03	0.03	0.04
Fe3+	0.26	0.30	0.29	0.24	0.46	0.49	0.52	0.15
Mg	2.83	2.84	2.60	2.82	2.75	2.69	2.70	2.53
Fe2+	1.72	1.71	1.93	1.73	1.64	1.68	1.59	2.02
Mn	0.04	0.05	0.04	0.05	0.04	0.05	0.05	0.04
[Mn	0.00	0.00	0.00	0.00	0.00	0.00	0.00	0.00
Fe2+	0.00	0.00	0.00	0.00	0.00	0.00	0.00	0.00
Mg	0.00	0.00	0.00	0.00	0.00	0.00	0.00	0.00
Fe3+	0.00	0.00	0.00	0.00	0.00	0.00	0.00	0.00
Ca	1.77	1.80	1.82	1.75	1.73	1.71	1.64	1.75
Na	0.23	0.20	0.18	0.25	0.27	0.29	0.36	0.25
Na	0.08	0.08	0.22	0.12	0.10	0.15	0.14	0.27
Ca	0.00	0.00	0.00	0.00	0.00	0.00	0.00	0.00
K	0.07	0.08	0.12	0.09	0.09	0.11	0.11	0.14
F	0.00	0.00	0.00	0.00	0.00	0.00	0.00	0.00
Cl	0.01	0.00	0.00	0.00	0.00	0.01	0.01	0.01
OH	1.99	2.00	2.00	2.00	2.00	1.99	1.99	1.99
Fe/Fe+Mg	0.41	0.41	0.46	0.41	0.43	0.45	0.44	0.46

3E: EPMA analyses of biotite. Recalculated formula on the basis of 22 oxygens

Analysis	1	2	3	4	5	6	7	8	9	10	11	12
Color	brown	brown	brown	brown	brown	brown	brown	brown	brown	brown	brown	brown
Sample	GRA	GRA	GRA	GRA	GRA	GRA	GRA	GRA	GRA	GRA01	GRA01	GRA01
Alteration	Mag	Mag	Mag	Mag	Mag	Mag	Mag	Mag	Mag	Mag	Mag	Mag
SiO2	33.83	33.30	34.63	35.49	34.30	34.76	34.77	34.15	34.17	33.10	33.54	33.63
TiO2	3.24	3.15	3.15	2.83	2.72	2.55	2.57	2.51	2.61	2.42	2.18	2.65
Al2O3	13.13	13.03	13.41	12.61	12.81	13.17	13.49	14.00	13.39	13.71	13.86	13.51
Fe2O3	0.00	0.00	0.00	0.00	0.00	0.00	0.00	0.00	0.00	0.00	0.00	0.00
FeO	31.36	32.08	32.19	32.22	33.20	34.03	34.67	35.38	33.63	33.42	35.12	33.59
MnO	0.30	0.34	0.26	0.36	0.31	0.26	0.36	0.40	0.44	0.00	0.00	0.00
MgO	2.66	2.65	2.71	2.61	2.49	1.80	1.90	1.92	1.88	1.03	1.06	1.09
CaO	0.08	0.18	0.09	0.01	0.10	0.01	0.01	0.06	0.22	0.06	0.06	0.06
Na2O	0.10	0.19	0.09	0.09	0.08	0.06	0.03	0.06	0.10	0.04	0.09	0.09
K2O	9.52	9.42	9.42	9.17	8.24	9.31	8.90	8.13	9.36	8.81	8.22	8.95
F	0.26	0.03	0.59	0.55	0.43	1.07	0.33	0.87	0.49	0.36	0.31	0.61
Cl	0.54	0.50	0.58	0.56	0.54	0.43	0.39	0.37	0.40	0.79	0.74	0.75
Si	2.81	2.78	2.82	2.90	2.85	2.85	2.83	2.78	2.82	2.82	2.81	2.83
Al(IV)	1.19	1.22	1.18	1.10	1.15	1.15	1.17	1.22	1.19	1.18	1.19	1.17
Al(VI)	0.10	0.06	0.11	0.11	0.10	0.13	0.13	0.13	0.12	0.19	0.18	0.17
Ti	0.20	0.20	0.19	0.17	0.17	0.16	0.16	0.15	0.16	0.16	0.14	0.17
Fet	0.09	0.14	0.10	0.02	0.22	0.05	0.17	0.33	0.05	0.03	0.15	0.02
Fed	2.09	2.10	2.10	2.18	2.08	2.29	2.19	2.08	2.27	2.35	2.31	2.34
Fe3+(T)	0.00	0.00	0.00	0.00	0.00	0.00	0.00	0.00	0.00	0.00	0.00	0.00
Fe3+(M)	0.09	0.14	0.10	0.02	0.22	0.05	0.17	0.33	0.05	0.03	0.15	0.02
Mn	0.02	0.02	0.02	0.03	0.02	0.02	0.03	0.03	0.03	0.00	0.00	0.00
Mg	0.33	0.33	0.33	0.32	0.31	0.22	0.23	0.23	0.23	0.13	0.13	0.14
Ca	0.01	0.02	0.01	0.00	0.01	0.00	0.00	0.01	0.02	0.01	0.01	0.01
Na	0.02	0.03	0.01	0.01	0.01	0.01	0.01	0.01	0.02	0.01	0.02	0.02
K	1.01	1.00	0.98	0.96	0.87	0.98	0.92	0.85	0.98	0.96	0.88	0.96
OH	1.86	1.92	1.77	1.78	1.81	1.66	1.86	1.72	1.82	1.79	1.81	1.73
F	0.07	0.01	0.15	0.14	0.11	0.28	0.09	0.22	0.13	0.10	0.08	0.16
Cl	0.08	0.07	0.08	0.08	0.08	0.06	0.05	0.05	0.06	0.11	0.11	0.11
mgli	0.30	0.33	0.27	0.21	0.26	0.15	0.16	0.19	0.19	0.14	0.12	0.12
feal	2.31	2.40	2.30	2.29	2.40	2.38	2.42	2.46	2.39	2.34	2.42	2.36
Mg#	0.13	0.13	0.13	0.13	0.12	0.09	0.09	0.09	0.09	0.05	0.05	0.06
Name	Lep	Lep	Lep	Lep	Lep	Lep	Lep	Lep	Lep	Lep	Lep	Lep
Fe/Fe+Mg	0.87	0.87	0.87	0.87	0.88	0.91	0.91	0.91	0.91	0.95	0.95	0.95
fet	2.26	2.38	2.29	2.22	2.53	2.39	2.53	2.74	2.37	2.41	2.62	2.38

Analysis	13	14	15	16	17	18	19	20	21	22	23	24	25	26
Color	brown	brown	brown	brown	brown	brown	brown	brown	brown	brown	brown	brown	brown	brown
Sample	GRA01	GRA01	GRA01	GRA01	GRA01	GRA01	GRA01	GRA01	35GNA	35GNA	35GNA	35GNA	35GNA	35GNA
Alteration	Mag	Mag	Mag	Mag	Mag	Mag	Mag	Mag	Mag	Mag	Mag	Mag	Mag	Mag
SiO2	34.28	34.56	34.02	34.12	34.89	34.97	32.49	33.97	34.81	33.96	34.80	34.54	35.20	34.61
TiO2	2.45	2.67	2.46	2.23	2.75	2.68	2.38	2.55	2.84	2.63	2.32	2.77	2.46	2.56
Al2O3	13.50	13.45	13.94	14.00	14.30	14.30	13.30	14.65	14.63	14.60	14.29	14.55	15.08	14.22
Fe2O3	0.00	0.00	0.00	0.00	0.00	0.00	0.00	0.00	0.00	0.00	0.00	0.00	0.00	0.00
FeO	33.63	33.90	33.41	33.04	35.04	34.84	34.59	33.15	34.89	35.62	35.97	35.44	35.41	34.01
MnO	0.00	0.00	0.00	0.00	0.00	0.00	0.00	0.00	0.00	0.00	0.00	0.00	0.00	0.00
MgO	1.07	1.06	1.15	1.14	1.33	1.21	1.26	1.08	1.07	1.09	1.06	1.08	1.09	1.09
CaO	0.05	0.06	0.06	0.03	0.07	0.01	0.04	0.21	0.03	0.00	0.03	0.01	0.04	0.03
Na2O	0.09	0.04	0.09	0.13	0.07	0.03	0.05	0.05	0.03	0.07	0.10	0.05	0.13	0.02
K2O	8.95	9.01	8.81	8.77	9.07	9.33	9.28	8.95	8.96	9.25	9.43	9.21	9.23	8.93
F	0.49	0.50	0.12	0.14	0.56	0.43	0.27	0.17	0.40	0.25	0.42	0.14	0.20	0.44
Cl	0.70	0.77	0.74	0.73	0.75	0.69	0.76	0.77	0.55	0.54	0.52	0.60	0.53	0.56
Si	2.86	2.87	2.84	2.86	2.81	2.83	2.77	2.81	2.81	2.77	2.81	2.79	2.81	2.84
Al(IV)	1.14	1.14	1.16	1.14	1.19	1.18	1.23	1.19	1.19	1.23	1.19	1.21	1.20	1.16
Al(VI)	0.19	0.18	0.21	0.24	0.17	0.19	0.11	0.24	0.20	0.17	0.17	0.18	0.22	0.22
Ti	0.15	0.17	0.15	0.14	0.17	0.16	0.15	0.16	0.17	0.16	0.14	0.17	0.15	0.16
Fet	0.05	0.02	0.02	0.08	0.09	0.03	0.14	0.06	0.09	0.14	0.04	0.11	0.01	0.00
Fed	2.30	2.33	2.31	2.23	2.28	2.32	2.33	2.24	2.27	2.28	2.40	2.28	2.35	2.33
Fe3+(T)	0.00	0.00	0.00	0.00	0.00	0.00	0.00	0.00	0.00	0.00	0.00	0.00	0.00	0.00
Fe3+(M)	0.05	0.02	0.02	0.08	0.09	0.03	0.14	0.06	0.09	0.14	0.04	0.11	0.01	0.00
Mn	0.00	0.00	0.00	0.00	0.00	0.00	0.00	0.00	0.00	0.00	0.00	0.00	0.00	0.00
Mg	0.13	0.13	0.14	0.14	0.16	0.15	0.16	0.13	0.13	0.13	0.13	0.13	0.13	0.13
Ca	0.00	0.01	0.01	0.00	0.01	0.00	0.00	0.02	0.00	0.00	0.00	0.00	0.00	0.00
Na	0.02	0.01	0.02	0.02	0.01	0.01	0.01	0.01	0.01	0.01	0.02	0.01	0.02	0.00
K	0.95	0.95	0.94	0.94	0.93	0.96	1.01	0.94	0.92	0.96	0.97	0.95	0.94	0.94
OH	1.77	1.76	1.86	1.86	1.76	1.80	1.82	1.85	1.82	1.86	1.82	1.88	1.88	1.81
F	0.13	0.13	0.03	0.04	0.14	0.11	0.07	0.04	0.10	0.06	0.11	0.04	0.05	0.11
Cl	0.10	0.11	0.11	0.10	0.10	0.09	0.11	0.11	0.08	0.08	0.07	0.08	0.07	0.08
mgli	0.09	0.07	0.11	0.10	0.09	0.07	0.20	0.10	0.06	0.10	0.06	0.07	0.04	0.07
feal	2.31	2.34	2.28	2.22	2.36	2.33	2.51	2.21	2.33	2.42	2.40	2.39	2.29	2.28
Mg#	0.05	0.05	0.06	0.06	0.06	0.06	0.06	0.06	0.05	0.05	0.05	0.05	0.05	0.05
Name	Lep	Lep	Lep	Lep	Lep	Lep	Lep	Lep	Lep	Lep	Lep	Lep	Lep	Lep
Fe/Fe+Mg	0.95	0.95	0.94	0.94	0.94	0.94	0.94	0.95	0.95	0.95	0.95	0.95	0.95	0.95
fet	2.40	2.37	2.35	2.40	2.45	2.39	2.61	2.35	2.44	2.57	2.47	2.51	2.37	2.33

Analysis	27	28	29	30	31	32	33	34	35	36	37	38
Color	brown	brown	brown	brown	brown	brown	brown	brown	brown	brown	brown	brown
Sample	35GNA	35GNA	35GNA	35GNA	35GNA	35GNA	35GNA	35GNA	35GNA	35GNA	35GNA	35GNA
Alteration	Mag	Mag	Mag	Mag	Mag	Mag	Mag	Mag	Mag	Mag	Mag	Mag
SiO2	34.86	35.28	34.83	34.92	34.36	34.18	34.12	33.72	33.97	34.17	33.44	33.41
TiO2	2.58	2.54	3.13	2.83	2.57	2.52	2.55	2.32	2.33	2.69	2.51	2.38
Al2O3	14.26	14.39	14.70	14.44	14.81	14.55	14.17	14.10	14.34	14.78	14.66	14.62
Fe2O3	0.00	0.00	0.00	0.00	0.00	0.00	0.00	0.00	0.00	0.00	0.00	0.00
FeO	36.14	35.76	35.03	35.77	35.11	34.67	34.83	35.32	35.64	36.04	36.56	36.51
MnO	0.00	0.00	0.00	0.00	0.00	0.00	0.00	0.00	0.00	0.00	0.00	0.00
MgO	1.08	1.06	1.13	1.13	1.10	1.25	1.01	1.15	1.62	1.12	1.07	1.02
CaO	0.00	0.01	0.01	0.08	0.01	0.03	0.09	0.04	0.06	0.01	0.01	0.00
Na2O	0.09	0.09	0.11	0.13	0.00	0.29	0.11	0.00	0.39	0.00	0.00	0.00
K2O	9.36	9.38	9.15	9.29	8.08	7.99	8.79	9.25	9.19	8.87	9.26	8.94
F	0.47	0.45	0.47	0.07	0.14	0.36	0.34	0.37	0.24	0.35	0.36	0.14
Cl	0.58	0.59	0.55	0.50	0.50	0.48	0.51	0.51	0.52	0.53	0.53	0.54
Si	2.81	2.83	2.79	2.80	2.80	2.80	2.81	2.79	2.76	2.76	2.73	2.74
Al(IV)	1.20	1.18	1.21	1.20	1.20	1.20	1.19	1.21	1.24	1.24	1.27	1.26
Al(VI)	0.16	0.18	0.18	0.16	0.22	0.21	0.19	0.16	0.14	0.17	0.14	0.16
Ti	0.16	0.15	0.19	0.17	0.16	0.16	0.16	0.14	0.14	0.16	0.15	0.15
Fet	0.09	0.03	0.12	0.09	0.20	0.15	0.07	0.10	0.12	0.22	0.24	0.25
Fed	2.34	2.37	2.23	2.30	2.19	2.23	2.33	2.34	2.31	2.22	2.26	2.26
Fe3+(T)	0.00	0.00	0.00	0.00	0.00	0.00	0.00	0.00	0.00	0.00	0.00	0.00
Fe3+(M)	0.09	0.03	0.12	0.09	0.20	0.15	0.07	0.10	0.12	0.22	0.24	0.25
Mn	0.00	0.00	0.00	0.00	0.00	0.00	0.00	0.00	0.00	0.00	0.00	0.00
Mg	0.13	0.13	0.14	0.14	0.13	0.15	0.12	0.14	0.20	0.14	0.13	0.13
Ca	0.00	0.00	0.00	0.01	0.00	0.00	0.01	0.00	0.01	0.00	0.00	0.00
Na	0.01	0.01	0.02	0.02	0.00	0.05	0.02	0.00	0.06	0.00	0.00	0.00
K	0.96	0.96	0.94	0.95	0.84	0.84	0.92	0.98	0.95	0.92	0.97	0.94
OH	1.80	1.81	1.81	1.91	1.90	1.84	1.84	1.83	1.87	1.84	1.83	1.89
F	0.12	0.11	0.12	0.02	0.04	0.09	0.09	0.10	0.06	0.09	0.09	0.04
Cl	0.08	0.08	0.08	0.07	0.07	0.07	0.07	0.07	0.07	0.07	0.07	0.08
mgli	0.06	0.03	0.06	0.06	0.08	0.11	0.08	0.12	0.16	0.09	0.12	0.12
feal	2.43	2.37	2.36	2.41	2.33	2.32	2.37	2.43	2.43	2.43	2.51	2.50
Mg#	0.05	0.05	0.05	0.05	0.05	0.06	0.05	0.06	0.08	0.05	0.05	0.05
Name	Lep	Lep	Lep	Lep	Lep	Lep	Lep	Lep	Lep	Lep	Lep	Lep
Fe/Fe+Mg	0.95	0.95	0.95	0.95	0.95	0.94	0.95	0.95	0.93	0.95	0.95	0.95
fet	2.53	2.42	2.46	2.49	2.59	2.53	2.47	2.54	2.54	2.66	2.74	2.75

Analysis	39	40	41	42	43	44	45	46	47	48	49	50
Color	brown	brown	brown	brown	brown	brown	brown	brown	brown	brown	brown	brown
Sample	35GNA	35GNA	34GNA01	34GNA01	34GNA01	34GNA01	34GNA01	34GNA01	34GNA01	34GNA01	GNA02	GNA02
Alteration	Mag	Mag	Mag	Mag	Mag	Mag	Mag	Mag	Mag	Mag	Ca-Fe	Ca-Fe
SiO2	31.72	33.44	32.79	34.73	29.01	31.74	31.02	32.78	31.56	34.54	38.26	38.67
TiO2	2.51	2.28	2.23	2.42	2.54	2.29	2.36	2.71	2.81	2.37	1.21	1.10
Al2O3	14.89	14.09	17.05	16.52	16.48	17.06	16.76	16.02	15.60	15.73	12.28	12.08
Fe2O3	0.00	0.00	0.00	0.00	0.00	0.00	0.00	0.00	0.00	0.00	0.00	0.00
FeO	37.33	37.07	33.08	33.49	32.47	33.56	32.90	35.02	35.05	34.62	26.86	26.54
MnO	0.00	0.00	0.43	0.57	0.38	0.42	0.46	0.48	0.44	0.44	0.00	0.00
MgO	1.41	1.23	0.37	0.41	0.41	0.35	0.41	0.45	0.45	0.44	10.23	10.78
CaO	0.12	0.03	0.04	0.03	0.00	0.01	0.03	0.01	0.02	0.03	0.02	0.02
Na2O	0.00	0.00	0.07	0.12	0.10	0.20	0.20	0.08	0.05	0.06	0.00	0.07
K2O	8.04	9.00	9.53	9.51	8.97	9.14	9.42	9.29	9.11	9.29	8.68	8.65
F	0.32	0.43	0.00	0.09	0.12	0.01	0.00	0.20	0.32	0.18	1.68	1.98
Cl	0.53	0.56	0.46	0.48	0.47	0.42	0.47	0.50	0.46	0.47	0.05	0.08
Si	2.64	2.75	2.70	2.78	2.56	2.64	2.63	2.68	2.65	2.78	2.94	2.95
Al(IV)	1.36	1.25	1.31	1.22	1.45	1.36	1.38	1.32	1.35	1.22	1.06	1.05
Al(VI)	0.10	0.11	0.35	0.33	0.27	0.32	0.30	0.23	0.19	0.28	0.05	0.04
Ti	0.16	0.14	0.14	0.15	0.17	0.14	0.15	0.17	0.18	0.14	0.07	0.06
Fet	0.57	0.28	0.09	0.15	0.23	0.05	0.03	0.15	0.27	0.05	0.25	0.24
Fed	2.03	2.27	2.19	2.09	2.16	2.29	2.30	2.25	2.19	2.28	1.48	1.45
Fe3+(T)	0.00	0.00	0.00	0.00	0.00	0.00	0.00	0.00	0.00	0.00	0.00	0.00
Fe3+(M)	0.57	0.28	0.09	0.15	0.23	0.05	0.03	0.15	0.27	0.05	0.25	0.24
Mn	0.00	0.00	0.03	0.04	0.03	0.03	0.03	0.03	0.03	0.03	0.00	0.00
Mg	0.18	0.15	0.05	0.05	0.05	0.04	0.05	0.06	0.06	0.05	1.17	1.23
Ca	0.01	0.00	0.00	0.00	0.00	0.00	0.00	0.00	0.00	0.00	0.00	0.00
Na	0.00	0.00	0.01	0.02	0.02	0.03	0.03	0.01	0.01	0.01	0.00	0.01
K	0.85	0.94	1.00	0.97	1.01	0.97	1.02	0.97	0.98	0.96	0.85	0.84
OH	1.84	1.81	1.94	1.91	1.90	1.94	1.93	1.88	1.85	1.89	1.59	1.51
F	0.08	0.11	0.00	0.02	0.03	0.00	0.00	0.05	0.09	0.05	0.41	0.48
Cl	0.08	0.08	0.06	0.07	0.07	0.06	0.07	0.07	0.07	0.06	0.01	0.01
mgli	0.25	0.14	0.07	-0.02	0.27	0.12	0.16	0.08	0.14	-0.01	0.95	0.99
feal	2.65	2.58	2.10	2.09	2.32	2.19	2.22	2.37	2.48	2.23	1.75	1.72
Mg#	0.06	0.06	0.02	0.02	0.02	0.02	0.02	0.02	0.02	0.02	0.40	0.42
Name	Lep	Lep	Lep	Lep	Lep	Lep	Lep	Lep	Lep	Lep	Fe-biot	Fe-biot
Fe/Fe+Mg	0.94	0.94	0.98	0.98	0.98	0.98	0.98	0.98	0.98	0.98	0.60	0.58
fet	3.17	2.83	2.36	2.39	2.62	2.39	2.36	2.55	2.73	2.38	1.97	1.93

Analysis	51	52	53	54	55	56	57	58	59	60	61	62
Color	brown	brown	brown	brown	brown	brown	brown	brown	brown	brown	brown	brown
Sample	GNA02	GNA02	GNA02	GNA02	GNA02	GNA02	GNA02	GNA02	GNA02	GNA02	GNA02	GNA02
Alteration	Ca-Fe	Ca-Fe	Ca-Fe	Ca-Fe	Ca-Fe	Ca-Fe	Ca-Fe	Ca-Fe	Ca-Fe	Ca-Fe	Ca-Fe	Ca-Fe
SiO2	37.66	39.19	39.53	38.76	36.65	36.33	37.82	37.98	36.36	36.13	37.49	38.80
TiO2	1.11	1.11	1.01	0.97	1.24	1.25	1.29	1.00	1.10	1.26	1.16	1.20
Al2O3	12.08	12.24	13.03	12.03	12.57	12.31	12.40	12.57	12.41	12.62	12.85	13.10
Fe2O3	0.00	0.00	0.00	0.00	0.00	0.00	0.00	0.00	0.00	0.00	0.00	0.00
FeO	25.99	25.96	26.35	25.89	24.16	25.50	26.27	26.37	25.85	26.12	24.57	24.57
MnO	0.00	0.00	0.00	0.00	0.00	0.00	0.00	0.00	0.00	0.00	0.00	0.00
MgO	10.47	11.06	10.26	10.81	10.61	10.39	10.72	10.84	11.29	10.35	10.98	10.86
CaO	0.04	0.01	0.04	0.07	0.13	0.12	0.02	0.02	0.03	0.09	0.09	0.04
Na2O	0.00	0.00	0.00	0.28	0.49	0.04	0.10	0.00	0.00	0.00	0.00	0.00
K2O	8.33	8.70	8.78	8.59	9.23	9.05	8.98	9.09	9.29	9.36	9.60	9.92
F	2.02	2.08	2.12	1.71	1.76	1.83	2.04	1.75	1.55	1.49	2.13	2.18
Cl	0.09	0.08	0.07	0.09	0.08	0.10	0.06	0.07	0.05	0.08	0.10	0.05
Si	2.94	2.96	2.97	2.96	2.88	2.87	2.90	2.91	2.84	2.84	2.89	2.93
Al(IV)	1.06	1.04	1.03	1.04	1.12	1.13	1.10	1.09	1.14	1.16	1.11	1.07
Al(VI)	0.05	0.06	0.12	0.05	0.05	0.02	0.03	0.04	0.00	0.01	0.06	0.10
Ti	0.07	0.06	0.06	0.06	0.07	0.07	0.07	0.06	0.07	0.08	0.07	0.07
Fet	0.27	0.21	0.10	0.15	0.08	0.25	0.26	0.24	0.36	0.28	0.13	0.02
Fed	1.43	1.43	1.55	1.51	1.51	1.44	1.43	1.45	1.33	1.43	1.46	1.53
Fe3+(T)	0.00	0.00	0.00	0.00	0.00	0.00	0.00	0.00	0.01	0.00	0.00	0.00
Fe3+(M)	0.27	0.21	0.10	0.15	0.08	0.25	0.26	0.24	0.35	0.28	0.13	0.02
Mn	0.00	0.00	0.00	0.00	0.00	0.00	0.00	0.00	0.00	0.00	0.00	0.00
Mg	1.22	1.25	1.15	1.23	1.24	1.23	1.23	1.24	1.32	1.21	1.26	1.22
Ca	0.00	0.00	0.00	0.01	0.01	0.01	0.00	0.00	0.00	0.01	0.01	0.00
Na	0.00	0.00	0.00	0.04	0.08	0.01	0.02	0.00	0.00	0.00	0.00	0.00
K	0.83	0.84	0.84	0.84	0.93	0.91	0.88	0.89	0.93	0.94	0.95	0.96
OH	1.49	1.49	1.49	1.58	1.55	1.53	1.50	1.57	1.61	1.62	1.47	1.47
F	0.50	0.50	0.50	0.41	0.44	0.46	0.50	0.42	0.38	0.37	0.52	0.52
Cl	0.01	0.01	0.01	0.01	0.01	0.01	0.01	0.01	0.01	0.01	0.01	0.01
mgli	1.02	0.99	0.88	0.99	1.09	1.09	1.03	1.03	1.18	1.09	1.08	0.98
feal	1.71	1.65	1.59	1.66	1.62	1.74	1.74	1.71	1.76	1.78	1.59	1.52
Mg#	0.42	0.43	0.41	0.43	0.44	0.42	0.42	0.42	0.44	0.41	0.44	0.44
Name	Fe-biot	Fe-biot	Fe-biot	Fe-biot	Mg-biot	Mg-biot	Mg-biot	Mg-biot	Mg-biot	Mg-biot	Mg-biot	Mg-biot
Fe/Fe+Mg	0.58	0.57	0.59	0.57	0.56	0.58	0.58	0.58	0.56	0.59	0.56	0.56
fet	1.97	1.85	1.76	1.80	1.66	1.93	1.95	1.93	2.05	2.00	1.72	1.57

Analysis	63	64	65	66	67	68	69	70	71	72	73	74	75
Color	brown	brown	brown	brown	brown	brown	brown	brown	brown	brown	brown	brown	brown
Sample	GNA02	GNA02	GNA02	ALB04	ALB04	ALB04	ALB04	ALB04	ALB04	ALB04	ALB04	ALB04	ALB04
Alteration	Ca-Fe	Ca-Fe	Ca-Fe	Ca-Fe	Ca-Fe	Ca-Fe	Ca-Fe	Ca-Fe	Ca-Fe	Ca-Fe	Ca-Fe	Ca-Fe	Ca-Fe
SiO2	37.81	38.81	37.95	39.23	38.16	38.01	38.27	39.58	40.53	38.57	38.82	38.53	39.31
TiO2	1.51	1.22	1.14	1.88	1.86	1.86	1.91	1.95	1.86	1.90	1.64	1.78	1.69
Al2O3	12.70	12.40	12.55	13.27	12.43	12.69	13.26	13.34	13.64	12.69	13.06	12.68	13.12
Fe2O3	0.00	0.00	0.00	0.00	0.00	0.00	0.00	0.00	0.00	0.00	0.00	0.00	0.00
FeO	22.81	22.64	22.91	21.12	21.28	20.84	22.09	20.88	22.14	20.69	19.44	20.02	20.65
MnO	0.00	0.00	0.00	0.00	0.03	0.11	0.01	0.03	0.05	0.07	0.15	0.00	0.12
MgO	10.49	11.22	11.27	12.47	11.32	11.45	11.99	12.25	12.52	11.63	12.98	12.33	12.64
CaO	0.15	0.08	0.05	0.01	0.02	0.03	0.06	0.02	0.02	0.07	0.03	0.03	0.02
Na2O	0.01	0.00	0.00	0.14	0.11	0.11	0.03	0.10	0.10	0.06	0.10	0.09	0.05
K2O	9.29	9.61	9.16	8.89	9.34	9.07	8.64	9.36	8.88	8.69	9.34	9.11	9.32
F	2.16	2.58	2.06	0.00	0.00	0.00	0.00	0.00	0.00	0.00	0.00	0.00	0.00
Cl	0.07	0.10	0.08	0.07	0.10	0.05	0.06	0.08	0.07	0.10	0.06	0.07	0.05
Si	2.95	2.98	2.95	2.94	2.96	2.95	2.91	2.95	2.95	2.97	2.95	2.96	2.95
Al(IV)	1.05	1.02	1.05	1.06	1.04	1.05	1.09	1.05	1.05	1.03	1.06	1.04	1.05
Al(VI)	0.11	0.10	0.10	0.11	0.10	0.11	0.09	0.12	0.12	0.12	0.11	0.11	0.11
Ti	0.09	0.07	0.07	0.11	0.11	0.11	0.11	0.11	0.10	0.11	0.09	0.10	0.10
Fet	0.01	0.06	0.06	0.12	0.01	0.03	0.22	0.03	0.12	0.05	0.03	0.03	0.06
Fed	1.47	1.40	1.43	1.21	1.38	1.32	1.18	1.28	1.23	1.29	1.20	1.25	1.24
Fe3+(T)	0.00	0.00	0.00	0.00	0.00	0.00	0.00	0.00	0.00	0.00	0.00	0.00	0.00
Fe3+(M)	0.01	0.06	0.06	0.12	0.01	0.03	0.22	0.03	0.12	0.05	0.03	0.03	0.06
Mn	0.00	0.00	0.00	0.00	0.00	0.01	0.00	0.00	0.00	0.01	0.01	0.00	0.01
Mg	1.22	1.28	1.31	1.39	1.31	1.32	1.36	1.36	1.36	1.34	1.47	1.41	1.41
Ca	0.01	0.01	0.00	0.00	0.00	0.00	0.01	0.00	0.00	0.01	0.00	0.00	0.00
Na	0.00	0.00	0.00	0.02	0.02	0.02	0.00	0.01	0.01	0.01	0.02	0.01	0.01
K	0.92	0.94	0.91	0.85	0.92	0.90	0.84	0.89	0.83	0.85	0.90	0.89	0.89
OH	1.46	1.36	1.48	1.99	1.99	1.99	1.99	1.99	1.99	1.99	1.99	1.99	1.99
F	0.53	0.63	0.51	0.00	0.00	0.00	0.00	0.00	0.00	0.00	0.00	0.00	0.00
Cl	0.01	0.01	0.01	0.01	0.01	0.01	0.01	0.01	0.01	0.01	0.01	0.01	0.01
mgli	1.02	1.04	1.10	1.14	1.09	1.11	1.14	1.09	1.06	1.10	1.23	1.18	1.15
feal	1.46	1.42	1.46	1.32	1.40	1.36	1.42	1.29	1.33	1.32	1.22	1.28	1.29
Mg#	0.45	0.47	0.47	0.51	0.49	0.50	0.49	0.51	0.50	0.50	0.54	0.52	0.52
Name	Mg-biot	Mg-biot	Mg-biot	Mg-biot	Mg-biot	Mg-biot	Mg-biot	Mg-biot	Mg-biot	Mg-biot	Mg-biot	Mg-biot	Mg-biot
Fe/Fe+Mg	0.55	0.53	0.53	0.49	0.51	0.51	0.51	0.49	0.50	0.50	0.46	0.48	0.48
fet	1.50	1.51	1.55	1.44	1.39	1.38	1.62	1.33	1.47	1.38	1.26	1.32	1.35

Analysis	75	76	77	78	79	80	81	82	83	84	85	86
Color	brown	brown	brown	brown	brown	brown	brown	green	green	green	green	green
Sample	ALB04	ALB04	ALB04	ALB04	ALB04	ALB04	ALB04	ALBGNA1	ALBGNA1	ALBGNA1	ALBGNA1	ALBGNA1
Alteration	Ca-Fe	Ca-Fe	Ca-Fe	Ca-Fe	Ca-Fe	Ca-Fe	Ca-Fe	Ca-Mg	Ca-Mg	Ca-Mg	Ca-Mg	Ca-Mg
SiO2	39.31	39.30	38.61	39.38	39.65	38.95	39.10	40.21	40.17	40.11	40.15	40.67
TiO2	1.69	1.77	1.73	1.64	1.62	1.67	1.72	0.29	0.40	0.31	0.29	0.46
Al2O3	13.12	12.82	13.22	13.45	13.61	12.87	13.07	11.81	11.45	11.49	11.55	11.74
Fe2O3	0.00	0.00	0.00	0.00	0.00	0.00	0.00	0.00	0.00	0.00	0.00	0.00
FeO	20.65	19.86	19.65	19.71	20.22	20.66	20.39	16.30	17.16	16.90	16.80	16.51
MnO	0.12	0.00	0.09	0.07	0.05	0.16	0.06	0.00	0.00	0.00	0.00	0.00
MgO	12.64	12.38	12.73	13.20	13.71	12.58	12.48	16.80	16.96	16.77	17.11	16.36
CaO	0.02	0.05	0.03	0.00	0.01	0.02	0.02	0.05	0.09	0.02	0.05	0.01
Na2O	0.05	0.11	0.09	0.13	0.05	0.06	0.11	0.00	0.00	0.00	0.00	0.00
K2O	9.32	8.93	9.06	9.36	8.89	9.69	9.52	9.17	8.87	8.44	8.06	7.74
F	0.00	0.00	0.00	0.00	0.00	0.00	0.00	2.44	2.62	2.80	3.11	2.98
Cl	0.05	0.06	0.06	0.06	0.05	0.07	0.07	0.05	0.02	0.03	0.03	0.02
Si	2.95	2.98	2.94	2.94	2.93	2.94	2.95	3.02	3.02	3.03	3.03	3.07
Al(IV)	1.05	1.02	1.06	1.06	1.07	1.06	1.05	0.98	0.99	0.97	0.97	0.93
Al(VI)	0.11	0.13	0.12	0.12	0.11	0.09	0.11	0.07	0.03	0.06	0.05	0.11
Ti	0.10	0.10	0.10	0.09	0.09	0.10	0.10	0.02	0.02	0.02	0.02	0.03
Fet	0.06	0.01	0.06	0.04	0.17	0.03	0.00	0.03	0.14	0.14	0.21	0.12
Fed	1.24	1.25	1.19	1.19	1.08	1.27	1.28	1.00	0.94	0.92	0.85	0.92
Fe3+(T)	0.00	0.00	0.00	0.00	0.00	0.00	0.00	0.00	0.00	0.00	0.00	0.00
Fe3+(M)	0.06	0.01	0.06	0.04	0.17	0.03	0.00	0.03	0.14	0.14	0.21	0.12
Mn	0.01	0.00	0.01	0.00	0.00	0.01	0.00	0.00	0.00	0.00	0.00	0.00
Mg	1.41	1.40	1.44	1.47	1.51	1.42	1.40	1.88	1.90	1.89	1.92	1.84
Ca	0.00	0.00	0.00	0.00	0.00	0.00	0.00	0.00	0.01	0.00	0.00	0.00
Na	0.01	0.02	0.01	0.02	0.01	0.01	0.02	0.00	0.00	0.00	0.00	0.00
K	0.89	0.87	0.88	0.89	0.84	0.93	0.92	0.88	0.85	0.81	0.78	0.74
OH	1.99	1.99	1.99	1.99	1.99	1.99	1.99	1.41	1.38	1.33	1.25	1.29
F	0.00	0.00	0.00	0.00	0.00	0.00	0.00	0.58	0.62	0.67	0.74	0.71
Cl	0.01	0.01	0.01	0.01	0.01	0.01	0.01	0.01	0.00	0.00	0.00	0.00
mgli	1.15	1.14	1.21	1.21	1.24	1.17	1.15	1.58	1.60	1.59	1.62	1.52
feal	1.29	1.23	1.23	1.20	1.23	1.32	1.28	0.97	1.07	1.03	1.02	0.96
Mg#	0.52	0.53	0.54	0.54	0.55	0.52	0.52	0.65	0.64	0.64	0.65	0.64
Name	Mg-biot	Mg-biot	Mg-biot	Mg-biot	Mg-biot	Mg-biot	Mg-biot	Mg-biot	Mg-biot	Mg-biot	Mg-biot	Mg-biot
Fe/Fe+Mg	0.48	0.47	0.46	0.46	0.45	0.48	0.48	0.35	0.36	0.36	0.36	0.36
fet	1.35	1.27	1.31	1.27	1.42	1.34	1.29	1.06	1.22	1.21	1.26	1.16

Analysis	87	88	89	90	91	92	93	94	95	96	97	98	99
Color	green	green	green	green	green	green	green	green	brown	brown	brown	brown	brown
Sample	ALBGNA1	ALBGNA1	ALBGNA1	ALBGNA1	ALBGNA1	ALBGNA1	ALBGNA1	ALBGNA1	34BALB02	34BALB02	34BALB02	34BALB02	34BALB02
Alteration	Ca-Mg	Ca-Mg	Ca-Mg	Ca-Mg	Ca-Mg	Ca-Mg	Ca-Mg	Ca-Mg	Ca-Mg	Ca-Mg	Ca-Mg	Ca-Mg	Ca-Mg
SiO2	38.98	39.93	40.60	40.57	42.02	39.71	40.57	40.34	39.52	38.76	37.48	38.05	38.69
TiO2	0.37	0.21	0.37	0.15	0.18	0.24	0.23	0.19	1.92	1.88	1.64	1.82	1.69
Al2O3	12.18	11.66	11.75	12.11	12.64	12.14	11.73	11.76	12.77	12.89	12.75	13.08	13.13
Fe2O3	0.00	0.00	0.00	0.00	0.00	0.00	0.00	0.00	0.00	0.00	0.00	0.00	0.00
FeO	17.86	17.44	16.98	17.01	16.71	17.17	17.12	17.43	17.69	17.92	17.26	17.55	17.54
MnO	0.00	0.00	0.00	0.00	0.00	0.00	0.00	0.00	0.14	0.14	0.11	0.06	0.17
MgO	15.84	16.82	16.44	16.06	15.36	16.83	16.53	16.71	15.25	14.95	15.39	15.43	15.18
CaO	0.00	0.00	0.00	0.00	0.00	0.02	0.07	0.07	0.04	0.00	0.05	0.00	0.02
Na2O	0.00	0.00	0.00	0.00	0.00	0.00	0.00	0.00	0.09	0.05	0.08	0.03	0.08
K2O	9.86	9.74	9.79	9.06	9.06	8.89	9.37	7.61	9.98	9.91	9.99	10.07	10.10
F	2.11	2.72	2.88	2.94	3.29	2.34	3.04	2.59	1.73	1.77	1.81	2.03	1.95
Cl	0.00	0.00	0.00	0.01	0.00	0.00	0.00	0.01	0.04	0.06	0.04	0.05	0.05
Si	2.96	3.00	3.03	3.04	3.10	2.98	3.03	3.04	2.92	2.90	2.86	2.86	2.89
Al(IV)	1.04	1.01	0.97	0.96	0.90	1.02	0.97	0.96	1.08	1.10	1.14	1.14	1.11
Al(VI)	0.05	0.03	0.06	0.11	0.19	0.06	0.06	0.08	0.04	0.04	0.01	0.02	0.05
Ti	0.02	0.01	0.02	0.01	0.01	0.01	0.01	0.01	0.11	0.11	0.09	0.10	0.10
Fet	0.06	0.07	0.03	0.03	0.21	0.15	0.00	0.22	0.11	0.16	0.19	0.21	0.12
Fed	1.08	1.02	1.03	1.04	0.82	0.93	1.07	0.88	0.98	0.97	0.91	0.89	0.98
Fe3+(T)	0.00	0.00	0.00	0.00	0.00	0.00	0.00	0.00	0.00	0.00	0.00	0.00	0.00
Fe3+(M)	0.06	0.07	0.03	0.03	0.21	0.15	0.00	0.22	0.11	0.16	0.19	0.21	0.12
Mn	0.00	0.00	0.00	0.00	0.00	0.00	0.00	0.00	0.01	0.01	0.01	0.00	0.01
Mg	1.79	1.88	1.83	1.80	1.69	1.89	1.84	1.88	1.68	1.67	1.75	1.73	1.69
Ca	0.00	0.00	0.00	0.00	0.00	0.00	0.01	0.01	0.00	0.00	0.00	0.00	0.00
Na	0.00	0.00	0.00	0.00	0.00	0.00	0.00	0.00	0.01	0.01	0.01	0.00	0.01
K	0.96	0.93	0.93	0.87	0.85	0.85	0.89	0.73	0.94	0.95	0.97	0.97	0.96
OH	1.49	1.35	1.32	1.30	1.23	1.44	1.28	1.38	1.59	1.57	1.56	1.51	1.53
F	0.51	0.65	0.68	0.70	0.77	0.56	0.72	0.62	0.41	0.42	0.44	0.48	0.46
Cl	0.00	0.00	0.00	0.00	0.00	0.00	0.00	0.00	0.01	0.01	0.01	0.01	0.01
mgli	1.54	1.59	1.51	1.48	1.32	1.61	1.53	1.57	1.42	1.43	1.57	1.52	1.46
feal	1.11	1.08	1.02	0.96	0.85	1.03	1.02	1.03	1.17	1.20	1.19	1.19	1.15
Mg#	0.61	0.63	0.63	0.63	0.62	0.64	0.63	0.63	0.61	0.60	0.61	0.61	0.61
Name	Mg-biot	Mg-biot	Mg-biot	Mg-biot	Mg-biot	Mg-biot	Mg-biot	Mg-biot	Mg-bio	Mg-bio	Mg-bio	Mg-bio	Mg-bio
Fe/Fe+Mg	0.39	0.37	0.37	0.37	0.38	0.36	0.37	0.37	0.39	0.40	0.39	0.39	0.39
fet	1.19	1.17	1.09	1.10	1.24	1.23	1.07	1.31	1.21	1.28	1.30	1.32	1.22

Analysis	100	101	102	103	104	105	106	107	108	109	110	111	112
Color	brown	brown	brown	brown	brown	brown	brown	brown	brown	brown	brown	brown	brown
Sample	34BALB02	34BALB02	MAAB03	MAAB03	MAAB03	ALBGNA2M	ALBGNA2M	ALBGNA2M	ALBGNA2M	ALBGNA2M	ALBGNA2M	ALBGNA2M	ALBGNA2M
Alteration	Ca-Mg	Ca-Mg	Ca-Mg	Ca-Mg	Ca-Mg	Lit c	Lit c	Lit c	Lit c	Lit c	Lit c	Lit c	Lit c
SiO2	38.52	35.97	40.10	39.94	40.72	35.85	36.41	35.34	36.19	36.23	35.70	35.41	36.23
TiO2	1.78	2.32	0.80	0.72	0.61	2.81	3.16	2.98	3.05	3.07	2.20	2.51	2.57
Al2O3	12.97	12.41	13.63	13.57	13.66	15.30	14.77	13.80	14.86	14.59	14.44	14.55	14.65
Fe2O3	0.00	0.00	0.00	0.00	0.00	0.00	0.00	0.00	0.00	0.00	0.00	0.00	0.00
FeO	17.31	16.87	14.45	14.33	14.52	25.85	26.02	25.75	25.35	25.31	25.50	24.91	25.11
MnO	0.16	0.04	0.06	0.14	0.21	0.00	0.00	0.00	0.00	0.00	0.00	0.00	0.00
MgO	15.13	15.18	17.88	17.36	17.54	8.00	8.02	8.31	8.00	7.95	7.89	7.22	7.89
CaO	0.02	0.48	0.05	0.01	0.03	0.00	0.03	0.20	0.01	0.05	0.45	0.73	0.09
Na2O	0.09	0.03	0.11	0.05	0.06	0.00	0.00	0.00	0.00	0.38	0.62	0.57	0.30
K2O	10.17	9.89	9.94	10.32	9.41	9.72	9.76	9.45	9.57	9.70	9.50	9.78	9.73
F	2.02	1.50	1.80	1.81	2.13	0.46	0.25	0.31	0.25	0.42	0.24	0.13	0.28
Cl	0.04	0.04	0.02	0.04	0.02	0.12	0.12	0.16	0.12	0.14	0.13	0.13	0.16
Si	2.89	2.81	2.93	2.94	2.97	2.76	2.79	2.78	2.79	2.80	2.80	2.79	2.82
Al(IV)	1.11	1.14	1.08	1.06	1.04	1.24	1.21	1.22	1.21	1.20	1.20	1.21	1.19
Al(VI)	0.04	0.00	0.10	0.11	0.14	0.15	0.12	0.06	0.15	0.12	0.13	0.15	0.16
Ti	0.10	0.14	0.04	0.04	0.03	0.16	0.18	0.18	0.18	0.18	0.13	0.15	0.15
Fet	0.11	0.27	0.04	0.04	0.02	0.19	0.20	0.26	0.17	0.09	0.06	0.20	0.01
Fed	0.98	0.84	0.84	0.84	0.87	1.47	1.47	1.44	1.46	1.55	1.61	1.45	1.63
Fe3+(T)	0.00	0.05	0.00	0.00	0.00	0.00	0.00	0.00	0.00	0.00	0.00	0.00	0.00
Fe3+(M)	0.11	0.21	0.04	0.04	0.02	0.19	0.20	0.26	0.17	0.09	0.06	0.20	0.01
Mn	0.01	0.00	0.00	0.01	0.01	0.00	0.00	0.00	0.00	0.00	0.00	0.00	0.00
Mg	1.70	1.77	1.94	1.90	1.90	0.92	0.92	0.98	0.92	0.92	0.92	0.85	0.91
Ca	0.00	0.04	0.00	0.00	0.00	0.00	0.00	0.02	0.00	0.00	0.04	0.06	0.01
Na	0.01	0.01	0.02	0.01	0.01	0.00	0.00	0.00	0.00	0.06	0.09	0.09	0.05
K	0.98	0.98	0.93	0.97	0.87	0.96	0.95	0.95	0.94	0.96	0.95	0.98	0.96
OH	1.52	1.62	1.58	1.57	1.51	1.87	1.92	1.90	1.92	1.88	1.92	1.95	1.91
F	0.48	0.37	0.42	0.42	0.49	0.11	0.06	0.08	0.06	0.10	0.06	0.03	0.07
Cl	0.01	0.01	0.00	0.01	0.00	0.02	0.02	0.02	0.02	0.02	0.02	0.02	0.02
mgli	1.47	1.64	1.66	1.62	1.59	0.81	0.78	0.88	0.79	0.78	0.81	0.75	0.78
feal	1.16	1.24	0.83	0.82	0.79	1.68	1.73	1.81	1.67	1.69	1.67	1.65	1.63
Mg#	0.61	0.62	0.69	0.68	0.68	0.36	0.36	0.37	0.36	0.36	0.36	0.34	0.36
Name	Mg-bio	Mg-bio	Mg-biot	Mg-biot	Mg-biot	Fe-biot	Fe-biot	Fe-biot	Fe-biot	Fe-biot	Fe-biot	Fe-biot	Fe-biot
Fe/Fe+Mg	0.39	0.38	0.31	0.32	0.32	0.64	0.65	0.63	0.64	0.64	0.64	0.66	0.64
fet	1.20	1.37	0.93	0.92	0.90	1.86	1.87	1.95	1.81	1.72	1.73	1.84	1.64

Analysis	113	114	115	116	117	118	119	120	121	122	123	124	125
Color	brown	brown	brown	brown	brown	brown	brown	brown	brown	brown	brown	brown	brown
Sample	ALBG NA2M	ALBG NA2M	ALBG NA2M	ALBG NA2M	ALBG NA2M	ALBG NA2M	ALBG NA2M	ALBG NA2M	ALBG NA2M	ALBG NA2M	ALBG NA2M	ALBG NA2M	ALBG NA2M
Alteration	Lit c	Lit c	Lit c	Lit c	Lit c	Lit c	Lit c	Lit c	Lit c	Lit c	Lit c	Lit c	Lit c
SiO2	35.94	35.82	35.93	36.08	36.32	35.63	36.64	36.30	36.39	36.15	36.22	35.84	35.81
TiO2	3.06	2.74	2.52	2.42	2.27	1.83	2.40	2.59	2.20	2.37	2.19	2.23	2.48
Al2O3	14.44	14.50	14.94	14.57	14.94	14.74	15.02	15.49	15.45	15.06	15.05	14.96	15.04
Fe2O3	0.00	0.00	0.00	0.00	0.00	0.00	0.00	0.00	0.00	0.00	0.00	0.00	0.00
FeO	25.14	25.70	27.03	26.86	26.53	27.27	27.01	26.88	27.22	27.42	27.63	27.13	27.72
MnO	0.00	0.00	0.00	0.00	0.00	0.00	0.00	0.00	0.00	0.00	0.00	0.00	0.00
MgO	8.32	8.34	5.90	6.14	5.69	5.94	6.28	5.71	6.09	6.38	6.32	5.86	5.82
CaO	0.03	0.24	0.16	0.02	0.08	0.01	0.02	0.02	0.01	0.00	0.01	0.04	0.13
Na2O	0.00	0.17	0.06	0.00	0.35	0.00	0.00	0.00	0.00	0.00	0.00	0.09	0.00
K2O	9.72	9.72	8.61	8.65	8.45	8.87	8.76	8.72	8.62	8.62	8.43	8.98	9.35
F	0.25	0.40	0.33	0.29	0.27	0.30	0.42	0.06	0.27	0.45	0.17	0.31	0.32
Cl	0.11	0.11	0.12	0.18	0.11	0.14	0.13	0.10	0.11	0.14	0.19	0.13	0.14
Si	2.79	2.78	2.84	2.86	2.88	2.85	2.86	2.84	2.84	2.83	2.84	2.84	2.82
Al(IV)	1.21	1.22	1.16	1.14	1.13	1.15	1.14	1.16	1.16	1.17	1.16	1.16	1.18
Al(VI)	0.11	0.10	0.23	0.22	0.27	0.24	0.24	0.27	0.27	0.22	0.23	0.24	0.21
Ti	0.18	0.16	0.15	0.14	0.14	0.11	0.14	0.15	0.13	0.14	0.13	0.13	0.15
Fet	0.19	0.15	0.04	0.06	0.10	0.01	0.04	0.02	0.04	0.13	0.12	0.01	0.02
Fed	1.44	1.52	1.75	1.73	1.66	1.82	1.72	1.75	1.74	1.67	1.69	1.79	1.80
Fe3+(T)	0.00	0.00	0.00	0.00	0.00	0.00	0.00	0.00	0.00	0.00	0.00	0.00	0.00
Fe3+(M)	0.19	0.15	0.04	0.06	0.10	0.01	0.04	0.02	0.04	0.13	0.12	0.01	0.02
Mn	0.00	0.00	0.00	0.00	0.00	0.00	0.00	0.00	0.00	0.00	0.00	0.00	0.00
Mg	0.96	0.96	0.70	0.73	0.67	0.71	0.73	0.67	0.71	0.75	0.74	0.69	0.68
Ca	0.00	0.02	0.01	0.00	0.01	0.00	0.00	0.00	0.00	0.00	0.00	0.00	0.01
Na	0.00	0.03	0.01	0.00	0.05	0.00	0.00	0.00	0.00	0.00	0.00	0.01	0.00
K	0.96	0.96	0.87	0.88	0.85	0.91	0.87	0.87	0.86	0.86	0.84	0.91	0.94
OH	1.92	1.89	1.90	1.90	1.92	1.91	1.88	1.97	1.92	1.87	1.93	1.91	1.90
F	0.06	0.10	0.08	0.07	0.07	0.08	0.10	0.02	0.07	0.11	0.04	0.08	0.08
Cl	0.01	0.01	0.02	0.02	0.02	0.02	0.02	0.01	0.02	0.02	0.03	0.02	0.02
mgli	0.84	0.85	0.57	0.60	0.53	0.60	0.58	0.53	0.57	0.62	0.61	0.58	0.57
feal	1.70	1.73	1.71	1.70	1.62	1.69	1.66	1.64	1.64	1.71	1.71	1.69	1.76
Mg#	0.37	0.37	0.28	0.29	0.28	0.28	0.29	0.28	0.29	0.29	0.29	0.28	0.27
Name	Fe-biot	Fe-biot	Fe-biot	Fe-biot	Fe-biot	Fe-biot	Fe-biot	Fe-biot	Fe-biot	Fe-biot	Fe-biot	Fe-biot	Fe-biot
Fe/Fe+Mg	0.63	0.63	0.72	0.71	0.72	0.72	0.71	0.73	0.72	0.71	0.71	0.72	0.73
fet	1.83	1.81	1.82	1.84	1.86	1.83	1.80	1.78	1.82	1.92	1.94	1.81	1.85

Analysis	126	127	128	129	130	131	132	133	134	135	136	137	138
Color	brown	brown	brown	brown	brown	green	green	green	green	green	green	green	green
Sample	ALBG NA2M	ALBG NA2M	ALBG NA2M	ALBG NA2M	ALBG NA2M	ALBG NA2V	ALBG NA2V	ALBG NA2V	ALBG NA2V	ALBG NA2V	ALBG NA2V	ALBG NA2V	ALBG NA2V
Alteration	Lit c	Lit c	Lit c	Lit c	Lit c	Lit c	Lit c	Lit c	Lit c	Lit c	Lit c	Lit c	Lit c
SiO2	34.50	34.50	34.51	35.29	34.82	36.85	36.61	35.68	35.84	35.11	36.13	36.12	35.78
TiO2	2.41	2.84	2.33	2.57	2.61	0.96	0.96	1.22	1.14	1.23	1.23	1.20	0.87
Al2O3	14.60	14.55	14.66	15.08	14.67	15.49	14.99	14.92	15.64	15.13	15.09	14.73	14.61
Fe2O3	0.00	0.00	0.00	0.00	0.00	0.00	0.00	0.00	0.00	0.00	0.00	0.00	0.00
FeO	28.06	28.07	27.67	28.95	28.34	25.71	25.82	26.05	25.85	27.10	26.31	25.89	26.30
MnO	0.00	0.00	0.00	0.00	0.00	0.00	0.00	0.00	0.00	0.00	0.00	0.00	0.00
MgO	5.79	6.03	6.07	6.14	6.25	7.81	8.06	8.23	7.58	8.10	7.95	7.71	7.78
CaO	0.29	0.08	0.01	0.03	0.00	0.05	0.03	0.03	0.04	0.06	0.15	0.04	0.04
Na2O	0.40	0.23	0.00	0.79	0.00	0.00	0.00	0.04	0.11	0.06	0.66	0.00	0.02
K2O	9.13	9.19	8.95	9.84	9.88	8.75	8.24	8.82	9.47	9.21	9.54	9.36	9.42
F	0.08	0.32	0.22	0.28	0.40	0.50	0.30	0.25	0.04	0.37	0.46	0.43	0.44
Cl	0.16	0.20	0.19	0.16	0.15	0.14	0.13	0.13	0.15	0.15	0.16	0.18	0.16
Si	2.77	2.76	2.78	2.74	2.76	2.87	2.88	2.82	2.81	2.77	2.81	2.85	2.85
Al(IV)	1.23	1.24	1.22	1.26	1.24	1.13	1.13	1.18	1.19	1.23	1.19	1.15	1.16
Al(VI)	0.15	0.13	0.18	0.12	0.13	0.29	0.26	0.21	0.26	0.17	0.19	0.23	0.21
Ti	0.15	0.17	0.14	0.15	0.16	0.06	0.06	0.07	0.07	0.07	0.07	0.07	0.05
Fet	0.05	0.19	0.17	0.05	0.17	0.05	0.05	0.12	0.07	0.17	0.10	0.04	0.04
Fed	1.83	1.68	1.69	1.83	1.71	1.62	1.65	1.60	1.63	1.62	1.61	1.67	1.71
Fe3+(T)	0.00	0.00	0.00	0.00	0.00	0.00	0.00	0.00	0.00	0.00	0.00	0.00	0.00
Fe3+(M)	0.05	0.19	0.17	0.05	0.17	0.05	0.05	0.12	0.07	0.17	0.10	0.04	0.04
Mn	0.00	0.00	0.00	0.00	0.00	0.00	0.00	0.00	0.00	0.00	0.00	0.00	0.00
Mg	0.69	0.72	0.73	0.71	0.74	0.91	0.94	0.97	0.89	0.95	0.92	0.91	0.92
Ca	0.03	0.01	0.00	0.00	0.00	0.00	0.00	0.00	0.00	0.01	0.01	0.00	0.00
Na	0.06	0.04	0.00	0.12	0.00	0.00	0.00	0.01	0.02	0.01	0.10	0.00	0.00
K	0.94	0.94	0.92	0.98	1.00	0.87	0.83	0.89	0.95	0.93	0.95	0.94	0.96
OH	1.96	1.89	1.92	1.91	1.88	1.86	1.91	1.92	1.97	1.89	1.87	1.87	1.87
F	0.02	0.08	0.06	0.07	0.10	0.12	0.08	0.06	0.01	0.09	0.11	0.11	0.11
Cl	0.02	0.03	0.03	0.02	0.02	0.02	0.02	0.02	0.02	0.02	0.02	0.02	0.02
mgli	0.64	0.66	0.67	0.62	0.67	0.75	0.79	0.86	0.77	0.87	0.79	0.78	0.81
feal	1.88	1.92	1.83	1.91	1.90	1.44	1.49	1.59	1.50	1.69	1.59	1.56	1.59
Mg#	0.27	0.28	0.28	0.27	0.28	0.35	0.36	0.36	0.34	0.35	0.35	0.35	0.35
Name	Fe-biot	Fe-biot	Fe-biot	Fe-biot	Fe-biot	Fe-biot	Fe-biot	Fe-biot	Fe-biot	Fe-biot	Fe-biot	Fe-biot	Fe-biot
Fe/Fe+Mg	0.73	0.72	0.72	0.73	0.72	0.65	0.64	0.64	0.66	0.65	0.65	0.65	0.65
fet	1.93	2.07	2.04	1.93	2.05	1.73	1.74	1.84	1.76	1.96	1.81	1.75	1.78

Analysis	139	140	141	142	143	144	145	146	147	148	149	150	151
Color	green	green	green	green	green	green	green	green	green	green	green	brown	brown
Sample	ALBGNA2V	ALBGNA2V	ALBGNA2V	ALBGNA2V	ALBGNA2V	ALBGNA2V	ALBGNA2V	ALBGNA2V	ALBGNA2V	ALBGNA2V	ALBGNA2V	GNA09	GNA09
Alteration	Lit c	Lit c	Lit c	Lit c	Lit c	Lit c	Lit c	Lit c	Lit c	Lit c	Lit c	Lit c	Lit c
SiO2	35.08	35.48	35.54	34.67	35.40	34.23	34.54	34.64	35.20	35.00	35.67	35.94	32.08
TiO2	1.26	1.06	1.24	1.08	1.15	1.06	1.08	1.12	1.11	0.95	1.04	2.94	2.91
Al2O3	15.20	14.48	15.17	14.91	15.41	15.41	15.41	14.44	15.57	14.66	15.76	14.56	13.50
Fe2O3	0.00	0.00	0.00	0.00	0.00	0.00	0.00	0.00	0.00	0.00	0.00	0.00	0.00
FeO	26.23	26.75	28.06	26.69	26.95	26.91	26.90	25.88	26.39	26.26	25.73	28.06	24.76
MnO	0.00	0.00	0.00	0.00	0.00	0.00	0.00	0.00	0.00	0.00	0.00	0.38	0.33
MgO	7.77	8.37	7.98	8.41	7.72	8.35	7.79	8.15	7.81	7.89	7.70	4.98	4.66
CaO	0.05	0.03	0.03	0.10	0.06	0.19	0.13	0.44	0.05	0.30	0.22	0.01	0.03
Na2O	0.00	0.06	0.18	0.00	0.00	0.00	0.44	0.52	0.00	0.11	0.20	0.05	0.19
K2O	9.11	9.04	9.53	8.58	9.06	8.72	8.34	9.10	9.23	8.78	9.30	9.59	8.80
F	0.22	0.17	0.45	0.41	0.42	0.41	0.39	0.44	0.26	0.40	0.57	0.00	0.00
Cl	0.15	0.14	0.14	0.16	0.14	0.17	0.16	0.19	0.16	0.14	0.13	0.16	0.27
Si	2.79	2.81	2.76	2.77	2.79	2.73	2.75	2.78	2.78	2.81	2.80	2.84	2.80
Al(IV)	1.21	1.19	1.24	1.23	1.21	1.27	1.25	1.22	1.22	1.19	1.20	1.17	1.20
Al(VI)	0.22	0.16	0.16	0.17	0.22	0.18	0.20	0.15	0.23	0.20	0.26	0.19	0.18
Ti	0.08	0.06	0.07	0.07	0.07	0.06	0.07	0.07	0.07	0.06	0.06	0.17	0.19
Fet	0.09	0.15	0.15	0.25	0.11	0.27	0.16	0.02	0.08	0.05	0.09	0.00	0.00
Fed	1.65	1.62	1.67	1.53	1.67	1.53	1.64	1.72	1.67	1.72	1.60	1.85	1.80
Fe3+(T)	0.00	0.00	0.00	0.00	0.00	0.00	0.00	0.00	0.00	0.00	0.00	0.00	0.00
Fe3+(M)	0.09	0.15	0.15	0.25	0.11	0.27	0.16	0.02	0.08	0.05	0.09	0.00	0.00
Mn	0.00	0.00	0.00	0.00	0.00	0.00	0.00	0.00	0.00	0.00	0.00	0.03	0.02
Mg	0.92	0.99	0.93	1.00	0.91	0.99	0.93	0.98	0.92	0.94	0.90	0.59	0.61
Ca	0.00	0.00	0.00	0.01	0.01	0.02	0.01	0.04	0.00	0.03	0.02	0.00	0.00
Na	0.00	0.01	0.03	0.00	0.00	0.00	0.07	0.08	0.00	0.02	0.03	0.01	0.03
K	0.92	0.91	0.95	0.87	0.91	0.89	0.85	0.93	0.93	0.90	0.93	0.97	0.98
OH	1.92	1.94	1.87	1.88	1.88	1.87	1.88	1.86	1.91	1.88	1.84	1.98	1.96
F	0.06	0.04	0.11	0.10	0.11	0.10	0.10	0.11	0.07	0.10	0.14	0.00	0.00
Cl	0.02	0.02	0.02	0.02	0.02	0.02	0.02	0.03	0.02	0.02	0.02	0.02	0.04
mgli	0.84	0.89	0.82	0.94	0.81	0.95	0.87	0.91	0.83	0.86	0.79	0.47	0.67
feal	1.61	1.67	1.74	1.68	1.63	1.68	1.66	1.66	1.58	1.63	1.49	1.86	1.84
Mg#	0.35	0.36	0.34	0.36	0.34	0.36	0.34	0.36	0.35	0.35	0.35	0.24	0.25
Name	Fe-biot	Fe-biot	Fe-biot	Fe-biot	Fe-biot	Fe-biot	Fe-biot	Fe-biot	Fe-biot	Fe-biot	Fe-biot	Fe-biot	Fe-biot
Fe/Fe+Mg	0.65	0.64	0.66	0.64	0.66	0.64	0.66	0.64	0.65	0.65	0.65	0.76	0.75
fet	1.84	1.92	1.98	2.04	1.88	2.06	1.95	1.76	1.82	1.81	1.78	1.85	1.81

Analysis	152	153	154	155	156	157	158	159	160	161	162	163	164
Color	brown	brown	brown	brown	brown	brown	brown	brown	brown	brown	brown	brown	brown
Sample	GNA09	GNA09	GNA09	GNA09	GNA09	GNA09	GNA09	GNA09	GNA09	GNA09	GNA09	GNA09	GNA09
Alteration	Lit c	Lit c	Lit c	Lit c	Lit c	Lit c	Lit c	Lit c	Lit c	Lit c	Lit c	Lit c	Lit c
SiO2	34.12	32.40	34.18	34.75	35.36	35.63	35.12	35.81	35.19	35.69	35.02	34.26	35.91
TiO2	2.91	2.94	3.00	2.98	3.11	3.11	2.93	2.92	3.11	2.65	2.77	2.95	3.18
Al2O3	14.50	14.39	14.20	13.85	14.30	14.36	15.12	15.10	15.10	14.94	14.81	13.89	14.82
Fe2O3	0.00	0.00	0.00	0.00	0.00	0.00	0.00	0.00	0.00	0.00	0.00	0.00	0.00
FeO	28.51	25.16	28.06	24.74	27.51	28.44	28.02	27.67	26.66	27.24	27.29	27.62	27.61
MnO	0.40	0.25	0.35	0.48	0.32	0.27	0.24	0.36	0.34	0.25	0.31	0.41	0.34
MgO	4.58	5.11	4.56	4.77	4.74	4.88	5.10	4.91	5.04	4.95	4.80	4.59	5.01
CaO	0.02	0.00	0.01	0.00	0.03	0.01	0.01	0.00	0.01	0.02	0.01	0.01	0.02
Na2O	0.08	0.13	0.06	0.14	0.11	0.12	0.12	0.04	0.06	0.23	0.19	0.15	0.11
K2O	9.68	9.38	9.49	9.36	9.44	9.14	9.58	9.72	9.56	9.29	9.33	9.52	9.62
F	0.00	0.00	0.00	0.00	0.00	0.00	0.00	0.00	0.00	0.00	0.00	0.00	0.00
Cl	0.15	0.18	0.17	0.17	0.15	0.16	0.17	0.20	0.17	0.18	0.18	0.15	0.16
Si	2.77	2.75	2.79	2.88	2.84	2.83	2.78	2.82	2.81	2.84	2.82	2.81	2.82
Al(IV)	1.23	1.25	1.21	1.12	1.17	1.17	1.22	1.18	1.20	1.16	1.18	1.19	1.18
Al(VI)	0.16	0.19	0.16	0.23	0.19	0.17	0.19	0.22	0.22	0.24	0.22	0.16	0.20
Ti	0.18	0.19	0.18	0.19	0.19	0.19	0.18	0.17	0.19	0.16	0.17	0.18	0.19
Fet	0.08	0.04	0.07	0.18	0.02	0.08	0.05	0.03	0.02	0.09	0.04	0.02	0.01
Fed	1.85	1.75	1.84	1.53	1.83	1.81	1.80	1.79	1.76	1.72	1.80	1.88	1.81
Fe3+(T)	0.00	0.00	0.00	0.00	0.00	0.00	0.00	0.00	0.00	0.00	0.00	0.00	0.00
Fe3+(M)	0.08	0.04	0.07	0.18	0.02	0.08	0.05	0.03	0.02	0.09	0.04	0.02	0.01
Mn	0.03	0.02	0.02	0.03	0.02	0.02	0.02	0.02	0.02	0.02	0.02	0.03	0.02
Mg	0.55	0.65	0.56	0.59	0.57	0.58	0.60	0.58	0.60	0.59	0.58	0.56	0.59
Ca	0.00	0.00	0.00	0.00	0.00	0.00	0.00	0.00	0.00	0.00	0.00	0.00	0.00
Na	0.01	0.02	0.01	0.02	0.02	0.02	0.02	0.01	0.01	0.04	0.03	0.02	0.02
K	1.00	1.02	0.99	0.99	0.97	0.93	0.97	0.98	0.97	0.94	0.96	1.00	0.97
OH	1.98	1.97	1.98	1.98	1.98	1.98	1.98	1.97	1.98	1.98	1.98	1.98	1.98
F	0.00	0.00	0.00	0.00	0.00	0.00	0.00	0.00	0.00	0.00	0.00	0.00	0.00
Cl	0.02	0.03	0.02	0.02	0.02	0.02	0.02	0.03	0.02	0.02	0.03	0.02	0.02
mgli	0.52	0.69	0.51	0.52	0.47	0.47	0.52	0.46	0.51	0.48	0.50	0.52	0.47
feal	1.98	1.80	1.97	1.70	1.87	1.92	1.85	1.80	1.76	1.75	1.80	1.95	1.83
Mg#	0.22	0.27	0.23	0.26	0.24	0.23	0.25	0.24	0.25	0.25	0.24	0.23	0.24
Name	Fe-biot	Fe-biot	Fe-biot	Fe-biot	Fe-biot	Fe-biot	Fe-biot	Fe-biot	Fe-biot	Fe-biot	Fe-biot	Fe-biot	Fe-biot
Fe/Fe+Mg	0.78	0.73	0.78	0.74	0.76	0.77	0.76	0.76	0.75	0.76	0.76	0.77	0.76
fet	2.02	1.82	1.99	1.90	1.86	1.97	1.91	1.86	1.79	1.90	1.87	1.91	1.82

Analysis	165	166	167	168	169	170	171	172	173	174	175	176	177
Color	brown	brown	brown	brown	brown	brown	brown	brown	brown	brown	brown	brown	brown
Sample	GNA09	GNA09	GNA09	GNA09	GNA09	GNA09	GNA09	GNA09	GNA09	GNA09	GNA09	GNA09	GNA09
Alteration	Lit c	Lit c	Lit c	Lit c	Lit c	Lit c	Lit c	Lit c	Lit c	Lit c	Lit c	Lit c	Lit c
SiO2	36.82	35.62	35.69	34.91	35.68	36.48	34.46	35.40	35.03	34.85	35.22	35.20	35.52
TiO2	3.09	3.45	3.26	3.25	3.09	3.21	3.04	3.05	3.08	3.22	3.21	3.17	2.92
Al2O3	15.51	14.51	14.48	14.34	14.17	14.83	13.94	14.68	14.31	14.35	14.19	14.31	15.02
Fe2O3	0.00	0.00	0.00	0.00	0.00	0.00	0.00	0.00	0.00	0.00	0.00	0.00	0.00
FeO	27.30	26.79	27.63	27.60	27.94	27.79	28.55	28.05	28.65	28.66	28.21	28.47	27.82
MnO	0.33	0.25	0.31	0.40	0.24	0.40	0.31	0.30	0.50	0.39	0.41	0.38	0.34
MgO	5.16	4.71	4.81	4.46	5.01	4.84	4.36	4.71	4.50	4.50	4.67	4.67	4.78
CaO	0.03	0.01	0.02	0.01	0.03	0.03	0.04	0.05	0.00	0.03	0.01	0.05	0.04
Na2O	0.23	0.25	0.11	0.14	0.08	0.20	0.08	0.07	0.09	0.08	0.10	0.08	0.33
K2O	9.64	9.55	9.53	9.73	9.49	9.54	9.12	9.36	9.57	9.77	9.45	9.51	9.68
F	0.00	0.00	0.00	0.00	0.00	0.00	0.00	0.00	0.00	0.00	0.00	0.00	0.00
Cl	0.16	0.17	0.20	0.19	0.20	0.20	0.19	0.16	0.15	0.19	0.21	0.17	0.17
Si	2.83	2.84	2.83	2.81	2.84	2.84	2.81	2.82	2.81	2.79	2.82	2.81	2.81
Al(IV)	1.17	1.16	1.17	1.19	1.16	1.16	1.19	1.18	1.19	1.21	1.18	1.19	1.19
Al(VI)	0.24	0.20	0.19	0.18	0.17	0.21	0.16	0.20	0.16	0.15	0.16	0.16	0.21
Ti	0.18	0.21	0.20	0.20	0.19	0.19	0.19	0.18	0.19	0.19	0.19	0.19	0.17
Fet	0.09	0.07	0.01	0.02	0.02	0.05	0.09	0.02	0.06	0.06	0.06	0.06	0.07
Fed	1.67	1.71	1.83	1.84	1.84	1.76	1.86	1.84	1.86	1.86	1.83	1.84	1.77
Fe3+(T)	0.00	0.00	0.00	0.00	0.00	0.00	0.00	0.00	0.00	0.00	0.00	0.00	0.00
Fe3+(M)	0.09	0.07	0.01	0.02	0.02	0.05	0.09	0.02	0.06	0.06	0.06	0.06	0.07
Mn	0.02	0.02	0.02	0.03	0.02	0.03	0.02	0.02	0.03	0.03	0.03	0.03	0.02
Mg	0.59	0.56	0.57	0.54	0.59	0.56	0.53	0.56	0.54	0.54	0.56	0.56	0.56
Ca	0.00	0.00	0.00	0.00	0.00	0.00	0.00	0.00	0.00	0.00	0.00	0.00	0.00
Na	0.03	0.04	0.02	0.02	0.01	0.03	0.01	0.01	0.01	0.01	0.02	0.01	0.05
K	0.95	0.97	0.97	1.00	0.96	0.95	0.95	0.95	0.98	1.00	0.97	0.97	0.98
OH	1.98	1.98	1.97	1.97	1.97	1.97	1.97	1.98	1.98	1.97	1.97	1.98	1.98
F	0.00	0.00	0.00	0.00	0.00	0.00	0.00	0.00	0.00	0.00	0.00	0.00	0.00
Cl	0.02	0.02	0.03	0.03	0.03	0.03	0.03	0.02	0.02	0.03	0.03	0.02	0.02
mgli	0.44	0.45	0.46	0.46	0.48	0.42	0.48	0.46	0.46	0.47	0.47	0.47	0.46
feal	1.72	1.81	1.86	1.91	1.89	1.82	2.00	1.88	1.98	1.99	1.95	1.96	1.83
Mg#	0.25	0.24	0.24	0.22	0.24	0.24	0.21	0.23	0.22	0.22	0.23	0.23	0.23
Name	Fe-biot	Fe-biot	Fe-biot	Fe-biot	Fe-biot	Fe-biot	Fe-biot	Fe-biot	Fe-biot	Fe-biot	Fe-biot	Fe-biot	Fe-biot
Fe/Fe+Mg	0.75	0.76	0.76	0.78	0.76	0.76	0.79	0.77	0.78	0.78	0.77	0.77	0.77
fet	1.85	1.86	1.84	1.88	1.88	1.86	2.04	1.89	1.98	1.99	1.95	1.96	1.91

Analysis	178	179	180	181	182	183	184	185	186	187	188	189
Color	brown	brown	brown	brown	brown	brown	brown	brown	brown	brown	brown	brown
Sample	GNA09	GNA09	GNA09	GNA09	GNA09	GNA09	GNA09	GNA09	BCAB	BCAB	BCAB	BAB129
Alteration	Lit c	Lit c	Lit c	Lit c	Lit c	Lit c	Lit c	Lit c	K-Mg	K-Mg	K-Mg	K-Mg
SiO2	36.02	35.20	35.90	35.10	35.19	35.54	35.32	35.57	39.69	40.32	40.73	42.98
TiO2	3.02	2.91	3.08	3.15	3.17	3.26	3.22	3.20	1.32	1.36	1.44	1.56
Al2O3	15.33	14.69	14.93	14.59	14.58	14.55	14.55	14.92	14.63	14.40	14.21	14.08
Fe2O3	0.00	0.00	0.00	0.00	0.00	0.00	0.00	0.00	0.00	0.00	0.00	0.00
FeO	28.04	28.45	27.62	27.74	28.06	27.63	28.09	26.80	9.36	9.04	8.96	10.57
MnO	0.34	0.49	0.34	0.28	0.31	0.32	0.32	0.37	0.16	0.04	0.20	0.11
MgO	4.83	4.79	4.64	4.54	4.67	4.55	4.70	4.97	20.83	20.37	20.42	20.10
CaO	0.02	0.02	0.03	0.04	0.04	0.00	0.00	0.00	0.04	0.02	0.02	0.05
Na2O	0.13	0.14	0.24	0.15	0.05	0.09	0.15	0.08	0.08	0.16	0.11	0.09
K2O	9.61	9.41	9.47	9.46	9.49	9.72	9.73	9.44	9.99	10.08	10.18	9.72
F	0.00	0.00	0.00	0.00	0.00	0.00	0.00	0.00	0.41	0.63	0.49	0.00
Cl	0.17	0.18	0.17	0.18	0.17	0.21	0.20	0.21	0.02	0.02	0.01	0.04
Si	2.81	2.80	2.83	2.82	2.81	2.83	2.81	2.82	2.86	2.90	2.92	2.98
Al(IV)	1.19	1.20	1.17	1.19	1.19	1.17	1.19	1.18	1.14	1.10	1.08	1.02
Al(VI)	0.22	0.18	0.22	0.19	0.18	0.20	0.17	0.22	0.10	0.13	0.12	0.14
Ti	0.18	0.17	0.18	0.19	0.19	0.20	0.19	0.19	0.07	0.07	0.08	0.08
Fet	0.02	0.06	0.07	0.01	0.04	0.04	0.01	0.02	0.16	0.03	0.02	0.00
Fed	1.81	1.83	1.75	1.85	1.83	1.80	1.86	1.76	0.41	0.52	0.52	0.61
Fe3+(T)	0.00	0.00	0.00	0.00	0.00	0.00	0.00	0.00	0.00	0.00	0.00	0.00
Fe3+(M)	0.02	0.06	0.07	0.01	0.04	0.04	0.01	0.02	0.16	0.03	0.02	0.00
Mn	0.02	0.03	0.02	0.02	0.02	0.02	0.02	0.03	0.01	0.00	0.01	0.01
Mg	0.56	0.57	0.55	0.54	0.56	0.54	0.56	0.59	2.24	2.19	2.18	2.08
Ca	0.00	0.00	0.00	0.00	0.00	0.00	0.00	0.00	0.00	0.00	0.00	0.00
Na	0.02	0.02	0.04	0.02	0.01	0.01	0.02	0.01	0.01	0.02	0.02	0.01
K	0.96	0.96	0.95	0.97	0.97	0.99	0.99	0.96	0.92	0.93	0.93	0.86
OH	1.98	1.98	1.98	1.98	1.98	1.97	1.97	1.97	1.90	1.85	1.89	2.00
F	0.00	0.00	0.00	0.00	0.00	0.00	0.00	0.00	0.09	0.14	0.11	0.00
Cl	0.02	0.02	0.02	0.02	0.02	0.03	0.03	0.03	0.00	0.00	0.00	0.01
mgli	0.44	0.48	0.43	0.46	0.47	0.44	0.46	0.48	1.97	1.90	1.87	1.69
feal	1.81	1.92	1.81	1.88	1.90	1.86	1.91	1.78	0.55	0.49	0.51	0.57
Mg#	0.24	0.23	0.23	0.23	0.23	0.23	0.23	0.25	0.80	0.80	0.80	0.77
Name	Fe-biot	Fe-biot	Fe-biot	Fe-biot	Fe-biot	Fe-biot	Fe-biot	Fe-biot	Mg-biot	Mg-biot	Mg-biot	Mg-biot
Fe/Fe+Mg	0.77	0.77	0.77	0.77	0.77	0.77	0.77	0.75	0.20	0.20	0.20	0.23
fet	1.85	1.96	1.89	1.87	1.91	1.88	1.88	1.80	0.72	0.57	0.56	0.62

Analysis	190	191	192	193	194	195	196	197	198	199
Color	brown	brown	brown	brown	brown	brown	brown	brown	brown	brown
Sample	BAB129	BAB129	BAB129	BAB129	BAB129	BAB129	BAB129	BAB129	BAB129	BAB129
Alteration	K-Mg	K-Mg	K-Mg	K-Mg	K-Mg	K-Mg	K-Mg	K-Mg	K-Mg	K-Mg
SiO2	43.06	41.92	41.24	42.46	42.20	42.06	42.10	40.68	41.61	40.95
TiO2	1.44	1.49	1.52	1.63	1.69	1.73	1.67	1.49	1.63	1.67
Al2O3	14.04	13.18	13.44	13.59	13.13	13.16	12.96	13.00	12.97	12.70
Fe2O3	0.00	0.00	0.00	0.00	0.00	0.00	0.00	0.00	0.00	0.00
FeO	10.55	10.56	10.58	10.34	10.40	10.38	10.72	10.53	10.60	10.36
MnO	0.25	0.13	0.16	0.23	0.13	0.19	0.11	0.12	0.19	0.12
MgO	20.32	19.30	18.83	18.74	19.24	19.10	19.33	18.25	19.29	18.99
CaO	0.06	0.03	0.06	0.03	0.03	0.02	0.04	0.09	0.02	0.04
Na2O	0.13	0.05	0.06	0.11	0.05	0.06	0.08	0.14	0.06	0.09
K2O	9.70	10.11	10.26	9.77	10.03	9.83	9.89	9.68	9.91	9.92
F	0.00	0.06	0.67	0.42	0.11	0.49	0.73	0.32	0.73	1.12
Cl	0.03	0.01	0.04	0.02	0.04	0.02	0.02	0.02	0.03	0.03
Si	2.98	3.00	2.98	3.02	3.01	3.01	3.01	3.00	3.00	3.00
Al(IV)	1.02	1.00	1.02	0.98	0.99	0.99	0.99	1.00	1.00	1.01
Al(VI)	0.13	0.11	0.12	0.16	0.12	0.12	0.10	0.13	0.10	0.09
Ti	0.08	0.08	0.08	0.09	0.09	0.09	0.09	0.08	0.09	0.09
Fet	0.01	0.08	0.10	0.14	0.08	0.06	0.04	0.12	0.02	0.04
Fed	0.60	0.56	0.54	0.48	0.54	0.56	0.60	0.53	0.62	0.59
Fe3+(T)	0.00	0.00	0.00	0.00	0.00	0.00	0.00	0.00	0.00	0.00
Fe3+(M)	0.01	0.08	0.10	0.14	0.08	0.06	0.04	0.12	0.02	0.04
Mn	0.02	0.01	0.01	0.01	0.01	0.01	0.01	0.01	0.01	0.01
Mg	2.10	2.06	2.03	1.99	2.05	2.04	2.06	2.01	2.07	2.07
Ca	0.00	0.00	0.01	0.00	0.00	0.00	0.00	0.01	0.00	0.00
Na	0.02	0.01	0.01	0.02	0.01	0.01	0.01	0.02	0.01	0.01
K	0.86	0.92	0.95	0.89	0.91	0.90	0.90	0.91	0.91	0.93
OH	2.00	1.99	1.84	1.90	1.97	1.89	1.83	1.92	1.83	1.74
F	0.00	0.01	0.15	0.10	0.03	0.11	0.17	0.08	0.17	0.26
Cl	0.00	0.00	0.01	0.00	0.01	0.00	0.00	0.00	0.00	0.00
mgli	1.71	1.70	1.70	1.61	1.68	1.68	1.70	1.69	1.72	1.75
feal	0.57	0.61	0.61	0.55	0.60	0.61	0.64	0.61	0.64	0.64
Mg#	0.77	0.77	0.76	0.76	0.77	0.77	0.76	0.76	0.76	0.77
Name	Mg-biot	Mg-biot	Mg-biot	Mg-biot	Mg-biot	Mg-biot	Mg-biot	Mg-biot	Mg-biot	Mg-biot
Fe/Fe+Mg	0.23	0.23	0.24	0.24	0.23	0.23	0.24	0.24	0.24	0.23
fet	0.62	0.71	0.74	0.75	0.70	0.69	0.68	0.77	0.66	0.68

3F: EPMA analyses of garnet. Recalculated formula on the basis of 12 oxygens

	1	2	3	4	5	6	7	8	9	10	11	12
Analysis (wt%)	F10-7-1B-C4-1	F10-7-1B-C4-2	F10-7-1B-C4-3	F10-7-1B-C1-4	F10-7-1B-C1-5	F10-7-1B-C1-6	LR35-F10-7-28-C2-1	LR35-F10-7-28-C2-2	LR35-F10-7-28-C2-3	LR35-F10-7-28-C2-4	LR35-F10-7-28-C2-5	LR35-F10-7-28-C2-6
SiO_2	35.62	35.98	35.98	35.89	35.78	35.87	36.00	36.35	36.42	35.88	34.83	36.19
TiO_2	0.77	0.72	0.87	0.94	0.81	0.76	0.62	0.74	0.72	0.72	0.53	0.69
Al_2O_3	3.98	3.70	3.93	4.42	4.04	3.75	3.80	3.54	3.95	3.88	3.37	3.67
FeO / FeO_{tot}	23.66	25.67	25.11	23.07	24.78	25.66	24.77	24.03	24.95	24.18	25.83	25.35
MnO	0.37	0.62	0.51	0.52	0.47	0.41	0.64	0.28	0.50	0.31	0.65	0.75
MgO	0.00	0.00	0.00	0.00	0.00	0.00	0.01	0.00	0.00	0.00	0.03	0.01
CaO	32.45	31.27	32.33	33.07	32.56	31.84	32.69	34.17	32.98	33.29	32.01	32.08
Na_2O	0.04	0.03	0.00	0.00	0.03	0.05	0.03	0.03	0.06	0.01	0.07	0.01
F	0.48	0.18	0.44	0.74	0.75	0.62	0.35	0.50	0.18	0.79	0.15	0.34
O=F (calc)	-0.20	-0.07	-0.18	-0.31	-0.32	-0.26	-0.15	-0.21	-0.07	-0.33	-0.06	-0.14
Total (calc)	97.16	98.10	99.01	98.35	98.91	98.69	98.94	99.50	99.74	98.77	97.47	98.94
Recalculated (wt%)												
final FeO	1.61	3.02	2.28	1.57	1.89	2.74	1.25	0.38	1.31	1.30	0.21	2.29
final Fe_2O_3	24.51	25.17	25.37	23.90	25.43	25.47	26.14	26.28	26.27	25.43	28.46	25.63
final MnO	0.37	0.62	0.51	0.52	0.47	0.41	0.64	0.28	0.50	0.31	0.65	0.75
final Mn_2O_3	0.00	0.00	0.00	0.00	0.00	0.00	0.00	0.00	0.00	0.00	0.00	0.00
Total	99.61	100.62	101.55	100.74	101.45	101.24	101.56	102.13	102.37	101.33	100.31	101.51
TSi	2.96	2.98	2.95	2.94	2.93	2.95	2.95	2.95	2.96	2.94	2.90	2.97
Ti	0.05	0.05	0.05	0.06	0.05	0.05	0.04	0.04	0.04	0.04	0.03	0.04
Tal	0.01	0.01	0.03	0.01	0.02	0.01	0.03	0.02	0.03	0.01	0.09	0.01
Al	0.38	0.35	0.35	0.42	0.36	0.35	0.34	0.32	0.35	0.36	0.24	0.35
Fe2+VI	0.04	0.03	0.03	0.05	0.02	0.03	0.01	0.02	0.00	0.03	0.00	0.03
Fe2+	0.08	0.18	0.13	0.06	0.11	0.16	0.08	0.00	0.09	0.06	0.01	0.13
Fe3+	1.53	1.57	1.56	1.47	1.57	1.58	1.61	1.61	1.61	1.57	1.79	1.58
Mn2+	0.03	0.04	0.04	0.04	0.03	0.03	0.04	0.02	0.03	0.02	0.05	0.05
Mg	0.00	0.00	0.00	0.00	0.00	0.00	0.00	0.00	0.00	0.00	0.00	0.00
Ca	2.89	2.78	2.84	2.91	2.85	2.80	2.87	2.97	2.87	2.92	2.86	2.82
Na	0.01	0.00	0.00	0.00	0.00	0.01	0.00	0.00	0.01	0.00	0.01	0.00
End-members												
FCa garnet	0.01	0.00	0.01	0.02	0.02	0.01	0.01	0.01	0.00	0.02	0.00	0.01
Schorlomite-Al	0.00	0.00	0.01	0.00	0.01	0.01	0.01	0.01	0.02	0.01	0.02	0.00
Morimotoite	0.04	0.03	0.03	0.05	0.02	0.03	0.01	0.02	0.00	0.03		0.03
NaTi garnet	0.00	0.00			0.00	0.00	0.00	0.00	0.01	0.00		0.00
Spessartine	0.01	0.01	0.01	0.01	0.01	0.01	0.01	0.01	0.01	0.01	0.02	0.02
Pyrope	0.00	0.00	0.00	0.00	0.00	0.00	0.00	0.00	0.00	0.00	0.00	0.00
Almandine	0.03	0.06	0.04	0.02	0.04	0.05	0.03	0.00	0.03	0.02	0.00	0.04
Grossular	0.15	0.10	0.11	0.16	0.12	0.10	0.12	0.14	0.13	0.14	0.10	0.11
Andradite	0.77	0.78	0.78	0.74	0.78	0.79	0.81	0.80	0.80	0.78	0.84	0.79

	13	14	15	16	17	18	19	20	21	22
Analysis (wt%)	F10-7-2B	F10-7-2B	3409GALB04-C1-1	3409GALB04-C9-22	3409GALB04-C9-24	3516-PAAB01-C1-38	3516-PAAB01-C1-39	3516-PAAB01-C1-40	3516-PAAB01-C2-41	3516-PAAB01-C2-42
SiO_2	36.03	36.11	36.07	34.79	34.93	37.01	36.87	36.90	33.00	32.62
TiO_2	0.79	0.58	0.68	1.38	0.55	0.35	0.89	0.35	0.60	0.64
Al_2O_3	4.19	3.92	3.70	5.47	4.00	1.95	3.90	1.81	1.31	1.37
FeO / FeO_{tot}	23.01	24.26	25.77	21.99	24.68	26.26	23.50	26.78	26.42	25.54
MnO	0.39	1.15	0.89	0.38	0.84	1.28	0.15	1.17	0.92	0.89
MgO	0.00	0.00	0.00	0.03	0.01	0.02	0.00	0.06	1.11	1.15
CaO	33.94	31.74	30.70	33.37	31.26	31.88	33.68	31.64	24.95	24.70
Na_2O	0.00	0.05	0.04	0.07	0.06	0.04	0.01	0.00	0.20	0.23
F	0.00	0.00	0.23	0.77	0.33	0.32	0.44	0.00	0.27	0.00
O=F (calc)			-0.10	-0.32	-0.14	-0.13	-0.19		-0.11	
Total (calc)	98.40	97.80	97.98	97.93	96.52	98.97	99.26	98.70	88.67	87.14
Recalculated (wt%)										
final FeO	0.00	1.65	3.54	0.05	1.38	2.49	1.95	2.61	4.47	3.92
final Fe_2O_3	25.57	25.13	24.70	24.38	25.90	26.42	23.95	26.85	24.40	24.02
final MnO	0.29	1.15	0.89	0.38	0.84	1.28	0.15	1.17	0.92	0.89
final Mn_2O_3	0.11	0.00	0.00	0.00	0.00	0.00	0.00	0.00	0.00	0.00
Total	100.97	100.32	100.45	100.37	99.12	101.63	101.65	101.39	91.12	89.55
TSi	2.96	2.99	2.99	2.85	2.93	3.00	3.00	3.00	3.00	3.00
Ti	0.05	0.04	0.04	0.09	0.03	0.02	0.05	0.02	0.04	0.05
Tal	0.04	0.01	0.00	0.10	0.05	0.00	0.00	0.00	0.00	0.00
Al	0.36	0.38	0.36	0.43	0.35	0.19	0.37	0.18	0.14	0.15
Fe2+VI	0.00	0.02	0.05	0.00	0.00	0.10	0.11	0.08	0.05	0.00
Fe2+	0.00	0.09	0.19	0.00	0.10	0.07	0.03	0.11	0.30	0.30
Fe3+	1.58	1.57	1.54	1.50	1.64	1.64	1.47	1.67	1.69	1.69
Mn2+	0.02	0.08	0.06	0.03	0.06	0.09	0.01	0.08	0.07	0.07
Mg	0.00	0.00	0.00	0.00	0.00	0.00	0.00	0.01	0.11	0.11
Ca	2.98	2.82	2.73	2.93	2.81	2.81	2.93	2.81	2.46	2.48
Na	0.00	0.01	0.01	0.01	0.01	0.01	0.00	0.00	0.04	0.04
End-members										
FCa garnet			0.01	0.02	0.01	0.01	0.01		0.01	
Schorlomite-Al	0.02	0.00		0.04	0.02					
Morimotoite		0.02	0.04			0.02	0.05	0.02	0.04	0.00
NaTi garnet	0.00	0.00								0.02
Spessartine	0.00	0.03	0.02	0.01	0.02	0.03	0.00	0.03	0.02	0.02
Pyrope	0.00	0.00	0.00	0.00	0.00	0.00	0.00	0.00	0.00	0.00
Almandine	0.00	0.03	0.06	0.00	0.03	0.02	0.01	0.04	0.04	0.05
Grossular	0.18	0.13	0.09	0.19	0.12	0.03	0.16	0.02	0.00	0.00
Andradite	0.79	0.78	0.77	0.73	0.80	0.82	0.73	0.84	0.77	0.82

	23	24	25	26	27	28	29
Analysis (wt%)	3516-PAAB01-C2-43	3516-PAAB01-C2-44	3516-PAAB01-C2-45	3516-PAAB01-C2-46	poab05-C4-01	poab05-C4-3	poab05-C4-4
SiO_2	36.30	36.62	32.41	36.08	36.01	35.00	35.34
TiO_2	0.42	0.41	0.89	1.77	0.43	0.39	0.48
Al_2O_3	1.78	1.76	1.25	1.84	3.01	2.55	2.46
FeO / FeO_{tot}	26.46	26.73	25.71	24.76	23.77	23.83	24.24
MnO	0.97	0.85	0.90	0.57	0.72	0.35	0.57
MgO	0.19	0.09	1.17	0.05	0.29	0.23	0.26
CaO	30.88	31.74	24.41	32.46	31.80	32.18	32.07
Na_2O	0.10	0.05	0.22	0.02	0.00	0.00	0.03
F	0.25	0.44	0.39	0.02	0.00	0.01	0.32
O=F (calc)	-0.10	-0.18	-0.16	-0.01		0.00	-0.13
Total (calc)	97.23	98.49	87.19	97.55	96.04	94.53	95.64
Recalculated (wt%)							
final FeO	2.69	2.67	4.65	2.40	1.43	0.21	0.73
final Fe_2O_3	26.42	26.73	23.41	24.84	24.82	26.26	26.13
final MnO	0.97	0.85	0.90	0.57	0.72	0.35	0.57
final Mn_2O_3	0.00	0.00	0.00	0.00	0.00	0.00	0.00
Total	99.87	101.16	89.54	100.04	98.51	97.17	98.26
TSi	3.00	3.00	3.00	3.00	3.00	3.00	2.99
Ti	0.03	0.03	0.00	0.11	0.03	0.02	0.03
Tal	0.00	0.00	0.00	0.00	0.00	0.00	0.00
Al	0.18	0.17	0.14	0.18	0.30	0.26	0.25
Fe2+VI	0.09	0.11	0.08	0.13	0.03	0.00	0.00
Fe2+	0.10	0.08	0.28	0.04	0.07	0.01	0.05
Fe3+	1.67	1.67	1.65	1.56	1.57	1.69	1.67
Mn2+	0.07	0.06	0.07	0.04	0.05	0.03	0.04
Mg	0.02	0.01	0.13	0.01	0.00	0.02	0.03
Ca	2.77	2.82	2.45	2.91	2.87	2.96	2.91
Na	0.02	0.01	0.04	0.00	0.00	0.00	0.00
End-members							
FCa garnet	0.01	0.01	0.01	0.00		0.00	0.01
Schorlomite-Al						0.00	
Morimotoite	0.03	0.03	0.06	0.11	0.03	0.01	0.03
NaTi garnet					0.00		
Spessartine	0.02	0.02	0.02	0.01	0.02	0.01	0.01
Pyrope	0.01	0.00	0.01	0.00	0.00	0.01	0.01
Almandine	0.03	0.03	0.03	0.01	0.02	0.00	0.00
Grossular	0.02	0.03	0.00	0.06	0.11	0.11	0.09
Andradite	0.83	0.83	0.74	0.78	0.79	0.85	0.83

3G: EPMA analyses of titanite. Recalculated formula on the basis of 5 oxygens

	1	2	3	4	5	6	7	8	9	10	11	12
Sample	8_11	8_11	8_11	8_11	8_11	8_11	8_11	8_11	8_11	8_11	8_11	8_11
Mineralization	UNM	UNM	UNM	UNM	UNM	UNM	UNM	UNM	UNM	UNM	UNM	UNM
Alteration	Mag	Mag	Mag	Mag	Mag	Mag	Mag	Mag	Mag	Mag	Mag	Mag
Anomaly	31	31	31	31	31	31	31	31	31	31	31	31
SiO2	31.45	30.95	30.71	31.15	31.20	30.83	31.08	31.44	31.05	31.32	31.19	31.21
TiO2	31.38	30.98	31.10	32.08	32.43	32.19	32.65	32.98	32.97	32.45	32.72	32.38
Al2O3	4.81	4.76	4.51	4.19	4.01	4.08	3.82	4.11	4.08	4.18	4.08	4.33
Fe2O3	1.33	1.59	1.31	1.23	1.57	1.50	1.71	1.73	1.49	1.49	1.39	1.29
MnO	0.09	0.07	0.06	0.12	0.07	0.03	0.00	0.06	0.06	0.15	0.05	0.07
MgO	0.01	0.00	0.01	0.02	0.00	0.00	0.00	0.00	0.00	0.01	0.04	0.00
CaO	28.28	27.21	26.81	26.05	27.26	27.54	27.86	28.15	28.03	27.48	26.93	26.95
Na2O	0.03	0.02	0.01	0.06	0.08	0.07	0.07	0.06	0.02	0.10	0.04	0.05
K2O	0.02	0.12	0.03	0.03	0.02	0.04	0.01	0.00	0.02	0.02	0.02	0.02
F	0	0	0	0	0	0	0	0	0	0	0	0
Cl	0.02	0.00	0.01	0.00	0.00	0.00	0.00	0.01	0.00	0.00	0.00	0.00
TOTAL	97.41	95.69	94.56	94.93	96.64	96.27	97.20	98.54	97.71	97.19	96.47	96.30
Si	1.05	1.05	1.05	1.06	1.05	1.04	1.04	1.04	1.03	1.05	1.05	1.05
Al	0.19	0.19	0.18	0.17	0.16	0.16	0.15	0.16	0.16	0.16	0.16	0.17
Ti	0.79	0.79	0.80	0.82	0.82	0.82	0.82	0.82	0.83	0.81	0.83	0.82
Fe	0.02	0.03	0.03	0.02	0.03	0.03	0.03	0.03	0.03	0.03	0.03	0.02
Mn	0.00	0.00	0.00	0.00	0.00	0.00	0.00	0.00	0.00	0.00	0.00	0.00
Mg	0.00	0.00	0.00	0.00	0.00	0.00	0.00	0.00	0.00	0.00	0.00	0.00
Ca	1.01	0.99	0.98	0.95	0.98	1.00	1.00	1.00	1.00	0.98	0.97	0.97
Na	0.00	0.00	0.00	0.00	0.01	0.00	0.00	0.00	0.00	0.01	0.00	0.00
K	0.00	0.01	0.00	0.00	0.00	0.00	0.00	0.00	0.00	0.00	0.00	0.00
F(at)	0.00	0.00	0.00	0.00	0.00	0.00	0.00	0.00	0.00	0.00	0.00	0.00
Cl	0.00	0.00	0.00	0.00	0.00	0.00	0.00	0.00	0.00	0.00	0.00	0.00
Al/Al+Ti+Fe	0.19	0.19	0.18	0.17	0.16	0.16	0.15	0.16	0.16	0.16	0.16	0.17
Total	3.06	3.05	3.05	3.03	3.04	3.05	3.05	3.05	3.05	3.05	3.04	3.04
Fe+Al	0.21	0.22	0.21	0.19	0.19	0.19	0.18	0.19	0.19	0.19	0.19	0.20
Al+Fe/TiO2	0.20	0.20	0.19	0.17	0.17	0.17	0.17	0.18	0.17	0.17	0.17	0.17
OH	-	-	-	-	-	-	-	-	-	-	-	-
Ttn	-	-	-	-	-	-	-	-	-	-	-	-
F(at)	-	-	-	-	-	-	-	-	-	-	-	-

	13	14	15	16	17	18	19	20	21	22	23	24	25
Sample	8_11	8_11	31BIAB	31BIAB	31BIAB	31BIAB	ALB03	ALB03	ALB03	ALB03	ALB03	ALB03	ALB03
Mineralization	UNM	UNM	MIN	MIN	MIN	MIN	UNM	UNM	UNM	UNM	UNM	UNM	UNM
Alteration	Mag	Mag	Ca-Mg	Ca-Mg	Ca-Mg	Ca-Mg	Ca-Mg	Ca-Mg	Ca-Mg	Ca-Mg	Ca-Mg	Ca-Mg	Ca-Mg
Anomaly	31	31	31	31	31	31	31	31	31	31	31	31	31
SiO2	31.43	31.39	30.11	30.68	30.45	30.56	31.10	31.37	30.74	31.35	30.78	31.05	31.44
TiO2	33.14	33.62	31.57	30.35	32.00	31.41	33.26	32.53	34.38	33.67	34.21	33.05	34.68
Al2O3	3.95	3.77	2.64	3.10	2.53	3.24	2.71	3.22	2.34	3.01	2.62	2.97	2.33
Fe2O3	1.61	2.02	2.13	2.34	2.61	2.35	2.08	2.37	2.08	2.07	1.98	2.17	1.78
MnO	0.13	0.12	0.00	0.05	0.00	0.02	0.09	0.00	0.02	0.06	0.01	0.10	0.10
MgO	0.00	0.00	0.05	0.07	0.01	0.03	0.00	0.01	0.00	0.00	0.03	0.00	0.00
CaO	27.52	27.44	27.71	28.02	28.08	28.29	27.97	28.02	28.44	28.53	28.15	28.05	28.11
Na2O	0.06	0.08	0.04	0.03	0.03	0.00	0.06	0.01	0.09	0.03	0.02	0.02	0.04
K2O	0.01	0.01	0.00	0.00	0.01	0.00	0.01	0.00	0.00	0.01	0.00	0.02	0.01
F	0	0	1.09	1.25	1.45	1.33	0.00	0.00	0.00	0.00	0.00	0.00	0.00
Cl	0.01	0.00	0.00	0.01	0.00	0.00	0.01	0.01	0.00	0.00	0.01	0.01	0.00
TOTAL	97.85	98.46	94.88	95.38	96.55	96.66	97.29	97.53	98.10	98.74	97.81	97.44	98.48
Si	1.04	1.04	1.02	1.03	1.01	1.01	1.04	1.05	1.03	1.04	1.03	1.04	1.04
Al	0.15	0.15	0.11	0.12	0.10	0.13	0.11	0.13	0.09	0.12	0.10	0.12	0.09
Ti	0.83	0.84	0.81	0.77	0.80	0.78	0.84	0.82	0.86	0.84	0.86	0.83	0.86
Fe	0.03	0.04	0.04	0.04	0.05	0.04	0.04	0.04	0.04	0.04	0.04	0.04	0.03
Mn	0.00	0.00	0.00	0.00	0.00	0.00	0.00	0.00	0.00	0.00	0.00	0.00	0.00
Mg	0.00	0.00	0.00	0.00	0.00	0.00	0.00	0.00	0.00	0.00	0.00	0.00	0.00
Ca	0.98	0.97	1.01	1.01	1.00	1.01	1.01	1.00	1.02	1.01	1.01	1.01	1.00
Na	0.00	0.01	0.00	0.00	0.00	0.00	0.00	0.00	0.01	0.00	0.00	0.00	0.00
K	0.00	0.00	0.00	0.00	0.00	0.00	0.00	0.00	0.00	0.00	0.00	0.00	0.00
F(at)	0.00	0.00	0.12	0.13	0.15	0.14	0.00	0.00	0.00	0.00	0.00	0.00	0.00
Cl	0.00	0.00	0.00	0.00	0.00	0.00	0.00	0.00	0.00	0.00	0.00	0.00	0.00
Al/Al+Ti+Fe	0.15	0.14	0.11	0.13	0.10	0.13	0.11	0.13	0.09	0.12	0.10	0.12	0.09
Total	3.04	3.04	3.10	3.12	3.11	3.12	3.04	3.05	3.05	3.05	3.04	3.05	3.03
Fe+Al	0.18	0.18	0.15	0.17	0.15	0.17	0.15	0.17	0.13	0.16	0.14	0.16	0.12
Al+Fe/TiO2	0.17	0.17	0.15	0.18	0.16	0.18	0.14	0.17	0.13	0.15	0.13	0.16	0.12
OH	-	-	0.03	0.03	-0.01	0.03	-	-	-	-	-	-	-
Ttn	-	-	0.85	0.83	0.85	0.83	-	-	-	-	-	-	-
F(at)	-	-	0.12	0.13	0.15	0.14	-	-	-	-	-	-	-

Sample	26 ALB03	27 ALB03	28 ALB03	29 ALB03	30 ALB03	31 ALB03	32 ALB03	33 ALB03	34 ALB03	35 ALB03	36 ALB03	37 ALB03
Mineralization	UNM	UNM	UNM	UNM	UNM	UNM	UNM	UNM	UNM	UNM	UNM	UNM
Alteration	Ca-Mg	Ca-Mg	Ca-Mg	Ca-Mg	Ca-Mg	Ca-Mg	Ca-Mg	Ca-Mg	Ca-Mg	Ca-Mg	Ca-Mg	Ca-Mg
Anomaly	31	31	31	31	31	31	31	31	31	31	31	31
SiO2	31.27	31.43	31.27	30.83	30.99	31.14	30.95	30.61	29.99	31.00	30.59	31.09
TiO2	34.72	32.97	35.40	36.83	35.41	35.50	36.34	37.42	36.23	36.06	36.68	36.64
Al2O3	2.34	2.94	1.61	1.23	1.84	2.01	1.77	1.24	1.76	1.72	1.29	1.14
Fe2O3	1.56	2.05	2.06	0.99	1.52	1.55	1.32	1.10	1.28	1.33	2.55	1.57
MnO	0.02	0.06	0.04	0.06	0.08	0.08	0.15	0.00	0.00	0.00	0.00	0.00
MgO	0.00	0.01	0.00	0.00	0.01	0.00	0.02	0.00	0.00	0.00	0.01	0.00
CaO	27.91	27.82	28.61	27.83	27.89	27.81	27.74	27.93	27.84	28.36	28.80	28.50
Na2O	0.02	0.06	0.05	0.07	0.06	0.10	0.09	0.08	0.00	0.00	0.00	0.00
K2O	0.00	0.01	0.01	0.00	0.02	0.03	0.03	0.00	0.00	0.00	0.00	0.00
F	0.00	0.00	0.00	0.00	0.00	0.00	0.00	0.00	0.00	0.00	0.00	0.00
Cl	0.00	0.00	0.00	0.00	0.01	0.00	0.00	0.00	0.01	0.00	0.01	0.01
TOTAL	97.84	97.35	99.05	97.84	97.81	98.21	98.42	98.37	97.18	98.47	99.98	98.99
Si	1.04	1.05	1.03	1.03	1.03	1.03	1.03	1.02	1.01	1.03	1.01	1.03
Al	0.09	0.12	0.06	0.05	0.07	0.08	0.07	0.05	0.07	0.07	0.05	0.04
Ti	0.87	0.83	0.88	0.92	0.89	0.89	0.91	0.93	0.92	0.90	0.91	0.91
Fe	0.03	0.04	0.04	0.02	0.03	0.03	0.02	0.02	0.02	0.02	0.05	0.03
Mn	0.00	0.00	0.00	0.00	0.00	0.00	0.00	0.00	0.00	0.00	0.00	0.00
Mg	0.00	0.00	0.00	0.00	0.00	0.00	0.00	0.00	0.00	0.00	0.00	0.00
Ca	1.00	1.00	1.01	0.99	1.00	0.99	0.99	0.99	1.00	1.01	1.02	1.01
Na	0.00	0.00	0.00	0.00	0.00	0.01	0.01	0.01	0.00	0.00	0.00	0.00
K	0.00	0.00	0.00	0.00	0.00	0.00	0.00	0.00	0.00	0.00	0.00	0.00
F(at)	0.00	0.00	0.00	0.00	0.00	0.00	0.00	0.00	0.00	0.00	0.00	0.00
Cl	0.00	0.00	0.00	0.00	0.00	0.00	0.00	0.00	0.00	0.00	0.00	0.00
Al/Al+Ti+Fe	0.09	0.12	0.06	0.05	0.07	0.08	0.07	0.05	0.07	0.07	0.05	0.05
Total	3.03	3.04	3.04	3.02	3.03	3.03	3.02	3.02	3.03	3.03	3.03	3.02
Fe+Al	0.12	0.15	0.10	0.07	0.10	0.11	0.09	0.07	0.09	0.09	0.10	0.07
Al+Fe/TiO2	0.11	0.15	0.10	0.06	0.09	0.10	0.08	0.06	0.08	0.08	0.10	0.07
OH	-	-	-	-	-	-	-	-	-	-	-	-
Ttn	-	-	-	-	-	-	-	-	-	-	-	-
F(at)	-	-	-	-	-	-	-	-	-	-	-	-

Sample	38 ALB03	39 ALB03	40 ALB03	41 ALB03	42 ALB03	43 ALB02	44 ALB02	45 ALB02	46 ALB02	47 ALB02	48 ALB02	49 ALB02
Mineralization	UNM	UNM	UNM	UNM	UNM	UNM	UNM	UNM	UNM	UNM	UNM	UNM
Alteration	Ca-Mg	Ca-Mg	Ca-Mg	Ca-Mg	Ca-Mg	Ca-Mg	Ca-Mg	Ca-Mg	Ca-Mg	Ca-Mg	Ca-Mg	Ca-Mg
Anomaly	31	31	31	31	31	31	31	31	31	31	31	31
SiO2	31.46	29.76	29.49	29.45	30.04	30.62	30.18	30.89	30.35	29.95	29.79	29.39
TiO2	35.55	35.68	38.09	37.30	35.98	36.50	36.35	37.86	37.86	37.74	36.81	36.16
Al2O3	1.54	2.16	0.57	1.99	1.46	1.05	0.80	0.70	0.77	0.87	1.20	1.45
Fe2O3	1.48	1.76	1.47	1.62	1.52	1.60	1.45	1.30	1.27	1.47	1.57	1.52
MnO	0.00	0.00	0.00	0.00	0.00	0.07	0.08	0.00	0.07	0.07	0.10	0.08
MgO	0.00	0.00	0.01	0.00	0.00	0.03	0.00	0.05	0.03	0.05	0.00	0.04
CaO	28.80	28.43	28.25	28.32	28.50	27.79	27.92	28.66	28.29	28.18	28.10	27.69
Na2O	0.00	0.00	0.00	0.00	0.00	0.06	0.09	0.03	0.05	0.04	0.04	0.07
K2O	0.00	0.00	0.00	0.00	0.00	0.01	0.01	0.00	0.02	0.01	0.02	0.01
F	0.00	0.00	0.00	0.00	0.00	0.44	0.13	0.22	0.41	0.50	0.39	0.53
Cl	0.01	0.00	0.00	0.00	0.01	0.00	0.00	0.00	0.00	0.00	0.01	0.00
TOTAL	98.87	97.80	97.87	98.68	97.50	97,979	97	99.64	98.94	98.68	97.87	96.70
Si	1.04	1.00	0.99	0.98	1.01	1.02	1.02	1.01	1.00	0.99	0.99	0.99
Al	0.06	0.09	0.02	0.08	0.06	0.04	0.03	0.03	0.03	0.03	0.05	0.06
Ti	0.88	0.90	0.96	0.93	0.91	0.91	0.92	0.93	0.94	0.94	0.92	0.92
Fe	0.03	0.03	0.03	0.03	0.03	0.03	0.03	0.02	0.02	0.03	0.03	0.03
Mn	0.00	0.00	0.00	0.00	0.00	0.00	0.00	0.00	0.00	0.00	0.00	0.00
Mg	0.00	0.00	0.00	0.00	0.00	0.00	0.00	0.00	0.00	0.00	0.00	0.00
Ca	1.02	1.02	1.02	1.01	1.03	0.99	1.01	1.01	1.00	1.00	1.00	1.00
Na	0.00	0.00	0.00	0.00	0.00	0.00	0.01	0.00	0.00	0.00	0.00	0.00
K	0.00	0.00	0.00	0.00	0.00	0.00	0.00	0.00	0.00	0.00	0.00	0.00
F(at)	0.00	0.00	0.00	0.00	0.00	0.05	0.01	0.02	0.04	0.05	0.04	0.06
Cl	0.00	0.00	0.00	0.00	0.00	0.00	0.00	0.00	0.00	0.00	0.00	0.00
Al/Al+Ti+Fe	0.06	0.08	0.02	0.07	0.06	0.04	0.03	0.03	0.03	0.03	0.05	0.06
Total	3.03	3.04	3.02	3.03	3.04	3.04	3.03	3.03	3.04	3.04	3.05	3.05
Fe+Al	0.09	0.12	0.05	0.11	0.09	0.07	0.06	0.05	0.05	0.06	0.08	0.09
Al+Fe/TiO2	0.08	0.11	0.05	0.10	0.08	0.07	0.06	0.05	0.05	0.06	0.08	0.08
OH	-	-	-	-	-	0.03	0.05	0.03	0.01	0.01	0.04	0.03
Ttn	-	-	-	-	-	0.93	0.94	0.95	0.95	0.94	0.92	0.91
F(at)	-	-	-	-	-	0.05	0.01	0.02	0.04	0.05	0.04	0.06

	50	51	52	53	54	55	56	57	58	59	60	61
Sample	ALB02	3409GNA01	3409GNA01	3409GNA01	3409GNA01	3409GNA01	GALB04	GALB04	GALB04	GALB04	GALB04	GALB04
Mineralization	UNM	UNM	UNM	UNM	UNM	UNM	UNM	UNM	UNM	UNM	UNM	UNM
Alteration	Ca-Mg	Mag	Mag	Mag	Mag	Mag	Ca-Fe	Ca-Fe	Ca-Fe	Ca-Fe	Ca-Fe	Ca-Fe
Anomaly	31	34	34	34	34	34	34	34	34	34	34	34
SiO2	30.68	31.19	29.77	29.74	30.92	28.19	30.04	30.49	30.75	30.03	30.29	30.00
TiO2	35.65	29.06	29.77	28.93	29.05	31.27	30.47	30.93	30.07	31.02	30.02	31.91
Al2O3	1.63	6.93	7.14	7.30	6.85	6.05	3.97	4.17	4.23	3.95	4.18	3.87
Fe2O3	1.40	1.31	1.09	1.28	1.17	1.17	3.16	3.10	3.01	3.40	3.32	2.96
MnO	0.09	0.11	0.08	0.18	0.13	0.19	0.05	0.00	0.04	0.03	0.00	0.03
MgO	0.01	0.00	0.00	0.00	0.01	0.00	0.01	0.00	0.00	0.02	0.02	0.01
CaO	27.81	27.89	28.00	27.51	27.25	28.35	27.81	28.21	28.19	28.19	28.34	28.46
Na2O	0.07	0.05	0.07	0.08	0.09	0.09	0.06	0.06	0.03	0.05	0.00	0.07
K2O	0.01	0.01	0.02	0.01	0.01	0.02	0.00	0.01	0.01	0.00	0.00	0.02
F	0.56	2.81	2.04	1.96	1.78	1.55	1.90	1.58	2.04	1.55	2.18	1.31
Cl	0.00	0.00	0.00	0.01	0.01	0.00	0.00	0.00	0.00	0.01	0.00	0.01
TOTAL	97.67	98,184	97,104	96,168	96,506	96,213	96,663	97,875	97,495	97,579	97,428	98,086
Si	1.02	0.98	0.96	0.97	1.01	0.94	0.99	1.00	1.00	0.99	0.99	0.99
Al	0.06	0.26	0.27	0.28	0.26	0.24	0.15	0.16	0.16	0.15	0.16	0.15
Ti	0.89	0.69	0.72	0.71	0.71	0.78	0.76	0.76	0.74	0.77	0.74	0.79
Fe	0.03	0.02	0.02	0.02	0.02	0.02	0.06	0.06	0.05	0.06	0.06	0.05
Mn	0.00	0.00	0.00	0.01	0.00	0.01	0.00	0.00	0.00	0.00	0.00	0.00
Mg	0.00	0.00	0.00	0.00	0.00	0.00	0.00	0.00	0.00	0.00	0.00	0.00
Ca	0.99	0.94	0.97	0.96	0.95	1.01	0.98	0.99	0.98	0.99	0.99	1.00
Na	0.00	0.00	0.00	0.01	0.01	0.01	0.00	0.00	0.00	0.00	0.00	0.00
K	0.00	0.00	0.00	0.00	0.00	0.00	0.00	0.00	0.00	0.00	0.00	0.00
F(at)	0.06	0.28	0.21	0.20	0.18	0.16	0.20	0.16	0.21	0.16	0.22	0.14
Cl	0.00	0.00	0.00	0.00	0.00	0.00	0.00	0.00	0.00	0.00	0.00	0.00
Al/Al+Ti+Fe	0.07	0.27	0.27	0.28	0.26	0.23	0.16	0.16	0.17	0.16	0.17	0.15
Total	3.05	3.19	3.17	3.17	3.14	3.16	3.15	3.13	3.15	3.14	3.16	3.12
Fe+Al	0.09	0.28	0.29	0.30	0.28	0.26	0.21	0.22	0.22	0.22	0.22	0.20
Al+Fe/TiO2	0.08	0.28	0.28	0.30	0.28	0.23	0.23	0.23	0.24	0.24	0.25	0.21
OH	0.03	0.00	0.08	0.10	0.10	0.10	0.01	0.05	0.01	0.05	0.00	0.07
Ttn	0.91	0.72	0.71	0.70	0.72	0.74	0.79	0.78	0.78	0.78	0.78	0.80
F(at)	0.06	0.28	0.21	0.20	0.18	0.16	0.20	0.16	0.21	0.16	0.22	0.14

	62	63	64	65	66	67	68	69	70	71	72	73
Sample	GALB 04	GALB 04	GALB 04	MALB 02	MALB 02	MALB 02	MALB 02	MALB 02	MALB 02	BALB 02	BALB 02	BALB 02
Mineralization	UNM	UNM	UNM	UNM	UNM	UNM	UNM	UNM	UNM	MIN	MIN	MIN
Alteration	Ca-Fe	Ca-Fe	Ca-Fe	Ca-Fe	Ca-Fe	Ca-Fe	Ca-Fe	Ca-Fe	Ca-Fe	Ca-Mg	Ca-Mg	Ca-Mg
Anomaly	34	34	34	34	34	34	34	34	34	34	34	34
SiO2	30.20	30.78	29.01	31.13	31.00	31.22	30.77	31.04	31.04	30.12	29.65	30.02
TiO2	29.80	31.32	31.00	27.41	28.26	27.71	27.10	28.62	27.86	35.57	35.39	35.63
Al2O3	4.55	3.82	4.04	5.80	5.40	5.50	6.29	6.42	5.66	1.42	0.71	0.90
Fe2O3	3.32	2.95	3.83	2.87	3.16	3.13	2.89	2.39	2.57	1.76	2.70	2.29
MnO	0.09	0.17	0.07	0.19	0.25	0.28	0.22	0.19	0.27	0.01	0.02	0.00
MgO	0.03	0.00	0.00	0.05	0.02	0.01	0.00	0.03	0.00	0.02	0.19	0.04
CaO	28.82	28.43	27.10	27.46	26.34	26.56	26.33	26.44	26.39	25.99	26.11	26.66
Na2O	0.04	0.05	0.05	0.06	0.08	0.07	0.06	0.11	0.07	0.18	0.09	0.20
K2O	0.01	0.00	0.04	0.03	0.01	0.02	0.01	0.00	0.01	0.01	0.05	0.00
F	1.76	1.50	1.27	2.16	2.31	1.89	1.58	2.37	1.65	0.51	0.73	0.41
Cl	0.00	0.01	0.00	0.02	0.01	0.01	0.01	0.00	0.00	0.00	0.01	0.05
TOTAL	97,865	98,378	95,875	96.26	95.87	95.59	94.58	96.61	94.82	95	95	96
Si	0.99	1.00	0.98	1.02	1.02	1.03	1.03	1.00	1.04	1.02	1.01	1.02
Al	0.18	0.15	0.16	0.22	0.21	0.21	0.25	0.24	0.22	0.06	0.03	0.04
Ti	0.73	0.77	0.79	0.67	0.70	0.69	0.68	0.70	0.70	0.91	0.91	0.91
Fe	0.06	0.05	0.07	0.05	0.06	0.06	0.05	0.04	0.05	0.03	0.05	0.04
Mn	0.00	0.00	0.00	0.01	0.01	0.01	0.01	0.01	0.01	0.00	0.00	0.00
Mg	0.00	0.00	0.00	0.00	0.00	0.00	0.00	0.00	0.00	0.00	0.01	0.00
Ca	1.01	0.99	0.98	0.96	0.92	0.94	0.94	0.92	0.94	0.94	0.95	0.97
Na	0.00	0.00	0.00	0.00	0.00	0.00	0.00	0.01	0.00	0.01	0.01	0.01
K	0.00	0.00	0.00	0.00	0.00	0.00	0.00	0.00	0.00	0.00	0.00	0.00
F(at)	0.18	0.15	0.14	0.22	0.24	0.20	0.17	0.24	0.17	0.05	0.08	0.04
Cl	0.00	0.00	0.00	0.00	0.00	0.00	0.00	0.00	0.00	0.00	0.00	0.00
Al/Al+Ti+Fe	0.18	0.15	0.16	0.24	0.22	0.22	0.25	0.25	0.23	0.06	0.03	0.04
Total	3.16	3.13	3.12	3.17	3.16	3.15	3.14	3.16	3.13	3.03	3.05	3.04
Fe+Al	0.24	0.20	0.23	0.28	0.27	0.27	0.30	0.29	0.27	0.09	0.08	0.08
Al+Fe/TiO2	0.26	0.22	0.25	0.32	0.30	0.31	0.34	0.31	0.30	0.09	0.10	0.09
OH	0.05	0.05	0.10	0.05	0.03	0.07	0.13	0.04	0.10	0.04	0.00	0.04
Ttn	0.76	0.80	0.77	0.72	0.73	0.73	0.70	0.71	0.73	0.91	0.92	0.92
F(at)	0.18	0.15	0.14	0.22	0.24	0.20	0.17	0.24	0.17	0.05	0.08	0.04

	74	75	76	77	78	79	80	81	82	83	84	85
Sample	BALB02	BALB02	BALB02	BALB02	BALB02	BALB02	BALB02	BALB02	GRA01	GRA01	GRA01	GRA01
Mineralization	MIN	MIN	MIN	MIN	MIN	MIN	MIN	MIN	UNM	UNM	UNM	UNM
Alteration	Ca-Mg	Ca-Mg	Ca-Mg	Ca-Mg	Ca-Mg	Ca-Mg	Ca-Mg	Ca-Mg	Mag	Mag	Mag	Mag
Anomaly	34	34	34	34	34	34	34	34	35	35	35	35
SiO2	27.70	29.83	24.36	27.53	28.67	31.16	31.32	31.65	31.34	31.75	30.63	31.11
TiO2	34.88	35.28	34.64	35.73	34.78	38.42	37.25	37.10	31.56	31.04	32.90	32.69
Al2O3	1.36	1.29	1.22	1.39	1.38	0.42	0.62	0.73	4.61	5.10	4.55	4.47
Fe2O3	2.00	1.99	2.05	1.98	2.28	1.20	1.59	1.24	1.32	1.57	1.64	1.40
MnO	0.06	0.03	0.00	0.01	0.11	0.00	0.03	0.08	0.00	0.00	0.00	0.00
MgO	0.01	0.03	0.00	0.02	0.01	0.00	0.00	0.01	0.01	0.02	0.03	0.00
CaO	26.17	24.35	26.91	26.68	25.34	27.79	27.83	28.33	28.51	28.40	28.03	28.06
Na2O	0.13	0.18	0.12	0.13	0.14	0.10	0.09	0.13	0.08	0.12	0.04	0.02
K2O	0.00	0.01	0.01	0.01	0.00	0.01	0.00	0.01	0.00	0.00	0.01	0.02
F	0.20	0.00	0.72	0.35	0.33	0.29	0.37	0.38	1.69	1.95	1.33	1.36
Cl	0.00	0.00	0.01	0.00	0.01	0.00	0.00	0.01	0.01	0.00	0.01	0.00
TOTAL	92	93	90	94	93	99	99	100	97.41	95.69	94.93	96.64
Si	0.98	1.04	0.90	0.96	1.01	1.02	1.03	1.03	1.01	1.01	0.99	1.00
Al	0.06	0.05	0.05	0.06	0.06	0.02	0.02	0.03	0.17	0.19	0.17	0.17
Ti	0.93	0.93	0.96	0.94	0.92	0.95	0.92	0.91	0.76	0.74	0.80	0.79
Fe	0.04	0.04	0.04	0.04	0.04	0.02	0.03	0.02	0.02	0.03	0.03	0.03
Mn	0.00	0.00	0.00	0.00	0.00	0.00	0.00	0.00	0.00	0.00	0.00	0.00
Mg	0.00	0.00	0.00	0.00	0.00	0.00	0.00	0.00	0.00	0.00	0.00	0.00
Ca	1.00	0.91	1.06	1.00	0.95	0.98	0.98	0.99	0.98	0.97	0.97	0.97
Na	0.01	0.01	0.01	0.01	0.01	0.01	0.01	0.01	0.00	0.01	0.00	0.00
K	0.00	0.00	0.00	0.00	0.00	0.00	0.00	0.00	0.00	0.00	0.00	0.00
F(at)	0.02	0.00	0.08	0.04	0.04	0.03	0.04	0.04	0.17	0.20	0.14	0.14
Cl	0.00	0.00	0.00	0.00	0.00	0.00	0.00	0.00	0.00	0.00	0.00	0.00
Total	3.04	2.99	3.10	3.05	3.03	3.02	3.03	3.04	3.13	3.14	3.11	3.11
Fe+Al	0.10	0.09	0.09	0.10	0.10	0.04	0.05	0.05	0.20	0.22	0.20	0.20
OH	0.07	0.09	0.01	0.06	0.07	0.01	0.01	0.01	0.03	0.02	0.07	0.06
Ttn	0.90	0.91	0.91	0.90	0.90	0.96	0.95	0.95	0.80	0.78	0.80	0.80
F(at)	0.02	0.00	0.08	0.04	0.04	0.03	0.04	0.04	0.17	0.20	0.14	0.14

Sample	86 GRA01	87 GRA01	88 GRA01	89 GRA01	90 GRA01	91 GRA01	92 GRA01	93 GRA01	94 GRA01	95 5-8a	96 5-8a	97 5-8a
Mineralization	UNM	UNM	UNM	UNM	UNM	UNM	UNM	UNM	UNM	UNM	UNM	UNM
Alteration	Mag	Mag	Mag	Mag	Mag	Mag	Mag	Mag	Mag	Mag	Mag	Mag
Anomaly	35	35	35	35	35	35	35	35	35	35	35	35
SiO2	30.38	30.90	29.64	31.42	30.26	30.69	31.26	31.00	31.10	30.99	32.03	29.95
TiO2	31.61	30.26	29.91	29.50	31.89	31.32	31.03	30.77	30.84	30.47	30.78	31.56
Al2O3	4.60	4.78	5.01	6.42	4.57	4.72	5.00	5.29	5.79	3.63	3.94	3.56
Fe2O3	1.37	1.29	1.73	1.13	1.16	1.39	1.51	1.40	1.63	2.06	2.20	2.39
MnO	0.00	0.00	0.00	0.00	0.00	0.00	0.00	0.00	0.00	0	0	0
MgO	0.00	0.02	0.05	0.01	0.00	0.00	0.05	0.04	0.03	0.00	0.01	0.00
CaO	28.27	28.57	27.53	28.92	27.91	28.22	28.12	28.49	28.75	28.35	28.72	28.17
Na2O	0.03	0.12	0.15	0.08	0.05	0.13	0.13	0.09	0.10	0	0	0
K2O	0.00	0.00	0.02	0.00	0.00	0.00	0.02	0.00	0.01	0	0	0
F	1.20	1.03	0.94	1.84	1.39	2.05	1.35	1.90	1.50	0	0	0
Cl	0.00	0.01	0.00	0.00	0.00	0.01	0.02	0.00	0.00	0.00	0.01	0.01
TOTAL	96.27	97.20	98.54	97.71	97.19	96.30	97.85	98.46	96.86	95.58	97.75	95.63
Si	1.00	1.02	1.01	1.00	1.00	0.99	1.02	1.00	1.00	1.06	1.07	1.03
Al	0.18	0.19	0.20	0.24	0.18	0.18	0.19	0.20	0.22	0.15	0.15	0.14
Ti	0.78	0.75	0.76	0.71	0.79	0.76	0.76	0.74	0.74	0.78	0.77	0.81
Fe	0.03	0.02	0.03	0.02	0.02	0.03	0.03	0.03	0.03	0.04	0.04	0.05
Mn	0.00	0.00	0.00	0.00	0.00	0.00	0.00	0.00	0.00	0.00	0.00	0.00
Mg	0.00	0.00	0.00	0.00	0.00	0.00	0.00	0.00	0.00	0.00	0.00	0.00
Ca	1.00	1.01	1.00	0.99	0.98	0.98	0.98	0.98	0.99	1.04	1.03	1.03
Na	0.00	0.01	0.01	0.00	0.00	0.01	0.01	0.01	0.01	0.00	0.00	0.00
K	0.00	0.00	0.00	0.00	0.00	0.00	0.00	0.00	0.00	0.00	0.00	0.00
F(at)	0.13	0.11	0.10	0.19	0.15	0.21	0.14	0.19	0.15	0.00	0.00	0.00
Cl	0.00	0.00	0.00	0.00	0.00	0.00	0.00	0.00	0.00	0.00	0.00	0.00
Total	3.11	3.12	3.12	3.16	3.12	3.15	3.12	3.15	3.14	3.07	3.06	3.06
Fe+Al	0.20	0.21	0.23	0.26	0.20	0.20	0.22	0.23	0.25	0.19	0.20	0.19
OH	0.08	0.10	0.13	0.08	0.05	-0.01	0.08	0.03	0.10	-	-	-
Ttn	0.80	0.79	0.77	0.74	0.80	0.80	0.78	0.77	0.75	-	-	-
F(at)	0.13	0.11	0.10	0.19	0.15	0.21	0.14	0.19	0.15	-	-	-

	98	99	100	101	102	103	104	105	106	107	108	109
Sample	5-8a	5-8a	5-8a	5-8a	5-8a	5-8a	5-8a	5-8a	5-8a	5-8a	5-8a	5-8a
Mineralization	UNM	UNM	UNM	UNM	UNM	UNM	UNM	UNM	UNM	UNM	UNM	UNM
Alteration	Mag	Mag	Mag	Mag	Mag	Mag	Mag	Mag	Mag	Mag	Mag	Mag
Anomaly	35	35	35	35	35	35	35	35	35	35	35	35
SiO2	31.10	31.01	31.33	31.63	30.99	28.71	31.71	30.36	31.14	30.61	28.81	30.93
TiO2	30.03	30.09	31.18	29.43	31.84	31.83	30.72	31.00	31.67	30.71	29.89	30.78
Al2O3	3.53	4.15	3.77	4.28	4.18	3.91	4.22	4.76	4.19	4.09	4.68	4.23
Fe2O3	2.20	2.08	1.88	2.10	1.72	2.26	2.30	1.88	1.64	1.86	1.93	2.23
MnO	0	0	0	0	0	0	0	0	0	0	0	0
MgO	0.00	0.00	0.00	0.00	0.00	0.00	0.00	0.00	0.01	0.00	0.01	0.00
CaO	28.08	28.60	28.49	28.60	29.28	28.23	28.69	28.63	28.56	28.73	28.66	28.32
Na2O	0	0	0	0	0	0	0	0	0	0	0	0
K2O	0	0	0	0	0	0	0	0	0	0	0	0
F	0	0	0	0	0	0	0	0	0	0	0	0
Cl	0.01	0.00	0.01	0.00	0.00	0.00	0.00	0.00	0.00	0.00	0.02	0.00
TOTAL	94.95	95.94	96.71	96.05	98.02	95.01	97.65	96.66	97.21	96.11	94.06	96.58
Si	1.07	1.05	1.06	1.07	1.03	0.99	1.06	1.03	1.04	1.04	1.01	1.05
Al	0.14	0.17	0.15	0.17	0.16	0.16	0.17	0.19	0.17	0.16	0.19	0.17
Ti	0.78	0.77	0.79	0.75	0.80	0.83	0.77	0.79	0.80	0.79	0.78	0.78
Fe	0.04	0.04	0.04	0.04	0.03	0.04	0.04	0.04	0.03	0.04	0.04	0.04
Mn	0.00	0.00	0.00	0.00	0.00	0.00	0.00	0.00	0.00	0.00	0.00	0.00
Mg	0.00	0.00	0.00	0.00	0.00	0.00	0.00	0.00	0.00	0.00	0.00	0.00
Ca	1.03	1.04	1.03	1.04	1.05	1.05	1.03	1.04	1.02	1.05	1.07	1.03
Na	0.00	0.00	0.00	0.00	0.00	0.00	0.00	0.00	0.00	0.00	0.00	0.00
K	0.00	0.00	0.00	0.00	0.00	0.00	0.00	0.00	0.00	0.00	0.00	0.00
F(at)	0.00	0.00	0.00	0.00	0.00	0.00	0.00	0.00	0.00	0.00	0.00	0.00
Cl	0.00	0.00	0.00	0.00	0.00	0.00	0.00	0.00	0.00	0.00	0.00	0.00
Total	3.06	3.07	3.06	3.07	3.07	3.07	3.07	3.07	3.06	3.07	3.09	3.07
Fe+Al	0.18	0.21	0.19	0.21	0.20	0.20	0.21	0.22	0.20	0.20	0.23	0.21
OH	-	-	-	-	-	-	-	-	-	-	-	-
Ttn	-	-	-	-	-	-	-	-	-	-	-	-
F(at)	-	-	-	-	-	-	-	-	-	-	-	-

	110	111	112	113	114	115	116	117	118	119	120	121
Sample	5-8a	5-8a	5-8a	5-8a	5-8a	5-8a	5-8a	5-1B	5-1B	5-1B	9_4	9_4
Mineralization	UNM	UNM	UNM	UNM	UNM	UNM	UNM	UNM	UNM	UNM	UNM	UNM
Alteration	Mag	Mag	Mag	Mag	Mag	Mag	Mag	Mag	Mag	Mag	Mag	Mag
Anomaly	35	35	35	35	35	35	35	35	35	35	35	35
SiO2	30.94	30.92	31.96	31.62	31.05	31.27	31.54	30.77	31.21	31.49	31.21	31.23
TiO2	28.62	29.55	27.98	30.29	28.64	31.69	31.08	29.20	29.58	30.93	32.35	30.80
Al2O3	5.25	4.72	5.92	4.23	5.06	3.94	3.97	6.55	5.17	4.77	4.61	5.61
Fe2O3	1.55	1.57	1.65	1.29	1.94	1.95	2.28	1.32	1.87	1.59	1.26	1.59
MnO	0	0	0	0	0	0.11	0.10	0.12	0.08	0.04	0	0
MgO	0.00	0.00	0.00	0.00	0.00	0.00	0.00	0.00	0.00	0.00	0.02	0.00
CaO	28.99	28.76	29.69	28.95	28.37	28.27	28.43	29.07	28.25	28.36	29.23	29.09
Na2O	0	0	0	0	0	0.13	0.11	0.01	0.11	0.07	0.06	0.05
K2O	0	0	0	0	0	0.01	0.01	0.00	0.01	0.00	0.02	0.00
F	0	0	0	0	0	0.95	1.94	2.50	1.85	1.88	0.77	1.67
Cl	0.01	0.00	0.00	0.01	0.01	0.01	0.00	0.01	0.02	0.01	0.00	0.01
TOTAL	95.37	95.52	97.20	96.39	95.07	97.91	98.65	98.50	97.35	98.36	95.79	96.73
Si	1.06	1.05	1.07	1.07	1.06	1.03	1.01	0.98	1.01	1.01	1.01	1.00
Al	0.21	0.19	0.23	0.17	0.20	0.15	0.15	0.25	0.20	0.18	0.18	0.21
Ti	0.73	0.76	0.70	0.77	0.74	0.78	0.75	0.70	0.72	0.75	0.79	0.74
Fe	0.03	0.03	0.03	0.02	0.04	0.04	0.04	0.02	0.03	0.03	0.02	0.03
Mn	0.00	0.00	0.00	0.00	0.00	0.00	0.00	0.00	0.00	0.00	0.00	0.00
Mg	0.00	0.00	0.00	0.00	0.00	0.00	0.00	0.00	0.00	0.00	0.00	0.00
Ca	1.06	1.05	1.06	1.05	1.04	0.99	0.98	0.99	0.98	0.98	1.02	1.00
Na	0.00	0.00	0.00	0.00	0.00	0.01	0.01	0.00	0.01	0.00	0.00	0.00
K	0.00	0.00	0.00	0.00	0.00	0.00	0.00	0.00	0.00	0.00	0.00	0.00
F(at)	0.00	0.00	0.00	0.00	0.00	0.10	0.20	0.25	0.19	0.19	0.08	0.17
Cl	0.00	0.00	0.00	0.00	0.00	0.00	0.00	0.00	0.00	0.00	0.00	0.00
Total	3.09	3.08	3.10	3.07	3.08	3.10	3.14	3.19	3.15	3.14	3.10	3.14
Fe+Al	0.24	0.22	0.26	0.19	0.24	0.19	0.19	0.27	0.23	0.21	0.20	0.24
OH	-	-	-	-	-	0.09	-0.01	0.02	0.04	0.02	0.12	0.07
Ttn	-	-	-	-	-	0.81	0.81	0.73	0.77	0.79	0.80	0.76
F(at)	-	-	-	-	-	0.10	0.20	0.25	0.19	0.19	0.08	0.17

	122	123	124	125	126	127	128	129	130	131	132	133	134
Sample	9_4	9_4	9_4	9_4	9_4	9_4	9_4	9_4	9_4	9_4	GNA05	GNA05	GNA05
Mineralization	UNM	UNM	UNM	UNM	UNM	UNM	UNM	UNM	UNM	UNM	UNM	UNM	UNM
Alteration	Mag	Mag	Mag	Mag	Mag	Mag	Mag	Mag	Mag	Mag	Mag	Mag	Mag
Anomaly	35	35	35	35	35	35	35	35	35	35	35	35	35
SiO2	32.03	30.53	30.99	31.64	31.26	31.33	31.35	30.82	30.78	31.10	30.18	30.09	30.40
TiO2	32.92	31.46	30.57	30.67	31.41	32.26	31.60	31.48	33.06	32.00	33.56	33.37	33.14
Al2O3	5.21	5.29	6.07	5.76	5.10	4.59	5.52	4.71	5.02	5.03	2.91	2.97	3.09
Fe2O3	0.91	1.44	1.53	1.44	1.39	2.01	1.19	1.64	1.31	1.38	2.12	1.81	1.89
MnO	0	0	0	0	0	0	0	0	0	0	0	0	0
MgO	0.00	0.00	0.00	0.02	0.00	0.01	0.02	0.00	0.00	0.27	0.00	0.00	0.00
CaO	29.54	28.28	28.77	29.17	29.28	29.09	29.48	29.00	28.44	28.44	28.01	28.05	28.25
Na2O	0.00	0.09	0.05	0.04	0.06	0.11	0.05	0.02	0.42	0.00	0	0	0
K2O	0.02	0.02	0.00	0.01	0.00	0.00	0.01	0.03	0.00	0.00	0	0	0
F	1.65	1.48	1.88	1.66	2.18	1.44	1.71	2.03	1.69	1.59	0	0	0
Cl	0.00	0.00	0.00	0.01	0.00	0.00	0.00	0.00	0.01	0.00	0.00	0.00	0.00
TOTAL	96.47	94.98	96.10	96.05	95.70	95.84	94.93	96.01	96.39	95.07	96.90	96.31	96.79
Si	1.00	0.99	0.99	1.00	0.99	1.00	0.99	0.99	0.98	1.00	1.02	1.02	1.03
Al	0.19	0.20	0.23	0.22	0.19	0.17	0.21	0.18	0.19	0.19	0.12	0.12	0.12
Ti	0.77	0.77	0.73	0.73	0.75	0.77	0.75	0.76	0.79	0.77	0.85	0.85	0.84
Fe	0.02	0.03	0.03	0.03	0.02	0.04	0.02	0.03	0.02	0.02	0.04	0.03	0.04
Mn	0.00	0.00	0.00	0.00	0.00	0.00	0.00	0.00	0.00	0.00	0.00	0.00	0.00
Mg	0.00	0.00	0.00	0.00	0.00	0.00	0.00	0.00	0.00	0.01	0.00	0.00	0.00
Ca	0.99	0.98	0.98	0.99	0.99	0.99	1.00	0.99	0.97	0.97	1.02	1.02	1.02
Na	0.00	0.01	0.00	0.00	0.00	0.01	0.00	0.00	0.03	0.00	0.00	0.00	0.00
K	0.00	0.00	0.00	0.00	0.00	0.00	0.00	0.00	0.00	0.00	0.00	0.00	0.00
F(at)	0.16	0.15	0.19	0.17	0.22	0.15	0.17	0.21	0.17	0.16	0.00	0.00	0.00
Cl	0.00	0.00	0.00	0.00	0.00	0.00	0.00	0.00	0.00	0.00	0.00	0.00	0.00
Total	3.13	3.13	3.15	3.14	3.16	3.13	3.14	3.15	3.14	3.13	3.05	3.05	3.05
Fe+Al	0.21	0.23	0.26	0.24	0.21	0.21	0.23	0.21	0.21	0.21	0.16	0.15	0.16
OH	0.04	0.08	0.07	0.07	0.00	0.06	0.06	0.00	0.04	0.05	-	-	-
Ttn	0.79	0.77	0.74	0.76	0.79	0.79	0.77	0.79	0.79	0.79	-	-	-
F(at)	0.16	0.15	0.19	0.17	0.22	0.15	0.17	0.21	0.17	0.16	-	-	-

Sample	135 GNA05	136 GNA05	137 GNA05	138 GNA05	139 GNA05	140 GNA05	141 GNA05	142 GNA05	143 GNA05	144 GNA02	145 GNA02	146 GNA02	147 GNA02
Mineralization	UNM	UNM	UNM	UNM	UNM	UNM	UNM	UNM	UNM	UNM	UNM	UNM	UNM
Alteration	Mag	Mag	Mag	Mag	Mag	Mag	Mag	Mag	Mag	Mag	Mag	Mag	Mag
Anomaly	35	35	35	35	35	35	35	35	35	35	35	35	35
SiO2	30.46	30.90	30.42	30.27	30.52	30.78	30.60	30.29	30.79	31.69	31.17	31.93	31.81
TiO2	33.33	31.65	31.84	32.43	33.10	33.39	33.25	33.58	33.15	31.77	32.23	30.33	33.95
Al2O3	3.05	4.05	3.76	3.28	3.97	3.84	3.18	3.41	3.82	4.31	4.10	4.72	3.20
Fe2O3	2.08	2.08	1.94	2.10	1.68	1.51	1.87	1.58	1.95	2.27	2.39	2.68	2.12
MnO	0	0	0	0	0	0	0	0	0	0.29	0.09	0.08	0.17
MgO	0.00	0.00	0.00	0.00	0.00	0.00	0.00	0.00	0.00	0.05	0.03	0.02	0.00
CaO	28.23	28.45	28.69	27.96	28.75	28.86	28.47	28.74	28.47	28.64	28.57	28.92	28.79
Na2O	0	0	0	0	0	0	0	0	0	0.08	0.09	0.05	0.09
K2O	0	0	0	0	0	0	0	0	0	0.03	0.01	0.01	0.00
F	0	0	0	0	0	0	0	0	0	1.83	2.04	1.69	1.55
Cl	0.00	0.00	0.01	0.00	0.00	0.00	0.00	0.01	0.00	0.00	0.00	0.00	0.00
TOTAL	97.20	97.19	96.66	96.03	98.07	98.49	97.44	97.62	98.18	#####	99,853	99,720	#####
Si	1.03	1.04	1.03	1.03	1.02	1.02	1.03	1.01	1.02	1.01	0.99	1.02	1.01
Al	0.12	0.16	0.15	0.13	0.16	0.15	0.13	0.13	0.15	0.16	0.15	0.18	0.12
Ti	0.84	0.80	0.81	0.83	0.83	0.83	0.84	0.85	0.83	0.76	0.77	0.73	0.81
Fe	0.04	0.04	0.04	0.04	0.03	0.03	0.04	0.03	0.04	0.04	0.04	0.05	0.04
Mn	0.00	0.00	0.00	0.00	0.00	0.00	0.00	0.00	0.00	0.01	0.00	0.00	0.00
Mg	0.00	0.00	0.00	0.00	0.00	0.00	0.00	0.00	0.00	0.00	0.00	0.00	0.00
Ca	1.02	1.02	1.04	1.02	1.03	1.03	1.02	1.03	1.01	0.97	0.97	0.99	0.98
Na	0.00	0.00	0.00	0.00	0.00	0.00	0.00	0.00	0.00	0.00	0.01	0.00	0.01
K	0.00	0.00	0.00	0.00	0.00	0.00	0.00	0.00	0.00	0.00	0.00	0.00	0.00
F(at)	0.00	0.00	0.00	0.00	0.00	0.00	0.00	0.00	0.00	0.18	0.20	0.17	0.16
Cl	0.00	0.00	0.00	0.00	0.00	0.00	0.00	0.00	0.00	0.00	0.00	0.00	0.00
Total	3.05	3.06	3.07	3.05	3.06	3.06	3.05	3.06	3.05	3.14	3.14	3.14	3.11
Fe+Al	0.16	0.20	0.19	0.17	0.19	0.18	0.16	0.16	0.19	0.20	0.20	0.23	0.16
OH	-	-	-	-	-	-	-	-	-	0.02	-0.01	0.05	0.00
Ttn	-	-	-	-	-	-	-	-	-	0.80	0.80	0.77	0.84
F(at)	-	-	-	-	-	-	-	-	-	0.18	0.20	0.17	0.16

	148	149	150	151	152	153	154	155	156	157	158	159	160
Sample	7-1B	7-1B	7-1B	7-1B	7-1B	7-1B	7-9B	7-9B	7-9B	7-9B	7-9B	7-9B	7-9B
Mineralization	UNM	UNM	UNM	UNM	UNM	UNM	UNM	UNM	UNM	UNM	UNM	UNM	UNM
Alteration	Ca-Fe	Ca-Fe	Ca-Fe	Ca-Fe	Ca-Fe	Ca-Fe	Ca-Fe	Ca-Fe	Ca-Fe	Ca-Fe	Ca-Fe	Ca-Fe	Ca-Fe
Anomaly	35	35	35	35	35	35	35	35	35	35	35	35	35
SiO2	30.87	30.74	30.49	29.85	30.78	30.56	29.85	30.70	30.72	29.65	29.70	30.34	29.92
TiO2	30.67	31.30	31.72	34.38	34.32	31.97	33.74	33.60	33.66	32.81	32.73	32.93	33.01
Al2O3	3.50	3.87	3.13	1.76	1.89	3.39	3.82	3.58	3.71	3.77	3.69	3.90	3.76
Fe2O3	3.34	2.78	3.43	2.19	2.35	2.86	2.94	2.89	2.85	2.91	2.91	3.00	2.77
MnO	0.00	0.09	0.09	0.11	0.08	0.02	0.00	0.00	0.00	0.00	0.00	0.00	0.00
MgO	0.00	0.00	0.00	0.00	0.00	0.00	0.00	0.13	0.00	0.09	0.09	0.00	0.00
CaO	28.29	28.74	28.09	28.70	28.54	28.34	28.97	28.91	28.61	29.07	29.10	29.09	29.39
Na2O	0.00	0.00	0.00	0.02	0.02	0.02	0.00	0.35	0.00	0.00	0.00	0.00	0.00
K2O	0.06	0.04	0.07	0.07	0.06	0.04	0.00	0.00	0.00	0.00	0.01	0.01	0.01
F	1.85	1.61	2.26	1.49	0.85	1.71	1.48	1.61	1.39	1.17	1.12	0.89	1.73
Cl	0.00	0.00	0.00	0.00	0.00	0.01	0.00	0.00	0.00	0.00	0.00	0.01	0.00
TOTAL	97.80	98.49	98.33	97.93	98.54	98.18	96.99	96.84	95.61	96.46	95.75	96.56	95.63
Si	1.01	1.00	0.99	0.98	1.01	1.00	0.96	0.98	0.98	0.97	0.97	0.99	0.96
Al	0.13	0.15	0.12	0.07	0.07	0.13	0.15	0.13	0.14	0.15	0.14	0.15	0.14
Ti	0.75	0.77	0.77	0.85	0.85	0.78	0.82	0.80	0.81	0.81	0.81	0.81	0.80
Fe	0.06	0.05	0.06	0.04	0.04	0.05	0.05	0.05	0.05	0.05	0.05	0.05	0.05
Mn	0.00	0.00	0.00	0.00	0.00	0.00	0.00	0.00	0.00	0.00	0.00	0.00	0.00
Mg	0.00	0.00	0.00	0.00	0.00	0.00	0.00	0.01	0.00	0.00	0.00	0.00	0.00
Ca	0.99	1.00	0.97	1.01	1.01	0.99	1.00	0.98	0.98	1.02	1.02	1.01	1.01
Na	0.00	0.00	0.00	0.00	0.00	0.00	0.00	0.02	0.00	0.00	0.00	0.00	0.00
K	0.00	0.00	0.00	0.00	0.00	0.00	0.00	0.00	0.00	0.00	0.00	0.00	0.00
F(at)	0.19	0.17	0.23	0.15	0.09	0.18	0.15	0.16	0.14	0.12	0.12	0.09	0.18
Cl	0.00	0.00	0.00	0.00	0.00	0.00	0.00	0.00	0.00	0.00	0.00	0.00	0.00
Total	3.14	3.14	3.15	3.11	3.08	3.13	3.12	3.14	3.11	3.12	3.12	3.10	3.14
Fe+Al	0.20	0.20	0.18	0.11	0.12	0.18	0.20	0.19	0.19	0.20	0.20	0.20	0.19
OH	0.00	0.03	-0.05	-0.05	0.03	0.01	0.05	0.02	0.05	0.08	0.08	0.11	0.02
Ttn	0.80	0.80	0.82	0.89	0.88	0.82	0.80	0.81	0.81	0.80	0.80	0.80	0.81
F(at)	0.19	0.17	0.23	0.15	0.09	0.18	0.15	0.16	0.14	0.12	0.12	0.09	0.18

	161	162	163	164	165	166	167	168	169	170	171	172	173
Sample	7-9B	7-9B	GNA02	GNA02	GNA02	GNA02	GNA02	GNA02	GNA02	GNA02	GNA02	GNA02	GNA02
Mineralization	UNM	UNM	UNM	UNM	UNM	UNM	UNM	UNM	UNM	UNM	UNM	UNM	UNM
Alteration	Ca-Fe	Ca-Fe	Ca-Fe	Ca-Fe	Ca-Fe	Ca-Fe	Ca-Fe	Ca-Fe	Ca-Fe	Ca-Fe	Ca-Fe	Ca-Fe	Ca-Fe
Anomaly	35	35	35	35	35	35	35	35	35	35	35	35	35
SiO2	30.22	28.75	28.84	29.13	28.85	28.31	28.60	28.89	30.72	30.53	30.64	30.80	30.65
TiO2	32.66	33.47	35.72	35.81	35.74	34.67	36.26	35.47	35.47	35.70	36.29	34.84	34.26
Al2O3	3.81	3.78	2.27	2.24	2.07	2.32	1.97	2.29	2.10	1.85	1.66	2.38	2.42
Fe2O3	3.30	2.97	2.49	3.03	2.71	2.94	3.00	3.22	2.92	2.76	2.47	2.94	2.82
MnO	0.00	0.00	0.00	0.00	0.00	0.00	0.00	0.00	0.00	0.00	0.00	0.00	0.00
MgO	0.07	0.00	0.21	0.00	0.08	0.03	0.00	0.13	0.17	0.14	0.01	0.16	0.15
CaO	29.05	29.06	28.57	28.59	28.55	28.16	28.41	28.05	27.09	26.91	26.78	26.71	27.07
Na2O	0.00	0.00	0.00	0.00	0.07	0.00	0.00	0.28	0.05	0.00	0.00	0.00	0.11
K2O	0.00	0.00	0.00	0.00	0.00	0.01	0.00	0.00	0.02	0.01	0.00	0.01	0.02
F	1.66	1.71	0.98	1.51	1.03	0.58	0.80	0.75	1.77	1.01	1.48	1.26	1.43
Cl	0.01	0.00	0.00	0.00	0.00	0.00	0.00	0.00	0.00	0.00	0.01	0.00	0.01
TOTAL	94.95	95.94	96.05	98.02	95.01	97.65	96.66	97.21	96.11	94.06	96.58	95.37	95.52
Si	0.97	0.94	0.95	0.95	0.95	0.96	0.95	0.96	0.99	1.00	0.99	1.00	1.00
Al	0.14	0.14	0.09	0.09	0.08	0.09	0.08	0.09	0.08	0.07	0.06	0.09	0.09
Ti	0.79	0.82	0.89	0.87	0.89	0.88	0.90	0.88	0.86	0.88	0.88	0.85	0.84
Fe	0.06	0.05	0.05	0.05	0.05	0.06	0.06	0.06	0.05	0.05	0.04	0.05	0.05
Mn	0.00	0.00	0.00	0.00	0.00	0.00	0.00	0.00	0.00	0.00	0.00	0.00	0.00
Mg	0.00	0.00	0.01	0.00	0.00	0.00	0.00	0.01	0.01	0.01	0.00	0.01	0.01
Ca	1.00	1.01	1.01	0.99	1.01	1.02	1.01	1.00	0.93	0.94	0.93	0.93	0.95
Na	0.00	0.00	0.00	0.00	0.00	0.00	0.00	0.02	0.00	0.00	0.00	0.00	0.01
K	0.00	0.00	0.00	0.00	0.00	0.00	0.00	0.00	0.00	0.00	0.00	0.00	0.00
F(at)	0.17	0.18	0.10	0.16	0.11	0.06	0.08	0.08	0.18	0.10	0.15	0.13	0.15
Cl	0.00	0.00	0.00	0.00	0.00	0.00	0.00	0.00	0.00	0.00	0.00	0.00	0.00
Total	3.14	3.14	3.10	3.11	3.10	3.08	3.08	3.09	3.09	3.06	3.07	3.07	3.09
Fe+Al	0.20	0.20	0.13	0.14	0.13	0.15	0.13	0.15	0.13	0.12	0.11	0.14	0.14
OH	0.03	0.02	0.03	-0.01	0.02	0.09	0.05	0.07	-0.05	0.02	-0.04	0.02	0.00
Ttn	0.80	0.80	0.87	0.86	0.87	0.85	0.87	0.85	0.87	0.88	0.89	0.86	0.86
F(at)	0.17	0.18	0.10	0.16	0.11	0.06	0.08	0.08	0.18	0.10	0.15	0.13	0.15

Sample	174 ALB05	175 ALB05	176 ALB05	177 ALB05	178 ALB05	179 ALB05	180 ALB05	181 ALB05	182 ALB05	183 ALB05	184 ALB05	185 ALB05	186 ALB05
Mineralization	MIN	MIN	MIN	MIN	MIN	MIN	MIN	MIN	MIN	MIN	MIN	MIN	MIN
Alteration	Ca-Mg	Ca-Mg	Ca-Mg	Ca-Mg	Ca-Mg	Ca-Mg	Ca-Mg	Ca-Mg	Ca-Mg	Ca-Mg	Ca-Mg	Ca-Mg	Ca-Mg
Anomaly	35	35	35	35	35	35	35	35	35	35	35	35	35
SiO2	30.77	30.79	30.87	31.29	30.60	31.12	31.04	30.85	30.61	30.42	30.73	30.73	30.74
TiO2	35.71	37.07	37.40	38.38	37.69	38.60	38.38	37.03	37.78	36.66	36.82	37.16	37.81
Al2O3	0.62	0.43	0.63	0.22	0.28	0.27	0.30	0.37	0.25	0.36	0.91	0.42	0.34
Fe2O3	1.67	1.12	1.19	0.76	0.78	0.70	0.84	1.35	0.70	1.61	1.60	1.28	1.32
MnO	0.03	0.10	0.03	0.00	0.10	0.00	0.09	0.03	0.09	0.00	0.07	0.06	0.04
MgO	0.01	0.03	0.03	0.00	0.00	0.00	0.00	0.00	0.00	0.00	0.00	0.03	0.00
CaO	27.20	27.28	27.46	28.34	27.67	28.43	28.43	28.05	28.28	27.47	27.73	28.03	28.51
Na2O	0.11	0.15	0.04	0.05	0.08	0.05	0.07	0.09	0.17	0.02	0.07	0.13	0.07
K2O	0.04	0.01	0.04	0.02	0.02	0.01	0.01	0.00	0.01	0.02	0.00	0.02	0.00
F	0	0	0	0	0	0	0	0	0	0	0	0	0
Cl	0.00	0.00	0.00	0.00	0.00	0.00	0.00	0.00	0.00	0.00	0.00	0.00	0.00
TOTAL	96.05	98.02	95.01	97.65	97.21	96.11	94.06	96.58	95.37	95.17	95.02	94.87	94.72
Si	1.05	1.04	1.03	1.03	1.03	1.02	1.02	1.03	1.02	1.03	1.03	1.03	1.02
Al	0.02	0.02	0.02	0.01	0.01	0.01	0.01	0.01	0.01	0.01	0.04	0.02	0.01
Ti	0.91	0.94	0.94	0.95	0.95	0.96	0.95	0.93	0.95	0.93	0.93	0.94	0.94
Fe	0.03	0.02	0.02	0.01	0.01	0.01	0.02	0.03	0.01	0.03	0.03	0.02	0.02
Mn	0.00	0.00	0.00	0.00	0.00	0.00	0.00	0.00	0.00	0.00	0.00	0.00	0.00
Mg	0.00	0.00	0.00	0.00	0.00	0.00	0.00	0.00	0.00	0.00	0.00	0.00	0.00
Ca	0.99	0.98	0.98	1.00	1.00	1.00	1.00	1.01	1.01	1.00	0.99	1.00	1.01
Na	0.01	0.01	0.00	0.00	0.01	0.00	0.00	0.01	0.01	0.00	0.00	0.01	0.00
K	0.00	0.00	0.00	0.00	0.00	0.00	0.00	0.00	0.00	0.00	0.00	0.00	0.00
F(at)	0.00	0.00	0.00	0.00	0.00	0.00	0.00	0.00	0.00	0.00	0.00	0.00	0.00
Cl	0.00	0.00	0.00	0.00	0.00	0.00	0.00	0.00	0.00	0.00	0.00	0.00	0.00
Total	3.02	3.01	3.01	3.01	3.01	3.01	3.01	3.02	3.02	3.01	3.02	3.02	3.02
Fe+Al	0.06	0.04	0.05	0.02	0.03	0.02	0.03	0.04	0.02	0.04	0.07	0.04	0.04
OH	-	-	-	-	-	-	-	-	-	-	-	-	-
Ttn	-	-	-	-	-	-	-	-	-	-	-	-	-
F(at)	-	-	-	-	-	-	-	-	-	-	-	-	-

Sample	187 ALB05	188 ALB05	189 ALB05	190 ALB05	191 ALB05	192 ALB05	193 ALB05	194 ALB05	195 PAB03	196 PAB03	197 PAB03	198 PAB03	199 PAB03
Mineralization	MIN	MIN	MIN	MIN	MIN	MIN	MIN	MIN	MIN	MIN	MIN	MIN	MIN
Alteration	Ca-Mg	Ca-Mg	Ca-Mg	Ca-Mg	Ca-Mg	Ca-Mg	Ca-Mg	Ca-Mg	Ca-Mg	Ca-Mg	Ca-Mg	Ca-Mg	Ca-Mg
Anomaly	35	35	35	35	35	35	35	35	35	35	35	35	35
SiO2	31.31	31.06	31.09	30.62	30.37	31.08	31.21	31.18	30.94	30.39	31.31	31.47	30.45
TiO2	37.63	37.27	37.36	37.01	36.52	37.61	37.84	37.94	35.27	37.29	36.38	36.57	34.88
Al2O3	0.47	0.49	0.44	0.33	0.64	0.47	0.43	0.39	0.55	0.37	1.16	0.68	0.34
Fe2O3	1.15	1.23	1.28	1.17	1.45	1.34	1.40	1.32	0.90	0.64	0.86	0.68	0.97
MnO	0.05	0.08	0.10	0.05	0.02	0.07	0.06	0.01	0.00	0.00	0.00	0.00	0.00
MgO	0.00	0.00	0.01	0.00	0.01	0.00	0.03	0.14	0.01	0.00	0.01	0.01	0.00
CaO	28.46	28.21	28.09	27.57	27.84	28.16	28.67	28.20	28.34	28.34	28.08	28.67	27.88
Na2O	0.05	0.08	0.10	0.15	0.07	0.06	0.10	0.15	0.05	0.02	0.04	0.03	0.04
K2O	0.00	0.00	0.00	0.02	0.02	0.00	0.01	0.01	0.01	0.01	0.01	0.00	0.00
F	0	0	0	0	0	0	0	0	0.27	0.06	0.45	0.32	0.21
Cl	0.00	0.00	0.00	0.00	0.00	0.00	0.00	0.00	0.00	0.01	0.00	0.00	0.00
TOTAL	94.58	94.43	94.28	94.13	93.98	93.84	93.69	93.54	96.20	97.10	98.10	98.30	94.69
Si	1.03	1.03	1.03	1.03	1.03	1.03	1.03	1.03	1.05	1.02	1.03	1.04	1.05
Al	0.02	0.02	0.02	0.01	0.03	0.02	0.02	0.02	0.02	0.01	0.04	0.03	0.01
Ti	0.93	0.93	0.93	0.94	0.93	0.94	0.93	0.94	0.90	0.94	0.90	0.91	0.90
Fe	0.02	0.02	0.02	0.02	0.03	0.02	0.03	0.02	0.02	0.01	0.02	0.01	0.02
Mn	0.00	0.00	0.00	0.00	0.00	0.00	0.00	0.00	0.00	0.00	0.00	0.00	0.00
Mg	0.00	0.00	0.00	0.00	0.00	0.00	0.00	0.01	0.00	0.00	0.00	0.00	0.00
Ca	1.01	1.00	1.00	1.00	1.01	1.00	1.01	1.00	1.03	1.02	0.99	1.01	1.03
Na	0.00	0.01	0.01	0.01	0.00	0.00	0.01	0.01	0.00	0.00	0.00	0.00	0.00
K	0.00	0.00	0.00	0.00	0.00	0.00	0.00	0.00	0.00	0.00	0.00	0.00	0.00
F(at)	0.00	0.00	0.00	0.00	0.00	0.00	0.00	0.00	0.03	0.01	0.05	0.03	0.02
Cl	0.00	0.00	0.00	0.00	0.00	0.00	0.00	0.00	0.00	0.00	0.00	0.00	0.00
Total	3.02	3.02	3.02	3.02	3.02	3.01	3.02	3.02	3.04	3.02	3.04	3.03	3.04
Fe+Al	0.04	0.04	0.04	0.04	0.05	0.04	0.04	0.04	0.04	0.03	0.06	0.04	0.03
OH	-	-	-	-	-	-	-	-	0.01	0.02	0.01	0.01	0.01
Ttn	-	-	-	-	-	-	-	-	0.96	0.97	0.94	0.96	0.97
F(at)	-	-	-	-	-	-	-	-	0.03	0.01	0.05	0.03	0.02

Sample	200 PAB 03	201 PAB 03	202 PAAB 01	203 PAAB 01	204 PAAB 01	205 PAAB 01	206 POAB 02	207 POAB 02	208 POAB 02	209 POAB 02	210 POAB 02	211 POAB 02	212 POAB 02
Mineralization	MIN	MIN	UNM	UNM	UNM	UNM	UNM	UNM	UNM	UNM	UNM	UNM	UNM
Alteration	Ca-Mg	Ca-Mg	Na-Ca	Na-Ca	Na-Ca	Na-Ca	Na-Ca	Na-Ca	Na-Ca	Na-Ca	Na-Ca	Na-Ca	Na-Ca
Anomaly	35	35	35	35	35	35	35	35	35	35	35	35	35
SiO2	31.49	31.47	31.12	31.39	31.50	31.28	30.28	29.80	30.55	31.14	30.99	30.85	30.26
TiO2	37.04	37.10	35.20	32.73	37.40	31.72	32.98	34.23	34.99	36.14	34.12	33.57	32.79
Al2O3	0.38	0.47	1.29	2.75	0.54	2.46	1.02	1.01	0.82	0.81	1.18	1.16	1.12
Fe2O3	0.47	0.54	2.71	3.53	1.92	3.99	3.74	3.80	2.82	2.57	3.42	3.75	4.08
MnO	0.01	0.00	0.00	0.06	0.01	0.02	0.41	0.44	0.56	0.49	0.49	0.54	0.58
MgO	0.00	0.01	0.03	0.02	0.01	0.04	0.11	0.06	0.03	0.03	0.07	0.05	0.09
CaO	28.91	28.93	28.53	28.00	28.65	28.26	26.32	25.91	27.06	27.03	26.88	26.40	25.84
Na2O	0.00	0.03	0.06	0.05	0.07	0.05	0.17	0.21	0.17	0.17	0.16	0.18	0.16
K2O	0.00	0.00	0.00	0.00	0.00	0.01	0.01	0.01	0.01	0.00	0.02	0.00	0.01
F	0.25	0.63	0.77	2.14	0.03	1.46	0.44	0.29	0.21	0.43	0.48	0.62	0.66
Cl	0.01	0.00	0.00	0.00	0.00	0.00	0.00	0.00	0.00	0.00	0.00	0.00	0.01
TOTAL	98.44	98.91	99.39	99.75	100.13	98.67	95.28	95.64	97.13	98.65	97.60	96.86	95.31
Si	1.04	1.03	1.02	1.00	1.03	1.02	1.04	1.02	1.03	1.03	1.04	1.04	1.04
Al	0.01	0.02	0.05	0.10	0.02	0.09	0.04	0.04	0.03	0.03	0.05	0.05	0.05
Ti	0.92	0.91	0.87	0.79	0.92	0.78	0.85	0.89	0.89	0.90	0.86	0.85	0.85
Fe	0.01	0.01	0.05	0.06	0.04	0.07	0.07	0.07	0.05	0.05	0.06	0.07	0.08
Mn	0.00	0.00	0.00	0.00	0.00	0.00	0.01	0.01	0.02	0.01	0.01	0.02	0.02
Mg	0.00	0.00	0.00	0.00	0.00	0.00	0.01	0.00	0.00	0.00	0.00	0.00	0.00
Ca	1.02	1.01	1.00	0.96	1.00	0.99	0.97	0.95	0.98	0.96	0.96	0.95	0.95
Na	0.00	0.00	0.00	0.00	0.00	0.00	0.01	0.01	0.01	0.01	0.01	0.01	0.01
K	0.00	0.00	0.00	0.00	0.00	0.00	0.00	0.00	0.00	0.00	0.00	0.00	0.00
F(at)	0.03	0.06	0.08	0.22	0.00	0.15	0.05	0.03	0.02	0.04	0.05	0.07	0.07
Cl	0.00	0.00	0.00	0.00	0.00	0.00	0.00	0.00	0.00	0.00	0.00	0.00	0.00
Total	3.03	3.05	3.07	3.13	3.02	3.12	3.05	3.04	3.04	3.04	3.05	3.06	3.06
Fe+Al	0.02	0.03	0.10	0.17	0.06	0.17	0.11	0.11	0.09	0.08	0.11	0.12	0.12
OH	0.00	-0.04	0.02	-0.05	0.05	0.02	0.06	0.08	0.06	0.03	0.06	0.05	0.05
Ttn	0.98	0.97	0.90	0.83	0.94	0.83	0.89	0.89	0.91	0.92	0.89	0.88	0.88
F(at)	0.03	0.06	0.08	0.22	0.00	0.15	0.05	0.03	0.02	0.04	0.05	0.07	0.07

Sample	213 POAB 02	214 MAAB 03	215 MAAB 03	216 MAAB 03	217 MAAB 03	218 MAAB 03	219 MAAB 03	220 MAAB 03	221 MAAB 03	222 MAAB 03	223 MAAB 03	224 BCAB	225 BCAB
Mineralization	UNM	MIN	MIN	MIN	MIN	MIN	MIN	MIN	MIN	MIN	MIN	MIN	MIN
Alteration	Na-Ca	Ca-Mg	Ca-Mg	Ca-Mg	Ca-Mg	Ca-Mg	Ca-Mg	Ca-Mg	Ca-Mg	Ca-Mg	Ca-Mg	K-Mg	K-Mg
Anomaly	35	35	35	35	35	35	35	35	35	35	35	35	35
SiO2	30.73	31.17	31.12	31.25	31.20	31.11	29.42	31.27	31.56	31.43	31.18	31.29	30.60
TiO2	31.95	33.56	33.09	33.81	33.53	38.61	34.62	33.22	34.44	38.01	37.46	38.42	37.46
Al2O3	1.41	2.85	3.13	2.33	2.56	0.32	0.57	2.70	2.73	0.79	0.72	1.02	1.33
Fe2O3	3.91	2.04	1.99	1.85	1.97	0.74	1.64	1.97	2.02	1.10	1.19	0.31	0.39
MnO	0.45	0.00	0.05	0.07	0.00	0.00	0.04	0.00	0.02	0.00	0.06	0.00	0.02
MgO	0.12	0.01	0.03	0.00	0.00	0.00	0.03	0.01	0.04	0.00	0.01	0.01	0.00
CaO	25.73	27.90	27.90	28.72	28.98	28.67	28.87	28.36	28.50	28.44	28.46	28.25	28.01
Na2O	0.16	0.05	0.03	0.06	0.01	0.03	0.05	0.02	0.05	0.07	0.04	0.06	0.04
K2O	0.01	0.00	0.00	0.00	0.01	0.01	0.01	0.01	0.01	0.00	0.00	0.01	0.01
F	0.92	1.09	1.10	0.09	0.58	0.00	1.14	0.72	1.05	0.32	0.14	0.06	0.00
Cl	0.00	0.00	0.00	0.01	0.00	0.00	0.01	0.00	0.00	0.00	0.00	0.00	0.00
TOTAL	94.98	98.20	97.97	98.14	98.60	99.47	95.92	97.97	99.98	100.02	99.21	99,424	97,848
Si	1.05	1.02	1.02	1.04	1.03	1.02	0.99	1.03	1.02	1.02	1.03	1.02	1.02
Al	0.06	0.11	0.12	0.09	0.10	0.01	0.02	0.10	0.10	0.03	0.03	0.04	0.05
Ti	0.82	0.82	0.81	0.85	0.83	0.95	0.88	0.82	0.83	0.93	0.93	0.94	0.94
Fe	0.07	0.04	0.04	0.03	0.04	0.01	0.03	0.04	0.04	0.02	0.02	0.01	0.01
Mn	0.01	0.00	0.00	0.00	0.00	0.00	0.00	0.00	0.00	0.00	0.00	0.00	0.00
Mg	0.01	0.00	0.00	0.00	0.00	0.00	0.00	0.00	0.00	0.00	0.00	0.00	0.00
Ca	0.94	0.98	0.98	1.02	1.02	1.01	1.05	1.00	0.98	0.99	1.00	0.99	1.00
Na	0.01	0.00	0.00	0.00	0.00	0.00	0.00	0.00	0.00	0.00	0.00	0.00	0.00
K	0.00	0.00	0.00	0.00	0.00	0.00	0.00	0.00	0.00	0.00	0.00	0.00	0.00
F(at)	0.10	0.11	0.11	0.01	0.06	0.00	0.12	0.08	0.11	0.03	0.01	0.01	0.00
Cl	0.00	0.00	0.00	0.00	0.00	0.00	0.00	0.00	0.00	0.00	0.00	0.00	0.00
Total	3.07	3.08	3.09	3.05	3.08	3.01	3.10	3.08	3.08	3.03	3.02	3.01	3.02
Fe+Al	0.13	0.15	0.16	0.13	0.14	0.03	0.05	0.14	0.14	0.05	0.05	0.05	0.06
OH	0.03	0.03	0.04	0.12	0.08	0.03	-0.07	0.07	0.03	0.02	0.04	0.04	0.06
Ttn	0.87	0.85	0.84	0.87	0.86	0.97	0.95	0.86	0.86	0.95	0.95	0.95	0.94
F(at)	0.10	0.11	0.11	0.01	0.06	0.00	0.12	0.08	0.11	0.03	0.01	0.01	0.00

Sample	226 BCAB	227 BCAB	228 BAB129	229 BAB129	230 BAB129	231 BAB129	232 BAB129	233 BAB129	234 BAB129	235 POAB05	236 POAB05	237 POAB05	238 POAB05
Mineralization	MIN	MIN	MIN	MIN	MIN	MIN	MIN	MIN	MIN	MIN	MIN	MIN	MIN
Alteration	K-Mg	K-Mg	K-Mg	K-Mg	K-Mg	K-Mg	K-Mg	K-Mg	K-Mg	Ca-Mg	Ca-Mg	Ca-Mg	Ca-Mg
Anomaly	35	35	35	35	35	35	35	35	35	35	35	35	35
SiO2	31.15	30.87	29.40	29.84	30.26	30.43	30.37	30.82	30.16	29.90	30.23	30.31	30.02
TiO2	37.68	37.02	39.13	38.14	37.34	36.96	38.49	37.33	38.58	34.64	33.49	34.58	35.14
Al2O3	1.20	1.33	0.54	0.65	0.77	0.68	0.52	0.72	0.75	1.79	2.35	1.52	0.92
Fe2O3	0.28	0.38	0.13	0.20	0.34	0.20	0.21	0.31	0.15	2.24	2.40	1.67	1.72
MnO	0.07	0.05	0.00	0.00	0.00	0.00	0.00	0.00	0.00	0.05	0.03	0.02	0.07
MgO	0.01	0.00	0.00	0.00	0.00	0.01	0.00	0.00	0.00	0.02	0.02	0.01	0.03
CaO	27.55	27.91	28.33	28.47	28.61	28.55	28.73	28.62	28.66	26.96	26.58	27.76	27.04
Na2O	0.07	0.03	0.00	0.00	0.00	0.00	0.00	0.00	0.00	0.07	0.09	0.06	0.02
K2O	0.00	0.00	0.00	0.00	0.00	0.00	0.00	0.00	0.00	0.00	0.02	0.00	0.00
F	0.17	0.00	0.00	0.00	0.00	0.00	0.00	0.00	0.00	0.52	0.69	0.80	0.22
Cl	0.00	0.00	0.01	0.01	0.00	0.00	0.02	0.00	0.00	0.00	0.00	0.00	0.00
TOTAL	98,106	97,596	97.56	97.46	97.35	96.83	98.34	97.82	98.31	95.96	95.61	96.37	95.09
Si	1.03	1.03	0.99	1.00	1.02	1.03	1.01	1.03	1.00	1.01	1.02	1.02	1.03
Al	0.05	0.05	0.02	0.03	0.03	0.03	0.02	0.03	0.03	0.07	0.09	0.06	0.04
Ti	0.94	0.93	0.99	0.96	0.94	0.94	0.96	0.94	0.96	0.88	0.85	0.87	0.91
Fe	0.01	0.01	0.00	0.00	0.01	0.00	0.00	0.01	0.00	0.04	0.05	0.03	0.03
Mn	0.00	0.00	0.00	0.00	0.00	0.00	0.00	0.00	0.00	0.00	0.00	0.00	0.00
Mg	0.00	0.00	0.00	0.00	0.00	0.00	0.00	0.00	0.00	0.00	0.00	0.00	0.00
Ca	0.97	1.00	1.02	1.02	1.03	1.03	1.02	1.02	1.02	0.98	0.96	1.00	0.99
Na	0.00	0.00	0.00	0.00	0.00	0.00	0.00	0.00	0.00	0.00	0.01	0.00	0.00
K	0.00	0.00	0.00	0.00	0.00	0.00	0.00	0.00	0.00	0.00	0.00	0.00	0.00
F(at)	0.02	0.00	0.00	0.00	0.00	0.00	0.00	0.00	0.00	0.06	0.07	0.08	0.02
Cl	0.00	0.00	0.00	0.00	0.00	0.00	0.00	0.00	0.00	0.00	0.00	0.00	0.00
Total	3.01	3.01	3.02	3.02	3.02	3.02	3.02	3.02	3.02	3.05	3.06	3.07	3.03
Fe+Al	0.05	0.06	0.02	0.03	0.04	0.03	0.02	0.03	0.03	0.11	0.14	0.09	0.07
OH	0.03	-	-	-	-	-	-	-	-	0.06	0.07	0.01	0.05
Ttn	0.95	-	-	-	-	-	-	-	-	0.89	0.86	0.91	0.93
F(at)	0.02	-	-	-	-	-	-	-	-	0.06	0.07	0.08	0.02

3H: EPMA analyses of epidote. Recalculated formula on the basis of 12.5 oxygens

	MAAB03	MAAB03	MAAB03	MAAB03
SiO2	37.49	38.25	36.91	35.20
TiO2	0.07	0.02	0.01	0.14
Al2O3	21.27	21.14	20.99	17.86
FeO	13.83	13.81	13.72	12.76
MgO	0.08	0.07	0.05	0.22
MnO	0.06	0.05	0.03	0.03
CaO	22.22	22.62	21.61	19.32
Na2O	0.01	0.00	0.01	0.15
K2O	0.00	0.00	0.00	0.01
F	0.07	0.11	0.00	0.36
Cl	0.00	0.00	0.01	0.11
H2O	0.00	0.00	0.00	0.00
Total]wt%	95.07	96.02	93.34	85.98
[Si	3.00	3.00	3.00	3.00
Al(IV)	0.00	0.00	0.00	0.00
[Ti	0.00	0.00	0.00	0.01
Al(VI)	2.01	1.95	2.01	1.79
Cr	0.00	0.00	0.00	0.00
V	0.00	0.00	0.00	0.00
Fe3+	0.10	0.12	0.13	0.22
Fe2+	0.83	0.79	0.81	0.69
Mg	0.01	0.01	0.01	0.03
Mn3+	0.00	0.00	0.00	0.00
Mn2+	0.00	0.00	0.00	0.00
Ni	0.00	0.00	0.00	0.00
Zn	0.00	0.00	0.00	0.00
Cu	0.00	0.00	0.00	0.00
Nb	0.00	0.00	0.00	0.00
Sn	0.00	0.00	0.00	0.00
[Mn2+	0.00	0.00	0.00	0.00
Fe2+	0.00	0.00	0.00	0.00
Ca	1.91	1.90	1.88	1.76
Sr	0.00	0.00	0.00	0.00
Ba	0.00	0.00	0.00	0.00
Pb	0.00	0.00	0.00	0.00
Na	0.00	0.00	0.00	0.03
K	0.00	0.00	0.00	0.00
P	0.00	0.00	0.00	0.00
REE	0.00	0.00	0.00	0.00
Th	0.00	0.00	0.00	0.00
U	0.00	0.00	0.00	0.00
[Epidote name]	Epidote	Epidote	Epidote	Epidote

3I: EPMA analyses of uraninite. Recalculated formula on the basis of 1 cation.

	1	2	3	4	5	6	7	8	9
AMOSTRA	POAB05	POAB05	POAB05	POAB05	POAB05	POAB05	POAB05	POAB05	POAB05
ANOMALIA	AN35	AN35	AN35	AN35	AN35	AN35	AN35	AN35	AN35
class	veinlets	veinlets	veinlets	veinlets	veinlets	veinlets	veinlets	veinlets	veinlets
SiO2	0.93	2.96	1.85	1.90	0.06	1.04	0.52	1.29	0.08
TiO2	0.00	0.07	0.08	0.05	0.12	0.44	0.50	0.46	0.28
CaO	3.48	3.44	3.52	3.39	1.43	2.18	1.92	3.02	1.98
Al2O3	0.10	0.27	0.16	0.16	0.00	0.05	0.02	0.02	0.00
MgO	0.03	0.02	0.01	0.04	0.03	0.04	0.00	0.00	0.03
Y2O3	3.86	4.36	4.48	4.54	9.30	6.46	7.85	5.83	7.47
FeO	0.23	0.13	0.10	0.17	0.30	0.51	0.11	0.15	0.10
ZrO2	0.13	0.53	0.22	0.46	0.00	0.11	0.04	0.32	0.05
V2O3	0.00	0.08	0.05	0.04	0.00	0.04	0.05	0.02	0.00
P2O5	0.09	0.13	0.11	0.14	0.30	0.14	0.20	0.15	0.18
UO2	75.57	74.06	76.26	75.12	73.48	75.44	75.34	74.56	76.23
ThO2	0.000	0.11	0.08	0.06	0.03	0.00	0.11	0.15	0.10
PbO	5.68	5.57	6.02	6.16	5.19	5.77	5.85	5.76	5.91
Total	94.18	91.74	92.93	92.26	90.24	92.23	92.51	91.75	92.40
Si (apfu)	0.042	0.120	0.078	0.080	0.003	0.045	0.023	0.055	0.003
Ti	0.000	0.003	0.003	0.002	0.005	0.018	0.020	0.018	0.012
Ca	0.084	0.075	0.079	0.076	0.034	0.050	0.044	0.069	0.047
Al	0.004	0.010	0.006	0.006	0.000	0.002	0.001	0.001	0.000
Mg	0.001	0.001	0.000	0.001	0.001	0.001	0.000	0.000	0.001
Y	0.069	0.071	0.075	0.076	0.167	0.110	0.135	0.099	0.132
Fe	0.004	0.002	0.002	0.003	0.006	0.009	0.002	0.003	0.002
Zr	0.003	0.011	0.004	0.009	0.000	0.002	0.001	0.007	0.001
V	0.000	0.002	0.001	0.001	0.000	0.001	0.001	0.001	0.000
P	0.005	0.007	0.006	0.008	0.018	0.008	0.012	0.009	0.011
U	0.754	0.668	0.711	0.702	0.735	0.720	0.725	0.705	0.754
Th	0.000	0.001	0.001	0.001	0.000	0.000	0.001	0.001	0.001
Pb	0.034	0.030	0.034	0.035	0.031	0.033	0.034	0.033	0.035
U/Th	7389066666.67	658.33	909.27	1184.72	2477.59	737596444.44	701.62	476.48	784.62
Si+Ti+Ca+Mg+Y+Fe+Zr	14.17	17.31	16.41	16.71	16.13	16.05	16.81	16.86	15.86
Age	0.54	0.54	0.57	0.59	0.51	0.55	0.56	0.55	0.55

	10	11	12	13	14	15	16	17	18
AMOSTRA	POAB05	POAB05	POAB05	POAB05	POAB05	POAB05	POAB05	POAB05	POAB05
ANOMALIA	AN35	AN35	AN35	AN35	AN35	AN35	AN35	AN35	AN35
class	veinlets	veinlets	veinlets	veinlets	veinlets	veinlets	veinlets	veinlets	veinlets
SiO2	0.09	0.16	0.16	0.08	0.06	0.07	0.07	0.09	0.23
TiO2	0.09	0.16	0.07	0.04	0.05	0.10	0.08	0.09	0.40
CaO	1.75	2.40	1.99	2.20	1.93	2.03	2.30	2.44	2.45
Al2O3	0.00	0.00	0.00	0.00	0.00	0.00	0.00	0.00	0.00
MgO	0.00	0.00	0.01	0.03	0.03	0.01	0.02	0.00	0.02
Y2O3	7.81	6.10	7.32	5.09	6.20	5.17	6.27	6.08	7.14
FeO	0.11	0.11	0.21	0.31	0.53	0.40	0.06	0.09	0.09
ZrO2	0.00	0.27	0.07	0.05	0.10	0.05	0.00	0.00	0.07
V2O3	0.00	0.00	0.00	0.00	0.01	0.00	0.00	0.03	0.00
P2O5	0.19	0.15	0.20	0.12	0.15	0.10	0.13	0.16	0.17
UO2	77.80	75.72	75.80	79.62	79.15	80.58	79.80	79.10	76.65
ThO2	0.09	0.09	0.14	0.03	0.00	0.03	0.12	0.06	0.12
PbO	5.94	6.89	6.27	6.52	6.16	5.99	5.60	5.98	5.66
Total	93.96	92.08	92.23	94.09	94.36	94.51	94.46	94.11	92.99
Si (apfu)	0.004	0.007	0.007	0.003	0.003	0.003	0.003	0.004	0.010
Ti	0.004	0.007	0.003	0.002	0.002	0.004	0.003	0.004	0.016
Ca	0.041	0.058	0.048	0.053	0.046	0.049	0.054	0.058	0.057
Al	0.000	0.000	0.000	0.000	0.000	0.000	0.000	0.000	0.000
Mg	0.000	0.000	0.000	0.001	0.001	0.000	0.001	0.000	0.001
Y	0.137	0.109	0.131	0.091	0.110	0.092	0.111	0.107	0.124
Fe	0.002	0.002	0.004	0.006	0.010	0.007	0.001	0.002	0.002
Zr	0.000	0.006	0.001	0.001	0.002	0.001	0.000	0.000	0.001
V	0.000	0.000	0.000	0.000	0.000	0.000	0.000	0.001	0.000
P	0.011	0.009	0.012	0.007	0.009	0.006	0.008	0.009	0.010
U	0.764	0.759	0.755	0.796	0.781	0.801	0.785	0.779	0.744
Th	0.001	0.001	0.001	0.000	0.000	0.000	0.001	0.001	0.001
Pb	0.035	0.042	0.038	0.039	0.037	0.036	0.033	0.036	0.033
U/Th	864.41	841.34	521.93	2780.49	7739208888.89	3151.57	661.28	1267.97	635.15
Si+Ti+Ca+Mg+Y+Fe+Zr	15.78	16.06	16.02	14.00	14.50	13.43	14.44	14.74	16.06
Age	0.55	0.65	0.59	0.59	0.56	0.53	0.51	0.54	0.53

	19	20	21	22	23	24	25	26	27	28
AMOSTRA	POAB05	MAAB03	MAAB03	MAAB03	MAAB03	MAAB03	MAAB03	MAAB03	BIAB01	BIAB01
ANOMALIA	AN35	AN35	AN35	AN35	AN35	AN35	AN35	AN35	AN35	AN35
class	veinlets	veinlets	veinlets	veinlets	veinlets	veinlets	veinlets	veinlets	disseminated	disseminated
SiO2	0.39	0.49	0.29	0.07	0.11	0.07	0.38	0.25	0.20	0.32
TiO2	0.54	0.11	0.39	0.15	0.07	0.01	0.27	0.00	0.19	0.23
CaO	1.89	2.93	3.41	2.15	2.61	2.52	3.22	2.92	0.97	0.96
Al2O3	0.00	0.02	0.01	0.00	0.00	0.00	0.01	0.00	0.03	0.07
MgO	0.04	0.00	0.00	0.00	0.06	0.04	0.03	0.06	0.02	0.00
Y2O3	7.89	1.62	2.16	2.23	3.00	2.57	1.75	2.09	0.27	0.57
FeO	0.09	0.03	0.00	0.34	0.16	0.14	0.00	0.06	0.04	0.29
ZrO2	0.04	0.01	0.14	0.07	0.11	0.07	0.23	0.11	0.01	0.02
V2O3	0.00	0.00	0.00	0.00	0.01	0.00	0.00	0.00	0.03	0.00
P2O5	0.17	0.02	0.06	0.00	0.00	0.00	0.07	0.04	0.02	0.00
UO2	73.48	81.21	82.92	79.13	79.29	79.88	79.69	78.65	88.48	87.59
ThO2	0.17	0.02	0.04	0.08	0.09	0.14	0.03	0.06	0.20	0.28
PbO	5.27	5.94	5.53	5.42	5.70	6.08	6.19	5.75	6.29	6.37
Total	89.95	92.39	94.94	89.64	91.20	91.51	91.87	89.97	96.77	96.68
Si (apfu)	0.018	0.022	0.013	0.003	0.005	0.003	0.017	0.012	0.009	0.015
Ti	0.022	0.005	0.016	0.007	0.003	0.001	0.012	0.000	0.008	0.010
Ca	0.045	0.072	0.080	0.055	0.065	0.064	0.079	0.074	0.024	0.023
Al	0.000	0.001	0.000	0.000	0.000	0.000	0.000	0.000	0.001	0.003
Mg	0.001	0.000	0.000	0.000	0.002	0.001	0.001	0.002	0.001	0.000
Y	0.140	0.030	0.038	0.043	0.056	0.048	0.032	0.039	0.005	0.010
Fe	0.002	0.001	0.000	0.007	0.003	0.003	0.000	0.001	0.001	0.005
Zr	0.001	0.000	0.003	0.002	0.002	0.002	0.005	0.003	0.000	0.000
V	0.000	0.000	0.000	0.000	0.000	0.000	0.000	0.000	0.001	0.000
P	0.011	0.001	0.003	0.000	0.000	0.000	0.005	0.002	0.001	0.000
U	0.728	0.831	0.813	0.847	0.826	0.838	0.811	0.829	0.907	0.891
Th	0.002	0.000	0.000	0.001	0.001	0.001	0.000	0.001	0.002	0.003
Pb	0.032	0.037	0.033	0.035	0.036	0.039	0.038	0.037	0.039	0.039
U/Th	427.65	4179.18	1930.48	943.56	871.13	565.94	2782.83	1349.11	426.19	306.95
Si+Ti+Ca+Mg+Y+Fe+Zr	16.17	11.14	11.96	10.17	11.69	11.46	12.08	11.18	8.17	8.81
Age	0.52	0.53	0.48	0.49	0.52	0.55	0.56	0.53	0.51	0.52

	29	30	31	32	33	34	35	36
AMOSTRA	BIAB01	BIAB01	BIAB01	BIAB129	BIAB129	BIAB129	BIAB129	BIAB129
ANOMALIA class	AN35 disseminated	AN35 disseminated	AN35 disseminated	AN35 disseminated	AN35 disseminated	AN35 disseminated	AN35 disseminated	AN35 disseminated
SiO2	0.31	0.11	0.02	0.16	0.13	2.84	0.12	0.32
TiO2	0.13	0.17	0.16	0.06	0.00	0.88	0.06	0.00
CaO	0.61	1.06	0.65	0.70	1.52	1.18	1.43	3.04
Al2O3	0.30	0.01	0.01	0.00	0.00	0.63	0.00	0.07
MgO	0.02	0.00	0.00	0.04	0.03	0.05	0.03	0.11
Y2O3	0.63	0.72	0.40	0.77	0.86	0.55	0.70	0.24
FeO	0.32	0.90	0.06	0.05	0.11	0.45	0.06	0.07
ZrO2	0.02	0.03	0.06	0.03	0.05	0.07	0.01	0.06
V2O3	0.10	0.03	0.00	0.07	0.04	0.00	0.01	0.00
P2O5	0.00	0.01	0.01	0.00	0.00	0.00	0.00	0.01
UO2	89.09	91.07	91.01	84.80	81.17	74.12	85.96	71.79
ThO2	0.02	0.07	0.11	1.01	0.64	0.35	0.40	0.23
PbO	6.39	6.41	6.24	5.98	9.23	6.19	6.53	9.50
Total	97.94	100.58	98.72	93.67	93.78	87.30	95.30	85.44
Si (apfu)	0.014	0.005	0.001	0.008	0.006	0.125	0.005	0.016
Ti	0.006	0.007	0.007	0.003	0.000	0.036	0.003	0.000
Ca	0.015	0.025	0.016	0.018	0.039	0.028	0.036	0.083
Al	0.012	0.000	0.000	0.000	0.000	0.025	0.000	0.003
Mg	0.001	0.000	0.000	0.002	0.001	0.002	0.001	0.004
Y	0.011	0.013	0.007	0.015	0.016	0.010	0.013	0.005
Fe	0.006	0.017	0.001	0.001	0.002	0.008	0.001	0.001
Zr	0.000	0.001	0.001	0.001	0.001	0.001	0.000	0.001
V	0.003	0.001	0.000	0.002	0.001	0.000	0.000	0.000
P	0.000	0.001	0.001	0.000	0.000	0.000	0.000	0.001
U	0.893	0.893	0.926	0.902	0.866	0.725	0.895	0.816
Th	0.000	0.001	0.001	0.011	0.007	0.003	0.004	0.003
Pb	0.039	0.038	0.038	0.039	0.060	0.037	0.041	0.065
U/Th	4355.61	1349.19	780.60	82.50	124.40	210.06	209.08	302.54
Si+Ti+Ca+Mg+Y+Fe+Zr	8.42	8.56	7.65	8.71	12.42	12.68	9.25	13.46
Age	0.52	0.51	0.49	0.51	0.79	0.60	0.54	0.91

	37	38	39	40	41	42	43	44
AMOSTRA	BIAB129	BIAB129	BCAB	BCAB	BCAB	BCAB	BCAB	BCAB
ANOMALIA class	AN35 disseminated	AN35 disseminated	AN35 disseminated	AN35 disseminated	AN35 disseminated	AN35 disseminated	AN35 disseminated	AN35 disseminated
SiO2	0.27	0.18	0.06	0.10	0.04	0.09	0.08	0.46
TiO2	0.04	0.00	0.00	0.00	0.10	0.13	0.10	0.19
CaO	1.23	1.49	0.52	0.65	0.50	0.55	0.50	0.57
Al2O3	0.03	0.00	0.00	0.00	0.00	0.01	0.01	0.31
MgO	0.05	0.03	0.01	0.03	0.03	0.00	0.03	0.19
Y2O3	0.54	0.40	0.43	0.49	0.57	0.72	0.61	0.70
FeO	0.04	0.11	0.23	0.36	0.41	0.17	0.45	0.27
ZrO2	0.01	0.00	0.01	0.00	0.00	0.04	0.00	0.06
V2O3	0.01	0.15	0.00	0.05	0.00	0.04	0.02	0.08
P2O5	0.02	0.00	0.00	0.00	0.00	0.00	0.00	0.00
UO2	86.33	79.97	88.09	86.02	87.03	84.73	85.87	84.87
ThO2	0.18	0.17	0.12	0.36	0.05	0.19	0.17	0.25
PbO	6.14	9.20	6.29	6.18	6.30	6.48	6.22	6.19
Total	94.88	91.71	95.78	94.28	95.03	93.17	94.06	94.13
Si (apfu)	0.013	0.009	0.003	0.005	0.002	0.005	0.004	0.021
Ti	0.002	0.000	0.000	0.000	0.005	0.006	0.005	0.008
Ca	0.031	0.039	0.013	0.017	0.013	0.014	0.013	0.014
Al	0.001	0.000	0.000	0.000	0.000	0.001	0.000	0.013
Mg	0.002	0.001	0.000	0.001	0.001	0.000	0.001	0.006
Y	0.010	0.008	0.008	0.009	0.011	0.014	0.012	0.013
Fe	0.001	0.002	0.005	0.007	0.008	0.003	0.009	0.005
Zr	0.000	0.000	0.000	0.000	0.000	0.001	0.000	0.001
V	0.000	0.004	0.000	0.001	0.000	0.001	0.000	0.002
P	0.001	0.000	0.000	0.000	0.000	0.000	0.000	0.000
U	0.899	0.873	0.929	0.916	0.920	0.911	0.914	0.874
Th	0.002	0.002	0.001	0.004	0.001	0.002	0.002	0.003
Pb	0.039	0.061	0.040	0.040	0.040	0.042	0.040	0.039
U/Th	458.77	449.37	694.65	232.98	1810.45	427.05	499.74	338.73
Si+Ti+Ca+Mg+Y+Fe+Zr	8.43	11.44	7.43	7.77	7.56	8.22	7.69	8.72
Age	0.51	0.80	0.51	0.52	0.52	0.55	0.52	0.52

	45	46	47	48	49	50	51	52
AMOSTRA	BCAB	BCAB	BCAB	BCAB	BCAB	BCAB	BCAB	BCAB
ANOMALIA	AN35	AN35	AN35	AN35	AN35	AN35	AN35	AN35
class	disseminated	disseminated	disseminated	disseminated	disseminated	disseminated	disseminated	disseminated
SiO2	0.21	0.09	0.23	0.04	0.09	0.09	0.06	0.04
TiO2	0.14	0.00	0.00	0.04	0.04	0.00	0.00	0.09
CaO	0.41	0.42	0.95	0.62	0.79	0.49	0.43	0.49
Al2O3	0.02	0.00	0.01	0.00	0.00	0.00	0.01	0.00
MgO	0.09	0.03	0.02	0.04	0.01	0.00	0.02	0.01
Y2O3	0.59	0.65	0.67	0.60	0.67	0.66	0.64	0.60
FeO	0.22	0.28	0.03	0.12	0.02	0.37	0.42	0.45
ZrO2	0.03	0.03	0.00	0.00	0.03	0.02	0.00	0.00
V2O3	0.04	0.00	0.09	0.04	0.00	0.00	0.01	0.00
P2O5	0.00	0.00	0.00	0.00	0.01	0.01	0.00	0.00
UO2	82.07	83.80	86.42	88.84	88.28	87.80	87.66	86.23
ThO2	0.30	0.28	0.22	0.26	0.27	0.44	0.33	0.36
PbO	5.88	5.75	6.04	6.72	6.85	6.43	6.42	6.30
Total	90.01	91.38	94.80	97.33	97.04	96.34	95.99	94.57
Si (apfu)	0.010	0.004	0.011	0.002	0.004	0.004	0.003	0.002
Ti	0.007	0.000	0.000	0.002	0.002	0.000	0.000	0.004
Ca	0.011	0.011	0.024	0.016	0.020	0.012	0.011	0.012
Al	0.001	0.000	0.000	0.000	0.000	0.000	0.000	0.000
Mg	0.003	0.001	0.001	0.001	0.000	0.000	0.001	0.000
Y	0.012	0.013	0.013	0.011	0.013	0.012	0.012	0.011
Fe	0.005	0.006	0.001	0.002	0.000	0.007	0.008	0.009
Zr	0.001	0.001	0.000	0.000	0.001	0.000	0.000	0.000
V	0.001	0.000	0.003	0.001	0.000	0.000	0.000	0.000
P	0.000	0.000	0.000	0.000	0.000	0.001	0.000	0.000
U	0.907	0.922	0.907	0.920	0.915	0.917	0.921	0.917
Th	0.003	0.003	0.002	0.003	0.003	0.005	0.004	0.004
Pb	0.039	0.038	0.038	0.042	0.043	0.041	0.041	0.041
U/Th	264.83	290.54	377.23	335.39	317.33	195.10	259.73	232.92
Si+Ti+Ca+Mg+Y+Fe+Zr	7.59	7.22	8.13	8.28	8.74	8.13	7.88	7.88
Age	0.52	0.49	0.50	0.54	0.56	0.53	0.53	0.52

	53	54	55	56	57	58	59	60
AMOSTRA	BCAB	BCAB	BCAB	BCAB	BCAB	BCAB	BCAB	BCAB
ANOMALIA	AN35	AN35	AN35	AN35	AN35	AN35	AN35	AN35
class	disseminated	disseminated	disseminated	disseminated	disseminated	disseminated	disseminated	disseminated
SiO2	0.02	0.07	0.16	0.06	0.13	0.09	0.09	0.12
TiO2	0.04	0.04	0.00	0.00	0.06	0.00	0.02	0.00
CaO	0.47	0.34	0.59	0.49	0.46	0.85	0.35	0.39
Al2O3	0.00	0.00	0.00	0.00	0.02	0.05	0.00	0.02
MgO	0.00	0.02	0.03	0.03	0.01	0.02	0.03	0.03
Y2O3	0.82	0.80	0.65	0.58	0.58	0.57	0.58	0.52
FeO	0.06	0.20	0.25	0.27	0.18	0.17	0.49	0.55
ZrO2	0.00	0.02	0.00	0.03	0.00	0.07	0.00	0.00
V2O3	0.00	0.01	0.03	0.05	0.00	0.00	0.01	0.03
P2O5	0.00	0.00	0.00	0.00	0.00	0.00	0.00	0.01
UO2	87.82	88.76	87.94	89.35	88.11	89.57	88.04	86.95
ThO2	1.20	0.53	0.38	0.36	0.39	0.29	0.43	0.47
PbO	6.32	6.75	6.71	6.66	6.44	6.84	6.51	6.32
Total	96.75	97.59	96.76	97.87	96.38	98.52	96.54	95.41
Si (apfu)	0.001	0.003	0.007	0.003	0.006	0.004	0.004	0.006
Ti	0.002	0.002	0.000	0.000	0.003	0.000	0.001	0.000
Ca	0.012	0.009	0.015	0.012	0.012	0.021	0.009	0.010
Al	0.000	0.000	0.000	0.000	0.001	0.002	0.000	0.001
Mg	0.000	0.001	0.001	0.001	0.000	0.001	0.001	0.001
Y	0.015	0.015	0.012	0.011	0.011	0.010	0.011	0.010
Fe	0.001	0.004	0.005	0.005	0.004	0.003	0.010	0.011
Zr	0.000	0.000	0.000	0.001	0.000	0.002	0.000	0.000
V	0.000	0.000	0.001	0.001	0.000	0.000	0.000	0.001
P	0.000	0.000	0.000	0.000	0.000	0.000	0.000	0.001
U	0.916	0.918	0.913	0.921	0.919	0.912	0.919	0.915
Th	0.013	0.006	0.004	0.004	0.004	0.003	0.005	0.005
Pb	0.040	0.042	0.042	0.042	0.041	0.042	0.041	0.040
U/Th	71.62	164.99	225.68	241.33	221.48	298.90	202.55	182.05
Si+Ti+Ca+Mg+Y+Fe+Zr	8.87	8.55	8.49	8.18	8.08	8.76	7.97	7.84
Age	0.52	0.54	0.55	0.53	0.52	0.55	0.53	0.52

	61	62	63	64	65	66	67	68
AMOSTRA	BALB02	BALB02	BALB02	BALB02	BALB02	BALB02	BALB02	BALB02
ANOMALIA	AN34	AN34	AN34	AN34	AN34	AN34	AN34	AN34
class	disseminated	disseminated	disseminated	disseminated	disseminated	disseminated	disseminated	disseminated
SiO2	0.07	0.04	0.11	0.04	0.05	0.08	0.10	0.06
TiO2	0.02	0.03	0.03	0.02	0.14	0.08	0.09	0.10
CaO	0.39	0.43	0.77	0.40	0.49	0.48	0.44	0.53
Al2O3	0.00	0.00	0.00	0.00	0.00	0.03	0.00	0.00
MgO	0.01	0.02	0.02	0.02	0.02	0.01	0.02	0.00
Y2O3	2.87	2.52	2.80	2.55	2.46	2.78	2.48	2.56
FeO	0.22	0.05	0.05	0.14	0.26	0.34	0.15	0.41
ZrO2	0.00	0.00	0.02	0.04	0.03	0.00	0.00	0.00
V2O3	0.00	0.08	0.00	0.00	0.03	0.07	0.00	0.02
P2O5	0.05	0.04	0.06	0.12	0.02	0.03	0.06	0.05
UO2	82.03	83.20	81.76	84.19	83.72	84.07	83.92	82.90
ThO2	1.12	1.10	1.07	1.05	1.41	1.22	1.48	0.91
PbO	6.01	6.21	6.05	6.14	6.12	6.06	6.21	6.23
Total	92.80	93.72	92.73	94.72	94.72	95.26	94.94	93.78
Si (apfu)	0.003	0.002	0.005	0.002	0.002	0.004	0.005	0.003
Ti	0.001	0.001	0.001	0.001	0.006	0.003	0.004	0.004
Ca	0.010	0.011	0.020	0.010	0.012	0.012	0.011	0.013
Al	0.000	0.000	0.000	0.000	0.000	0.001	0.000	0.000
Mg	0.000	0.001	0.001	0.001	0.001	0.000	0.001	0.000
Y	0.055	0.048	0.053	0.048	0.046	0.051	0.046	0.048
Fe	0.004	0.001	0.001	0.003	0.005	0.007	0.003	0.008
Zr	0.000	0.000	0.000	0.001	0.001	0.000	0.000	0.000
V	0.000	0.002	0.000	0.000	0.001	0.002	0.000	0.001
P	0.004	0.002	0.004	0.008	0.001	0.002	0.004	0.003
U	0.872	0.880	0.865	0.877	0.872	0.867	0.872	0.870
Th	0.012	0.012	0.012	0.011	0.015	0.013	0.016	0.010
Pb	0.039	0.040	0.039	0.039	0.039	0.038	0.039	0.040
U/Th	71.94	73.69	74.50	78.55	58.26	67.21	55.55	89.17
Si+Ti+Ca+Mg+Y+Fe+Zr	10.48	10.33	10.85	10.25	10.69	10.74	10.79	10.39
Age	0.52	0.53	0.53	0.52	0.52	0.52	0.53	0.54

	69	70	71	72	73	74	75	76
AMOSTRA	BALB02	BALB02	BALB02	BALB02	BALB02	BALB02	BALB02	BALB02
ANOMALIA	AN34	AN34	AN34	AN34	AN34	AN34	AN34	AN34
class	disseminated	disseminated	disseminated	disseminated	disseminated	disseminated	disseminated	disseminated
SiO2	0.07	0.08	0.08	0.14	0.08	0.06	0.10	0.09
TiO2	0.00	0.04	0.00	0.10	0.00	0.08	0.00	0.00
CaO	0.45	0.59	0.63	0.49	0.42	0.47	0.45	0.51
Al2O3	0.00	0.00	0.00	0.00	0.00	0.00	0.00	0.00
MgO	0.01	0.01	0.04	0.00	0.02	0.00	0.03	0.02
Y2O3	2.51	2.91	3.11	2.46	3.02	3.19	2.49	2.69
FeO	0.27	0.11	0.33	0.21	0.37	0.55	0.18	0.30
ZrO2	0.00	0.02	0.00	0.00	0.02	0.00	0.06	0.00
V2O3	0.00	0.00	0.00	0.06	0.06	0.01	0.03	0.00
P2O5	0.00	0.05	0.04	0.03	0.04	0.07	0.02	0.05
UO2	84.06	83.78	82.74	81.12	83.10	83.34	84.16	84.46
ThO2	1.42	1.12	1.12	1.26	0.95	0.86	1.17	1.05
PbO	6.07	6.44	6.26	5.79	6.10	6.11	6.18	6.23
Total	94.86	95.15	94.36	91.67	94.18	94.80	94.85	95.41
Si (apfu)	0.003	0.004	0.004	0.007	0.004	0.003	0.004	0.004
Ti	0.000	0.002	0.000	0.005	0.000	0.003	0.000	0.000
Ca	0.011	0.015	0.016	0.013	0.011	0.012	0.011	0.013
Al	0.000	0.000	0.000	0.000	0.000	0.000	0.000	0.000
Mg	0.000	0.000	0.001	0.000	0.001	0.000	0.001	0.001
Y	0.047	0.054	0.058	0.047	0.057	0.059	0.047	0.050
Fe	0.005	0.002	0.006	0.004	0.007	0.011	0.004	0.006
Zr	0.000	0.000	0.000	0.000	0.000	0.000	0.001	0.000
V	0.000	0.000	0.000	0.002	0.002	0.000	0.001	0.000
P	0.000	0.003	0.003	0.002	0.003	0.005	0.001	0.003
U	0.879	0.867	0.861	0.869	0.868	0.861	0.878	0.873
Th	0.015	0.012	0.012	0.014	0.010	0.009	0.012	0.011
Pb	0.038	0.040	0.039	0.038	0.039	0.038	0.039	0.039
U/Th	58.00	73.14	71.98	62.95	85.71	94.86	70.58	78.57
Si+Ti+Ca+Mg+Y+Fe+Zr	10.52	11.20	11.20	10.25	10.59	10.76	10.43	10.57
Age	0.52	0.55	0.54	0.51	0.53	0.53	0.53	0.53

	77	78	79	80	81	82	83	84	85
AMOSTRA	BALB02	BALB02	BALB02	BALB02	GALB02	GALB02	GALB02	GALB02	GALB02
ANOMALIA	AN34	AN34	AN34	AN34	AN34	AN34	AN34	AN34	AN34
class	disseminated	disseminated	disseminated	disseminated	veinlets	veinlets	veinlets	veinlets	veinlets
SiO2	0.06	0.02	0.08	0.04	1.98	0.78	0.45	0.08	0.14
TiO2	0.04	0.08	0.00	0.06	0.33	1.97	1.35	0.03	0.08
CaO	0.42	0.46	0.52	0.54	1.83	2.32	2.15	0.35	0.81
Al2O3	0.00	0.00	0.00	0.00	0.07	0.03	0.05	0.00	0.05
MgO	0.01	0.05	0.03	0.00	0.01	0.03	0.04	0.03	0.02
Y2O3	2.59	2.88	3.05	2.70	1.49	0.99	0.94	2.31	1.48
FeO	0.20	0.43	0.38	0.12	0.12	0.32	0.19	0.00	0.10
ZrO2	0.00	0.03	0.01	0.05	0.00	0.14	0.09	0.00	0.00
V2O3	0.00	0.09	0.02	0.00	0.00	0.00	0.04	0.00	0.05
P2O5	0.05	0.05	0.04	0.06	0.00	0.00	0.00	0.08	0.01
UO2	83.10	83.26	83.36	82.82	68.31	71.22	76.17	78.70	76.98
ThO2	1.02	1.08	0.99	1.16	0.83	0.80	0.68	0.96	1.05
PbO	5.85	6.28	6.16	6.05	5.48	5.96	6.59	5.99	5.83
Total	93.33	94.71	94.66	93.60	80.47	84.57	88.77	88.51	86.62
Si (apfu)	0.003	0.001	0.004	0.002	0.098	0.037	0.021	0.004	0.007
Ti	0.002	0.004	0.000	0.003	0.015	0.087	0.059	0.001	0.004
Ca	0.011	0.011	0.013	0.014	0.049	0.058	0.054	0.009	0.022
Al	0.000	0.000	0.000	0.000	0.003	0.001	0.002	0.000	0.002
Mg	0.000	0.002	0.001	0.000	0.001	0.001	0.001	0.001	0.001
Y	0.049	0.053	0.057	0.051	0.030	0.019	0.017	0.046	0.030
Fe	0.004	0.008	0.007	0.002	0.003	0.006	0.004	0.000	0.002
Zr	0.000	0.001	0.000	0.001	0.000	0.003	0.002	0.000	0.000
V	0.000	0.002	0.001	0.000	0.000	0.000	0.001	0.000	0.001
P	0.003	0.003	0.002	0.004	0.000	0.000	0.000	0.005	0.001
U	0.880	0.864	0.866	0.873	0.755	0.742	0.790	0.881	0.877
Th	0.011	0.011	0.011	0.012	0.009	0.009	0.007	0.011	0.012
Pb	0.037	0.039	0.039	0.039	0.037	0.038	0.041	0.041	0.040
U/Th	79.74	75.52	82.08	69.87	80.18	87.05	109.05	80.40	71.48
Si+Ti+Ca+Mg+Y+Fe+Zr	9.97	10.83	10.81	10.60	12.02	12.99	12.30	9.71	9.45
Age	0.51	0.54	0.53	0.52	0.57	0.60	0.61	0.54	0.54

	86	87	88	89	90	91	92	93
AMOSTRA	GALB02	GALB02	GALB02	GALB02	GALB02	GALB02	31BIAB01	31BIAB01
ANOMALIA	AN34	AN34	AN34	AN34	AN34	AN34	AN31	AN31
class	veinlets	veinlets	veinlets	veinlets	veinlets	veinlets	dissemiated	dissemiated
SiO2	0.19	0.50	0.08	0.08	0.50	0.37	0.15	0.16
TiO2	0.00	0.16	0.04	0.18	0.07	0.05	0.08	0.00
CaO	0.62	0.93	6.60	0.46	0.52	2.62	2.26	2.54
Al2O3	0.01	0.00	0.02	0.00	0.01	0.05	0.02	0.00
MgO	0.02	0.02	0.00	0.01	0.01	0.05	0.00	0.00
Y2O3	1.49	1.65	1.11	2.10	1.75	1.35	0.55	0.69
FeO	0.04	0.29	0.01	0.07	0.03	0.06	0.52	0.53
ZrO2	0.00	0.11	0.04	0.05	0.00	0.00	0.01	0.00
V2O3	0.02	0.00	0.01	0.00	0.01	0.08	0.00	0.11
P2O5	0.06	0.03	0.03	0.08	0.04	0.00	0.00	0.01
UO2	76.46	74.11	73.94	77.81	70.82	71.52	87.48	86.73
ThO2	1.01	0.89	1.24	1.32	1.14	1.34	0.15	0.33
PbO	5.49	5.95	6.42	6.20	4.84	6.03	5.59	5.85
Total	85.43	84.67	89.53	88.36	79.74	83.56	96.81	96.94
Si (apfu)	0.010	0.026	0.004	0.004	0.027	0.019	0.007	0.008
Ti	0.000	0.008	0.002	0.009	0.004	0.002	0.004	0.000
Ca	0.017	0.025	0.162	0.012	0.015	0.072	0.001	0.000
Al	0.001	0.000	0.001	0.000	0.001	0.002	0.000	0.000
Mg	0.001	0.001	0.000	0.000	0.000	0.002	0.000	0.000
Y	0.031	0.034	0.020	0.042	0.038	0.028	0.010	0.013
Fe	0.001	0.006	0.000	0.002	0.001	0.001	0.010	0.011
Zr	0.000	0.003	0.001	0.001	0.000	0.000	0.000	0.000
V	0.001	0.000	0.000	0.000	0.000	0.002	0.000	0.003
P	0.004	0.002	0.002	0.006	0.003	0.000	0.000	0.001
U	0.885	0.845	0.756	0.868	0.861	0.814	0.930	0.923
Th	0.012	0.010	0.013	0.015	0.014	0.016	0.002	0.004
Pb	0.038	0.041	0.040	0.042	0.036	0.042	0.036	0.038
U/Th	73.88	81.05	58.30	57.86	60.64	52.03	585.89	259.34
Si+Ti+Ca+Mg+Y+Fe+Zr	8.82	10.20	15.54	10.39	8.83	11.81	8.81	9.56
Age	0.51	0.57	0.61	0.57	0.49	0.60	0.46	0.49

	94	95	96	97	98
AMOSTRA	31BIAB01	31BIAB01	31BIAB01	31BIAB01	31BIAB01
ANOMALIA	AN31	AN31	AN31	AN31	AN31
class	dissemiated	dissemiated	dissemiated	dissemiated	dissemiated
SiO2	0.12	0.11	0.10	0.30	0.22
TiO2	0.00	0.12	0.10	0.00	0.04
CaO	1.68	1.76	3.18	3.05	3.02
Al2O3	0.00	0.00	0.02	0.29	0.04
MgO	0.00	0.05	0.05	0.00	0.00
Y2O3	0.63	0.46	0.71	0.21	0.30
FeO	1.11	0.51	0.58	2.96	1.71
ZrO2	0.00	0.01	0.00	0.54	0.49
V2O3	0.05	0.00	0.08	0.04	0.00
P2O5	0.02	0.01	0.12	0.00	0.00
UO2	86.92	85.27	87.04	78.16	79.27
ThO2	0.09	0.10	0.16	0.01	0.01
PbO	6.61	6.80	6.63	8.53	8.88
Total	97.22	95.19	98.77	94.10	93.95
Si (apfu)	0.006	0.005	0.005	0.015	0.011
Ti	0.000	0.005	0.004	0.000	0.002
Ca	0.000	0.000	0.000	0.007	0.001
Al	0.000	0.002	0.002	0.000	0.000
Mg	0.000	0.000	0.000	0.000	0.000
Y	0.012	0.009	0.013	0.004	0.006
Fe	0.022	0.010	0.011	0.060	0.035
Zr	0.000	0.000	0.000	0.013	0.012
V	0.001	0.000	0.002	0.001	0.000
P	0.001	0.001	0.008	0.000	0.000
U	0.915	0.922	0.910	0.844	0.874
Th	0.001	0.001	0.002	0.000	0.000
Pb	0.042	0.044	0.042	0.056	0.059
U/Th	988.20	833.74	525.35	5878.85	15500.71
Si+Ti+Ca+Mg+Y+Fe+Zr	9.13	9.36	10.90	12.93	12.98
Age	0.55	0.57	0.55	0.76	0.78

3J: Other uranium minerals

N.º	8	9	27	28	29	33	30	31	32
MgO	0.06	0.02	0.00	0.00	0.02	0.03	0.04	0.03	0.07
TiO2	0.04	0.03	0.00	0.00	0.00	0.04	12.89	14.59	13.65
Y2O3	0.00	0.00	0.00	0.00	0.15	0.02	0.00	0.06	0.00
Al2O3	0.03	0.06	0.32	0.26	0.42	0.03	0.07	0.09	0.15
V2O3	0.02	0.13	0.00	0.00	0.05	0.14	0.53	0.44	0.49
P2O5	0.02	0.01	0.00	0.00	0.05	0.03	0.39	0.36	0.34
SiO2	15.48	15.05	33.50	30.74	32.93	13.46	2.70	3.29	3.38
FeO	0.07	0.07	0.15	0.04	0.00	0.01	0.49	0.44	0.65
ZrO2	0.00	0.00	0.01	0.01	0.00	0.01	0.30	0.10	0.09
PbO	0.10	0.00	1.54	1.54	1.59	0.04	5.96	7.07	6.17
ThO2	0.07	0.00	0.02	0.01	0.00	0.00	0.00	0.07	0.00
UO2	65.17	67.21	54.40	54.30	57.23	67.54	58.29	55.34	56.10
CaO	5.24	5.57	0.43	0.32	0.17	4.87	1.92	2.33	2.25
Total	86.29	88.15	90.37	87.22	92.59	86.21	83.57	84.21	83.34
Comment	F11BIAB129-C1-1	F11BIAB129-C1-2	3533PAB03-C2-1	3533PAB03-C2-2	3533PAB03-C2-3	3533PAB03-C4-1	3533PAB03-C3-1	3533PAB03-C3-2	3533PAB03-C3-3
	uranofana	uranofana	uranofana	uranofana	uranofana	uranofana	U-Si-Ti specie	U-Si-Ti specie	U-Si-Ti specie

4A: Anomalia 35 – Depósito Gameleira I

ANOMALIA 35					
	LOG EMPRESA		COLETADAS		LÂMINAS
FURO 33	0-8,70	SOLO			
	8,70-17,85	RAAR			
	17,85-39	MAQM	AM 01	28,08-28,48	GNA01
		MAQM	AM 02	28,92-29,12	
		MAQM	AM 03	30,80-31,42	MAAB01
		MAQM	AM 04	32,87-33,27	POAB01
	39-43,35	POAB/EPAB			
		POAB/EPAB	AM 05	40,08-40,49	POAB02
	43,35-44,75	MAQM	AM 06	44,68-45,06	
	44,75-47,85	PAAB/BAAB	AM 07	45,97-46,30	PAB03
	47,85-70	AMQM/MAQM	AM 08	49,10-49,54	BIAB01
		AMQM/MAQM	AM 09	59,11-59,43	GNA02
FURO 12	19-34,70	MAQM	AM 01	34,06 - 34,44	GNA01
	34,70-36,40	MAAB	AM 02	35,48-35,90	MAB01
	36,40-71,50	MAQM	AM 03	50,94-51,95	GNA02
		MAQM	AM 04	71,00-71,34	
	71,50-73	MAAB/POAB	AM 05	71,72-71,93	MAB02
	73-81	MAQM	AM 06	74,26-74,93	POAB01
	81-105,50	MAAB/POAB	AM 07	80-,87-81,40	GNA03
		MAAB/POAB	AM 08	82,75-83,41	POAB02
		MAAB/POAB	AM 09	85,50-85,96	POAB03
		MAAB/POAB	AM 10	87,90-88,20	POAB04
		MAAB/POAB	AM 11	90,54-90,74	
		MAAB/POAB	AM 12	94,09-94,45	POAB05
		MAAB/POAB	AM 13	103,34-103,74	
	105,50-106,5	MAAB/dique?	AM 14	105,86-106,15	MAAB03
	106,5-119	MAAB/BIAB	AM 15	107,50-107,87	
		MAAB/BIAB	AM 16	117,84-118,19	BIAB01
	119-122,50	BIAB	AM 17	121,49-121,84	
	122,5-130	MAQM	AM 18	123,68-124,07	POAB06
		MAQM	AM 19	128,06-128,47	GNA04
FURO 16	17,50-32,50	RX ALTERADA			
	32,50-82,70	MAQM			
		MAQM	AM 01	81,51-81,85	GNA01
	82,70-84,70	MAAB fino	AM 02	82,84-83.23	
	82,70-84,70	MAAB	AM 03	84,25-85,19	POAB01/MAAB01
	84,70-124	MAQM	AM 03	84,25-85,19	POAB01/MAAB01
	124-131	MAAB/PAAB	AM 04	124,10-124,63	MAAB02
	124-131	MAAB/PAAB	AM 05	125,85-127,35	PAAB01
	131-137	MAAB/BIAB	AM 06	131,63-131,91	MAAB03
	131-137	MAAB/BIAB	AM 07	135,20-135,68	
	137-141,25	MAQM/dique?	AM 08	140,85-141,57	GNA02
	141,25-143	MAAB/dique?	AM 09	142,8-143,25	
	143-148	BCAB	AM 10	147,30-147,77	BCAB
	148-150	MAAB/BIAB	AM 11	147,99-148,25	
		MAAB/BIAB	AM 12	149,52-150,02	BIAB
	150-152	BRECHA	AM 13	151,05-151,69	
	152-170	MAQM	AM 14	159,22-159,54	GNA03

	COLETADAS		LÂMINAS	
FURO 10	AMT 01	52,14 - 53,10	GNA/GRA	GNA 01; GRA 01
	AMT 01	53,11 - 53,22	GRA CIN	
	AMT 02	55,16 - 55,87	GRA CIN	
	AMT 03	55,96 - 56,15	GRA CIN	
	AMT 04	56,15 - 56,60	GRA CIN	
	AMT 05	56,87 -57,8	GRA CIN/FOL	5_1; 5_2; 5_7
	AMT 06	57,8 - 58,85	GNA	5-8(GNA)
	AMT 07	58,75 - 59,66	ALB	7_1; 7_2; 7_3; 7_9
	AMT 08	59,66 - 60,60	GNA	8_3; 8_4A; 8_4B; 8_6; 8_8A ; 8_8B
	AMT 09	60,60 - 61,65	GNA	8_9A; 8_9B
	AMT 02	84,05 - 84,95	GNA/ALB	GNA 02; ALB 01
	AMT 04	91,7 - 92,3	ALB/GNA	ALB 02; ALB/GNA 01; GNA 03
	AMT 03	93,65 - 94	ALB	
	AMT 09	119,9 - 119,55	GNA/ALB n min	GNA 04
	AMT 05	119,72 - 119,92	ALB MAAB?	ALB 03
	AMT 10	121,2 - 121,5	ALB N MIN	ALB 04
	AMT 11	124,25 - 124,8	ALB MIN	ALB 05
	AMT 13		ALB	ALB 06
	AMT 12	130,73 - 130,84	ALB	
	AMT 06	132,12 - 132,39	ALB - GNA	ALB 07; ALB/GNA 02
	AMT 07	142,01 - 142,35	GNA PROTOM	
	AMT 08	143,1 - 143,72	GNA PROTOM	GNA 05; GNA 06; GNA 07

4B: Anomalia 34 – Depósito Barrinha

	ANOMALIA 34				
	LOG EMPRESA		COLETADAS		LÂMINAS
	0-5	SOLO			
	5-15	RAAR			
	15-23,9	MAQM	AM 01	17,45-17,95	
	23,9-84,50	AMQM	AM 02	25,9-26,15	GNA01
		AMQM	AM 03	49,45-50,02	GNA02
		AMQM	AM 04	83,95-84,42	MALB01
	84,5-87	MAAB/POAB	AM 05	85,27-85,8	
FURO 09	87-92	GPAB	AM 06	86,82-87,40	GALB01
	92-111	BPAB	AM 07	91,45-92,27	
		BPAB	AM 08	96,65-93,35	BALB01
		BPAB	AM 09	95,25-95,66	
		BPAB	AM 10	103,98-104,51	BALB02
	111-120	ALB/GRAAB	AM 11	111,21-111,95	
		ALB/GRAAB	AM 12	112,45-113,21	GALB02
	120-126	BIAB	AM 13	122,77-123,67	BALB03
	126-133	PGAB	AM 15	128,17-129	GALB04
		PGAB	AM 14	130-130,61	GALB03
	133-140	MAQM	AM 16	134,29-134,84	GALB05

4C: Anomalia 31 – Depósito Barreiro

	ANOMALIA 31				
FURO 04	LOG EMPRESA		COLETADAS		LÂMINAS
	6,5-10,45	RAAR			
	10,45-12,50	ANF	AM01	11,13-11,60	ANF01
	12,50-27,15	MAQM	AM02	25,09-25,42	GNA01
	27,15-33,50	ALB	AM03	31,64-32,09	
	33,50-77	MAQM	AM04	35,20-35,77	
			AM05	75,47-75,95	GNA02
	77-87	BIAB	AM06	77,52-77,96	
			AM07	83,29-83,81	BIAB01
	87-92	MAGN	AM08	90,36-90,89	
	92-100	MAQM	AM09	93,50-93,90	
			AM10	94,34-94,79	MAGN01
			AM11	97,95-98,24	

FURO 11	COLETADO			LÂMINAS
	16,4 - 16,8	GNA	AMT 01	3111GNA01
	17,4 - 18	ALB (PAAB)	AMT 02	3111PALB01
	20,62 - 21	ALB (MAAB)	AMT 03	
	21,18 - 21,52	AUG GNA	AMT 04	3111GNA02
	31,2 - 31,5	AUG GNA	AMT 05	
	32 - 32,45	ALB (BIAB)	AMT 06	3111MALB01
	32,71 - 33,17	ALB (BIAB)	AMT 07	3111BALB01
	33,73 - 34,10	AUG GNA	AMT 08	
	39,15 - 40,12	GNA/ANF	AMT 09	
	41,3 - 41,78	ANF/GNA	AMT 10	3111GNA03/ANF01
	48,90 - 49,10	GNA	AMT 01	1_1
	49,61 - 49,68	GNA	AMT 02	
	49,80 - 49,98	GNA	AMT 03	3_1
	50,48 - 51	GNA/GRA	AMT 11	
	51,00 - 51,20	GRA	AMT 04	
	51,85 - 52	GRA	AMT 05	5_3
	53,38 - 53,75	GRA	AMT 12	
	53,75 - 54	GRA	AMT 06	
	54 - 54,35	GRA	AMT 13	GRA 01
	57,6 - 59,9	GRA	AMT 07	
	60,71 - 61,65	GRA ROS	AMT 08	8_11
	65,8 - 66,75	GRA ROS	AMT 14	
	66,75 - 67,85	GRA ROS	AMT 09	9-7 GRA ROS;9-9
	68,90 - 69,05	GRA ROS/GNA	AMT 10	
	86,28 - 87,16	GNA	AMT 15	GNA 01
	132 - 132,8	GNA/PIAB/ALB	AMT 16	
	132,8 - 134,75		AMT 17	ALB 01; ALB 02;ALB 03
	132,8 - 134,75		AMT 17	3111GNA04
	141,2 - 141,79	GNA	AMT 19	